Numerical Analysis of the Reuse of Piled Raft Foundations

by

Konstantinos Giannopoulos
MEng, ACGI, MSc, DIC

A thesis submitted to Imperial College London
in partial fulfilment of the requirements for the degree
of Doctor of Philosophy in the Faculty of Engineering

Department of Civil and Environmental Engineering
Imperial College London
London SW7 2AZ

July 2011

Declaration

I declare that the work presented in this thesis was carried out in the Department of Civil and Environmental Engineering at Imperial College London from October 2007. I also declare that this thesis is the result of my own work and any quotation or description of the work of others is acknowledged herein by reference to the sources, whether published or unpublished.

Konstantinos Giannopoulos

July 2011

Abstract

This thesis considers the reuse and the optimum design of piled raft foundations using numerical analysis. The solution proposed for reusing foundations is the design of a piled raft foundation capable of supporting successive buildings. A raft foundation, with a limited number of piles located strategically beneath the raft and utilising a high proportion of the ultimate load capacity, is considered the most efficient design when the raft foundation alone provides sufficient load capacity, but at the same time settlements are excessive. This is the case in high plasticity stiff clays such as London Clay.

When building on old piles, these piles had to sustain a certain load from the previous structure over a period of time, during which the soil is subjected to the time-related processes of consolidation and creep. A time dependent constitutive model, capable of reproducing several aspects of the time dependent behaviour of soils including creep and isotach viscosity, is employed in the finite element analyses. The model parameters are calibrated with the results of laboratory tests on London Clay, whose time dependent behaviour in its natural state is characterised by isotach viscosity, rate dependent peak strength and rate independent critical state line.

Preliminary analyses of single piles indicate that the consolidation processes in the ground result in little gain in capacity in the long term, whereas creep results in increased capacity. A back-analysis of documented piled load tests in London Clay is performed, where the effects of pile installation are quantified. Numerical model calibration is performed with the documented observations of a well instrumented piled raft foundation at Stonebridge Park, London. 3D parametric analyses of piled raft foundations are then performed, in order to assess the appropriate location and dimensions of piles and raft thickness. The performance of piled raft foundations with time is assessed parametrically at different levels of preloading. Optimisation of the performance of the piled raft foundation at Stonebridge Park is attempted by examining several pile arrangements, where a central pile support with a limited number of piles is more cost-effective than the original design.

Acknowledgments

Initially, I would like to express my gratitude to my supervisors Dr. L. Zdravkovic and Prof. D. M. Potts for their guidance through my PhD career and their continuous support from the beginning until the end of this 'marathon'. I would like to express to them my appreciation for offering me the opportunity to perform research and be a proud member of the numerical group of the Geotechnics section of the Civil and Environmental Engineering Department at Imperial College London. I would like also to express my gratitude to Empirikion Foundation for supporting financially my PhD studies. Without this support, I would not be able to complete my studies.

Next, I would like to thank all the members of the research group, the academic staff, the technicians, and of course all the people making this place work, for enhancing my academic and personal life. Many special thanks to my officemates Katerina, Teresa and Marianna, and the other ICFEP users David and Reini, who made this place feel like home from the beginning. Special thanks to Antonio, Bo, Shen, Freya, Loizos and Vasilis and many wishes to them for a successful PhD thesis.

I would like also to thank Imperial as an institution and the civil engineering department for giving me the opportunity to study science, integrate me as a personality and equip me with valuable skills for the future. I cannot forget the Hellenic Society, the IC Football and Basketball teams, the SSL league, the Friday evenings. It has been 9 years since 2002 and I feel that an era is closing.

I also thank my friends in London for hanging out, playing football, and making this time especially enjoyable. I would like also to express my appreciation to my parents, who offered me the chance to spend almost a decade in London and always wanted the best for me. Many thanks to my brother Giannis, who was always there to help. Special thanks to Iro for her patience and continuous support.

Table of Contents

DECLARATION 2
ABSTRACT 3
ACKNOWLEDGMENTS 4
TABLE OF CONTENTS 5
LIST OF FIGURES 11
LIST OF TABLES 24
SYMBOLS AND ABBREVIATIONS 26

CHAPTER 1 INTRODUCTION 33
1.1. BACKGROUND 33
1.2. REDEVELOPMENT OPTIONS 34
1.3. REUSE OF OLD PILES – CASE HISTORIES 36
1.4. DESIGN OF NEW FOUNDATIONS FOR FUTURE REUSE 40
1.5. OBJECTIVES AND METHODOLOGY 41
1.6. LAYOUT OF THE THESIS 42

CHAPTER 2 PILED FOUNDATIONS 46
2.1. INTRODUCTION 46
2.2. SINGLE PILES 47
2.2.1. INTRODUCTION 47
2.2.2. LIFE CYCLE OF PILES 48
2.2.2.1. Installation and Equilibration 48
2.2.2.2. Loading phase 52
2.2.2.3. Elapsed time 56
2.2.2.4. Unloading and reloading 57
2.2.3. AXIAL LOAD CAPACITY OF PILES 58
2.2.3.1. End-bearing resistance 59
2.2.3.2. Shaft friction 60

2.2.4. OBSERVED LONG TERM PERFORMANCE OF PILES 62
2.2.4.1. Load tests on displacement piles 63
2.2.4.2. Load tests on replacement piles 64
2.2.4.3. Conclusions from load tests 66
2.3. PILED RAFT FOUNDATIONS 67
2.3.1. INTRODUCTION 67
2.3.2. DESIGN CONCEPTS 68
2.3.2.1. Design philosophies 68
2.3.2.2. Conditions for efficient design 71
2.3.2.3. Effective choice of foundation type 71
2.3.3. DESIGN APPROACHES AND CASE HISTORIES 72
2.3.3.1. 'Conventional' piled rafts 72
2.3.3.2. Piles as 'settlement reducers' and 'creep piling' rafts 79
2.3.3.3. An attempt for optimum design: Piled rafts to control differential settlements 91
2.3.4. METHODS OF ANALYSIS 98
2.3.4.1. Simplified calculation methods 99
2.3.4.2. Approximate computer based methods 104
2.3.4.3. More rigorous numerical methods 106
2.3.5. NUMERICAL STUDIES 109
2.3.5.1. Parametric studies on hypothetical piled raft foundations 109
2.3.5.2. Hiscocks House: Stonebridge Park (London) by Viggiani (1998) 120
2.3.5.3. Torhaus der Messe: Frankfurt by Reul and Randolph (2003) 122
2.3.5.4. Five-storey building: Urawa (Japan) by Poulos (2001) 125
2.4. SUMMARY AND CONCLUDING REMARKS 127

CHAPTER 3 TIME DEPENDENT BEHAVIOUR OF SOILS 131
3.1. INTRODUCTION 131
3.2. CONSOLIDATION 132
3.2.1. The process of consolidation 132
3.2.2. Definition of primary and secondary consolidation 133
3.2.3. Time dependency of consolidation 135
3.3. VISCOUS BEHAVIOUR OF SOILS AND SOIL AGEING 136
3.3.1. CREEP AND STRESS RELAXATION 137
3.3.1.1. Definition of creep and stress relaxation 137
3.3.1.2. Definition of creep phases 138

3.3.1.3. Quantification of creep behaviour *139*
3.3.2. RATE EFFECTS 141
3.3.2.1. Definition of rate effects *141*
3.3.2.2. Isotach vs. non-isotach viscosity *141*
3.3.3. ACCUMULATED EFFECTS 144
3.3.3.1. Observed volumetric creep behaviour in clays *145*
3.3.3.2. Observed deviatoric creep behaviour in clays *150*
3.4. CONCLUDING REMARKS 156

CHAPTER 4 CONSTITUTIVE MODELS 158
4.1. INTRODUCTION 158
4.2. FINITE ELEMENT METHOD 159
4.2.1. Finite element theory for linear materials *159*
4.2.2. Non-linearity in finite element analysis *161*
4.2.3. Finite element formulation for coupled problems *163*
4.3. MODIFIED CAM CLAY MODEL 165
4.3.1. Formulation in general stress space *165*
4.3.2. Undrained strength *170*
4.3.3. Model parameters *171*
4.4. EQUIVALENT TIME CREEP MODEL 172
4.4.1. Fundamental assumption *172*
4.4.2. The concept of equivalent time *174*
4.4.3. Constitutive equation for isotropic loading conditions *176*
4.4.4. Extension to general stress space *180*
4.4.5. Plastic potential and loading surface *181*
4.4.6. Soil structure *183*
4.4.7. Model parameters *184*
4.5. VALIDATION OF ET CREEP MODEL FOR NATURAL SOILS 188
4.5.1. Model parameters *189*
4.5.2. Incremental load 24-hour oedometer tests *190*
4.5.3. Constant rate of strain oedometer tests *193*
4.5.4. Drained creep tests under 1D conditions *194*
4.5.5. Undrained triaxial compression tests *196*
4.5.6. Undrained triaxial creep tests *198*
4.6. CONCLUDING REMARKS 201

CHAPTER 5 CONSTITUTIVE MODEL CALIBRATION 203

5.1. INTRODUCTION 203

5.2. DESCRIPTION OF LONDON CLAY: BACKGROUND 204

5.2.1. History of the London Clay Formation 204

5.2.2. Geology, lithological units and index properties at Heathrow 209

5.2.3. Macrofabric and shear strength 211

5.3. VISCOUS BEHAVIOUR OF INTACT LONDON CLAY AND THE CAPABILITIES OF THE ET CREEP MODEL 213

5.4. DETERMINATION OF TIME DEPENDENT PARAMETER C_α 219

5.4.1. Intact samples of London Clay 219

5.4.2. Reconstituted samples of London Clay 223

5.5. LOADING SURFACES: DERIVATION OF THE ET CREEP MODEL PARAMETERS . 225

5.6. SHEAR STIFFNESS FOR LABORATORY TESTS AND PILED FOUNDATIONS PROBLEMS 229

5.7. MONOTONIC RATE BEHAVIOUR: CALIBRATION OF THE ET CREEP MODEL PARAMETERS 231

5.7.1. Oedometer tests: Units C, $B_{2(c)}$, $B_{2(b)}$, $B_{2(a)}$, A_3 231

5.7.2. Triaxial tests: Units C, $B_{2(c)}$, $B_{2(b)}$, $B_{2(a)}$, A_3 236

5.8. TIME DEPENDENT BEHAVIOUR: CALIBRATION OF THE ET CREEP MODEL PARAMETERS 240

5.8.1. Oedometer creep test: Unit $B_{2(b)}$ 240

5.8.2. Triaxial creep tests: Unit $B_{2(b)}$ 242

5.9. SUMMARY AND CONCLUDING REMARKS 244

CHAPTER 6 NUMERICAL MODEL CALIBRATION 246

6.1. INTRODUCTION 246

6.2. PRELIMINARY FINITE ELEMENT ANALYSES ON SINGLE PILES 246

6.2.1. Model parameters and soil conditions 248

6.2.2. Problem geometry and boundary conditions 252

6.2.3. Description of the analyses 253

6.2.4. Soft clay analyses 255

6.2.5. Stiff clay analyses 260

6.2.6. Discussion 264

6.3. BACK-ANALYSIS: PILE LOAD TEST AT HEATHROW 265

6.3.1. Description of the pile load test 265

6.3.2. The stiff clay test site in Heathrow 268

6.3.3. Model parameters *273*
6.3.4. Considerations for the back-analysis *273*
6.3.5. Problem geometry and boundary conditions *276*
6.3.6. Description of analysis *277*
6.3.7. Results and discussion *278*
6.4. CASE HISTORY: HISCOCKS HOUSE, STONEBRIDGE PARK 280
6.4.1. Description of Hiscocks House *280*
6.4.2. The stiff clay site in Stonebridge Park, London *281*
6.4.3. Model parameters *288*
6.4.4. Calibration of soil profile for long term analysis *290*
6.4.5. PILE LOAD TEST PRIOR CONSTRUCTION: 1972 294
6.4.5.1. Description of the pile load test *294*
6.4.5.2. Problem geometry and boundary conditions *295*
6.4.5.3. Description of analysis *296*
6.4.5.4. Results and discussion *297*
6.4.6. 3D MODELLING OF PILED RAFT FOUNDATION 299
6.4.6.1. Problem geometry and boundary conditions *299*
6.4.6.2. Description of analysis *301*
6.4.6.3. Results and discussion *304*
6.4.7. PILE LOAD TEST AFTER DEMOLITION: 2005 314
6.4.7.1. Description of the pile load test *314*
6.4.7.2. Description of analysis *314*
6.4.7.3. Results and discussion *315*
6.5. CONCLUDING REMARKS 320

CHAPTER 7 PARAMETRIC ANALYSES OF PILED RAFT FOUNDATIONS 322
7.1. INTRODUCTION 322
7.2. HYPOTHETICAL PILED RAFT FOUNDATION IN LONDON CLAY 323
7.2.1. Problem geometry and boundary conditions *323*
7.2.2. Description of analyses *325*
7.2.3. Results and discussion *326*
7.3. OPTIMISED FOUNDATION DESIGN OF HISCOCKS HOUSE 335
7.3.1. DESIGN OF RAFT FOUNDATION: *parametric study of raft thickness* 337
7.3.1.1. Problem geometry and boundary conditions *338*
7.3.1.2. Description of analysis *339*

7.3.1.3. Results and discussion *340*
7.3.2. ORIGINAL DESIGN OF PILED RAFT FOUNDATION 346
7.3.2.1. Description of analysis *346*
7.3.2.2. Results and discussion *347*
7.3.3. DESIGN OF PILED RAFT FOUNDATION: *parametric study varying the number and length of piles* 349
7.3.3.1. Parametric cases *350*
7.3.3.2. Problem geometry and boundary conditions *351*
7.3.3.3. Description of analysis *353*
7.3.3.4. Results and discussion *354*
7.4. SUMMARY AND CONCLUDING REMARKS 360
CHAPTER 8 CONCLUSIONS AND RECOMMENDATIONS 363
8.1. GENERAL REMARKS ON THE RESEARCH 363
8.2. TIME DEPENDENCY AND CONSITUTIVE MODELLING OF NATURAL STIFF CLAYS 365
8.3. TIME EFFECTS AND OPTIMUM DESIGN OF PILED RAFT FOUNDATIONS 367
8.4. RECOMMENDATIONS FOR FURTHER RESEARCH 377
REFERENCES 380

List of Figures

Figure 1.1: (a) Empress State Building (skyscrapernews, 2008), (b) Juxon House (EAG, 2008) 36
Figure 1.2: Empress State Building in (a) 1961 (Chapman et al. 2007), and (b) 2003 (wikipedia, 2008) 37
Figure 1.3: Empress State Building: plan of original foundations (St John and Chow, 2006) 37
Figure 1.4: Empress State Building: plan of new piles under the extended part (St John and Chow, 2006) 38
Figure 1.5: Juxon House: (a) layout of the original foundations, (b) plan of original foundation with new piles to augment capacity (St John and Chow, 2006) 39
Figure 1.6: Juxon House: plan of five pile caps (St John and Chow, 2006) 39
Figure 1.7: Foundation platform to support successive buildings (Chapman et al., 2007) 41
Figure 2.1: Life cycle of a pile over two building lives. 48
Figure 2.2: Variations with time of radial effective stresses at four ICP clay test sites (Jardine et al., 2005) 50
Figure 2.3: Schematic diagram for the evolution of radial stress around a pile during equilibration. 52
Figure 2.4: Shaft and base contribution to load capacity of a ‘friction’ pile. 53
Figure 2.5: Load transfer from head of pile to shaft for (a) small loading, (b) in working conditions and (c) at failure 54
Figure 2.6: Failure surfaces for piles in compression. 54
Figure 2.7: Load settlement response of single pile in compression. (Randolph, 2003) 55
Figure 2.8: Load-displacement behaviour of a pile loaded-unloaded-reloaded in short and long term 57
Figure 2.9: Load capacity of a single pile 58
Figure 2.10: API (1986) recommendations for the variation of α with undrained shear strength 61

Figure 2.11: Normalised capacity against time of re-tested displacement piles (Powel et al. 2003).....64
Figure 2.12: Load displacement curves for a typical tested pile at Canons Park (Powel et al. 2003).....64
Figure 2.13: Load displacement response of virgin piles tested (a) 2.5 and (b) 46 months old after installation (Powel and Skinner, 2006).....65
Figure 2.14: Comparison of archive (1972) and recent (2005) pile load tests (Butcher et al. 2006).....66
Figure 2.15: Transition from raft to pile group to piled raft foundation (Randolph, 2003) 68
Figure 2.16: Load-settlement curves for piled rafts according to various design philosophies (Poulos, 2001).....70
Figure 2.17: Main (east) elevation of Hiscocks House (Cooke et al., 1981).....73
Figure 2.18: Foundation plan and longitudinal cross-sections of Hiscocks House (Cooke et al., 1981).....74
Figure 2.19: Foundation plan of north-east quarter showing positions of instruments and cable runs (Cooke et al., 1981).....75
Figure 2.20: Development of load during construction, and borehole magnet extensometer readings; also mean settlement given by precise levelling round the completed building (Cooke et al., 1981).....75
Figure 2.21: Development of pile loading during erection of the building, showing the difference between the loads carried by the various characteristic piles (Cooke *et al.*, 1981) 76
Figure 2.22: Peak raft pressures: (a) at approximately 45% of full load; (b) at 100% of full load (Cooke et al., 1981) 77
Figure 2.23: Proportion of the total foundation load carried by the piles at various stages of construction (Cooke *et al.*, 1981).....78
Figure 2.24: Levelling observations made around the building at various dates after completion (Cooke *et al.*, 1981).....79
Figure 2.25: Contours of settlement (mm): (a) 2 years of measurements; (b) 4 years of measurements (Cooke *et al.*, 1981).....79
Figure 2.26: Raft without piles: load – settlement derivation (Burland, 1995).....80
Figure 2.27: Schematic relationship between settlement and number of piles beneath a raft foundation on clay (Burland, 1995).....81
Figure 2.28: Profile view of Torhaus der Messe building (Reul and Randolph, 2003) 82
Figure 2.29: Ground plan of raft (Reul and Randolph, 2003).....83

Figure 2.30: Influence of pile length on the computed settlements (Sommer et al., 1985)..... 84
Figure 2.31: Settlement profile. Measurements after Sommer (1991) and finite element analysis (Reul and Randolph, 2003) 85
Figure 2.32: Pile loads (Sommer, 1991)..... 85
Figure 2.33: Schematic of the building and summary of soil investigation (Yamashita et al., 1994)..... 86
Figure 2.34: Foundation plan and specification of piles (Yamashita et al., 1994)..... 87
Figure 2.35: Measured settlements (Yamashita et al., 1994) 88
Figure 2.36: Development of pile-head loads (Yamashita et al., 1994)..... 88
Figure 2.37: Measured pile loads at the time of building completion (Yamashita et al., 1994)..... 89
Figure 2.38: Sum of the measured pile-head loads and the building load (Yamashita et al., 1994)..... 89
Figure 2.39: View of residential buildings, Olskroken. The building on creep piles seen to the left, the one on conventional piles to the right (Hansbo, 1984) 90
Figure 2.40: Settlement contours in mm and average settlement versus time for the two buildings (Hansbo, 1993)..... 91
Figure 2.41: Central piles to reduce differential settlement (Randolph, 1994) 92
Figure 2.42: Schematic design approach for settlement reducing piles (Randolph, 1994)..... 93
Figure 2.43: Messe Turm building in Frankfurt (Sommer et al., 1991)..... 94
Figure 2.44: Soil profile and undrained shear strength (Sommer et al., 1991) 94
Figure 2.45: Plan and side elevation of piled raft foundation (Sommer et al., 1991) 95
Figure 2.46: Load development and settlement versus time (Sommer et al., 1991) 96
Figure 2.47: Settlements of the foundation raft (Sommer et al., 1991)..... 97
Figure 2.48: Pile loads and skin friction distribution after completion of structural frame (Sommer et al., 1991)..... 97
Figure 2.49: Load distribution between piles and raft (Sommer et al., 1991)..... 98
Figure 2.50: Simplified load-settlement curve for preliminary analysis (Poulos, 2001) 102
Figure 2.51: Definition of piled raft problem (Poulos, 1994) 106
Figure 2.52: Parameters of hypothetical pile raft (Poulos, 2001)..... 110
Figure 2.53: Effect of number of piles on piled raft behaviour (Poulos, 2001) 111
Figure 2.54: Effect of raft thickness on piled raft behaviour (Poulos, 2001)..... 112
Figure 2.55: Load-settlement curves for various piled raft configurations (Poulos, 2001).... 113
Figure 2.56: Models analyzed in the numerical simulation (Katzenbach et al., 1998) 114

Figure 2.57: Load-settlement curves of a piled raft with n= 13 piles (Katzenbach et al., 1998)..... 115
Figure 2.58: Distribution of (a) pile load and (b) skin friction along the pile shaft (Katzenbach et al., 1998) 116
Figure 2.59: Foundation layouts for piled raft analysis (Randolph, 1994)..... 117
Figure 2.60: Settlement profiles for different pile layouts (Randolph, 1994) 118
Figure 2.61: Parameters of numerical study (Viggiani, 2001) 119
Figure 2.62: Maximum decrease of the maximum differential settlement of the raft following the addition of piles as a function of the total quantity of piles (Viggiani, 2001)..... 120
Figure 2.63: Increase of average settlement and load share of the raft with decreasing number of piles (Viggiani, 1998)..... 121
Figure 2.64: Effect of the number and layout of piles on the differential settlement (Viggiani, 1998)..... 122
Figure 2.65: Modified pile configurations A and B (Reul and Randolph, 2003)..... 123
Figure 2.66: Coefficient for (a) maximum settlement, (b) differential settlement and (c) load share of piles depending on the total pile length (Reul and Randolph, 2003) 124
Figure 2.67: (a) Computed settlement and (b) moment distribution with and without piles (Poulos, 2001)..... 126
Figure 2.68: Effect of raft thickness on (a) computed settlement and (b) moment profiles (Poulos, 2001) 127
Figure 3.1: Definition of consolidation phases during 1D oedometer compression test: (a) Stress versus log (time); (b) log (strain rate) versus log (time) (Augustesen et al., 2004)..... 134
Figure 3.2: Creep test: (a) stress-strain relationship; (b) stress history; and (c) strain history..... 137
Figure 3.3: Relaxation test: (a) stress-strain relationship; (b) strain history; and (c) stress history..... 138
Figure 3.4: Definition of creep phases: (a) strain versus time; (b) strain rate versus log (time)..... 139
Figure 3.5: One-dimensional step load creep test: vertical strain versus log (time) 140
Figure 3.6: Relationship between the parameter m and the evolution of creep strain with time..... 140
Figure 3.7: CRS test: (a) strain history; (b) stress-strain response 141

Figure 3.8: Isotach viscosity vs non-isotach viscosity: clays vs sands (Augustesen et al, 2004)..... 142
Figure 3.9: Isotach viscosity: unique stress-strain-strain rate relation (Augustesen et al, 2004)..... 143
Figure 3.10: Non-isotach behaviour of clays: (a) at very slow rates, (b) after long period of creep (Augustesen et al, 2004)..... 144
Figure 3.11: Concept of isochrones or time lines for the 1D compression of soft clays (Bjerrum, 1967)..... 146
Figure 3.12: Influence of drained creep on subsequent one-dimensional compression behaviour in CRS oedometer tests on reconstituted Fujinomori clay (Tatsuoka, 2003) 146
Figure 3.13: Schematic diagram of the behaviour of a soil element following a drained creep period; (a) pure viscous behaviour; (b) viscous and structure effects. (Bodas Freitas, 2008)..... 147
Figure 3.14: Influence of drained creep on one-dimensional compression behaviour in tests on artificially sedimented Jonquiere clay (Leroueil et al., 1996; after Perret et al, 1995)..... 148
Figure 3.15: Influence on drained creep on the compression behaviour of reconstituted Fujinomori clay and change in initial constraint modulus M_0 for different ageing periods (Tatsuoka et al., 1998; after Momoya, 1998) 149
Figure 3.16: Effect of slow rate on straining on the one-dimensional compression behaviour of artificially sedimented Jonquiere clay (Leroueil et al, 1996) 150
Figure 3.17: Influence of creep time on the yield envelope in triaxial stress space in tests on San Francisco Bay mud (Arulanandan et al, 1971) 151
Figure 3.18: Influence of volumetric creep rate on the limit state curve from drained triaxial tests on undisturbed lightly overconsolidated St. Alban clay (Tavenas et al, 1978)..... 151
Figure 3.19: Proposed general model of the effects of time on the yield envelope of clays (Tavenas and Leroueil, 1977) 152
Figure 3.20: Influence of deviator stress in drained triaxial creep tests on undisturbed London Clay (Bishop, 1966)..... 153
Figure 3.21: (a) Variation of creep rate with time in constant stress creep; (b) influence of deviator stress level on the rupture life in undrained triaxial compression of undisturbed Haney clay (Vaid and Campanella, 1977) 153

Figure 3.22: Influence of drained creep on subsequent undrained shearing behaviour in triaxial compression of undisturbed Vallerica clay (Santucci de Magistris et al., 1998) 154
Figure 3.23: Influence of undrained creep on subsequent stress-strain behaviour in undrained triaxial compression on Fujinomori clay (Tatsuoka et al., 1998; after Momoya, 1998) 155
Figure 3.24: Influence of drained creep on subsequent stress-strain behaviour in undrained triaxial compression of Fujinomori clay (Tatsuoka et al., 1998; after Momoya, 1998) 155
Figure 3.25: The three types of post-aging stress-strain relationships (Tatsuoka et al, 1998) 156
Figure 4.1: Schematic representation of the modified Newton-Raphson algorithm for a one-dimensional non-linear problem (Potts and Zdravkovic, 1999) 163
Figure 4.2: Behaviour under isotropic compression 166
Figure 4.3: Yield surface on J-p′ plane 167
Figure 4.4: Yield surface in v-J-p′ space 168
Figure 4.5: State boundary surface 168
Figure 4.6: Failure surfaces in the deviatoric plane 168
Figure 4.7: Volumetric behaviour of Cam clay models 169
Figure 4.8: Definition of primary and secondary consolidation and instant and delayed compression 173
Figure 4.9: Equivalent Time Creep model in isotropic conditions 174
Figure 4.10: Extension to general stress space 181
Figure 4.11: Framework for the consideration of soil structure 184
Figure 4.12: Incremental load 24-hours oedometer tests 190
Figure 4.13: Incremental load 24-hours oedometer tests on structured soil – ET Creep model predictions for p_{s0} equal to (a) 10.0 kPa, (b) 40.0 kPa, and (c) 100 kPa 192
Figure 4.14: Constant rate of strain and stepwise change of strain rate oedometer tests 193
Figure 4.15: Drained creep tests under 1D conditions at different stress levels 194
Figure 4.16: Change in void ratio during drained creep in 1D conditions 195
Figure 4.17: Stress paths for undrained triaxial and stepwise change of strain rate compression tests 197
Figure 4.18: Stress-strain paths for undrained triaxial and stepwise change of strain rate compression tests 197
Figure 4.19: Stress paths for undrained triaxial creep tests at different stress levels 198

Figure 4.20: Development of pore water pressure with time during undrained creep 199
Figure 4.21: Stress-strain paths for undrained triaxial creep at different stress levels 200
Figure 4.22: Axial strain rate during undrained creep for different stress levels 200
Figure 5.1: Palaeogeographical reconstruction of the 'London Clay Sea' in the Early Eocene (Ziegler, 1990) 206
Figure 5.2: Eocene stratigraphy of the London Clay Formation in Southern Britain (King, 1981) 207
Figure 5.3: The London Clay Formation: idealised depositional sequences linked to sea level changes (King, 1981) 207
Figure 5.4: Palaeocene and Eocene sections of the London Clay Formation (King, 1981) 208
Figure 5.5: Geology of London Clay at Heathrow Airport Terminal 5 (Hight et al. 2003) 210
Figure 5.6: Water content profile and profile of index properties with lithological unit and sub-unit boundaries (Hight et al. 2003) 211
Figure 5.7: General normalised viscous behaviour of London Clay in triaxial compression – illustration of conceptual behaviour (Sorensen, 2006) 215
Figure 5.8: Influence of deviatoric stress in drained triaxial creep tests on undisturbed London Clay (Bishop, 1966) 217
Figure 5.9: Strain rate vs. time relationships during drained triaxial creep on London Clay (Mitchell et al., 1997, replotted data from Bishop, 1966) 217
Figure 5.10: Consolidation curves of incremental load oedometer test on samples of undisturbed London Clay from Ongar (Som, 1968) 218
Figure 5.11: Oedometer creep tests on London Clay samples from (a) Ongar and (b) Oxford Circus (Som, 1968) 220
Figure 5.12: Isochrones observed for in-situ OC soils merging with those for normal consolidation (Nash, 2010) 221
Figure 5.13: ET Creep model and stress paths in isotropic conditions 222
Figure 5.14: 1D compression and swelling path resulting from step loading, step unloading and constant rate of strain compression/swelling in test on reconstituted London Clay (Sorensen, 2006) 223
Figure 5.15: Constant total stress consolidation curves for each load step increment in 1D compression test on reconstituted London Clay (Sorensen, 2006) 224
Figure 5.16: Axial strain rate reduction during consolidation for each step load increment in 1D compression test on reconstituted London Clay (Sorensen, 2006) 224

Figure 5.17: Peak and post-rupture failure envelopes for different lithological units (Hight et al., 2007) 226
Figure 5.18: Loading surfaces along with the normalised effective stress paths for lithological units (a) $B_{2,}$ (b) A_3, and (c) C 227
Figure 5.19: Normalised loading surfaces for lithological units $B_{2,}$ A_3, and C 228
Figure 5.20: Characteristics stiffness-strain behaviour of soil with typical strain ranges for typical strain ranges for laboratory tests and structures (Atkinson, 2000) 229
Figure 5.21: Variation with depth of shear moduli in vertical and horizontal planes (Gasparre, 2005) 230
Figure 5.22: Single element boundary conditions for oedometer test 232
Figure 5.23: IL oedometer test on natural sample from unit C (7m) 233
Figure 5.24: IL oedometer test on natural sample from unit $B_{2(c)}$ (10m) 233
Figure 5.25: IL oedometer test on natural sample from unit $B_{2(b)}$ (17m) 234
Figure 5.26: IL oedometer test on natural sample from unit $B_{2(a)}$ (28m) 234
Figure 5.27: IL oedometer test on natural sample from unit A_3 (36m) 235
Figure 5.28: Single element displacement boundary conditions for triaxial test 237
Figure 5.29: Undrained triaxial test on natural sample from unit C (7m) 238
Figure 5.30: Undrained triaxial test on natural sample from unit $B_{2(c)}$ (11m) 238
Figure 5.31: Undrained triaxial test on natural sample from unit $B_{2(b)}$ (17.5m) 238
Figure 5.32: Undrained triaxial test on natural sample from unit $B_{2(a)}$ (28.5m) 239
Figure 5.33: Undrained triaxial test on natural sample from unit A_3 (38m) 239
Figure 5.34: FE simulation of IL oedometer creep test 241
Figure 5.35: Development of viscoplastic strains with time at constant vertical effective stress 241
Figure 5.36: Effect of stepwise change in strain rate on undrained stress-strain shearing path of OC intact London Clay 243
Figure 5.37: Effect of stain rate on undrained stress-strain shearing path of London Clay from unit B2b 243
Figure 5.38: Effect of stain rate on undrained stress path of London Clay from unit B2b 244
Figure 6.1: S_u, OCR and K_o profiles for soft clay site 250
Figure 6.2: Mesh for preliminary finite element analyses on single piles 252
Figure 6.3: Soft clay analysis: definition of failure load for ET Creep analyses 254
Figure 6.4: MCC soft clay analysis: load-settlement response for undrained loading 256

Figure 6.5: MCC soft clay analysis: contours at failure of (a) vertical shear stress, (b) excess pore water pressures 256
Figure 6.6: MCC soft clay analysis: load-settlement response for different levels of preloading 257
Figure 6.7: ET Creep soft clay analysis: load-settlement response for different levels of preloading 258
Figure 6.8: Soft clay analysis: gain in load capacity for different levels of preloading 260
Figure 6.9: Gain in bearing capacity for preloaded footing (Bodas Freitas et al., 2007) 260
Figure 6.10: ET Creep stiff clay analysis: contours at failure of excess pore water pressures 261
Figure 6.11: Stiff clay analysis: load-settlement response for different levels of preloading 262
Figure 6.12: Stiff clay analysis: gain in load capacity for different levels of preloading 262
Figure 6.13: Deviatoric stress vs. deviatoric strain for elements adjacent to pile shaft: (a) below the failure load (66%), (b) at failure load, (c) after failure load 264
Figure 6.14: Test pile details performed in Heathrow Airport Terminal 5 (Unwin and Jessep, 2004) 266
Figure 6.15: Pile head movement against load for test pile (Unwin and Jessep, 2004) 268
Figure 6.16: Pile load test site in Heathrow Airport T5: (a) suggested soil profile and, (b) adopted soil profile for the finite element simulation 269
Figure 6.17: Ko profile estimated on basis of suction measurements (Hight et al., 2007) 270
Figure 6.18: Permeability measurements at T5 using self-boring pressuremeter compared with database (Hight et al., 2007) 271
Figure 6.19: Variation with depth of shear moduli in vertical and horizontal planes (Gasparre, 2005) 272
Figure 6.20: Single pile mesh for pile load test in Heathrow Airport Terminal 5 276
Figure 6.21: Predicted vs. measured load-settlement response of pile load test 279
Figure 6.22: Predicted load-settlement response for original conditions vs. calibrated 279
Figure 6.23: Plan view of Stonebridge Park and Wembley stadium area (Google Earth, 2010) 282
Figure 6.24: Schematic of the site geology in Wembley (Cheong, 2007) 282
Figure 6.25: Hiscocks House: adopted soil profile for finite element simulation 283
Figure 6.26: Stonebridge Park: undrained shear strength profile 284
Figure 6.27: Wembley: undrained shear strength profile (O'Brien, 2010) 285

Figure 6.28: Shear modulus profile: (a) Wembley (O'Brien et al., 2004), (b) Stonebridge Park 286
Figure 6.29: Assumed profiles in St James Park (Wongsaroj et al., 2007) and Stonebridge Park 288
Figure 6.30: Determination of OCR profile in Stonebridge Park 290
Figure 6.31: Column mesh used for calibration of soil profile for long term analysis 291
Figure 6.32: Pore water pressure profiles: (a) initial permeability, (b) calibrated permeability 292
Figure 6.33: Isotropic permeability profile in Stonebridge Park 292
Figure 6.34: Initial and calibrated horizontal stress and K_o profiles 293
Figure 6.35: (a) Load-time and settlement-time curves from the incremental pile loading test; (b) load-settlement curves from the incremental and CRP tests (Cooke et al., 1981) 294
Figure 6.36: Single pile mesh for pile load test in Stonebridge Park 295
Figure 6.37: Load vs. settlement for the incremental and CRP pile load tests 297
Figure 6.38: Load vs. time plot for the incremental pile load test 298
Figure 6.39: Settlement vs. time plot for the incremental pile load test 298
Figure 6.40: Load vs. settlement for the original conditions and calibrated CRP pile load tests 299
Figure 6.41: 3D mesh for the piled raft foundation of Hiscocks House 300
Figure 6.42: 3D view of the piled raft foundation of Hiscocks House 300
Figure 6.43: Plan view of piles detail of the piled raft foundation of Hiscocks House 301
Figure 6.44: Structural load during construction of Hiscocks House 305
Figure 6.45: Development of absolute settlement for a range of depths below the underside of the raft 305
Figure 6.46: Foundation plan of north-east quarter showing positions of piles instrumented and of magnet extensometer (Cooke et al., 1981) 306
Figure 6.47: Contours of accumulated displacement for the period during which measurements have been reported by Cooke et al. (1981) (units in metres) 306
Figure 6.48: Comparison between FE predicted settlements with measured settlements from Cooke et al. (1981) at representative depths below the underside of the raft 307
Figure 6.49: Development of absolute settlement for a range of depths below the underside of the raft in the long term 307
Figure 6.50: Contours of settlement at raft level between 12 July 1976 and 24 June 1980: (a) predicted, (b) measured 309

Figure 6.51: Predicted contours of settlement at raft level (a) at occupation of Hiscocks House, (b) after 29 years of occupation 309
Figure 6.52: Development of predicted pile loading during erection of Hiscocks House, showing the distribution of loads carried by characteristic piles 310
Figure 6.53: Comparison between the predicted average pile loading of characteristic piles and the measured values published by Cooke et al. (1981) 311
Figure 6.54: Development of predicted average pile loading of characteristic piles in the long term, showing the distribution of loads carried by characteristic piles 312
Figure 6.55: Contours of vertical effective stress at the raft-soil interface at occupation of Hiscocks House (units in kPa; sign convention tension positive) 313
Figure 6.56: Proportion of total structural load carried by piles at various stages of construction 314
Figure 6.57: Comparison between the predicted and the documented (Burcher et al, 2006) load-settlement response of the pile tested in 2005 316
Figure 6.58: Comparison of the predicted load-settlement response of the pile testes in original conditions (Curve 1), with no reduced lateral stresses and OCR (Curve 2), and reduced elapsed time (Curve 3) 317
Figure 6.59: Predicted load-settlement response for pile load tests in 1972 and 2005 318
Figure 6.60: Predicted load-settlement response of a CRP test on a working pile in 1972 and in 2005 319
Figure 7.1: 3D mesh for hypothetical foundation problem 324
Figure 7.2: 3D view of the discretised (a) raft foundation, (b) uniform piled raft foundation, and (c) piled raft foundation with central pile support 324
Figure 7.3: Plan view of piles detail of hypothetical piled foundations 325
Figure 7.4: Load-settlement response of hypothetical foundations up to failure load 327
Figure 7.5: Load on piles for piled raft foundations with 25 and 5 piles 328
Figure 7.6: Load share of piles for piled raft foundations with 25 and 5 piles 328
Figure 7.7: Contours of settlement at a load level of 41.2 MN for the (a) raft foundation, (b) piled raft foundation with 25 piles, and (c) piled raft foundation with 5 piles (units in m) 331
Figure 7.8: Contours of settlement at a load level of 41.2 MN for the (a-b) raft foundation (c-d) piled raft foundation with 25 piles, and (e-f) piled raft foundation with 5 piles (units in mm) 332
Figure 7.9: Load-settlement response for different levels of preloading for raft foundation 333

Figure 7.10: Load-settlement response for different levels of preloading for piled raft foundation with 25 piles uniformly distributed 334
Figure 7.11: Load-settlement response for different levels of preloading for piled raft foundation with 5 piles in the central region of the raft 334
Figure 7.12: Gain in overall load capacity after 50 years of preloading for the raft foundation, the piled raft foundation with 25 piles and the piled raft foundation with 5 piles 335
Figure 7.13: Definitions of foundation movement 336
Figure 7.14: 3D mesh for the raft foundation 338
Figure 7.15: 3D view of the raft foundation (0.9 m thick case) 339
Figure 7.16: Load-settlement response of raft foundation loaded to failure 341
Figure 7.17: Development of structural load with time for the raft foundation with the original thickness 342
Figure 7.18: Development of absolute settlements at the centre of the raft for a range of depths below the underside of the raft for the original raft thickness 342
Figure 7.19: Contours of excess pore water pressures at the end of the structural load application for the raft foundation with the original raft thickness (units in kPa) 343
Figure 7.20: Settlement profile with depth in the long term for the raft foundation with the original raft thickness 343
Figure 7.21: Contours of settlement of the raft foundation with raft thickness equal to: (a) 0.9 m, (b) 1.5 m, and (c) 2.5 m (units in mm) 345
Figure 7.22: Development of differential settlement centre-to-corner with time for the raft foundation examined parametrically 345
Figure 7.23: Development of maximum angular distortion with time for the raft foundation examined parametrically 346
Figure 7.24: Load-settlement response of original piled raft foundation loaded to failure 347
Figure 7.25: Development of differential settlement centre-to-corner with time for the raft foundation examined parametrically 348
Figure 7.26: Development of maximum angular distortion with time for the raft foundation examined parametrically 348
Figure 7.27: Load-settlement response of original piled raft foundation loaded to failure during construction and after 30 years of elapsed time at working conditions 349
Figure 7.28: Location of piles for parametric case with (a) 185 piles, (b) 107 piles, and (c) 55 piles 351
Figure 7.29: 3D mesh for the piled raft foundation 352

Figure 7.30: Contours of settlement for the parametric cases with 185 piles and pile length (a) 17.5 m, (b) 13.0 m, and (c) 8.75 m (units in mm) 356
Figure 7.31: Contours of settlement for the parametric cases with 107 piles and pile length (a) 17.5 m, (b) 13.0 m, and (c) 8.75 m (units in mm) 356
Figure 7.32: Contours of settlement for the parametric cases with 55 piles and pile length (a) 17.5 m, (b) 13.0 m, and (c) 8.75 m (units in mm) 357
Figure 7.33: Differential settlement centre-to-corner for each parametric case against total pile length..... 359
Figure 7.34: Load share of piles for each parametric case study against total pile length 360

List of Tables

Table 3.1: Coefficient of permeability (m/s) (BS 8004: 1986) 135
Table 3.2: Viscous characteristics of soils (Sorensen, 2006) 143
Table 4.1: Modified Cam Clay model parameters as input in ICFEP 171
Table 4.2: Equivalent Time Creep model parameters 185
Table 4.3: Model parameters for the validation analyses 189
Table 5.1: Summary of the observed viscous behaviour of London Clay in reconstituted and intact states (Sorensen, 2006) 214
Table 5.2: ET Creep model parameters for London Clay: Parameters defining CSL and loading surface 228
Table 5.3: ET Creep model parameters for London Clay: Shear modulus G 231
Table 5.4: Main characteristics of London Clay samples tested in IL oedometer tests (Gasparre, 2005) 231
Table 5.5: ET Creep model parameters for London Clay: Parameters defining compressibility 235
Table 5.6: Triaxial tests on natural samples (Gasparre, 2005) 236
Table 5.7: Calibrated OCR values in terms of mean effective stress for London Clay 239
Table 5.8: ET Creep model parameters for London Clay: Parameters defining time dependency 242
Table 5.9: Summary of ET Creep model parameters for London Clay 245
Table 6.1: Basic material properties for soft clay 249
Table 6.2: ET Creep model parameters for soft clay 249
Table 6.3: ET Creep model parameters for stiff clay 251
Table 6.4: ET Creep model parameters employed for the back-analysis of pile load test at Heathrow Airport Terminal 5 273
Table 6.5: ET Creep model parameters for Stonebridge Park units 289
Table 6.6: Sequence of FE analysis for the piled raft foundation problem 302

Table 7.1: Summary of limiting values of angular distortion for framed buildings and reinforced load bearing walls (Institution of Structural Engineers, 1989) 337
Table 7.2: Angular distortion limits after Bjerrum (1963) 337
Table 7.3: Parametric cases with varying number of piles and pile length 350

Symbols and Abbreviations

Symbol

A	activity
A_b	area of the base
A_g	area occupied by the pile group
A_r	area of the raft
A_s	area of the shaft
c'	effective cohesion
c_s'	effective interface cohesion
c_{vr}	coefficient of consolidation
C	constant that depends on M
C_α	coefficient of secondary consolidation
$C_{\alpha e}$	coefficient of secondary compression defined in terms of void ratio
$C_{\alpha\varepsilon}$	coefficient of secondary compression defined in terms of strain
$[D]$	constitutive matrix
$\{\Delta d\}_{nG}$	vector of incremental nodal displacements
$\{\Delta d_E\}$	vector of incremental element nodal displacements
$\{\Delta d_G\}$	vector of global incremental nodal displacements
d	pile diameter
e	void ratio
e_o	initial void ratio
Δe	change in void ratio
E	Young's modulus
F	yield function
$g(\theta)$	the slope of the critical state line in J-p′ stress space
G	shear modulus
G_{hv}	shear modulus in the horizontal direction action of vertical facet

G_{hh}	shear modulus in the horizontal direction action of horizontal facet
h	hour(s)
i	increment number
j	the iteration number
J	deviatoric stress
$J_{2\eta}$	stress ratio squared
$J_{2\eta,failure}$	stress ratio at failure squared
k	permeability
k_c	reduction factor
k_p	stiffness of the pile group
k_r	stiffness of the raft
k_{pr}	combined stiffness of the piled raft
K	elastic bulk modulus
K_1	constant
K_2	constant
K_o	coefficient of earth pressures at rest
K_s	coefficient of earth pressure for the pile shaft
K_{rs}	relative raft-soil stiffness
$[K_E]$	element stiffness matrix
$[K_G]$	global stiffness matrix
$[K_G]^i$	incremental global system stiffness matrix
L	length
$[L_G]$	off diagonal coupling submatrix
m	creep parameter
M	gradient of the critical state line in p' - q space under triaxial compression
M_f	the value of M for the loading surface
M_g	the value of M for the plastic potential surface
n	number of piles
N_c	bearing capacity factor
$[n_G]$	submatrix associated with the direction of gravity
p'	mean effective stress
p^*_e	equivalent intrinsic pressure
p'_m	mean effective stress
p'_{mio}	mean effective stress at $\varepsilon_{vm} = 0$ on the intrinsic reference time line

$p_o^{'}$	hardening/softening parameter defining the current size of the surface
p_s	increase in $p'_{mi\,0}$ due to soil structure
p_{s0}	initial increase in $p'_{mi\,0}$ due to soil structure
P	plastic potential function
P_1	total applied load at which the pile group capacity is reached
P_p	ratio of the load carried by the pile group to the total load
P_r	ratio of the load carried by the raft to the total load
P_u	ultimate load capacity of the piled raft
$\{\Delta p_f\}_{nG}$	vector of prescribed nodal pore fluid pressures
r_c	radius of circular pile cap
r_o	radius of pile
q	deviatoric stress
q_b	end-bearing resistance of pile
q_c	cone resistance of pile tip
$\overline{q_c}$	average cone resistance of pile tip
Q	nodal flow values
Q	total applied load
Q_{bf}	base load capacity
Q_{bf}	ultimate load capacity of the piled group as a block
Q_f	ultimate load capacity of a pile
Q_i	initial load capacity of a pile
Q_0	working load
Q_{pf}	average load carried by a pile within a group
Q_{prf}	ultimate load capacity of the piled raft
Q_r	load taken by the raft
Q_{rf}	ultimate load capacity of the raft alone
$Q_{r'f}$	ultimate load capacity of the raft around the periphery of piles
Q_{sf}	pile shaft capacity
$\{\Delta R_E\}$	vector of incremental element nodal forces
$\{\Delta R_G\}$	vector of global incremental nodal forces
$\{\Delta R_G\}^i$	vector of incremental nodal forces
R	pile radius
R	resistance
$R_{d,sf}$	permissible working load of an un-piled raft

S	settlement
S_{sf}	settlement for an un-piled raft
S_u	undrained shear strength
$S_{u,base}$	undrained shear strength of the soil at pile base
$\bar{S}_{u,shaft}$	average undrained shear strength measured over the length of the pile
t	raft thickness
t	time
Δt	time increment
t_e	equivalent time
t_0	real time associated with the reference time line
T	non-dimensional time factor
v	specific volume
v_1	the specific volume on the virgin consolidation line at unit pressure
v_s	the specific volume of swelling lines at unit pressure
v	Poisson's ratio
V	specific volume
ΔV	change in specific volume
w	settlement
Δw	differential settlement
w_o	initial water content
X	the proportion of load carried by the raft
Y_0	yield envelope
α	shaft adhesion factor
α_f	loading surface parameter
α_g	plastic potential parameter
α_{pr}	load share of the piles
α_{rp}	interaction factor between the raft and the pile group
β	angular distortion
β	integration parameter
δ	differential settlement
δ_r	max diff. settlement for an un-piled raft
δ'	effective angle of interface friction
Δ	deflection
ε	strain

ε_{vm}	volumetric strain
ε_{vm}^{r}	volumetric strain on the reference time line
ε_{vmo}^{r}	volumetric strain at a reference mean effective stress p'_{mo}
ε_{vm}^{el}	elastic volumetric strain at the isotropic effective stress p'_{m}
ε_{vmu}^{el}	elastic volumetric strain at a reference mean effective stress p'_{u},
$d\varepsilon_{v}^{e}$	change in elastic volumetric strain
$\Delta\varepsilon_{vm}^{el}$	incremental elastic volumetric strain
ε_{v}^{p}	plastic volumetric strain
ε_{vm}^{vp}	visco-plastic volumetric strain
$\Delta\varepsilon_{vm}^{vp}$	incremental visco-plastic volumetric strain
$\log \dot{\varepsilon}$	logarithm of creep strain rate
ε_{d}	deviatoric strain
$\varepsilon_{vm,limit}^{vp}$	limit for the amount of volumetric visco-plastic strain
$\dot{\varepsilon}_{vm}^{vp}$	visco-plastic volumetric strain rate
$\{\Delta\varepsilon\}$	vector of strains
$\{\Delta\varepsilon^{el}\}$	incremental elastic strains
$\{\Delta\varepsilon^{T}\}$	incremental total strains
$\{\Delta\varepsilon^{vp}\}$	incremental visco-plastic strains
ζ	parameter depending on maximum radius of influence and pile diameter
$\bar{\eta}$	generalised normalised stress ratio
θ	Lode's angle
ξ_{s}	settlement reduction coefficient for the maximum settlement
$\xi_{\Delta s}$	settlement reduction coefficient for the differential settlement
κ	slope of swelling line on v-ln p' plane
κ/V	slope of the instant time line on ε_{vm} - ln p'_{m} space
λ	slope of virgin consolidation line on v-ln p' plane
λ/V	slope of the reference time line in ε_{vm} - ln p'_{m} space
μ	Poisson's ratio
μ_{f}	loading surface parameter
μ_{g}	plastic potential parameter
ν	angle of dilation
ρ	settlement
ρ_{0}	settlement for the un-piled raft

ρ_s	parameter that controls the rate of destructuration
$\sigma_1^{'}$	major principal effective stress
$\sigma_2^{'}$	intermediate principal effective stress
$\sigma_3^{'}$	minor principal effective stress
$\sigma_h^{'}$	effective horizontal stress
$\sigma_{hs}^{'}$	effective horizontal stress on the shaft at failure
σ_r'	radial effective stress
σ_{ri}'	initial radial effective stress
$\sigma_{r(t)}'$	time dependent radial effective stress
σ_{rc}'	final radial effective stress
σ'_v	vertical effective stress
σ'_{vi}	initial vertical effective stress
$\{\Delta\sigma\}$	the vector of incremental total stresses
$\{\Delta\sigma'\}$	the vector of incremental effective stresses
$\{\Delta\sigma_f\}$	vector of incremental pore fluid pressure
τ_{sf}	skin friction at failure
φ'	angle of shearing resistance
$\varphi_{cs}^{'}$	critical state angle of shearing resistance
$\varphi_{cv}^{'}$	constant volume angle of shearing resistance
Φ	visco-plastic scalar multiplier
$[\Phi_G]$	permeability submatrix
ψ	creep parameter
ψ_0/V	time dependent parameter for equivalent time creep model
$\{\psi\}^j$	residual load vector
ψ^1	residual vector for iteration 1

Abbreviation

1D	one-dimensional
2D	two-dimensional
3D	three-dimensional
CF	clay fraction
CPT	cone penetration test
CRP	constant rate of penetration

CRS	constant rate of strain
CSL	critical state line
EOP	end of primary consolidation
ET	equivalent time
FE	finite element
ICFEP	Imperial College finite element program
ICL	intrinsic compression line
ICP	Imperial College pile
IL	incremental load
LL	liquid limit
LVDT	linear variable differential transformers
MCC	modified Cam Clay
NC	normally consolidated
NCL	normal compression line
OC	overconsolidated
OCR	overconsolidation ratio
PI	plasticity index
PL	plastic limit
RC	rotary core sample
SBP	self-boring pressuremeter
SPT	standard penetration test
SRS	step-wise change in rate of strain
T5	terminal 5
TESRA	temporary effect of strain rate and strain acceleration
TW	thin wall sample
U100 QUT	quick undrained triaxial test (on 100 mm diameter sample)
YSR	yield stress ratio

Chapter 1

Introduction

1.1. BACKGROUND

The development of new construction sites, for either residential or commercial buildings, in urban areas is often hampered by the existence of old foundations, congested underground space and archaeological artefacts. This is currently an important issue in London and in other big cities around the world.

Recent developments in major urban centres, such as the Juxon House near St Paul's Cathedral in London (St John and Chow, 2006) and many others, have highlighted the increasing problems faced with several generations of redevelopment on the site and the resulting number of old foundations remaining in the ground. Old piles, underground infrastructure and archaeological artefacts are posing threats for future urban developments and, therefore, it has been of major importance to develop new processes to provide environmentally sustainable foundations for future developments.

The importance of the problem is demonstrated by the fact that geotechnical companies around Europe, led by the Building Research Establishment (BRE) in the UK, recently instigated an industry based project, partly funded by the EU 5th Framework, on the Reuse of Foundations for Urban Sites (RuFUS). The aim of the project was to facilitate sharing of experience in the reuse of foundations across Europe, enable research into a wide range of technical issues, and provide innovative technical developments for construction in inner cities. A conference was held (RuFUS 2006, Butcher et al., 2006a) and a 'best practice handbook' (Butcher et al., 2006b) was published by the project partners in 2006, where some typical case histories are summarized.

1.2. REDEVELOPMENT OPTIONS

The current redevelopment options, when dealing with old foundations on a site, can be summarized into three basic options: (a) avoid, (b) remove, and (c) reuse. (Starzec et al., 2006)

Avoiding old foundations is the easiest option. This implies new foundations to be located in such positions that they do not clash with old foundations. This option allows the redevelopment to proceed, however it adds to the detritus in the ground. As the number of old piles in the ground increases, the option to completely avoid old piles in future redevelopments becomes increasingly expensive. Larger transfer structures and piles with larger capacity may be required and, in addition, the need for space in future redevelopments may be hampered by the reduced available space in the ground. Therefore, this option is considered as non-sustainable for future redevelopments.

Another important constraint that may make avoidance unfeasible is the presence of archaeological artefacts as described by Williams (2006), which is very common in large European cities. In many urban cities, foundations have been installed into archaeological deposits. These are the foundations of buildings which were constructed in the last half century, when there was less protection for cultural heritage. Recently, archaeological artefacts have drawn attention, leading to a common European policy for the protection of archaeology, the Valletta Convention in 1992. This Convention indicates that the preferred method of dealing with archaeology is the in situ preservation of archaeological heritage rather than the removal by excavating it, which is both time-consuming and uneconomical. This implies that the option to avoid current pile installations is unfeasible and another option should be adopted; either removal or reuse of old piles.

Removal of old piles is possible, but the cost is high. It may be achieved by overcoring and progressive removal of pile lengths from the ground, in the case of a fully reinforced pile, as described by Chapman et al. (2007). This technique involves the separation of the pile from the surrounding soil, by cutting out a cylinder of soil around the pile perimeter, and allowing the pile to be lifted out of the ground. If the pile is not reinforced though, this technique may be problematic, since the pile may break during lifting. Therefore, rock boring equipment may be used to break the pile up into small pieces and bring them to the surface while boring.

In addition to the high cost and the difficulties involved, the process of removal may have an effect on the soil surrounding the piles as indicated by Chapman et al. (2007). As the piles are

removed, the soil adjacent to the pile may be disturbed. This disturbance may result in a reduction in the capacity of the new piles due to the resulting softening or relaxation of the ground, which needs to be considered as part of the pile design.

Reuse of old foundations is the third option. This option should be followed if ground congestion from previous foundations, utilities, tunnels and archaeology restricts new foundations to such an extent that their installation is extremely difficult or exceptionally costly. The main benefits of foundation reuse are (Anderson et al., 2006):

(a) *sustainability benefits* from the reduction in foundation construction and the resulting reduction in energy requirements for construction materials and processes;
(b) *financial benefits* from the potential savings in construction cost and programme duration;
(c) *future development potential* of the site from the conservation of free ground space left and the resulting increase of property value due to the future development flexibility.

Nowadays, existing retaining walls, strip foundations and raft foundations are often reused. However, the reuse of pile foundations for new structures has been less common, despite the strong benefits. This may be due to uncertainties over construction quality and concrete durability, as well as to the concerns of all involved parties, including funders and insurers, according to Starzec et al. (2006). Nevertheless, some experience has already built up on the reuse of piles. In particular, experience has been gained in the combination of new and old piles, where new piles are installed to supplement the capacity of existing foundations which are being considered for reuse. Several typical case histories, involving refurbishment or redevelopment of buildings across Europe and where such a technique has been applied, are presented in the conference proceedings and the 'best practice handbook' produced by the partners of the RuFUS project.

The main issues that have to be addressed when considering the reuse of old piled foundations, and where uncertainties arise, are (Vaziri and Windle, 2006):

(a) quality of design information on the existing piles;
(b) integrity of existing piles;
(c) design responsibility and insurances;
(d) impact of demolition of existing building on the piles;
(e) pile deterioration and design life of the piles;
(f) the new column grid location in relation to the existing piles;
(g) load carrying capacity of existing piles;

(h) load-settlement response of existing piles.

The lack of confidence to deal with these issues and the lack of a body to take responsibility over these issues results in engineers hesitating over the reuse of old foundations as indicated by Chapman et al. (2001). Therefore, there has been an increasing effort to develop new processes to provide environmentally sustainable foundations for future developments, and tackle all the obstacles for the reuse of old piles.

1.3. REUSE OF OLD PILES – CASE HISTORIES

Two case histories in London, where old piles have been reused, are briefly described, in order to highlight current practice. The first case history is the Empress State Building (Figure 1.1a) located in Earl's Court, which involves refurbishing of the building. The second case history is the Juxon House (Figure 1.1b) located near St Paul's Cathedral, which involves demolition of the old building and reconstruction of a new one on top of the old piles with the addition of new piles at required locations. Both projects have been presented by St John and Chow (2006) in the International Conference organised by the Building Research Establishment (BRE) in the UK on the "Reuse of Foundations for Urban Sites" (RuFUS).



Figure 1.1: (a) Empress State Building (Skyscrapernews, 2008), (b) Juxon House (EAG, 2008)

(a) Earl's Court (refurbishing)

The Empress State Building in Earl's Court was originally completed in 1961 and it was eventually redeveloped after four decades, between 2001 and 2003. Two photographs from the same view point, but with a time difference of 42 years are presented in Figure 1.2. The

building is founded in London Clay and a plan of the original foundations is shown in Figure 1.3, where the piles are under-reamed. The project involved the reuse of the existing 28 storey building, adding three extra floors on the top. Also, an extension southwards of 6 m was required. Such a development is regarded as 'refurbishment'.

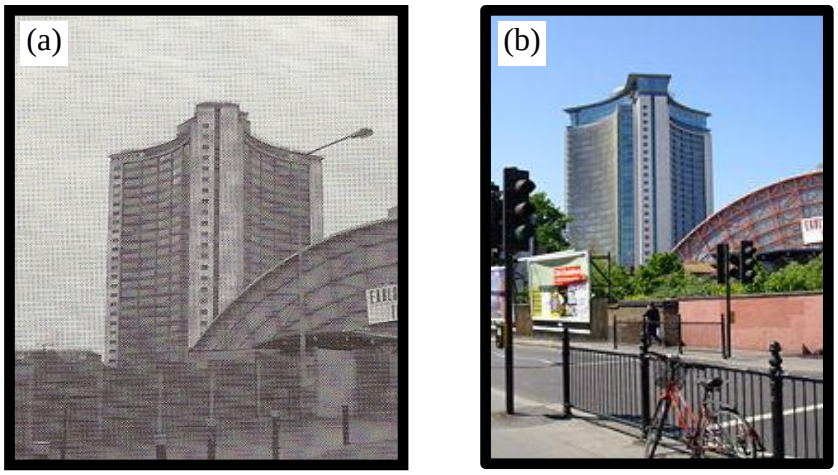


Figure 1.2: Empress State Building in (a) 1961 (Chapman et al. 2007), and (b) 2003 (Wikipedia, 2008)

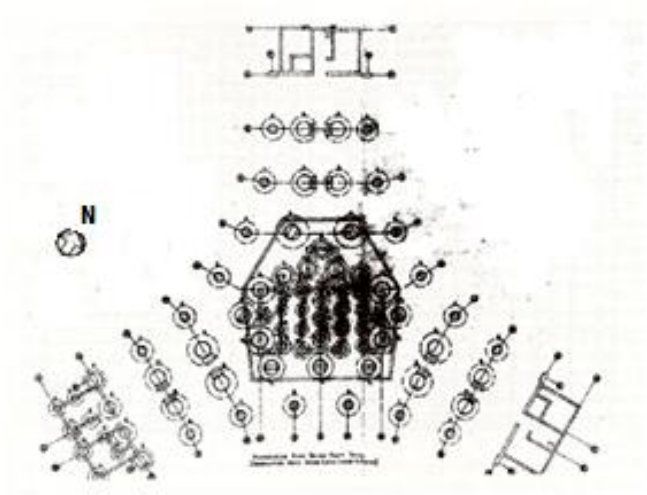


Figure 1.3: Empress State Building: plan of original foundations (St John and Chow, 2006)

The initial desire of the developers was the proposed extension on top and on the southside to be fully supported by the existing old piles. However, it was determined that the proposed development would result in an addition of around 33% of load on the existing under-reamed piles on the southside of the building, which was not acceptable, due to the lack of confidence in the long-term capacity of the piles. The foundation design principle adopted was to limit the new pile loads below the maximum load they have experienced previously, in order to ensure that the existing piles remain stiff in reloading.

Generally in current practice, an allowance of extra load capacity in old piles is acceptable. For instance, the BCA/BSRIA document 'refurbishment of concrete buildings: structural and services options' (BCA/BSRIA, 1995) states that:

> *"Extra load capacity is generally built into foundations of older buildings and in the 1970s District Surveyors would commonly allow an additional 10% of the total building loading to be added to the foundations at a later date, provided the building was sound and no settlement had occurred."*

Due to the fact that the predicted new loads on existing piles were larger than what would be accepted, the solution implemented was to add new piles under the extending part of the building (Figure 1.4). This involved the design of a stiff beam linking the old piles to a new foundation system, which would also carry the new line of columns, in order to reduce the risk of unacceptable settlements occurring to the old piles. The final pile loads were determined at maximum 12 % larger than before, which were judged to be acceptable.

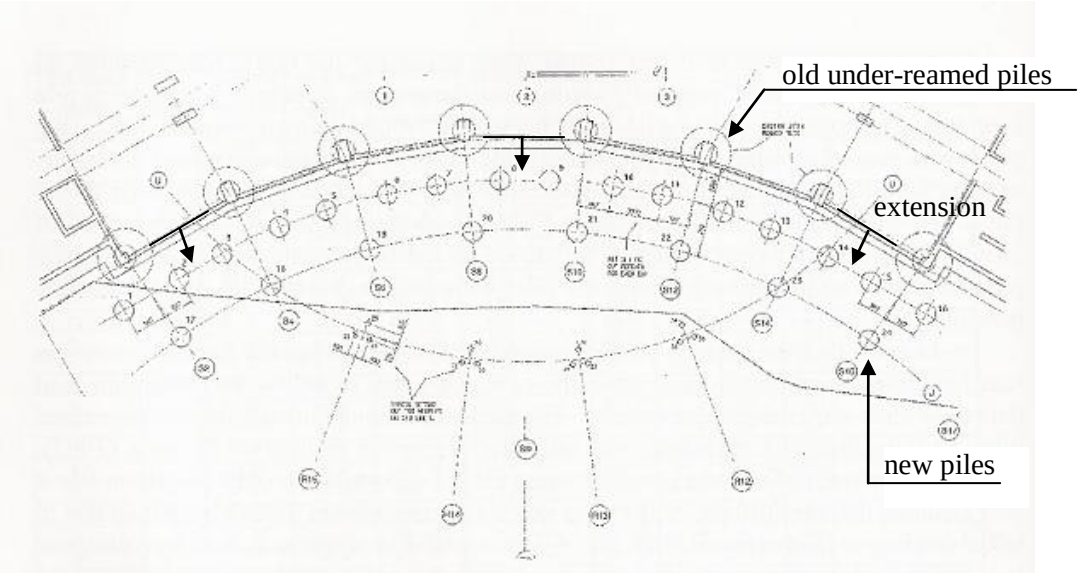


Figure 1.4: Empress State Building: plan of new piles under the extended part (St John and Chow, 2006)

(b) Juxon House (redevelopment)

The Juxon House in St Paul's Churchyard in London was originally developed in the early 1960s and it was redeveloped after 40 years. It is founded in London Clay and the layout of the original foundations is shown in Figure 1.5a. Original piles are mainly under-reamed piles with base diameters of up to 3.2 m.

The project involved demolition of an existing 10 storey building, founded on a number of under-reamed and straight shafted piles, and then reconstruction of a new eight storey building in its place. The new development covers a larger floor plan than the earlier building, as shown in Figure 1.5b, requiring new piles to supplement existing old piles. Like the Empress State Building, the foundation design principle was once again to limit the new pile loads on existing piles to below the maximum load they have experienced previously, due to the lack of confidence of their long-term capacity. Also, due to uncertainties on the combined response of the new and old piles, design loads on the new piles remained low, in order that the new piles remain stiff and consequently compatible with the stiff response of the reused piles.

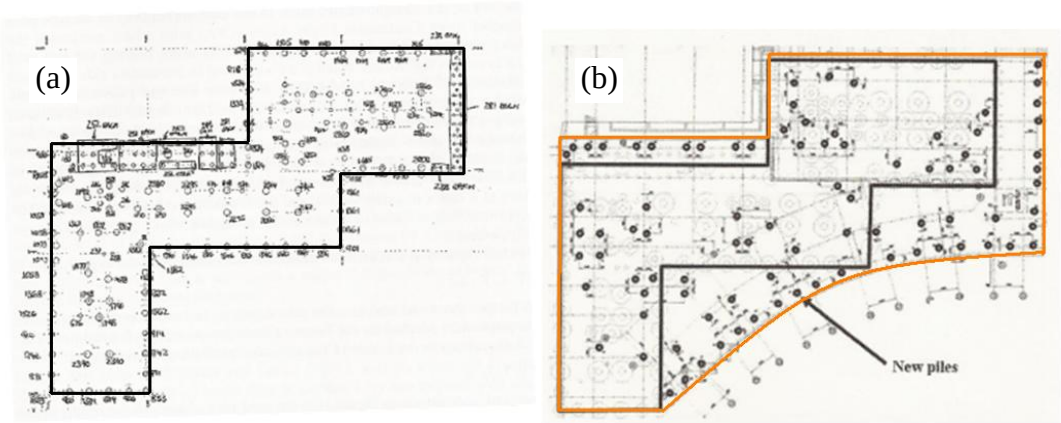


Figure 1.5: Juxon House: (a) layout of the original foundations, (b) plan of original foundation with new piles to augment capacity (St John and Chow, 2006)

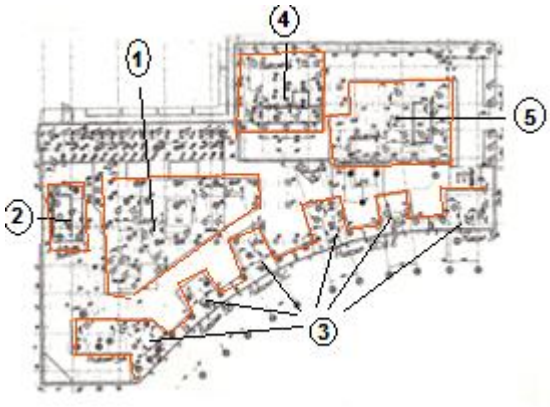


Figure 1.6: Juxon House: plan of five pile caps (St John and Chow, 2006)

In the design for the new building, the foundations were divided into five main pile caps, numbered 1 to 5 (Figure 1.6). The new loads were calculated for each raft, and if greater than the previously applied load, additional piles were added. Pile caps were designed on the basis

of providing sufficient load capacity, and the piles were designed with high factors of safety, in order to obtain a stiff response.

Both projects show that, despite the uncertainties involved, old piles have been reused successfully in practice. However, it is recognised that it is very difficult to determine what the actual capacity and stiffness of existing piles is on reloading. Consequently, old piles are reloaded at a lower level than previously experienced, in order to remain stiff. At the same time, new piles are designed with higher factors of safety, resulting in conservative and more costly designs. Furthermore, it has to be considered that many risks are involved and very often new developments are completely different to the older ones, making reuse of foundations less economical and more risky.

1.4. DESIGN OF NEW FOUNDATIONS FOR FUTURE REUSE

It is recognised that the best way to deal with congested underground space in urban sites is to be proactive through the application of methods that facilitate the reuse of foundations. Keeping detailed records for the construction and operation of the structure and its foundations, as well as the use of instrumentation, able to record the structural loading and the performance of the foundations during the lifespan of the structure (‘smart foundations’), are regarded as a means to reduce uncertainties in the reuse of foundations according to Chapman et al. (2007).

Reducing the number of foundations in the ground from successive superstructures is regarded very important as well. A proactive measure against congested underground space is designing foundations for an extended working life. A solution that has been put forward by the RuFUS project (2006) is the design of a foundation platform to support successive structures and able to accommodate variable load combinations from successive structures. A foundation platform, for instance see Figure 1.7, increases the reuse potential of foundations allowing new foundations to be reused in the future, limiting the requirements of raw material and construction work, and thus contributing to a sustainable design.

It is recognised by Chapman et al. (2007) that, despite the fact that such a foundation system may be feasible to construct, it may not be possible to predict future requirements. At the same time, the cost of designing a foundation platform for all possible future buildings requirements may be extremely high. However, wherever there are planning restrictions, such as maximum building height, a prediction for the most suitable foundations may be made.

Nevertheless, designing foundations that allow flexibility in the layout of the structure that it can carry increases the potential for future reuse of the foundations. The foundation platform described could have the form of a piled raft foundation, as shown in Figure 1.7.

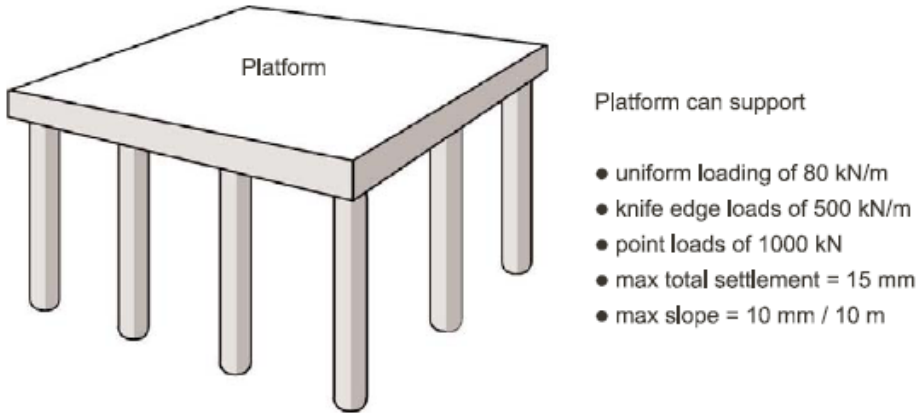


Figure 1.7: Foundation platform to support successive buildings (Chapman et al., 2007)

1.5. OBJECTIVES AND METHODOLOGY

The overall objective of the research presented in this thesis is to contribute towards the optimum design of foundations considering their past, their present and their future. Foundations of old buildings are taken into account, in order to examine the time effects on them, and at the same time an effort is made to provide environmentally sustainable foundation solutions for future developments, considering their geometry and the time factor as well. Several geotechnical aspects of the reuse of piled foundations and of the design of optimum foundations are investigated, which are detailed below. Also, the method employed to deal with these geotechnical problems is outlined.

One of the main geotechnical questions that arises when having to build on old foundations is estimating how much load can be sustained by such foundations, as new developments usually tend to be larger than the previous ones (e.g. multi-storey buildings compared to previous low-rise buildings, heavier loads, deeper basements, etc.). Clearly, these foundations had to sustain a certain load from the previous structure over a period of time, during which the soil was subjected to time-related processes of consolidation, as well as creep. Both of these processes would have enhanced the soil strength and stiffness compared to the initial ones, but it is recognised that the difficulty is in quantifying this enhancement. This is one of the main issues identified in the RuFUS project, but for which no solution was put forward by

the project partners. One of the aims of the present research is to provide an answer to this issue.

The most efficient design for piled foundations is recognised to be the piled raft foundation system, which can be used as a foundation platform to support successive structures. The major geotechnical issues concern the optimum location of the piles underneath the raft and the foundation response with time. It is known that the most optimum design is achieved when piled rafts are founded in stiff clays, since piles may be utilised as 'settlement reducers', rather than as a means to provide additional load capacity. London Clay is a stiff clay, where extensive research has been performed on its behaviour, and where several documented case histories are found. An objective of this research is to optimise the design of foundations in stiff clays, in particular in London Clay.

The research involves advanced finite element analyses using the Soil Mechanics Section's finite element program ICFEP (Potts and Zdravkovic, 1999). The analysis is coupled, thus taking account of consolidation processes in the ground. It also employs an advanced constitutive model that can reproduce soil behaviour due to creep. Creep falls into a broad group of soil behaviour which is related to the viscosity of the soil. A geotechnical issue is how to quantify the time dependent behaviour of natural stiff clays. Another objective of this research is to realistically reproduce the time dependent behaviour of natural stiff clays, and in particular of London Clay.

A number of case histories are used to calibrate both the constitutive and numerical models of the foundations. Case histories involve single isolated piles as well as more complex piled foundations. In continuation, a series of parametric studies is performed, with the aim of providing guidance for the likely enhancement of soil properties and hence foundation capacity. Foundation types involve fully piled foundations as well as piled rafts.

1.6. LAYOUT OF THE THESIS

This thesis consists of four main parts: (a) a literature review on piles, piled raft foundations and time dependent behaviour of soils, (b) a description of an appropriate constitutive model and calibration of the model parameters with laboratory tests on London Clay, (c) preliminary finite element analyses of single piles and calibration of numerical models, including single piles and piled raft foundations, with field data from case histories in London clay, and (d)

parametric analyses to optimise design and reuse of piled raft foundations. In the following, a detailed description of the layout of this thesis is presented.

In ***Chapter 2***, a literature review on single piles and on piled raft foundations is performed. Initially, the life cycle of a pile during the life span of a typical building founded in cohesive soil, which has been in place for a long period of time before being redeveloped is assessed. Methods for determining the axial load capacity are presented. A literature review of the long term performance of single piles through pile load tests is performed, where the time dependent mechanisms involved are explored.

Then, focus is given on piled raft foundations, where a literature review on the design concepts of piled raft foundations is performed; conditions for efficient design are explored. The design approaches and the types of piled raft foundations adopted in current practice are described along with the description of characteristic case histories. The design process for piled raft foundations and the factors required to be considered in the design are explored, along with methods of analysis. Finally, a literature review on the numerical analyses performed on piled raft foundations is performed, in order to identify the critical aspects of piled raft foundations.

A literature review on the time dependent behaviour of soils then follows in ***Chapter 3***, focusing on the behaviour of saturated clays. The behaviour of soils under compressive load in the short term and long term, during primary and secondary consolidation, is identified and the mechanisms that trigger this behaviour are explored. Consolidation, soil viscosity and soil ageing are classified and their significance in engineering practice is highlighted. The results from several laboratory tests examining volumetric and deviatoric creep in clays are assessed, from which the accumulated effects of soil viscosity and soil ageing on the behaviour of clays are determined.

In ***Chapter 4***, a description of the finite element method and of the constitutive models employed in this thesis is given. In particular, the theory behind the finite element method for linear and non-linear materials is presented, as well as pore water pressure considerations due to the coupled nature of the finite element analyses performed. A description of the Modified Cam Clay model is made by considering its formulation in triaxial stress space and its extension to general stress space. The Equivalent Time (ET) Creep model, a time dependent model that can reproduce isotach viscosity, is then described by considering the assumptions involved, its formulation in isotopic stress conditions and its extension to general stress space. Several features of the model are described, including the modelling of destructuration upon

loading. Finally, a validation of the ET Creep model is performed, in order to examine the accuracy of the model in mimicking the time dependent behaviour of natural clays.

In ***Chapter 5***, the ET Creep model parameters are calibrated with the results of laboratory tests on London Clay sampled from Heathrow Airport Terminal 5, in order to reproduce the time dependent behaviour of London Clay. Initially, a description of the London Clay is made by highlighting the geological history of the London Clay Formation and by describing the local geology, lithological units and index properties at Heathrow. The macrofabric of London Clay is also discussed along with its effects on shear strength. Subsequently, the viscous behaviour of London Clay, along with the capabilities of the ET Creep model to reproduce this time dependent behaviour, is described. Then, the model parameters are obtained and calibrated by employing oedometer, triaxial and creep test results. The compressibility, strength and stiffness, and time dependent behaviour of London Clay are reproduced for each individual lithological unit and sub-unit identified at Heathrow Airport Terminal 5.

In ***Chapter 6***, finite element analyses of piled foundations are performed, in order to calibrate the numerical models of piled foundations installed in London Clay. Initially, a preliminary analysis of the short-term and long-term behaviour of single piles founded in typical soft clay and stiff clay ground conditions is performed, in order to assess the time effects on the performance of single piles. Then, documented case histories in London Clay, on the response of single piles under axial loading and on the performance of a piled raft foundation, are utilised, in order to calibrate the numerical models of piled raft foundations; the ET Creep model parameters calibrated for London Clay are employed in the analyses. In particular, a documented single pile load test from Heathrow Airport Terminal 5 is initially back-analysed, by considering several aspects of the CRP pile load test and the effects of installation. Then, the focus moves to a documented large scale project, the Hiscocks House in Stonebridge Park founded on a piled raft foundation, where a series of pile load tests before the erection of the building and after its demolition are utilised to validate the numerical and constitutive models; single pile load tests involve both maintained and CRP load tests. The performance of the piled raft foundation is also compared with the predicted results by employing a three-dimensional (3D) finite element analysis.

In ***Chapter 7***, 3D parametric analyses on piled raft foundations are performed. An initial study on a hypothetical piled raft foundation in London Clay is performed in order to assess the concept of locating piles centrally under the raft. Three different foundations are examined: a raft foundation, a piled raft foundation with a uniform distribution of piles and a piled raft

foundation with central pile support. The effect of preloading and the potential for increased load capacity are also assessed. Subsequently, optimisation of the performance of the piled raft foundation at Stonebridge Park is attempted by examining several pile arrangements, consistent with the findings from the literature review on piled raft foundations. In particular, the limitations of employing a raft foundation for Hiscocks House and the lack of cost-efficiency of the original design are highlighted. A parametric study of the foundations of Hiscocks House is performed by varying the raft thickness, the number of piles and the pile length, as well as the pile geometry underneath the raft. Finally, the effects of time on the performance of the original piled raft foundation for Hiscocks House are examined.

Chapter 2

Piled Foundations

2.1. INTRODUCTION

The overall objective of the research presented in this thesis is to contribute to the understanding of the mechanisms involved in the optimum design of piled foundations. It is considered that a raft foundation, with a limited number of piles beneath it, is the most efficient design, where the raft contributes in the load sharing and the piles contribute in the reduction of settlements and differential settlements.

This chapter presents a limited literature review on piled foundations. Single piles are considered first and in particular their axial load capacity, since this is the main loading pattern from residential and commercial buildings. The life cycle of a pile, during the life span of a typical building founded in cohesive soil, which has been in place for a long period of time before being redeveloped, from installation to reloading, is assessed. Methods for determining the axial load capacity of piles are briefly described. Finally, the observed time effects on piles are presented and assessed through several documented pile load tests.

The focus then moves to piled raft foundations and the design philosophy of piled foundations. The advantages of piled raft foundations are highlighted and eventually the design process of such foundations is presented. Different design approaches and case histories, along with numerical studies, are presented from which several conclusions about the critical aspects, the current practice and knowledge on piled raft foundations, are drawn.

2.2. SINGLE PILES

2.2.1. INTRODUCTION

Piles are slender elements in a foundation whose function is to transfer load from the superstructure, through weak compressible strata, onto stiffer or more compact and less compressible soils or rocks. Piles are also used as a means to resist uplift loads in the case where tall structures are subjected to overturning forces from winds (e.g. skyscrapers, wind turbines) or waves (e.g. marine structures). Different combinations of loading may be involved including vertical and horizontal loads, when piles are used to support retaining walls, bridge piers and abutments, and machinery foundations (Tomlinson and Woodward, 2009).

The focus in this research is on piles which are loaded vertically and are in compression. Such conditions arise when piles are used to support residential or commercial buildings where the main concern for the designers is to provide sufficient load capacity and ensure the settlements are within the design limits.

Several types of piles have been employed in industry, depending on the design requirements and local conditions. The most common ways to classify piles are with respect to load transmission, functional behaviour, type of material and effect on the soil during installation. These may include end-bearing or friction piles, or a combination of both with respect to load transmission, conventional or 'settlement (or stress) reducing' piles with respect to functional behaviour, timber, concrete, steel or composite piles with respect to material type, and displacement (driven) or replacement (bored) piles with respect to the effect on the soil during installation.

It is widely accepted that the performance of axially loaded piles depends on several factors, which have to be considered when designing piled foundations:

- The *soil media* in which the pile is installed, e.g. sand, clay, rock, presence of water etc.;
- The *physical properties* of the pile, e.g. length, diameter, material, cross-section etc.;
- The *method of installation*, e.g. boring, driving, jacking etc.;
- The *loading conditions*, e.g. piled loaded vertically and statically in compression or tension, rate of loading, cycling loading, dynamic loading etc.;
- The *time elapsed* since the end of installation.

However, it should be acknowledged that the determination of the pile load capacity is of a complex nature and currently it is mainly based on empirical methods and partly on theoretical concepts of soil mechanics. Methods to determine the axial load capacity of piles are described in section 2.2.3.

2.2.2. LIFE CYCLE OF PILES

The life cycle of a pile during the life span of a typical building founded in cohesive soil which has been in place for a long period of time before being redeveloped, from installation to reloading, is assessed in order to consider the processes and the mechanisms involved which may affect the short and long-term performance of piles. In Figure 2.1, a schematic diagram of a typical life cycle of a pile over two building lives is presented, where typical variations of loading and settlement with time are shown. Several phases during the pile life cycle may be identified including the installation, equilibration, loading, elapsed time, unloading and reloading phases.

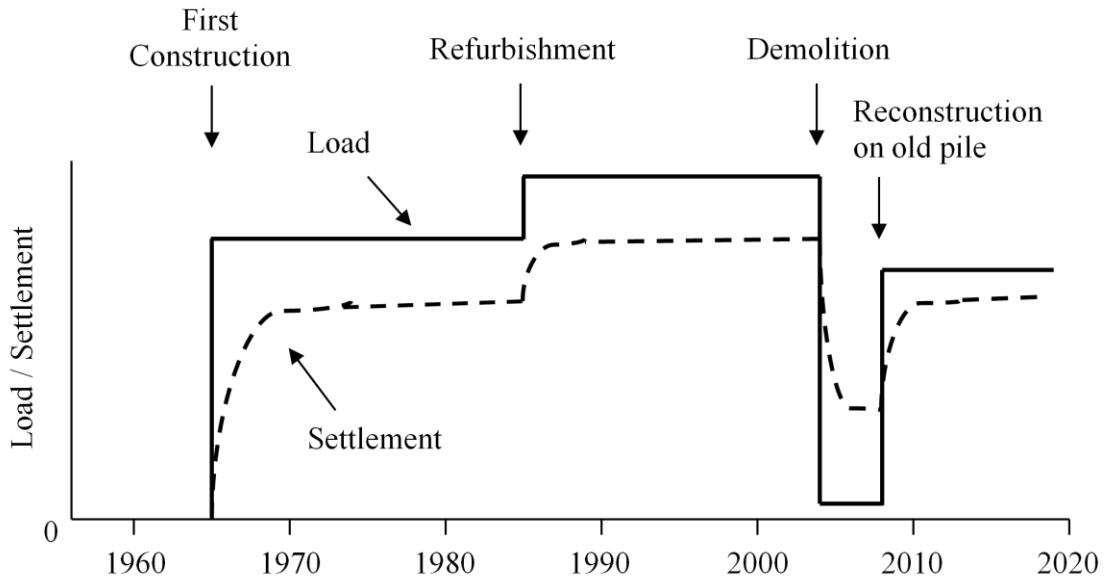


Figure 2.1: Life cycle of a pile over two building lives.

2.2.2.1. Installation and Equilibration

The first phase of the pile life cycle is the installation phase during which the pile is installed in the ground either by displacement or replacement. Pile behaviour during loading is significantly affected by installation and it is a matter that has been investigated and described thoroughly by Tomlinson and Woodward (2009), Jardine et al. (2005), Randolph (2003),

Pellew (2002) and others. Following the installation phase a period of equilibration continues. Equilibration may last for weeks or months, depending on the amount of disturbance in the surrounding soil during installation. Different processes take place during installation and equilibration depending (a) on the medium the pile is installed within and (b) on the method of installation. In this research, the focus is on clays, which are known to have variable behaviour depending on their type.

(a) Displacement piles

Considering displacement piles (or driven piles) in soft and firm clays, Randolph (2003) describes that during driving the soil is displaced laterally initially to an extent equal to the volume of the pile entering the soil. The clay close to the pile-soil interface is extensively remoulded and high pore water pressures are generated. During equilibration, the excess pore water pressures developed during installation dissipate into the surrounding clay, resulting in a gradual restoration of the radial effectives stresses around the pile shaft. More particularly, as the driving induced pore water pressures dissipate, the soil consolidates. This leads to the horizontal effective stresses acting against the pile wall gradually increasing with time implying increased mobilised skin friction.

Regarding displacement piles in stiff clays, Tomlinson and Woodward (2009) state that during driving the soil is also displaced laterally and high excess pore water pressures are generated. In soft and firm clays, the excess pore water pressures are positive, whereas in stiff clays they are negative. In stiff clays, extensive cracking of the soil occurs in a radial direction around the pile during driving. If the clay has a fissured structure, the radial cracks around the pile propagate along the fissures, while beneath the pile toe the soil is extensively remoulded and therefore the fissure structure is destroyed. Driving may also result in the soil surrounding the upper part of the pile breaking away without the gaining contact with the pile in the future. During equilibration, dissipation of the excess pore water pressures developed during installation occurs rapidly into the surrounding crack system. However, due to the negative excess pore water pressures developed in the soil during installation, high radial effective stresses are initially mobilised. These reduce with time as the negative pore water pressures dissipate.

Imperial College model Pile (ICP) tests performed by the Imperial College Soil Mechanics research group at different test sites have shown how the radial effective stresses vary with time during the equilibration phase. Figure 2.2 shows the variation of the radial effective stress normalised to the final equalised radial effective stress with time for different types of

clay ranging from very stiff (London Clay) to soft (Bothkennar Clay). In stiff clays, during installation the radial effective stresses on piles increase due to the development of negative pore water pressures, which can be up to 40% for instance for London Clay (see Figure 2.2), and then they drop during equilibration to the in-situ pre-installation value. In soft clays, due to the development of excess pore water pressures during installation, initially the radial effective stresses on piles reduce and then they increase during equilibration to the in-situ pre-installation value.

The duration of the equilibration period is very important when considering the capacity of a pile, since capacity estimations are often made considering data from pile load tests, which usually take place several days after the pile installation. According to Jardine et al. (2005), the duration of the equilibration period (t) depends on pile radius (R^2) in addition to the coefficient of consolidation (c_{vr}) for radially draining soil ($T = c_{vr}t/R^2$ for closed-ended or fully plugged piles, where T is a non-dimensional time factor – equilibration is effectively complete when T=100). For the ICP pile with a diameter of 100 mm, it seems that 3,000 minutes (see Figure 2.2) or 2 days approximately are required for equilibration to occur in a soft Bothkennar clay. Considering this, for a close-ended driven pile with diameter of 1000 mm, equilibration may last up to 200 days approximately.

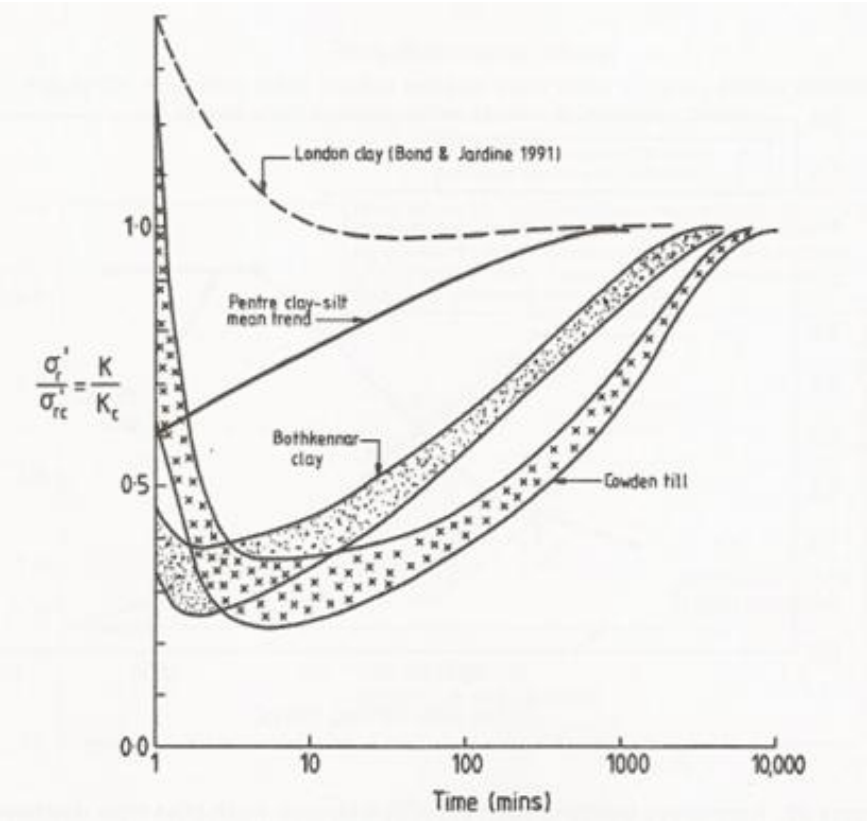


Figure 2.2: Variations with time of radial effective stresses at four ICP clay test sites. (Jardine et al., 2005)

(b) Replacement piles

In case of replacement or bored piles, installation causes changes in properties on the walls of the pile borehole, which have a significant effect on the skin-frictional resistance of the piles, as described by Tomlinson and Woodward (2009). For example, the shear strength of the clay immediately adjacent to the pile shaft is almost always less than that of the surrounding clay. More particularly, drilling of the pile borehole causes the relief of lateral pressure on the borehole walls, resulting in swelling of the clay and migration of the pore water towards the exposed clay face. Flow of water may be restricted if bentonite is used to support the sides of the borehole, however softening of the clay will still occur due to the relief of lateral pressures on the wall. Further softening of the adjacent soil after placing the concrete in the pile borehole may occur because of the migration of water from the unset concrete into the clay.

Meyerhof and Murdoch (1953) observed a rise in water content close to the pile interface due to the combined effects of drilling and placing concrete. They measured an increase of 4% in the water content of London Clay close to the interface of a 760 mm diameter shaft, which extended for a distance of approximately 70 mm from the interface. Similar trends have been observed by Taylor (1966) for piles in stiff Humber Till, however this rise in moisture content lasted for a period of one month, after which the moisture content dropped and remained depressed for at least 10 months.

A schematic diagram from Pellew (2002) for the evolution of the radial stress around a pile in a high plasticity stiff clay such as London Clay, during equilibration, is shown in Figure 2.3. As indicated, a minimum effective radial pressure is developed during the early curing process following concreting and this is denoted by σ_{ri}'. A period of time-dependent change ($\sigma_{r(t)}'$) follows, leading to a final state (σ_{rc}') after full equalisation of pore pressures. The σ_{rc}' value will tend to a level for which the in-situ Ko stress provides an upper bound, according to Chandler (1968) and Burland (1973), providing that the pile is formed promptly after excavation of the shaft. Fleming et al. (2009) claim that the final σ_{rc}' value may be reduced by 20% in heavily overconsolidated clay, where the value of K_o is large, due to stress relaxation. Delays in pouring the concrete may reduce the in-situ horizontal effective stress considerably according to Fleming et al. (2009). Back analysis of tests of bored piles in heavily overconsolidated London Clay show values of K below unity (K_o for London Clay is usually regarded as exceeding 1.0), where delays have occurred between augering and forming the piles (Fleming and Thorburn, 1983).

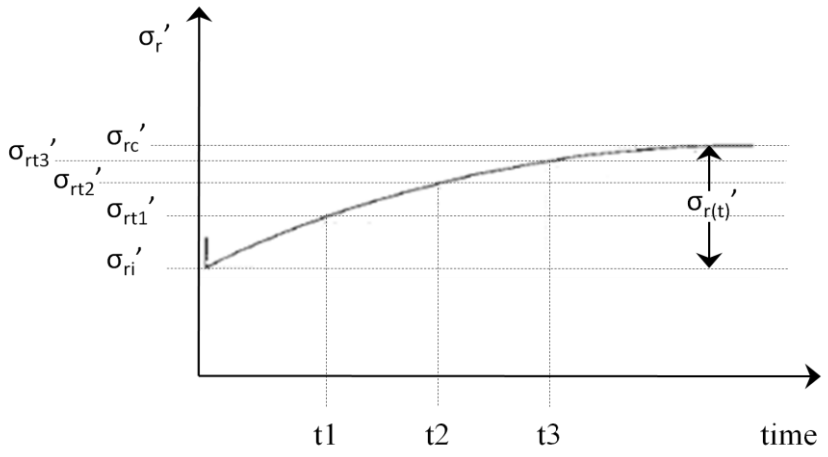


Figure 2.3: Schematic diagram for the evolution of radial stress around a pile during equilibration.

Tests from Whitaker and Cooke (1966) on 940 mm diameter piles in London Clay have shown that the equilibration period and the recovery in stresses may last for 40 to 60 weeks. Pellew (2002) describes that the evolution of $\sigma_{r(t)}'$ is dependent on the drainage condition provided by the pile concrete at the interface. Pile load tests performed by Pellew (2002) on small diameter piles in London Clay have shown that a period of 50 days was required for pore pressure equalisation. It was also recognised by Pellew (2002) that the equalisation period for typical large diameter bored piles would theoretically be significantly larger.

Both changes in water content with time and equalisation of radial effective stresses with time may result in increased shaft capacity with time according to Pellew (2002). This has to be taken into account when assessing the load capacity of a pile by load tests, since commercial pile load tests usually take place after a short period after the pile installation, perhaps within a couple of weeks when the pile concrete is deemed sufficiently strong. Pile load tests on similar piles at different time intervals, including those of Taylor (1966) and Whitaker and Cooke (1966), have shown a significant rise in load capacity after several months. More pile load tests are described in section 2.2.5.

2.2.2.2. Loading phase

During the loading phase, the pile is loaded from the structure which is built on top. The loading phase spans from the moment the pile is first loaded to the moment the pile is fully loaded, i.e. the construction period. Excess pore water pressures are generated near the pile-soil interface and around the pile toe, a mechanism regarded as undrained loading. Load capacity in piles is derived from a combination of friction along the pile shaft and end bearing

at the pile base. The relative magnitude of the shaft and base capacities depends on the geometry of the pile and the soil profile. Piles which derive most of their capacity from the base capacity are referred to as ‘end-bearing’ piles, whereas those which derive most of their capacity from shaft friction are known as ‘friction’ or ‘floating’ piles. The behaviour of a ‘friction’ pile is shown schematically in Figure 2.4.

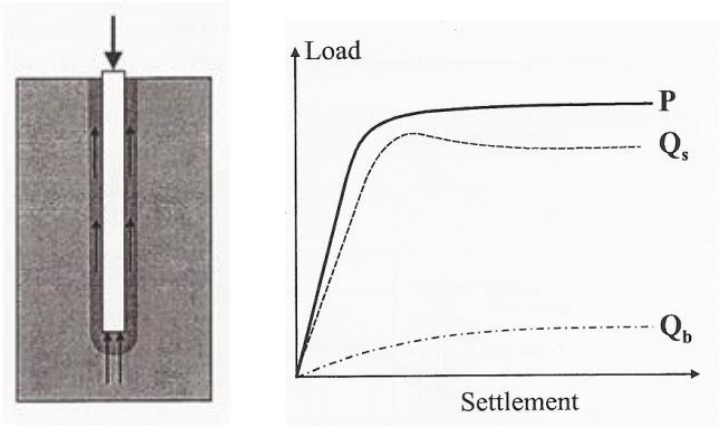


Figure 2.4: Shaft and base contribution to load capacity of a ‘friction’ pile.

According to Tomlinson and Woodward (2009), full shaft mobilisation is usually fully developed at small displacements, of the order of 0.3% to 1.0% of the pile diameter, whereas the mobilisation of the full base resistance requires much larger movements, of the order of 10% to 20% of the pile diameter. In a similar manner, Fleming et al. (2009) claim that full shaft mobilisation is developed at displacements of the order of 0.5% to 2% of the pile diameter, whereas the base capacity is mobilised at displacements of the order of 5% to 10% of the pile diameter.

Tomlinson and Woodward (2009) produced a theoretical plot shown in Figure 2.5, which shows the transfer of load from the pile to the soil at characteristic stages of loading. At low levels of loading the majority of the load is carried by frictional resistance of the pile shaft, whereas the base resistance is very low. When loaded to some working load, the frictional resistance in the pile shaft is already fully mobilised and at the same time the pile toe is carrying some load. Finally, at failure there is no additional resistance from shaft friction, but the base load is reaching its ultimate value. An additional sketch of the failure surfaces, developed around the pile shaft in skin friction and around the pile toe in end bearing, is plotted in Figure 2.6.

The ultimate pile resistance is defined by Tomlinson and Woodward (2009) as the stage at which there is a general shear failure of the soil beneath the pile toe. However, it should be

acknowledged that failure in engineering can also depend on relative displacements between piles causing intolerable distortion to the structure supported rather than to bearing failure.

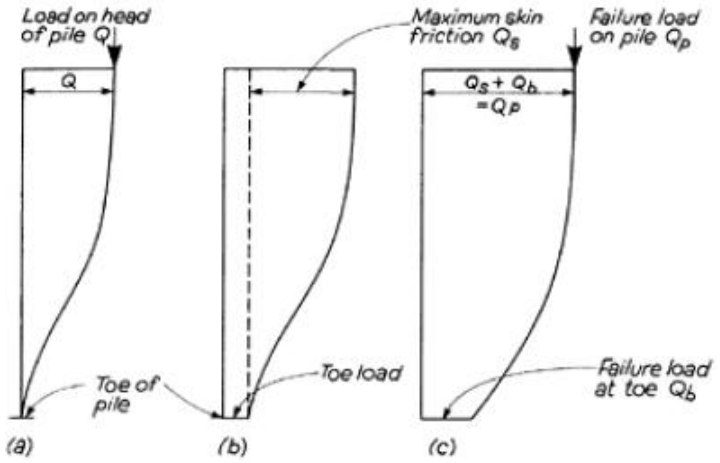


Figure 2.5: Load transfer from head of pile to shaft for (a) small loading, (b) in working conditions and (c) at failure.

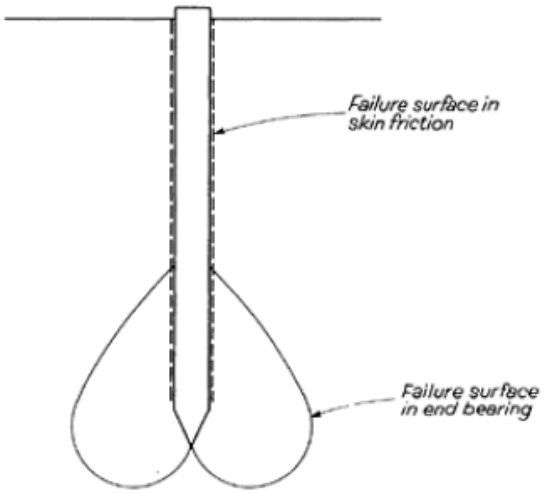


Figure 2.6: Failure surfaces for piles in compression.

A numerical simulation performed by Randolph (2003) and presented by Fleming et al. (2009) illustrates the contribution of the shaft and base to pile capacity and the displacement level at which each component is fully mobilised. A load transfer approach has been applied and the results are compared with those from a load test on a bored pile, 0.8 m diameter and 20 m long, in Figure 2.7. The contributions of the pile shaft and pile base are also shown in Figure 2.7, and conclusions can be drawn about the required displacements to mobilise full capacity of each component. This is important due to the fact that since the shaft capacity is fully mobilised, the stiffness of the pile-soil system reduces to that of the pile base, and the displacements start to increase rapidly. According to Randolph (2003), the shaft capacity of

4.1 MN is mobilised at a displacement of less than 6 mm (0.75% of the pile diameter), while the base resistance is still rising for movements in excess of 80 mm (10% of the pile diameter). The ultimate load capacity is taken as 7 MN, with the shaft contributing 60% of the total capacity at failure. However, at a working load of 3.5 MN, Fleming et al. (2009) conclude that 95% of the resistance is provided by the shaft and only 5% of the load is carried by the base. Such differences in pile-soil stiffness due to different levels of loading are of fundamental importance in the design of piled foundations.

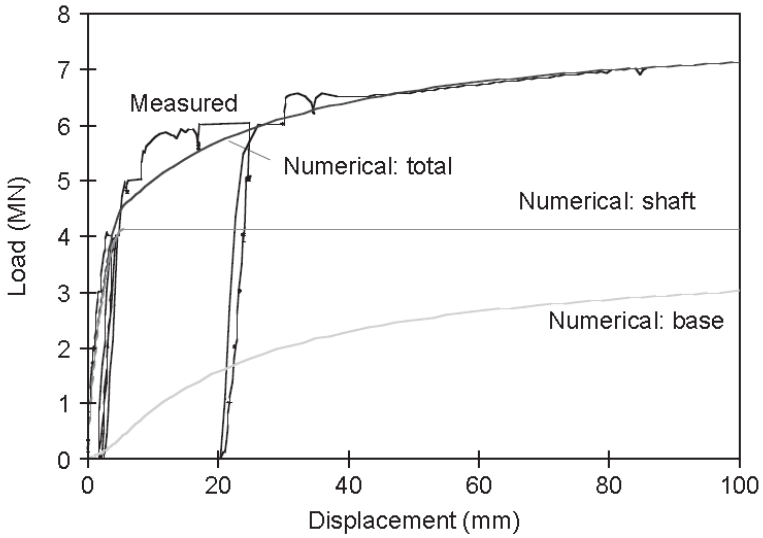


Figure 2.7: Load settlement response of single pile in compression. (Randolph, 2003)

Generally, the capacity of single piles can be determined by testing (e.g. static and dynamic pile load tests) and calculation. Methods to calculate the ultimate capacity of a single pile fall broadly into two categories according to Fleming et al. (2009), those based on fundamental soil properties such as shear strength and angle of friction, and those based on in-situ measurements such as standard penetration tests or cone penetration tests.

In current methods to determine the ultimate capacity of piles, calculations are based on the physical properties of the soil in the undisturbed state and therefore several correlations are made. Such conditions have led Randolph (2003) to postulate that "we may never be able to estimate axial pile capacity in many soil types more accurately than about $\pm$ 30%". Therefore, this uncertainty usually results in large factor of safety in the design of piled foundations, ranging typically from 2 to 3. Methods to estimate the ultimate capacity of a single pile are described in section 2.2.3.

2.2.2.3. Elapsed time

The elapsed time phase is the period after the pile has been fully loaded from the building on top and lasts for the whole life span of the building during which refurbishment may take place and, therefore, an increase in the loading of the piles may be observed, as shown in Figure 2.1. During that period the time related processes of consolidation and creep take place. Consolidation takes place due to the dissipation of excess pore water pressures generated near the pile-soil interface and around the pile toe during the loading period, whereas soil creep results from the application of long-term stress to the surrounding soil. Both of these processes result in additional settlement referred as consolidation and creep settlement respectively.

Both consolidation and creep are expected to enhance the strength and stiffness of the soil adjacent to the pile with time, resulting in increased load capacity and stiffness of the pile with time. Tomlinson and Woodward (2009) describe that, based on Bjerrum (1973) reports on piles driven into soft clays, if a pile has an adequate safety factor as shown by a conventional short-term loading test, the effect of the permanent (i.e. long term) working load will be to increase the safety factor with time as a result of creep and consolidation of the clay. For stiff clays on the other hand, Tomlinson and Woodward (2009) state that no conclusive observations for the effects of sustained loading on piles have been published, as described in section 2.2.5.3, however enhancement of the pile capacity by a lesser amount than in soft clays at working load is expected. Consolidation and soil creep are fully described in Chapter 3.

In addition to the time dependent mechanical changes in the surrounding soil due to consolidation and creep, time dependent thixotropy, cementing and bonding of the disturbed interface soils may influence the frictional behaviour of a pile during its lifespan according to Chow (1997). It is expected that this time dependent structuration enhances the physical properties of the interface soils.

Other processes that may take place during the lifespan of a building are physiochemical processes, such as corrosion, which may alter the interface roughness of the pile. The absence of air may play a role as well. Pellew (2002) discusses steel displacement piles at Canons Park, London, where significant physiochemical processes were observed on the pile-soil interface, affecting the frictional behaviour of the piles tested. Such processes are out of the scope of this thesis.

Finally, changes in the ground conditions may also take place during the life span of a building, such as changes in the water table, which may affect the behaviour of a piled foundation. According to Butcher et al. (2006b), many major European cities are experiencing rising groundwater tables which can reduce both end-bearing and skin friction components of pile capacity, and affect displacement behaviour. Such effects may be significant; however they are also out of the scope of this thesis.

2.2.2.4. Unloading and reloading

Figure 2.8 shows the schematic behaviour of a pile which is loaded, unloaded, and then reloaded. The unloading phase is the phase during which the building on top of the piles is demolished in order to allow for redevelopment as shown in Figure 2.1. The load on the piles is removed, resulting in an elastic rebound of the piles and a 'permanent set' according to Tomlinson and Woodward (2009), as shown schematically in Figure 2.8.

Then, when the new building is built on top of the old piles, the piles are re-loaded and their response is stiffer than initially. Such a response has several implications, in particular in terms of differential settlements, in the case where old and new piles are combined in order for new piles to provide sufficient support to the new building load (Chapman et al, 2007).

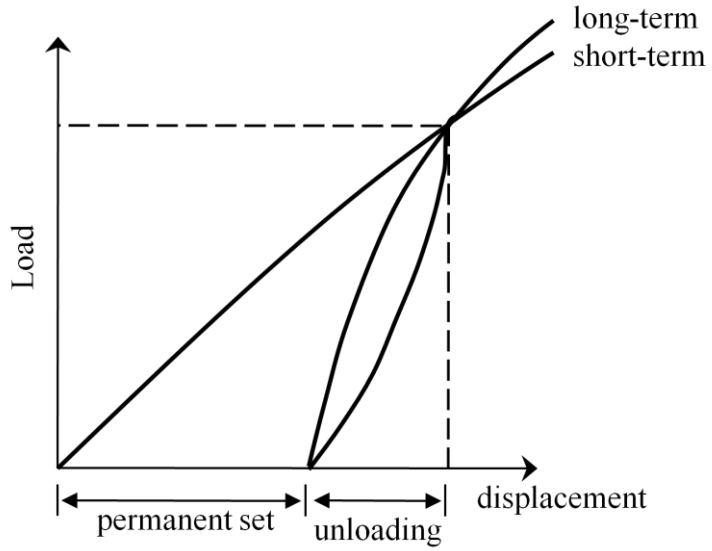


Figure 2.8: Load-displacement behaviour of a pile loaded-unloaded-reloaded in short and long term

The unload-reload effect is visible up to the past maximum load applied to the pile. If the pile is loaded, unloaded, and then reloaded to a higher load level during a small time step (short-term), the load-settlement response of a reused pile follows eventually the response of a fresh

pile after the initial stiff response. However, if the pile had been loaded for a long period of time before being unloaded, the stiffness of the pile would have increased due to the effects of time. This additional stiffness due to elapsed time is visible at the moment when the new load on the pile exceeds the previous load the pile had to sustain, where if no time effects took place, the load-settlement path would follow the original path (short-term) as shown in Figure 2.8. This behaviour is shown on a pile load test in section 2.2.4.

2.2.3. AXIAL LOAD CAPACITY OF PILES

Determination of axial pile capacity has been controversial for many years due to the empirical nature of the design methods developed. Therefore, the design of piles has remained a constant source of research attention. As a result several design methods are proposed in the literature, including Jardine and Chow (1996), De Cock and Legrand (1997), API (1986) and many others.

Generally, a pile subjected to an axial load is carrying the load partly by shear generated along the shaft, and partly by the normal stress generated at the base of the pile. The ultimate load capacity of a pile (Q_f) (Figure 2.9) is equal to the sum of the base capacity (Q_{bf}) and the shaft capacity (Q_{sf}):

Equation 2.1 $$Q_f = Q_{bf} + Q_{sf}$$

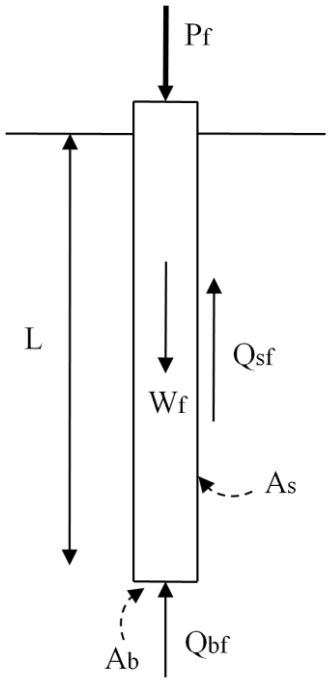


Figure 2.9: Load capacity of a single pile

The total base capacity can be determined by multiplying the maximum end-bearing pressure (q_b) with the base area (A_b),

Equation 2.2 $$Q_{bf} = A_b \cdot q_b$$

and, the total shaft capacity may be calculated by multiplying the average maximum skin friction ($\bar{\tau}_{sf}$) with the shaft area (A_s):

Equation 2.3 $$Q_{sf} = A_s \cdot \bar{\tau}_{sf}$$

Design methods to calculate end-bearing resistance and the shaft friction of a pile in cohesive soils, such as clays, are briefly described in the following sections.

2.2.3.1. End-bearing resistance

Regarding the end-bearing resistance of a pile founded in cohesive soils, it is conventionally calculated in terms of the undrained shear strength of the soil at the pile base ($S_{u,base}$), using a bearing capacity factor (N_c). Hence, the end-bearing pressure is determined by:

Equation 2.4 $$q_b = N_c \cdot S_{u,base}$$

where N_c is approximately equal to 9, according to Skempton (1951) for depths relevant to piles.

It is not strictly correct to use the undrained shear strength of the soil at the pile base level according to Tomlinson and Woodward (2009), since some remoulding due to installation may have altered the S_u at the base level. However, it is commonly accepted that the in-situ S_u may be employed to determine the end-bearing resistance, due to the fact that most of the failure surface mobilised below the pile toe (Figure 2.6) is not significantly distributed by the installation of the pile. Regarding the N_c value, it is commonly taken as equal to 9 if the pile penetrates the bearing stratum by three diameters or more according to Fleming et al. (2009), however values ranging between 5 and 20 have been measured for large and small diameter piles respectively (Jardine and Christoulas, 1991).

Another approach to determine the end-bearing resistance of a pile is to correlate it with the results from a CPT test. Bustamante and Gianeselli (1982) developed an approach based on a CPT test, where the base capacity is calculated by applying a reduction factor k_c to q_c. The value of q_c is averaged over 1.5 pile diameters above and below the base level, and the value of the reduction factor k_c varies between 0.45 and 0.55 depending on the soil (0.5 for soft

clay, 0.45 for moderately firm clay and 0.55 for firm to stiff clay). Hence, the end-bearing pressure is determined by:

Equation 2.5 $$q_b = k_c \cdot \overline{q_c}$$

A more recent design approach is the ICP design method (Jardine et al. 2005), where the q_b is also based solely on the CPT resistance. According to Jardine et al. (2005), recent research demonstrates that q_b can be collated more accurately with the CPT resistance q_c developed at the pile tip level than the conventional method in terms of undrained shear strength. The following has been suggested for closed-ended piles, which distinguishes between drained and undrained loading:

Equation 2.6

$$q_b = 0.8 \cdot \overline{q_c} \quad \text{for undrained loading}$$

$$q_b = 1.3 \cdot \overline{q_c} \quad \text{for drained loading}$$

where $\overline{q_c}$ is the average cone resistance over 1.5 pile diameters above and below the pile tip.

2.2.3.2. Shaft friction

Several design methods have been developed to determine the shaft friction. These are commonly categorised as the "α-method" and "β-method" depending on the way the skin friction is determined. For the "α-method", the skin friction is related to the undrained shear strength by the factor α, whereas the "β-method" is an effective-stress-based method and the skin friction is related to the vertical effective free field stress, multiplied by the factor β.

(a) α-method

The α-method is a total stress approach where the shaft capacity of a pile is determined by averaging the maximum skin friction (τ_{sf}) around the pile shaft:

Equation 2.7 $$\bar{\tau}_{sf} = \alpha \cdot \bar{S}_{u,shaft}$$

where $\bar{S}_{u,shaft}$ is the average undrained shear strength measured over the length of the pile, and α is the 'shaft adhesion factor'. This is an empirical factor which is based on a large number of pile tests. The value of α can range from between 1.5 for soft sensitive clays to as low as 0.2 for very stiff clays. Several values of α for different types of soil, depending on their shear strength, have been proposed in the literature (e.g. the American Petroleum Institute (API 1986) recommendation in Figure 2.10). The past stress history, overconsolidation ratio, and slenderness ratio of the pile may play a role along with the

undrained shear strength of the soil according to Fleming et al. (2009). The installation process may also play an important role in the value of α. For example, for bored piles lower values of α are recommended by Tomlinson and Woodward (2009), if there is long delay between drilling and placing of the concrete.

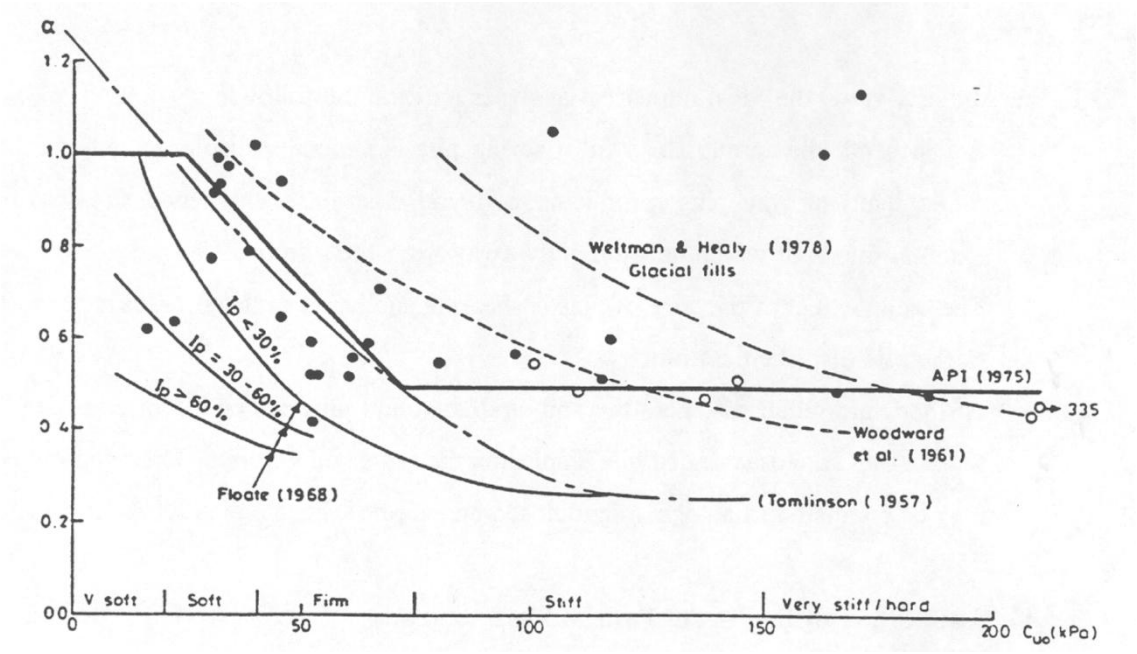


Figure 2.10: API (1986) recommendations for the variation of $\boldsymbol{\alpha}$ with undrained shear strength

(b) β-method

The β-method is an effective stress approach where the skin friction at failure (τ_{sf}) is expressed in terms of effective stress:

Equation 2.8 $$\tau_{sf} = \sigma_{hs}^{'} \cdot \tan\delta^{'} + c_s^{'}$$

where $\delta^{'}$ is the effective angle of interface friction, $c_s^{'}$ is the effective interface cohesion and $\sigma_{hs}^{'}$ is the effective horizontal stress on the shaft at failure. Failure is assumed to take place in the remoulded soil close to the pile shaft and therefore the effective interface cohesion is usually taken as zero (Burland, 1973). If now $\sigma_{hs}^{'}$ is related to the effective overburden pressure $\sigma_v^{'}$ by the earth pressure coefficient for the shaft K_s, then:

Equation 2.9 $$\tau_{sf} = K_s\sigma_v^{'} \cdot \tan\delta^{'} = \beta \cdot \sigma_v^{'}$$

where β is the product ($K_s \tan\delta^{'}$), and can be obtained empirically, from pile tests, in a similar way as the value of α.

According to Fleming et al. (2009), the value of K_s will vary depending on the type of pile (driven or bored) and the past stress history of the soil. Burland (1973) proposes a lower bound for normally consolidated soils with $K_s = K_o$ and $\delta' = \phi'_{cv}$ at failure, which gives a value of β ranging from 0.25 to 0.3, however it is claimed by Fleming et al. (2009) that it does not take into account the stress changes that occur during and after pile installation. For overconsolidated clays, the value of β is significantly higher. Meyerhof (1976) has shown that for driven piles the value of K_s varies between 1 and 2 times the value of K_o and that the value of β depends also on the Yield Stress Ratio of the soil. More recently, Jardine and Chow (1996) have shown that for driven piles the value of $\delta'$is equal to the angle measured from interface ring shear tests, which is equal to the residual angle of friction. On the other hand, for bored piles the friction angle that should be used is still subject to debate, according to Fleming et al. (2009). However, they claim that it has been suggested, notably by Burland and Twine (1988), that a residual angle of friction is appropriate, at least for bored piles in heavily overconsolidated clay.

2.2.4. OBSERVED LONG TERM PERFORMANCE OF PILES

This section uses examples of pile load tests to explain the long-term performance of a single pile, but does not describe in detail different available types of pile testing and how these are used to estimate pile capacity. Such a review allows the experimental assessment of the possible time-dependent mechanisms involved, which may affect the behaviour of piles when they are re-used. In the following, a collection of results from load tests on displacement piles in clays from Powell et al. (2003), results from tests on bored piles at a London Clay site from Powell and Skinner (2006), and a large scale pile load test on a bored pile in London Clay by Butcher and Skinner (2006) are presented.

The majority of pile load tests in the literature are on first-time loaded (‘virgin’ piles) and on re-tested piles which have already failed. These tests allow the assessment of the time effects which are due to pile installation and to the effects that take place at the pile-soil interface with time during equilibration. In this thesis, the point of interest is on piles which have been loaded under working conditions for a long period of time, for instance a pile which is loaded from a building. Tests on piles under working conditions in the long term unfortunately have not been recorded extensively in the literature, and therefore no conclusive observations have been published on the effects of sustained loading under working conditions.

2.2.4.1. Load tests on displacement piles

The load tests on displacement piles in clays from Powell et al. (2003) are static constant rate of penetration (CRP) tests, performed on steel piles initially tested to failure and then re-tested after a certain period of time. Testing sites include Cowden, Canons Park, Brent and Bothkennar, all in the UK. Detailed information about the piles and the soil characteristics are given by Powell et al. (2003).

In Figure 2.11, a collection of results from Powell et al. (2003) of the variation of the normalised capacity with time of the piles tested is presented. The normalised capacity is equal to capacity at time *t* over the capacity at initial testing. According to Powell et al. (2003), initial testing is performed after equalisation of pore water pressures around the pile has occurred, in order to avoid any increase or decrease of the pile capacity with time which would be due to equalisation. However, no justification for this statement has been provided.

Also, tests with similar rates of loading (no rate effects) initially and at time *t* are examined. Rate effects on piles are known to be quite significant (Bjerrum, 1973, has reported tests on displacement piles in soft clay in Mexico City and in Gothenburg, where a 50% reduction on shaft adhesion was observed, when the loading rate was reduced from 10 to 0.001 mm per minute and from 1 to 0.001 per minute respectively).

Results from the different test sites on re-tested driven or jacked piles indicate that typically 10-20% improvement in capacity is achieved within 1-3 months and up to 30-40% within 3-4 years. Also, piles at Canons Park, a London Clay site, show improvements of 50% to 80% after 30 years. Progressive stiffening in the load displacement response with time is also observed in a typical pile tested at Canons Park, as shown in Figure 2.12. The improvement of capacity and the stiffening in the load settlement response with time is regarded by Powell et al. (2003) to be due to ageing; however, the reasons for such improvement have not yet been fully explored according to Powell et al. (2003). The mechanisms that may be involved have been discussed in Section 2.2.2.3 and are further assessed in Section 2.2.4.3.

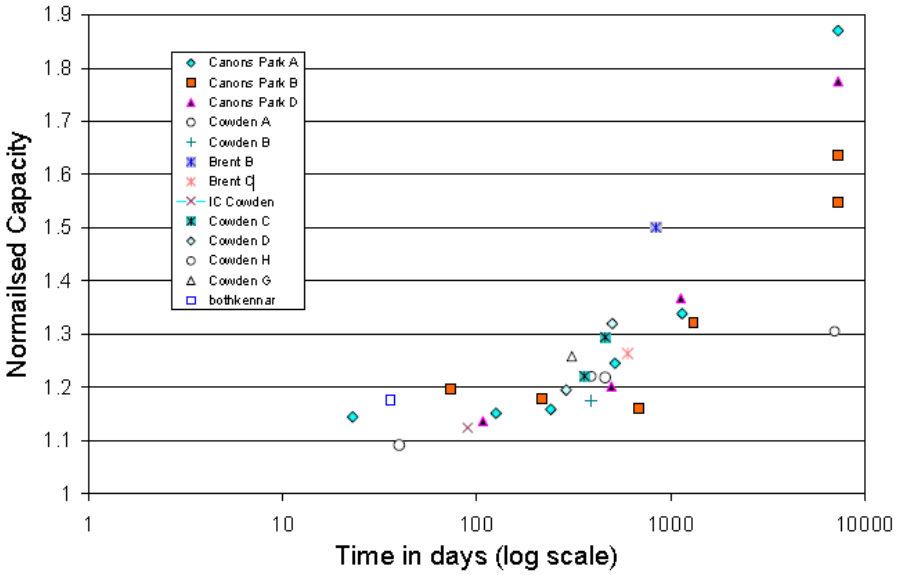


Figure 2.11: Normalised capacity against time of re-tested displacement piles (Powell et al. 2003)

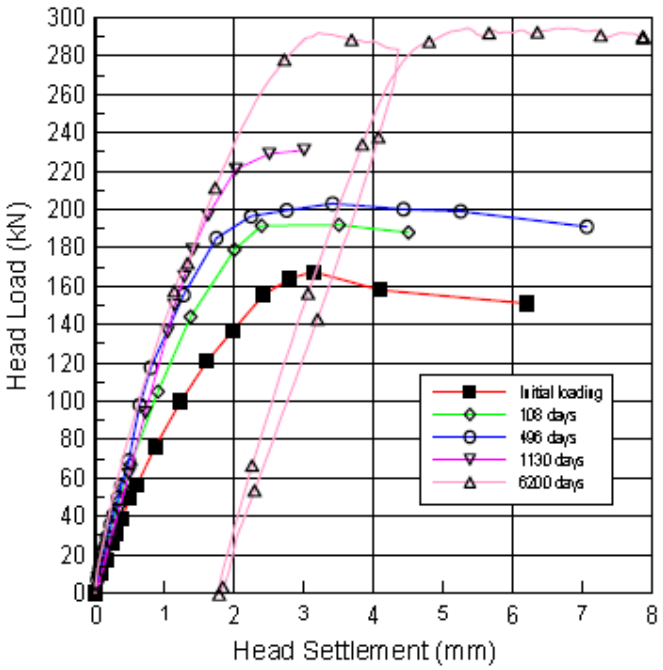


Figure 2.12: Load displacement curves for a typical tested pile at Canons Park (Powell et al. 2003)

2.2.4.2. Load tests on replacement piles

The static load tests on replacement (or bored) piles at a London Clay site, from Powell and Skinner (2006), have been performed on 'virgin' Continuous Flight Auger piles, in order to assess the long-term performance of piles which are first time loaded. First time loading of

bored piles is important due to the brittle failure of piles in London Clay. The brittle behaviour is visualised from the load-settlement response of the pile loaded to failure which reaches a peak and then drops towards a residual value. If the pre-failed piles were tested again, a lower capacity would be expected upon reloading, as shown on pile load tests performed by Unwin and Jessep (2004) and as described by Tomlinson and Woodward (2009), since residual surfaces would have been formed during first-time failure. Therefore, reliable conclusions about the long-term behaviour can be made only on first-time loaded piles and not on re-tested piles. This is not the case for displacement piles, due to the formation of residual surfaces in the soil during driving.

A series of identical piles, with 300 mm diameter and 10 m length, have been installed in stiff London Clay and were tested at different time intervals. A detailed description of the site, the pile installation and the testing are given by Powell and Skinner (2006).

Results of two sets of pile load tests on identical 'virgin' piles 2.5 months and 46 months old respectively (Figure 2.13) show that capacity has increased by 25 %. Also, some increase in stiffness is observed, which is more evident in the large scale pile load test performed at a London Clay site which is discussed below. The reason for such enhancement in capacity and stiffness is attributed to soil ageing by Powell and Skinner (2006).

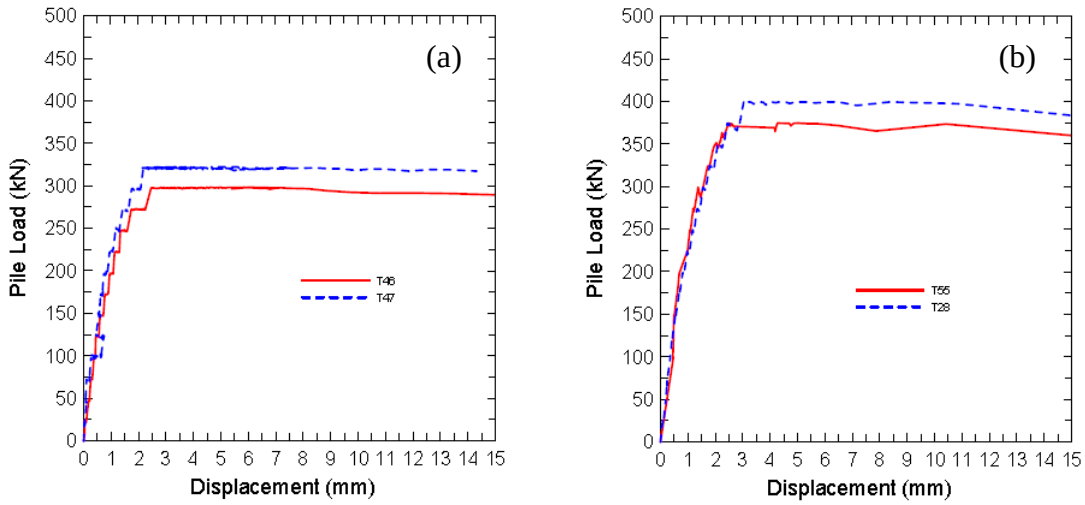


Figure 2.13: Load displacement response of virgin piles tested (a) 2.5 and (b) 46 months old after installation (Powell and Skinner, 2006)

The large scale pile load test presented by Butcher and Skinner (2006) was performed in 2005 on a bored pile (d= 450 mm, L= 13 m) of a demolished building in Stonebridge Park, a London clay site. The load-settlement behaviour of this pile is compared to the load-

settlement behaviour of an identical pile tested in 1972 before being loaded by the building. In this case, the re-loaded pile had been under working load for a period of 33 years.

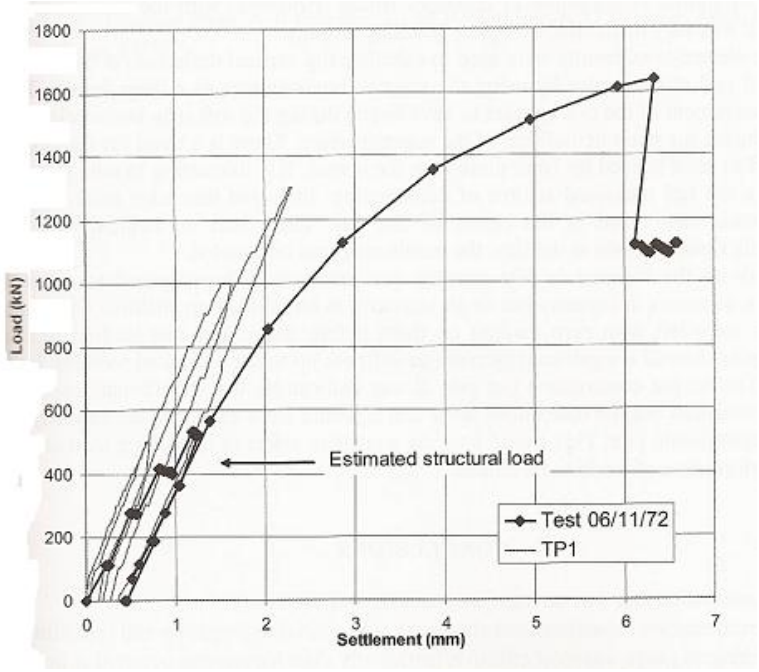


Figure 2.14: Comparison of archive (1972) and recent (2005) pile load tests (Butcher and Skinner, 2006)

The load-settlement response of the 2005 and the 1972 pile load tests is shown in Figure 2.14. The 2005 test has been designed to approximate the 1972 test. Unfortunately, the recent pile load test (TP1 in Figure 2.14) failed due to a failure of an anchor pile. Still, the 2005 pile test shows a much stiffer response than the 1972 test up to the estimated structural load that it had sustained during its lifespan. This is expected due to the unloading-loading effect described in Section 2.2.2.4. However, this increase in stiffness continues at higher loads than previously experienced by the pile, indicating that re-used piles are stiffer, even if the load exceeds the previous working load. Also, Butcher and Skinner (2006) conclude that if the test had been completed, it would have exceeded the initial 1972 bearing capacity. Therefore, from these tests it may be concluded that re-used piles have stiffer load-displacement response and have larger capacity than new piles.

2.2.4.3. Conclusions from load tests

From the above, several conclusions may be drawn about the behaviour of piles in the long term. In particular, it has been observed that pile load capacity and stiffness increases with time for both displacement and replacement piles, 'virgin' and re-tested piles, after a long period of time, and also for a large scale pile load test which is typical of a pile which is re-

used. The reason for such an enhancement is not clear and it tends to vary with soil type. Different processes seem to take place according to the pile type and the history of the pile prior to reloading or first time loading.

However, in continuation with the processes identified in Section 2.2.2.3, there is a common belief according to Augustesen (2006) that the capacity and stiffness increase with time due to changes in the characteristics of the soil skeleton, changes in the pile-soil interaction and/or changes in the stress regime in the soil surrounding a given pile. Installation effects and equalisation may play a role as described in detail in Section 2.2.2.1 since, despite the common belief that these effects heal within a couple of weeks, they may last longer.

Also, it is worth noting that the increase in shaft friction is much bigger than the increase in end bearing for straight-shafted piles, as shown by several studies, including Bullock et al. (2005a), Bullock et al. (2005b) and Komurka et al. (2003).

2.3. PILED RAFT FOUNDATIONS

2.3.1. INTRODUCTION

In foundation design, it is common to consider first the use of a shallow foundation system, such as a raft, to support a structure and then, if this is not adequate, to consider the use of a fully piled foundation system, consisting of a large number of piles, inter-connected through a pile cap and forming a pile group. Adequacy of a foundations performance is defined as the ability of a foundation system to provide sufficient load capacity and to reduce settlements, both average and differential, and bending stress in the raft within the design limits. Traditionally, if any of the criteria is not fulfilled for a shallow foundation, the choice is to support the structure on a fully piled foundation, where the entire design loads are resisted by the piles.

Recently there has been an increasing recognition that the behaviour of a mat or raft can be enhanced effectively by the addition of a limited number of piles, giving rise to the concept of a pile-enhanced raft or a piled raft (Figure 2.15). The piled raft foundation is a geotechnical composite construction consisting of three bearing elements: piles, raft and subsoil. Compared to the traditional foundation design where the structural load is transferred either by the raft or by the piles, this is an innovative design concept where both the raft and the piles contribute to the foundation performance. In particular, both the raft and the piles are able to transmit

loads directly to the subsoil and, therefore, piles are usually not required to ensure the overall stability of the foundation, but to act as 'settlement reducers' (Burland et al., 1977), since the raft alone usually provides sufficient load capacity (Randolph, 1994). Therefore, a piled raft foundation can reduce settlements, differential settlements and bending stresses in the raft in a very economic way, compared to the traditional concepts.

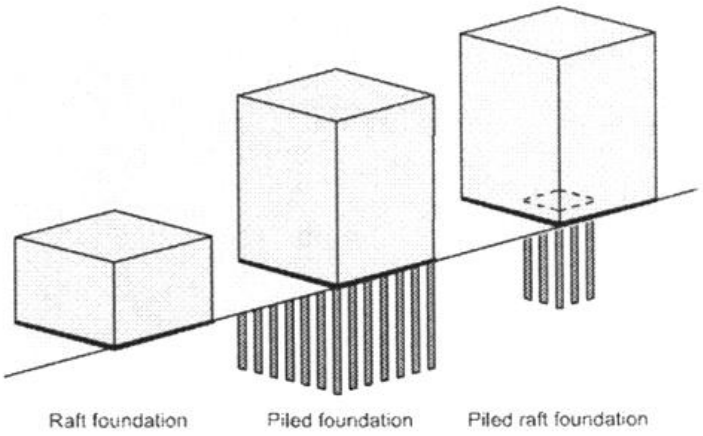


Figure 2.15: Transition from raft to pile group to piled raft foundation (Randolph, 2003)

Key questions that arise in the design of piled rafts, after Randolph (1994), concern the relative proportion of load carried by raft and piles, and the effect of the additional pile support on absolute and differential settlements. These may be determined by considering the response of each component together with the interaction between the components.

2.3.2. DESIGN CONCEPTS

2.3.2.1. Design philosophies

Three different design approaches for piled rafts, that usually apply in practice, have been identified by Randolph (1994):

(a) *the 'Conventional' approach*, where the foundation is designed essentially as a conventional pile group; however, some allowance is made for the contribution of the raft to the foundation performance, primarily to the ultimate load capacity.

(b) *the 'Creep Piling' approach*, where (i) piles are designed to operate at a working load at which significant creep in the soil starts to occur, typically 70-80% of the ultimate load capacity, and (ii) sufficient piles are included beneath the raft to reduce the net contact pressure between the raft and the soil.

(c) *the 'Differential Settlement Control' approach*, in which piles are not uniformly distributed, but are located strategically beneath the raft in order to reduce differential settlements.

Moreover, Poulos (2001) describes a more extreme version of the creep piling approach that may be used for the design of piled raft foundations. This involves the utilisation of the full load capacity of the piles, i.e. some or all piles are designed to operate at 100% of their ultimate load capacity. Such a design concept is only applicable if the raft alone provides adequate load capacity, but at the same time it fails the settlement criterion. Therefore, this approach is regarded to give rise to the concept of using piles in piled rafts primarily as 'settlement reducers', while recognising their contribution to the ultimate load capacity of the foundation system as well.

Both the 'creep piling' and the 'differential settlement control' approaches, identified by Randolph (1994), are considered to use piles as 'settlement reducers', since in both cases piles are included to enhance the foundation performance in terms of settlement rather than to provide load capacity.

Piles designed to utilise their full load capacity may also be used in order to reduce excessive bending stresses in the raft, as well as local yielding and settlement in the underlying soil, according to Burland (1995). Such piles are referred to as 'stress reducing piles'. Such piles have been included in the foundations of the Queen Elizabeth Conference Centre in London (Burland and Karla, 1986) under the most heavily loaded columns, in order to apply a constant upward force beneath each column, thus reducing the loads transferred from the columns into the raft. 'Stress reducing piles' may also reduce settlements.

The concept of using piles as 'settlement reducers' is schematically presented by Poulos (2001) in Figure 2.16, where the load-settlement behaviour of piled rafts for each approach identified is presented, except the 'differential settlement control' approach, which has to do more with the strategic location of piles rather than the utilisation of their load capacity. Curve 0 shows the behaviour of the raft alone, which fails to satisfy the settlement criterion for the design load applied. Curve 1 illustrates the behaviour of a 'conventional' piled raft, whose behaviour is governed by the pile group behaviour. In this case, the piled raft load-settlement behaviour is linear at the design load and, despite the fact that it satisfies the settlement criterion, there is a lot of room for optimisation in the design. Curve 2 represents the case using 'creep piling', where the piles are designed with a lower factor of safety and are fewer; therefore, the raft carries more load than for curve 1. Again, despite the fact that the

design satisfies the settlement criterion for the design load applied, there is still room for optimisation. Finally, curve 3 represents the case where piles are fully mobilised at the design load, i.e. they work as 'settlement reducers', and therefore the number of piles included is very small. In this case, the load-settlement behaviour may not be linear, however the foundation seems to have an adequate margin of safety and the settlement criterion is satisfied. Therefore, this case is considered as the optimum one, since maximum economy is achieved, while maintaining a satisfactory behaviour.

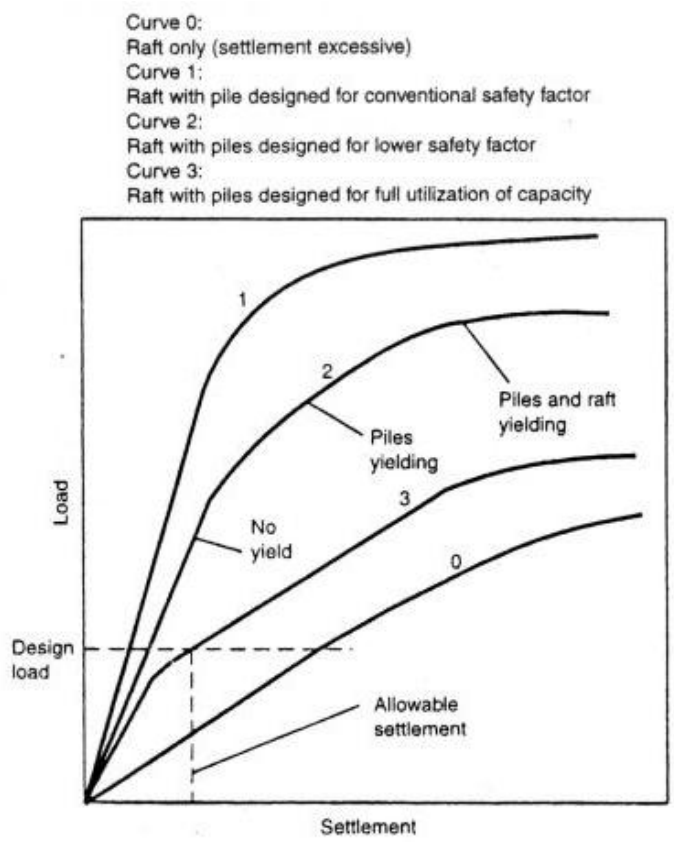


Figure 2.16: Load-settlement curves for piled rafts according to various design philosophies (Poulos, 2001)

Extensive research, including Burland et al. (1977), Cooke (1986), Randolph (1994), Burland (1995), Poulos (2001) and Love (2003), has been performed in order to support the concept of using piles as 'settlement reducers', rather than as a means to provide load capacity to the piled raft foundation. Also, there has been an attempt by several researchers to identify the appropriate location and geometry of piles, in order to achieve the most optimum design. These are presented through several numerical studies in Section 2.3.5, where the performance of piled rafts, which were initially designed using the conventional approach, is examined using a settlement based design approach with less piles, rather than a capacity based design approach with more piles. Finally, all the design approaches identified are

discussed in Section 2.3.3, where several case histories based on each design approach are described.

2.3.2.2. Conditions for efficient design

The most efficient application of a piled raft foundation occurs when the raft alone has adequate load capacity (‘large’ raft), but does not satisfy the settlement or differential settlement criteria. As foresaid, under these conditions the piles may work as ‘settlement reducers’, usually utilising their full or almost full load capacity, in order to enhance the foundation performance, rather than to provide additional means of support.

The soil profiles, which may be favourable for such a design according to Poulos (2001), are those which either consist of (a) relatively stiff clays or (b) relatively dense sands. This is the reason behind the fact that most case histories involving piled raft foundations are founded on stiff clays, as discussed in Section 2.3.4.

On the other hand, as discussed by Poulos (2001), there are some situations which are unfavourable for the design of a piled raft. These include (a) soil profiles containing soft clays or loose sands near the surface, or (b) soil profiles containing soft compressible layers at relative shallow depths. In the first case, the raft may not have the ability to provide adequate load capacity and stiffness (‘small’ raft). Therefore, a ‘conventional’ design will have to be applied. In the second case, the problem is that the long-term settlement of these compressible layers may reduce the contribution of the raft to the long-term stiffness of the piled raft. Thus, the full load capacity of piles will not be able to be mobilized in the initial design, since in the long-term piles will have to support additional load. Moreover, according to Poulos (2001) there are some other soil profiles not suitable for the design of piled rafts, which have to be treated with considerable caution. These are the ones that are likely to undergo consolidation settlements or swelling movements due to external causes. In particular, consolidation settlements may result in lost contact pressure between the raft and the soil. This will result in transfer of additional load to the piles and, consequently, increased settlement of the foundation system.

2.3.2.3. Effective choice of foundation type

The effective choice of foundation type to support a structure is of fundamental importance in geotechnical engineering. Significant economics in design may be achieved depending on the

foundation solution and, therefore, there has been a continuous effort to develop efficient and cost-effective foundation designs.

The conceptual design of foundations involves initially the assessment of the performance of the raft foundation alone, without piles, according to Poulos (2001). In particular, vertical and lateral bearing capacity, as well as settlement and differential settlement, of the raft alone may be determined using conventional methods. Bending stress in the raft due to concentrated loading from columns is another criterion, which may play a role in the conceptual design of the foundations. In the case where the raft alone satisfies all the design requirements, then the foundation may be designed conventionally as a shallow foundation.

However, if the raft alone does not provide enough load capacity, or settlements and bending stress in the raft exceed the design limits, then piles may be introduced to enhance the performance of the raft foundation, giving rise to the piled raft foundation. An alternative option is to provide a group of piles, inter-connected through a pile cap, under concentrated column loads.

The addition of a number of piles below the raft foundation results in reduced settlements as well as to a smaller raft thickness (due to the reduction of bending stress in the raft) since piles carry part of the structural load. In the same manner, the contribution of a raft to the piled foundation performance results in a smaller number of piles and reduced pile lengths since the raft carries part of the total load.

2.3.3. DESIGN APPROACHES AND CASE HISTORIES

2.3.3.1. ‘Conventional’ piled rafts

In the ‘conventional’ design approach, the piled raft foundation is designed as a conventional pile group, with regular spacing of piles over the raft area. The majority of the load is carried by the piles, which are designed with a conventional factor of safety against failure of about 2 to 3. At the same time, some allowance for the contribution of the raft (usually 20-40%) to the foundation performance is made, allowing the reduction of the total number of piles and resulting in significant savings in piling costs. (Randolph, 1994)

This approach is considered as the first attempt to include the raft in the foundation performance. It is a capacity based design, where the effort is to provide a considerable factor of safety against bearing failure. One of the first applications of such a design in the United

Kingdom is considered to be Hiscocks House in Stonebridge Park, London. It was heavily instrumented and its performance is detailed below, as this case is analysed subsequently as part of this research.

(a) Hiscocks House, London, UK

An important case history, where the performance of a conventional piled raft foundation is thoroughly examined (Cooke et al., 1981), is the Hiscocks House (Figure 2.17), a 16 storey building located in the Stonebridge Park area of London. Instrumentation was put in place in order to assess the behaviour of the foundations. Works started in early 1973 and the building was occupied at the end of 1975. In 2004, Hiscocks House was demolished, after 29 years of occupation, in order to re-develop the site (Butcher and Skinner, 2006).

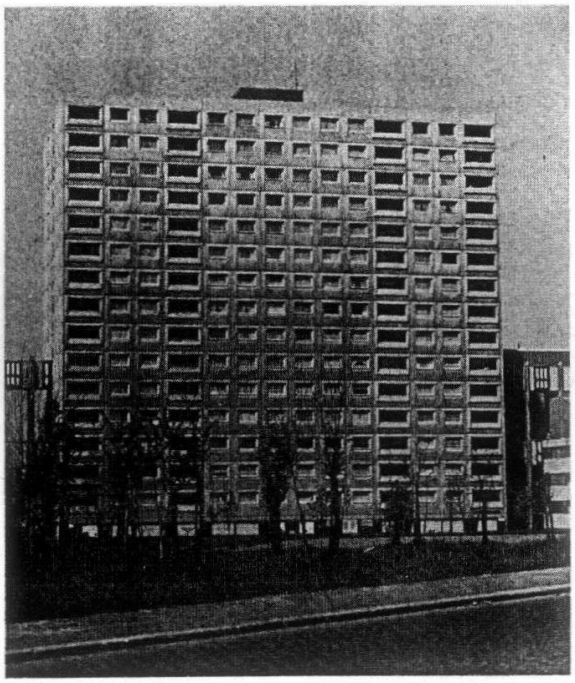


Figure 2.17: Main (east) elevation of Hiscocks House (Cooke et al., 1981)

Hiscocks House was 43.3 m long by 19.2 m wide. It was founded on London Clay, with an estimated undrained shear strength profile of 100 kPa at 3 m depth and increasing to 260 kPa at a depth of 25 m. The foundations consisted of a heavily reinforced concrete raft (0.9 m thick) linking 351 bored concrete piles, which were installed on a square grid of 1.6 m centre to centre spacing. Piles were 13 m long and 0.45 m in diameter. (Figure 2.18) (Cooke et al., 1981)

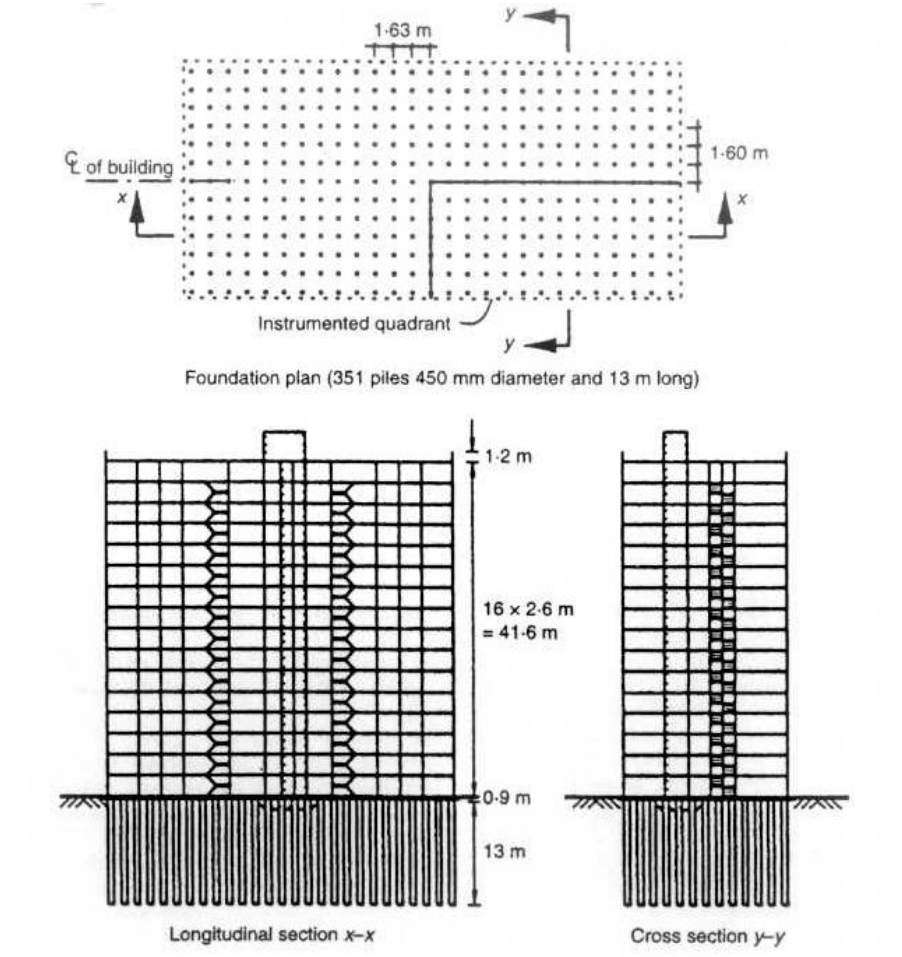


Figure 2.18: Foundation plan and longitudinal cross-sections of Hiscocks House (Cooke et al., 1981)

Cooke et al. (1981) make several observations about the performance of the Hiscocks House foundations and present data regarding the distribution of load between piles, the contribution of the raft to the foundation as a whole, and the building settlements during construction and the first years of occupation, which are detailed below. Also, the instrumentation put in place is described (Figure 2.19) and the method to record the data required to assess the performance of the piled raft foundation. It should be noted that Figure 2.19 shows only a quarter of the foundation.

In particular, a multi-point magnet extensometer at the central corridor, being accessible during construction and occupation, was used to record the settlement of the building and the vertical strains of the clay at different depths. Cooke et al. (1981) produced a settlement/load versus time plot (Figure 2.20), which indicates that the initial settlement at the end of construction in 1975 was about 10 mm and increased, after 4 years, by about 70% to 17 mm. This 10 mm settlement is considered as the immediate settlement and the next 7 mm is

considered as consolidation settlement; however, these should be regarded as upper and lower limits respectively, since some consolidation occured while construction was going on.

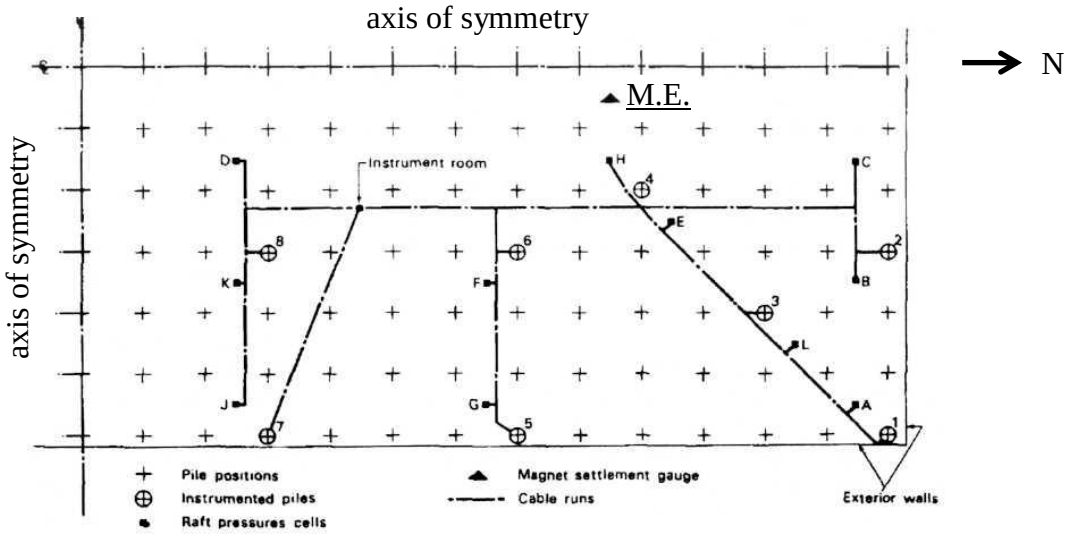


Figure 2.19: Foundation plan of north-east quarter showing positions of instruments and cable runs (Cooke et al., 1981)

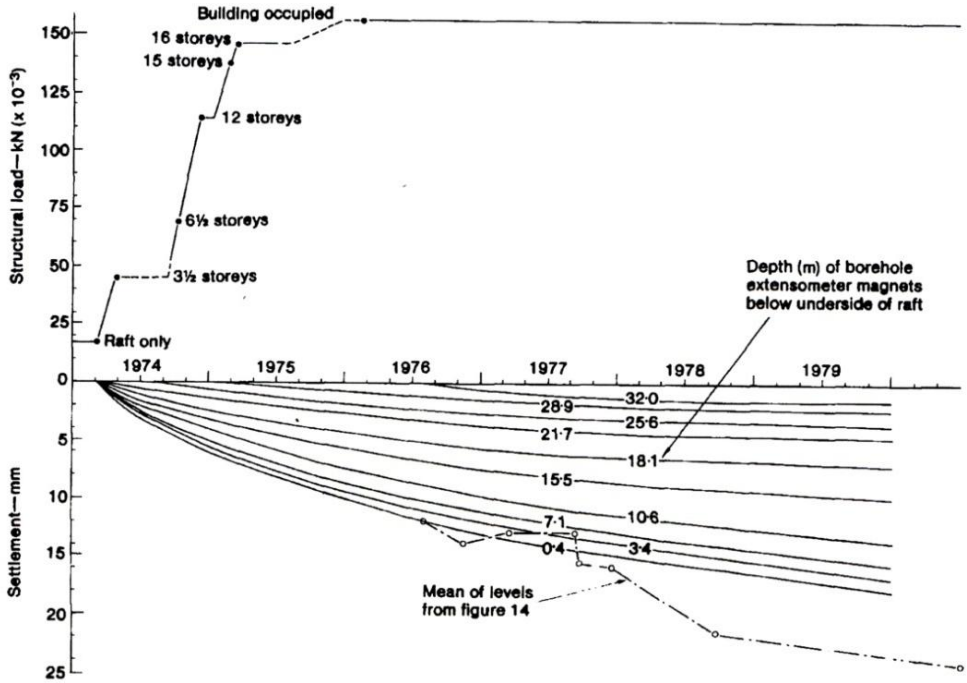


Figure 2.20: Development of load during construction, and borehole magnet extensometer readings; also mean settlement given by precise levelling round the completed building (Cooke et al., 1981)

The pile loads were measured with load cells placed at the head of the characteristic piles marked as crosses (from 1 to 8) in Figure 2.19. These indicated that the corner piles carried larger loads than the other piles in the group at all stages of construction (see Figure 2.21).

The measurements also showed that the edge piles carried almost twice the load of the internal piles. Cooke et al. (1981) discuss that the distribution of load between piles is affected by the rigidity of the raft and the structure, as well as by the number of piles and their geometry. In particular, it is described that in the case of a uniform and completely flexible building, all piles would carry equal loads, which was not the case at Hiscocks House. The raft/soil stiffness of Hiscocks House is not known, however it is claimed that it is more likely to be towards the rigid end of the stiffness range.

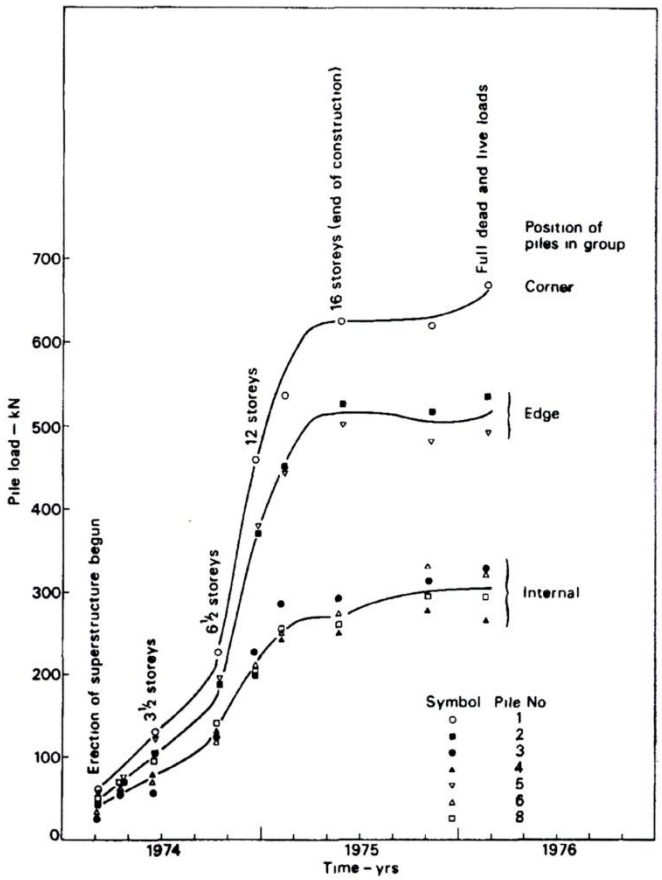


Figure 2.21: Development of pile loading during erection of the building, showing the difference between the loads carried by the various characteristic piles (Cooke *et al.*, 1981)

The pressures developed at the soil-raft interface were measured using several pressure cells, placed at the centre of squares formed by four adjacent piles. These are marked by points A to L in Figure 2.19. It is postulated that the clay immediately against the pile shaft is dragged down by the shaft and that therefore the contact pressure is minimal near piles and that it is maximum between the piles. The measurements presented in Figure 2.22 indicated that the peak pressures were related to the variation of pile loading. In particular, they were highest at the corners of the building and decreased towards the centre. These results were commented

on by Cooke et al. (1981) as being representative of a rigid foundation on top of an elastic medium.

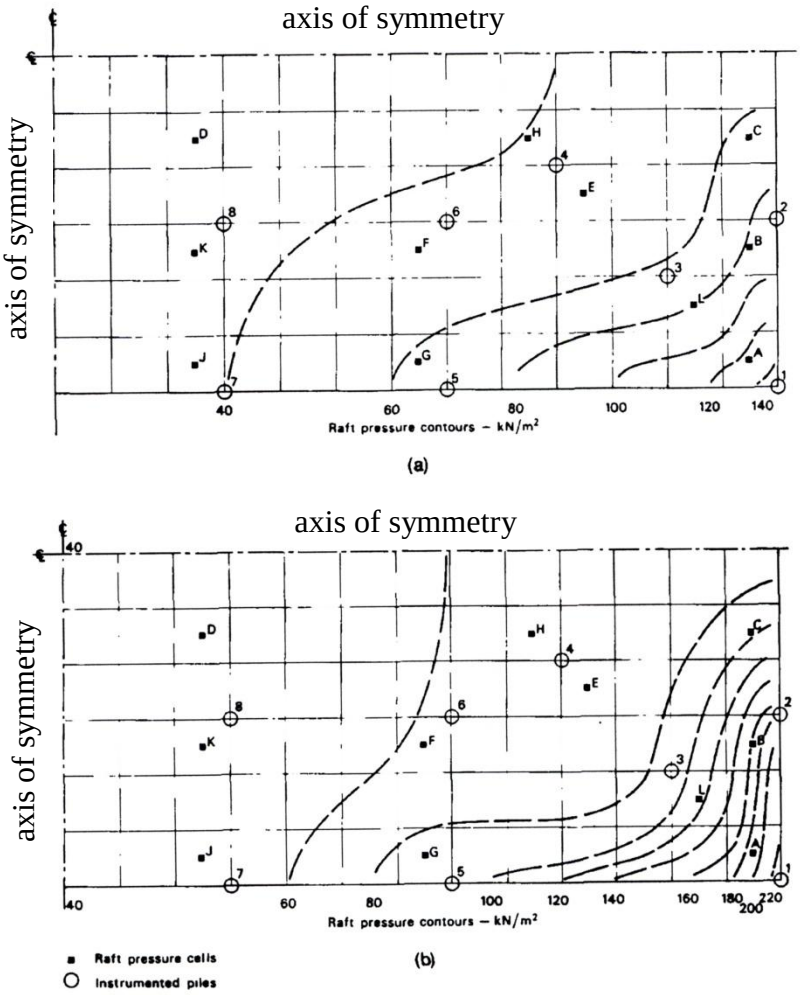


Figure 2.22: Peak raft pressures: (a) at approximately 45% of full load; (b) at 100% of full load (Cooke et al., 1981)

Cooke et al. (1981) were also able to calculate the mean load share between piles and raft during construction and until occupation, taking advantage of the load and pressure cells installed at characteristic locations. The results showed that the load carried directly by the raft varied from about 45% of the total at early stages of construction to 25% at the time of occupation. Figure 2.23 was produced to present the results.

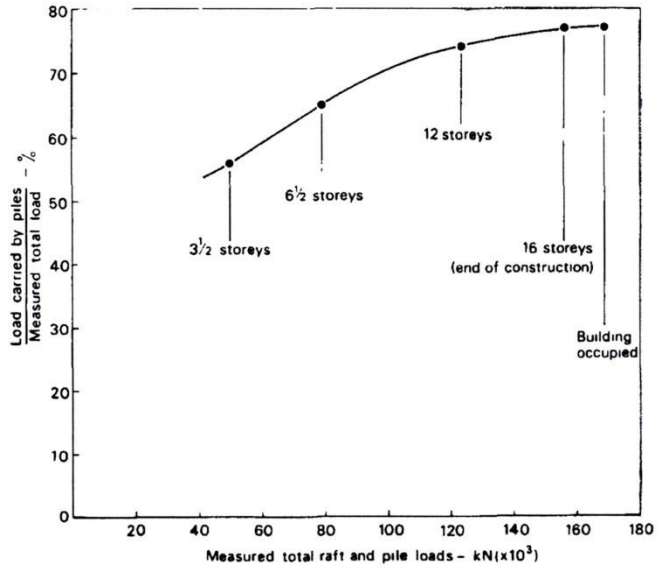


Figure 2.23: Proportion of the total foundation load carried by the piles at various stages of construction (Cooke *et al.*, 1981)

In terms of differential settlements, Cooke et al. (1981) describe that no records could be taken during the construction and some months after the occupation for various reasons. Nevertheless, reliable recordings at the eight stud positions (levelling ponts), as shown in Figure 2.24, were obtained using a precision level from the moment the average settlement of the building was 12 mm, i.e. consolidation processes had had already started. The measurements taken were collected by Cooke et al. (1981) and Figure 2.25 was produced, in order to discuss the differential settlements of the building. In particular, it was observed that after 2 years of measurements the settlements of the western side and northern end were larger than those around the south-eastern corner. However, after 4 years the settlements were more symmetrical being larger at the middle of the building, and amounted to +5 mm approximately from the northern/southern end in respect to the middle. Nevertheless, differential settlements were regarded as very small and therefore they were considered insignificant.

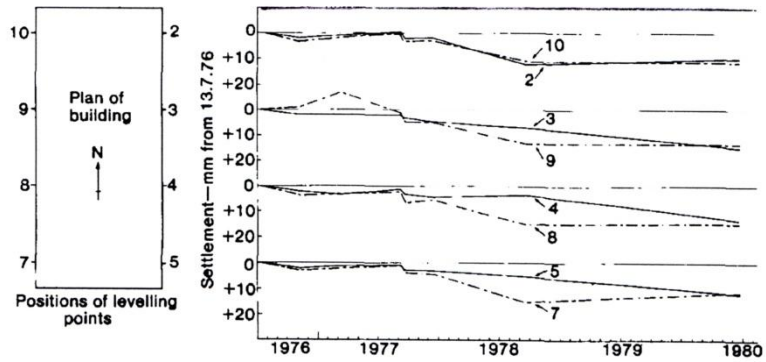


Figure 2.24: Levelling observations made around the building at various dates after completion (Cooke *et al.*, 1981)

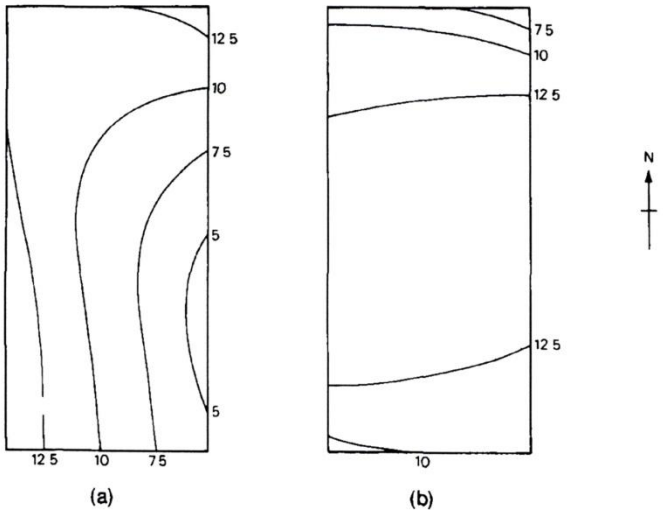


Figure 2.25: Contours of settlement (mm) after: (a) 2 years of measurements; (b) 4 years of measurements (Cooke *et al.*, 1981)

2.3.3.2. Piles as 'settlement reducers' and 'creep piling' rafts

Piles may be used as 'settlement reducers' when the raft alone is able to provide adequate load capacity, but at the same time the settlements exceed the design limits. According to Randolph (1994), in the majority of cases where piles form part of the foundation for a structure, the primary reason for inclusion of the piles is to reduce settlements, since the raft alone has sufficient load capacity. Such piles are designed to mobilise their full capacity at working conditions (Burland et al., 1977). Settlements in this case are reduced by allowing piles to move plastically relative to the surrounding soil. This approach is considered as a step towards the development of an optimum design approach for piled foundations, since fewer piles are required to limit settlements than to provide load capacity to a foundation.

Cooke (1986) defined a design approach for piled raft foundations, where piles are used for settlement limitation. He postulated that a satisfactory design is achieved if sufficient piles are included for the ultimate bearing capacity of the group to match the required working load. Thus, the factor of safety on the piles alone is unity, while the real safety factor is provided by the capacity of the raft, resulting in a smaller number of piles than if the piles were designed with a conventional factor of safety.

An improved approach that would produce a more optimum number of piles beneath a raft according to Cooke (1986), which was supported by Burland (1995), would be to turn the attention to settlement rather than to capacity. In particular, with reference to Figure 2.26 they both suggest a similar procedure; to derive first the load-settlement profile for an un-piled raft up to failure, then determine the settlement (ρ_0) for the un-piled raft at working load (Q_0), and eventually determine the required load to be carried by the piles ($Q_0 - Q_1$) in order to reduce the settlement of the foundation to within the design limit (ρ_1). Piles are then designed with a factor of safety of one.

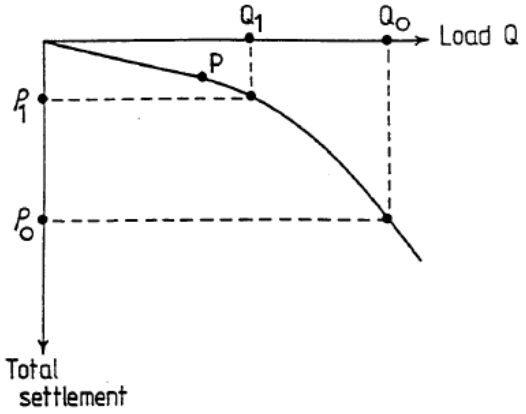


Figure 2.26: Raft without piles: load – settlement derivation (Burland, 1995)

In both approaches piles are uniformly distributed over the raft area, usually below column points, with a large spacing between them. This ensures that a pile-soil block behaviour is not reached, a case where the contribution and the performance of each individual pile drops, due to the larger number of piles with closer spacing. Burland (1995) has produced Figure 2.27, where it is shown that as the number of piles increases in a piled raft foundation, the spacing between them reduces until there comes a point where interaction begins to become significant. The relationship between settlement and number of piles then becomes non-linear and approaches the settlement of the solid block asymptotically. It is also claimed by Burland (1995) that usually the number of piles required to reduce the settlement to an acceptable amount is small enough for there to be negligible interaction between them.

Several piled rafts in practice have been designed with piles mobilising their full load capacity in order to reduce settlements. Examples of these are the Tohaus der Messe in Frankfurt and a five-storey building in Urawa, Japan. Both buildings foundation design and performance are described in detail subsequently.

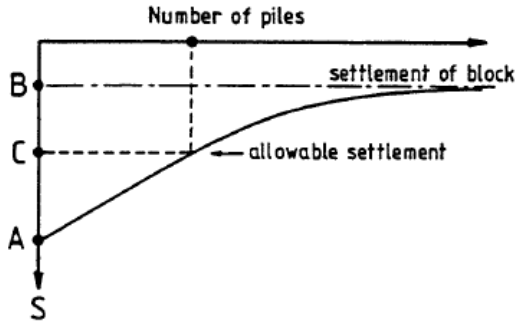


Figure 2.27: Schematic relationship between settlement and number of piles beneath a raft foundation on clay (Burland, 1995)

A design approach for piled rafts, mainly adopted in Scandinavian countries, is the 'creep piling' design approach, described by Randolph (1994), where piles are designed to operate at a working load at which significant creep starts to occur. The creep load can be determined, after Hansbo (1993), on a theoretical basis from the undrained long-term shear strength of the soil, which is usually at about 70 – 80% of the undrained shear strength. In the 'creep piling' approach, piles are uniformly distributed over the raft area with large spacings.

Moreover, in the 'creep piling' approach when the piles are loaded and reach the creep state, they penetrate into the soil and, consequently, the contact pressure between the raft and the soil increases. Therefore, sufficient piles must be included in order to keep the net contact pressure below the preconsolidation pressure of the soil. In cases where the average net load increase exceeds the preconsolidation pressure of the clay, the objective of creep piling is obviously not to eliminate but to reduce consolidation settlement. This is achieved by the fact that the stress increment exceeding the preconsolidation pressure of the clay is transferred to greater depths where the preconsolidation pressure is higher.

The creep piling approach works well in relatively soft cohesive soils. The country in which this approach was first developed is Sweden, where such soils are usually encountered, and therefore most literature is based on buildings constructed in Sweden. Hansbo (1984) presents three case histories. These include two residential buildings, an office building and a factory in Olskroken, Stampen and Gullbergsvass respectively. The Olskroken case history is presented in this thesis in order to highlight the potential savings on piles, by comparing two

similar buildings, the one founded on ‘conventional’ friction piles and the other one on ‘creep’ piles. The other two case histories, not presented in this thesis, show the applicability of piles designed with a very low factor of safety on (a) supporting net load increase over the preconsolidation pressure and (b) supporting peak pressures developed on raft-soil interface from columns.

(a) Torhaus der Messe, Frankfurt, Germany

A case history, where piles are utilised as ‘settlement reducers’, is the Torhaus der Messe, a 130 m high building in Frankfurt (Figure 2.28). The Torhaus was constructed between 1983 and 1986, and it is the first building in Germany with a piled raft foundation. It is founded on two large twin piled rafts, where, according to Sommer et al. (1985), the piles were designed to utilise their ultimate bearing capacity, in order to force the supporting function of the raft. A uniform distribution of piles over the raft area is employed. The design of the foundations was based on the experience from piled raft foundations in London and therefore a pile enhanced raft was applied in order to reduce excessive settlement. Heavy instrumentation was employed, since it was the first structure in Germany built on such foundations, which allows the assessment of its performance in terms of average settlement, settlement profile, pile load distribution and load share between piles and raft (Sommer et al., 1985).

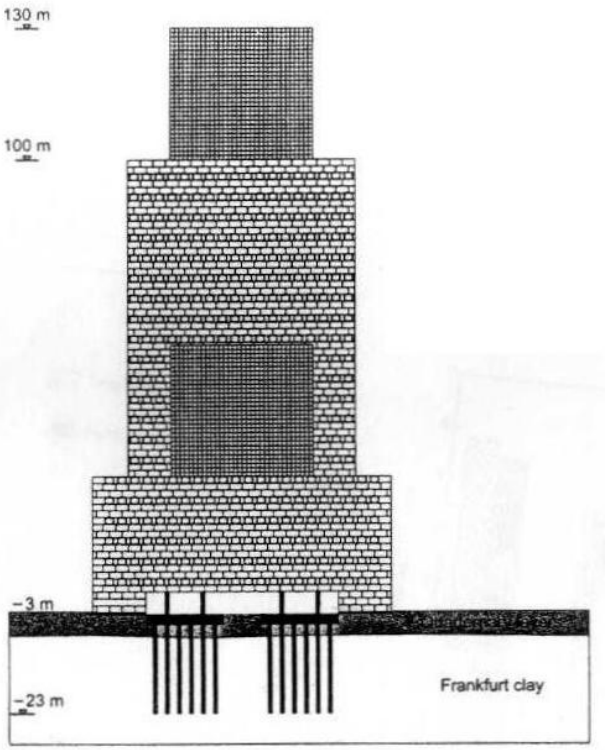


Figure 2.28: Profile view of Torhaus der Messe building (Reul and Randolph, 2003)

A ground investigation in the site revealed that the soil profile consists of quaternary sand and gravel down to 5.5 m depth, followed by the Frankfurt Clay. The Frankfurt Clay is inhomogeneous in general: it consists of an irregular and altering sequence of overconsolidated clays and silts accompanied with thin calcareous sand inclusions and isolated floating limestone layers. Moreover, the Frankfurt Clay is underlain by the Frankfurt Limestone; however it is considered to be outside the influence of the foundation. Finally, the groundwater level was found to be well below the raft level (Sommer et al., 1985).

The foundation layout of the Torhaus is shown in Figure 2.29. The building has no underground storeys, therefore it is founded near the ground surface, at a depth of 3 m. The rafts are rectangular, with 17.5 m × 24.5 m side lengths and 2.5 m thickness. A total number of 84 bored piles, with a length of 20 m and diameter of D = 0.9 m, are included beneath both rafts to support the structural loads. The pile spacing varies from 3.5 D to 3 D. The distance between the two rafts is 10 m edge to edge (Sommer et al., 1985).

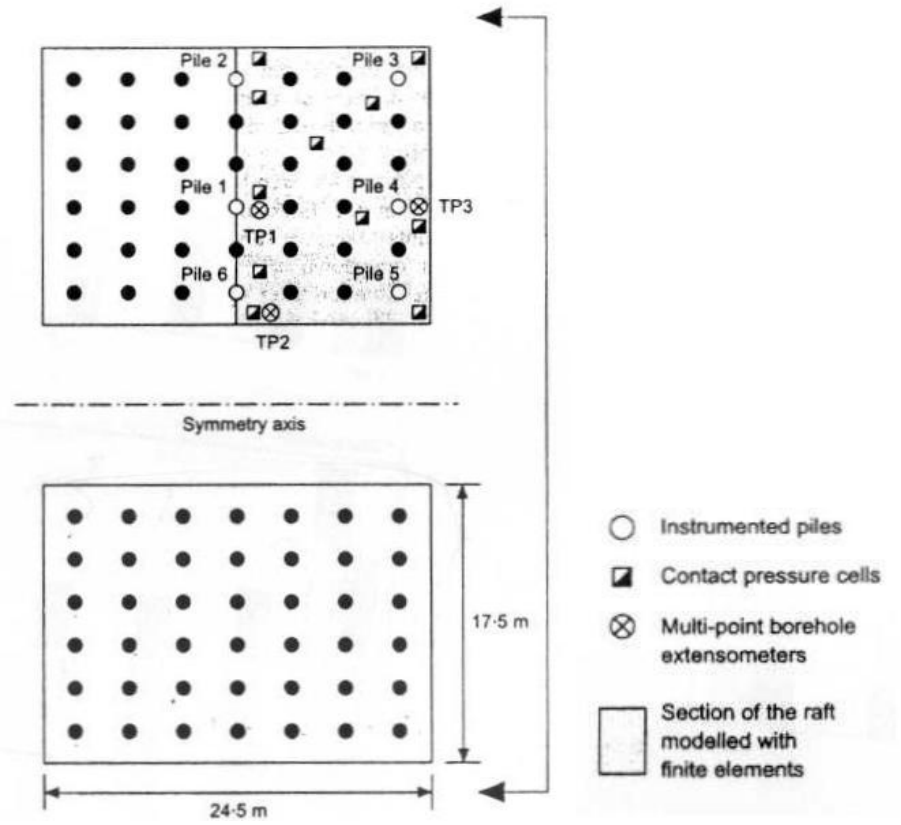


Figure 2.29: Ground plan of raft (Reul and Randolph, 2003)

The critical decision for the foundations was the length of the piles according to Sommer et al. (1985). The number of piles, spacing and diameter was fixed in the design process, and a set of finite element analyses was performed with varying pile lengths in order to determine the

maximum settlement. Based on the results (Figure 2.30), the decision was to choose a pile length beyond which greater lengths would not offer a significant decrease in settlement. According to this, 20 m long piles were employed. This approach however potentially results in pile-soil block behaviour (see Figure 2.27), and therefore the efficiency of each individual pile is likely to drop in the pile group. Therefore, despite the fact that piles were designed as 'settlement reducers' with uniform distribution, spacing between piles was small enough to initiate a pile-soil block behaviour as shown later, which is common for 'conventional' piled rafts.

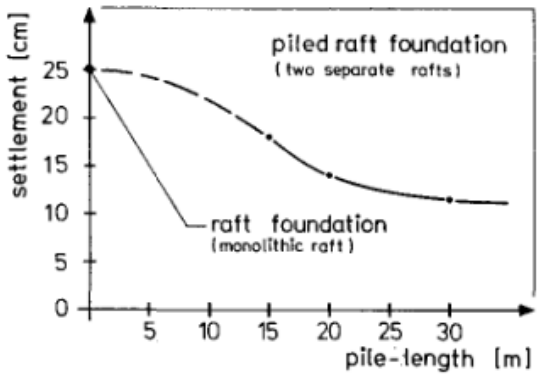


Figure 2.30: Influence of pile length on the computed settlements (Sommer et al., 1985)

Regarding the performance of the foundations, as shown in Figure 2.29, heavy instrumentation was put in place in one of the piled rafts, including six instrumented piles, eleven contact pressure cells and three multi-point borehole extensometers. From these, an average centre settlement for the two rafts of 124 mm was measured. Also, measured settlement profiles with depth from extensometers (Figure 2.31) located at the centre and the edge of the raft show a significant block deformation of the pile group and the surrounding soil, which is due to the large number of piles and the relatively small pile spacing, as described by Reul and Randolph (2003). This is also revealed by the results of a numerical analysis performed by Reul and Randolph (2003) of an equivalent un-piled raft (Figure 2.31), which shows a strong decrease of settlements with increasing depth.

Regarding the pile load distribution, as recorded by the six instrumented piles shown in Figure 2.32, it is observed that centre piles are the least loaded piles, whereas the corners piles are the most heavily loaded. In particular, edge and corner piles seem to carry two and three times more load than the central piles respectively. This is considered as a typical observation for 'conventional' piled rafts under working load conditions due to the pile-soil block behaviour. The variation of the loads with the pile position, after Reul and Randolph (2003),

is due to the varying mobilisation of shaft friction. Because of the block deformation of the pile group, there are only small differential displacements between the piles at the centre of the raft and the surrounding soil. Hence, the pile shaft loads of the centre piles are substantially smaller than the pile shaft loads of the edge or corner piles, while the base loads are similar. Finally, regarding the load share between the piles and the raft, piles seem to carry 67% of the total load, as recorded in February 1986 by Sommer (1991).

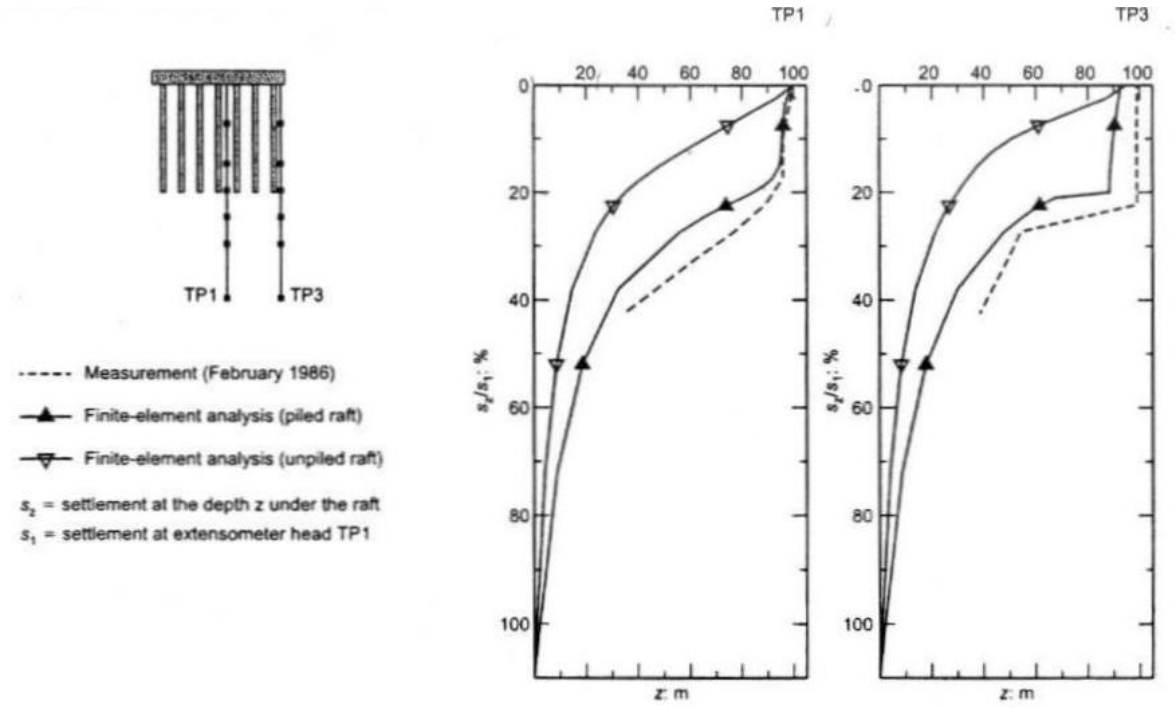


Figure 2.31: Settlement profile. Measurements after Sommer (1991) and finite element analysis (Reul and Randolph, 2003)

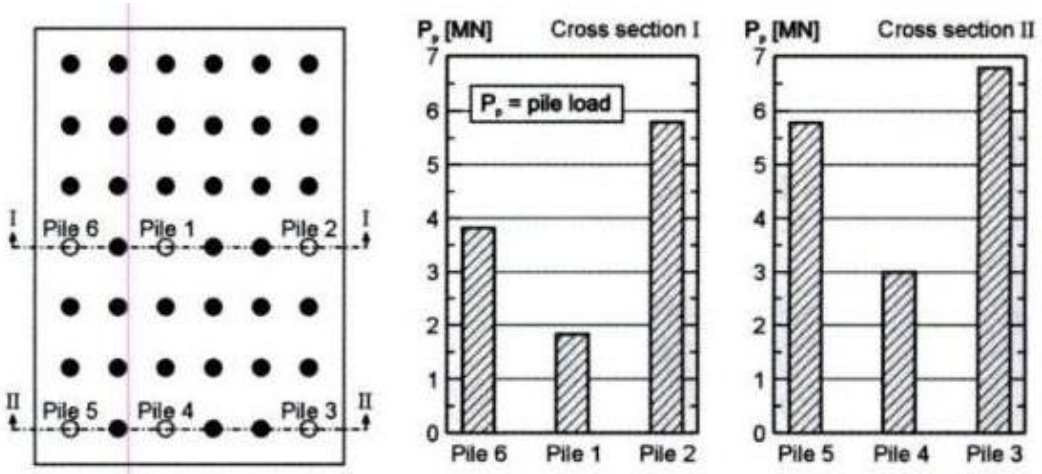


Figure 2.32: Pile loads (Sommer, 1991)

(b) 'Settlement reducing piles': Five storey building in Urawa, Japan

Yamashita et al. (1994) describe a well-instrumented and documented case of a piled raft foundation on a stiff clay deposit with 'settlement reducing piles' at large spacings to support a five-storey building in Urawa in Japan.

Figure 2.33 shows a schematic of the building and a summary of the soil investigation. This is a five-storey reinforced concrete structure and its plan is rectangular, with sides 24 m by 23 m. The design load is 47.5 MN and the average contact pressure is 84 kPa. The soil profile, down to a depth of 6m, is made of stiff over-consolidated clay labelled as Kanyo Loam. Down to 16 m the soil consists of loose to medium sands. From the depth of 16 m to 19 m, where the toes of the piles are set, the soil consists of medium to dense sands. Finally, a number of clay and silt layers appear alternately down to a depth of 42 m, below which dense sands and gravels lie.

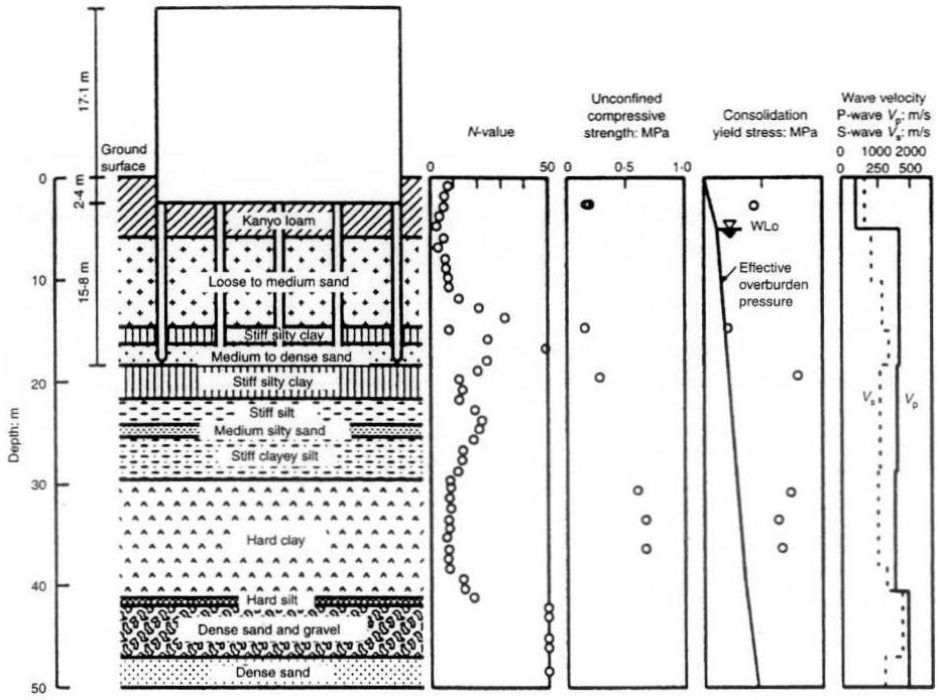
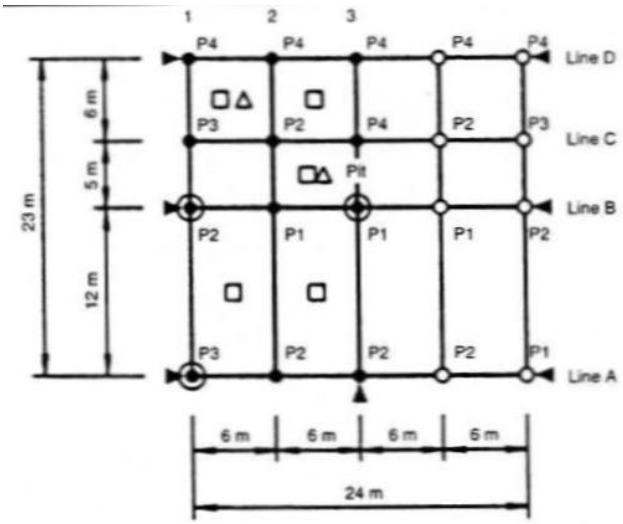


Figure 2.33: Schematic of the building and summary of soil investigation (Yamashita et al., 1994)

Regarding the foundations, Yamashita et al. (1994) describe that it was initially considered to found the structure on a raft foundation. However, despite the fact that the calculated maximum contact pressure was lower than the allowable bearing capacity (one-third of the ultimate value), settlement at the centre and differential settlement were too large and thus such a foundation design could not be accepted. In particular, an analysis showed that the

settlement would be 6 cm at the centre and 2 cm at the corner of the building, and the angle of distortion of the foundation would be 1/300 radian. Therefore, it was decided to introduce 'settlement reducing piles' in order to reduce settlements rather than to provide additional load capacity. Consequently, a total of twenty piles were placed beneath a 0.3 m thick raft at each column position (Figure 2.34), where the load was presumed to be concentrated. The piles were made of concrete, 16 m long and either 0.8 m or 0.7 m in diameter, with a central steel H-pile inserted. Both the pile diameter and the steel pile size depended on the column load, which ranged between 1.02 MN and 3.95 MN. Finally, the pile spacing was 6.3 to 8.6 times the pile diameter.



Pile no.	Borehole dia.: m	Size of steel-H: mm
P1	0·80	414 × 405 × 18 × 28
P2	0·80	400 × 400 × 13 × 21
P3	0·70	350 × 350 × 12 × 19
P4	0·70	300 × 300 × 10 × 15

Figure 2.34: Foundation plan and specification of piles (Yamashita et al., 1994)

During construction, instrumentation was put in place in order to monitor the behaviour of the foundations during construction and up to the completion of the building. In particular, the settlements of the building, axial loads on twelve selected piles, the earth contact pressure and pore water pressure on the underside of the raft were monitored.

Figure 2.35 was produced by Yamashita et al. (1994) to present the measured settlement of the building. At the time of completion of the building, the settlements amount to 1.0 cm to 2.0 cm. These are considerably lower than the estimated values for an un-piled raft (2.0 cm to 6.0 cm). Therefore, the piled raft foundation was effective in reducing the overall and differential settlement.

Figure 2.36 shows the development of the axial pile head load on the typical piles against time. Also, Figure 2.37 presents the pile loads and the ratios of the head loads to design column loads at the time of completion of the building. It is observed that the ratio of the pile-head load to the design column load at the corners piles is less than those for the piles at the

edges and in the interior of the raft. This is not consistent with the pattern observed in other piled raft structures, such as at Hiscocks House and Torhaus der Messe, where corner piles carry more than twice the load of the central piles. This may be due to, after Yamashita et al. (1994), the fact that at the periphy of the building a part of the load from the superstructure is directly transferred to the soil through the basement walls when the building is settling.

Finally, Figure 2.38 was produced by Yamashita et al. (1994) to present the relationship between the sum of the measured pile-head loads of the twelve instrumented piles and the respective estimated building load during construction. From this, it is observed that the proportion of the load carried by the piles at the time of the building completion was 49%, indicating that the contribution of the 'settlement reducing piles' to the load capacity is quite significant.

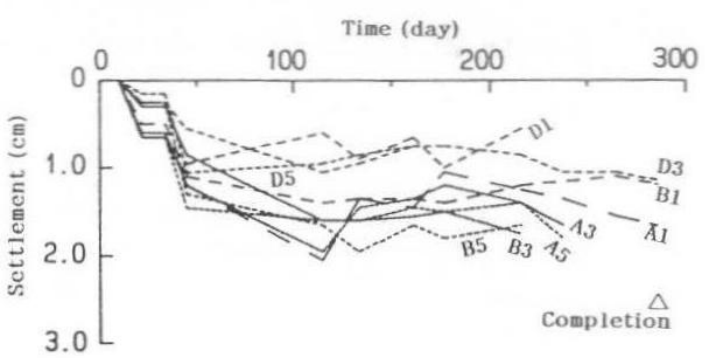


Figure 2.35: Measured settlements (Yamashita et al., 1994)



Figure 2.36: Development of pile-head loads (Yamashita et al., 1994)

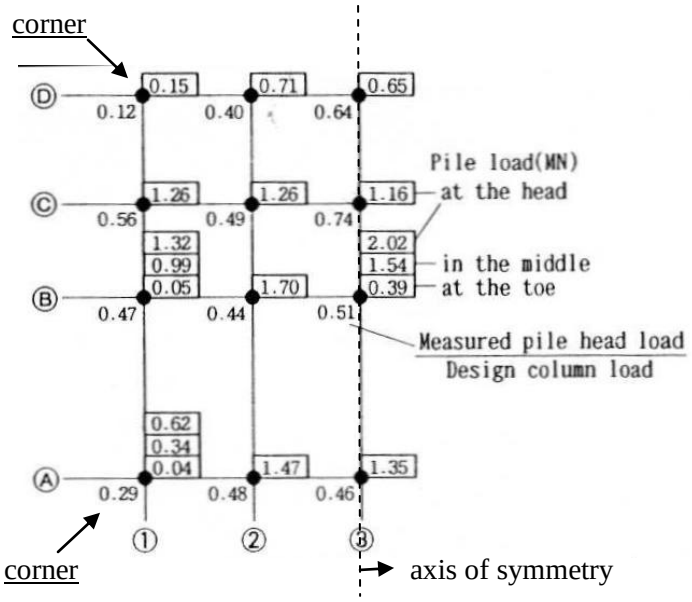


Figure 2.37: Measured pile loads at the time of building completion (Yamashita et al., 1994)

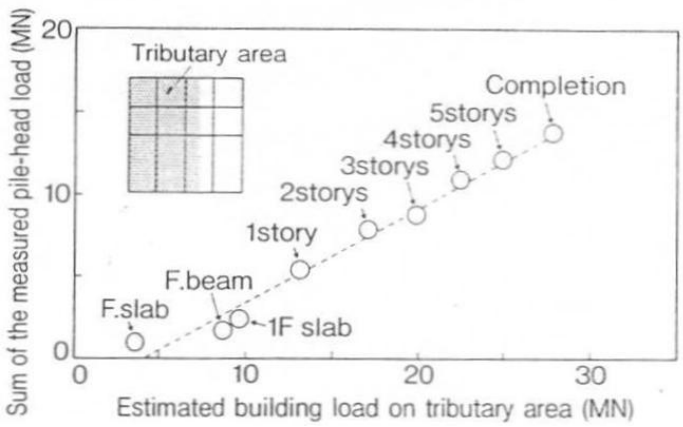


Figure 2.38: Sum of the measured pile-head loads and the building load (Yamashita et al., 1994)

(c) 'Creep piling' raft: Four storey building in Olskroken, Sweden

An important case history involving creep piles is the one described by Hansbo (1984) for a residential building in Olskroken in Sweden (Figure 2.39). Its importance is highlighted by the fact that extensive instrumentation was put in place in order to monitor and compare its performance, with a nearby similar building founded on conventional piles. This case history, therefore, gives the opportunity to assess and compare the effectiveness of piled rafts with creep piles with respect to conventional pile groups with friction piles.

A ground investigation performed at the site revealed that the upper layer of the soil profile consists of soft, highly plastic clay of 35 m to 55 m thickness, considered as normally consolidated, which is underlain by sand and gravel on till or rock.



Figure 2.39: View of residential buildings, Olskroken. The building on creep piles seen to the left, the one on conventional piles to the right (Hansbo, 1984)

The building on conventional friction piles is a 4-storey building with a base area of 50 m by 14 m. The building load applies approximately 65 kPa pressure to its foundations, or 46.4 MN total loads. The foundations are designed as fully piled, such that the pile foundation carries the total load of the structure with a safety factor of 3 against short-term pile failure. A total of 211 piles 28 m long were used.

The building founded on creep piles is also a 4-storey building, but its base area is larger, 75 m by 12 m. The building load applies approximately 60 kPa pressure to its foundations. The creep piles were designed to carry 47 kPa of the total pressure and the raft to carry the remaining pressure of 23 kPa (which is equal to the weight of the soil excavated to form the building basement). A total of 104 piles, 26 m long, were used, designed with a factor of safety in the order of 1.25, since the creep strength of the soil was estimated to be 70% of the conventional undrained shear strength. Therefore, each pile was designed each to carry a load of 330 kN.

Figure 2.40 was produced in order to present the measurements of settlement for both buildings and compare them. In particular, measured settlement contours for both buildings, as well as the measured relationship between average settlement and time, are presented. From these, it is concluded that despite the fact that the second building was supported on less than half the number of piles, it settled slightly less than the first building. This indicates that the potential economy that may be achieved by the use of piled rafts with piles as ‘settlement reducers’, without significant sacrifice of foundation performance.

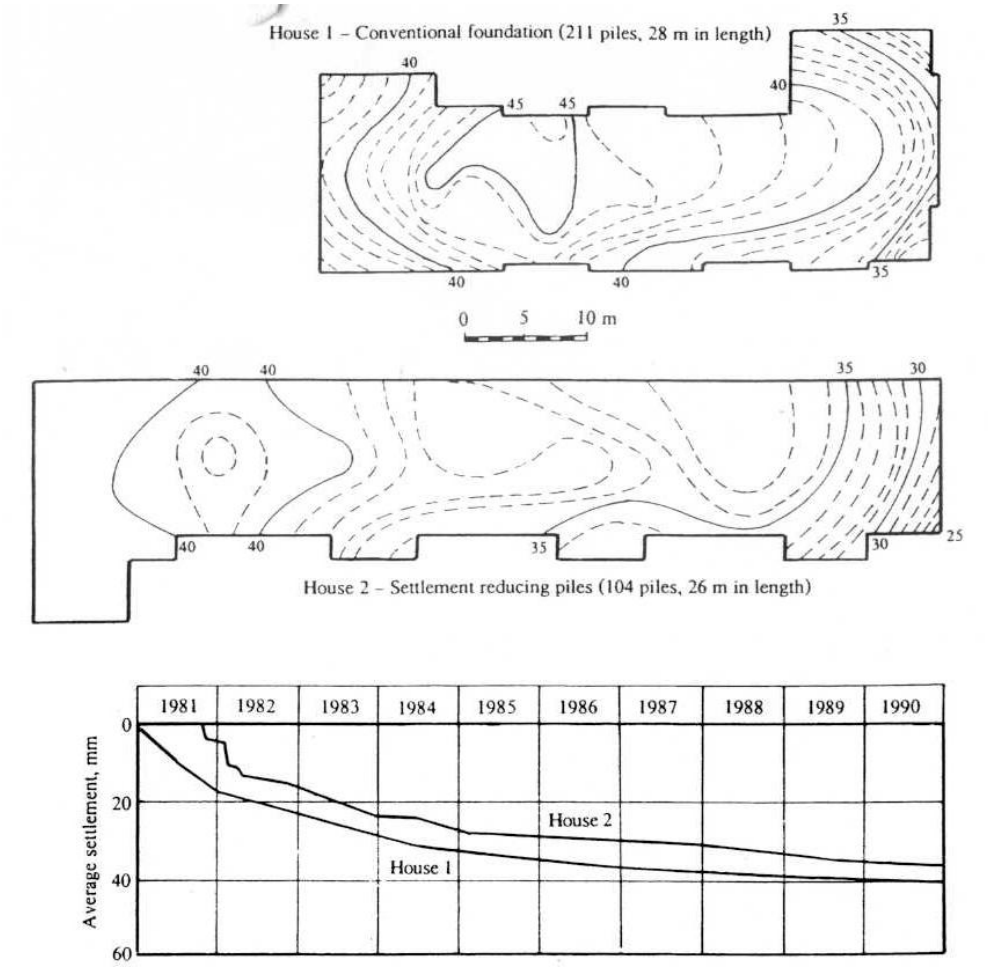


Figure 2.40: Settlement contours in mm and average settlement versus time for the two buildings (Hansbo, 1993)

2.3.3.3. An attempt for optimum design: Piled rafts to control differential settlements

The 'differential settlement control' design approach of piled raft foundations is the one where piles are located strategically beneath the raft in order to minimize differential settlements. This is due to the fact that differential settlement is usually a more critical criterion than absolute settlement in foundation designs. Therefore, if the location of piles is optimised, the differential settlements may be reduced with the minimum piling cost. The most efficient design is once again when the ultimate load capacity is provided by the raft with a large factor of safety against bearing failure, while recognising the contribution of the piles to reducing settlement and enhancing bearing capacity (Randolph, 1994).

So the question in this approach turns from "how many piles are needed to carry the load" (Burland, 1995) for conventional piled rafts, to "how many piles are needed to reduce the settlement to an acceptable amount" (Burland, 1995) for settlement reducing piles, to "how

many piles are needed to reduce the (differential) settlements to an acceptable level – and where they should be positioned?" (Fleming et al, 2009).

Deciding on the arrangement of piles beneath the raft is not an easy task. However, the principles of this design may be well defined if a raft foundation, loaded uniformly over its surface area, is considered, as shown in Figure 2.41. In particular, the un-piled raft has a tendency to sag in the centre; therefore, a few piles added in the central area of the foundation will reduce this tendency and, consequently, reduce differential settlements. (Randolph, 1994)

The required pile support in the central region may be estimated by considering the contact stress distribution beneath a rigid raft foundation and the average applied pressure to the foundation, where the central contact pressure is approximately half the average applied pressure (Figure 2.42). Therefore, the aim of the central piles should be to 'absorb' the difference between the applied structural load and the contact stress profile under a rigid raft foundation (50 – 70 % of the average applied pressure), in order to lead to a contact pressure distribution for a flexible raft (which is uniform without piles) that matches that of a rigid raft. If this contact pressure distribution was deliberately generated beneath a flexible raft, then the differential settlement would be reduced significantly.

The concept of including piles in the central region of the raft area to reduce differential settlement, rather than to reduce average settlement, is verified in the numerical studies performed, among others, by Randolph (1994) for a hypothetical piled raft, by Viggiani (1998), for Hiscocks House in Stonebridge Park, and by Reul and Randolph (2003), for the Torhaus der Messe in Frankfurt. These are described in detail in Section 2.3.5.

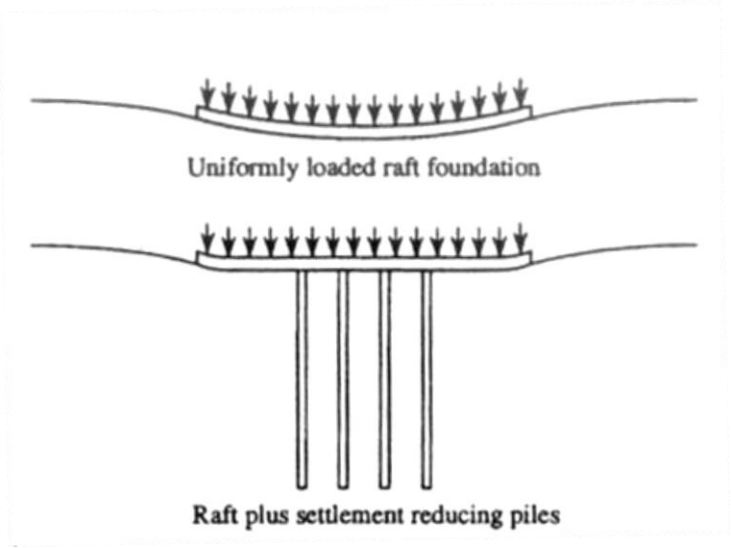


Figure 2.41: Central piles to reduce differential settlement (Randolph, 1994)

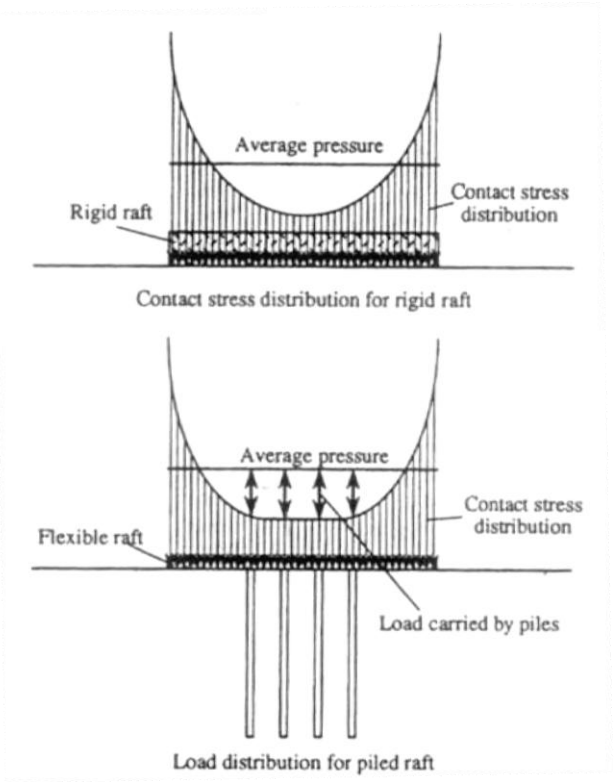


Figure 2.42: Schematic design approach for settlement reducing piles (Randolph, 1994)

(a) Messe Turm, Frankfurt, Germany

A case study, where the differential settlement control approach was adopted, is the MesseTurm building in Frankfurt (Figure 2.43) described by Sommer et al. (1991). MesseTurm is a high-rise building of 256 m height with 60 storeys, and it is ranked among the tallest buildings in Europe. Its importance is highlighted by the fact that it was one of the first high-rise buildings which were founded on a piled raft foundation and, therefore, significant instrumentation was installed in order to monitor the foundations' performance. Excavation work started in June 1988, and the complete piled raft foundation was in place by November 1988.

Experience in Frankfurt of high-rise buildings is significant. However, the majority of the buildings are supported on mat foundations. Mat foundations are not very effective in terms of serviceability. Settlements can be as much as 30 cm and usually they are uneven due to the inhomogeneities of the Frankfurt subsoil. Therefore, almost all these structures tilt (Sommer et al., 1991). The MesseTurm would be by far the tallest building in Frankfurt at that time, making potential tilt much more critical than any other structure. Settlements were estimated to be around 40 cm, if the building was designed on a mat foundation. Therefore, a different design approach was adopted, in order to reduce the settlements as much as possible. This was

the piled raft foundation, which involved the inclusion of piles beneath the raft in order to transfer part of the structural load down to the deeper soil deposits and, consequently, reduce overall settlements and tilt (Sommer et al., 1991).

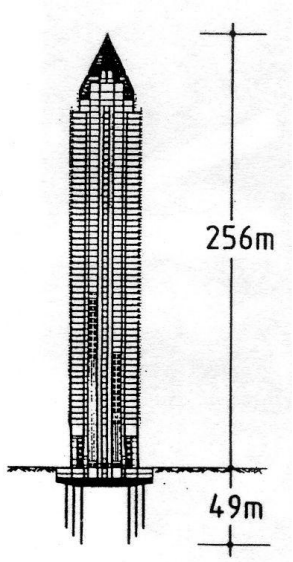


Figure 2.43: Messe Turm building in Frankfurt (Sommer et al., 1991)

The Frankfurt subsoil, as aforementioned, is quite inhomogeneous. A ground investigation in the area revealed that down to 8 m depth, the soil consists of gravels and sands, which are underlain down to 100 m by the Frankfurt Clay (Figure 2.44). The Frankfurt Clay consists of an irregular and altering sequence of clays and silts accompanied with thin calcareous sand inclusions and isolated floating limestone layers. In particular, the ground investigation revealed that the limestone layers have a maximum thickness of 1.4 m. The ground water table was found 5 m below the ground surface (Sommer et al., 1991).

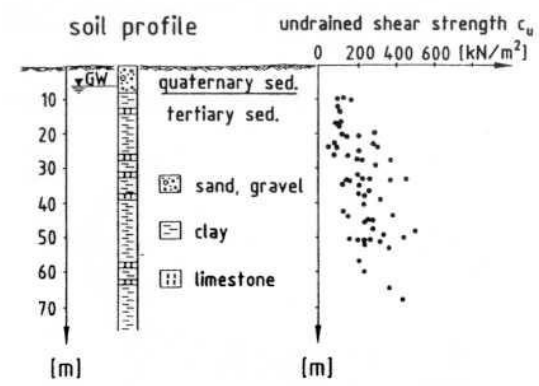


Figure 2.44: Soil profile and undrained shear strength (Sommer et al., 1991)

The foundation design of the MesseTurm is shown in Figure 2.45. The piled raft foundation is founded at a depth of 14 m below the ground surface. The raft is square in plan, of 58.8 m side length, and has a thickness of 6 m at the centre (core of the building), thinning to 3 m at the edges. A total of 64 bored piles of 1.3 m diameter and length varying from 26.9 m to 34.9 m are included beneath the raft in strategic locations. In particular, they are included in 3 approximate concentric circles of different pile length whose centreline distance varies from approximately 3.5 diameters to 6 diameters, starting from the outer to the inner circle (Sommer et al., 1991).

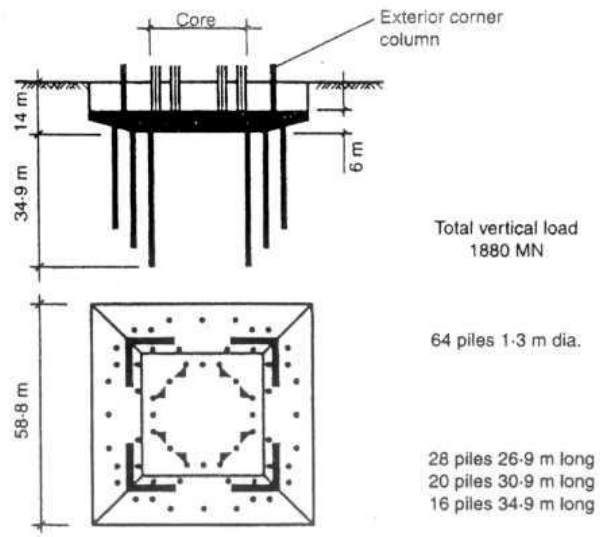


Figure 2.45: Plan and side elevation of piled raft foundation (Sommer et al., 1991)

The inner ring piles are designed to be longer than the outer ones. This is due to the fact that if they were equal in length, the outer piles would attract more load than the inner ones. Therefore, by adjusting the length, a more uniform loading distribution on the piles is achieved. The concentration of pile-loads towards the core has another advantage too. This is that the bending moments in the raft are reduced. Finally, piles were arranged in such a manner in order to optimise as much as possible the resistance against settlement and tilt, despite the lack, at that time, of knowledge and experience on load share between piles and raft, and their interaction (Sommer et al., 1991).

During construction instrumentation was installed, including instrumented piles (with strain gauges), extensometers and raft pressure cells, in order to monitor the foundation performance in terms of settlement, tilt, pile loads, bearing stresses, skin friction, and load share between piles and raft (Sommer et al., 1991).

Sommer et al. (1991) produced Figure 2.46 to present the average settlement of MesseTurm against time and structural load. This was measured around 9 cm at the completion of the superstructure, however it is considered that MesseTurm was built rapidly. Therefore settlement due to consolidation with time should be expected. Moreover, it should be noted that the settlement in Figure 2.46 does not count for the immediate settlement immediately after the pouring of the raft concrete. Sommer et al. (1991) state that subgrade settlements of 10 to 15 mm were measured, which were due to the "wet load" of the concrete carried directly by the soil below the raft. As the concrete hardened, part of the load was carried by the piles and, therefore, the load sharing between raft and piles developed.

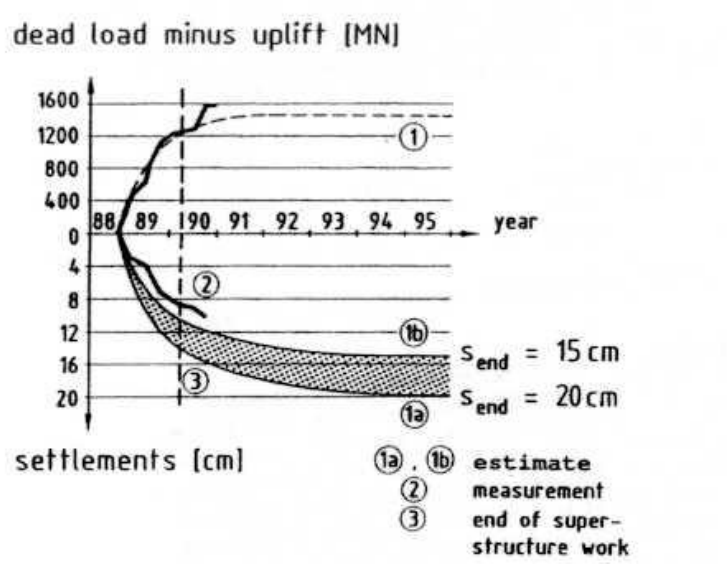


Figure 2.46: Load development and settlement versus time (Sommer et al., 1991)

Furthermore, Sommer et al. (1991) produced Figure 2.47 in order to present the differential settlements developed. In particular, contours of settlement were plotted at 90 % of the structural weight (disregarding settlements before the hardening of the raft concrete), where 4 cm settlement at the edges and 7 cm in the centre of the raft was measured. In addition, differential settlements for two sections (N-S and W-E) were plotted, where an angular distortion of 1:3500 was observed. It should be noted that most of the tilt of the structure occurred early in construction after the raft concrete was placed and amounted to approximately 1 cm toward the west.

Nevertheless, the MesseTurm was continuously checked for verticality. Therefore, it was constructed as nearly a vertical structure. However, if it had not been corrected, the horizontal movement at the top floor would have been 4.5 times larger due to the differential settlement of the raft.

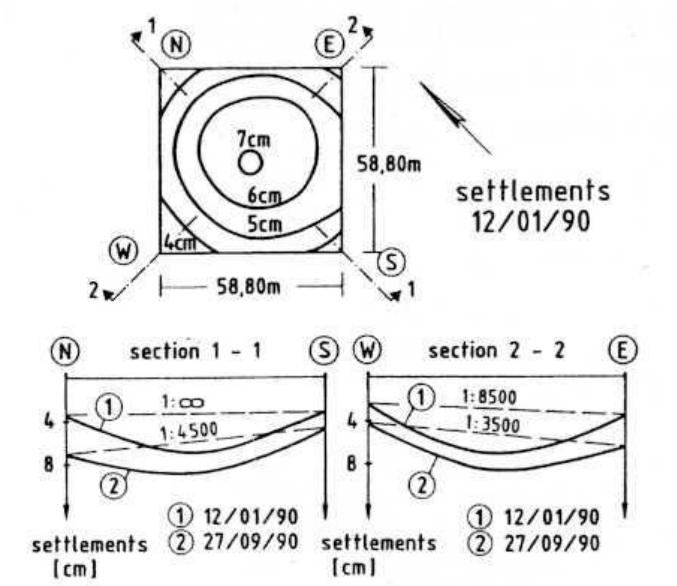


Figure 2.47: Settlements of the foundation raft (Sommer et al., 1991)

Regarding the pile loads, a uniform pile load distribution was almost achieved between the three different sets of piles after the completion of the structural frame. In particular, the load on piles in the outer and inner ring was measured at about 10-11 MN per pile, while the load on piles in the middle ring was measured at about 13 MN (Figure 2.48). Therefore, the strategy to vary the length of the piles proved to be successful, even though, with only some minor adjustments, a better pile load distribution could be achieved (Sommer et al., 1991).

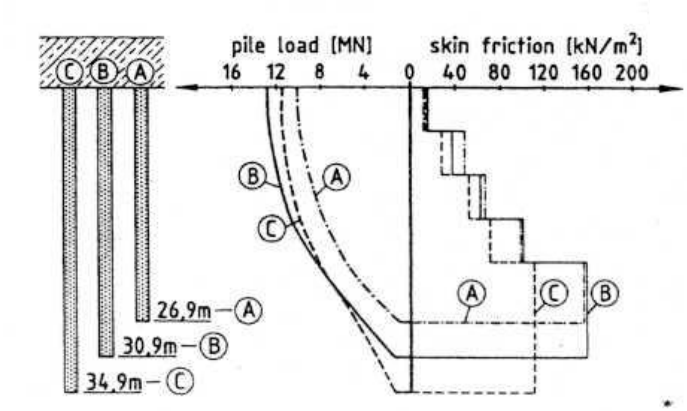


Figure 2.48: Pile loads and skin friction distribution after completion of structural frame (Sommer et al., 1991)

Regarding the load distribution between the piles and the raft, 55 % of the dead load was carried by the piles, while 45 % was carried by the raft, when the structural works were completed. The load share, however, was not the same during construction and was changing from the installation of the raft till the completion of the 60th floor. As shown in Figure 2.49,

when the huge raft was complete (407 MN out of 1880 MN of total load), the working raft carried 60 % of the load, whereas the piles only 40 % (Sommer et al., 1991).

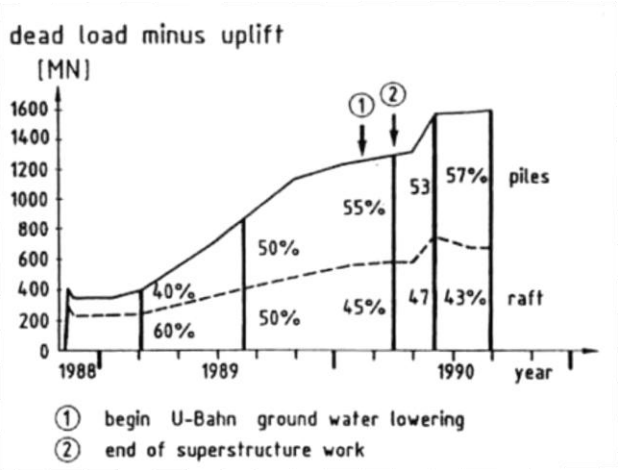


Figure 2.49: Load distribution between piles and raft (Sommer et al., 1991)

2.3.4. METHODS OF ANALYSIS

Key design decisions for the design of piled raft foundations, according to Poulos (2002), include (a) the required raft thickness, (b) the type of piles to be used, and (c) the required locations of the piles, and the pile diameter and length, to support a structure. These shape the performance of piled raft foundations and, therefore, the better the choice, the more efficient and optimum will be the design.

The design of piled raft foundations, as with any foundation system, requires the assessment of the following (Poulos, 2001):

(a) Ultimate load capacity for vertical, lateral and moment loadings
(b) Maximum settlement
(c) Differential settlement
(d) Raft moments and shears for the structural design of the raft
(e) Pile loads and moments, for the structural design of the piles

Poulos et al. (1997) have classified three broad classes of analysis method for piled raft foundations:

(a) Simplified calculation methods
(b) Approximate computer-based methods
(c) More rigorous numerical methods

Simplified calculation methods are performed in order to assess the feasibility of using a piled raft foundation. Relative simple calculations are involved where the required number, location and general characteristics of piles to satisfy the design requirements are determined using an iterative approach.

Approximate computer-based methods and more rigorous numerical methods of analysis are considered as more detailed design methods requiring significant computer resources. These allow the calculation of the detailed distribution of settlements and the determination of the optimum locations and arrangement of the piles. In addition, the bending moments and shear forces of the raft, as well as the pile loads, are estimated for the structural design of the piled raft.

2.3.4.1. Simplified calculation methods

Simplified methods found in the literature include those of Poulos and Davis (1980), Randolph (1983,1994) van Impe and Clerq (1995), and Burland (1995), where all involve simplifications in terms of soil profile and loading conditions on the foundation. A good example is the Poulos-Davis-Randolph (PDR) method, which is a combination of the Poulos and Davis (1980) and Randolph (1994) methods. This simplified method examines the interaction between piles within a pile group and piles with a raft in a combined piled raft foundation system, and eventually allows the determination of the load-settlement behaviour, as described in detail in Poulos (2001). This, along with the assessment of the vertical load capacity, differential settlements and localised behaviour under individual columns, allows the development of a conceptual model of a piled raft foundation.

(a) Vertical load capacity

The vertical load capacity can be determined, according to Poulos (2001), as the lesser of (i) the sum of the ultimate capacities of the raft and all the piles, or (ii) the ultimate capacity of the piled raft as a block, containing both the raft and the piles, and considering the raft contribution outside the periphery of the piles.

In case (i), the ultimate load capacity of the piled raft (Q_{prf}) is expressed as:

Equation 2.10 $$Q_{prf\,(i)} = Q_{rf} + n \cdot Q_{pf}$$

where Q_{rf} is the ultimate load capacity of the raft alone, Q_{pf} is the average load carried by a pile within the group and n the number of piles in the pile group. In some cases the capacity of individual piles within a closely spaced group may be lower than for equivalent isolated

piles. Therefore, a group efficiency factor is introduced, which represents the ratio of the load capacity of a pile in a group to the load capacity of an equivalent isolated pile. However, according to Fleming et al. (2009) the group efficiency is usually omitted in design due to the fact that its value is usually very close to unity. Also, it is stated that for closely spaced pile groups, a more common cause for concern is the block capacity of the group, which is usually less than the sum of the individual pile capacities.

In case (ii), the ultimate load capacity of the piled raft is expressed as:

Equation 2.11 $$Q_{prf\,(ii)} = Q_{bf} + Q_{r'f}$$

where Q_{bf} is the ultimate load capacity of the piled group as a block, and $Q_{r'f}$ is the ultimate load capacity of the raft around the periphery of piles which comes to direct contact with the soil. The vertical capacity of a pile group failing as a block can be calculated in a similar way to that for a single pile (Section 2.2.3), assuming that the full shear strength of the soil is mobilised around the periphery of the block. However, in this case A_b and A_s represent the base area of the block and surface area of the block respectively.

(b) Load-settlement behaviour

The load-settlement behaviour can be determined according to Poulos (2001) by considering the response of each component of the piled raft together with the interaction between the components, via elastic theory, and assuming uniform vertical loading (PDR method). In particular, the stiffness of the raft (k_r) and of the pile group (k_p), as well as the interaction factor (a_{rp}) between the raft and the pile group, must be estimated. From these, the combined stiffness of the piled raft (k_{pr}), as well as the load share between the two components of the piled raft, can be calculated, leading to the estimation of the load-settlement behaviour of the piled raft.

Using the approach by Randolph (1994), the combined stiffness of the piled raft, k_{pr}, can be determined as follows:

Equation 2.12 $$k_{pr} = \frac{k_p + (1 - 2a_{rp})k_r}{1 - {a_{rp}}^2(k_r/k_p)}$$

The raft stiffness k_r can be estimated using elastic theory. Examples include the solutions of Fraser and Wardle (1976) and Mayne and Poulos (1999). The pile group stiffness k_{pr} can also be determined using elastic theory, using the solutions of Poulos and Davis (1980), Fleming et al. (1992) or Poulos (1989), where the stiffness of a single pile is first computed, using for

example the approach by Randolph and Wroth (1978), and then multiplied by a group efficiency factor, both being approximated from elastic solutions.

The ratio of the load carried by the raft (P_r) to the total load can be estimated as follows:

Equation 2.13

$$\frac{P_r}{P_r + P_p} = \frac{(1 - a_{rp})k_r}{k_p + (1 - 2a_{rp})k_r} = X$$

Respectively, the ratio of the load carried by the pile group (P_p) to the total load is:

Equation 2.14

$$\frac{P_p}{P_r + P_p} = 1 - X = 1 - \frac{(1 - a_{rp})k_r}{k_p + (1 - 2a_{rp})k_r}$$

Now, regarding the determination of the interaction factor, Randolph (1983) suggests that, for single piles of radius r_o with circular caps of radius r_c, it is calculated as:

Equation 2.15

$$a_{rp} = 1 - \frac{\ln(r_c/r_o)}{\zeta}$$

where the parameter ζ depends on the maximum radius of influence of stress and the pile diameter.

This equation may also be used for large piled rafts according to Randolph (1994); however r_c in this case is an equivalent radius representing the area of the raft for each pile.

Furthermore, Clancy and Randolph (1993) performed some rigorous analyses in order to determine the value of the interaction factor. It was concluded that, as the number of piles increases, the value for a_{rp} converges to 0.8. This value, in particular, is independent of the pile spacing, slenderness ratio or stiffness ratio.

Therefore, for large groups the expression for the piled raft stiffness leads to:

Equation 2.16

$$k_{pr} = \frac{1 - 0.6(k_r/k_p)}{1 - 0.64(k_r/k_p)} k_p$$

Similarly, the expression for the ratio of the load carried by the raft to the load carried by the pile group is:

Equation 2.17

$$\frac{P_r}{P_p} = \frac{0.2}{1 - 0.8(k_r/k_p)} \frac{k_r}{k_p}$$

which for large groups typically lies between 0.3 – 0.5 times (k_r/k_p). (Randolph, 1994)

Considering the combined piled raft stiffness and the load share between the piles and the raft from Equations 2.12 and 2.13, a tri-linear load-settlement curve can be produced, like the one shown in Figure 2.50, in order to assess the load-settlement behaviour of a piled raft. (Poulos, 2001)

Looking at Figure 2.50, the stiffness of the piled raft is initially the dominant stiffness for the load-settlement behaviour of the foundation, which is the case until the pile group capacity is fully mobilised at point A. Assuming the pile capacity of each individual pile is mobilised simultaneously, then the total applied load at which the pile group capacity is reached, (P_1), is:

Equation 2.18 $$P_1 = \frac{P_u}{(1 - X)}$$

where P_u is the ultimate load capacity of the piled raft, and X is the proportion of load carried by the raft (Equation 2.13).

As soon as the pile group capacity is mobilised, i.e. after point A, the stiffness of the foundation is that of the raft alone. This stiffness remains operative until the ultimate load capacity of the piled raft foundation is reached, which is point B in Figure 2.50. Finally, the load-settlement curve becomes horizontal beyond point B, i.e. after the whole piled raft foundation has failed in bearing capacity.

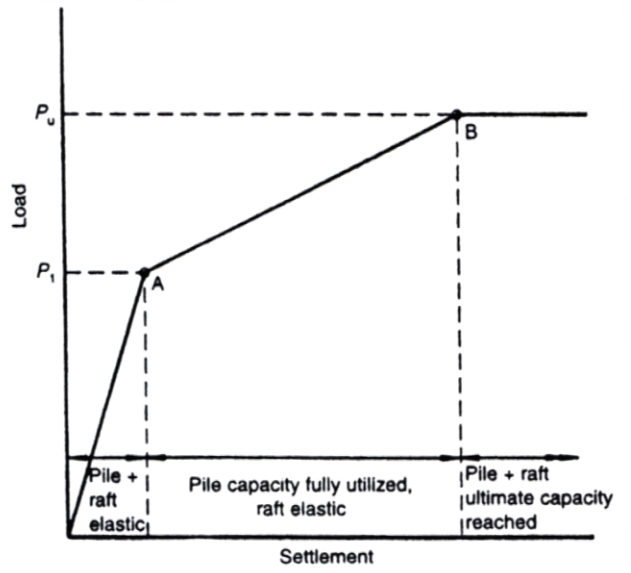


Figure 2.50: Simplified load-settlement curve for preliminary analysis (Poulos, 2001)

The PDR method is an iterative method. Figure 2.50 is produced for one case based on a particular number of piles. It can be re-produced for various numbers of piles, for example

using a spreadsheet, in order to determine the optimum number of piles, which satisfies the design requirements.

(c) Differential settlements

Differential settlements are usually a more critical criterion than absolute settlements in foundation design. Most approximate methods used to calculate the pile group settlement, according to Poulos (2002), make one of the two following extreme assumptions; either the pile cap is perfectly rigid or it is fully flexible. In the first case, all piles are expected to settle equally and therefore there is no differential settlement. On the other hand, if the pile cap is fully flexible and hence the load distribution onto the piles is known, the differential settlements can be determined ignoring the effect of the pile cap. Nevertheless, for piled rafts, where the pile cap is the raft, the raft is assumed to have a value of stiffness which is between the two extreme boundaries. Therefore, several adjustments are made.

An approach described by Randolph and Clancy (1993) to determine differential settlements for piled rafts is equivalent to the one for a typical pile group, where a fully flexible pile cap or raft is assumed. An improvement to the method has been suggested by Mayne and Poulos (1999), who developed a closed-form approximation in order to calculate a rigidity correction factor for pile caps of intermediate stiffness, which depends on the relative raft-soil stiffness. The solutions provided are for normalized differential settlements in respect to the mean piled raft settlement. Therefore, in order to calculate absolute differential settlements, the mean raft settlement is required.

(d) Design for localised behaviour under individual columns

Most analyses performed for piled raft foundations consider a uniformly distributed loading over the raft area. This may be adequate for preliminary analyses, however in a more detailed analysis where the location of piles is considered, an assessment of local requirements considering concentrated column loads is required, according to Poulos (2001). Foundations may satisfy the overall capacity and settlement requirements, however localised stress due to column loads may result in excessive bending stresses on the raft or excessive local settlement under the column position. Therefore, a pile, either termed as a ‘stress reducing’ or ‘settlement reducing’ pile depending on its required function, may be required under the point of interest.

Four minimum checks have to be performed in order to determine whether the raft alone can sustain the moments, shears etc., or if a pile is required below a column. These are:

(a) moment capacity of the raft

(b) shear capacity of the raft

(c) maximum contact pressure capacity of soil below the raft

(d) local settlement capacity

The above are estimated in order to examine whether the quantities developed due to the column loading exceed the allowable ones and whether a pile is required locally to provide either load capacity or additional stiffness. If the maximum moment, shear or contact pressure of the raft is the critical criteria, then the pile required has to be designed in order to provide load capacity. Such pile is referred as a 'stress reducing pile' by Burland (1995), in contrast to the 'settlement reducing piles' whose function is to provide additional stiffness. The required ultimate load capacity of the pile can be determined by considering the difference between the column load and the raft capacity, including the suggestion of Burland (1995) that approximately 90% of the ultimate pile load capacity should be considered as being mobilised below a piled raft. If the only critical criterion is local settlement, then a 'settlement reducing pile' should be included in order to provide an appropriate additional stiffness to the foundation.

2.3.4.2. Approximate computer based methods

Poulos et al. (1997) define as approximate computer-based methods the ones employing a 'strip on springs' or a 'plate on springs' approach. In both methods, the piles are represented by springs of appropriate stiffness, and the raft by a series of strip footings for the 'strip on springs' approach or by a plate for the 'plate on springs' approach.

(a) 'Strip on springs' approach

A typical method of the 'strip on springs' approach is presented by Poulos (1991). It combines (a) the boundary element method for the analysis of the strip and (b) a simplified analysis for axial pile response in order to simulate the piles response. This analysis is based on the one performed for a strip footing alone by Poulos (1984) and, then, it is extended in order to take account for the contribution of the piles in the performance of the foundation system. Approximate allowance is made for all components of interaction. The effects of the parts of the raft outside the strip section being analysed are also taken into account by computing the free-field soil movements due to these parts and the interaction of these with the strip section.

Verification of the analysis method has shown that it provides a reasonably satisfactory method of analysing the behaviour of piled strip foundations. Also, this analysis can provide an approximate solution for a piled raft, by analysing the behaviour of the piled raft in sections. Significant limitations are encountered, as described by Poulos et al. (1997). In particular, torsional moments within the raft cannot be considered, and also inconsistent settlements may be calculated at a point if strips in two directions through that point are analysed. However, according to Poulos et al. (1997) this method appears to provide a convenient means of rationally analysing complex foundations problems, and has the potential to provide a means of comparing the relative behaviour of alternative foundation configurations.

Other researchers who have employed the 'strip on springs' approach for a piled strip and have suggested how such solutions may be applied to a piled raft problem include Brown and Wiesner (1975) and Wiesner and Brown (1976).

(b) 'Plate on springs' approach

The 'plate on springs' approach is an approximate method, where the raft is modelled as a thin plate, the piles as interacting springs of appropriate stiffness and the soil as an equivalent elastic continuum, as described by Poulos (1994). This approach is considered to be an extension of the 'strip on springs' method presented by Poulos (1991).

Figure 2.51 portrays the problem involved; a rectangular raft with randomly distributed piles over the raft area and subjected to a combination of (a) concentrated vertical loading, (b) concentrated moment loading, (c) uniformly distributed loading over discrete areas, and (d) 'free-field' vertical soil movements.

The basis for the 'plate on springs' analysis is the boundary element method, where several idealisations and assumptions are made regarding:

(a) *the raft:* it is modelled as a thin elastic plate;
(b) *the piles:* they are modelled as springs whose stiffness is pre-determined from elastic theory and whose ultimate axial capacity in compression and tension is specified;
(c) *the soil:* it is assumed to be an isotropic elastic continuum consisting of horizontal layers;
(d) *the raft-soil contact pressure:* it is specified for both compression and tension on the basis of bearing capacity theory, allowing for local bearing failure or 'lift-off' of the raft from the soil.

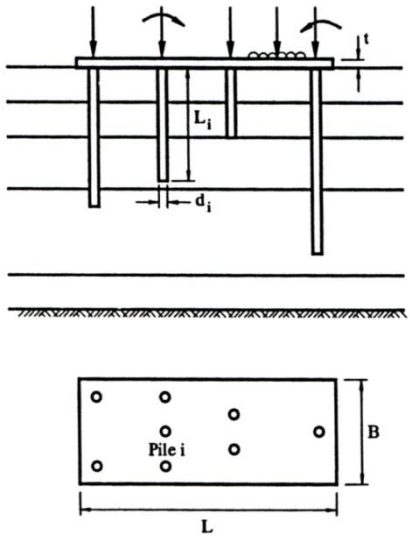


Figure 2.51: Definition of piled raft problem (Poulos, 1994)

Hence, this analysis allows for the consideration of both applied loading and free-field soil movements in the response of the foundation. Also, limiting pressures below the raft and ultimate load of the piles are set, allowing for the consideration of the non-linear behaviour of the piled raft.

Other researchers, including Clancy and Randolph (2003), Franke et al. (1994) and Yamashita et al. (1993), have adopted this approach by analysing the raft with finite elements; a more modern approach according to Poulos (1994). Clancy and Randolph (2003) limit the analysis to the elastic response of the foundation, whereas Franke et al. (1994) consider a nonlinear pile response via hyperbolic shaft and base response characteristics. In Yamashita et al. (1993), the means of interaction are not detailed.

2.3.4.3. More rigorous numerical methods

(a) Boundary element methods

The boundary element method is a numerical method of analysis, in which both the raft and the piles within the foundation system are discretised and use of elastic theory is made. Poulos et al. (1997) describe several efforts made to apply this method in a piled raft by several researchers.

One of the first examples employing this approach were those of Butterfield and Banerjee (1971). They performed an analysis of groups of piles founded in an elastic soil mass with a rigid cap on the ground surface. Later on, Kuwabara (1989) made an analysis for a piled raft in a homogeneous elastic soil mass using the boundary element method. In particular, the raft

was assumed rigid and the compressibility of the piles was considered. The results of this analysis indicated that the load share of the raft was very small at normal pile spacings. Eventually, Poulos (1993) made an analysis, considered as an extension of Kuwabara's, where the effects of free-field soil movements, limiting contact pressures between the raft and soil, and the development of ultimate compression or tensile loads in piles were taken into account. Despite these considerations, the limitation of the rigid raft remained, which is the case for most boundary element analyses.

(b) Methods combining boundary element and finite element analyses

These methods consist of a combination of boundary element analysis for the piles and of finite element analysis for the raft. One example employing such a method was performed by Hain and Lee (1978), after Poulos et al. (1997), where the raft was represented as a series of thin-plate finite elements, whereas the piles were partly discretised by boundary elements. The analysis involved several approximations, including the use of the interaction factor concept. Therefore, in this analysis the piles were not fully discretised. The analysis was considered elastic, despite the fact that ultimate loads for the piles were considered. Also, the soil was modelled as a homogeneous semi-infinite elastic mass. Despite these approximations, this analysis was referred to by many subsequent researchers, due to the fact that several important factors on piled raft response were highlighted.

Another analysis, where this time the piles were fully discretised, according to Poulos et al. (1997), was that of Sinha (1997). The soil was modelled as a homogeneous elastic soil mass. However, the non-linear soil behaviour was considered as well by applying limiting values for the raft-soil contact pressures in both compression and tension, as well as limiting stresses between the pile shafts and soil, and beneath the pile tips. In addition, the effects of soil swelling or consolidation were considered by taking into account the effects of free-field soil movements.

(c) Simplified finite element analyses

Simplified finite element analyses, where the piled raft is represented as either a plane strain problem (e.g. Desai, 1974) or an axi-symmetric problem (e.g. Hooper, 1973; Naylor and Hooper, 1974), have been employed, according to Poulos et al. (1997), in order to analyze a pile raft foundation system. In this approach, both the raft and the soil are discretised into finite elements.

Also, the non-linear behaviour of the soil and raft can be employed as well as time-dependent effects can be considered. In particular, the time-dependent settlement and the pile load distribution due to consolidation of the soil may be examined by implementing two-phase soil behaviour.

The main deficiency of this approach, after Poulos et al. (1997) is that simple loading patterns can be considered only and that torsional moments in the raft cannot be determined. In both plane strain and axi-symmetric problems, significant approximations have to be made, in particular with the piles, according to Poulos (2001). Piles must be "smeared" to a wall and given an equivalent stiffness equal to the total stiffness of the piles being represented by the wall. In addition, concentrated loadings have to be "smeared" as well. Unless uniform loading on a symmetric raft is considered, it may be required to run analyses for each of the directions in order to obtain estimates of the settlement profile and the raft moments.

Nevertheless, this method has been applied to several structures with piled raft foundations and the predictions made were quite similar to the observed behaviour (Poulos et al., 1997).

(d) Three-dimensional finite element analyses

According to Poulos et al. (1997), three-dimensional finite element analysis is the most 'powerful' tool at the moment in terms of modelling a real problem. The first attempt to model a piled foundation was made by Ottaviani (1975); however, more recent attempts for piled rafts were made by Katzenbach et al. (1998) and Reul and Randolph (2003), who produced parametric solutions for the settlement and load distribution within piled rafts. Parameters included the relative raft stiffness, the relative pile length and the number of piles.

Three-dimensional finite element analysis in principle removes the need for approximate assumptions made in all the above approaches. However, according to Poulos (2001) there are still some problems in relation to the modelling of the pile-soil interfaces. If interface elements are employed, there are some approximations in the assignment of joint stiffness properties. In addition, another major drawback is time. A complicated foundation system may need days to run, even with the most advanced computer resources available. Therefore, according to Poulos (2001) such analyses are usually used as benchmarks rather than as routine solution tools. However, it is recognised that nowadays three dimensional finite element analysis is used more and more often in design.

2.3.5. NUMERICAL STUDIES

In this section, results from numerical studies on piled raft foundations are presented, from which several observations about the behaviour of piled raft foundations are made. Initially, a series of parametric studies on hypothetical piled raft foundations is presented performed by Poulos (2001), Katzenbach et al. (1998), Randolph (1994) and Viggiani (2001), which consider the general behaviour of piled raft foundations, the concept to locate piles over the central region of the raft and the critical parameters for optimum design.

Subsequently, numerical studies on three case histories are presented, which were performed in order to assess the behaviour of different foundation arrangements, providing on indication on critical parameters for optimum design. The first two are for (a) Hiscocks House in Stonebridge Park, London and (b) the Torhaus der Messe building in Frankfurt, which were re-designed complying with the concept of locating the piles in the central region of the raft. The third case is for (c) a five-storey building in Urawa in Japan, where several characteristics of piled raft behaviour by varying, for example, the raft thickness, are examined.

2.3.5.1. Parametric studies on hypothetical piled raft foundations

(a) Hypothetical piled raft by Poulos (2001)

Poulos (2001) performed a numerical study on an idealised hypothetical problem, as shown in Figure 2.52, in order to examine some of the characteristics of piled raft behaviour. In particular, he examined the effects of a variation in (a) the number of piles, (b) the nature of loading (concentrated versus uniform distributed), (c) the raft thickness, and (d) the applied load level, on foundation behaviour, while keeping constant the length and the diameter of the piles.

The analysis was elastic and it was performed using the computer program GARP, which employs the 'plate on springs' approach of Poulos (1994). The raft (10m× 8m) in each case was discretised into 273 elements. The piles were assumed to exhibit elastic-plastic load-settlement behaviour, whose stiffness and interaction characteristics were computed using a separate analysis, performed using the computer program DEFPIG (Poulos, 1990).

The first analysis performed by Poulos (2001) was that of varying the number of piles. In particular, the analysis considered a piled raft with a number of piles ranging from 0, i.e. un-piled raft, to 45 piles (n=0, 9, 15, 25 and 45). Also, for each case either a uniform distributed load or a concentrated load applied to the foundation was considered. The raft thickness in

this analysis was 0.5 m, the pile length was 10 m, the pile diameter was 0.5 m, and the total applied load equalled 12 MN.

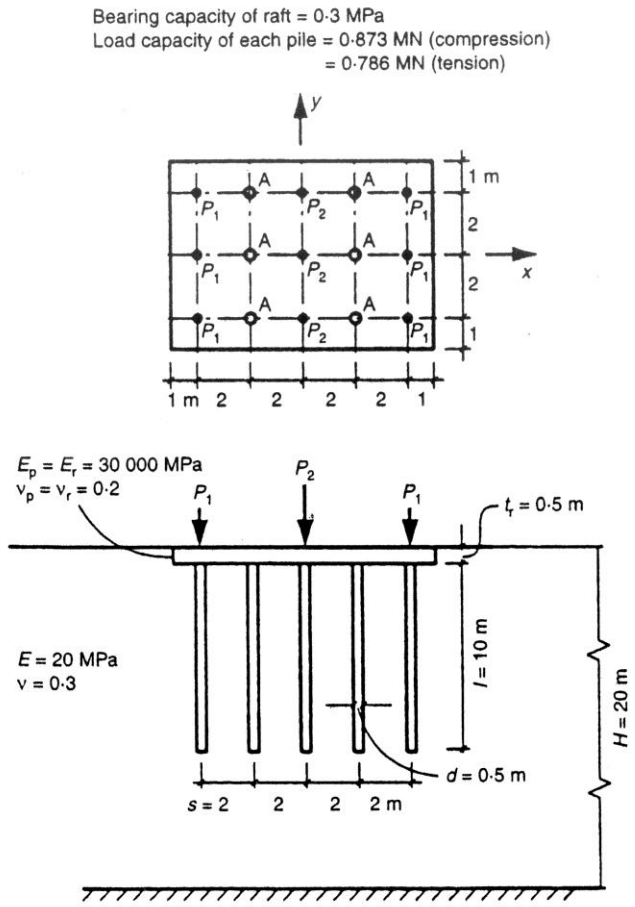


Figure 2.52: Parameters of hypothetical pile raft (Poulos, 2001)

The scope of this analysis was to examine the effect of the number of piles on the maximum settlement, differential settlement, maximum bending moment, as well as on the proportion of load carried by the piles, of a typical piled raft foundation. Figure 2.53 was produced to present the results of the analysis, from which several conclusions were drawn about the behaviour of piled raft foundations. In particular, Poulos (2001) states that:

(a) The *maximum settlement* decreases with increasing pile numbers (Figure 2.53a). This is the case for up to 20 piles. For more piles, the maximum settlement does not reduce further. Also, for small numbers of piles, the maximum settlement for concentrated loading is larger than the uniform loading. However, for ten or more piles this difference becomes very small.

(b) The *differential settlement* between the centre and corner piles does not have a regular pattern with the number of piles (Figure 2.53b). For the cases examined, the smallest differential settlement is obtained in the case of 3 piles centrally located, whereas the

largest one occurs in the case of 9 piles. The reason for the smallest differential settlement is that an un-piled raft 'dishes' with the maximum settlement being in the centre and therefore the piles centrally located reduce that tendency (see Section 2.3.3.3). For the largest differential settlement the reason is that, after Poulos (2001), the piles in the periphery of the raft 'hold up' the raft edges, which are not settling as much as the centre. For the other numbers of piles, the differential settlement is almost even, but less than the un-piled raft case. This due to the fact that the behaviour of the raft, in terms of contact pressure distribution, becomes stiffer with the addition of piles.

(c) The *maximum bending moments* are smaller again for the case of 3 piles centrally located. In addition, it is evident that the maximum bending moments are much larger for concentrated loading than uniform loading (Figure 2.53c).

(d) The *percentage of load carried by piles* increases with increasing number of piles, but the rate of increase is very small for more than about 15 piles. Also, the type of loading does not seem to have any effect on the load share (Figure 2.53d).

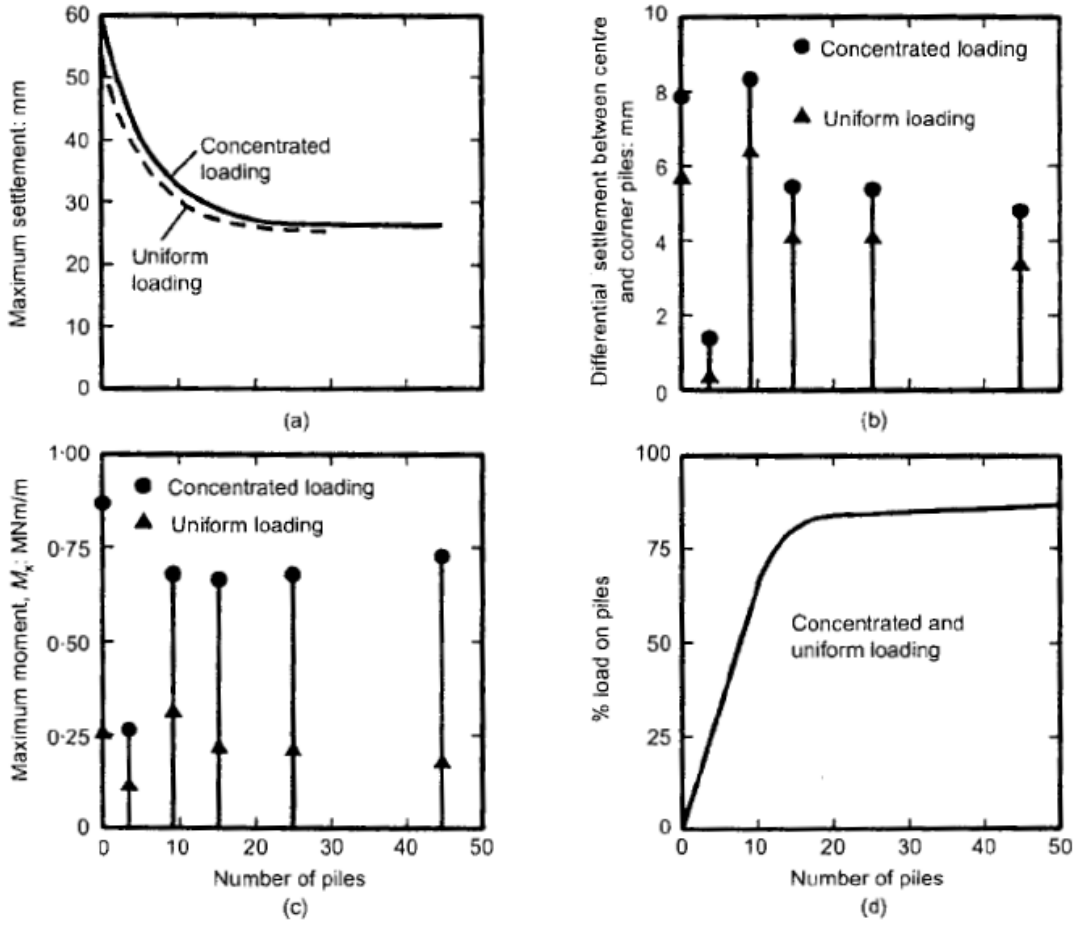


Figure 2.53: Effect of number of piles on piled raft behaviour (Poulos, 2001)

Next, Poulos (2001) performed analyses varying the raft thickness (t = 0.25 to 1.0 m), for the case of concentrated loading, for all pile number cases and for a total applied load of 12 MN, in order to examine the influence of the raft thickness on the piled raft behaviour. Figure 2.54 was produced in order to present the results, from which several characteristics of this variation may be determined. Poulos (2001) discusses that the variation of thickness for all numbers of piles has almost no effect on the maximum settlement and the load share of the piles. However, it does affect the differential settlement and the maximum bending moment. In particular, increasing the raft thickness reduces the differential settlement, but at the same time generally increases the maximum bending moment. A point worthy making is that, once again, the raft with only three piles centrally located below the raft is the optimum design for the whole range of thicknesses.

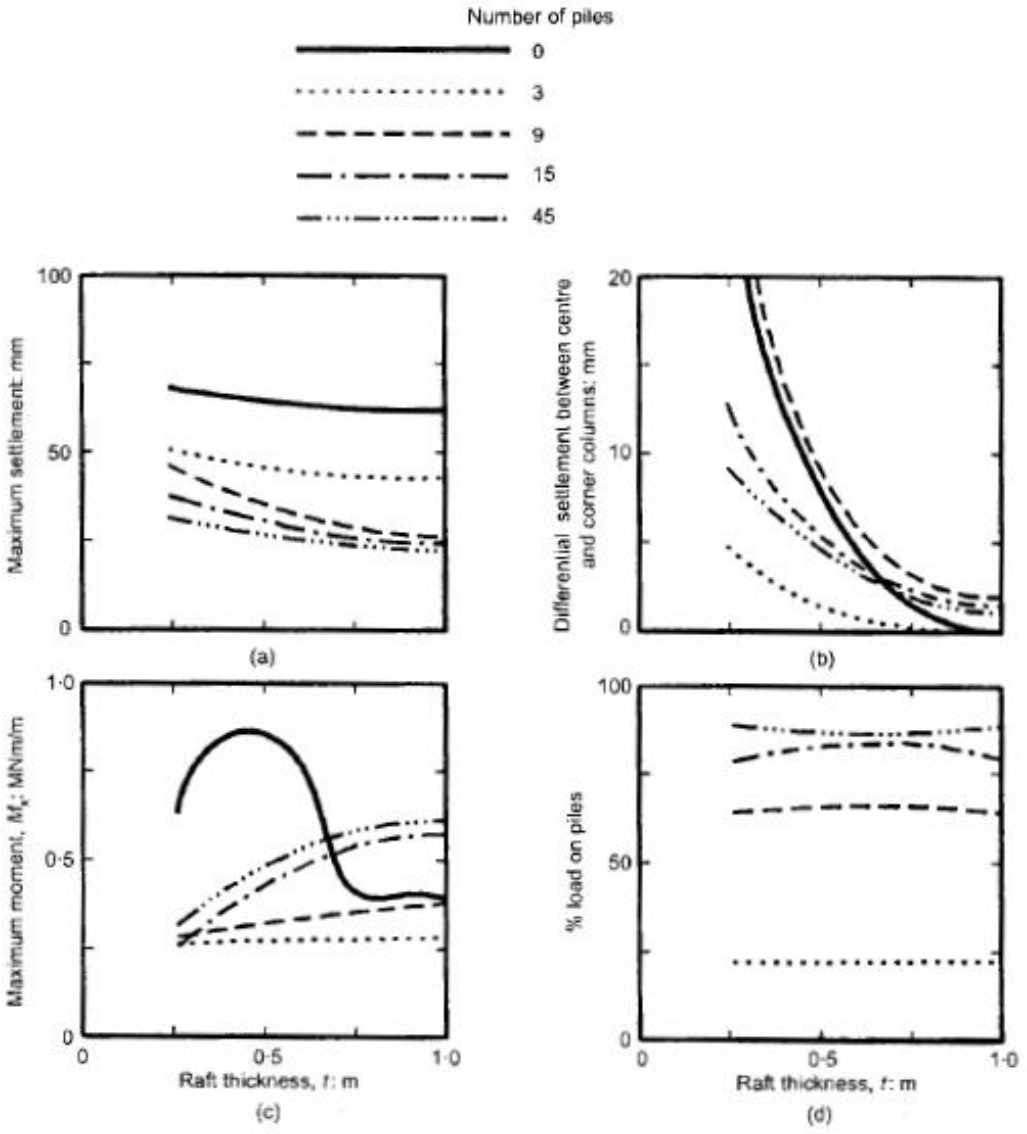


Figure 2.54: Effect of raft thickness on piled raft behaviour (Poulos, 2001)

The last set of analyses performed by Poulos (2001) involved varying the load level on the foundation. Figure 2.55 was produced to present the results from these analyses for various numbers of piles, from which it is obvious that settlement increases with increasing load level. Also, it is considered that the addition of piles is beneficial as the design load level increases, as well as that the addition of a small number of piles may be beneficial in the reduction of the maximum settlement of a foundation, provided that there is an adequate safety margin.

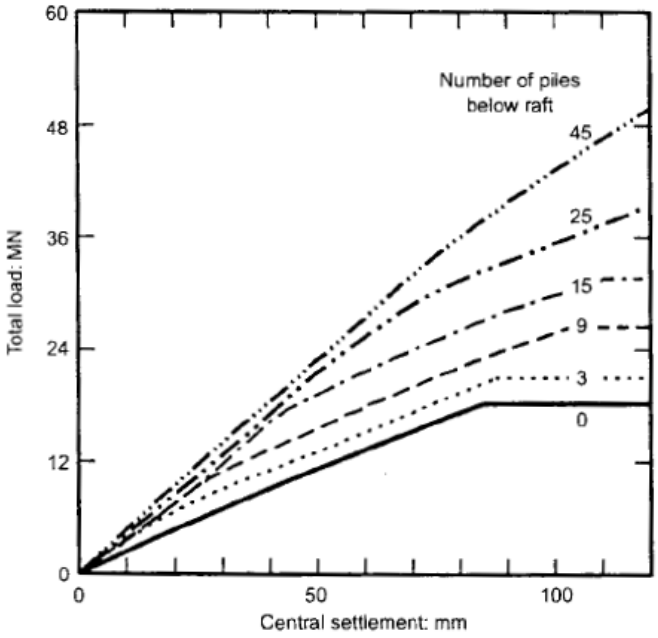


Figure 2.55: Load-settlement curves for various piled raft configurations (Poulos, 2001)

Finally, Poulos (2001) makes several recommendations about practical design of piled rafts, based on the analyses performed. In particular, he concludes that:

(a) Increasing the number of piles in a piled raft foundation is generally beneficial; however it does not always produce the best foundation performance. It is also recognized that beyond an upper limit in the number of piles very little additional benefit is obtained.

(b) The raft thickness affects differential settlement and bending moments, however it has little effect on load sharing and maximum settlement.

(c) In order to control differential settlement, the optimum performance is obtained by the strategic location of a relatively small number of piles, rather than by using a large number of piles, uniformly distributed over the raft area, or increasing the raft stiffness.

(d) The nature of loading applied, i.e. uniform or concentrated, is important for the maximum bending moment and the differential settlement, but not for the maximum settlement or load sharing between piles and raft.

(b) Hypothetical piled raft by Katzenbach et al. (1998)

Katzenbach et al. (1998) performed a three-dimensional finite element analysis on a typical piled raft system for various pile configurations and pile lengths. In particular, a square piled raft, with the number of piles varying between 1 and 49 and the pile length between 2D and 40D, was examined, as shown in Figure 2.56, in order to assess their influence on the load sharing between the piles and the raft, and on the settlement reduction provided by the piles. In the following, some of the results are presented, in order to highlight the positive contribution of the raft to the pile skin friction.

In these analyses, the geometrical model of the continuum and the piles consisted of 3-dimensional isoparametric finite elements, while the raft was modelled with shell elements. Due to the fourfold symmetry, the finite element mesh was reduced to an eighth of the area. The material behaviour of the piles was simulated as linear elastic, whereas the raft was considered as rigid. The subsoil was simulated using an elasto-plastic model with dual yield surfaces and a non-associated flow rule. The analysis was a fully drained analysis.

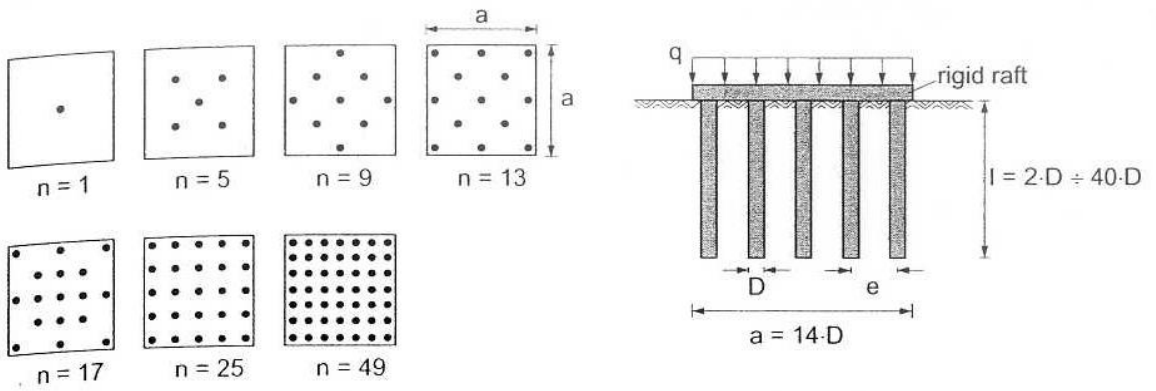


Figure 2.56: Models analyzed in the numerical simulation (Katzenbach et al., 1998)

Katzenbach et al. (1998) performed an analysis of a typical piled raft configuration with 13 piles and $l/D = 10$, in order to examine the load share between the piles and the raft during the loading process. Figure 2.57 was produced to present the load-settlement behaviour (R is resistance, $R_{d,sf}$ is permissible working load of an un-piled raft, S is settlement and S_{sf} is settlement for an un-piled raft at $R_{d,sf}$) and the contribution of the piles and the raft, where it is observed that, during the loading process, the contribution of the piles and the raft in resisting the applied load is not constant. Specifically, at low displacements the majority of the total load is transferred to the piles, but for increasing loads and settlements the contribution of the raft increases.

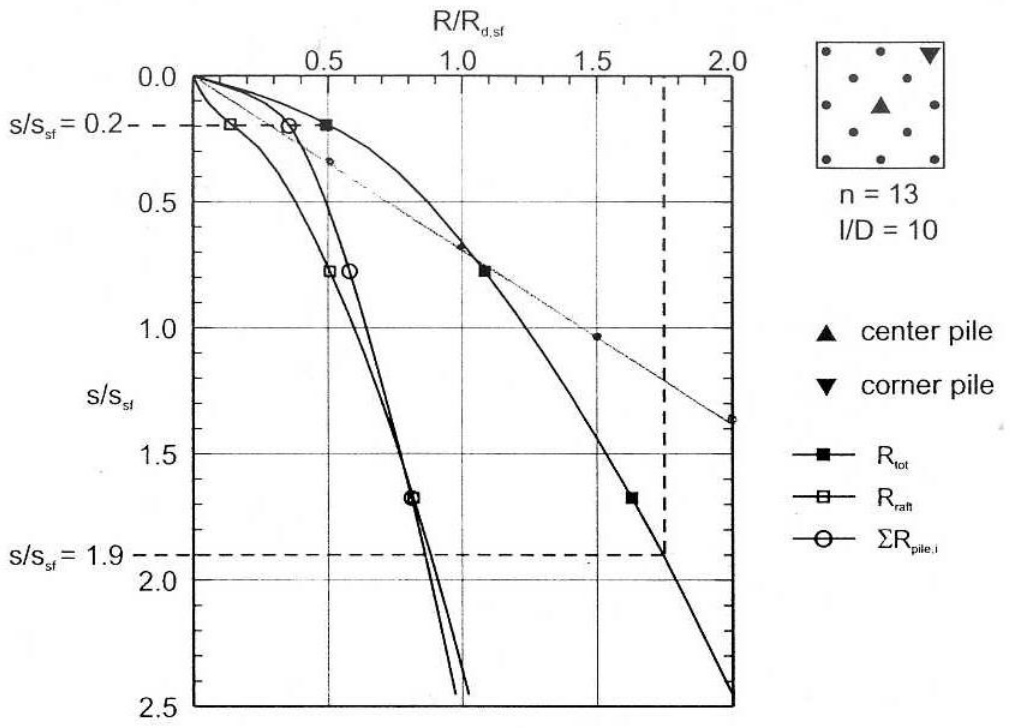


Figure 2.57: Load-settlement curves of a piled raft with n= 13 piles (Katzenbach et al., 1998)

Next, Katzenbach et al. (1998) presented results about the pile load and the skin friction distributions with depth of the centre and corner piles of the piled raft in Figure 2.58 for two levels of displacements (S/S_{sf} = 0.2 and 1.9, as noted in Figure 2.57), which are compared with a single pile and with the centre and corner piles of a fully piled foundation. For small settlements, the pile load distribution and the skin friction distribution was similar for all piles except the skin friction for the centre pile of the piled raft in the upper part, which was lower. This may be associated with the relative movement between pile and soil in this area, which is more or less equal to zero. For large settlements, the piles within the piled raft foundation develop more than twice the shaft resistance of the single isolated pile or the piles within a normal pile group, with the centre piles showing the largest values. This behaviour is due to the significant load share taken by the raft at such large settlement (as shown in Figure 2.57), which results in a higher soil stress state than fully piled foundations or single piles. Therefore the normal pressure on the pile shaft increases leading to higher effective skin friction. This gives rise to one of the main advantages of the piled raft: the bearing capacity of piles in piled rafts is larger than that of a single isolated pile due to the positive effect of the contact pressure, between the raft and the soil, on the pile skin friction in the long term.

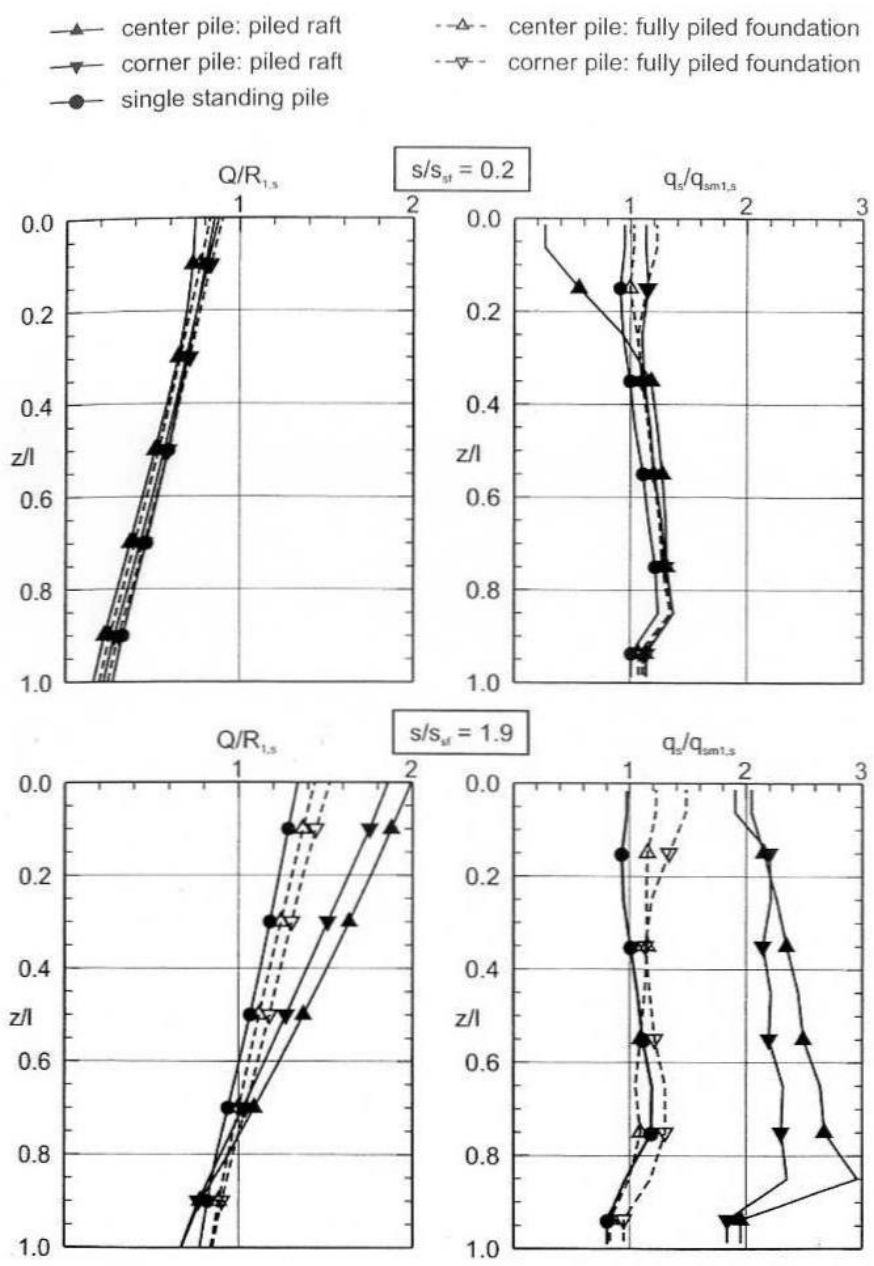


Figure 2.58: Distribution of (a) pile load and (b) skin friction along the pile shaft (Katzenbach et al., 1998)

(c) Typical piled raft analysis with central piles by Randolph (1994)

Randolph (1994) performed a numerical analysis of several pile configurations in order to illustrate the principles behind the concept of locating piles over the central region of the foundation (Section 2.3.3.3). In particular, he examined the behaviour, in terms of absolute settlement and differential settlement, of a shallow foundation, a 'conventional' piled raft and two piled rafts with piles located in the central region.

The foundation layouts are shown in Figure 2.59, with two different piling arrangements. The raft in all cases is a square raft with side length of 36 m. The first pile arrangement consists of

a 9x9 grid of piles at 4 m spacing, with pile length 20 m, diameter 0.8 m, and relative raft-soil stiffness of $K_{rs} = 0.01$. The second arrangement consists of a 3x3 group, at a spacing of 6 m, situated over the central region of the raft, with pile length 30 m, diameter either 1 m or 1.5 m, and a fully flexible raft. Also, in the second pile arrangement it is assumed that about 80 % of the pile capacity is mobilized under working conditions (600 kPa average loading). Therefore, the effective pressure carried by the piles over the central region is about 50% (300 kPa) and 80% (470 kPa) of the applied pressure, in respect to the pile diameters, according to Randolph (1994). The soil is assumed to be linear elastic with a shear modulus G = 100 MPa and a poisson ratio v = 0.4.

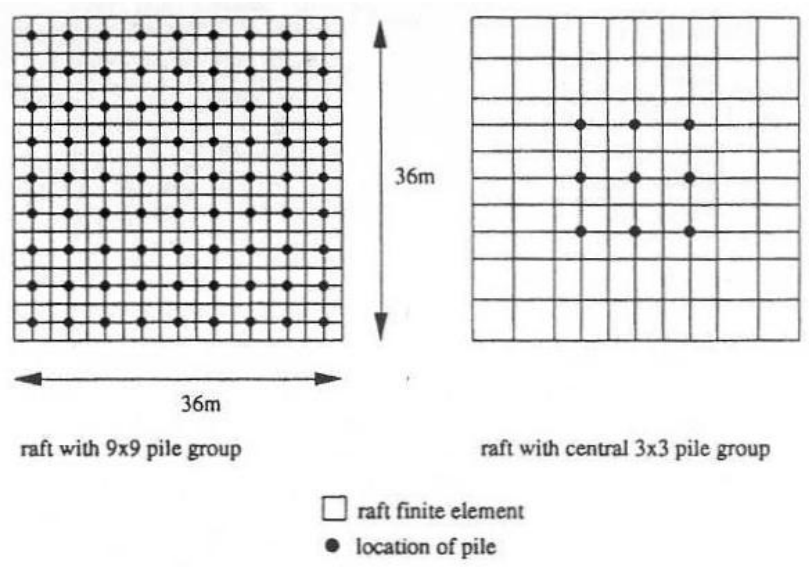


Figure 2.59: Foundation layouts for piled raft analysis (Randolph, 1994)

Figure 2.60 shows settlement profiles for the four cases of (a) un-piled raft (fully flexible), (b) 'conventional' piled raft (9x9), (c) central 3x3 pile group with 1 m pile diameter, and (d) central 3x3 pile group with 1.5 m pile diameter, subjected to an average pressure of 600 kPa or total load of 780 MN. It is observed that the central piles have very little effect on the corner (co-ordinate 0.0 in Figure 2.60) and edge (0.5 co-ordinate) settlement, and the average settlement is reduced by less than 5% compared to the raft foundation. However, the effectiveness of central piles in reducing differential settlement is evident, since the settlement in the central region of the raft (co-ordinate 1.0) is reduced while the mid-side and corner settlements remain almost unchanged. In the case of the fully piled raft foundation, the average settlement is reduced by about 20%, but almost no change to the differential settlement, compared to the raft foundation, is observed. This is due to the fact that both the edge, corner and central settlements are reduced almost by the same amount.

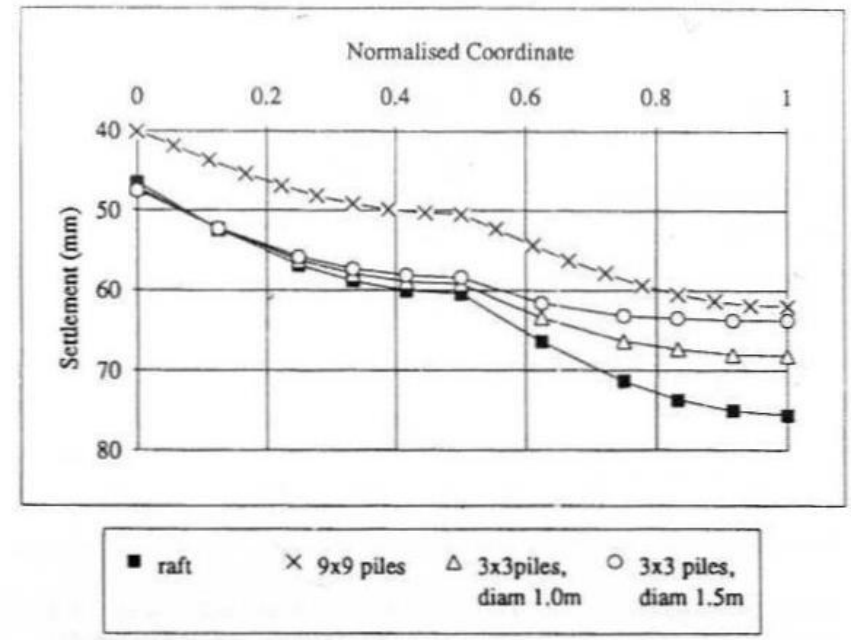


Figure 2.60: Settlement profiles for different pile layouts (Randolph, 1994)

(d) Parametric study by Viggiani (2001) for 'large piled rafts'

Viggiani (2001) performed a parametric study of a typical large piled raft foundation ('large piled raft': case where raft alone provides sufficient load capacity) using the computer program NAPRA (Boundary Element Method assuming linear elasticity), in order to examine some important characteristics of its behaviour and contribute towards the optimum design of piled rafts. In particular, he varied the number, the length, the diameter, the spacing of piles, the area occupied by the piles beneath a raft foundation and the relative raft-soil stiffness, and produced results regarding the load share between piles and raft, the average settlement and the maximum differential settlement. The parameters of this study are shown in Figure 2.61.

A subset of the results is presented in the following. In particular, the reduction of differential settlement of a typical piled raft foundation following the addition of piles is assessed for a constant spacing of piles equal to $s/d = 3$. The differential settlement δ between the centre and the corner was considered for a total load of 800 MN acting on the raft (the raft without pile has a bearing capacity equal to 2400 MN). Figure 2.62 was produced to present the results, where the values of δ/δ_r were plotted (δ_r is the max diff. settlement for an un-piled raft), for the various foundation layouts considered, as a function of the total pile length nL. The following observations were made by Viggiani (2001):

- The addition of piles to the raft is very effective in reducing the differential settlement. The maximum differential settlement δ may even reduce to zero.

- The longer the piles, the more effective they are in reducing the differential settlement. For the same total length of piles, a small number of longer piles is the most effective solution.
- For each curve of pile length, an optimum value of the total length of piles exists corresponding to the maximum reduction of the differential settlement. Also, this value corresponds to values of the ratio A_g/A in the range of 0.3 to 0.4 (A_g is the area occupied by the piles), where they represent groups of a few piles in the central zone of the foundation.

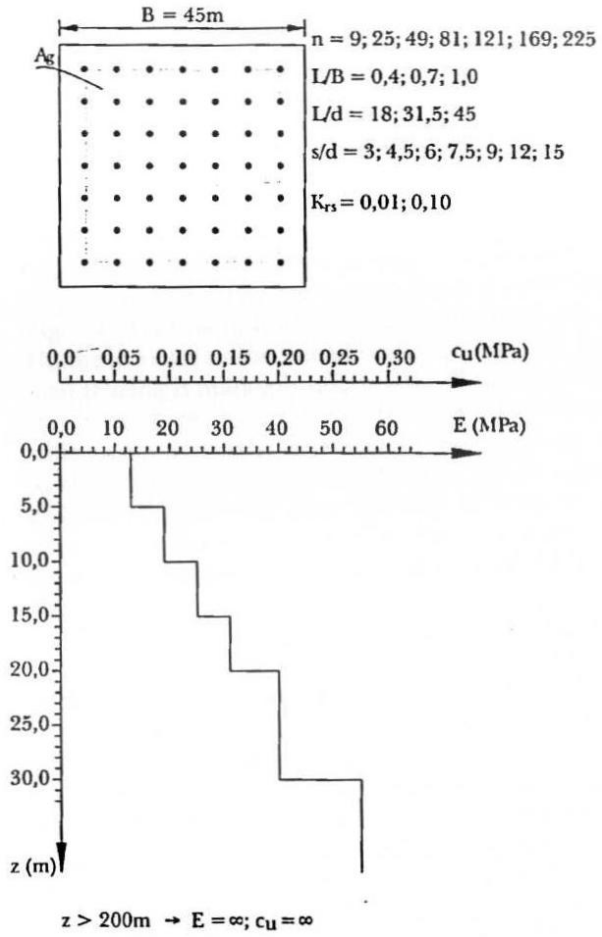


Figure 2.61: Parameters of numerical study (Viggiani, 2001)

An example is provided by Viggiani (2001) to support the use of fewer longer piles in the central zone of the foundation. More particularly, 81 piles with a length of 31.5 m (nL = 2552 m) reduce δ to 15% of δ_r with K_{rs} =0.01 and even to 2% of δ_r with K_{rs} =0.1. However, the same result may be obtained in both cases by using only 30 piles but with a length of 45 m (nL =1350m). Therefore, the addition of a relatively small number of relatively long piles in the central zone of a foundation is very effective in reducing or even cancelling the differential settlement.

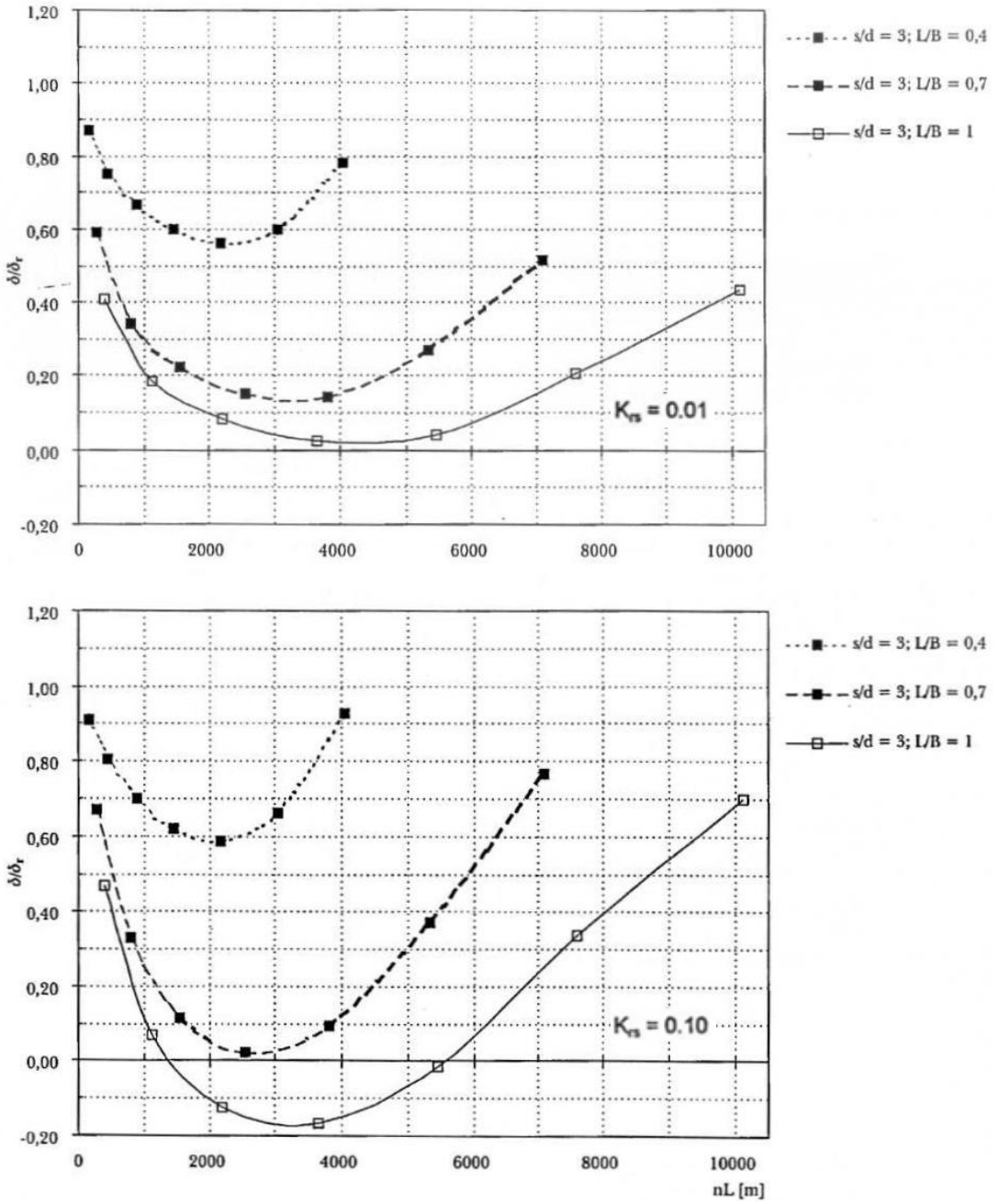


Figure 2.62: Maximum decrease of the maximum differential settlement of the raft following the addition of piles as a function of the total quantity of piles (Viggiani, 2001)

2.3.5.2. Hiscocks House: Stonebridge Park (London) by Viggiani (1998)

Viggiani (1998) performed a numerical study for the Hiscocks House in Stonebridge Park, in order to examine if a different pile arrangement than the original one would produce a more optimum design. As described before, Hiscocks House foundations were designed using the 'conventional' approach, i.e. with a uniform distribution of piles over the raft area, designed to carry the majority of the structural load. Therefore, in this analysis Viggiani examined the effects of reducing the number of piles and the ratio A_g/A_p(area of pile group over area of

raft) of the Hiscocks House, complying with the principle of locating piles centrally, on the average settlement, differential settlement and load sharing between the raft and the piles.

The original design of the Hiscocks House piled raft consisted of 351 piles, distributed uniformly over the raft area with a ratio A_g/A_p equal to 0.88. In this analysis, the different layouts examined, using the computer program NAPRA (Bounadry Element Method), were $A_g/A_p = 0.88$, 0.82, 0.54 and 0.30 for a varying number of piles for each A_g/A_p value.

The results of this study are presented in Figures 2.63 and 2.64. Plots of settlement, expressed by the ratio w/w_{351} where w is the settlement of the piled raft examined and w_{351} of the original piled raft, and of load share between the piles and the raft, expressed by the ratio Q_r/Q where Q_r is the load taken by the raft and Q the total applied load, in respect to the number of piles n are produced in Figure 2.63. Also, in Figure 2.64, plots of differential settlement Δw with respect to the number n and layout of piles A_g/A_p are presented.

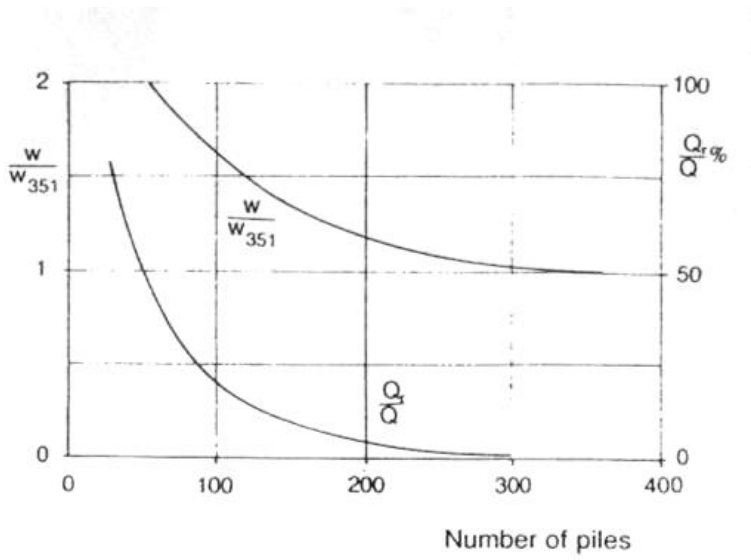


Figure 2.63: Increase of average settlement and load share of the raft with decreasing number of piles (Viggiani, 1998)

In Figure 2.63, it is observed that the average settlement increases with decreasing the number of piles. However, the rate of settlement increase is small for large pile groups. In particular, reducing the number of piles has very little effect on the settlement until the number of piles becomes less than about 200. Even with 117 piles, i.e. one-third of the actual number, the settlement increases by 50%, while the factor of safety against bearing failure reduces by about 58%. Regarding the load share between the piles and the raft, it is seen that, for the original foundation, virtually all of the load is carried by the piles, which is not the actual case recorded. Nevertheless, the less piles the more load carried by the raft.

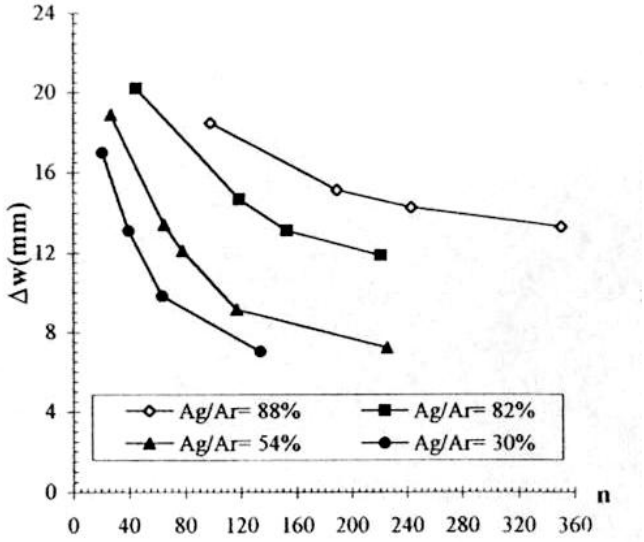


Figure 2.64: Effect of the number and layout of piles on the differential settlement (Viggiani, 1998)

In Figure 2.64, it can be observed that the effect of the number and layout of the piles is very significant in terms of differential settlement. Specifically, the differential settlement increases when decreasing the number of piles, but decreases dramatically when decreasing the ratio A_g/A_p, that is concentrating the piles in the central zone of the foundation.

Therefore, from this analysis it is concluded that a more optimum design could have been found for the foundation of the Hiscocks House. In particular, Viggiani (1998) states that the behaviour of the Hiscocks House foundation remains satisfactory in terms of absolute and differential settlement, when the number of piles is reduced to 1/2 or even 1/3 of the number of piles used in the original design. In addition, he suggests that the most optimum performance is obtained when the piles are located centrally in plan over the raft area.

2.3.5.3. Torhaus der Messe: Frankfurt by Reul and Randolph (2003)

Reul and Randolph (2003) performed a numerical study for the Torhaus der Messe building, using a three-dimensional elasto-plastic finite element analysis, in order to examine if a different pile arrangement compared to the original one would produce a more optimum design. As described before, the Torhaus foundations were designed using a 'settlement reducing' approach with a uniform distribution of piles over the raft area. However, as recorded due to the large number of piles the performance of foundations was similar to the behaviour of a 'conventional' piled raft. Therefore, two different pile configurations, complying with the principle of locating piles centrally to reduce differential settlement, were examined.

The original design of the twin Torhaus piled rafts included 84 piles, with a length of 20 m and diameter of 0.9 m, distributed uniformly over the raft area. For the modified pile configurations A and B (Figure 2.65), the number of piles was reduced to $n = 60$ and $n = 40$ respectively, and the pile length was varied between $L_p = 20$ m and $L_p = 27.5$ m, keeping the original pile diameter constant, for both modifications. Therefore, eight different cases were examined. The results of the analysis are shown in Figure 2.66, where plots of maximum settlement, differential settlement and load share between piles and raft against total pile length are presented.

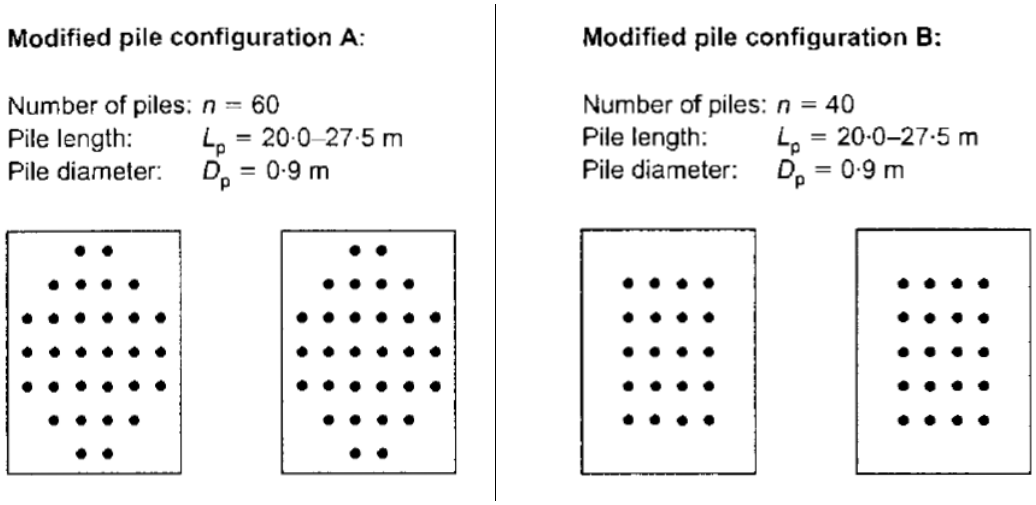


Figure 2.65: Modified pile configurations A and B (Reul and Randolph, 2003)

Regarding the maximum settlement (Figure 2.66a), it is observed that with a different pile configuration than the original one, and with longer piles, a more efficient design would have been achieved. In particular, the settlement reduction coefficient for the maximum settlement (ξ_s), defined as the ratio of maximum settlement of the piled raft to the maximum settlement of the corresponding un-piled raft, for the "real pile configuration" is 0.51 with a total pile length of 1680 m. However, the same value or better could have been achieved for "pile configuration A" with significantly a smaller total pile length, but with longer piles. For the same performance with the "real pile configuration" (n=84), for "pile configuration A" (n=60) the total pile length is equal to 1389 m (L = 23.1 m), and for "pile configuration B" (n=40) the total pile length is equal to only 1100 m (L = 27.5 m).

Regarding differential settlement (Figure 2.66b), the benefits of changing the pile configuration are more visible. For the "real pile configuration", the settlement reduction coefficient for the differential settlement ($\xi_{\Delta s}$), defined correspondingly to the maximum settlement, is equal to 0.50, whereas for the "pile configuration A", with the same maximum settlement, the coefficient is equal to only 0.16. In addition, for "pile configuration B", the coefficient is negative for all pile lengths examined, indicating that it causes hogging.

However, for a pile length less than 20 m, the differential settlement would approach zero, despite a small increase in the maximum settlement.

Regarding the load share between the piles and the raft (Figure 2.66c), the load share of the piles (α_{pr}) increases with increasing total pile length from 0.52 to 0.76. Obviously, the less the pile length the more load carried by the raft. Another important note is that, if this plot is related with the one for maximum settlement, then it is observed that the same maximum settlement can be achieved with a varying contribution of the piles in the load transfer.

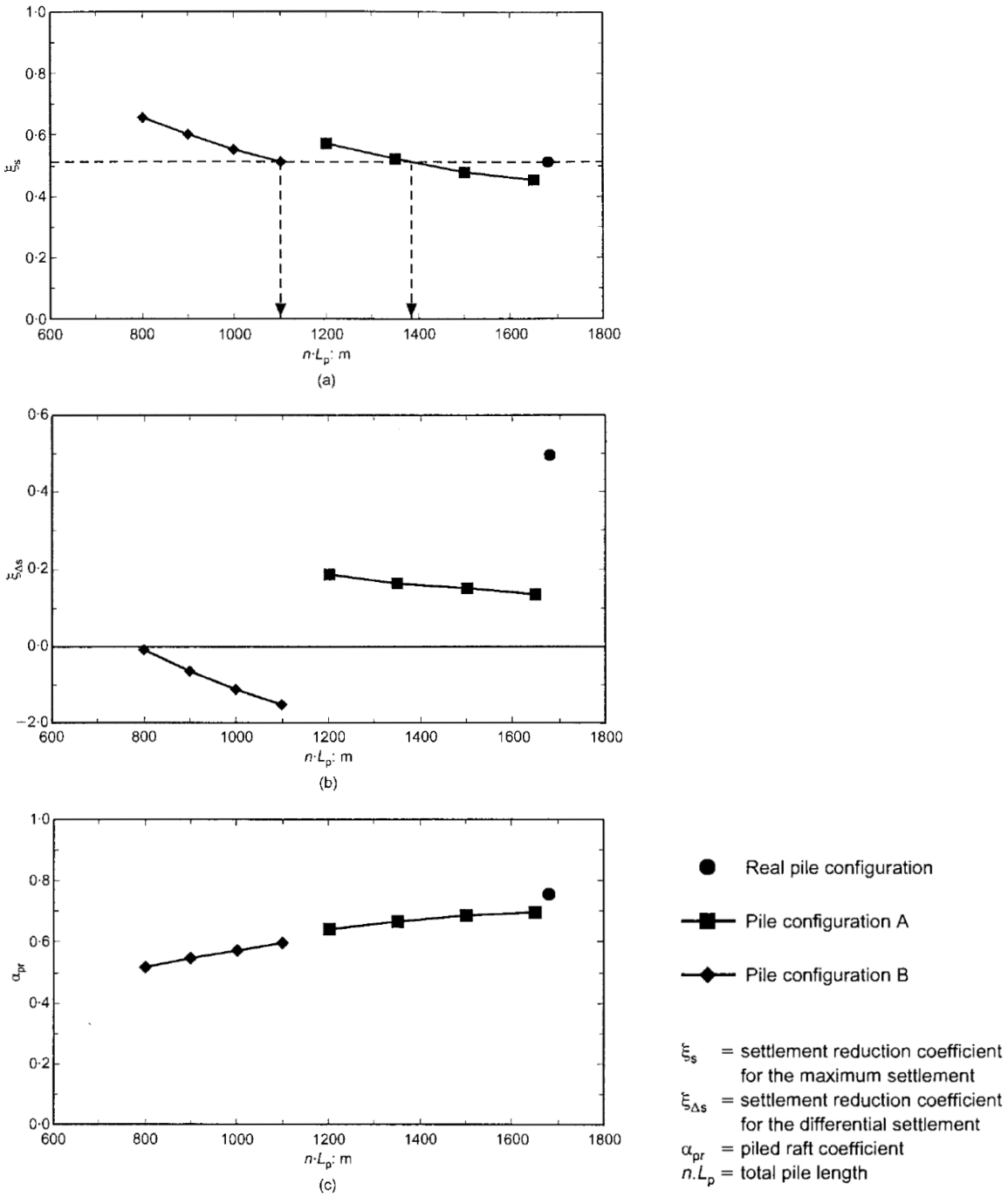


Figure 2.66: Coefficient for (a) maximum settlement, (b) differential settlement and (c) load share of piles depending on the total pile length (Reul and Randolph, 2003)

2.3.5.4. Five-storey building: Urawa (Japan) by Poulos (2001)

Poulos (2001) performed a numerical study using the program GARP ('plate on springs approach') for the foundations of the 5-storey building in Urawa in Japan described before. The aim of this analysis was to compare the calculated behaviour of the piled raft to the measured one, and examine some characteristics of the foundation by varying, for example, the raft thickness.

Initially, an analysis of the actual piled raft was performed. The results for settlement, load distribution etc. were compared with the measured values and it was concluded that the agreement between measured and computed piled raft behaviour was reasonable. Therefore, any further analysis would be considered reliable.

Poulos (2001) examined the maximum column loads that could be sustained by the raft alone, in order to check whether piles were required under the columns. These were calculated to be about 1.44 MN for internal columns and 0.50 MN for columns near the edge of the raft. From the analysis, it was concluded that piles were required under all columns, since the columns loads ranged between 1.02 MN and 3.95 MN which were larger than the loads the raft could sustain. Also, an investigation on how the foundation would behave, in the case of removal of some piles from below the least heavily loaded columns, was performed, where it was found that the foundation performance would be affected very adversely unless the raft became much thicker.

Furthermore, an examination of different foundation designs was performed using again the GARP program. In particular, two alternative foundations were compared with the actual piled raft in terms of settlement and bending moments: (a) a raft without piles, and (b) a piled raft with a thicker raft. The first analysis was that of the actual piled raft and of un-piled raft 0.3 m thick. Figure 2.67 was produced to present the computed settlement and bending moment profiles along column line B (Figure 2.34) for both cases. The un-piled raft produces substantially larger settlements, as well as larger bending moments at the column positions, than the piled one. In addition, it is observed that absolute settlement is more uniform distributed with the addition of piles, and therefore differential settlement is also reduced.

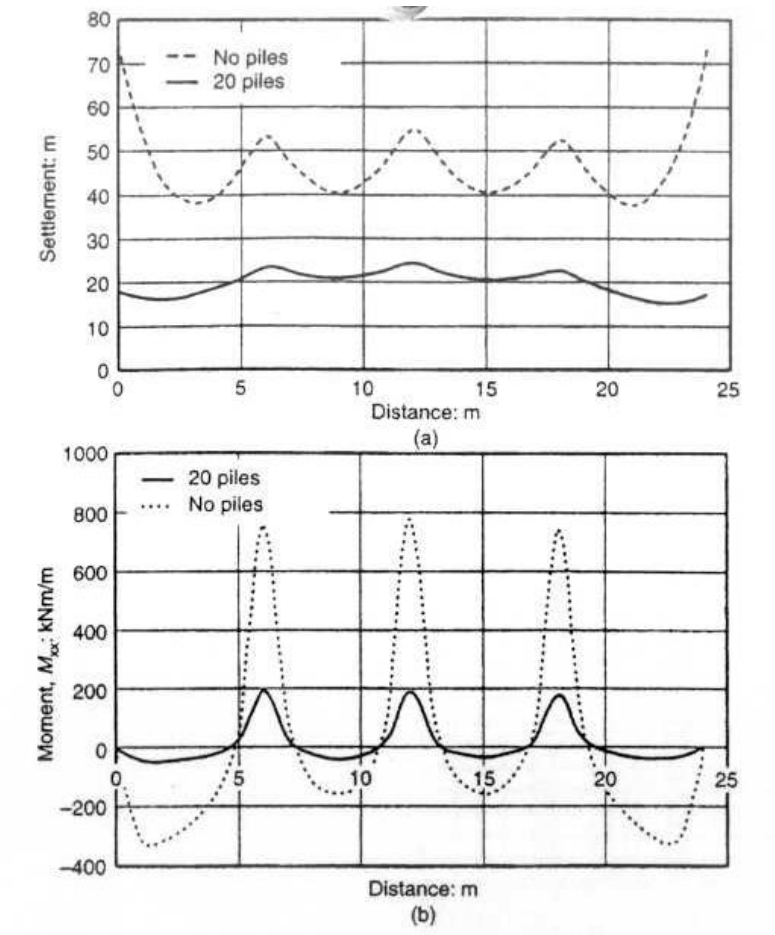


Figure 2.67: (a) Computed settlement and (b) moment distribution with and without piles (Poulos, 2001)

The second analysis was that of two piled rafts with 0.3 m and 0.75 m raft thicknesses respectively. Figure 2.68 shows the computed settlement and bending moment profiles along column line B (Figure 2.34) for both cases, where it is observed that the thicker raft produces a much more uniform settlement profile, and therefore the differential settlement is less. However, at the same time the bending moments on the thicker raft are increased significantly. This behaviour is the expected one, since the thicker the raft, the stiffer it is, and therefore the less differential settlement is produced.

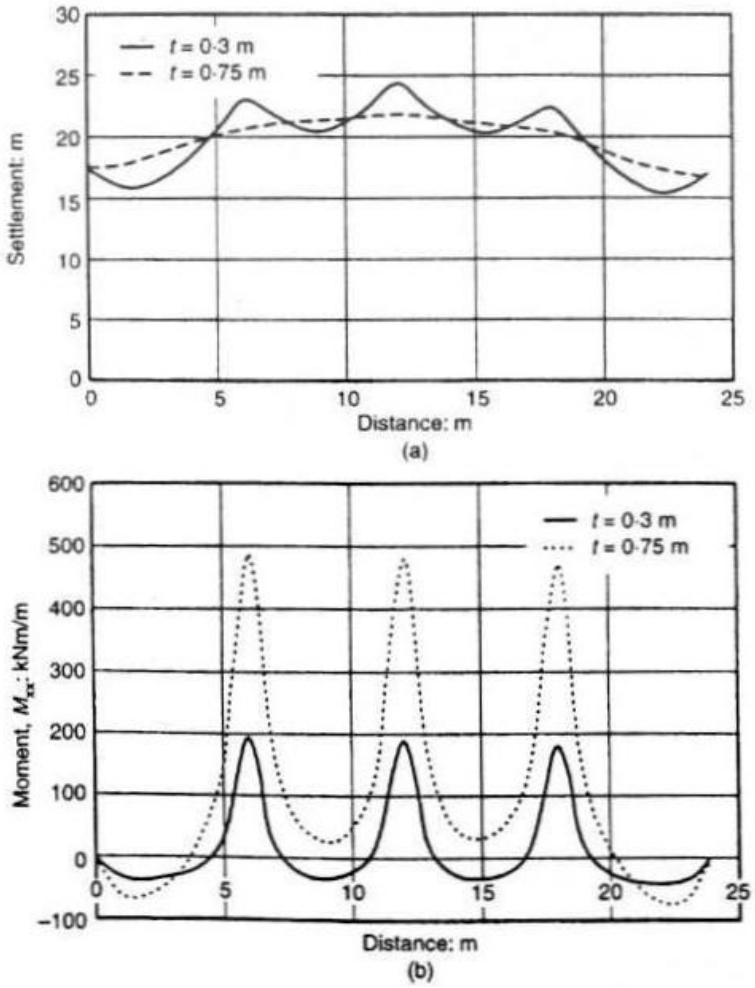


Figure 2.68: Effect of raft thickness on (a) computed settlement and (b) moment profiles (Poulos, 2001)

2.4. SUMMARY AND CONCLUDING REMARKS

The aim of this research is to contribute towards the optimum design of foundations. It is concluded that a raft foundation, with a limited number of piles located strategically beneath the raft and utilising their ultimate load capacity, is the most efficient design when the raft foundation alone provides sufficient load capacity, but at the same time settlements are excessive.

The pile-enhanced raft or piled raft foundation is an innovative design concept where both the raft and the piles are able to transmit loads directly to the subsoil, in contrast to the traditional design approach of piled foundations where the entire design loads are resisted by the piles. Piled raft foundations have a significant advantage over fully piled foundations, due to:

(a) the contribution of the raft to the foundation performance;

(b) the positive effect of the contact pressure, between the raft and the soil, on the piles' effective skin friction;
(c) the prospect of strategically locating piles below rafts in order to limit differential settlement, the main cause of structural damage, rather than to provide load capacity.

The life cycle of such piles, when they are reused for a new development, consists of the following phases:

(a) Installation and equilibration, whose effects on the surrounding soil depend on the construction method (either displacement or replacement) and on the medium the piles are installed. The period of equilibration depends on the pile geometry and may be longer than conventionally believed.
(b) Loading phase, where the piles are loaded from the structure being built on top. For friction piles, the majority of the resistance is provided by the shaft, however depending on the level of loading the contribution of the shaft and the base on the resistance changes, having an effect on the pile-soil stiffness.
(c) Elapsed time phase, during which the time related processes of consolidation and creep take place on the surrounding soil. Time dependent structuration may take place as well along with changes at the pile-soil interface due to physiochemical processes. These processes enhance the pile load capacity and stiffness with time.
(d) Unloading phase, where the piles rebound elastically and a permanent set is observed.
(e) Reloading phase, where the load response of piles reused for a new development is stiffer than the response of similar fresh piles, due to the loading-unloading effect as well as due to the stiffness enhancement with time. In the same manner, the load capacity of the reused piles is larger than the capacity of similar fresh piles.

For the design of piles in piled raft foundations, alternative design strategies have been identified. These include piles designed:

(a) conventionally, with a factor of safety against failure of the order of 2 to 3, and
(b) those designed to utilize a significant part ('creep piles') or the full load capacity of piles under working conditions, termed as 'settlement reducing piles' or 'stress reducing piles' in respect to their functional purpose.

In practice, several design approaches for piled rafts have been identified. These include:

(a) the 'conventional' approach, where conventional friction piles are uniformly distributed over the raft area with small spacings, in order to resist the majority of the design loads,

and the contribution of raft (usually 20-40%) is such that the piling requirements and costs are reduced;

(b) the ‘settlement reducing’ approach, where the piles are used as ‘settlement reducers’ uniformly distributed over the raft area usually with large spacings, and the raft provides sufficient load capacity;

(c) the ‘differential settlement control’ approach, where ‘settlement reducing piles’ are located strategically beneath the raft in order to minimize differential settlement, rather than to substantially reduce the overall average settlement, in an attempt to produce an optimum design.

The key design decisions for the design of a piled raft foundation include:

(a) the required raft thickness,
(b) the type of piles to be used, and
(c) the required location of the piles, and the pile diameter and length.

These design decisions shape the performance of the piled raft foundation and, therefore, the better they are, the more efficient and optimum the design. Several numerical studies have been performed in order to examine the behaviour of piled rafts, whose results lead towards some conclusions about efficient design of piled raft foundations. These are:

(a) Increasing the number of piles, while generally of benefit, does not always produce the best performance. There is an upper limit to the useful number of piles, beyond which very little additional benefit is obtained.

(b) The longer the piles, the more effective they are in reducing settlement, both absolute and differential. For the same total length of piles below a raft, a small number of longer piles is the most effective solution.

(c) The raft thickness has an effect on differential settlement and bending moments, however there is almost no effect on load sharing between the raft and the piles or on maximum settlement. Increasing the raft thickness reduces the differential settlements, however at the same time bending moments in the raft increase.

(d) In order to control differential settlement, optimum performance is likely to be achieved by the strategic location of a relatively small number of piles over the central region of the raft area, rather than using a large number of piles evenly distributed over the raft area or increasing the raft stiffness.

(e) The nature of the applied load, i.e. uniform or concentrated, is important for the differential settlement and bending moment, but not for the maximum settlement or load sharing between the raft and the piles.

Chapter 3

Time Dependent Behaviour of Soils

3.1. INTRODUCTION

The aim of this research is to consider the effects of time on the behaviour of piled foundations and contribute towards the optimum design of foundations considering their past, their present and their future. It is considered that the main mechanisms involved during the lifespan of a building are consolidation and creep, which result in increased settlement, stiffness and capacity, depending on the level of loading. Other time effects on the pile-soil interface, considered as ageing, may also affect the behaviour of piles in the long-term.

This chapter is a literature review of the time dependent behaviour of soils, focusing on the behaviour of saturated clays. The behaviour of soils under compressive load in the short and long term, during primary and secondary consolidation (or compression), is identified and the mechanisms that trigger this behaviour are explored. Consolidation due to stress changes in the soil is examined. In addition, the effects of time, including creep, stress relaxation and rate effects, not due to changes in stresses but due to elapsed time only, are classified and presented in order to highlight their significance in engineering practice. Finally, the accumulated effects of soil viscosity and ageing on the behaviour of clays are discussed through several documented laboratory tests, which examine the volumetric and deviatoric creep behaviour of clays, in order to form a better view on the time dependent behaviour of clays.

Particular attention to the time dependent behaviour of soils has been given since the 1950's. In particular, attention was given to the time-delayed deformation behaviour of soft clays and its creep characteristics with the aim of predicting the long-term settlement of foundations (e.g. Bjerrum, 1967). Another aspect of time dependent behaviour that also received

considerable attention is the time-dependent structuration in clays, in particular in very sensitive clays. Both aspects received particular attention until the 1990's, when it was realised that soils of varying nature might exhibit very different viscous effects (e.g. Mitchell et al., 1997; Tatsuoka et al., 1998). Since then, extensive work has been performed to characterise the viscous behaviour of soils and with the advance in numerical methods, efforts have been made to develop constitutive models that incorporate the viscous nature of soils, in particular for soils which are more susceptible to creep (e.g. Bodas Freitas, 2008).

3.2. CONSOLIDATION

3.2.1. The process of consolidation

In most textbooks (e.g. Craig, 1997), the process of consolidation is described through an example of a fully saturated soil column subjected to a change in vertical total stress, by considering the response of its effective stress to that change. For simplicity reasons, the lateral strain is assumed as zero and therefore the volume change in the soil is entirely due to deformation of the soil in the vertical direction (one-dimensional consolidation). Also, a static pore water pressure is assumed which is constant at a value governed by the position of the water table.

A change in the total vertical stress of a fully saturated soil results in an immediate rearrangement of the solid particles to positions closer to each other. However, if the water is incompressible and the soil is laterally confined, no such rearrangement is possible unless some of the pore water can escape. As a result, the pore water pressure is resisting the particle rearrangement and its value increases above the initial. The increase in pore water pressure, referred to as excess pore water pressure, is equal to the change of total stress. Such a process is referred to as undrained loading.

Eventually, the increase in the pore water pressure causes a pressure gradient resulting in a transient flow of pore water towards a free-draining boundary of the soil layer. Drainage lasts until the excess pore water pressure dissipates to the initial pore water pressure defined by the water table. As drainage takes place, the pore water is leaving free the solid particles to rearrange and take up new positions with a resulting increase in the interparticle forces and reduction in soil volume. Therefore, as the excess pore water pressure dissipates, the effective stress increases, while the soil volume reduces. When the process of consolidation is complete, the total stress is carried fully by the soil skeleton and the excess pore water

pressure is equal to zero. This process is time-dependent and the duration depends on the permeability and the stiffness of the soil.

One-dimensional consolidation is usually assessed through oedometer tests, where lateral strains are restricted. However, in practice one-dimensional consolidation can only occur when the loaded area of the soil layer, which is consolidating, is large compared with the thickness of the layer. If this is not the case, lateral strains arise from the rearrangement of soil particles in undrained conditions, resulting in an immediate settlement of the loaded area with no volume change. Eventually, when the soil volume consolidates with time, further settlement is observed due to the reduction of the pore water in the soil element, which is denoted as consolidation settlement.

3.2.2. Definition of primary and secondary consolidation

According to the classical theory, consolidation of saturated soils is divided into the primary and secondary phase (Figure 3.1), where the primary phase considers the pore pressure dissipation with time after a load application, and the secondary phase is mainly associated with the rearrangement and better packing of the soil particles and aggregates.

Primary consolidation is usually assessed through oedometer tests, where the soil specimen is loaded one-dimensionally in a number of increments, during which the load is maintained constant until all excess pore water pressure dissipates. Each load step usually lasts for 24 hours, during which strains develop due to the process of consolidation.

If the load increment is maintained longer than the period required for excess pore water pressures to dissipate, compressive strains are observed which cannot be explained by the dissipation of excess pore water pressures and the associated proportional increase in effective stress. These strains are explicitly due to time-dependent creep of the soil skeleton, rather than consolidation of the soil mass. Particle rearrangement takes place during creep due to the viscous nature of soils at constant effective stress conditions. This phase is denoted as secondary consolidation (or compression), during which creep strains develop at a reducing rate. The relationship between creep strain and the logarithm of time is usually characterised by a linear relationship. Sometimes a tertiary consolidation phase may be observed according to Augustesen et al. (2004), corresponding to pure creep too. The tertiary consolidation phase is characterized by a nonlinear relationship between strain and the logarithm of time, as schematically shown in Figure 3.1. This phenomenon has been reported by e.g. den Haan (1994) on oedometer tests on Portage peat.

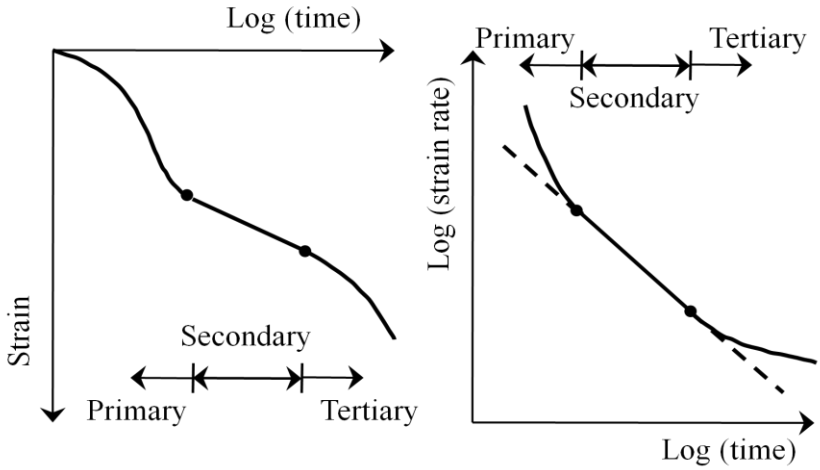


Figure 3.1: Definition of consolidation phases during 1D oedometer compression test: (a) Stress versus log (time); (b) log (strain rate) versus log (time) (Augustesen et al., 2004)

Whether the end of primary consolidation is unique or not is not clear in the literature. There has been significant debate about the moment at which secondary compression starts: at the beginning of loading or at the end of primary consolidation. The question is whether the void ratio at the end of primary consolidation under a given effective stress is unique or instead depends on the duration of primary consolidation, which would mean that the longer the duration the larger the effect of the mechanisms observed during secondary compression.

In the review done by Bodas Freitas (2008), there are two approaches that have been adopted in the literature, which include the End-Of-Primary (EOP) approach and the viscous approach. The first approach assumes that the secondary compression (creep) begins only after primary consolidation, whereas the second one assumes that creep occurs during the whole consolidation process, which in turn means that the strain at the EOP is not unique and that time-dependent creep strains take place during the primary consolidation.

Both approaches have been supported by experimental data, despite the fact that they are apparently contradictory. Leroueil (1995) performed a literature review for both approaches in order to examine the reasons for such a contradiction. This review claims that it is generally accepted that clays have viscous behaviour during primary consolidation, at least for strain rates encountered in the laboratory. However, when determining long-term field settlements from laboratory compression curves, the predicted settlements with the recorded ones are not in complete agreement. This is due to effects such as strain rate effects, structure development and temperature effects, which affect the soil deformation. Therefore, it is concluded that the true solution for long-term settlements deviates from the viscous approach and it is somewhere between the two extreme cases (Leroueil, 1995; Aboshi, 2004).

3.2.3. Time dependency of consolidation

Consolidation is a time dependent process, which is initiated by a pressure gradient resulting in a transient flow of pore water towards a free-draining boundary of the soil mass. The time taken for drainage of pore water to be completed depends on the permeability and the stiffness of the soil (both defining the coefficient of consolidation) and on the hydraulic boundary conditions. In soils of low permeability and/or low stiffness drainage is slow, whereas in soils of high permeability and/or stiffness drainage is rapid.

The permeability of soil is quantified through the coefficient of permeability, which depends primarily on the average size of the pores, which in turn is related to the distribution of particle sizes, particle shape and soil structure. In general, the smaller size the particles, the smaller is the average size of the pores and the lower is the coefficient of permeability. For a given soil, the coefficient of permeability is a function of void ratio and the smaller the void ratio the less permeable the soil is. Also, the presence of fissures in a clay affects the soil permeability. The water can flow quicker and, therefore, the permeability is higher than in an unfissured material.

The soil permeability also depends on temperature, which affects the viscosity of the pore water. Viscosity is a measure of the ability of a fluid to flow and its importance is highlighted in the following example given by Craig (1997). If the coefficient of permeability is measured at a room temperature of 20^oC, then at 10^oC and 0^oC the coefficient of permeability is 77% and 56% of the value at 20^oC respectively.

Typical values of the coefficient of permeability for different types of soil are given in Table 3.1, based on BS 8004:1986.

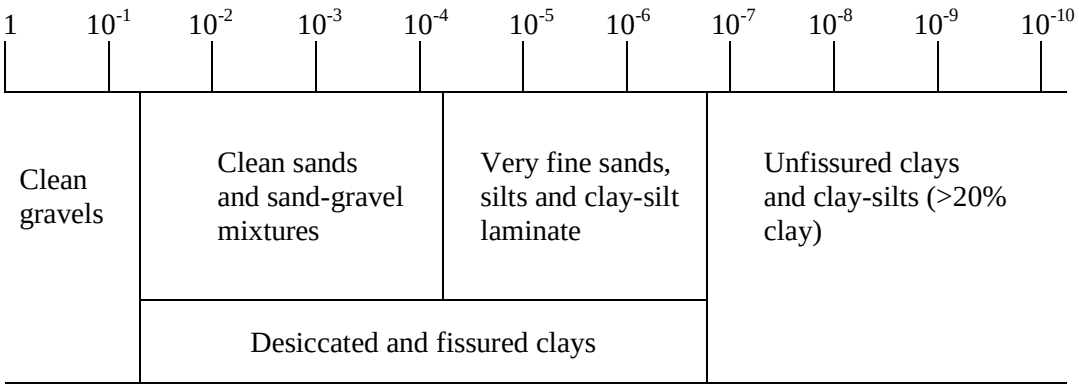


Table 3.1: Coefficient of permeability (m/s) (BS 8004: 1986)

3.3. VISCOUS BEHAVIOUR OF SOILS AND SOIL AGEING

Apart from consolidation, the time dependent behaviour of soils is usually divided into viscous effects and ageing effects. Viscous effects include time dependent processes such as:

(a) *Creep*: the development of strains at constant effective stresses;
(b) *Stress relaxation*: the continued decrease in effective stresses under constant strain conditions;
(c) *Rate effects*: the change in the stress-strain-strength soil response due to the rate of applied load/strain.

Viscous effects are believed to result mainly due to sliding at interparticle contacts and the associated particle re-arrangement, where the presence or absence of (free) water seems to have only a minor influence (Mitchell, 1993). Creep, stress relaxation and rate effects are time-dependent phenomena, which are all linked, and therefore they all fall into the same category of soil behaviour.

Ageing effects are the processes by which the soil gains structure, giving natural soil the additional components of strength and stiffness compared to the reconstituted soil, which cannot be accounted for by the void ratio and stress history alone. These are usually observed from the additional strength and stiffness of the soil after long periods of creep or stress relaxation, which cannot be accounted for by viscous effects. Ageing effects include the time-dependent structuration associated with physico-chemical processes such as thixotropy, bonding and cementation (Augustesen et al, 2004).

Viscous and ageing effects, after long periods of drained creep, are often difficult to distinguish, since both are time dependent and may take place simultaneously. Viscous effects may result in an apparent structuration upon loading after a drained creep period, which results in an increase in stiffness, yield stress and undrained shear strength as well. Both ageing and viscous effects after long periods of drained creep are coupled and are considered to show accumulated effects; however, there are fundamental differences between the apparent structuration associated with viscous effects and true ageing, as shown later.

Thixotropy, bonding and cementation of the soil are classified as inherent ageing effects in the review by Sorensen (2006), due to the fact that they do not require any interaction with the surrounding environment and may not in principle lead to any significant changes in the intrinsic properties of the soil (significant cementation will be an exemption). Other time

dependent changes to the soil structure may also rise due to the interaction with the surrounding environment, classified as environmental ageing effects by Sorensen (2006), which include weathering, chemical changes in pore water from external sources (e.g. leaching), heat, and pressure induced changes to the soil structure. Environmental ageing effects, in contrast to the inherent ageing effects, are considered to lead to changes in the soil composition and most likely to changes in the intrinsic properties of the soil as well.

There are three standard tests used to identify the time effects in soils: creep tests, stress relaxation tests, and constant rate of strain tests (CRS tests). In the following, the effects of such tests on soils, as well as the observed accumulated effects of soil viscosity and ageing in clays, will be discussed in order to distinguish various factors affecting the time dependent behaviour of clays.

3.3.1. CREEP AND STRESS RELAXATION

3.3.1.1. Definition of creep and stress relaxation

Creep is the development of strains at constant effective stresses and its characteristics can be fully determined from creep tests. Considering the stress-strain path of a soil during shearing to a stress-strain point A in Figure 3.2a, a creep test is defined as a test performed at constant effective stress conditions, i.e. from point A to B, where the stress is being kept constant with time (Figure 3.2b), while the strain is gradually increasing (Figure 3.2c). Such behaviour, i.e. from A to B in Figure 3.2c, indicates soil creep.

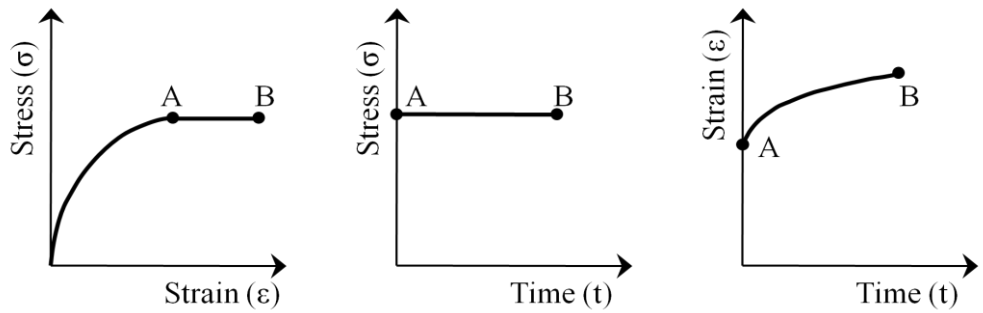


Figure 3.2: Creep test: (a) stress-strain relationship; (b) stress history; and (c) strain history

The rate of creep deformation is controlled by the viscous properties, or the viscous resistance, of the soil. The phenomenon of creep follows qualitatively similar trends for all soil types but, in general, the amount of creep deformation is found to increase with

increasing soil plasticity, water content and stress level, noting that larger creep deformation rates imply a decrease of the soils' viscous resistance (Sorensen, 2006).

On the other hand, stress relaxation is the continued decrease in effective stresses under constant strain conditions and its characteristics can be fully determined from stress relaxation tests. Considering the stress-strain path of a soil during shearing to a stress-strain point A in Figure 3.3a, a stress relaxation test is defined as a test performed at constant strain conditions, i.e. from point A to B, where the strain is being kept constant with time (Figure 3.3b), while the stress is gradually decreasing, i.e. relaxing (Figure 3.3c). Such behaviour, i.e. from A to B in Figure 3.3c, indicates soil stress relaxation.

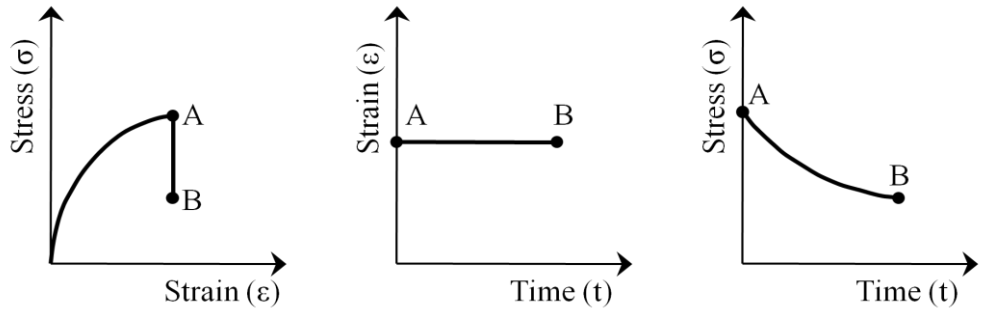


Figure 3.3: Relaxation test: (a) stress-strain relationship; (b) strain history; and (c) stress history

Creep and stress relaxation result from the same mechanism according to Lacerda and Houston (1973). The parameters that describe the stress relaxation process are equivalent to the creep parameters determined from the creep tests. Therefore, one could state that the reduction in effective stress during stress relaxation is directly linked to the creep potential at the same state.

3.3.1.2. Definition of creep phases

The creep process can be commonly divided into three phases: primary, secondary, and tertiary as shown in Figure 3.4. A decreasing, a constant, and an increasing strain rate define the three phases, respectively.

The primary phase is associated with the secondary compression, where the creep behaviour is characterised by reducing strain rates with time as described in Section 3.2.2. This behaviour is observed in one-dimensional oedometer tests or in triaxial tests at stress states far from failure.

For stress states close to failure during creep triaxial tests, secondary and tertiary creep phases may be observed, which are characterised by constant and accelerating strains rates with time respectively. The tertiary phase eventually leads to failure, a process referred to as creep rupture. It has been suggested by Mitchell et al. (1997) that creep rupture may be a result of progressive failure of interparticle bonds and associated reduction in effective stress caused by increases in water content or pore water pressure. Creep rupture is usually observed between the Critical State Line (CSL) and peak stress for overconsolidated (OC) soils according to Sorensen (2006).

It is noted that the creep phases described above are appropriate for deformations occurring after loading stages, and they are associated with an increase in the soil's mean effective stress. Creep behaviour following significant unloading stage is usually characterised by an initial phase of creep recovery, where creep strains give rise to further swelling, reversing to compression deformation after a period of time.

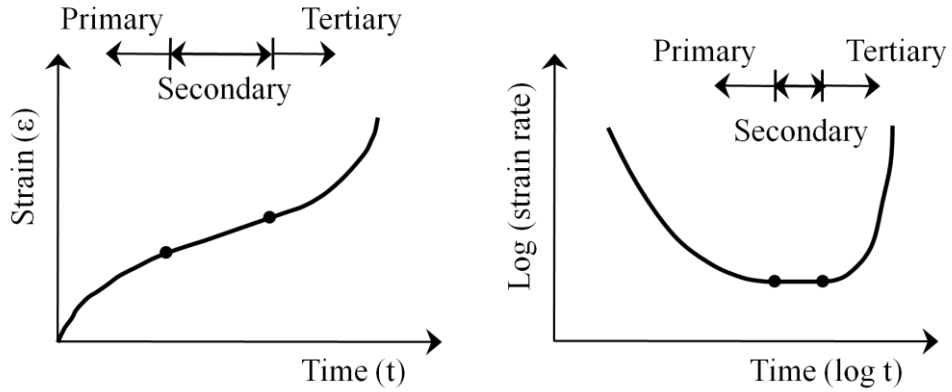


Figure 3.4: Definition of creep phases: (a) strain versus time; (b) strain rate versus log (time)

3.3.1.3. Quantification of creep behaviour

For engineering purposes, the compressibility of the soil with time during secondary compression can be quantified by the coefficient of secondary consolidation C_α, which is either expressed in terms of the relative change in void ratio Δe or the relative change in strain $\Delta \varepsilon$,

Equation 3.1 $$C_\alpha = \frac{\Delta e}{\Delta \log t}$$

Equation 3.2 $$C_{\alpha\varepsilon} = \frac{\Delta \varepsilon}{\Delta \log t}$$

The value of C_α is usually determined from oedometer tests, where load increments are maintained longer than 24 hours, the period required for excess pore water to fully dissipate, denoted as the end of primary consolidation in Figure 3.5. The value of C_α represents the change in e or ε with the logarithm of time, after EOP.

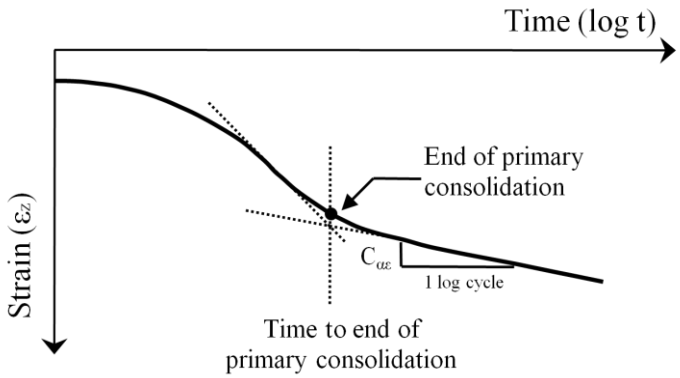


Figure 3.5: One-dimensional step load creep test: vertical strain versus log (time)

The relationship between creep strain and logarithm of time is usually assumed linear, however in many cases it has been found to deviate and show tendencies of either continuously increasing or decreasing gradients. To characterise that creep behaviour, Singh and Mitchell (1968) defined the parameter m, where:

Equation 3.3
$$m = \frac{\Delta \log \dot{\varepsilon}}{\Delta \log t}$$

The m parameter represents the relationship between the logarithm of creep strain rate ($\log \dot{\varepsilon}$) and logarithm of time ($\log t$) as shown schematically in Figure 3.6. The special case of m = 1 corresponds to a linear law between creep strain and the logarithm of time, i.e. a constant value of C_α.

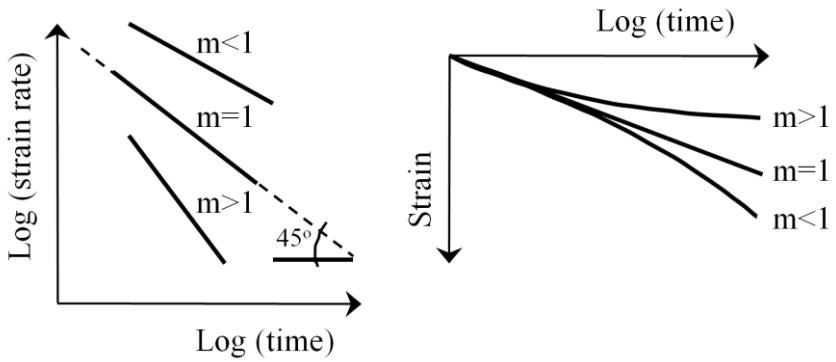


Figure 3.6: Relationship between the parameter $\boldsymbol{m}$ and the evolution of creep strain with time

3.3.2. RATE EFFECTS

3.3.2.1. Definition of rate effects

The effect of strain rate on the stress-strain-strength response can be investigated by means of CRS tests. A constant strain rate ($\dot{\varepsilon} = d\varepsilon/dt$) is enforced and kept constant throughout the experiment and the stress response is measured in order to obtain the stress-strain response. By comparing the soil stress-strain response at different values of strain rates, the rate effects can be evaluated.

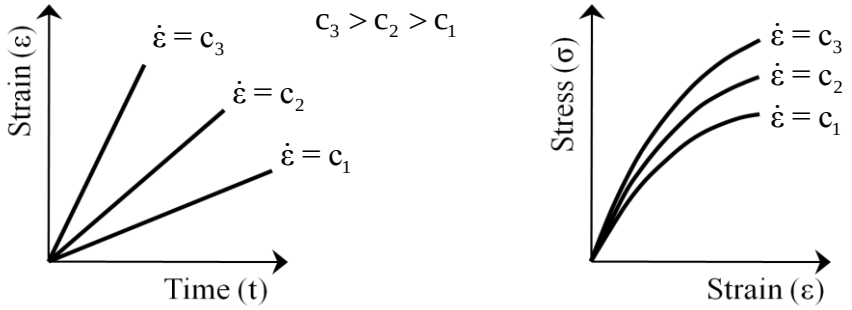


Figure 3.7: CRS test: (a) strain rate; (b) stress-strain response

In Figure 3.7, the stress-strain responses at three different strain rate values are shown. In general, it appears that the larger the strain rate, the larger the stress required to reach a certain level of strain. However, this is not the case for all soils; a fact that is explained by isotach and non-isotach viscosity.

3.3.2.2. Isotach vs. non-isotach viscosity

An important feature of soils in terms of rate effects is whether they exhibit isotach or non-isotach behaviour. Isotach behaviour is followed by soils which have rate effects and, therefore, they are characterised by a unique stress-strain-strain rate relation, whereas non-isotach behaviour is followed by soils not having rate effects. This means that isotach viscosity is symbolised by a unique relation between stresses and strains dependent on strain rate and the effects of change in strain rate are continuous, whereas in non-isotach viscosity the stress-strain relationship is independent of strain rate and effects of strain rate change are temporary. In general, clays are known to follow isotach behaviour, whereas sands do not (Augustesen et al, 2004).

In Figure 3.8, stress-strain plots of isotach and non-isotach viscosity are shown, from which their differences are explored. In particular, on the left hand plots (isotach behaviour), it is shown that a change in strain rate, for instance from $\dot{\varepsilon}_B$ to $\dot{\varepsilon}_A$, results in a different stress-strain path than the one followed initially. The new path is consistent with the one that would be followed if the soil was sheared from the beginning with $\dot{\varepsilon}_A$. In addition, a drop in the strain rate from $\dot{\varepsilon}_A$ to $\dot{\varepsilon}_B$ results in a shift of the stress-strain path to the path that was originally followed. On the right hand plots in Figure 3.8 (non-isotach behaviour), a change in strain rate results in a temporary shift of the stress-strain path, without a persistent effect. In addition, non-isotach viscosity is symbolised by a non-dependent stress-strain path on strain rate, i.e. no rate effects, as shown from the path followed for the strain rates $\dot{\varepsilon}_A$, $\dot{\varepsilon}_B$ and $\dot{\varepsilon}_C$.

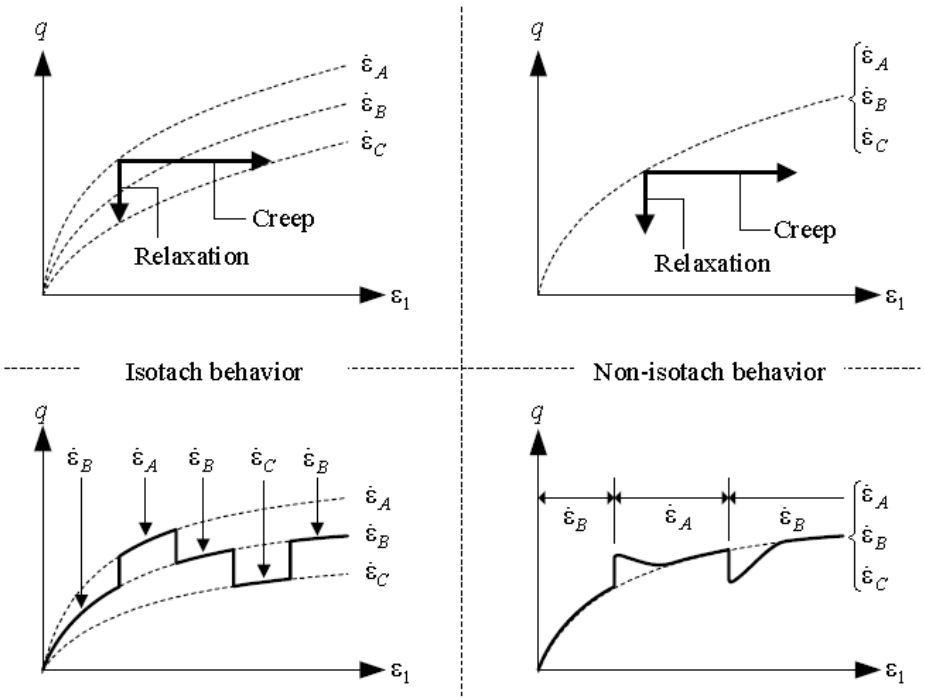


Figure 3.8: Isotach viscosity vs non-isotach viscosity: clays vs sands (Augustesen et al, 2004)

In isotach viscosity, the phenomena of creep, relaxation, and strain rate effects are governed by the same unique time-mechanism, implying that creep properties can be obtained by CRS tests and relaxation tests and vice versa. If the stress-strain paths for two different strain rates are considered in Figure 3.9, isotach viscosity implies that the unique stress-strain-strain rate relation at B can be reached by creep (OAB), relaxation (OA'B') or by enforcing a constant rate of strain (OB). This is not the case for soils exhibiting non-isotach viscosity, since the effects of change in strain rate are temporary as shown in Figure 3.8.

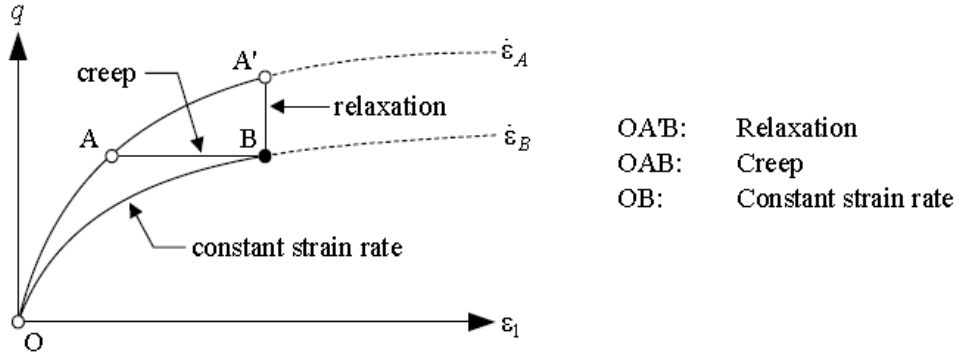


Figure 3.9: Isotach viscosity: unique stress-strain-strain rate relation (Augustesen et al, 2004)

According to Tatsuoka et al. (2002), viscosity of soils can be categorised into three groups: isotach behaviour, (pure) TESRA (Temporary Effect of Strain Rate and strain Acceleration) behaviour and General TESRA behaviour. The TESRA behaviour describes the viscous behaviour of soils which show temporary viscous effects (pure non-isotach behaviour), whereas the General TESRA behaviour describes the behaviour of soils which show a combination of temporary and persistent viscous effects and in general temporary effects are seen to increase with straining. The characteristics of each category and the soils which demonstrate this type of behaviour are summarised in Table 3.2 (after Sorensen, 2006).

Phenomenon	**Viscous characteristics**	**Observed in**
Isotach	• Separate CRS curves • Unique relationship between stress, plastic strain and its rate independently of strain history • Persistent effect of strain rate changes	• Soft clays (undisturbed and reconstituted) • Some soft rocks • Undisturbed stiff natural clays
(pure) TESRA	• Non-persistent temporary effect of strain rate changes • Overshooting and undershooting of the persistent CRS curve after changes in strain rate and subsequent decay towards a single unique CRS curve	• Clean sands
General TESRA	• Increasing TESRA effect with increasing strain • In the case of clays the TESRA effect is not observed at low stress levels, only at higher stress levels does the TESRA effect become increasingly apparent	• Cemented soils • Some dense gravels • Dense silty sands • Reconstituted stiff natural clays

Table 3.2: Viscous characteristics of soils (Sorensen, 2006)

Whether soils exhibit isotach or non-isotach viscosity is of fundamental importance when considering the modelling of the time-dependent behaviour of soils. Isotach viscosity is considered as appropriate to model the time effects in clays that result only from soil viscosity. However, there are some drawbacks according to Augustesen et al. (2004), which arise from the incapability of the isotach model to explain other simultaneous time effects that cause the development of soil structure. The first drawback is that isotach viscosity cannot explain the development of structure at very low strain rates. In Figure 3.10a, the effect of structuration at very low strain rates is shown, where the stress-strain path deviates from the unique stress-strain-strain rate relation denoted as isotach. The second drawback arises after long periods of ageing due to creep. As shown in Figure 3.10b, additional strength and stiffness is gained after a long period of creep in respect to what is expected by isotach behaviour, which is a result of structuration resulting from ageing. Structuration is mainly associated with the strengthening of the contacts between clay particles, which cannot be predicted by isotach viscosity as described next in detail. These phenomena are further described below.

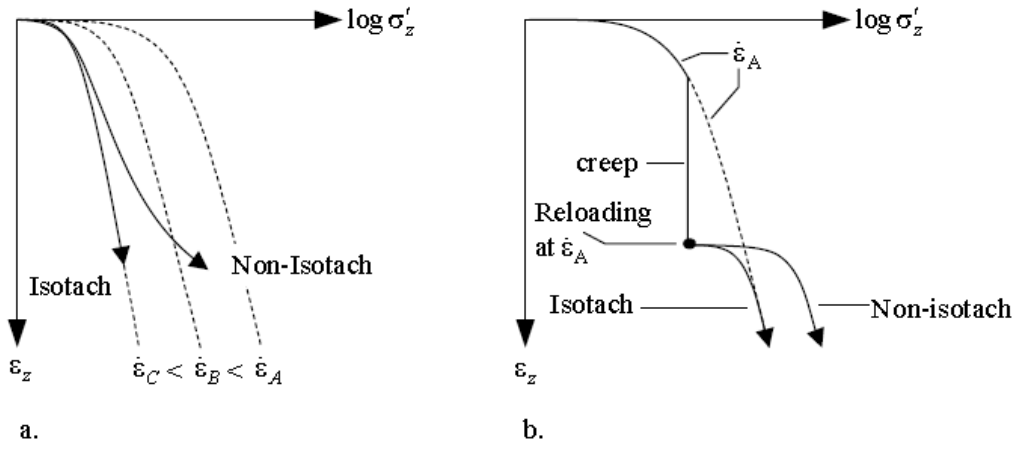


Figure 3.10: Non-isotach behaviour of clays: (a) at very slow rates, (b) after long period of creep (Augustesen et al, 2004)

3.3.3. ACCUMULATED EFFECTS

Accumulated effects are referred to as those effects which are observed after long periods of creep. They may include both viscous and ageing effects, and it is often difficult to distinguish them, since they are both time dependent and may take place simultaneously, according to Bodas Freitas (2008). Experimentally, accumulated effects take place in both one-dimensional and triaxial compression tests, and in particular they are observed through

changes of the yield locus, subsequent state paths and strength envelopes after long periods of ageing.

Depending on the creep test performed, Havel (2004) distinguishes the creep behaviour as either volumetric or deviatoric creep. Volumetric creep describes observations made in one-dimensional or isotropic compression, whereas deviatoric creep describes those made in triaxial compression tests under constant deviatoric stress. The main difference between volumetric creep and deviatoric creep is that the volumetric creep consists only of the primary phase of creep deformation, i.e. it tends to stabilise, whereas deviatoric creep may consist of all three phases defined in Section 3.3.1.2, depending on the shear mobilisation. If the deviator stress is low, then only the primary phase appears, but at higher deviatoric stress close to failure, the primary phase is followed by the secondary phase which eventually can lead to the tertiary phase and creep rupture. A literature review on the observed volumetric and deviatoric creep behaviour in clays is given below.

3.3.3.1. Observed volumetric creep behaviour in clays

In one-dimensional compression, the apparent preconsolidation pressure or yield stress increases during secondary compression. Bjerrum (1967) proposed the concept of isochrones or time lines as illustrated in Figure 3.11, which represent the equilibrium void ratios for specific times of sustained loading at various stress levels. The isochrones are parallel lines in the e-logσ_v' plane and represent also constant strain rate lines. The example illustrated in Figure 3.11 shows a soil which is subjected to a constant effective stress for a long period of time, where the void ratio and strain rate progressively decrease as a result of creep (denoted delayed compression). The concept elaborates that if the soil is reloaded, an increase in the yield pressure is observed, which is higher than the stress that the soil had been subjected to previously, without causing significant volumetric changes. This is referred to as apparent preconsolidation or quasi-overconsolidation by Bjerrum (1967). An example of such behaviour is shown in Figure 3.12, where Tatsuoka (2003) performed a typical constant rate of strain (CRS) oedometer test on reconstituted Fujinomori clay. The soil sample was left to creep for a period of 24 hours and it was then reloaded at the original rate. It is observed that the initial stiff response after creep is followed by gradual yield after which the state path rejoins the normal compression line defined by the original rate. Such behaviour is a result of pure volumetric creep and it is attributed to the reduction in void ratio with time.

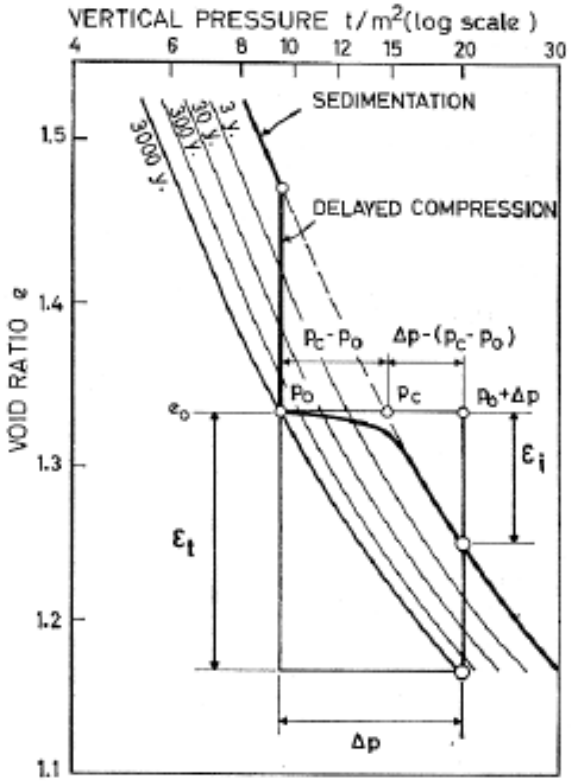


Figure 3.11: Concept of isochrones or time lines for the 1D compression of soft clays (Bjerrum, 1967)

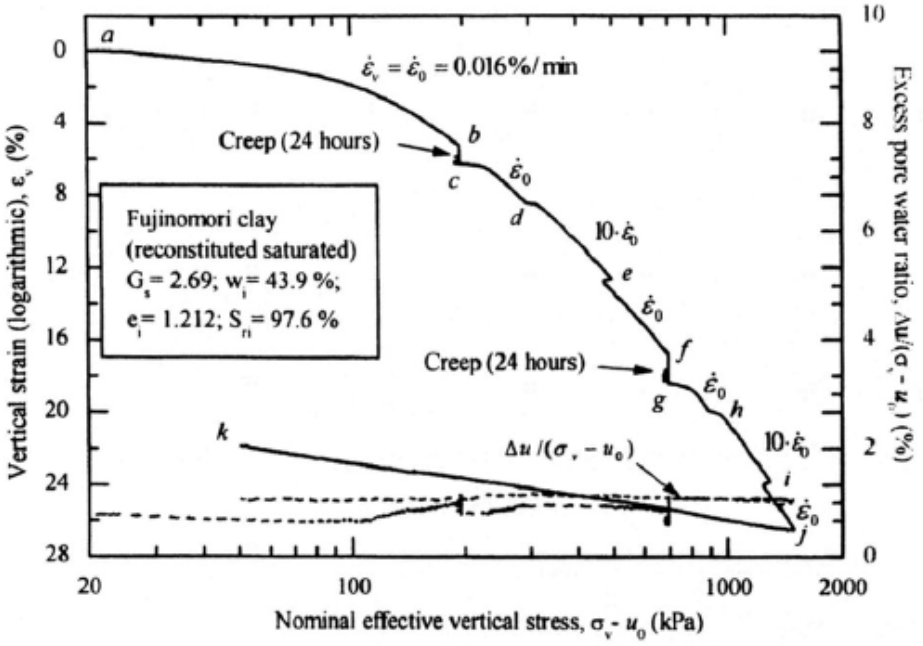


Figure 3.12: Influence of drained creep on subsequent one-dimensional compression behaviour in CRS oedometer tests on reconstituted Fujinomori clay (Tatsuoka, 2003)

Some studies in the literature, however, have shown that soils exhibit a preconsolidation pressure much higher than that due to its new void ratio only. This is attributed to the development of bonds between particles or aggregates due to soil ageing and is referred to as "structuration" by Augustesen et al. (2004). A schematic diagram in Figure 3.13 produced by Bodas Freitas (2008) shows the behaviour of a soil element following a drained creep period due to (a) viscous effects, and (b) viscous and structure effects. According to the isochrone concept for pure viscous behaviour, on reloading of a soil element after a creep period, it will have an initial stiff response due to its apparent preconsolidation, followed by a gradual yielding until the stress path rejoins the normal compression line (NCL) corresponding to the strain rate. However, when structuration (soil ageing) takes place during the creep period, on reloading an overshooting across the original NCL is observed, which can not be accounted for by rate effects. Eventually, destructuration may be observed at higher stresses where the stress path rejoins the original NCL.

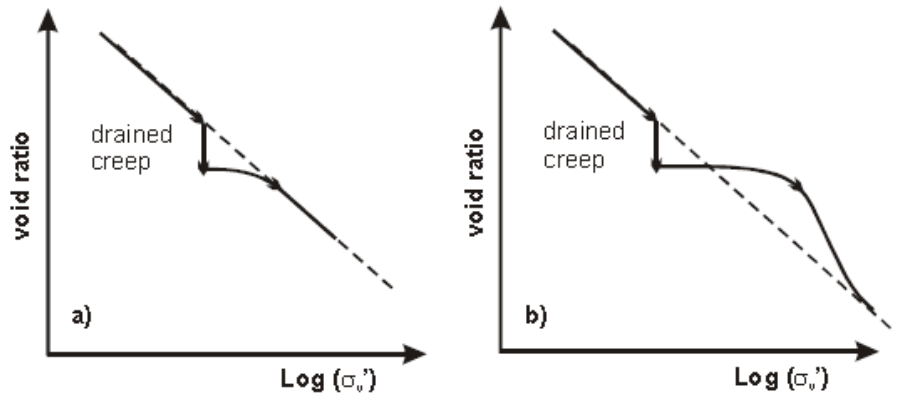


Figure 3.13: Schematic diagram of the behaviour of a soil element following a drained creep period; (a) pure viscous behaviour; (b) viscous and structure effects. (Bodas Freitas, 2008)

According to Augustesen et al. (2004), the structuration phenomenon is related both to time and strain rates. This means that the longer the duration of the secondary compression, the larger the development of structure in the soil. In addition, the slower the rate of loading is, the larger the potential for development of structure, as shown below.

A significant ageing effect has been observed among others by Perret et al. (1995), as reported by Leroueil et al. (1996), in tests on artificially sedimented Jonquiere clay, as shown in Figure 3.14, where the sample was left to creep for 120 days in drained conditions under a constant stress of 10 kPa, before being loaded again. As can be seen, the yield stress after ageing is significantly greater than that would be expected due to the reduction of void ratio due to the

viscous nature of the soil. Beyond this stress level, destructuration forces the compression curve back towards the unaged compression line with a steeper gradient than the original one.

A similar test reported by Tatsuoka et al. (1998) on Fujinomori clay (after Momoya, 1998) showed similar behaviour (Figure 3.15). Upon reloading the response is much stiffer, however the compression curve does not join the intrinsic compression, but it overshoots it, showing ageing effects on the yield pressure. The sample was left to creep for 30 days. A parallel study on the initial stiffness showed an increase in stiffness during creep as well. Initial stiffness M_0 was obtained for different periods of ageing up to 30 days as shown in Figure 3.15.

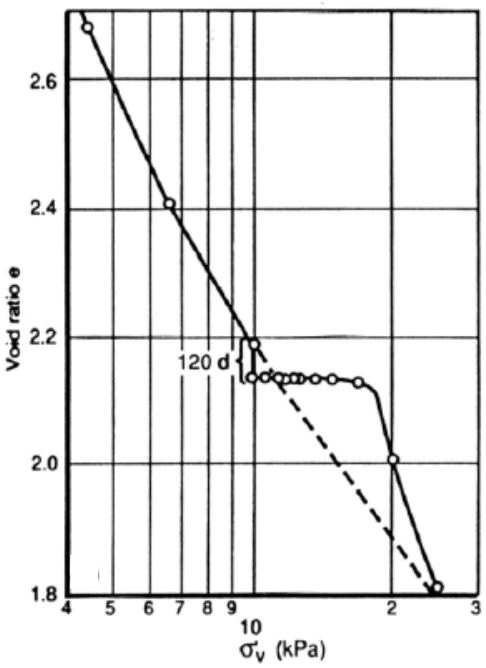


Figure 3.14: Influence of drained creep on one-dimensional compression behaviour in tests on artificially sedimented Jonquiere clay (Leroueil et al., 1996; after Perret et al, 1995)

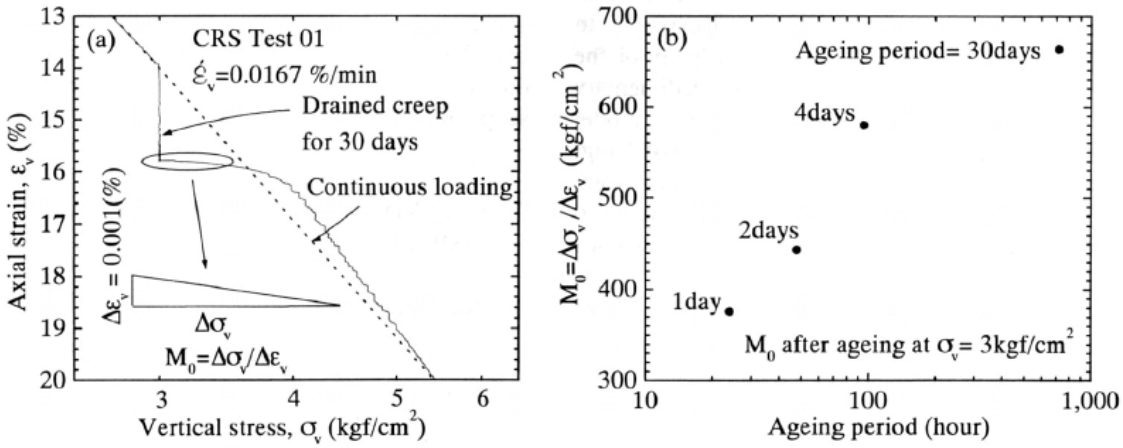


Figure 3.15: Influence on drained creep on the compression behaviour of reconstituted Fujinomori clay and change in initial constraint modulus M_0 for different ageing periods (Tatsuoka et al., 1998; after Momoya, 1998)

Regarding the development of structure at slow rates of loading, Leroueil et al. (1996) performed a series of oedometer compression tests on artificially sedimented Jonquiere clay, including a conventional 24-hours load step compression tests and CRS compression tests at two different strain rates of $1.27\text{x}10^{-5}$ s^{-1} (4.6%/hr) and $1.00\text{x}10^{-7}$ s^{-1} (0.036%/h); the conventional oedometer test corresponded to a strain rate of approximately $1.00\text{x}10^{-7}$ s^{-1}.The three tests were compared and a unique stress-strain-strain rate relationship was presumed being consisted with isotach viscosity, as discussed in Section 3.3.2.2. Therefore, it was expected that (a) the slow CRS compression test should coincide or at least should be very close to the conventional oedometer test and (b) the rapid CRS compression test should plot above the others. The expected trend was observed between the results of the conventional oedometer tests and the rapid CRS compression test. However, as shown in Figure 3.16 the slow CRS test turned out to be very different from the conventional oedometer test. In particular, it can been seen that the compression curve for the slowest strain rate is stiffer and it is even located above the higher strain rate curve and the curve for the conventional oedometer test. Such behaviour does not agree with the unique stress-strain-strain rate relationship and it was attributed to the progressive structuration (ageing), which takes place at slow strain rates. On the other hand, for the rapid test, insufficient time was available for structure to develop. Regarding the 24-hours oedometer test, structure might have formed during each load step, however it was destroyed after the application of a new load on the subsequent load step according to Leroueil et al. (1996). Structuration at slow rates has been described by Augustesen et al. (2004) as well, as already noted in section 3.3.2.2.

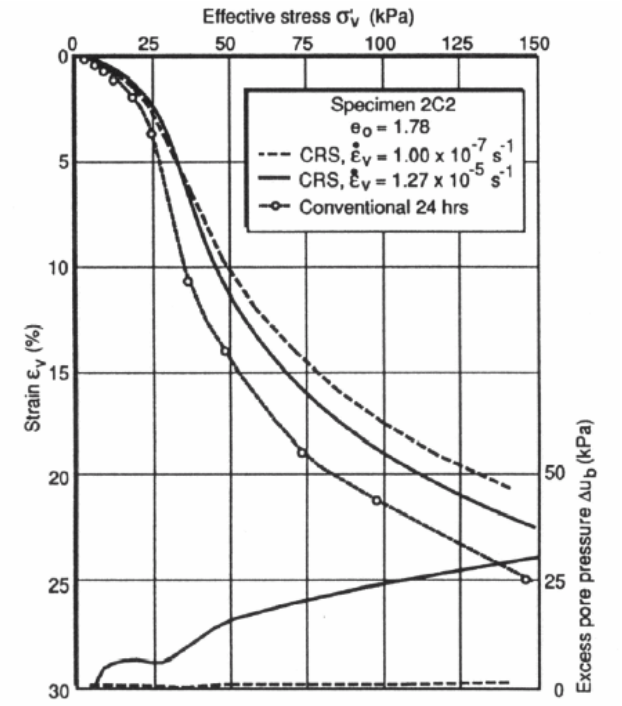


Figure 3.16: Effect of slow rate on straining on the one-dimensional compression behaviour of artificially sedimented Jonquiere clay (Leroueil et al, 1996)

3.3.3.2. Observed deviatoric creep behaviour in clays

Patterns similar to the observations in one-dimensional conditions have been reported in triaxial tests. Arulanandan et al. (1971) present results from undrained triaxial creep tests on San Francisco Bay mud at different stress levels in Figure 3.17, where it is seen that the isochrone concept proposed by Bjerrum (1967) in one-dimensional compression can extend to the entire yield surface in triaxial stress space. More particularly, stress loci at different creep times are plotted, where it is observed that the entire yield envelope in stress space progressively moves towards smaller stresses with time, while keeping the same shape. The decrease in stresses with time was attributed to the observed increase of pore water pressure with time.

Recently, the concept of isochrones has been replaced by the concept of constant rate of strain curves, which defines the framework for the influence of viscosity on the stress-strain behaviour as described in Section 3.3.2.2. Tavenas et al. (1978) performed drained triaxial tests on undisturbed lightly overconsolidated St. Alban clay, from which Figure 3.18 was deduced in order to show contours of equal volumetric strain rate at a creep time equal to 100 minutes. In particular, a series of creep tests were carried out at stresses located on the lines 0 to 5 shown in Figure 3.18 and at various stress levels progressively closer to the limit state surface, from which contours, containing the loci of the stress states that yield the same

volumetric strain rate after 100 minutes, were plotted. It is observed that the lines of equal volumetric strain rate have the same shape as the limit state surface and plot in parallel, with an ascending rate towards the limit state.

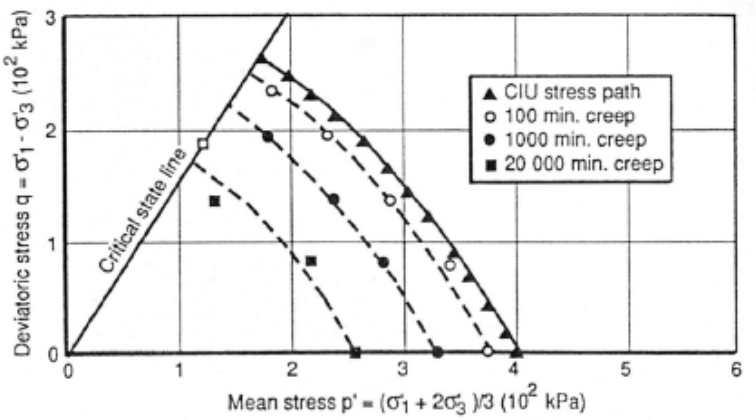


Figure 3.17: Influence of creep time on the yield envelope in triaxial stress space in tests on San Francisco Bay mud (Arulanandan et al, 1971)

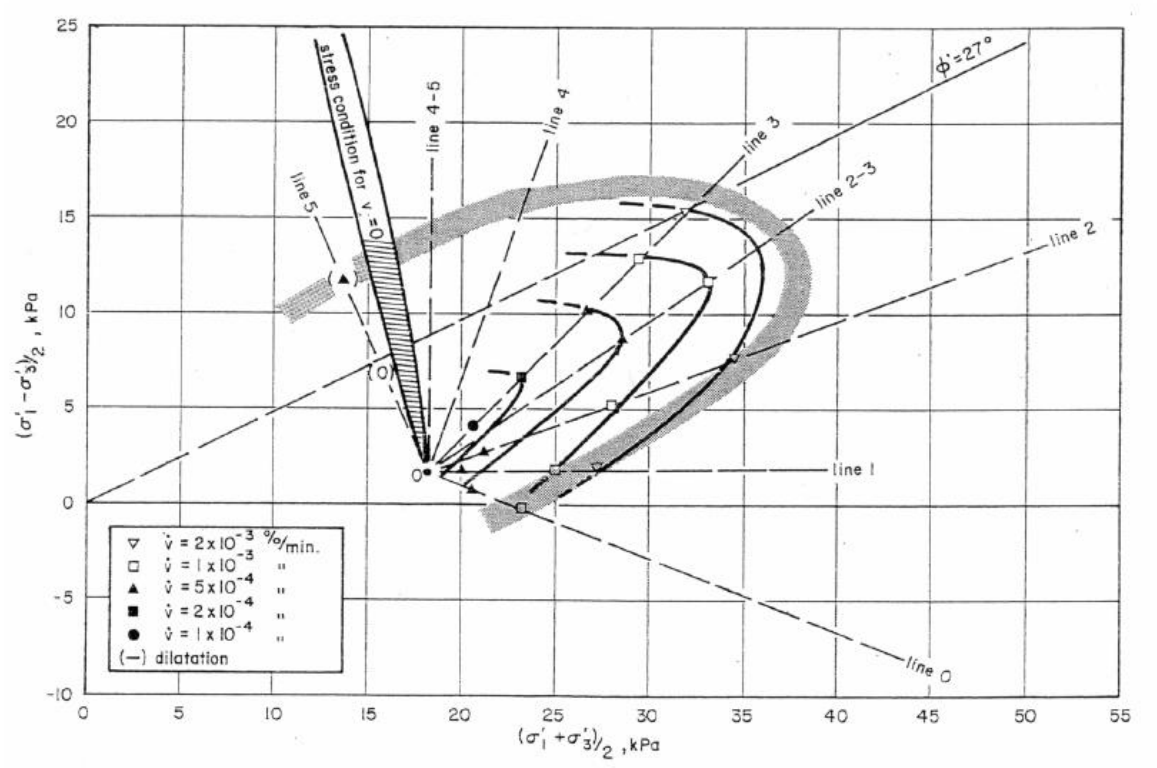


Figure 3.18: Influence of volumetric creep rate on the limit state curve from drained triaxial tests on undisturbed lightly overconsolidated St. Alban clay (Tavenas et al, 1978)

Furthermore, Tavenas et al. (1978), based on their findings, proposed a general model for the effect of time on the yield envelopes, as shown schematically in Figure 3.19. Yield envelopes and stress state zones I to IV, affecting the behaviour of clays during creep as described below, are shown in Figure 3.19a, along with the respective constant rate of strain lines in Figure 3.19b. This model assumes that if a soil element is loaded to state B on the Y_0 yield envelope, and then the soil element is left to creep for a period of time (from B to B' in Figure 3.19b), the current yield envelope expands to the 'aged' Y_1 envelope. Based on this model, creep rupture, a mechanism observed in triaxial compression (deviatoric creep conditions) and not in one-dimensional compression (volumetric creep conditions), is only observed if the stress state is moved to zones I or IV above the failure line and outside the Y_0 yield envelope.

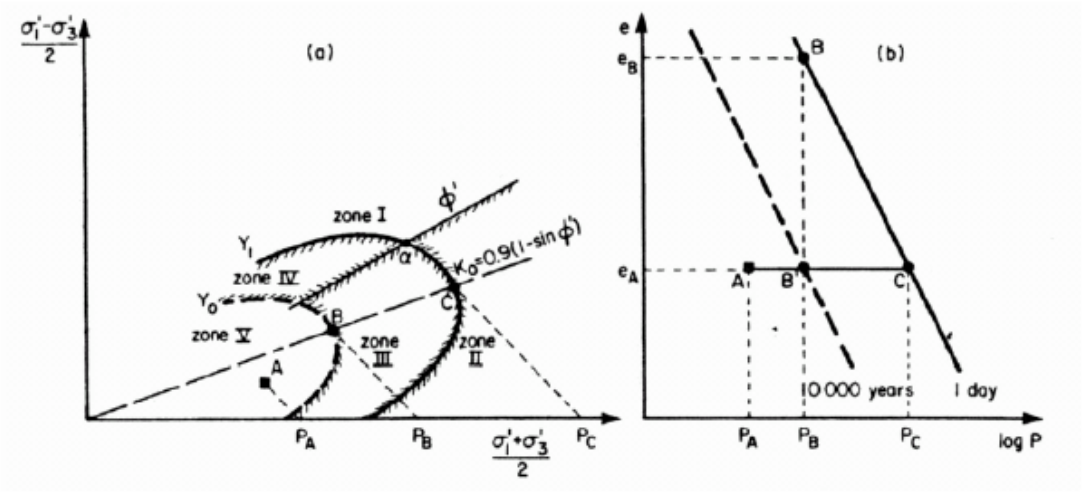


Figure 3.19: Proposed general model of the effects of time on the yield envelope of clays (Tavenas and Leroueil, 1977)

Creep rupture, as discussed in Section 3.3.1.2, occurs at soil states close to failure, where an acceleration of creep strain rate is observed leading eventually to failure. Results in the literature, which are in agreement with the proposed concept, include those of Bishop (1966) from drained triaxial creep tests on undisturbed London Clay (Figure 3.20) and of Vaid and Campanella (1977) from undrained triaxial creep tests on undisturbed Haney Clay (Figure 3.21). In Figure 3.20, the development of axial strain with time during a long-term period of creep under drained conditions for a series of drained triaxial creep tests on undisturbed London Clay is presented by Bishop (1966). It is observed that under constant deviatoric stress, there is a continuous development of axial strains for the majority of stress levels. However, at a stress level close to the peak stress, creep rupture takes place accompanied with acceleration in the creep strain rate. In Figure 3.21, the variation of axial strain rate with time under constant deviatoric stress for undrained triaxial creep tests on undisturbed Haney Clay

by Vaid and Campanella (1977) is shown, along with the influence of deviatoric stress on the rupture life. Vaid and Campanella (1977) suggest that an upper yield stress existed below which creep rupture would not occur. For stress levels above the yield stress the time taken to rupture was proportional to the applied stress, while for stress levels below the yield stress the samples showed a continuously decreasing creep rate. Also, they suggested that creep rupture in undrained conditions took place due to an increase in pore water pressure.

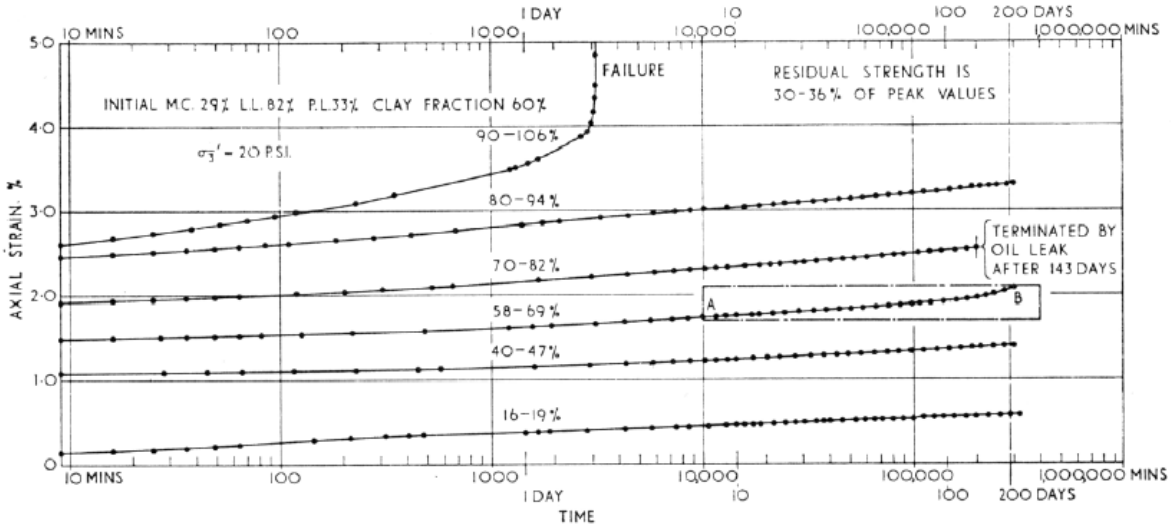


Figure 3.20: Influence of deviator stress in drained triaxial creep tests on undisturbed London Clay (Bishop, 1966)

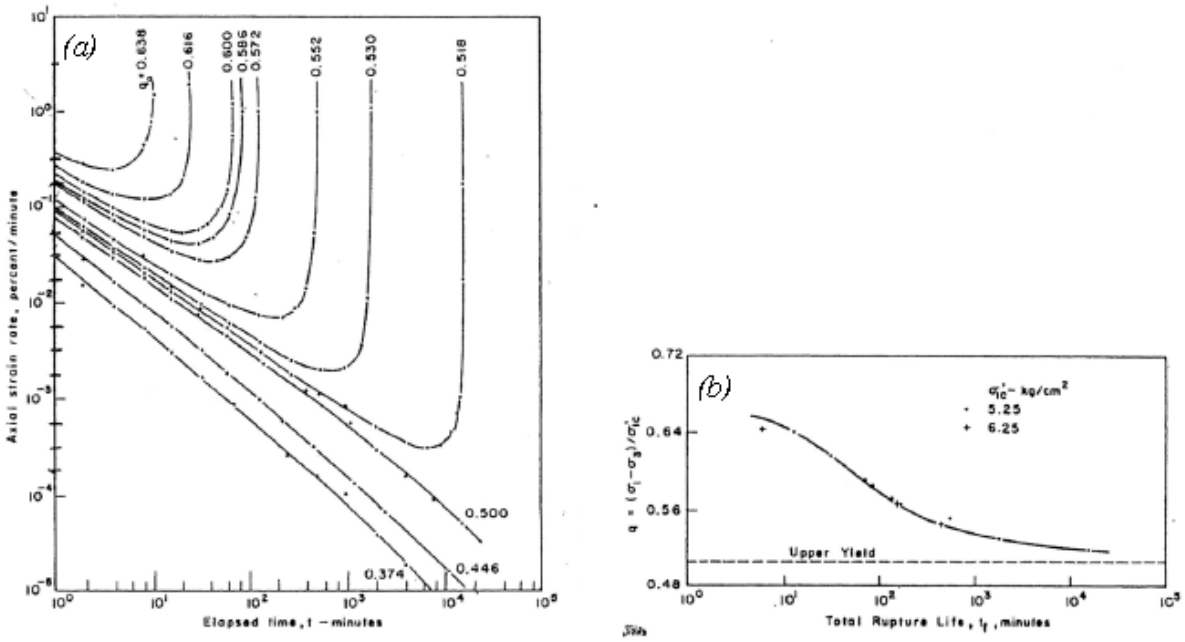


Figure 3.21: (a) Variation of creep rate with time in constant stress creep; (b) influence of deviator stress level on the rupture life in undrained triaxial compression of undisturbed Haney clay (Vaid and Campanella, 1977)

Next, Figure 3.22 shows results from undrained triaxial tests on undisturbed Vallerica clay performed by Santucci de Magistris et al. (1998), where a similar, stiffer, response to one-dimensional compression conditions is observed upon reloading after a period of drained creep under constant deviatoric stress. However, it is not clear whether the stress path rejoins that associated with the original strain rate or whether it overshoots it due to the coupled effect of creep (reduction in void ratio which results to increase of shear strength) and ageing.

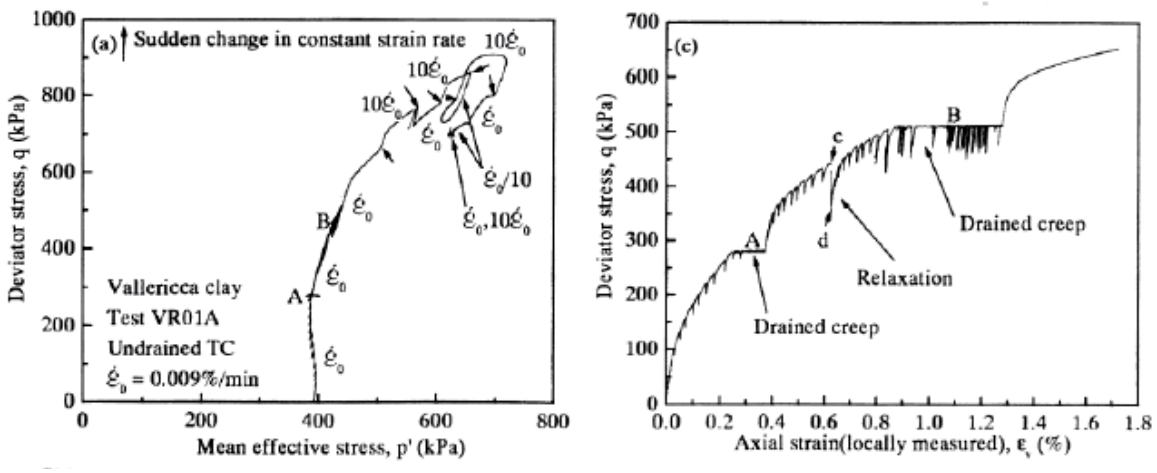


Figure 3.22: Influence of drained creep on subsequent undrained shearing behaviour in triaxial compression of undisturbed Vallerica clay (Santucci de Magistris et al., 1998)

Tatsuoka et al. (1998) report on undrained triaxial compression tests on normally consolidated reconstituted Fujinomori clay (after Momoya, 1998), where the effects of undrained and drained creep on subsequent reloading were examined. In Figures 3.23 and 3.24, the results of two samples, which were isotropically consolidated and then sheared under the same conditions, are presented. The difference between the two tests is that one sample was left to creep under undrained conditions for one day, whereas the other one in drained conditions for two days, before continuing undrained shearing to failure. From the q-p' plot in Figure 3.23, it can be seen that the stress state gradually moved to the left during undrained creep due to the increase in pore water pressure. On reloading at the same rate, an initial stiff response was observed and the stress-strain path then slightly overshot the original path. At failure, a gain in undrained shear strength is also observed for the sample which had experienced creep. The conclusion derived was that, since volume changes were absent during undrained creep and rate effects did not play a role, this gain in undrained strength was attributed to inherent ageing effects. Regarding drained creep, a similar set of tests, where the one sample was left to creep in drained conditions for two days, was performed by Momoya (1998). Results are

plotted in Figure 3.24 and this time they are normalised with respect to the changes in void ratio. Once again, it is seen that there is a gain in undrained shear strength due to soil ageing.

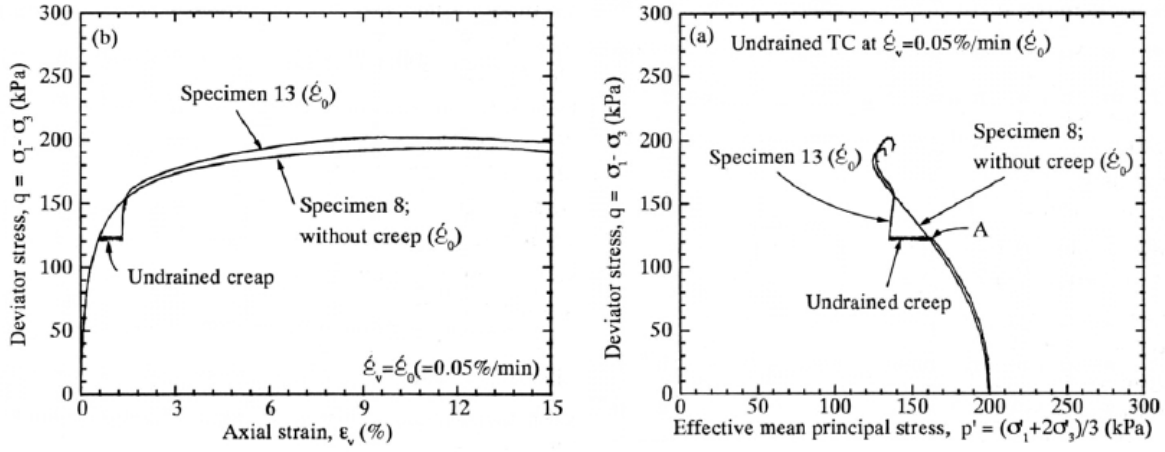


Figure 3.23: Influence of undrained creep on subsequent stress-strain behaviour in undrained triaxial compression on Fujinomori clay (Tatsuoka et al., 1998; after Momoya, 1998)

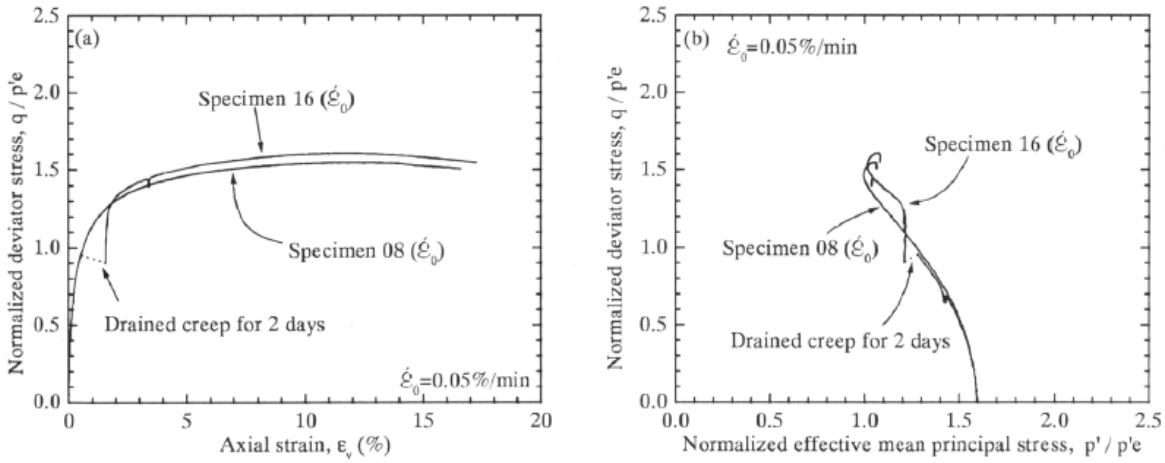


Figure 3.24: Influence of drained creep on subsequent stress-strain behaviour in undrained triaxial compression of Fujinomori clay (Tatsuoka et al., 1998; after Momoya, 1998)

Tatsuoka et al. (1998) prepared a summary of the accumulated phenomena due to the coupled effects of soil viscosity and ageing. They summarise three types of post ageing stress-strain relationships after a long period of constant deviatoric stress, when the soil is reloaded at the same strain rate as initial loading, without considering mechanical overconsolidation due to changes in void ratio during ageing. These are presented schematically in Figure 3.25, where they are classified as:

- Type 1, ageing without structuration: The stress-strain path after ageing rejoins the original path without exhibiting overshooting (B to C) (isotach viscosity)

- Type 2, temporary structuration effects: The stress-strain path after ageing rejoins the original path after exhibiting a temporary overshooting (B to D) (non-isotach viscosity)
- Type 3, persistent structuration effects: The stress-strain path after ageing does not rejoin the original path and there is a persistent overshooting. A larger peak strength is obtained due to the development of structure. It should be noted that this is the case for a constant strain rate before and after ageing.

In all cases, an initial stiff response is observed. However, whether the stress-strain path follows Type 1, 2 or 3, depends on the material tested and the loading conditions. It has been shown in the literature that natural clays follow isotach viscosity (Type 1), however when the soil is reloaded after periods of ageing, structuration effects have been observed. The additional stiffness due to structuration (Type 3) cannot be explained by isotach viscosity. On the other hand, sands are known to follow Type 2, as described in detail by Augustesen et al. (2004).

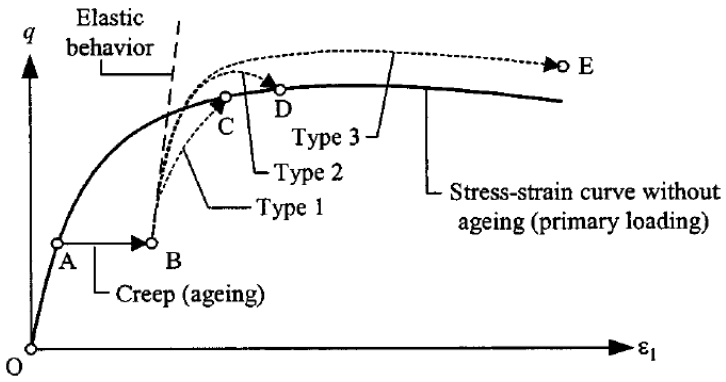


Figure 3.25: The three types of post-aging stress-strain relationships (Tatsuoka et al, 1998)

3.4. CONCLUDING REMARKS

Time effects on soil behaviour are an important element of this research. The aim of this chapter was to review the time dependent behaviour of soils, and in particular of saturated clays, in order to assess the main aspects required to be reproduced in numerical analysis of piled foundations. These include consolidation, soil viscosity and time dependent structuration (soil ageing), which are shown to have coupled effects on soil behaviour, despite the fact that different mechanisms drive these effects.

Consolidation results from a hydraulic gradient due to a stress change, whereas soil viscosity and ageing result purely due to time effects on soil behaviour. Viscous effects include phenomena such as creep, stress relaxation and strain rate effects, whereas soil ageing or structuration corresponds to a gain of additional components of strength and stiffness that cannot be accounted for by void ratio and stress history alone.

Most soils show identical behaviour during creep and stress relaxation, which is an increase in strain or a reduction in effective stress respectively with time. Several creep phases have been identified, which depend on the loading conditions. In deviatoric creep conditions, an acceleration in creep strain rate may be observed for stress states close to failure, leading to creep rupture, which is not observed in volumetric creep conditions where the stress state is far from failure.

An important feature of soils in terms of modelling is their strain rate effects and whether soils exhibit isotach or non-isotach viscosity. Isotach viscosity implies a unique stress-strain-strain rate relationship, whereas non-isotach viscosity, including pure and general TESRA behaviour, does not. In general, clays are known to exhibit isotach viscosity, whereas sands do not.

Chapter 4

Constitutive Models

4.1. INTRODUCTION

Two constitutive models, able to simulate the behaviour of saturated clays, are employed in the finite element analyses presented in this thesis. One is a form of the well known Modified Cam Clay model, whereas the other is the recently developed time-dependent Equivalent Time Creep model by Bodas Freitas (2008), which can account for soil viscous behaviour. The main focus in this work is on the latter model due to the fact that it can reproduce soil deformations due to creep.

In this chapter a brief summary of the finite element method is first presented. In particular, the theory behind the finite element method for linear and non-linear materials is presented, as well as pore water pressure considerations for the coupled nature of the finite element analyses performed. A description of the Modified Cam Clay model is then given, by considering its formulation in general stress space. The Equivalent Time Creep model, a time dependent model that can reproduce isotach viscosity, is then described by considering the assumptions involved, its formulation under isotopic stress conditions and its extension to general stress space. Several features of the model are described, including the modelling of destructuration upon loading. Finally, further validation of the Equivalent Time Creep model, in addition to that performed by Bodas Freitas (2008), is undertaken in order to examine the accuracy of the model in reproducing the behaviour of natural clays.

4.2. FINITE ELEMENT METHOD

The finite element method is a sophisticated form of numerical analysis, which has been used for the last forty years in many engineering fields, including geotechnical engineering. The main advantage of this method in respect to other methods of analysis is that it is able to satisfy, albeit approximately, the four fundamental requirements for a true theoretical solution. These are equilibrium of forces, compatibility of displacements, material constitutive behaviour and boundary conditions. In addition, the finite element method can satisfy the two additional requirements in coupled consolidation analyses, which are the continuity of flow and the generalised Darcy's law.

The accuracy of the finite element solution depends on the ability of the constitutive model to represent real soil behaviour and on the correctness of the boundary conditions imposed in the analysis. It is the responsibility of the geotechnical engineer to assess these parameters in design, in order to reflect accurately the field conditions. Time can be incorporated as well through coupled consolidation analyses, where the effect of time on the development of pore water pressures can be simulated.

The software package used for the finite element analyses in this thesis is the Imperial College Finite Element Program (ICFEP, Potts and Zdravkovic, 1999). This sophisticated code makes use of the displacement based finite element method and is able to perform two-dimensional (axi-symmetric, plane strain, plane stress), three-dimensional and Fourier series aided three-dimensional analyses. In this thesis, axi-symmetric analyses are performed for the single element runs and single pile runs, whereas for the complicated piled raft foundations three-dimensional analyses are applied.

A detailed description of the finite element method theory formulation, as well as practical applications, can be found in Potts and Zdravkovic (1999, 2001). In the following, a brief review of the finite element theory for linear materials is presented. Non-linearity in finite element analysis, and in particular in ICFEP, is then discussed, followed by a description of the finite element formulation for coupled problems.

4.2.1. Finite element theory for linear materials

The formulation of the finite element method, as described by Potts and Zdravkovic (1999) involves the following steps:

(a) Element discretisation

This is a process where the geometry of the problem under investigation is modelled. A number of finite elements comprise the finite element mesh. Finite elements have nodes on the element boundaries, or within the element, defined through a coordinate system. In this thesis, eight and twenty noded isoparametric elements are employed in ICFEP for the 2D and 3D analyses respectively.

(b) Primary variable approximation

A primary variable is selected (e.g. displacements, stresses etc.) and rules on how it varies over a finite element are established, where this variation is expressed in terms of nodal values. ICFEP adopts displacements as the primary variable, which is commonly adopted in engineering software. These are also referred to as degrees of freedom. Other quantities, such as stresses and strains, are then treated as secondary variables and can be determined once the primary variable has been calculated.

(c) Element equations

Element equations govern the deformational behaviour of each element, and their derivation is based on the conditions of compatibility, equilibrium and constitutive relations. Equilibrium and compatibility are linked through the material constitutive behaviour, which provides a relationship between the stresses and strains in the following form:

Equation 4.1 $$\{\Delta\sigma\} = [\mathrm{D}]\{\Delta\varepsilon\}$$

where $[\mathrm{D}]$ is the constitutive matrix, $\{\Delta\sigma\}$ is the vector of stresses and $\{\Delta\varepsilon\}$ is the vector of strains.

To determine the element equations an appropriate variational principle (e.g. Minimum potential energy) is invoked, resulting in the following formulation for the element equations:

Equation 4.2 $$[\mathrm{K_E}]\{\Delta\mathrm{d_E}\} = \{\Delta\mathrm{R_E}\}$$

where $[\mathrm{K_E}]$ is the element stiffness matrix, $\{\Delta\mathrm{d_E}\}$ is the vector of incremental element nodal displacements and $\{\Delta\mathrm{R_E}\}$ is the vector of incremental element nodal forces.

(d) Global equations

This involves the assemblage of the separate element equilibrium equations into a set of global equations:

Equation 4.3 $[K_G]\{\Delta d_G\} = \{\Delta R_G\}$

where $[K_G]$ is the global stiffness matrix, $\{\Delta d_G\}$ is the vector of all incremental nodal displacements and $\{\Delta R_G\}$ is the vector of all incremental nodal forces. The global stiffness matrix $[K_G]$ may be assembled using the direct stiffness method, which sums up the individual element contributions, while taking into consideration the degrees of freedom (i.e. nodal displacements) which are common between the elements. The terms of the right hand side load vector may be obtained in a similar manner by summing the individual loads acting at each node.

(e) Boundary conditions

The global equations are modified in order to include boundary conditions; these include loading conditions and displacement boundary conditions. Loading conditions, such as line and point loads, surcharge pressures, excavation, construction and body forces, affect the right hand side of the global system of equations $\{\Delta R_G\}$, while the displacement boundary conditions affect $\{\Delta d_G\}$.

(f) Solving the global equations

Global equations, which are in the form of a large system of simultaneous equations, are solved in order to determine the nodal displacements $\{\Delta d_G\}$. From these, secondary quantities, including stresses and strains, can be evaluated. There are various mathematical techniques for solving the simultaneous equations, including Gaussian elimination which is considered as the most common technique among finite element programs. The Gaussian elimination option that is available in ICFEP was adopted for the analysis presented in this thesis.

4.2.2. Non-linearity in finite element analysis

In the previous section, the finite element theory for linear materials was presented, where it was assumed that the soil is elastic and therefore the constitutive matrix $[D]$ is constant. Such an assumption results in a constant stiffness matrix $[K_G]$ during the finite element analysis. However, if the soil is non-linear, i.e. the constitutive model used to reproduce the soil behaviour is not linear elastic, then the equivalent constitutive matrix $[D]$ is no longer constant, but varies with stress and/or strain during the analysis. Consequently, on applying a change in the boundary conditions, either in terms of displacements $\{\Delta d\}$ or loads $\{\Delta R\}$, the stiffness matrix $[K_G]$ changes and therefore a solution strategy is required to account for the changing material behaviour.

To deal with this, Equation 4.3 is rewritten in an incremental form as:

Equation 4.4 $$[K_G]^i\{\Delta d\}^i_{nG} = \{\Delta R_G\}^i$$

where $[K_G]^i$ is the incremental global system stiffness matrix, $\{\Delta d\}^i_{nG}$ is the vector of incremental nodal displacements, $\{\Delta R_G\}^i$ is the vector of incremental nodal forces and i is the increment number. This global set of equations is solved for each increment and the final solution is then obtained by summing up the results for each increment.

However, due to the non-linearity of the stiffness matrix, it usually varies over an increment, unless a very large number of small increments are used. Therefore, the solution of Equation 4.4 is not considered as straightforward and a solution strategy is required to deal with this. Methods of solutions include for instance the tangent stiffness, the visco-plastic and the modified Newton-Raphson schemes. In ICFEP, the modified Newton-Raphson method is employed with an error controlled sub-stepping stress-point algorithm. This is considered to be the most robust and most economical method in terms of computer run-times and its basic principles are described below.

The modified Newton-Raphson method is a solution strategy that solves Equation 4.4 for each increment by adopting an iterative approach. Figure 4.1 illustrates graphically this approach for the simple problem of a uniaxially loaded bar of non-linear material. At the beginning of the first iteration, a global stiffness matrix $[K_G]^o$ is calculated from the current stress and strain state at the beginning of each increment. This is used in Equation 4.4 in order to obtain a solution, however it is recognised that it is likely to be in error due to the variation of the non-linear stiffness matrix over the increment. Therefore, the predicted displacement Δd^1 from the stiffness matrix $[K_G]^o$ is used to calculate a residual vector ψ^1, which is a measure of the error in the analysis. At the second iteration, Equation 4.4 is solved again using the residual vector ψ^1 as the right hand side vector, such that it can be rewritten as:

Equation 4.5 $$[K_G]^i\left(\{\Delta d\}^i_{nG}\right)^j = \{\psi\}^{j-1}$$

where the superscript j refers to the iteration number and $\{\psi\}^o = \{\Delta R_G\}^i$. This process is an iterative process and it ends when the calculated residual load is smaller than a pre-set tolerance. After convergence, the incremental solution of the unknown displacement quantities is then evaluated by summing up the calculated iterative displacements.

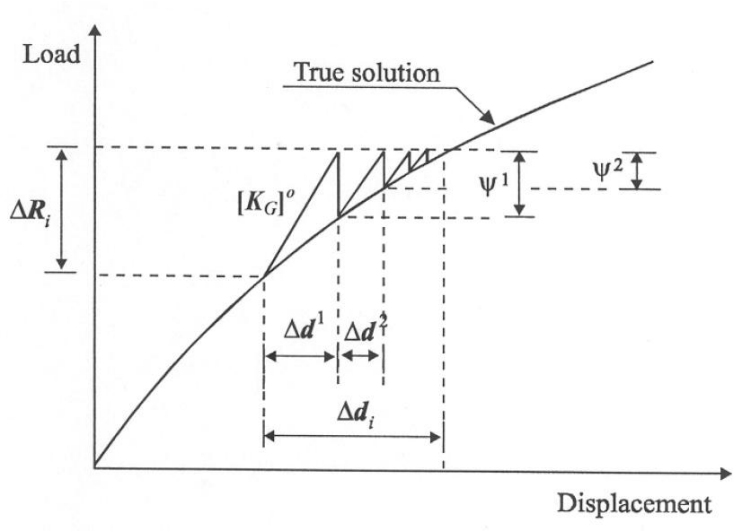


Figure 4.1: Schematic representation of the modified Newton-Raphson algorithm for a one-dimensional non-linear problem (Potts and Zdravkovic, 1999)

In ICFEP, convergence criteria are set on both the iterative displacements $\left(\{\Delta d\}^i_{nG}\right)^j$ and the residual loads $\{\psi\}^j$. These are expressed in terms of scalar norms:

Equation 4.6
$$\left\|\left(\{\Delta d\}^i_{nG}\right)^j\right\| = \sqrt{\left(\left(\{\Delta d\}^i_{nG}\right)^j\right)^T \left(\{\Delta d\}^i_{nG}\right)^j}$$

Equation 4.7
$$\left\|\{\psi\}^j\right\| = \sqrt{(\{\psi\}^j)^T\{\psi\}^j}$$

where they are compared with the respective accumulated and incremental values. The default convergence criterion in ICFEP is that the iterative quantities are within 2 % of both the accumulated and incremental ones.

One key step in the modified Newton-Raphson solution technique is the evaluation of the residual load vector $\{\psi\}^j$ for each iteration. This involves the employment of a stress point algorithm. In ICFEP, several options are available and for the analyses presented in this thesis an error-controlled substepping algorithm with a modified Euler integration scheme was adopted. A detailed presentation of this algorithm is out of the scope of this thesis but can be found in Potts and Zdravkovic (1999).

4.2.3. Finite element formulation for coupled problems

The finite element formulation presented so far can be used to analyse either fully drained or fully undrained problems. In the former case, the change in pore water pressures is zero and Equation 4.1 is a relationship between the effective stress vector and the corresponding

strains. In the latter case, the change of pore water pressures is not incorporated in Equation 4.1, and therefore it is a relationship between the total stress vector and the corresponding strains.

However, if it is necessary to observe how the pore water pressure changes from the short term (i.e. undrained) to the long term (i.e. drained) conditions, then a coupled analysis must be invoked, where the total stress vector is split into its effective and pore pressure parts, as in Equation 4.8:

Equation 4.8 $$\{\Delta\sigma\} = \{\Delta\sigma'\} + \{\Delta\sigma_f\} = [D']\{\Delta\varepsilon\} + \{\Delta\sigma_f\}$$

where $\{\Delta\sigma\}$ is the vector of incremental total stresses, $\{\Delta\sigma'\}$ the vector of incremental effective stresses and $\{\Delta\sigma_f\}$ the vector of incremental pore fluid pressure. Therefore, a further modification to the system of Equations 4.4 is required, which involves the combination of equations governing the flow of pore fluid through the soil skeleton with equations governing the deformation of the soil due to loading. Such an approach is called coupled, due to the fact that pore fluid flow and stress strain behaviour are coupled together.

The analysis of the time dependent consolidation requires therefore the solution of Biot's consolidation equations (Biot, 1941), coupled with the material constitutive model and the equilibrium equations. This means that (a) the equations of equilibrium, (b) the constitutive behaviour expressed in terms of effective stresses, (c) the equation of continuity, and (d) the generalised Darcy's law have to be satisfied, in order to formulate the equations for coupled consolidation analyses.

In a similar way as in an uncoupled formulation, for the element equations and subsequent global equations the principle of minimum potential energy is employed in order to formulate the equations for coupled consolidation analyses, resulting in the following system of equations:

Equation 4.9 $$\begin{bmatrix} [K_G] & [L_G] \\ [L_G]^T & -\beta\Delta t[\Phi_G] \end{bmatrix} \begin{Bmatrix} \{\Delta d\}_{nG} \\ \{\Delta p_f\}_{nG} \end{Bmatrix} = \begin{Bmatrix} \{\Delta R_G\} \\ ([n_G] + Q + [\Phi_G](\{p_f\}_{nG})_1)\Delta t \end{Bmatrix}$$

Equation 4.9 provides a set of simultaneous equations in terms of the incremental nodal displacements $\{\Delta d\}_{nG}$ and incremental nodal pore fluid pressures $\{\Delta p_f\}_{nG}$. Additional terms in respect to the uncoupled formulation include the off diagonal coupling submatrices $[L_G]$ and $[L_G]^T$, the permeability submatrix $[\Phi_G]$, and the submatrix associated with the direction of gravity $[n_G]$. Also β is an integration parameter that is introduced to indicate how the pore fluid pressure varies over the time increment Δt. (Potts and Zdravkovic, 1999)

Hydraulic boundary conditions need to be specified as well, in addition to displacement or loading boundary conditions, when considering coupled problems. These may take the form of prescribed nodal pore fluid pressures $\{\Delta p_f\}_{nG}$ or nodal flow values Q. Both are dealt with in a similar way to prescribed displacements and prescribed nodal forces respectively in solving the global equations.

4.3. MODIFIED CAM CLAY MODEL

The Modified Cam Clay model is an elasto-plastic constitutive model developed for saturated clays, within the framework of critical state soil mechanics. The first critical state models were developed at the University of Cambridge by Roscoe and his colleagues in the 1960's. The Modified Cam Clay model is an improvement of the original Cam Clay model, whose formulation was initially presented by Roscoe and Schofield (1963) and Schofield and Wroth (1968), while its improvement was presented by Roscoe and Burland (1968).

The Modified Cam Clay model can describe three important aspects of soil behaviour:

(a) strength,
(b) compression or dilatancy (the change of volume that occurs with shearing), and
(c) critical state in which soil elements can experience unlimited deformations without any changes in stress or volume.

In this thesis, a form of the Modified Cam Clay model is employed for the finite element analyses using the software package ICFEP. In the following, the formulation of the Modified Cam Clay model in general stress space is presented based on Potts and Zdravkovic (1999).

4.3.1. Formulation in general stress space

The Modified Cam Clay (MCC) model used in this thesis is generalised in 3D stress space considering the following:

(a) Virgin consolidation and swelling lines

The MCC model assumes that a sample of clay, which is slowly compressed under isotropic stress conditions ($\sigma_1' = \sigma_2' = \sigma_3' = p'$) and under perfectly drained conditions, moves along a trajectory in the v-ln p′ plane [$v = 1 + e$, $p' = (\sigma_1' + \sigma_2' + \sigma_3')/3$], which is known as the virgin consolidation line (path a-b-d in Figure 4.2). Subsequently, if the soil is unloaded from

point ‘b’ on the virgin consolidation line, it moves up the swelling line ‘bc’. If the soil is now re-loaded, it will first move down the swelling line until point ‘b’, from which it will move again down the virgin consolidation line. If the soil is unloaded again from point ‘d’, this time it will move up the swelling line ‘de’.

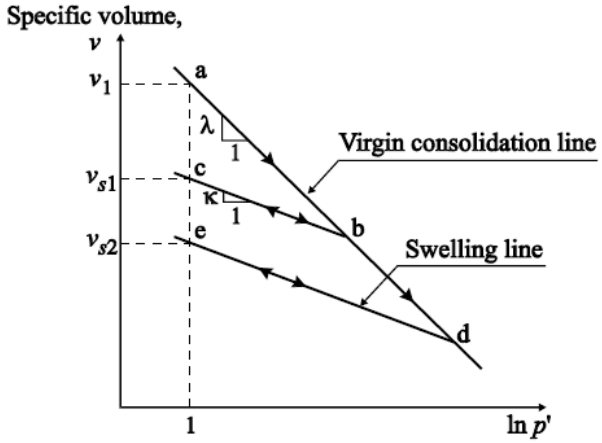


Figure 4.2: Behaviour under isotropic compression (Potts and Zdravkovic, 1999)

The MCC model assumes that the virgin consolidation line and the swelling lines are straight in v-ln p′ space. The virgin consolidation line, as shown in Figure 4.2, is defined by:

Equation 4.10 $$v + \lambda(\ln p') = v_1$$

while the swelling line is defined by:

Equation 4.11 $$v + \kappa(\ln p') = v_s$$

where λ is the slope of the virgin consolidation line in v-ln p′ space, κ is the slope of swelling lines in v-ln p′ space, v_1 is the specific volume on the virgin consolidation line at unit pressure, and v_s is the specific volume of swelling lines at unit pressure. The values of λ, κ and v_1 are characteristic properties of the particular type of clay, whereas the value of v_s is different for each swelling line and it depends on the loading history.

If the current state of the soil is on the virgin consolidation line, the soil is described as normally consolidated, and any volume change along the virgin consolidation line is mainly irreversible or plastic. On the other hand, if the soil is unloaded and its current state is on a swelling line, then the soil is described as overconsolidated, and any change along a swelling line is considered as reversible or elastic.

(b) Critical state line

Sustained shearing of a soil sample eventually leads to a state in which further shearing can occur without any changes in stress or volume. This is the final state for a soil taken to failure, independent of initial conditions. Such a state is called the critical state and it is considered as a basic feature of soil behaviour, which is reproduced in critical state models such as the MCC model. The critical state is characterised by the Critical State Line (CSL), which is the succession of critical state points for different yield surfaces in J-p'-v space. The CSL plots as a straight line in J-p' plane (Figure 4.3), with a slope $g(\theta)$.

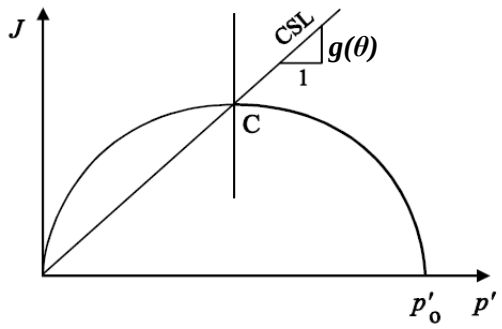


Figure 4.3: Yield surface on J-p' plane (Potts and Zdravkovic, 1999)

(c) Yield functions

It is assumed that under increasing deviatoric stress J, $[J = [(\sigma'_1 - \sigma'_2)^2 + (\sigma'_2 - \sigma'_3)^2 + (\sigma'_1 - \sigma'_3)^2]^{0.5} * (1/\sqrt{6})]$, the soil response is elastic until a yield value of J is attained, which can be obtained from the yield function:

Equation 4.12
$$F(\{\sigma'\},\{k\}) = \left(\frac{J}{p'g(\theta)}\right)^2 - \left(\frac{p'_o}{p'} - 1\right) = 0$$

where p' is the mean effective stress, J is the deviatoric stress, $g(\theta)$ is the slope of the CSL in J-p' space, and p'_o is the value of p' at the intersection of the current swelling line with the virgin consolidation line. Parameter p'_o is a hardening/softening parameter defining the current size of the surface.

In the J-p' plane, the MCC yield function plots as an ellipse (Figure 4.3), whose size is controlled by the parameter p'_o which has a different value for each swelling line (Figure 4.4). Considering this, in the three dimensional v-J-p' space, the yield function defines a surface called the Stable State Boundary Surface (Figure 4.5). Within this surface, the behaviour of

the model is elastic, whereas on the surface its behaviour is elasto-plastic. No state outside the surface is possible in the MCC model.

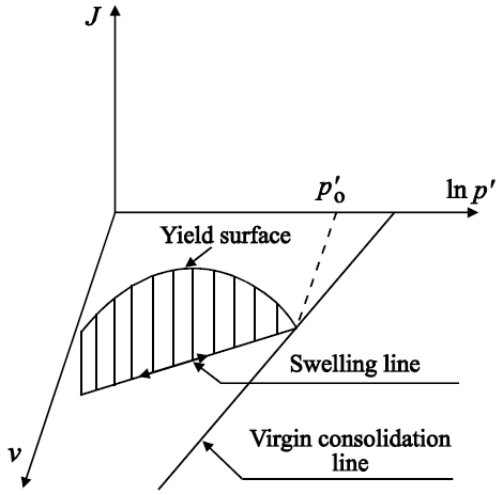


Figure 4.4: Yield surface in v-J-p′ space

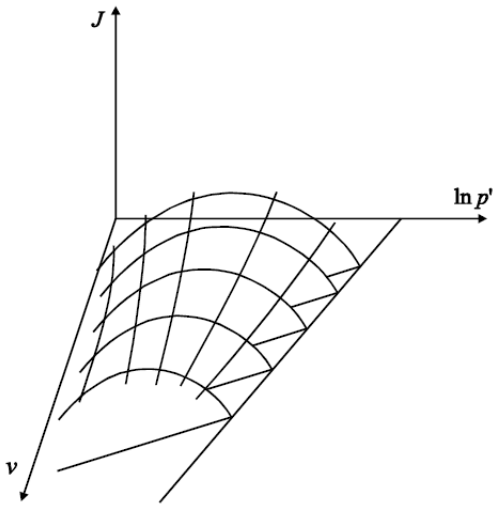


Figure 4.5: State boundary surface

The extension to general stress space is achieved by adopting a Mohr-Coulomb hexagon for the shape of the yield surface in the deviatoric plane (Figure 4.6). Parameter $g(\theta)$ is then given by:

Equation 4.13

$$g(\theta) = \frac{\sin \varphi'_{cs}}{\cos \theta + \frac{\sin \theta \sin \varphi'_{cs}}{\sqrt{3}}}$$

where φ'_{cs} is the critical state angle of shearing resistance and θ is the Lode's angle, $\theta = \tan^{-1}\left[\frac{1}{\sqrt{3}}\left(2\frac{(\sigma'_2-\sigma'_3)}{(\sigma'_1-\sigma'_3)}-1\right)\right]$, which defines the orientation of the stress state within the deviatoric plane. The limiting values of θ correspond to triaxial compression $\sigma_1 > \sigma_2 = \sigma_3$, which is identified by $\theta = -30^o$, and triaxial extension $\sigma_1 < \sigma_2 = \sigma_3$, which is identified by $\theta = +30^o$.

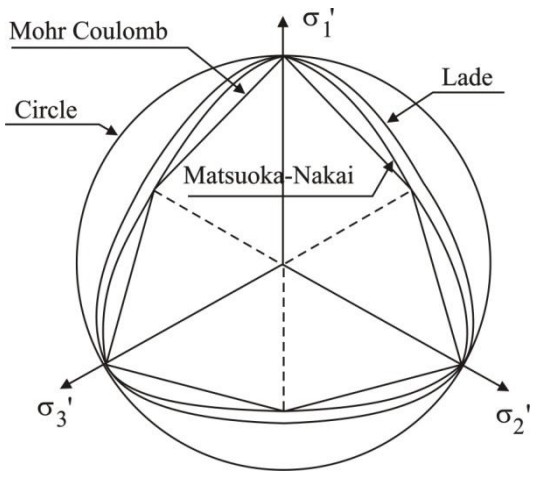


Figure 4.6: Failure surfaces in the deviatoric plane (Potts and Zdravkovic, 1999)

(d) Plastic potential function

The plastic potential function $P(\{\sigma'\},\{m\})$ has the same shape as the yield surface in J-p' space and is given also by Equation 4.12, i.e. $P(\{\sigma'\},\{m\}) = F(\{\sigma'\},\{k\})$. When the soil is plastic (i.e. when the soil state is on the stable state boundary surface) the plastic strain increment vector is taken normal to the plastic potential curve as shown in Figure 4.7. As the plastic potential and yield surface have the same shape in J-p' space, the plastic strain vector is also normal to the yield surface F in this space.

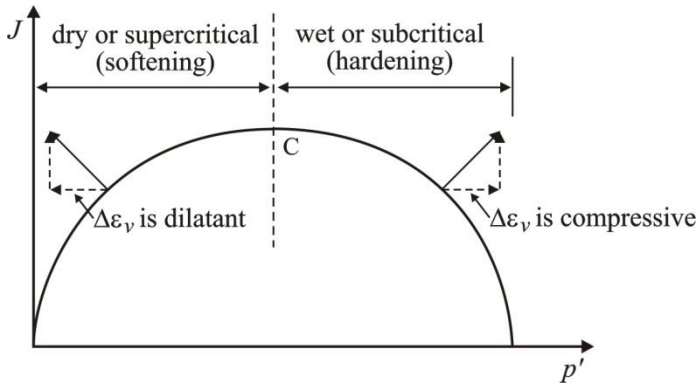


Figure 4.7: Volumetric behaviour of Cam clay models (Potts and Zdravkovic, 1999)

In this form of the MCC model, the extension to general stress space is achieved by adopting a circle for the plastic potential surface in the deviatoric plane, unlike the yield surface where a Mohr-Coulomb hexagon is adopted (Figure 4.6). Therefore, non-associated plasticity is assumed, meaning that the plastic potential surface has a different shape than the yield surface in general stress space. The extension of the plastic potential function is achieved by replacing the variable θ in Equation 4.12 by the parameter $\theta(\sigma')$, which represents the Lode's angle at the point in stress space at which the gradients of the plastic potential are required. Therefore, the plastic potential has rotational symmetry, and $P(\{\sigma'\},\{m\})$ is the surface of revolution generated by the intersection of $F(\{\sigma'\},\{k\})$ with the plane $\theta = \theta(\sigma')$.

(e) Hardening/softening rule

Hardening/softening is isotropic and is controlled by the parameter p_o', which gives the size of the yield surface in the J-p' plane. Both hardening and softening are provided by the following change in p_o':

Equation 4.14
$$\frac{dp_o'}{p_o'} = d\varepsilon_v^p \frac{v}{\lambda - \kappa}$$

where ε_v^p is the plastic volumetric strain.

In general, in the MCC model as shown in Figure 4.7, if yielding occurs to the right of the critical state point (wet or subcritical side), hardening behaviour, accompanied by contraction due to the positive incremental plastic volumetric strains, is followed. On the other hand, if yielding occurs to the left of the critical state point (dry or supercritical side), the soil exhibits softening behaviour, which is accompanied by dilatancy due to the negative incremental plastic volumetric strains.

(f) Definition of elastic component

In the MCC model, the behaviour of the soil within the yield surface and along a swelling line is elastic. Therefore, from Equation 4.11 for the swelling line, the elastic volumetric strain $d\varepsilon_v^e$ can be determined:

Equation 4.15 $$d\varepsilon_v^e = \frac{dv}{v} = \frac{k}{v}\frac{dp'}{p'}$$

from which the elastic bulk modulus K can be determined as:

Equation 4.16 $$K = \frac{dp'}{d\varepsilon_v^e} = \frac{vp'}{k}$$

which is proportional to v and p', and therefore this results in nonlinear elasticity. The elastic shear strains are then calculated from the elastic shear modulus G or from the Poisson's ratio μ.

4.3.2. Undrained strength

Although the input parameters for the MCC model include the drained strength, φ', in combination with other input parameters there is a closed form solution for the undrained strength S_u. It takes the following form:

Equation 4.17 $$\frac{S_u}{\sigma'_{vi}} = g(\theta)\cos\theta\frac{OCR}{6}(1+2K_o^{NC})[1+B^2]\left[\frac{2(1+2K_o^{OC})}{(1+2K_o^{NC})OCR[1+B^2]}\right]^{\frac{\kappa}{\lambda}}$$

where $B = \frac{\sqrt{3}(1-K_o^{NC})}{g(-30^o)(1+2K_o^{NC})}$. Consequently, the undrained shear strength is obtained by combining the input model parameters κ, λ and φ'_{cs} and initial stress conditions including the overconsolidation ratio (OCR), the coefficient of earth pressures at rest (K_o) and the initial vertical effective stress σ'_{vi}. The equation also indicates that the undrained strength varies

with the value of the Lode's angle. It will therefore be different under triaxial compression ($\theta = -30^o$) and plane strain ($\theta = 0^o$) conditions.

4.3.3. Model parameters

Specification of the MCC model in ICFEP requires five material parameters. These are the consolidation parameters (v_1, λ and κ), the drained strength parameter (φ'_{cs}) and the elastic parameter (μ or G). In addition, the initial stress conditions, as well as the OCR variation with depth, are required in order to determine the initial state of the soil and its position in respect to the yield surface. The model parameters are listed in Table 4.1.

Model Parameter	**Units**	**Description**
v_1	-	Specific volume at p' = 1 kPa on the isotropic virgin consolidation line
λ	-	Slope of virgin consolidation line on v-ln p′ plane
κ	-	Slope of swelling line on v-ln p′ plane
μ or G or G/p'_o	- kPa -	A second elastic parameter than can be either the Poisson's ratio μ, the elastic shear modulus G or the normalised shear modulus G/p'_o, which results in a stress dependent shear modulus
φ'_{cs}	degrees	Angle of shearing resistance

Table 4.1: Modified Cam Clay model parameters as input in ICFEP

4.4. EQUIVALENT TIME CREEP MODEL

The Equivalent Time Creep model is an elastic visco-plastic constitutive model that has been implemented in ICFEP as a generalised 3D model (Bodas Freitas, 2008). The model is able to simulate isotach viscosity, i.e. the phenomena of creep, stress relaxation and rate effects.

This is also a critical state model, which is based on the overstress theory and the Equivalent Time (ET) concept (Yin et al. 2002). The time-dependent behaviour of the model is characterised by the coefficient of secondary consolidation C_α. It incorporates a non-linear logarithmic function of visco-plastic strain with time, with a limit for the amount of visco-plastic volumetric strain that is attained at infinite time. It can predict soil ageing by accounting for viscoplastic strains, i.e. creep strains, however it is not able to determine any contribution to the soil strength and stiffness due to the development of structure with time.

The model is extended to general stress space by assuming that the current loading surface is a locus of constant visco-plastic scalar multiplier. Therefore, the incremental visco-plastic strains are calculated by evaluating the visco-plastic volumetric strain rate at the equivalent isotropic condition to enable the calculation of the scalar multiplier, with the incremental strain components being evaluated from a plastic potential function. In J-p′ stress space, the loading surface and plastic potential surface are described by a flexible equation proposed by Lagioia et al. (1996), and the extension to general stress space is done by adopting the Matsuoka-Nakai failure criterion in the deviatoric plane. A total of 15 input parameters are required for this model.

4.4.1. Fundamental assumption

The ET Creep model is based on the fundamental assumption that the total volumetric strain of a soil subjected to a stress increment is equal to the elastic component plus visco-plastic component. This is equivalent to the division of the soil compression, according to Bjerrum (1967), into an instant compression and a delayed (creep) compression (Figure 4.8). Instant strains are assumed to be elastic, time-independent and recoverable, whereas delayed (creep) strains are visco-plastic, time-dependent and irrecoverable. Such an assumption implies that creep occurs during the whole consolidation/compression process (viscous approach in Chapter 3), i.e. during both the primary and secondary consolidation, as shown in Figure 4.8. Therefore, it is assumed in the formulation of the ET Creep model in drained conditions that total settlement is equal to “instant” settlement plus “creep” (visco-plastic) settlement from the starting time. In reality, settlement is initially accompanied by flow of water from the soil

which is also time dependent (i.e. consolidation). Consequently, if a coupled formulation is employed, there are two time dependent phenomena occurring (i.e. consolidation and creep) and therefore the "instant" settlement is time-dependent and depends on the length of drainage path, the permeability and stiffness of the soil.

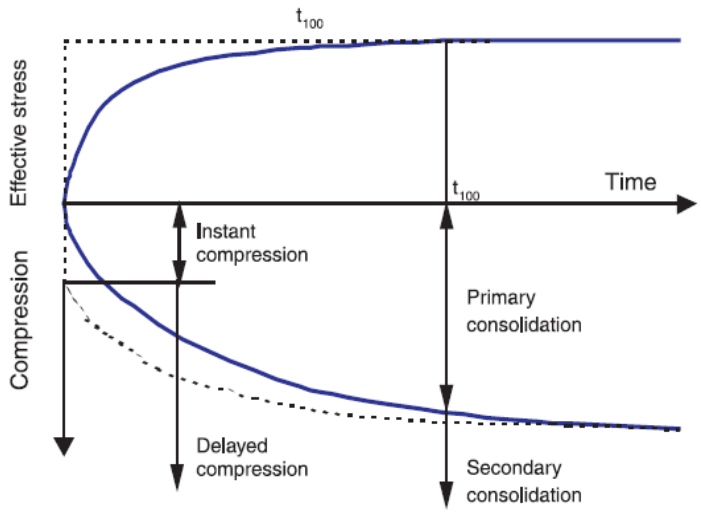


Figure 4.8: Definition of primary and secondary consolidation and instant and delayed compression

In incremental form, for an effective stress increment $\{\Delta\sigma'\}$ over a time increment Δt, the total incremental strains $\{\Delta\varepsilon^{T}\}$ are equal to:

Equation 4.18 $$\{\Delta\varepsilon^{T}\} = \{\Delta\varepsilon^{el}\} + \{\Delta\varepsilon^{vp}\}$$

where $\{\Delta\varepsilon^{el}\}$ are the elastic incremental strains and $\{\Delta\varepsilon^{vp}\}$ the visco-plastic incremental strains. The elastic incremental strains $\{\Delta\varepsilon^{el}\}$ can be determined by inverting the following equation:

Equation 4.19 $$\{\Delta\sigma'\} = [D]\{\Delta\varepsilon^{el}\}$$

where $\{\Delta\sigma'\}$ is the effective stress increment and [D] the elastic constitutive matrix. The visco-plastic incremental strains $\{\Delta\varepsilon^{vp}\}$ are calculated from the following flow rule, based on an extension of the overstress theory proposed by Perzyna (1963):

Equation 4.20 $$\{\Delta\varepsilon^{vp}\} = \langle\Phi\rangle\,\Delta t\,\frac{\partial P}{\partial\sigma'}$$

where Φ is a visco-plastic scalar multiplier representing the effects of strain rate on the material behaviour, Δt is the time elapsed, and P is the plastic potential function. The approach used to define and determine Φ is based on the equivalent time concept, in which a

non-linear logarithmic creep function with a limit is used, in order to fit the creep data of volumetric strain against time under isotropic conditions.

4.4.2. The concept of equivalent time

The concept of equivalent time, first introduced by Yin & Graham (1989), is applied in developing the elastic visco-plastic relationship. This concept indicates that the compression characteristics of a soil element can be described by reference to an equivalent creep time, which is defined as the time that a soil element in an isotropic state (ε_{vm}, p'_m) would take to creep from a reference line to the current stress state under constant mean effective stress. Equivalent time is related to a unique creep strain rate and not to real time; the larger the equivalent time, the smaller the creep strain rate. Equivalent time might be close to the real duration of the load increments in the normally consolidated range of incremental load oedometer tests; however this is not the case in the overconsolidated range.

The ET Creep model works in the volumetric strain (ε_{vm}) - mean effective stress ($\ln p'_m$) space (Figure 4.9). In order to determine the equivalent time, the following basic elements should be defined: (a) instant time line, (b) reference time line, (c) lines of constant equivalent time, and (d) limit time line.

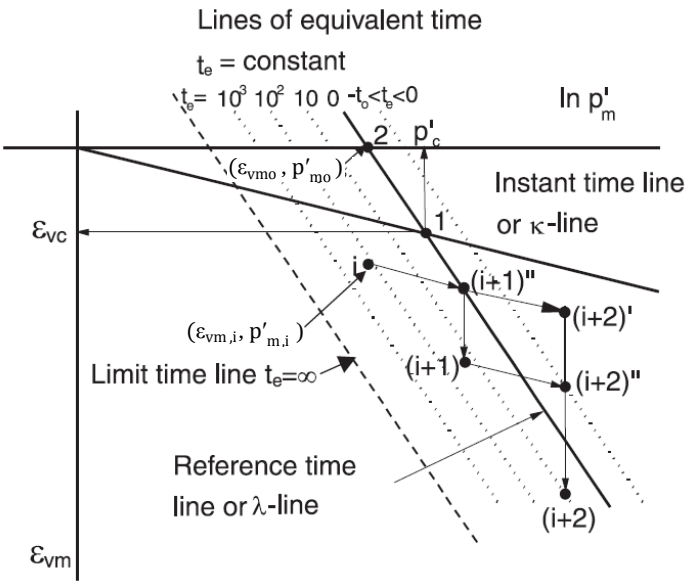


Figure 4.9: Equivalent Time Creep model in isotropic conditions

(a) Instant time line

The instant time line is used to define the instant elastic deformation at any point in Figure 4.9. The volumetric strain on the instant time line can be expressed as:

Equation 4.21 $$\varepsilon_{vm}^{el} = \varepsilon_{vmu}^{el} + \frac{\kappa}{V} \ln\left(\frac{p'_m}{p'_u}\right)$$

where ε_{vm}^{el} is the volumetric strain at the isotropic effective stress p'_m, ε_{vmu}^{el} is the volumetric strain at a reference mean effective stress p'_u, and κ/V is a model parameter. The instant time lines are a set of parallel lines with a slope of κ/V in the ε_{vm} - $\ln p'_m$ space. For instance, if a soil in an initial state at point i ($\varepsilon_{vm,i}$, $p'_{m,i}$) in Figure 4.9 is loaded to $p'_{m,i+1}$, the state of the soil will first instantly move along an instant time line from i to $(i+1)''$ and then it will experience creep, i.e. time dependent deformation to point $(i+1)$. A similar path (with a slope κ/V) is followed by every soil state which is loaded instantly (i.e. with no elapsed time).

(b) Reference time line

The reference time line is the locus of soil states that correspond to zero equivalent time (Figure 4.9). It is expressed as:

Equation 4.22 $$\varepsilon_{vm}^{r} = \varepsilon_{vmo}^{r} + \frac{\lambda}{V} \ln\left(\frac{p'_m}{p'_{mo}}\right)$$

where ε_{vm}^{r} is the volumetric strain at the isotropic effective stress p'_m, ε_{vmo}^{r} is the volumetric strain at a reference mean effective stress p'_{mo}, and λ/V and p'_{mo} are model parameters. The two parameters ε_{vmo}^{r} and p'_{mo} determine a point which the reference timeline passes through, i.e. they are used to position the reference timeline, and ε_{vmo}^{r} is usually assumed to be equal to zero.

(c) Lines of constant equivalent time

Lines of constant equivalent time are those parallel to the reference timeline (Figure 4.9) and represent a unique creep strain rate, with larger equivalent times associated with smaller creep strain rates. The equivalent time of states located below the reference timeline is always positive, whereas that of states above it is negative and varies between zero and $-t_o$, where t_o is a model parameter.

(d) Limit time line

The limit time line is the locus of the soil states, attained after drained creep for infinite time, and corresponding to an infinite equivalent time and a creep strain rate equal to zero (Figure 4.9). The limit time line is defined by the finite value of visco-plastic volumetric strain $\varepsilon_{vm,limit}^{vp}$, which represents the vertical distance between the limit time line and the reference

time line, i.e. the limit time line is a line of constant equivalent time at infinity. Such states are impossible to obtain, however in terms of the model formulation states below the limit time line are considered as pure elastic and time-independent.

Considering now an example where a soil element is in a state at point i in Figure 4.9. If it is loaded to $(i+1)''$, the state of the soil will move instantly to state $(i+1)''$ without any time dependency as described above, and then it will experience a time dependent visco-plastic deformation (creep) from $(i+1)''$ to $(i+1)$. The soil state at $(i+1)$ is on an equivalent time line with a unique creep strain rate depending on that equivalent time. It should be noted that the relationship between stress-strain-equivalent time is unique and, therefore, independent of the loading history. In other words, the same equivalent time, and therefore creep strain rate, is reached if a soil element is loaded from i to $(i+1)''$ and then left to creep to $(i+1)$, and if another soil element is loaded from i to $(i+2)'$, then left to creep to $(i+2)''$ and finally unloaded to $(i+1)$.

4.4.3. Constitutive equation for isotropic loading conditions

The elastic visco-plastic constitutive equation for isotropic loading conditions employs (a) a non-linear elastic part, which is time-independent, and (b) a non-linear logarithmic function of visco-plastic strain change with time, with a limit for the amount of visco-plastic volumetric strain that is attained at infinite time.

Considering an infinitesimal load increment $\Delta p'_m$ over a duration of time Δt, the associated incremental volumetric strain $\Delta\varepsilon_{vm}$ can be decomposed into an elastic and a visco-plastic component:

Equation 4.23 $$\Delta\varepsilon_{vm} = \Delta\varepsilon_{vm}^{el} + \Delta\varepsilon_{vm}^{vp}$$

where $\Delta\varepsilon_{vm}^{el}$ and $\Delta\varepsilon_{vm}^{vp}$ are the elastic and visco-plastic volumetric strain increments respectively.

The elastic part, which is instantaneous and time-independent, is stress level dependent and therefore non-linear. If it is assumed that the load increment is sufficiently small, then the elastic volumetric strain increment may be determined from the following equation:

Equation 4.24 $$\Delta\varepsilon_{vm}^{el} = \frac{\kappa}{V \cdot p'_m}\,\Delta p'_m$$

where the elastic bulk modulus K is:

Equation 4.25 $$K = \frac{V \cdot p'_m}{\kappa}$$

The visco-plastic volumetric strain increment may be determined by considering the visco-plastic volumetric strain rate $\dot{\varepsilon}_{vm}^{vp}$ over a time increment Δt which is sufficiently small:

Equation 4.26 $$\Delta\varepsilon_{vm}^{vp} = \Delta t \cdot \dot{\varepsilon}_{vm}^{vp}$$

where the visco-plastic volumetric strain rate $\dot{\varepsilon}_{vm}^{vp}$ can be determined by differentiating with respect to time the visco-plastic strains which are given by a linear logarithmic law (which is transformed to a non-linear relationship later to account for a limit to visco-plastic strains):

Equation 4.27 $$\varepsilon_{vm}^{vp} = \frac{\psi}{V} \ln\left(\frac{t_0 + t_e}{t_0}\right)$$

where ψ/V is a model parameter, t_e is the current equivalent time and t_0 is the real time associated with the reference time line. Therefore, by differentiating with respect to time t (where $t = t_0 + t_e$) the following visco-plastic volumetric strain rate $\dot{\varepsilon}_{vm}^{vp}$ is obtained:

Equation 4.28 $$\dot{\varepsilon}_{vm}^{vp} = \frac{d\varepsilon_{vm}^{vp}}{dt} = \frac{d\varepsilon_{vm}^{vp}}{dt_e} = \frac{\psi}{V} \cdot \frac{1}{t_0 + t_e}$$

Now, if we consider Figure 4.9, the volumetric strain at a generic stress state can be written as:

Equation 4.29 $$\varepsilon_{vm} = \varepsilon_{vm}^{r} + \varepsilon_{vm}^{vp}$$

where ε_{vm} is the current volumetric strain, ε_{vm}^{r} is the volumetric strain on the reference time line at the current mean effective stress p'_m and ε_{vm}^{vp} is the creep visco-plastic volumetric strain. Then, by substituting Equation 4.27 into Equation 4.29:

Equation 4.30 $$\varepsilon_{vm} = \varepsilon_{vm}^{r} + \frac{\psi}{V} \ln\left(\frac{t_0 + t_e}{t_0}\right)$$

which can be reworked to give the current equivalent time t_e as:

Equation 4.31 $$t_e = -t_0 + t_0 \cdot \exp\left[(\varepsilon_{vm} - \varepsilon_{vm}^{r})\frac{V}{\psi}\right]$$

Substituting Equation 4.31 into Equation 4.28, the visco-plastic volumetric strain rate can be determined by:

Equation 4.32

$$\dot{\varepsilon}_{vm}^{vp} = \frac{\psi}{V \cdot t_0} \cdot \exp\left[(\varepsilon_{vm}^{r} - \varepsilon_{vm})\frac{V}{\psi}\right]$$

Now, combining Equations 4.24 and 4.32, a general equation for the time dependent behaviour of soil under isotropic conditions, which is based on a linear logarithmic law is obtained:

Equation 4.33

$$\Delta\varepsilon_{vm} = \frac{\kappa}{V \cdot p'_m}\,\Delta p'_m + \frac{\psi}{V \cdot t_0} \cdot \exp\left[(\varepsilon_{vm}^{r} - \varepsilon_{vm})\frac{V}{\psi}\right] \cdot \Delta t$$

Furthermore, in order to consider a limit to the amount of visco-plastic volumetric strain that is attained at infinite time, a non-linear logarithmic function is employed to describe the creep deformation of soils (i.e. to replace Equation 4.27):

Equation 4.34

$$\varepsilon_{vm}^{vp} = \frac{\frac{\psi_0}{V}\ln\left(\frac{t_0 + t_e}{t_0}\right)}{1 + \frac{\psi_0}{V \cdot \varepsilon_{vm,limit}^{vp}}\ln\left(\frac{t_0 + t_e}{t_0}\right)}$$

The visco-plastic volumetric strain rate can be determined by differentiation with respect to time t (where $t = t_0 + t_e$):

Equation 4.35

$$\dot{\varepsilon}_{vm}^{vp} = \frac{d\varepsilon_{vm}^{vp}}{dt} = \frac{d\varepsilon_{vm}^{vp}}{dt_e} = \frac{\psi_0}{V} \cdot \frac{1}{t_0 + t_e} \cdot \frac{1}{\left(1 + \frac{\psi_0}{V \cdot \varepsilon_{vm,limit}^{vp}}\ln\frac{t_0 + t_e}{t_0}\right)^2}$$

The meaning of the parameter $\varepsilon_{vm,limit}^{vp}$ becomes clear when the equivalent time t_e tends to infinity, where:

Equation 4.36

$$\varepsilon_{vm}^{vp}\big|_{t_e = \infty} = \varepsilon_{vm,limit}^{vp}$$

Also, at t_e=0, the visco-plastic volumetric strain rate is:

Equation 4.37

$$(\dot{\varepsilon}_{vm}^{vp})_{t=t_0} = \frac{\psi_0}{V \cdot t_0}$$

Therefore, the parameters $\frac{\psi_0}{V}$ and t_0 define the visco-plastic strain rate on the reference time line.

Now, Equation 4.34 can be rewritten in the following format:

Equation 4.38

$$\varepsilon_{vm}^{vp} = \frac{\psi}{V}\ln\left(\frac{t_0 + t_e}{t_0}\right)$$

assuming that:

Equation 4.39

$$\frac{\psi}{V} = \frac{\frac{\psi_0}{V}}{1 + \frac{\psi_0}{V \cdot \varepsilon_{vm,limit}^{vp}} \ln\left(\frac{t_0 + t_e}{t_0}\right)}$$

where the parameter ψ/V is no longer constant (as it is for the linear logarithmic law), but varies with the equivalent time t_e, and $\frac{\psi_0}{V}$ is equal to the value of ψ/V at t_e=0.

Combining Equations 4.29 and 4.34:

Equation 4.40

$$\varepsilon_{vm} = \varepsilon_{vm}^{r} + \frac{\frac{\psi_0}{V} \ln\left(\frac{t_0 + t_e}{t_0}\right)}{1 + \frac{\psi_0}{V \cdot \varepsilon_{vm,limit}^{vp}} \ln\left(\frac{t_0 + t_e}{t_0}\right)}$$

where the equivalent time t_e may be obtained by reworking the above equation as for the linear case:

Equation 4.41

$$t_e = -t_0 + \exp\left[\frac{\varepsilon_{vm} - \varepsilon_{vm}^{r}}{\frac{\psi_0}{V}\left(1 - \frac{\varepsilon_{vm} - \varepsilon_{vm}^{r}}{\varepsilon_{vm,limit}^{vp}}\right)}\right]$$

Substituting Equation 4.41 into Equation 4.35, the visco-plastic volumetric strain rate can be determined by:

Equation 4.42

$$\dot{\varepsilon}_{vm}^{vp} = \frac{\psi_0}{V \cdot t_0} \cdot \left(1 + \frac{\varepsilon_{vm}^{r} - \varepsilon_{vm}}{\varepsilon_{vm,limit}^{vp}}\right)^2 \cdot \exp\left[\frac{V}{\psi_0} \frac{\varepsilon_{vm}^{r} - \varepsilon_{vm}}{\left(1 + \frac{\varepsilon_{vm}^{r} - \varepsilon_{vm}}{\varepsilon_{vm,limit}^{vp}}\right)}\right]$$

By considering an infinitesimal load increment $\Delta p'_m$ over a duration of time Δt, the elastic visco-plastic constitutive equation for isotropic loading conditions based on a non-linear logarithmic law becomes:

Equation 4.43

$$\Delta\varepsilon_{vm} = \frac{\kappa}{V \cdot p'_m} \Delta p'_m + \frac{\psi_0}{V \cdot t_0}\left(1 + \frac{\varepsilon_{vm}^{r} - \varepsilon_{vm}}{\varepsilon_{vm,limit}^{vp}}\right)^2 \exp\left[\frac{V}{\psi_0} \cdot \frac{\varepsilon_{vm}^{r} - \varepsilon_{vm}}{\left(1 + \frac{\varepsilon_{vm}^{r} - \varepsilon_{vm}}{\varepsilon_{vm,limit}^{vp}}\right)}\right] \cdot \Delta t$$

The elastic part, which is stress level dependent and therefore non-linear, is given from the following equation as already described:

Equation 4.44

$$\Delta\varepsilon_{vm}^{el} = \frac{\kappa}{V \cdot p'_m}\,\Delta p'_m$$

whereas the visco-plastic part, which is time-dependent, is given from the following equation:

Equation 4.45

$$\Delta\varepsilon_{vm}^{vp} = \frac{\psi_0}{V \cdot t_0}\left(1 + \frac{\varepsilon_{vm}^{r} - \varepsilon_{vm}}{\varepsilon_{vm,limit}^{vp}}\right)^2 \exp\left[\frac{V}{\psi_0} \cdot \frac{\varepsilon_{vm}^{r} - \varepsilon_{vm}}{\left(1 + \frac{\varepsilon_{vm}^{r} - \varepsilon_{vm}}{\varepsilon_{vm,limit}^{vp}}\right)}\right] \cdot \Delta t$$

4.4.4. Extension to general stress space

Recalling Equation 4.20 for the incremental visco-plastic strains $\{\Delta\varepsilon^{vp}\}$:

Equation 4.46

$$\{\Delta\varepsilon^{vp}\} = \langle\Phi\rangle\,\Delta t\,\frac{\partial P}{\partial\sigma'}$$

where $\langle\Phi\rangle = \Phi$ if the stress state lies above the limit line

$\langle\Phi\rangle = 0$ if the stress state lies on or below the limit line

and the elastic visco-plastic constitutive equation for isotropic loading conditions:

Equation 4.47

$$\Delta\varepsilon_{vm} = \frac{\kappa}{V \cdot p'_m}\,\Delta p'_m + \frac{\psi_0}{V \cdot t_0}\left(1 + \frac{\varepsilon_{vm}^{r} - \varepsilon_{vm}}{\varepsilon_{vm,limit}^{vp}}\right)^2 \exp\left[\frac{V}{\psi_0} \cdot \frac{\varepsilon_{vm}^{r} - \varepsilon_{vm}}{\left(1 + \frac{\varepsilon_{vm}^{r} - \varepsilon_{vm}}{\varepsilon_{vm,limit}^{vp}}\right)}\right] \cdot \Delta t$$

this section presents how the above constitutive relationship may be extended to general stress space and how the Φ value defined in Section 4.4.1 is determined.

In the ET Creep model, the incremental visco-plastic strains at a generic stress point are calculated by evaluating the visco-plastic volumetric strain rate at the equivalent isotropic condition, and assuming that the current loading surface is a locus of constant visco-plastic scalar multiplier with the incremental strain components being evaluated from a plastic potential function. Therefore, by comparing Equation 4.46 and Equation 4.47 the value of Φ can be evaluated as:

Equation 4.48

$$\Phi = \frac{\psi_0}{V \cdot t_0}\left(1 + \frac{\varepsilon_{vm}^{r} - \varepsilon_{vm}}{\varepsilon_{vm,limit}^{vp}}\right)^2 \exp\left[\frac{V}{\psi_0} \cdot \frac{\varepsilon_{vm}^{r} - \varepsilon_{vm}}{\left(1 + \frac{\varepsilon_{vm}^{r} - \varepsilon_{vm}}{\varepsilon_{vm,limit}^{vp}}\right)}\right] \cdot \frac{1}{\left|\frac{\partial P}{\partial p'}\right|_{\substack{p'=p'_m \\ J=0}}}$$

where $\left|\frac{\partial P}{\partial p'}\right|_{\substack{p'=p'_m \\ J=0}}$ is the absolute value of the partial differential of the plastic potential surface function P in relation to the mean effective stress, p', evaluated at the equivalent isotropic stress state $(p'_m, J = 0)$ as shown in Figure 4.10, the quantity ε_{vm}^{r} is the volumetric strain on the reference time line at the equivalent mean effective stress p'_m and the quantity ε_{vm} is the associated volumetric strain which is evaluated as:

Equation 4.49

$$\varepsilon_{vm} = \varepsilon_v + \frac{\kappa}{V}\ln\left(\frac{p'_m}{p'}\right)$$

where ε_v is the current total volumetric strain, p' is the current mean effective stress and p'_m is the size of the current loading surface, and corresponds to the mean effective stress at zero deviatoric stress on the current loading surface. Therefore, the problem of evaluating the visco-plastic incremental strains at a generic stress point $(p', J, \varepsilon_{vm})$ is reduced to evaluating the incremental volumetric visco-plastic strain, and thus the quantity Φ, at the equivalent stress point $(p'_m, J = 0, \varepsilon_{vm})$. The geometrical significance of the above is shown in Figure 4.10.

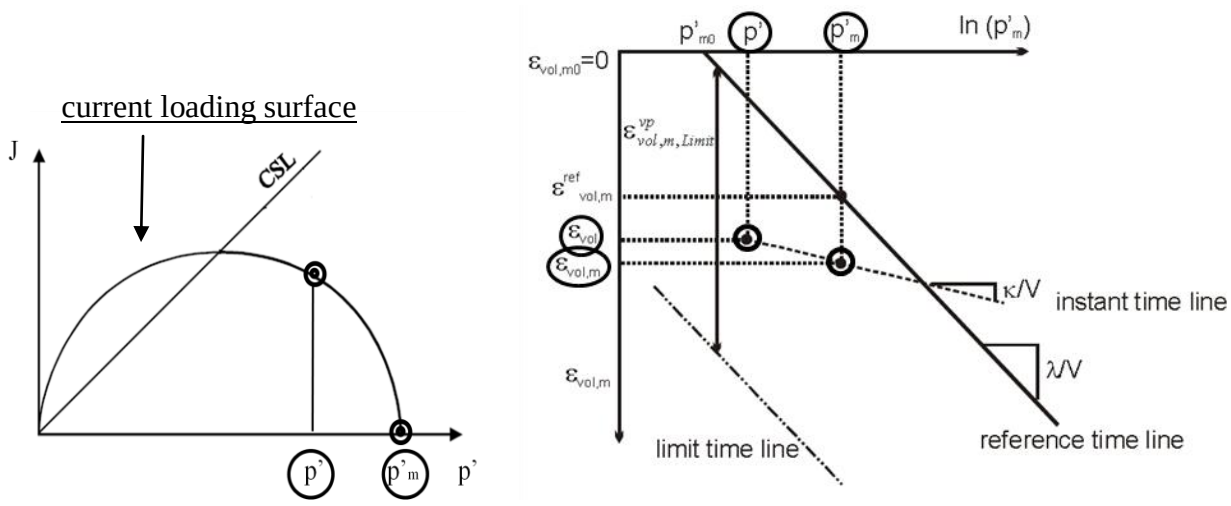


Figure 4.10: Extension to general stress space

4.4.5. Plastic potential and loading surface

In the triaxial stress space, the model is implemented by using a flexible function for the loading and plastic potential surfaces proposed by Lagioia et al. (1996), which can describe a

wide range of shapes including the Cam Clay "bullet shape" and the Modified Cam Clay "ellipse". The extension in the deviatoric plane to general stress space is done based on the Matsuoka-Nakai failure criterion, which is an improvement to the Mohr-Coulomb criterion, as it takes account of the effect of the intermediate principal stress. This shape of the yield and plastic potential surfaces in the deviatoric plane passes through the corners of the Mohr-Coulomb hexagon and follows closely its shape (Figure 4.6).

The expression proposed by Lagioia et al. (1996) for the loading and plastic potential surface is:

Equation 4.50

$$F = \frac{p'}{p'_m} - \frac{\left(1 + \frac{\bar{\eta}}{K_2}\right)^{\frac{K_2}{(1-\mu)(K_1-K_2)}}}{\left(1 + \frac{\bar{\eta}}{K_1}\right)^{\frac{K_1}{(1-\mu)(K_1-K_2)}}}$$

where K_1 and K_2 are constants given by (K_1 and K_2 denote a positive and a negative sign respectively in $\pm$):

Equation 4.51

$$K_{1/2} = \frac{\mu \cdot (1-\alpha)}{2 \cdot (1-\mu)} \cdot \left(1 \pm \sqrt{1 - \frac{4\alpha \cdot (1-\mu)}{\mu \cdot (1-\alpha)^2}}\right)$$

and $\bar{\eta}$ is the generalised normalised stress ratio:

Equation 4.52

$$\bar{\eta} = \sqrt{\frac{J_{2\eta}}{J_{2\eta,failure}}}$$

where $J_{2\eta}$ is the stress ratio squared:

Equation 4.53

$$J_{2\eta} = \left(\frac{J}{p'}\right)^2$$

and $J_{2\eta,failure}$ is the square of the stress ratio at failure. $J_{2\eta,failure}$ can be related to $g(\theta)$ according to the Matsuoka-Nakai failure surface by:

Equation 4.54

$$g(\theta) = \sqrt{J_{2\eta,failure}}$$

and can be obtained for a specific value of Lode's angle θ by solving the following cubic equation based on the Matsuoka-Nakai failure criterion (Potts and Zdravkovic, 1999):

Equation 4.55
$$\frac{2}{\sqrt{27}} C \cdot \sin(3\theta) \cdot \left(J_{2\eta,\text{failure}}\right)^{3/2} + (C-3) \cdot J_{2\eta,\text{failure}} - (C-9) = 0$$

where C is a constant that depends on M, the gradient of the critical state line in p' - q stress space under triaxial compression stress conditions (θ =-30^o), and it is given by:

Equation 4.56
$$C = \frac{9 - M^2}{\frac{2M^3}{27} - \frac{M^2}{3} + 1}$$

and M can be related to the angle of shearing resistance φ':

Equation 4.57
$$M = \frac{6 \sin \varphi'}{3 - \sin \varphi'}$$

Four parameters are required to fully define either the loading or plastic potential surface: M, μ, α and p'_m. More details can be found in Lagioia et al. (1996).

4.4.6. Soil structure

Soil structure is included in the ET Creep model by adopting an approach similar to Lagioia & Nova (1995). The model is able to mimic the existence of an initial structure, which is made to decrease during loading as a function of the accumulated visco-plastic volumetric strain, however it is not able to consider the development of structure with time. According to the framework described by Lagioia & Nova (1995), structure is included in the model by considering that the quantity p'_{m0} (used to position the reference time line) is decomposed into an intrinsic part (p'_{mi0}) and a transient part (p_s) associated with the existence of soil structure, as shown in Figure 4.11. Thus:

Equation 4.58
$$p'_{m0} = p'_{mi0} + p_s$$

where p'_{m0} is the mean effective stress on the reference time line of the natural material at ε_{vm}=0, p'_{mi0} is the mean effective stress on the intrinsic reference time line at ε_{vm}=0, and p_s is the current contribution due to soil structure. The parameter p_s varies from an initial value p_{s0} to zero at a very large volumetric visco-plastic strain, according to the following hardening rule:

Equation 4.59
$$\Delta p_s = -3.0 \cdot \rho_s \cdot p_s \cdot \varepsilon_d^2 \cdot \Delta\varepsilon_d$$

where ρ_s is a model parameter defining the rate of destructuration, p_s is the current value of the structure contribution, $\varepsilon_d = \int \left|\Delta\varepsilon_{vm}^{vp}\right|$ and $\Delta\varepsilon_d$ is the incremental value of ε_d.

The value of p'_{m0} is used to evaluate the value of ε_{vm}^{r} in Equation 4.22, which in turn is used to determine the value of the visco-plastic scalar multiplier Φ in Equation 4.48. Upon loading, destructuration is modelled according to Equation 4.59.

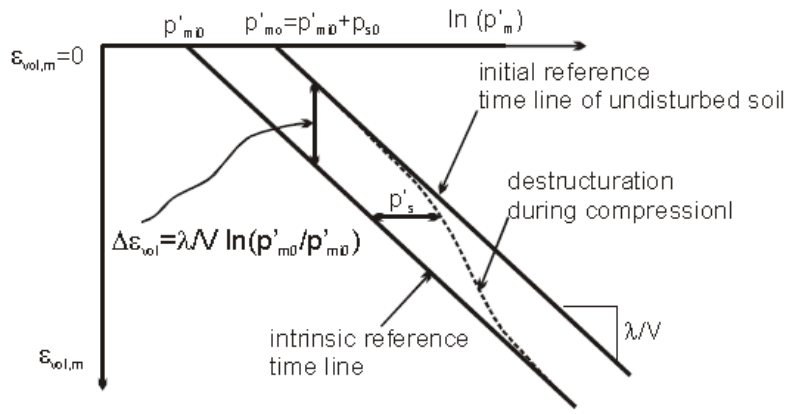


Figure 4.11: Framework for the consideration of soil structure

4.4.7. Model parameters

A total of 15 parameters, listed in Table 4.2, are required by the ET Creep model, in order for it to be employed in a boundary value problem. For analysis of a boundary value problem, it is also necessary for the user to specify the initial stress conditions, the initial void ratio and OCR variations with depth. In the following, a description of the geotechnical meaning of the model parameters is given.

Model Parameter	Units	Description
p'_{mio}	kPa	Mean effective stress at $\varepsilon_{vm} = 0$ on the intrinsic reference time line
λ/V	-	Slope of the reference time line in ε_{vm} - $\ln p'_m$ space
κ/V	-	Slope of the instant time line on ε_{vm} - $\ln p'_m$ space
μ or G or G/p'	- kPa -	A second elastic parameter than can be either the Poisson's ratio μ, the elastic shear modulus G or the normalised shear modulus G/p'_{mc}, which results in a stress dependent shear modulus
α_f	-	Loading surface parameter
μ_f	-	Loading surface parameter
M_f	-	Loading surface parameter

α_g	-	Plastic potential parameter
μ_g	-	Plastic potential parameter
M_g	-	Plastic potential parameter
ψ_0/V	-	Time dependent parameter
t_0	unit of time	Reference time; it should be expressed in the same units as that used to define the analysis time increments and permeability (in coupled consolidation analyses only)
$\varepsilon_{vm,limit}^{vp}$	-	Limit for the amount of volumetric visco-plastic strain
p_{s0}	kPa	Initial increase in p'_{mi0} due to structure, defining the position of the reference time line of the natural material
ρ_s	-	Parameter that controls the rate of destructuration

Table 4.2: Equivalent Time Creep model parameters

(a) Parameters λ/V and κ/V

The parameters λ/V and κ/V define the soil compressibility in the ε_{vm} - $\ln p'_m$ space, and they can be evaluated from an oedometer 24h step loading test. In particular, the parameter λ/V is the slope of the compression curve in the normally consolidated range of an undisturbed sample in the ε_{vm} - $\ln p'_m$ space. The parameter κ/V defines the instant time line and can be determined in approximation by the average slope of an unloading-reloading loop.

In the case of derivation of the model parameters from a reconstituted sample, due to differences in the initial void ratios between a reconstituted and an intact sample which affects the value of the specific volume V, the values of λ/V and κ/V may be evaluated as a first approximation by determining the values of λ and κ from the loading-unloading-reloading compression curve in V-$\ln p'$ space and then by using a value for the specific volume V representative of that in-situ.

(b) Second elastic parameter

A second elastic parameter is required in the model to fully characterize the isotropic elastic response of the soil, in addition to the stress dependent bulk modulus K defined by Equation

4.25. This parameter can be either the Poisson's ratio μ, the elastic shear modulus G or the normalized shear modulus G/p'.

(c) Parameters α_f, α_g,μ_f, μ_g, M_f and M_g

The parameters α, μ and M define the shape of the loading surface or plastic potential in general stress space. Two sets of parameters are employed, those denoted by the subscript "f" which refer to the loading surface, and those denoted by the subscript "g", which define the plastic potential. If the parameters with different subscripts are equal, the loading surface and plastic potential are equal and consequently the model is referred to as associated. The parameter M is the slope of the critical state line [$g(\theta)$] under triaxial compression stress conditions (θ=-30^o) in p'-q stress space and can be related to the angle of shearing resistance φ' through Equation 4.57. The parameters μ and α define the shape of the loading and plastic potential surfaces in J-p' stress space and can be evaluated by fitting the stress paths during undrained triaxial compression and extension tests.

(d) Time dependent parameters ψ_0/V, t_0 and $\varepsilon_{vm,limit}^{vp}$

The parameter ψ_0/V along with the parameter t_0 define the visco-plastic volumetric strain rate on the reference time line according to Equation 4.37. The parameter t_0 is the real time associated with the reference time, which represents the time at the end of primary consolidation (EOP), i.e. the time required for complete dissipation of excess pore water pressures. Usually, incremental load 24-hour oedometer tests are used to define the reference time line. Therefore, the parameter t_0 is usually set equal to 24 hours.

Regarding the parameter ψ_0/V, it is equal to the visco-plastic volumetric strain rate at a time equal to t_0. It can be determined from measurements of the volumetric strain rate at the end of load increments in an incremental load oedometer test. However, it is recommended to determine the parameter ψ_0/V from a test where the duration of the load increment, in the normally consolidated range, is extended beyond t_0 and during which secondary compression is only observed. The parameter ψ_0/V is then equal to the slope of the consolidation curve in ε_{vm}-ln t space at a time equal to t_0.

In engineering practice, it is common to represent secondary compression with the coefficient $C_{\alpha e}$. The coefficient of secondary compression $C_{\alpha e}$ is usually determined from incremental load 24-hour oedometer tests and it is expressed through the following function, which can be related to ψ_0:

Equation 4.60

$$C_{\alpha e} = \frac{\Delta e}{\log t_2 - \log t_1} = \frac{\Delta e}{\Delta \log t} = \frac{\Delta e \cdot \ln 10}{\Delta \ln t} = \psi_0 \cdot \ln 10$$

where if we consider the specific volume V, it becomes:

Equation 4.61

$$\frac{\psi_0}{V} = \frac{C_{\alpha e}}{V \cdot \ln 10}$$

The parameter $\varepsilon_{vm,limit}^{vp}$ is defined as the volumetric visco-plastic strain that is attained at infinite creep time under constant effective stress. This is evaluated by assuming that the infinite volumetric strain is reached when voids no longer exist in the soil. This can be determined by:

Equation 4.62

$$\varepsilon_{vm,limit}^{vp} = \frac{e_0}{1 + e_0}$$

where e_0 is the initial void ratio.

(e) Parameters p'_{mio}, p_{s0} and ρ_s

The parameter p'_{mio} is the mean effective stress at $\varepsilon_{vm} = 0$ on the intrinsic reference time line (Figure 4.11), i.e. the reference time line of the reconstituted unstructured soil. The value of p'_{mio} can be set arbitrarily. This is due to the fact that the viscoplastic strain rate is determined by the position of the current stress state to the reference line and not the absolute value of volumetric strain (refer to Equation 4.43). This applies for soils which have no structure.

When the soil is structured, the position of the current reference time line depends on the value of p_s, according to Equation 4.58, which varies from an initial value p_{s0} to zero at very large visco-plastic volumetric strains. The reduction of the value of p_s represents soil destructuration during compression, as graphically presented in Figure 4.11, and the value of ρ_s controls the rate of destructuration. Parameters p_{s0} and ρ_s can be determined by fitting an oedometer compression curve of a natural sample loaded up to full destructuration. The soil structure is evaluated by the ratio between the stress on the natural compression line and that on the reconstituted material at a given ratio or volumetric strain, and not by the absolute value of p_{s0}.

4.5. VALIDATION OF ET CREEP MODEL FOR NATURAL SOILS

Validation of the ET Creep model for the behaviour of natural materials under a variety of stress and strain paths was performed through a number of single element finite element analyses. The analyses were focused on the behaviour of overconsolidated and structured natural materials by mimicking common laboratory tests and by comparing the results with the observed experimental trends, as reported in Chapter 3.

Bodas Freitas (2008) validated the model through a series of finite element analyses, where the strengths and weaknesses of the ET Creep model were identified. The first set of analyses performed was on common laboratory tests on a typical soft clay. The second set included a series of laboratory tests on reconstituted samples of Hong-Kong marine deposits, a soft clay deposit, from which the ability of the model to mimic the behaviour of a real soil was assessed.

In particular, Bodas Freitas (2008) performed:

(a) finite element analyses of Ko stress paths for an unstructured soil in the normally consolidated range, including incremental loading (IL) 24-hour oedometer tests, constant rate of strain (CRS) oedometer tests, drained creep oedometer tests, and relaxation tests under Ko stress conditions;
(b) a coupled consolidation finite element analysis of IL 24-hour oedometer test on unstructured soil in the normally consolidated range;
(c) finite element analyses of CRS oedometer tests on structured soil in the normally consolidated range;
(d) finite element analyses of triaxial compression stress paths of an unstructured soil in both the normally and over consolidated range, including undrained triaxial compression and drained triaxial compression.

Also, finite element analyses were performed to simulate a wide range of laboratory tests on reconstituted samples of Hong-Kong marine deposits, where the analyses results were compared with the reported laboratory data. These included:

(a) undrained triaxial compression tests on normally consolidated samples at different values of constant axial strain rate;
(b) undrained triaxial compression tests on normally consolidated and overconsolidated samples sheared at a constant axial strain rate;

(c) undrained triaxial creep tests at different stress levels on normally consolidated samples;
(d) undrained triaxial compression test with stepwise change in strain rate combined with stress relaxation on a normally consolidated sample.

In this thesis, focus is given to natural materials which are in the overconsolidated range, and are known to developed significant viscoplastic strains under deviatoric conditions close to the peak deviatoric stress. A comparison of the predicted behaviour of natural overconsolidated soils with the observed experimental trends is performed. In particular, tests performed include:

(a) IL 24-hours oedometer tests on structured and unstructured soil in both the normally consolidated and overconsolidated range;
(b) CRS oedometer tests with a stepwise change in strain rate in the overconsolidated and normally consolidated range of an unstructured soil;
(c) drained creep tests under 1D conditions on unstructured overconsolidated soil;
(d) undrained triaxial compression tests with a stepwise change in strain rate on an unstructured overconsolidated soil;
(e) undrained triaxial creep tests on unstructured overconsolidated soil.

4.5.1. Model parameters

The model parameters employed for the single element analyses are listed in Table 4.3. The model parameters have been given values typical for stiff clays and they are equivalent to those employed in the analyses in Chapter 6 for the preliminary finite element analyses of piles in stiff clays.

p'_{mio}	λ/V	κ/V	$M_f = M_g$	$\alpha_f = \alpha_g$	$\mu_f = \mu_g$
kPa	-	-	-	-	-
10.0	0.060	0.030	0.8985	0.4	0.9
G	ψ_0/V	t_0	$\varepsilon^{vp}_{vm,limit}$	p_{s0}	ρ_s
kPa	-	day	-	kPa	-
70000.0	0.00409	1.0	0.412	0.0	0.0

Table 4.3: Model parameters for the validation analyses

4.5.2. Incremental load 24-hour oedometer tests

A series of incremental load (IL) 24-hour oedometer tests, by means of drained single element FE analyses, was performed, in order to examine the ET Creep model predictions in 1D compression. The first set of analyses includes tests on a normally consolidated, a lightly overconsolidated and a moderately overconsolidated unstructured soil sample with initial OCRs equal to 1.0, 1.5 and 4.0, respectively, following a loading-unloading-reloading-unloading path. The tests involve the application of a series of incremental loads with a load increment ratio $\Delta\sigma_v/\sigma'_v$ equal to unity for both loading and unloading, with the duration of each increment equal to 24 hours. Model parameters (see Table 4.3), initial stress conditions and initial void ratio for each test were identical, with the only variation being the OCR.

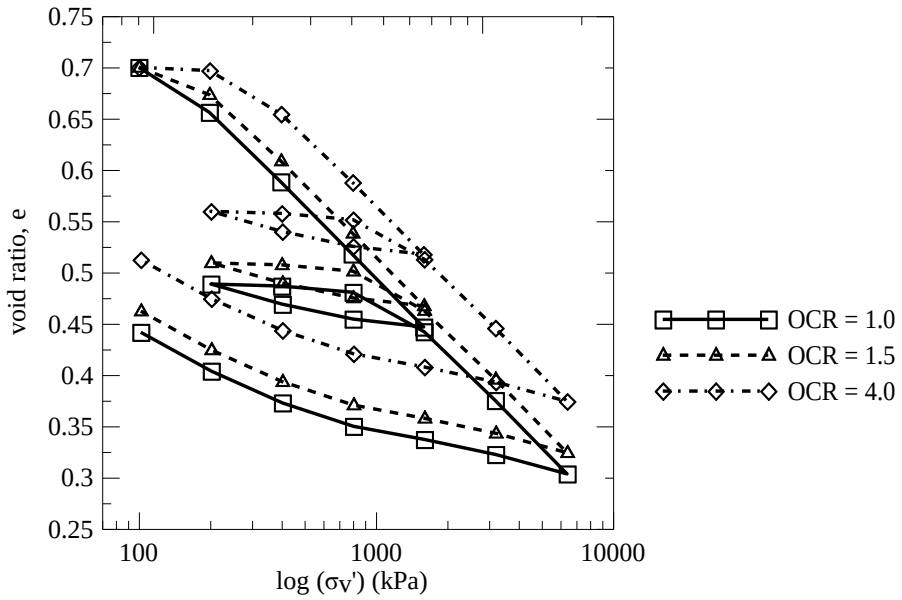


Figure 4.12: Incremental load 24-hours oedometer tests

The results are presented in Figure 4.12, from which it is observed that the behaviour between the different tests after initial 'yielding' (defined as the transitional zone between the overconsolidated and the normally consolidated range in the ET Creep model) is similar in both compression and swelling; the compression and swelling curves plot in parallel for the different tests. However, the slope of the initial compression curve (prior to initial 'yielding' for overconsolidated soils) for each test differs due to the variation in the initial values of OCR. For the heavily overconsolidated sample, it should be noted that, during initial loading, 'yielding' starts at a vertical effective stress representing an OCR larger than 1.0 and completes 'yielding' at OCR equal to 1.0; there is a transitional zone between swelling and compression lines, which is seen in all samples in reloading after unloading, and it is attributed to the fact that the closer the stress state to the reference time line (represented by

the compression line) the larger the development of viscoplastic strains. At the reference time line, strains develop according to the value of the model parameter λ/V, defined in Table 4.3.

The next set of finite element analyses include single element IL 24-hour oedometer tests of overconsolidated structured soils with an OCR equal to 4.0. Structure is defined by the parameters p_{s0} and ρ_s, which define the magnitude of structure and the rate of destructuration upon loading respectively. A parametric study was performed, where the parameter p_{s0} took the values of 10.0 kPa, 40.0 kPa and 100.0 kPa, and the parameter ρ_s the values of 500, 1000 and 2000, in order examine the effect of these parameters in 1D compression.

Figures 4.13a, 4.13b and 4.13c show the results for analyses with p_{s0} values of 10, 40 and 100 kPa respectively, where in each case the rate of destructuration is varied, and the compression lines plotted are compared with the compression curve of an unstructured soil. From Figure 4.13, it is observed that, depending on the values set to describe structure, different types of structure can be predicted, ranging from structures stable and difficult to break down to those that are unstable. For instance, in Figure 4.13a the limited deviation of the compression line of the structured soil in respect to the compression line of the unstructured soil indicates that the structure is very stable and it may be concluded that by adopting such values structure is not breaking down for stresses applied in engineering practice. On the other hand, in Figure 4.13c for high rates of destructuration, the structure is less stable. This is visualised by the significant change in the slope of the compression curve of the structured soil in respect to the compression curve of the unstructured soil. It should be acknowledged though that such high values of structure and rates of destructuration may be unrealistic and, therefore, not encountered in real soils.

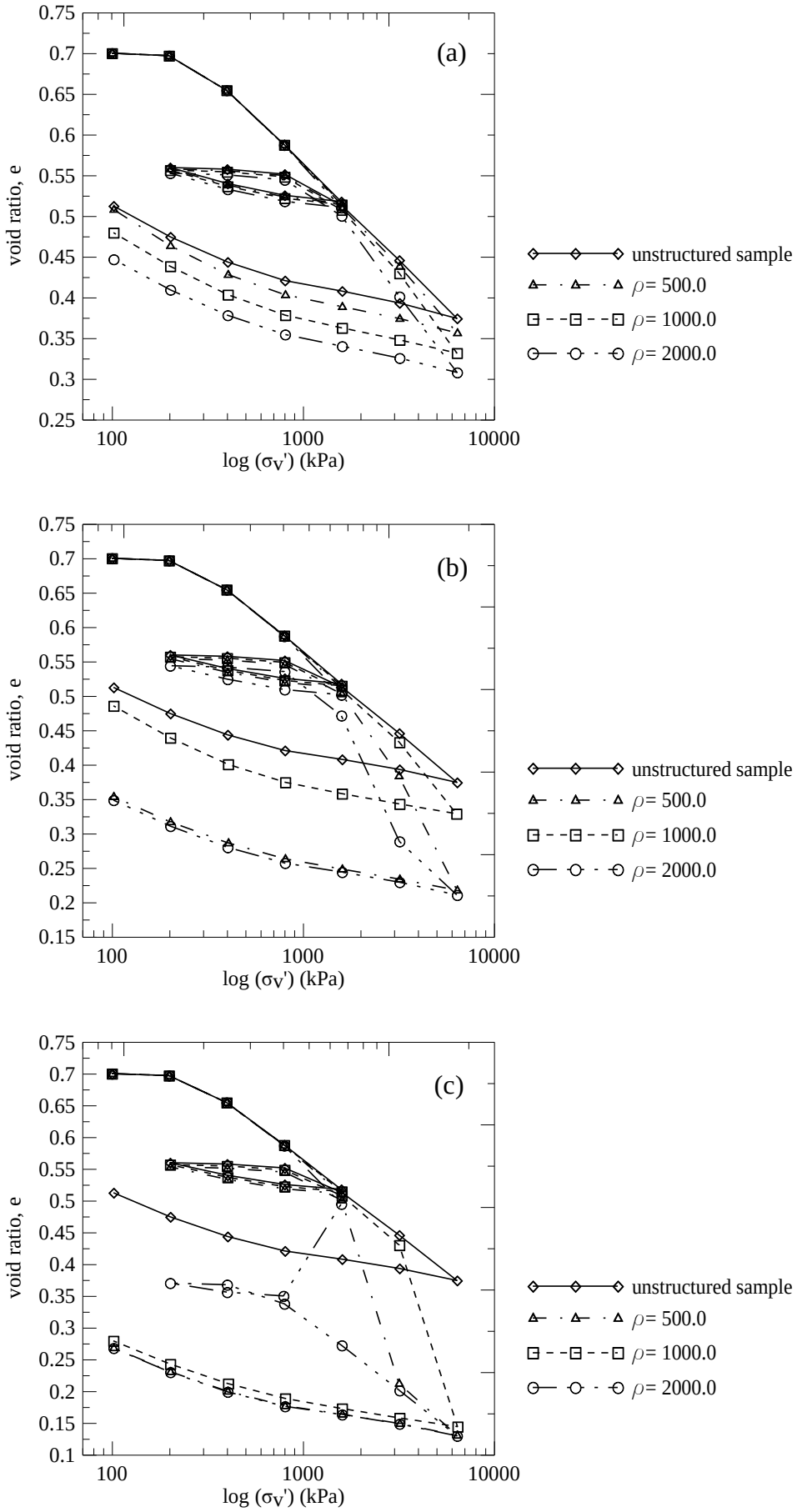


Figure 4.13: Incremental load 24-hour oedometer tests on structured soil – ET Creep model predictions for $\mathbf{p_{s0}}$ equal to (a) 10.0 kPa, (b) 40.0 kPa, and (c) 100 kPa

4.5.3. Constant rate of strain oedometer tests

A set of constant rate of strain (CRS) oedometer tests at four values of axial strain rate, by means of drained single element finite element analysis, was performed on an overconsolidated sample with OCR equal to 4.0, in order to examine the effect of strain rate in 1D compression in both the normally and overconsolidated range. The results are given in Figure 4.14, where $\dot{\varepsilon}_0$ is equal to 0.00409/day and corresponds to the value of the visco-plastic volumetric strain rate on the reference time line (see Equation 4.37). In the normally consolidated range, a different compression line is obtained for each strain rate. However this is not visualised in the overconsolidated range, where a common swelling line for each strain rate is plotted prior to 'yielding' (defined in Section 4.5.2).

The effect of strain rate change is observed in a CRS oedometer test, where the volumetric strain rate has been changed in a stepwise manner. It is observed that in the overconsolidated range of the ET Creep model (prior to 'yielding') there is no observable rate effect, despite the fact that the viscoplastic strains in the overconsolidated range are rate dependent. This is due to the fact that viscoplastic strains are very small in the overconsolidated range, resulting in a non-visible effect of strain rate change on strains. In the normally consolidated range, and close to it during 'yielding', a change in strain rate results in a noticeable change in the compression line in respect to the strain rate applied. A single stress-strain-strain rate relationship that is independent of the soil's previous loading history is obtained from the ET Creep model. This behaviour agrees with that of isotach viscosity.

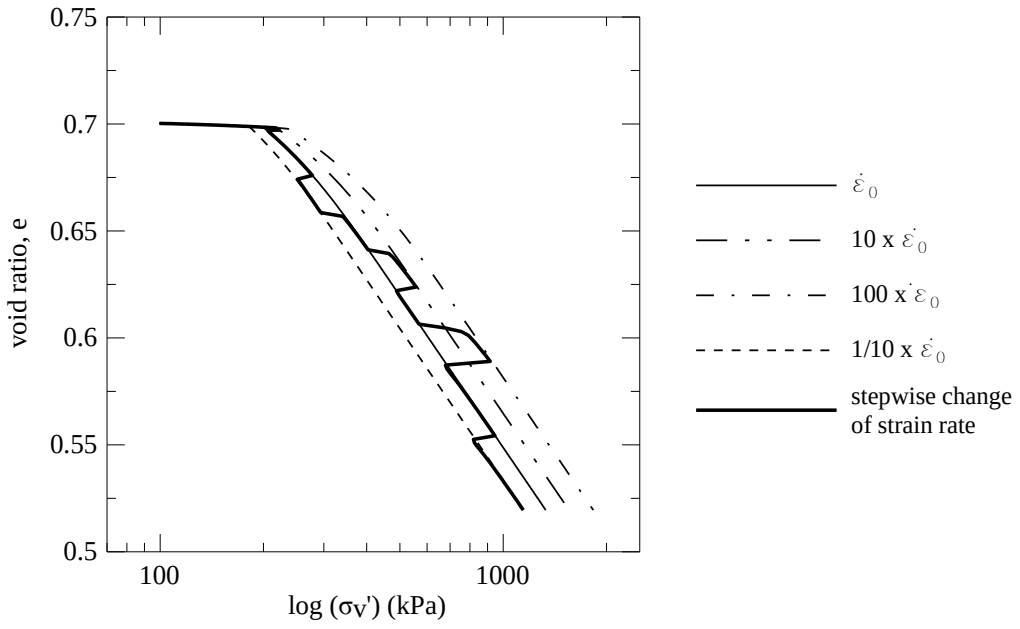


Figure 4.14: Constant rate of strain and stepwise change of strain rate oedometer tests

4.5.4. Drained creep tests under 1D conditions

A set of single element FE analyses that simulate CRS oedometer tests, during which a long creep period is applied at different stress levels, was performed on an overconsolidated soil sample with OCR equal to 4.0 under drained conditions, in order to examine the stress-strain response of the ET Creep model after a long period of creep. The applied strain rate was kept constant during the monotonic loading; it was equal to 0.00409/day and corresponded to the value of the visco-plastic volumetric strain rate on the reference time line (see Equation 4.37). The values at which a maintained vertical stress for a period of 510 days was applied correspond to OCR values of 3.0, 2.5, 2.0, 1.5 and 1.0. This allows the assessment of the development of visco-plastic volumetric strains (or creep strains) during drained creep for each case, in respect of the position of the current stress state to the reference time line.

In Figure 4.15, it is observed that following the drained creep period the compression curves are found to rejoin the original compression curve, with a stiffer response on reloading and with a gradual yield on rejoining the original compression curve. The yield stress is observed to be at a level well in excess of the magnitude of the stress that it had been subjected to during the drained creep period.

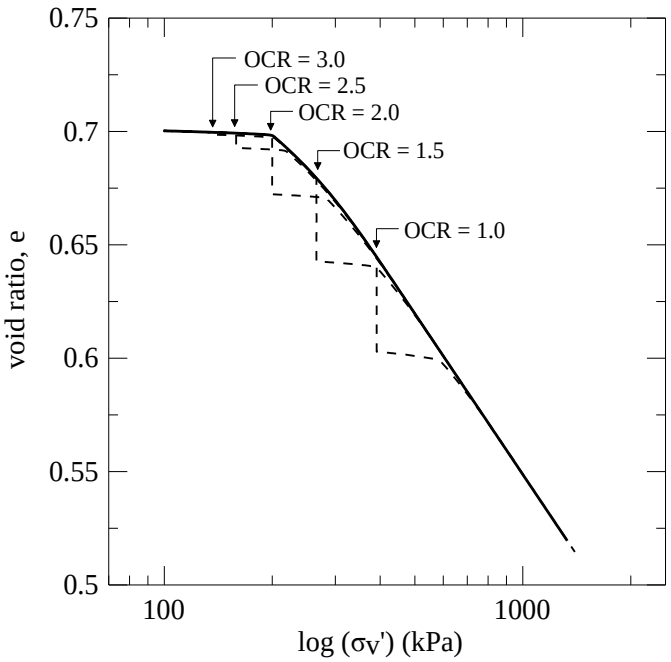


Figure 4.15: Drained creep tests under 1D conditions at different stress levels

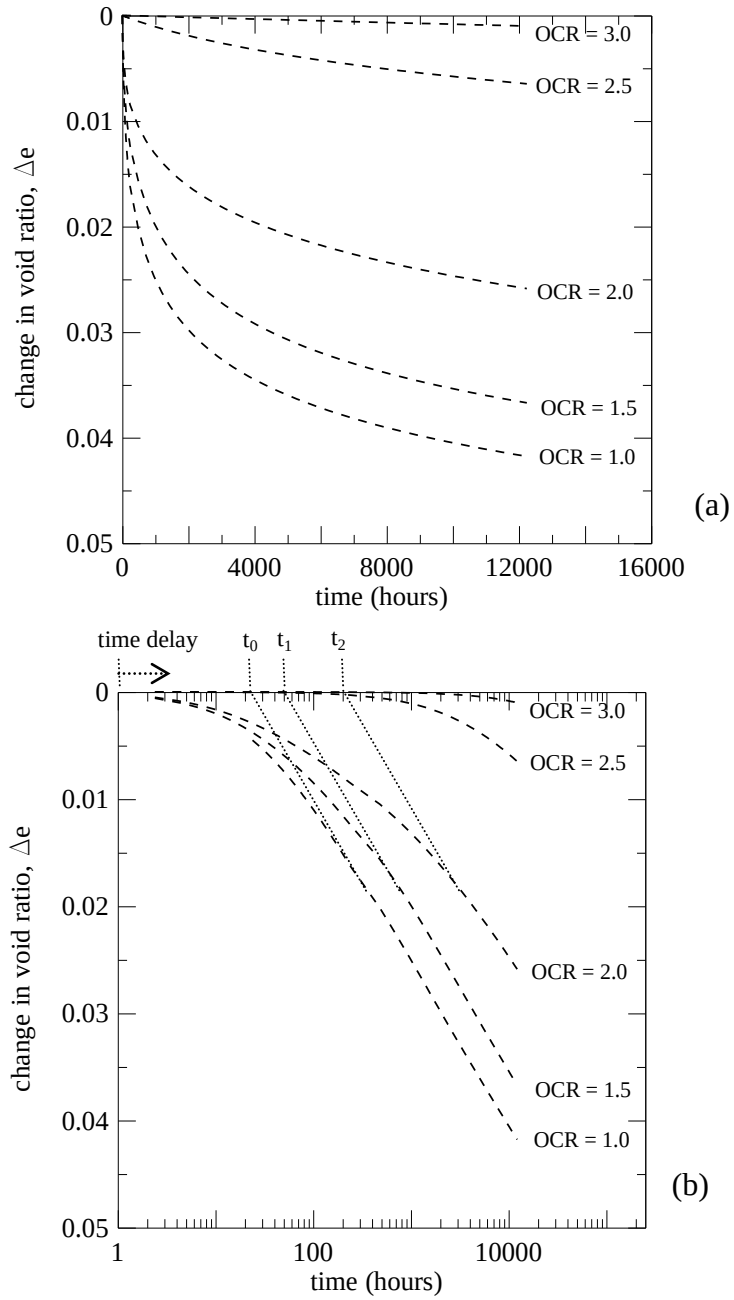


Figure 4.16: Change in void ratio during drained creep in 1D conditions

Figure 4.16a shows the change in void ratio with time during drained creep, due to the development of creep strains, for each level of maintained loading. It is observed that the larger the level of load during creep (i.e. the closer to the reference time line), the larger the development of viscoplastic strains. It would appear that at a load level of OCR equal to 3.0, creep strains are very small, indicating that, on the time scale examined in this set of tests, creep is insignificant at large values of OCR, whereas for values closer to 1.0, creep strains affect significantly the compressional behaviour of the sample.

Figure 4.16b shows the change in void ratio with time for each level of loading on a logarithmic scale of time. The change in void ratio is linear logarithmic, however a time delay between the start of the creep period and the establishment of the linear relationship between the void ratio change and the logarithm of time is observed. The time delay is obtained by the intersection between the tangent passing through the linear part of the Δe-log t curve and the time axis.

For the soil with OCR equal to 1.0, the time delay corresponds to the reference time t_0, which in this case is equal to 24 hours. This means that a period of 24 hours is required for viscoplastic strains to adopt a linear logarithmic relationship with time. Time delay is found to increase for higher values of OCR, which is associated with the position of the stress state in respect to the reference time line. The larger the OCR, the longer the time required for viscoplastic strains to adopt a linear logarithmic relationship with time.

4.5.5. Undrained triaxial compression tests

A set of undrained triaxial compression tests at various values of axial strain rate on an overconsolidated sample with OCR equal to 4.0 and isotropically consolidated to 300 kPa was performed, in order to examine the strain rate effects during shearing in the overconsolidated range of the ET Creep model.

The stress paths in J-p' space and the respective stress-strain paths are plotted in Figures 4.17 and 4.18 respectively for three axial strain rates ($\dot{\varepsilon}_0$ = 0.00409/day). In the J-p' space (Figure 4.17), the heavily overconsolidated samples follow initially a vertical effective stress path and the peak stress state is reached at stress ratios well above that at critical state line. The initial vertical stress path corresponds to the phase during which the behaviour is essentially 'elastic' (or pseudo-elastic). The stress path then bends to the right, with the soil yielding, as shown in the stress-strain response (Figure 4.18), towards the critical state line with a decreasing deviatoric stress until it reaches the critical state. It is observed that the larger the strain rate, the larger the peak undrained shear strength, indicating that the peak stress is strain rate dependent. Also, the fact that the initial vertical stress path is characterised as 'elastic' is because, at stress states at low deviatoric stress far from the reference time line, the amount of visco-plastic strains is limited. This results in a vertical pseudo-elastic response.

In addition, the effect of strain rate change was examined in an undrained triaxial compression test, where the axial strain rate has been changed in a stepwise manner. The results of this analysis are also plotted in Figures 4.17 and 4.18, from which it is observed that, despite the

fact the viscous behaviour is isotach for the whole stress path from initial shearing to yield and to critical state, the rate effects are not visualised at strains prior to yielding due to pseudo-elastic behaviour at stress states far from the reference time line. Close to yielding and up to the critical state, rate effects and isotach viscosity are visualised through the stepwise change in stress path.

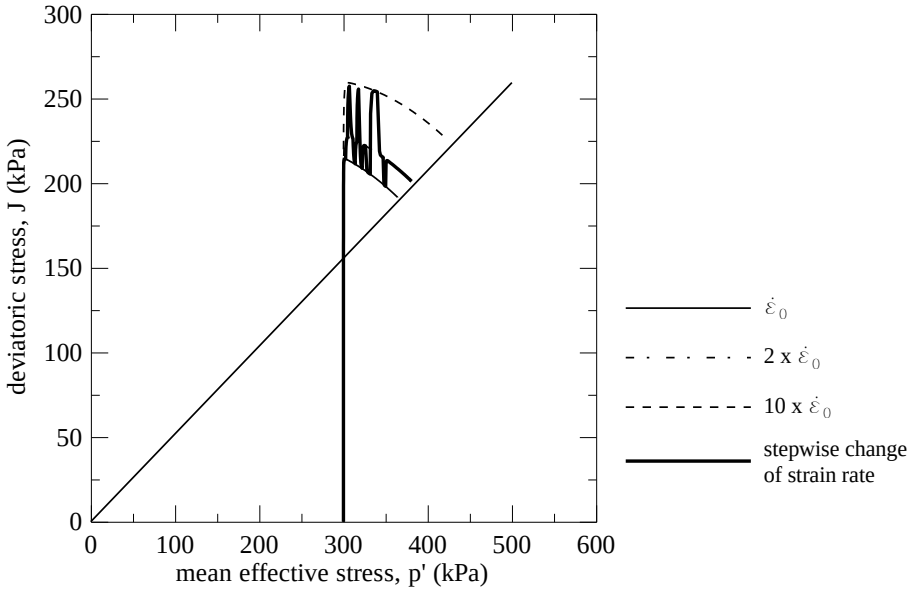


Figure 4.17: Stress paths for undrained triaxial and stepwise change of strain rate compression tests

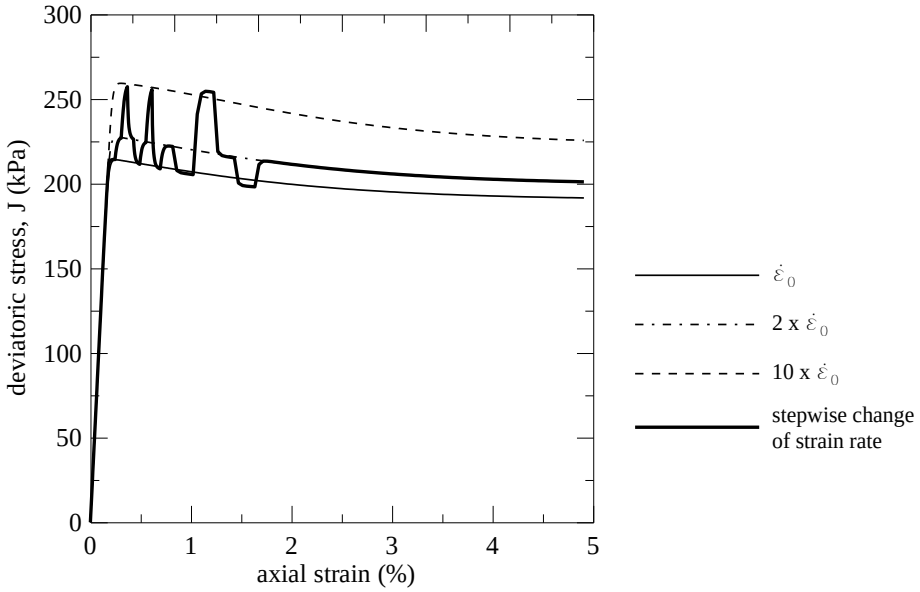


Figure 4.18: Stress-strain paths for undrained triaxial and stepwise change of strain rate compression tests

4.5.6. Undrained triaxial creep tests

A set of single element FE analyses that simulate undrained triaxial creep tests was performed on an overconsolidated sample with OCR equal to 4.0, in order to examine the ET Creep model response of natural soils when subjected to undrained creep under constant deviatoric stress conditions. The samples were loaded instantaneously to different levels of deviatoric stress with a constant axial strain rate of 0.00409/day, where at each stress level the samples were left to creep for a maximum period of 510 days under undrained conditions. Samples were restrained from undergoing any volume change, while the applied total stresses were kept constant, after which the samples were sheared to failure with the initial constant axial strain rate.

Figure 4.19 shows the stress paths followed by the samples which were left to creep at seven different levels of deviatoric stress, which are marked on the figure as percentage of the peak deviatoric stress obtained for the applied strain rate. It is observed that below the critical state line, the mean effective stress reduces during undrained creep, whereas above the critical state line the mean effective stress increases. This is due to the fact that the samples at stress states below the critical state line are trying to contract, resulting in an increase in pore water pressure during undrained shearing and subsequent undrained creep, as shown in Figure 4.20. On the other hand, for stress states above the critical state line, it is observed that the samples are trying to dilate, resulting to an increase in mean effective stress, due to the reduction in pore water pressure.

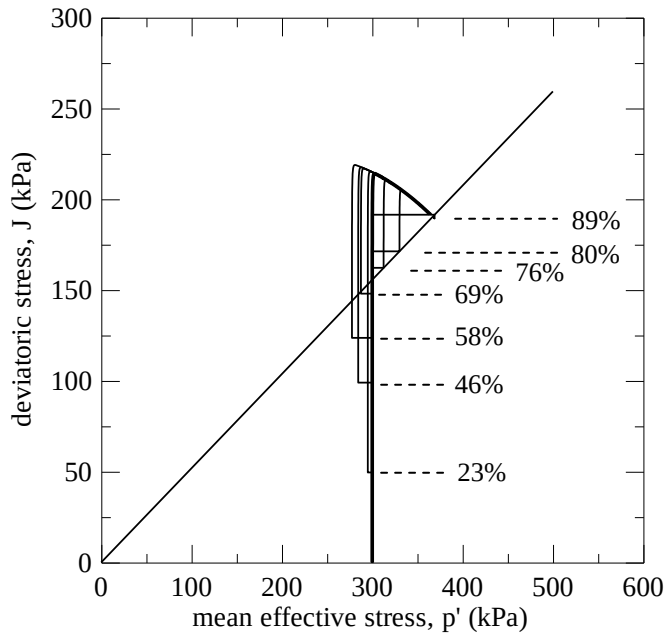


Figure 4.19: Stress paths for undrained triaxial creep tests at different stress levels

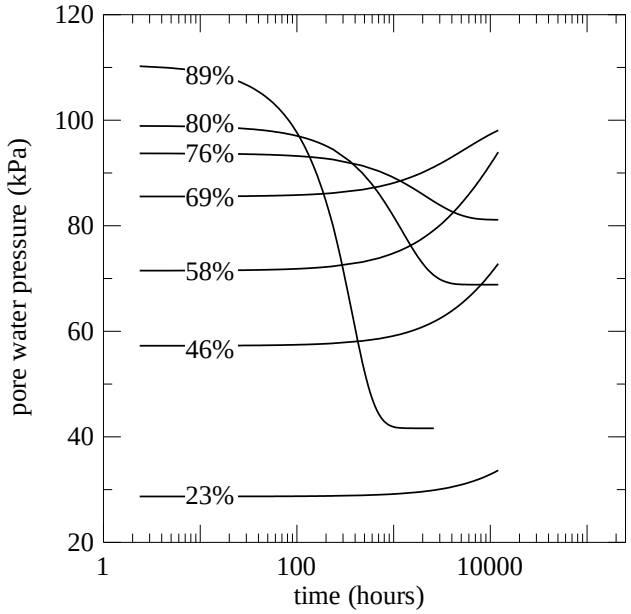


Figure 4.20: Development of pore water pressure with time during undrained creep

Moreover in Figure 4.19, it is observed that during creep the larger the deviatoric stress, the larger the gain in undrained shear strength. This is however the case up to a threshold value for stress ratios close to the critical state, above which undrained creep results in a reduced deviatoric peak stress on subsequent shearing. For larger stress ratios, at stress states close to the original peak deviatoric stress, undrained creep results in failure, due to the continuous straining towards the critical state. This is consistent with the behaviour of natural clays, where creep under constant deviatoric conditions (referred as deviatoric creep) at stress states close to the peak deviatoric stress may result in failure. This is equivalent to creep rupture, a phenomenon associated with the acceleration of the creep strain rate at stress states close to the peak deviatoric stress.

Figure 4.21 presents the stress-strain response for each test. It is observed that the viscoplastic strains developed at low levels of constant deviatoric stress during creep are significantly less than those developed close to the peak stress. Despite the fact that failure is initiated due to the development of large viscoplastic axial strains for stress states close to the peak deviatoric stress, on reloading it appears that a peak is reached before eventually the stress path reaches the critical state line. This peak on reloading is associated with a change in strain rate.

In Figure 4.22, the development of axial strain rate with time is presented. It is observed that the larger the deviatoric stress, the larger the axial strain rate during undrained creep, being consistent with the concept of equivalent time. Also, at stress states below the critical state line, it is observed that the axial strain rate reduces with time. For stress states above the

critical state line, the strain rate increases up to the point where the stress state reaches the critical state; at critical state the strain rate is constant. This fact indicates that the soil, at stress states above the critical state line and close to the peak deviatoric stress, is straining towards failure during undrained creep with an increasing strain rate. This increase in strain rate is observed on the 'dry' side of the loading surface of the ET Creep model (i.e. in OC soils) and not in NC soils (Bodas Freitas, 2008).

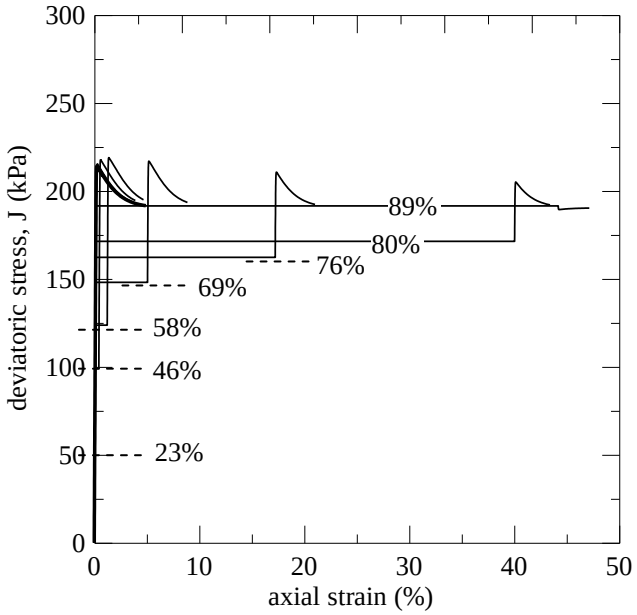


Figure 4.21: Stress-strain paths for undrained triaxial creep at different stress levels

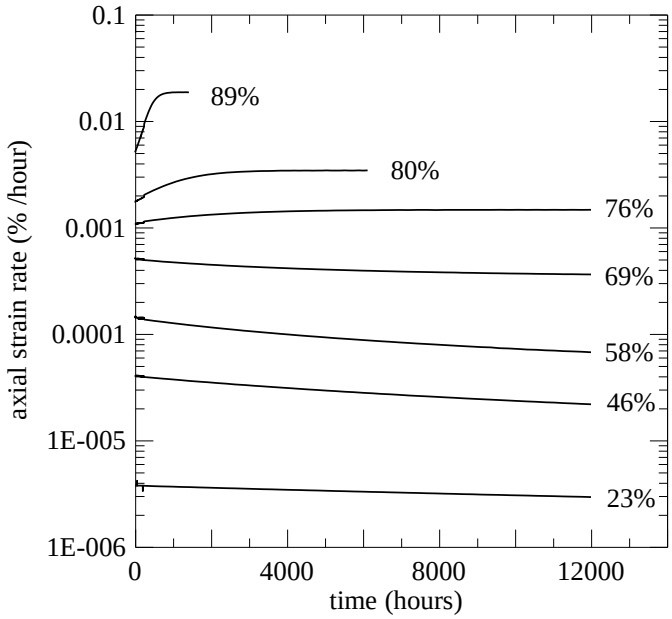


Figure 4.22: Axial strain rate during undrained creep for different stress levels

4.6. CONCLUDING REMARKS

The finite element method satisfies the four fundamental requirements for a true theoretical solution including the equilibrium of forces, compatibility of displacements, material constitutive behaviour and boundary conditions. Continuity of flow and generalised Darcy's law is satisfied as well, giving the opportunity to perform coupled finite element analysis, where time is incorporated. The software package used for the finite element analyses is the Imperial College Finite Element Program (ICFEP), which employs a modified Newton-Raphson approach with an error-controlled sub-stepping algorithm as a non-linear solver.

The accuracy of the finite element solution depends on the ability of the constitutive model to represent real soil behaviour and on the correctness of the boundary conditions imposed in the analysis. It is in the hands of the geotechnical engineer to assess these parameters in design, in order to reflect accurately the field conditions. In this thesis, two constitutive models are employed to model the behaviour of saturated clays, including a form of the elasto-plastic Modified Cam Clay model and the visco-plastic Equivalent Time (ET) Creep model developed by Bodas Freitas (2008), which can account for soil viscous behaviour and can reproduce soil deformations due to creep. Both models are critical state models.

A series of finite element analyses employing the ET Creep model have been performed by Bodas Freitas (2008), primarily for normally consolidated soft clays, in order to validate the formulation of the model by comparing the model predictions with the observed experimental trends. Further validation of the ET Creep model is performed by the author for the time dependent behaviour of natural overconsolidated stiff clays, such as London Clay, from which the following are concluded.

Isotach viscosity in the normally consolidated range in one-dimensional compression, as well as strain rate dependency of the peak deviatoric stress in undrained triaxial compression, is well predicted by the ET Creep model. Strain rate dependency at low deviatoric stresses during undrained triaxial compression and in the overconsolidated range during one-dimensional compression agrees also with isotach viscosity.

Development of creep strains in one-dimensional compression and undrained triaxial compression are well predicted, along with the failure initiated at stress states close to the peak deviatoric stress under constant deviatoric creep associated with creep rupture.

Finally, the presence of structure in natural overconsolidated stiff clays and it degradation upon loading can be employed in the ET Creep model; however no development of structure with time during creep can be predicted.

Chapter 5

Constitutive Model Calibration

5.1. INTRODUCTION

The Equivalent Time (ET) Creep model developed by Bodas Freitas (2008) is employed in this thesis to perform finite element analyses of piled raft foundations and contribute towards their optimum design. The soil that is under investigation is London Clay, a stiff overconsolidated clay formation, where recent building redevelopments in Central London have highlighted the emerging problem with old foundations and congested underground space.

Field investigations of London Clay, along with results from laboratory tests, allows the calibration of the ET Creep model parameters. Due to the time dependency of the model, both monotonic rate and time dependent behaviour of London Clay are simulated. Results from laboratory tests performed by Gasparre (2005) and Sorensen (2006) on London Clay samples from the site of the recently developed Heathrow Airport Terminal 5, west of London, are utilised, in order to obtain the model parameters. These are then employed in numerical analyses of piled foundations in Chapters 6 and 7. In addition, the extended soil investigation of the Terminal 5 Heathrow area performed by Hight et al. (2003) allows the definition of the geotechnical profile of the Heathrow T5 area.

Research on the behaviour of London Clay has been intense since the 1960s; however there has been a gap for several decades in this research. Important work conducted in the 1960s include Som (1968), Lovenbury (1969) and Davies (1975). Recently, with the development of Heathrow Airport Terminal 5, the opportunity arose to examine the behaviour of London Clay with more advanced laboratory equipment. In this thesis, the focus is on the results from this recent research, however research from the past is considered as well.

In this chapter, a description of the London Clay is made by highlighting the geological history of the London Clay Formation and by describing the local geology, lithological units and index properties at Heathrow, from which soil samples have been extracted in order to be tested in the laboratory. The macrofabric of London Clay is also discussed along with its effects on shear strength. Subsequently, the viscous behaviour of London Clay, along with the capabilities of the Equivalent Time Creep model to reproduce the time dependent behaviour, is described. The coefficient of secondary compression C_α, a major time-dependent parameter of the ET Creep model, is obtained. Loading surfaces of the ET Creep model for London Clay for each lithological unit are determined. The shear stiffness corresponding to pile loading in the field and that obtained from common laboratory tests, with relevance to the ET Creep model, are discussed. Finally, the ET Creep model parameters are calibrated by employing oedometer, triaxial and creep tests, allowing the calibration of the model parameters defining the compression, strength and stiffness, and time dependent behaviour of London Clay, respectively, for each individual lithological unit and sub-unit.

5.2. DESCRIPTION OF LONDON CLAY: BACKGROUND

The London Clay is a stiff overconsolidated bluish coloured marine clay (it becomes brown when weathered) of high plasticity and low sensitivity, whose macrofabric is characterised by the presence of fissures. It is heavily overconsolidated as a result of significant erosion events after deposition and also naturally structured from both sedimentation processes and post-sedimentation processes such as ageing.

According to the British Geological Survey (2004), "the London Clay is predominantly argillaceous and about 60 % of the formation consists of thoroughly bioturbated, slightly calcareous, silty clay to very silty clay". The London Clay Formation is divided into several lithological units, which depend on the historical deposition of the London Clay sediments.

In the following, a description of the history of the London Clay Formation is made and the local geology and lithological units at Heathrow are described. Also, the macrofabric of London Clay and its effect on shear strength are discussed.

5.2.1. History of the London Clay Formation

The London Clay Formation is a marine geological formation of the Early Eocene period, which was deposited in a basin that was subsiding and in which sea levels were raising. The

formation of London Clay is considered to be a sequence of deposition-erosion events; however in this thesis it is assumed for simplicity reasons, following Gasparre (2005), that processes such as erosion are taking place after the soil deposition is complete. Therefore, the geological history of the London Clay is divided into depositional and post-deposition processes, as described below.

The following summary of the geological history of the London Clay Formation is based on King (1981).

(a) Depositional processes: the London Basin and Hampshire Basin

The London Clay has a history of about 52 to 55 million years and it was deposited in the Early Eocene (Ypsesian age). The historical sequence starts in the Late Palaeocene, when the movement of the plate tectonics in the Northern Atlantic Sea created the conditions for the formation of a sedimentary basin, which originally included a large part of Northern and North-Eastern Europe, England and Scotland. In the Early Eocene, the London Clay deposition started in this sedimentary basin, due to a sea level rise over an area known as the Northern Sea Basin, where different geographical zones were formed afterwards, due to subsequent regional geological events mainly linked to sea level changes. The Northern Sea Basin included part of Southern England up to the Welsh Massif, Northern France, Western and Northern Belgium and Northern Germany (Figure 5.1).

In Southern England, two areas of the London Clay Formation are identified by King (1981): the Hampshire Basin and the London Basin. The sequence of deposition is shown in Figure 5.2, where the stratigraphy of the London Basin in Southern England is presented. The lowest and oldest unit is the Thanet Sand Formation, which is composed mainly of shallow marine sands. It was deposited in the Late Paleocene (Thanetian age) 56 to 58 million years ago on top of the Chalk. On top of the Thanet Sand Formation lies the Lambeth Group (a transgressional series of sands, silts and clays), which was deposited during the late Thanetian and early Ypsesian ages. It consists of the Upnor Formation, the Woolwich Formation and the Reading Formation. The Lambeth Group is overlain by the Thames Group, which consists of the older Harwich Formation (a glauconitic sand) to the younger London Clay Formation, which in turn underlies the Virginia Water Formation (a glauconitic sand with clay lamines and lenses), a formation encountered today at some localities in the North-West Surrey and East Berkshire.

The London Clay was deposited in a marine environment where the sea level was generally rising, however it involved several cycles of sea level changes, referred to as transgressive-

regressive cycles, where an initial marine transgression is followed by gradual shallowing of the sea. These cycles influenced the depositional process, resulting in the formation of different depositional sequences (stratigraphy) and features. A fall in sea level was related to the coarsening of the material being deposited, which was more evident at the edges of the depositional basin. The Hampshire Basin is located close to the edges of the depositional basin, where the effect of these cycles was more intense. This resulted in a varied stratigraphy, where all sea level cycles can be identified by the coarsening upwards of the sequences. On the other hand, the London Basin soil was deposited in deeper waters, in a lower energy environment than that in the Hampshire Basin, where there was not enough time for the sediments to deposit completely before the next sea level rise, resulting in a less evident stratigraphy of the deposited material. In order to illustrate these processes, King (1981) produced Figure 5.3, in order to present the depositional sequences in both areas linked to sea level variation.

The different cycles of sea level change and the equivalent changes in sedimentation are the basis for King's division of the London Clay into lithological units, based on the content of fossil fauna (biostratigraphy) and partly on the contents of sand and silt. Five major cycles are recognised in the London Clay, which are used to define its five divisions (divisions A to E, Figure 5.4). The total thickness of the London Clay Formation varies between 50 m and 150 m in the London Basin and between 50 m and 130 m in the Hampshire Basin. The full sequence of units or divisions is found only in some areas of the London Basin, such as in Southern Essex or Hampstead heath. However, in most areas, including Heathrow in west London, only the lower parts of the sequence are encountered today, from unit C and below.

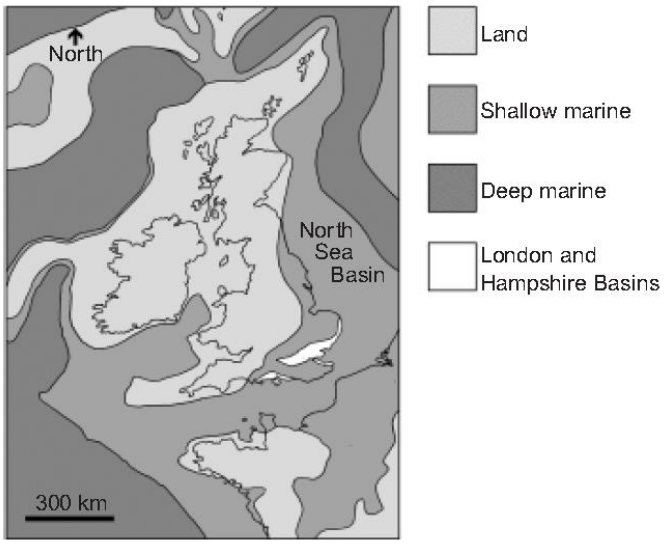


Figure 5.1: Palaeogeographical reconstruction of the 'London Clay Sea' in the Early Eocene (Ziegler, 1990)

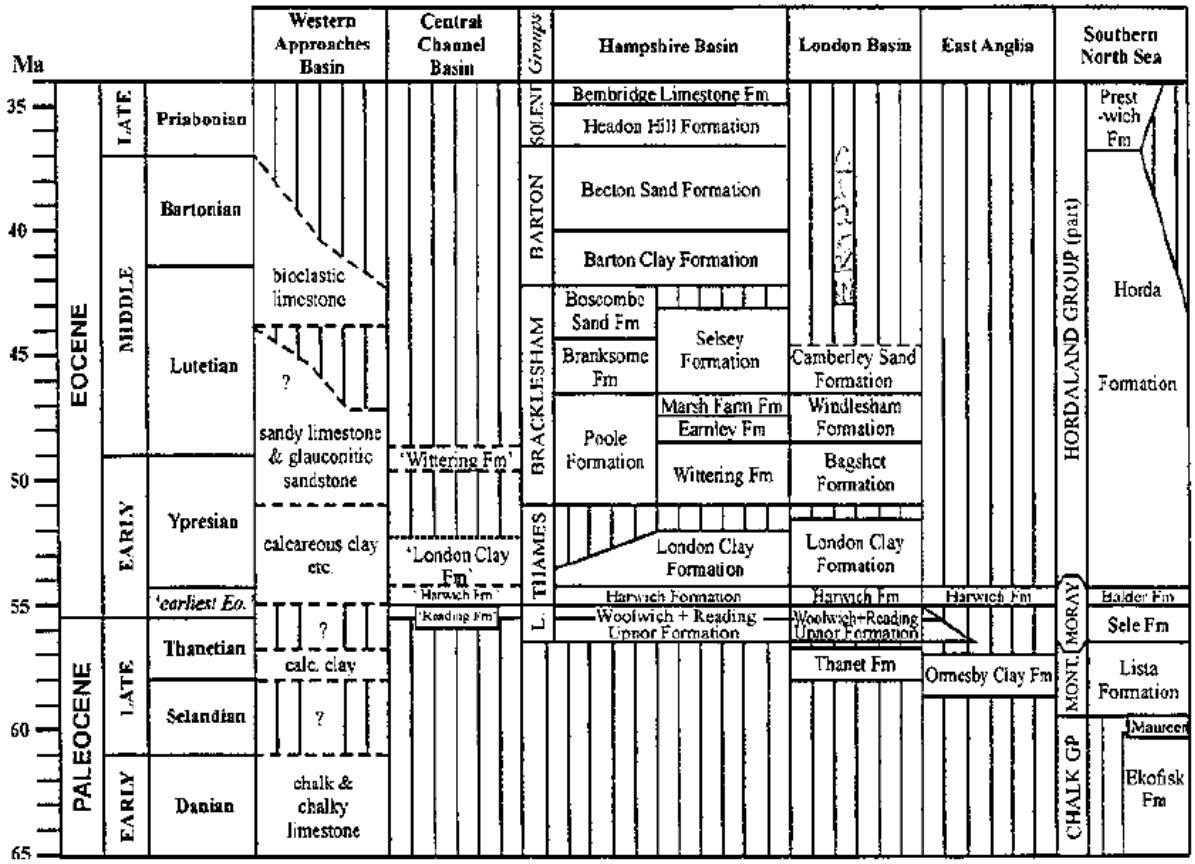


Figure 5.2: Eocene stratigraphy of the London Clay Formation in Southern Britain (King, 1981)

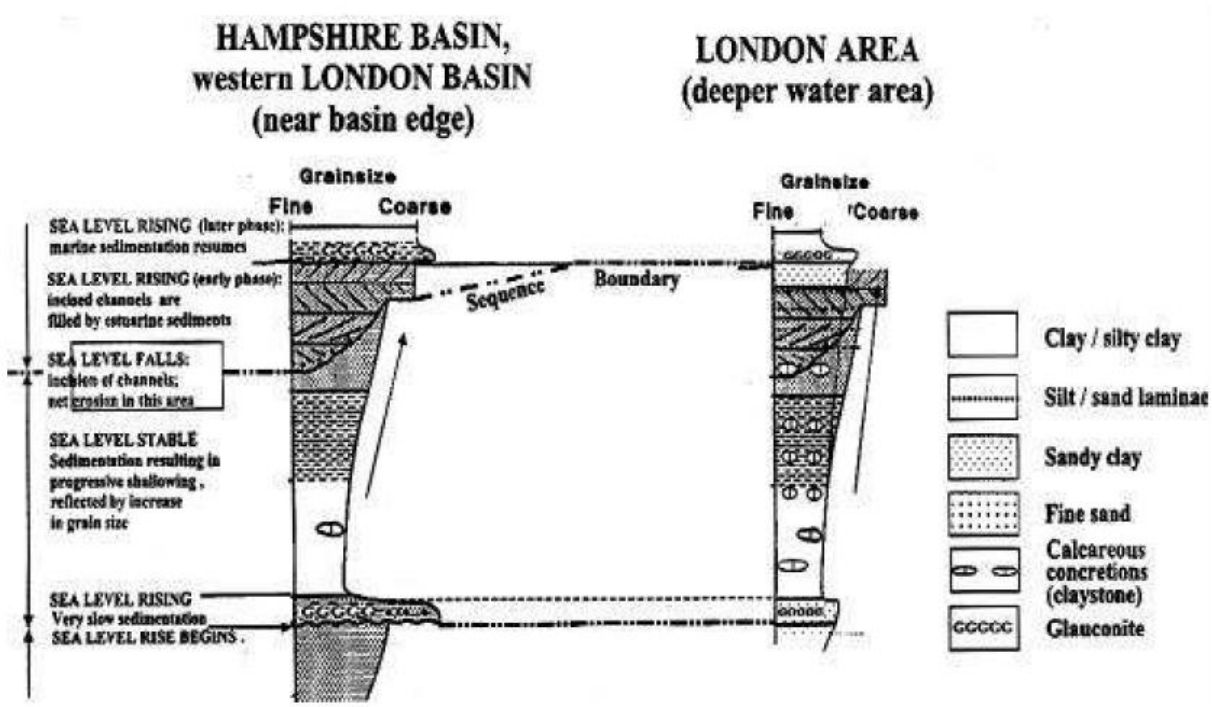


Figure 5.3: The London Clay Formation: idealised depositional sequences linked to sea level changes (King, 1981)

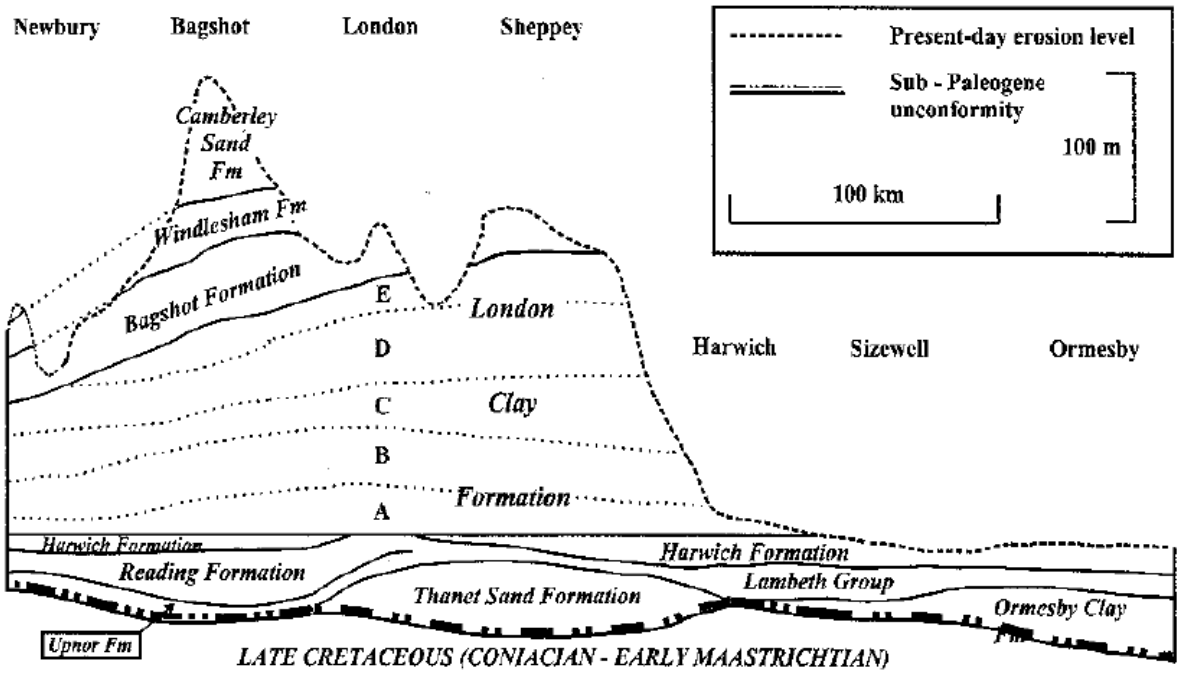


Figure 5.4: Palaeocene and Eocene sections of the London Clay Formation (King, 1981)

(b) Post-depositional processes: influence of the Alpine orogeny, erosion and weathering

The Alpine orogeny, erosion and weathering have played a role in the geology of Southern England and are processes that have formed the current geology in the London area. The Alpine orogeny has influenced the formation of the London Basin, whereas erosion and subsequent weathering have influenced the thickness of London Clay and the properties of the weathered London Clay respectively.

The formation of the London Basin has been influenced by the Alpine orogeny, whose compression of the subsiding London Platform and its sediment have resulted in the eastward plunging syncline of the London Basin. This syncline is very gentle, however several local faults have been identified, with dips no more than 3 degrees. It is considered that the Alpine orogeny is responsible for the formation of fault-blocks by the wave of energy developed in this process. These fault-blocks are believed to be responsible for the formation of discontinuities in the London Clay layer, due to the relative slippage between each other.

Erosion is a process that has been very influential on the current geology of the London Clay. Erosion took place in the Tertiary and Pleistocene epochs, during which a substantial thickness of London Clay was eroded. In particular, it is estimated that erosion ranges from 150 m in Essex (Skempton, 1961) to 300 m in the Wraysbury district (Bishop et al., 1965), and it has involved all the overlying deposits, and in some areas including the Thames Valley,

a large part of the London Clay itself, where Quaternary gravel sheets have been deposited after erosion (King, 1981). An important process associated with this erosion is the mechanical overconsolidation of the London Clay, which influences its current behaviour in its undisturbed state.

Weathering is a more recent process that followed erosion. The effect of weathering on London Clay can be visualised by the changing colour of the clay from blue-grey to brown due to oxidation, which is evident in areas where the London Clay outcrops. The thickness of London Clay which has been affected by weathering varies between 3 m and 6 m depending on the lithology. Weathering is stronger close to the surface, where the clay has a granulated or fragmented texture. On the other hand, with increasing depth weathering is less obvious and the structure of the clay becomes increasingly clear. In the case where Terrace Gravels overly London Clay, the weathered layer is limited to a very small stratum immediately below the base of the gravel, and unweathered material is found usually at about 1 m below the gravel. (Chandler, 2000)

5.2.2. Geology, lithological units and index properties at Heathrow

Heathrow is located in the west of the London Basin, where the London Clay Formation is covered by late Quaternary Terrace Gravels. Geological evidence suggests that these were deposited after erosion of perhaps 200 m of the upper part of the London Clay Formation.

Hight et al. (2003) present the geological section at Heathrow Airport Terminal 5 in Figure 5.5, where a 6 m layer of terrace gravel is evident on top of London Clay. The thickness of London Clay is found, from borings, to be 52 m and includes units A, B and C. Units A and B can be divided into sub-units A_2, A_3 and B_1, B_2 respectively, as shown in Figure 5.5. The thickness of units A, B and C is approximately 25m, 23m and 5m respectively. The water table was found to be at 1.5 m above the top of the clay and the pore water pressure was found to be hydrostatic.

The lithological units and their respective sub-units within the London Clay can also be identified also by utilising the water content profile with depth (Standing and Burland, 2006; Hight et al., 2003). Figure 5.6 shows the water content profile with depth for the Terminal 5 area ranging between 22.5 and 27%, where different units and sub-units are identified by Hight et al. (2003) using graphical means. In Figure 5.6, profiles of Atterberg limits by Hight et al. (2003) are presented, along with the lithological unit and sub-unit boundaries, where liquid and plastic limits range between 60-70% and 24-29% respectively depending on depth.

Also, it is observed that unit B_2 and its sub-units are generally more plastic than units A_3 and A_2.

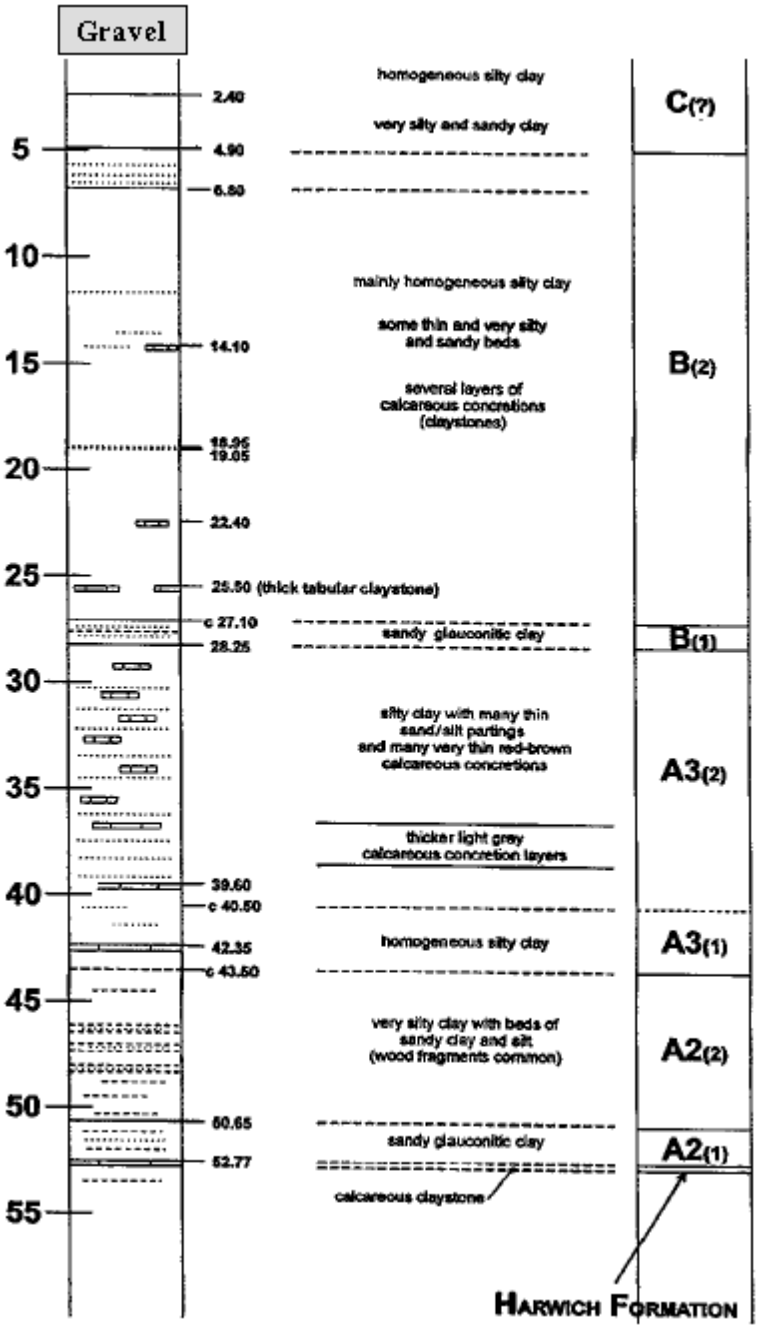


Figure 5.5: Geology of London Clay at Heathrow Airport Terminal 5 (Hight et al. 2003)

Gasparre (2005) and Sorensen (2006) performed laboratory tests on London Clay samples for the majority of the lithological units encountered at the Heathrow T5 site to characterise the profile of the London Clay in terms of engineering properties. In particular, Gasparre (2005) performed tests on samples from units C, $B_{2(c)}$, $B_{2(b)}$, $B_{2(a)}$ and A_3, whereas Sorensen (2006)

only from unit $B_{2(b)}$. More details about the tests performed are given in Sections 5.7 and 5.8, where the results are compared with the predictions of the ET Creep Model.

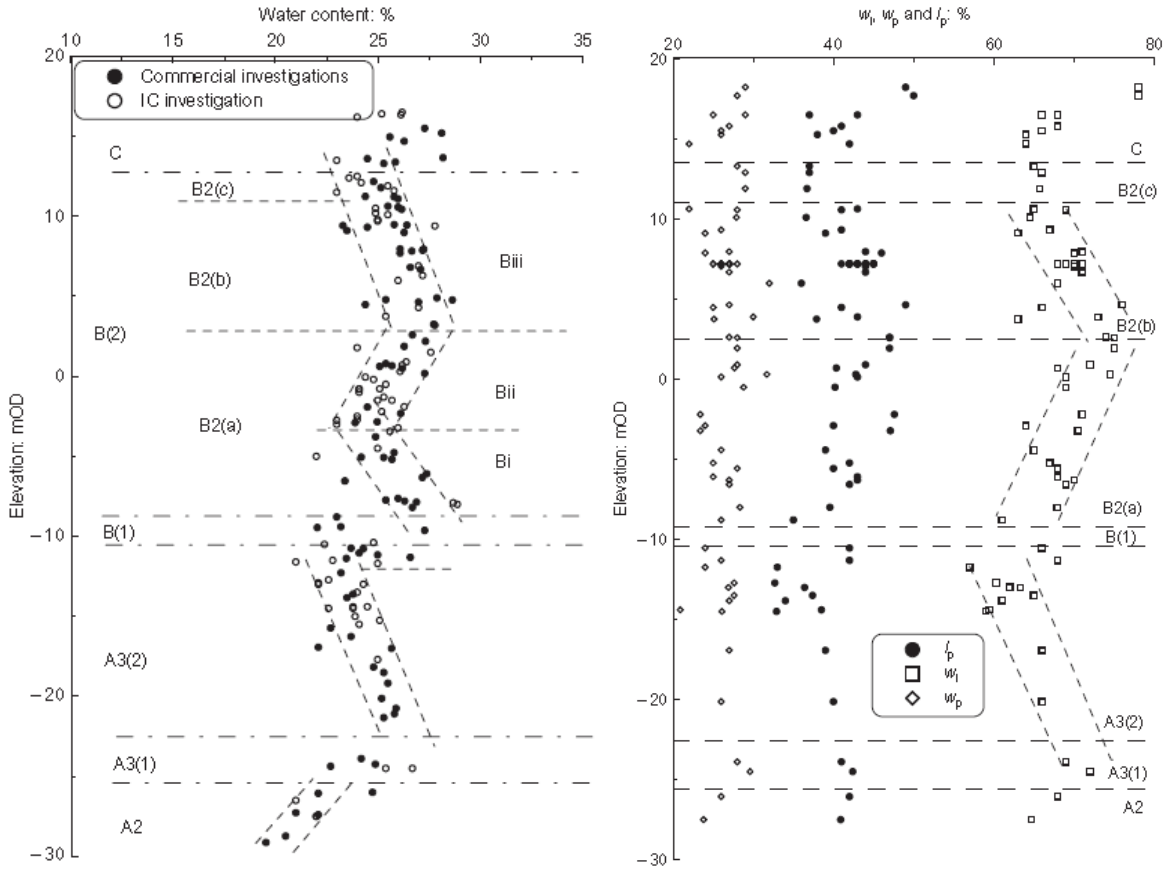


Figure 5.6: Water content profile and profile of index properties with lithological unit and sub-unit boundaries (Hight et al. 2003)

5.2.3. Macrofabric and shear strength

The macrofabric of the London Clay is characterised by natural discontinuities, whose engineering importance is significant. Gasparre (2005) describes that discontinuities in the London Clay are classified as laminations, backs (or joints) and fissures, whose distribution and orientation are considered to reflect the structural bedding and the erosion history of the clay. Laminations (or bedding) are characterised by a thin parting of more silty material and correspond to the boundaries between the lithological units. Joints (or backs) are large fractures, predominantly vertical, forming a series of intersecting curved surfaces. Fissures are small fractures existing in the clay, which are randomly oriented and have an irregular area.

Fissures in the London Clay tend to have variable spacing, from a few centimetres to a few tens of centimetres. They tend to be discontinuous and extend up to around 15 cm with orientations that are horizontal to sub-horizontal and vertical to sub-vertical (Skempton et al.,

1969). Their geometry and surface allow the identification of the possible causes of their formation according to Gasparre (2005), including fissures due to shear (smooth surfaces and curved conchoidal geometry) and tension (planar and rough) having orientations related to tectonic stress folding at the time of formation possibly during Alpine orogeny, fissures influenced by depositional variations (planar and rough), which are parallel to the bedding, and fissures influenced by the stress release during erosion and are parallel to the present ground surface.

It has been reported by Skempton et al. (1969) that the fissure intensity reduces with increasing depth, which is consistent with the observations made by Hight et al. (2007) at Heathrow. In particular, it was observed that unit A_2 is not fissured, whereas in unit A_3 one out of the eight samples tested failed along a pre-existing fissure; a much lower proportion than in the overlying units indicating the larger intensity of fissures closer to the ground surface.

The fissures are known to have an important effect on the mass behaviour of the clay and in particular it has been shown in the literature that they have an effect on shear strength. According to Hight et al. (2007), the shear strength of a clay (not subjected to shearing before) can range between two bounds: an upper bound, which is the peak stress for the intact clay without fissures where a brittle behaviour is observed, and a lower bound, which is the stress that causes the soil to fail along a pre-existing fissure, this indicating the fissure strength. Generally, the effective stress parameters of a clay lie between these two bounds depending on the spacing, extent and orientation of the fissures, on the direction of shearing, and on kinematic constraints. Gasparre (2005) concluded that natural fissures only affected large strain behaviour if they were oriented in directions compatible with the shearing mode. On the other hand, for clays that have been sheared before there is a lower bound, which is the residual strength, which lies between 10 and 12 degrees according to Hight et al. (2007), and it depends on the amount of the past displacement on the shear surface. Fissure strength is considered to be equivalent to post-rupture strength of the initially intact samples according to Gasparre et al. (2007), indicating that the natural fissures have not been subjected to large movements.

5.3. VISCOUS BEHAVIOUR OF INTACT LONDON CLAY AND THE CAPABILITIES OF THE ET CREEP MODEL

The viscous behaviour of London Clay in both the undisturbed and reconstituted state has been examined by Sorensen (2006) through laboratory tests on intact and reconstituted samples of London Clay from the Heathrow Airport Terminal 5 area. In particular, Sorensen (2006) conducted a series of advanced triaxial and oedometer tests, from which a framework of the viscous behaviour of London Clay was produced. In addition, research on the time dependent behaviour of London Clay performed in the past by Som (1968), Lovenbury (1969) and Davies (1975) through laboratory tests on intact London Clay samples, allows the review of the viscous behaviour of London Clay and the subsequent assessment of the capability of the ET Creep model to reproduce this behaviour.

Sorensen (2006) conducted a series of triaxial tests on intact samples of London Clay, reconstituted samples and overconsolidated reconstituted samples of London Clay. This work examined the influence of natural structure on the viscous behaviour and it compared it with the viscous behaviour of NC reconstituted samples. Also, the effect of mechanical overconsolidation as opposed to that of natural structure on the viscous behaviour was isolated. This allowed the development of a framework for the viscosity of London Clay by examining the influence of strain rate effects. From the tests performed, Sorensen (2006) drew Table 5.1 to compare the experimental findings. Figure 5.7 was also produced to present the conceptual viscous behaviour of intact, NC reconstituted and OC reconstituted samples of London Clay in a common plot during undrained shearing.

Regarding the tests on intact samples, which are the interest of this thesis, two triaxial compression tests were performed by Sorensen (2006), one drained and one undrained (see Section 5.8), with step changes in the axial strain rate, from which it was summarized that the viscous behaviour is isotach, with persistent effects of strain rate changes on the stress-strain path. In particular, it was observed that there is a unique stress-strain curve for a given strain rate. This is the case for both drained and undrained tests and for both small and large strains in the pre-peak and post-peak regions. Regarding the strain rate change, it was also observed that the immediate response is very stiff and nearly elastic, followed by a gradual yield, and with continued shearing the stress-strain path approaches and follows the path for the new strain rate without overshooting. Such viscous behaviour is referred to as isotach and it is observed both pre- and post-peak during shearing; it is similar to the behaviour of soft rocks, soft clays and other undisturbed stiff natural clays, according to Sorensen et al. (2007).

Sorensen (2006) also concludes, from the triaxial compression tests on intact samples of London Clay, that the peak strength envelope is affected significantly by strain rate, and therefore it is strain rate dependent, while the critical state appears to be independent of strain rate and unique in the e-p'-q space. These conclusions are visualised in Figure 5.7, where the normalised conceptual viscous behaviour in triaxial compression is plotted.

	OC intact	**NC reconstituted**	**OC reconstituted**
Monotonic rate behaviour	Very brittle	Ductile	Slightly brittle
Viscous behaviour – small strains	Isotach		
Viscous behaviour – large strains	Isotach	Non-isotach	Non-isotach
Persistent stress jump for given ratio of axial strain rate change until peak	Increases with increasing stress level	Reduces with increasing stress level	Constant?
Temporary stress jump for given ratio of axial strain rate change until peak	None	Increases with increasing stress level	Increases with increasing stress level
Total immediate stress jump for given ratio of axial strain rate change until peak	Increases with increasing stress level	Constant	Increases with increasing stress level
Immediate stiffness response to axial strain rate increases	Very stiff		
Strain rate dependency of …			
Peak strength envelope / state boundary surface	Dependent	N/A	Dependent
Critical State Line	?	Independent	Independent
Shear stiffness against shear strain	Independent?	Dependent	?
Pore water pressure (u.d.) against shear strain	Dependent	Independent	(In)dependent
Volumetric strain (d.) against shear strain	Independent	Independent	?

Table 5.1: Summary of the observed viscous behaviour of London Clay in reconstituted and intact states (Sorensen, 2006)

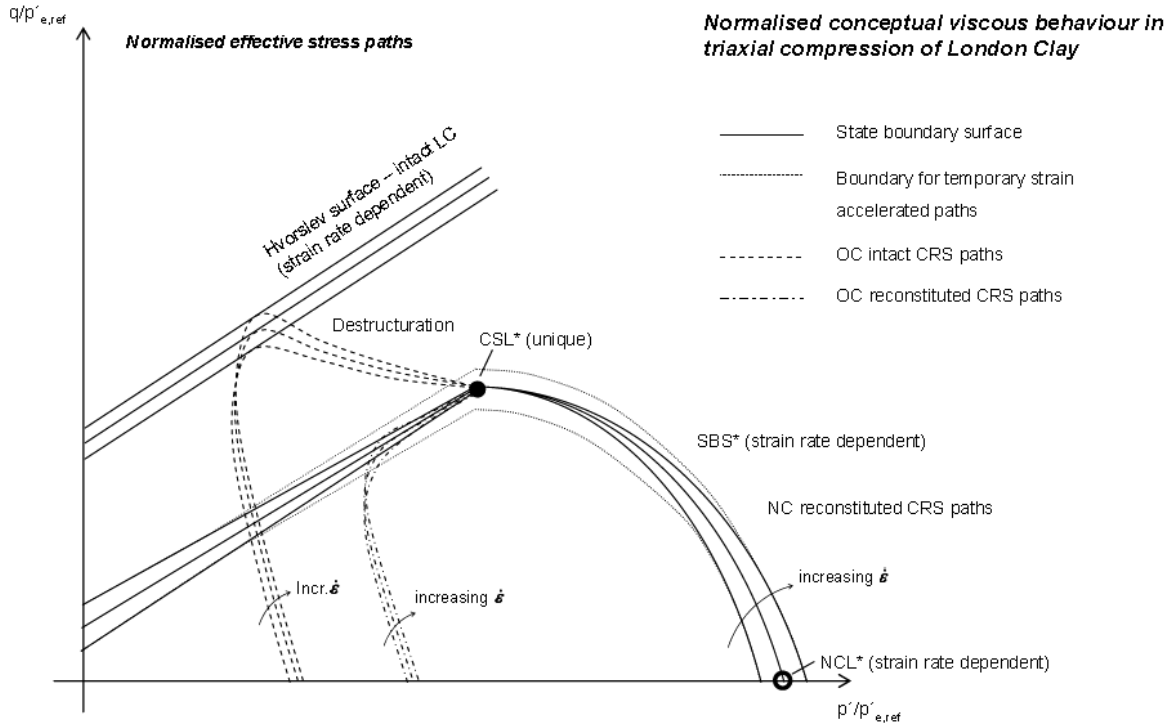


Figure 5.7: General normalised viscous behaviour of London Clay in triaxial compression – illustration of conceptual behaviour (Sorensen, 2006)

The experimental study on the viscous behaviour of intact London Clay and the conclusions drawn by Sorensen (2006) regarding the basic features of the viscosity and the rate dependency of intact London Clay allows the assessment of the capability of the ET Creep model to reproduce the time dependent behaviour of intact London Clay. Referring to Chapter 4, where the ET Creep model is validated for the time dependent behaviour of natural soils, the ET Creep model can reproduce well the persistent strain rate effects on the stress-strain response at large strains close to the peak deviatoric stress (i.e. isotach viscosity). At small strains, isotach viscosity is also simulated by the ET Creep model. It has also been shown that the ET Creep model reproduces well the strain rate dependency of the peak strength envelope in triaxial compression. Regarding the rate independency of the critical state line, it has been shown in Chapter 4 that the ET Creep model is a critical state model whose formulation implies that the critical state is rate independent.

Another series of laboratory tests, drained triaxial creep tests this time, on samples of undisturbed London Clay from Hendon performed by Lovenbury (1969) and presented by Bishop (1966), allows the evaluation of the characteristic relationship between strain rate and time during creep, expressed through the parameter m (see Section 3.3.1.3). This set of experiments examines the development of creep strains under constant deviatoric conditions, i.e. deviatoric creep. It is recognised by Bishop (1966) that technical difficulties arise when

performing creep tests, due to the fact that constant effective stress conditions have to be maintained for a long period of time, in the range of months. Nevertheless, a series of tests on samples of intact London Clay were performed, where samples were kept under sustained shear stresses for a period of about seven months. The stress levels were approximately 16%, 40%, 60%, 70%, 80%, and 90% of the peak drained strength obtained in a test of five days duration.

In Figure 5.8, the development of axial strains with time during deviatoric creep under constant shear stress conditions for the different stress levels is presented. It is observed that under constant deviatoric stress, there is a continuous development of axial strains for the majority of stress levels. However, at a stress level close to the peak stress, creep rupture takes place accompanied by acceleration in the creep strain rate. The respective plot of axial strain rate against time, from which the parameter m can be derived, is presented in Figure 5.9. It is observed that for the tests where creep rupture is not reached (i.e. no acceleration of strain rate leading to failure), the logarithm of creep rate decreases linearly with increase in the logarithm of time. This is the case for any stress level, since with an increase in deviator stress the lines shift vertically upwards, indicating that the slope of this relationship is independent of stress level. Therefore, it may be concluded that the parameter m is equal 1, which means essentially that the coefficient of secondary compression C_α is constant with time for any stress level, except when the soil reaches creep rupture. The evaluation of C_α for intact London Clay is discussed in Section 5.4.1.

Another series of laboratory tests, incremental load oedometer tests, on samples of undisturbed London Clay from Ongar to the north-east of London, where load increments were held longer than the customary 24 hours to enable full dissipation of excess pore water pressures to occur, was performed by Som (1968). In these tests, the development of strains with time after full dissipation is measured, indicating whether the development of creep strains is linear logarithmic or not and, respectively, whether the value of parameter m is equal to 1 or not. More particularly, in the test shown in Figure 5.10 the sample was left to creep for a period of 93 days, showing a linear relationship between strains, both axial and volumetric, with the logarithm of time. This behaviour is quantified with a constant C_α and m = 1 (Equation 3.3). Therefore, it may be concluded that the value of C_α remains constant with the development of creep strains.

Similar observations are made by Davies (1975), who performed creep tests on three different undisturbed stiff clays, including London Clay. The creep tests on London Clay involved

triaxial creep tests, where the long-term deformation of London Clay at different deviatoric stress levels was examined. Also, Davies concludes from his detailed study on creep effects on undisturbed clays, that the value of C_α is constant for values of the effective overburden pressure exceeding the apparent preconsolidation pressure.

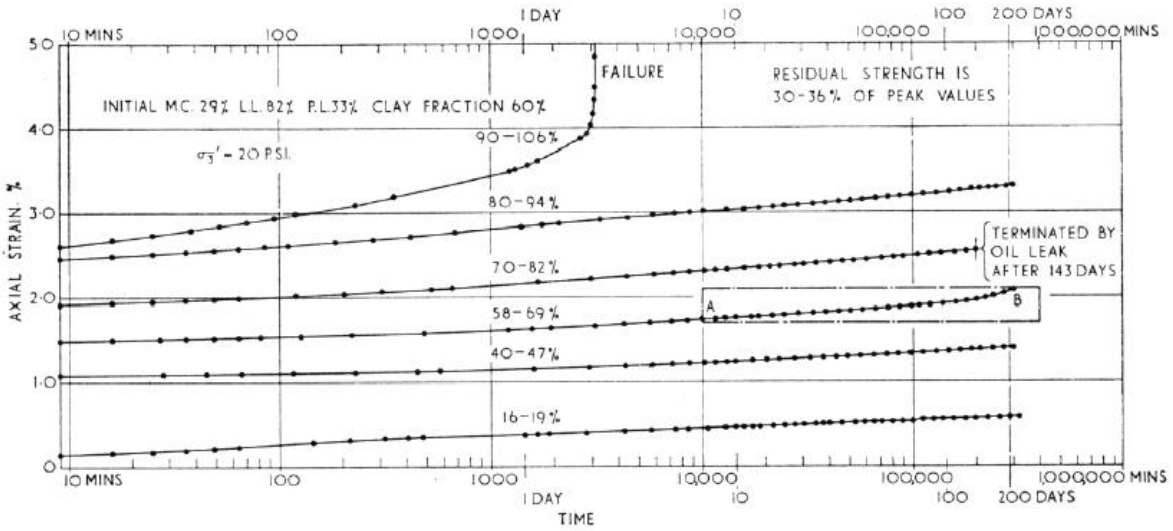


Figure 5.8: Influence of deviatoric stress in drained triaxial creep tests on undisturbed London Clay (Bishop, 1966)

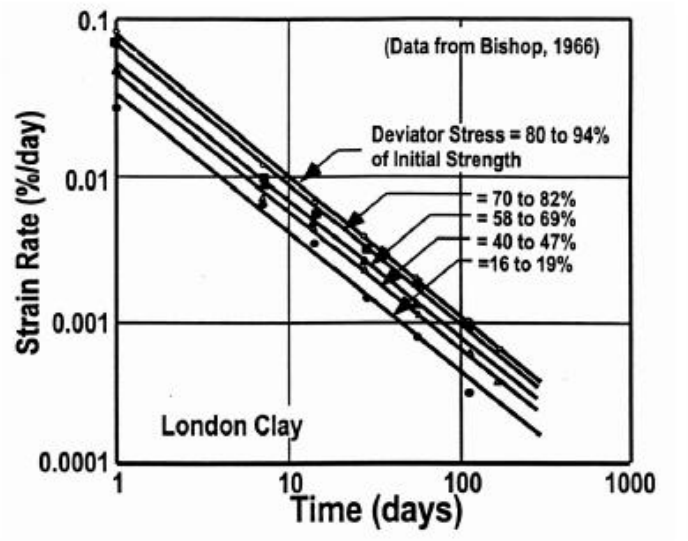


Figure 5.9: Strain rate vs. time relationships during drained triaxial creep on London Clay (Mitchell et al., 1997, replotted data from Bishop, 1966)

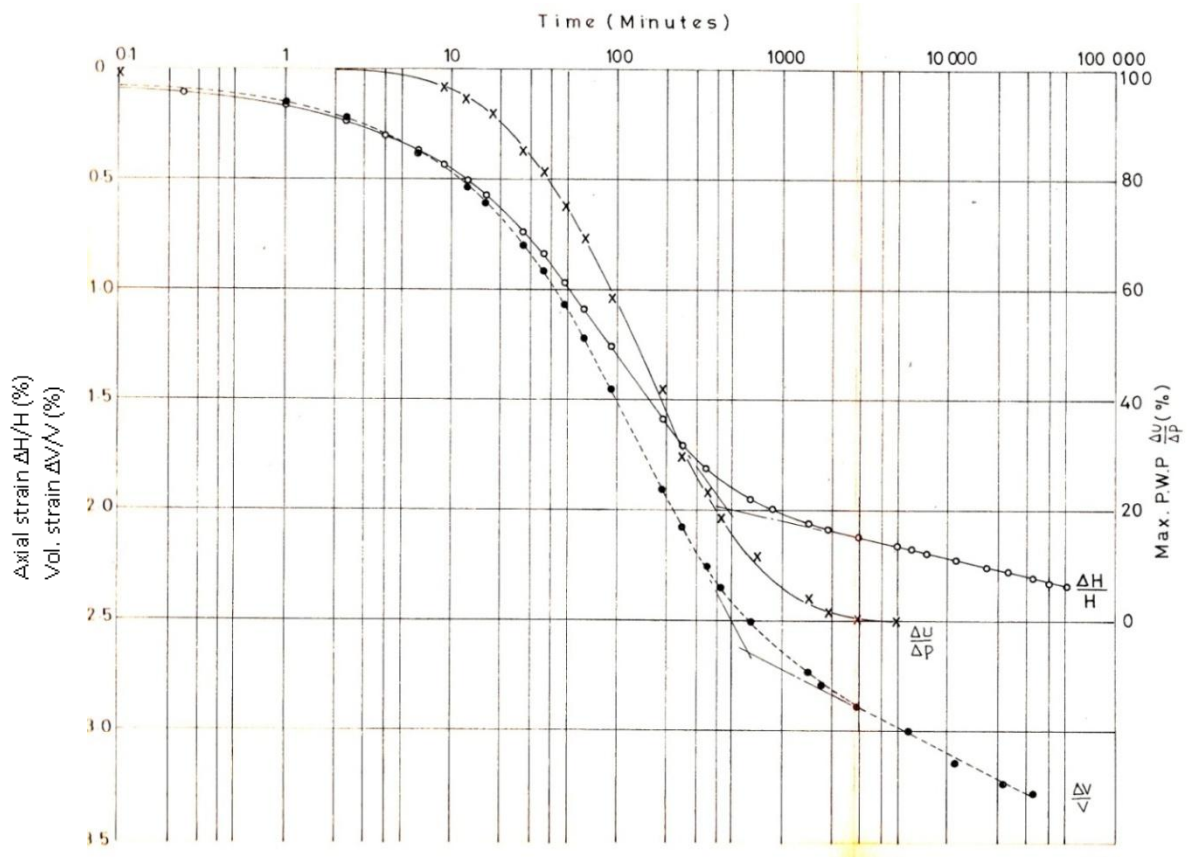


Figure 5.10: Consolidation curves of incremental load oedometer test on samples of undisturbed London Clay from Ongar (Som, 1968)

The value of the parameter m is regarded as an important parameter for the quantification of the creep behaviour in geotechnical problems. The calculated creep strains may be larger or smaller than the real ones, if an inappropriate parameter m is employed. If the value of the parameter m is equal to 1, this implies that the relationship of the logarithm of strain rate with the logarithm of time is linear. On the other hand, if the value of the parameter m is higher or lower than 1, then the relationship deviates from the linear relationship (see Figure 3.6).

The ET Creep model incorporates a non-linear logarithmic function of visco-plastic strain with time, with a limit for the amount of visco-plastic volumetric strain ($\varepsilon_{vm,limit}^{vp}$) that is attained at infinite time. This formulation allows flexibility in the proposed model for adopting either a linear or a non-linear logarithmic relationship of visco-plastic strain with time. Bodas Freitas (2008) performed parametric analyses of the limit value parameter, showing that, if a limit of the visco-plastic strains required to result in no voids in the soil is prescribed, then the relationship of visco-plastic strain with time becomes approximately linear. Such a formulation allows the user of the ET Creep model to employ different values of the parameter m in the analyses, and offers the option of employing a linear logarithmic creep law (i.e. $m = 1$).

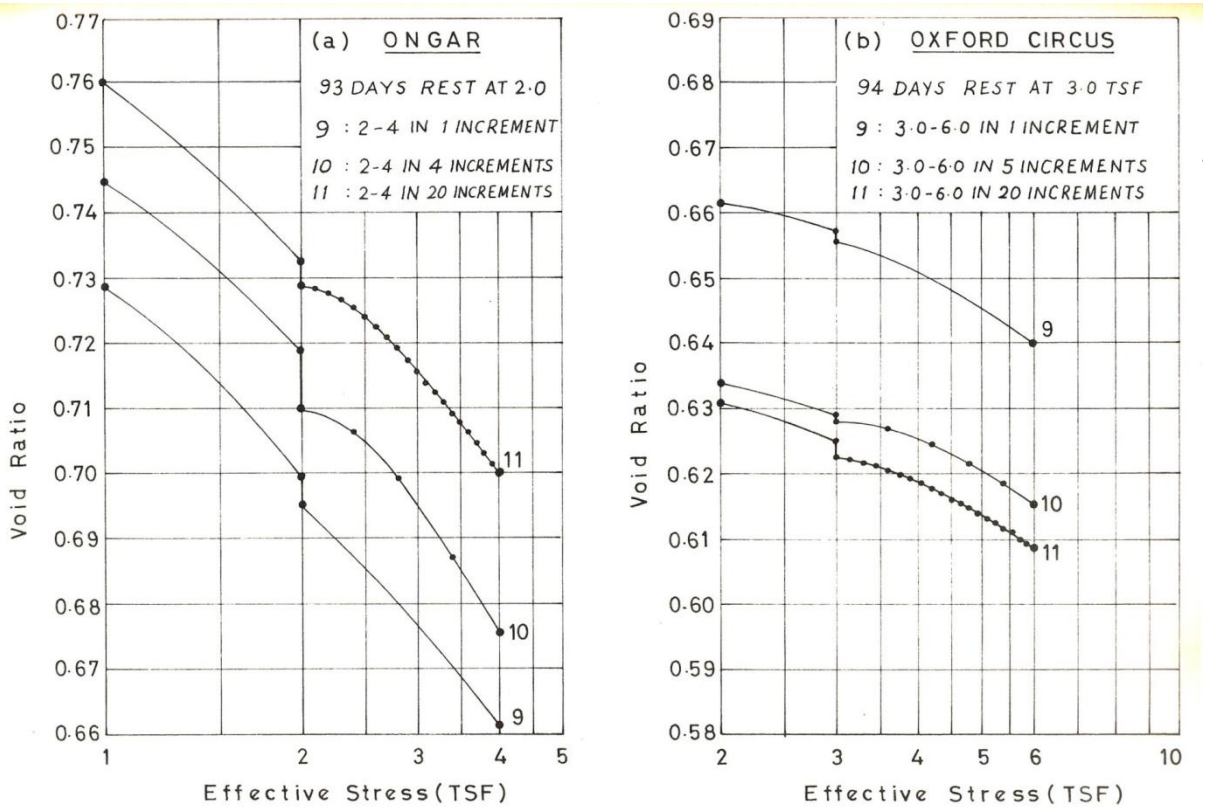
5.4. DETERMINATION OF TIME DEPENDENT PARAMETER C_α

The time-dependent behaviour of the ET Creep model is characterised by the coefficient of secondary consolidation C_α through the time-dependent model parameter ψ_0/V (see Section 4.4.7), which is used to quantify the development of visco-plastic volumetric strains at the reference time t_0 defined in Section 4.4.2. In engineering practice, the coefficient of secondary consolidation C_α is usually determined from incremental load oedometer tests, where the load increments are maintained longer than 24 hours, in order to allow excess pore water pressures to fully dissipate. The value of C_α represents the change in Δe or $\Delta\varepsilon$ with the logarithm of time during secondary compression, at an effective stress level larger than the apparent preconsolidation stress level (see Section 3.3.1.3).

It has been shown that the viscous behaviour of intact London Clay is affected by the presence of structure. Therefore, it is anticipated that the value of C_α should be ideally calculated from oedometer tests on intact samples of London Clay. The recent work of Sorensen (2006) did not involve any oedometer creep testing of intact London Clay. Therefore, only the work of Som (1968), which involved incremental load oedometer tests on samples of undisturbed London Clay from Ongar and Oxford Circus, could be used for estimating the value of C_α. Load increments were held longer than the 24 hours in these tests, and several conclusions about the value of C_α may be drawn.

5.4.1. Intact samples of London Clay

Figure 5.11 shows results from oedometer tests on intact London Clay where the maintained stress level was similar to the in-situ stress. It is apparent that significant creep deformations take place during elapsed time at stress levels which are similar to the in-situ stresses. Such recorded deformations were not expected, due to the fact that at the in-situ stress level the soil would have already experienced creep for a long period of time. This implies that the soil tested should produce insignificant creep strains due to the time delay which is observed in OC soils (see Figure 4.16). Som (1968) discusses that swelling of the samples during sampling and the initial swelling stage of the experiments may have affected the soil structure and therefore, during the creep period, the soil is trying to recover the lost structure by straining under constant stress conditions. Such disturbance of intact samples results in samples creeping under stress conditions that they have already experienced during their history.



Note: 1 TSF = 95.8 kPa

Figure 5.11: Oedometer creep tests on London Clay samples from (a) Ongar and (b) Oxford Circus (Som, 1968)

Similar effects have also been observed by Lovenbury (1969), where comparisons were made between strain rates in the laboratory and in-situ, at relevant stresses and time scales. In particular, the settlement records at Chelsea and Waterloo Bridges (MacDonald and Skempton, 1955; Cooling and Gibson, 1955) are compared with results from creep tests. The correlation from this comparison is that, if the secondary settlement in-situ is considered to become dominant 2-3 years after loading, it amounts to 15-25% of the primary settlement after 16 years of records. On the other hand, in the creep tests secondary compression amounts to 30% of primary compression at 2 years and if this is extrapolated to 16 years, it would amount to approximately 40% of primary compression. In addition, the strain rate measured in the creep tests at 2 years was an order of magnitude higher than the minimum average settlement rates exhibited at Chelsea and Waterloo Bridges, according to Lovenbury (1969). This indicates that the amount of secondary compression and the strain rates recorded in the laboratory are larger than the recorded in-situ. However, it was recognised by Lovenbury (1969) that the correlation was approximate due to the difficulty in interpreting the settlement records.

The discrepancy between laboratory and field observations has been recorded in the behaviour of other natural soils as well. Nash (2010) makes a conceptual approach to this in Figure 5.12, by illustrating isochrones for overconsolidated intact clays based on the approach of Bjerrum (1967) for normally consolidated clays. If a soil element creeps from state A, when it was initially deposited 10000 years ago, to state B today, the soil element would currently be undergoing creep at a very slow rate that can be evaluated assuming that parallel isochrones apply. Therefore, it would be expected that if a high quality sample is reloaded to the in-situ state B from state E, then the creep rate should be equivalent to the one observed in-situ after 10000 years of creep.

However, in laboratory incremental load oedometer tests on high quality samples that are reloaded to the in-situ state B, creep is observed at rates that are initially comparable with those in the normally consolidated range, with the creep rate falling off rapidly. Therefore, as the soil element is loaded towards the yield stress, a more appropriate relationship for isochrones, according to Nash (2010), is for them to be curved rather than parallel, as shown by the dashed lines in Figure 5.12. Therefore, at state B in the laboratory test the creep rate is equivalent to the in-situ creep rate at state A. The soil in-situ is considered to creep in practice at a slower rate than in the laboratory, being at state B* if the curved isochrones are adopted. This difference between B and B* is accounted for by sample disturbance.

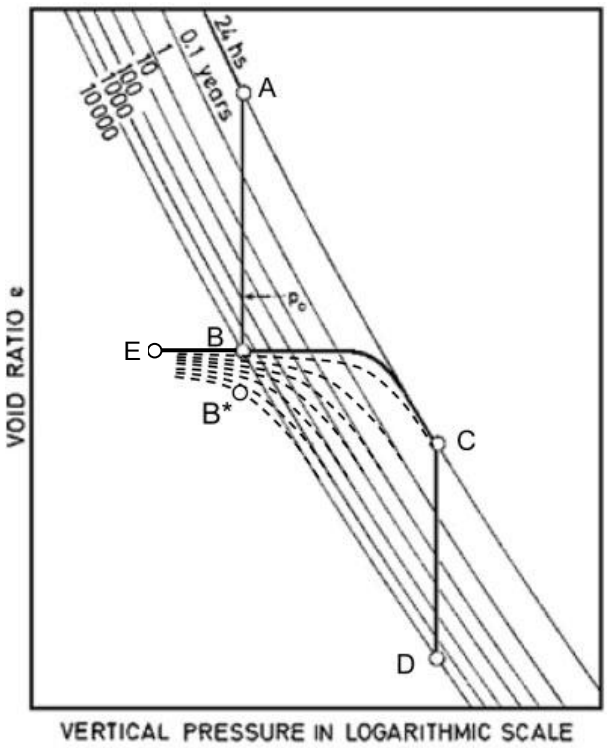


Figure 5.12: Isochrones observed for in-situ OC soils merging with those for normal consolidation (Nash, 2010)

Regarding the determination of C_α for the application of the ET Creep model in finite element analyses, it would appear that the value of C_α cannot be calibrated from creep tests on intact samples at stress levels which are similar to the in-situ stresses, due to swelling and sample disturbance during sampling, affecting the soil structure and subsequent creep during loading. No time delay due to creep history is observed (see Figure 4.16) and therefore if the strain development with time is fitted with the computed strains, then the value of C_α will not be realistic. Considering these facts, in order to determine an appropriate value for C_α for intact London Cay to employ in the ET Creep model, it is assumed that the value of C_α in in-situ problems is common for soils in both the undisturbed and the reconstituted states, implying that the creep potential of a soil is independent of its stress history and depends on its current stress state. Therefore, considering the formulation of the ET Creep model in Figure 5.13, it is assumed that the same creep potential (i.e. visco-plastic strain rate) is reached for (a) a soil element which is loaded from i to $(i+1)''$ and then left to creep to $(i+1)$, and (b) for another soil element which is loaded from i to $(i+2)'$, then left to creep to $(i+2)''$ and finally unloaded to $(i+1)$. Example (a) represents a NC clay which is left to creep to state i having an apparent overconsolidation, then loaded to state $(i+1)''$ due to overburden stress and finally left to creep to state $(i+1)$. On the other hand, example (b) represents a NC soil which initially is left to creep to state i, then loaded to state $(i+2)'$ due to a larger overburden stress than example (a), then left to creep to state $(i+2)''$ and finally unloaded to a stress state $(i+1)$ due to erosion events, and thus becomes OC, during which significant structure is developed.

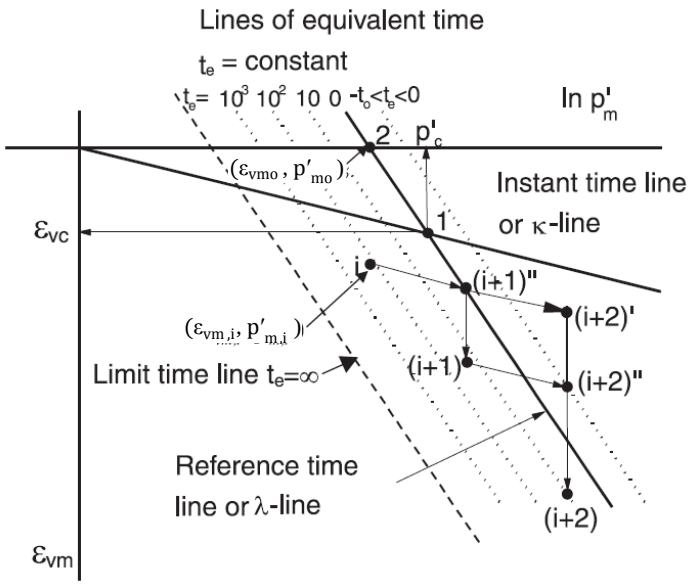


Figure 5.13: ET Creep model and stress paths in isotropic conditions

5.4.2. Reconstituted samples of London Clay

The evolution of creep strains during secondary compression on reconstituted samples of London Clay from Heathrow Terminal 5 (unit B2b) has been examined by Sorensen (2006). In particular, an incremental load (IL) oedometer test was performed on reconstituted London Clay where the sample was step-loaded to 785 kPa in six increments, with each load increment being double the previous load (i.e. 3-28-52-101-199-394-785 kPa). After each load step the sample was left to consolidate for 24 hours, during which most of the excess pore water pressures dissipated. At the last load increment of 785 kPa, the sample was left to creep for period of 30 days after the end of primary consolidation (EOP), in order to examine the characteristics of pure creep. Following the creep period, the sample was compressed with a constant rate of strain (CRS) up to a vertical stress of around 2000 kPa, where it was left to relax for 4 days (i.e. no strains allowed). Subsequently, the sample was unloaded to 785 kPa with a constant rate of strain, from which point the sample was fully unloaded in steps. Figure 5.14 shows the compression resulting from the combined IL and CRS oedometer test.

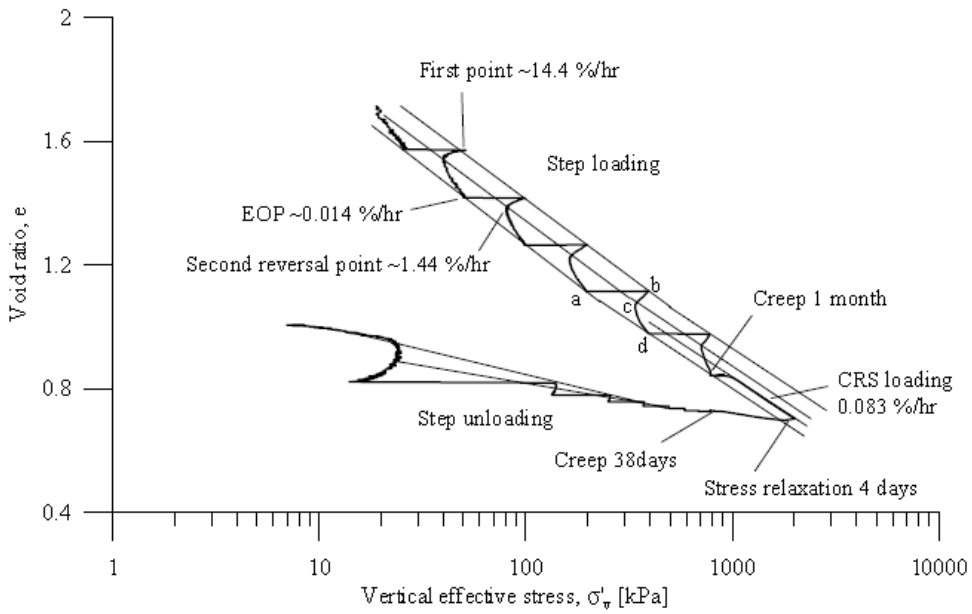


Figure 5.14: 1D compression and swelling path resulting from step loading, step unloading and constant rate of strain compression/swelling in test on reconstituted London Clay (Sorensen, 2006)

The consolidation curves for each load increment are plotted in Figure 5.15, where for the increment of 785 kPa the load was maintained for a period of 30 days, during which creep strains developed representing secondary compression. The creep behaviour observed after EOP is characterised according to Sorensen (2006) by a near-linear reduction in void ratio

with the logarithm of time, with a coefficient of secondary compression $C_\alpha = \Delta e/(\Delta \log t) = 0.016$, where C_α is the inclination to the horizontal of the relative change in void ratio with time after EOP. In addition, it is noted that a logarithmic linear reduction in strain rate with time is followed with a value of m being close to 1 (Figure 5.16), which is the same as the case of intact samples of London Clay shown in Section 5.3.

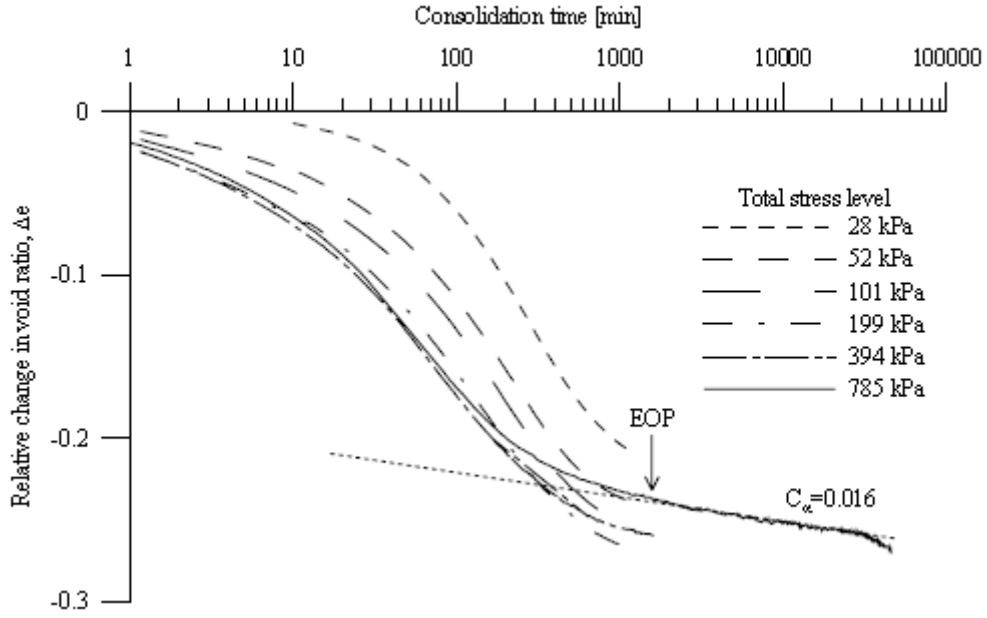


Figure 5.15: Constant total stress consolidation curves for each load step increment in 1D compression test on reconstituted London Clay (Sorensen, 2006)

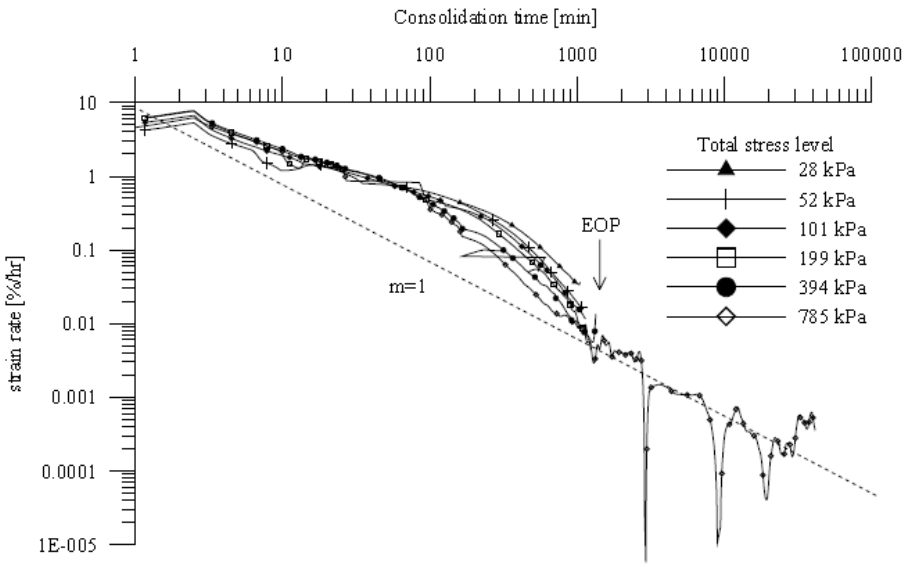


Figure 5.16: Axial strain rate reduction during consolidation for each step load increment in 1D compression test on reconstituted London Clay (Sorensen, 2006)

5.5. LOADING SURFACES: DERIVATION OF THE ET CREEP MODEL PARAMETERS

The ET Creep model is a critical state model. Therefore, the critical state angle of shearing resistance in triaxial compression, expressed in terms of $M = (6\sin\varphi')/(3 - \sin\varphi')$, is required along with the parameters α and μ, in order to define the shapes of the loading and plastic potential surfaces in the J-p' plane. Gasparre (2005) performed a series of triaxial compression tests on intact London Clay samples from several units at Heathrow Terminal 5, where the stress paths for each unit were plotted together in a normalised way, allowing the derivation of the α, μ and M parameters required for the ET Creep Model.

Hight et al. (2007) present in Figure 5.17 failure envelopes in triaxial compression and extension for the different units encountered in Heathrow Terminal 5. Two failure envelopes are drawn for each unit or sub-unit: one representing a peak envelope to the stress paths and one representing the post-rupture strength. Sufficient data from a series of triaxial compression and extension tests performed by Gasparre (2005) have been gathered for units $B_{2(c)}$, $B_{2(b)}$, $B_{2(a)}$ and A_3. However, according to Hight et al. (2007) failure envelopes for these units are somewhat subjective due to the fact that their identification is not clear-cut. In addition, failure envelopes for the remaining units C and A_2, due to the lack of sufficient data, are suggested by Hight et al. (2007).

A linear approximation for the peak envelopes has been adopted Hight et al. (2007), despite the fact that peak envelopes are considered to be curved at small stresses. Despite this, a comparison between peak envelopes allows the conclusion that peak strength envelopes rise with increasing depth and therefore they differ between lithological units. It is evident that the deeper units $B_{2(a)}$, A_3 and A_2 have a significant cohesion intercept, reflecting increasing structure and higher peak strength envelopes in these units. Regarding the post-rupture envelopes, Hight et al. (2007) claim that the envelope is effectively common for all sub-units of unit B_2.

Referring to Section 4.4.5, the parameter M is the gradient of the critical state line in p'-q stress space under triaxial compression stress conditions. It can be related to the angle of shearing resistance φ' by Equation 4.58. It is assumed to be equivalent to the post-rupture strength envelope, therefore a constant stress ratio at the post-rupture strength level tending to converge towards a unique critical state value for each unit is obtained.

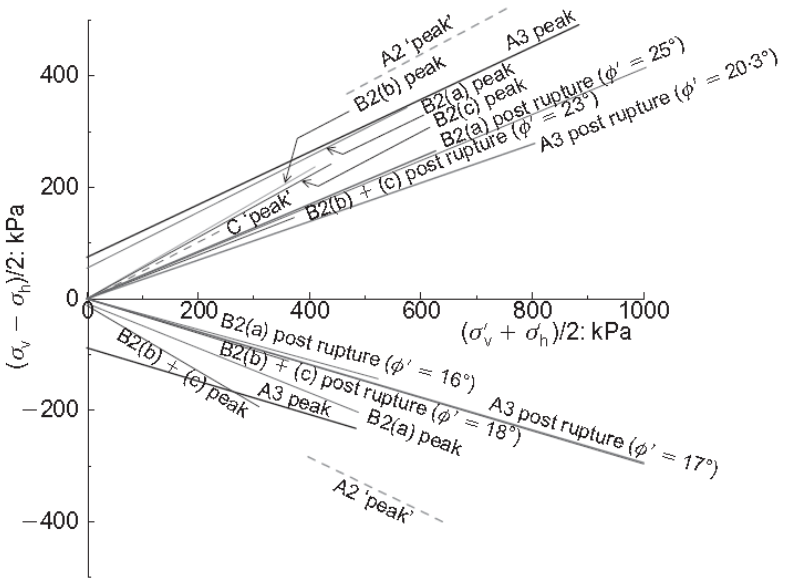


Figure 5.17: Peak and post-rupture failure envelopes for different lithological units (Hight et al., 2007)

Gasparre (2005) took the effective stress paths from undrained triaxial compression tests on samples from the different lithological units and normalised them to eliminate the influence of void ratio by using the equivalent intrinsic pressure p^*_e, which was calculated considering the appropriate isotropic NCL* for each unit or sub-unit. The normalised effective stress paths and the State Boundary Surfaces formed allow the determination of the shape parameters α and μ of the loading surface for each unit and sub-unit. Also, the post-rupture envelope allows the determination of the M parameter.

The parameters α and μ are determined by fitting the experimental data, more specifically, the stress paths during undrained triaxial compression. By suitable selection of the values of α and μ, the model is able to reproduce a wide range of surfaces. In Figure 5.18, the loading surfaces calculated from parameters M, α and μ, using the equations for the plastic potential and loading surface in Section 4.4.5 [$F(\{\sigma'\},\{k\}) = P(\{\sigma'\},\{m\}) = \left(\frac{J}{p'M}\right)^2 - \left(\frac{p'_o}{p'} - 1\right) = 0$], are plotted along with the effective stress paths for each unit. Effective stress paths which are on the dry side are utilised in order to obtain the appropriate loading surface profile, since London Clay is overconsolidated. Finally, a collective plot for all units is presented in Figure 5.19, where it is evident that the loading surface for unit A_3 plots above that for the other units on the dry side reflecting increasing structure and a higher peak strength envelope. It should also be considered that due to the lack of sufficient data for unit C, the loading surface is suggestive.

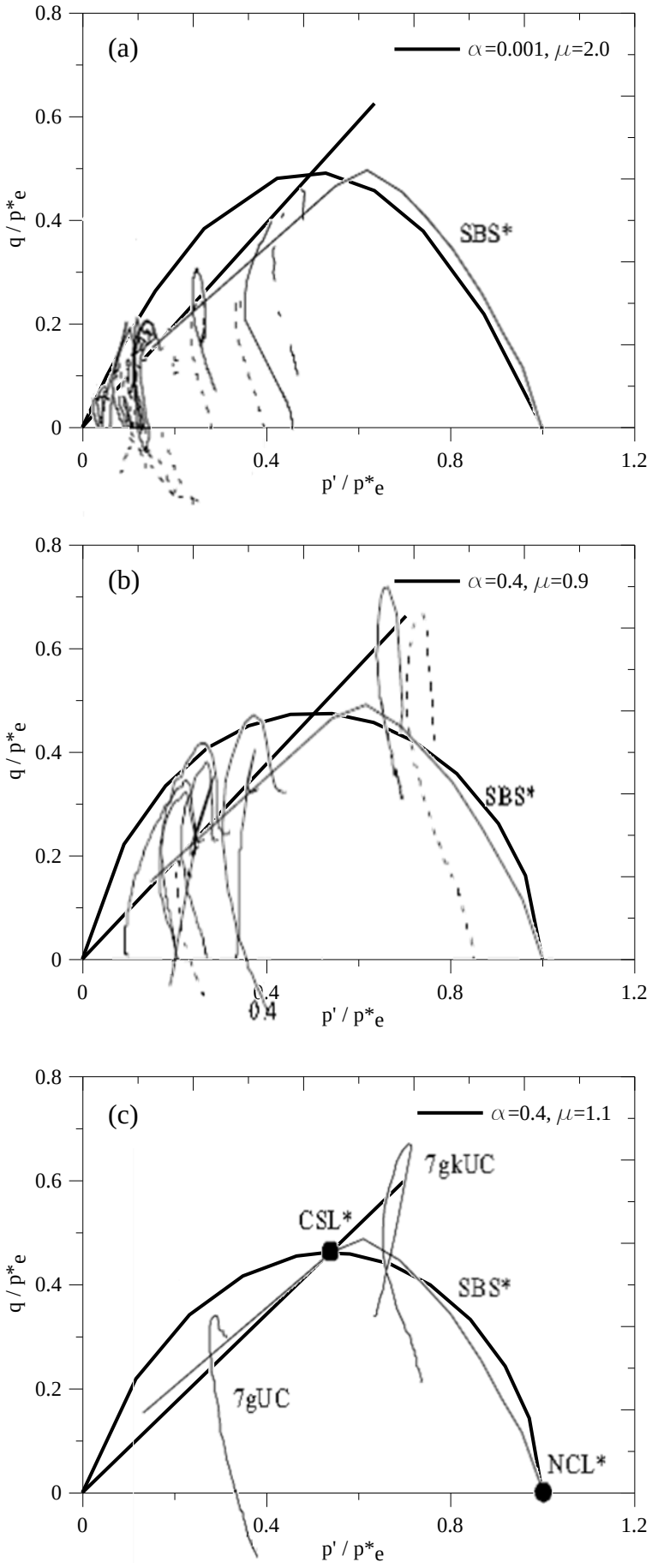


Figure 5.18: Loading surfaces along with the normalised effective stress paths for lithological units (a) B_2, (b) A_3, and (c) C

Associated plasticity is assumed in the ET Creep model for the model calibration, meaning that the plastic potential surface has the same shape as the loading surface in triaxial loading conditions. In this case, $M_f = M_g$, $\alpha_f = \alpha_g$ and $\mu_f = \mu_g$.

The loading surface parameters and the plastic potential parameters for units C, B_2 and A_3 of London Clay are presented in Table 5.2.

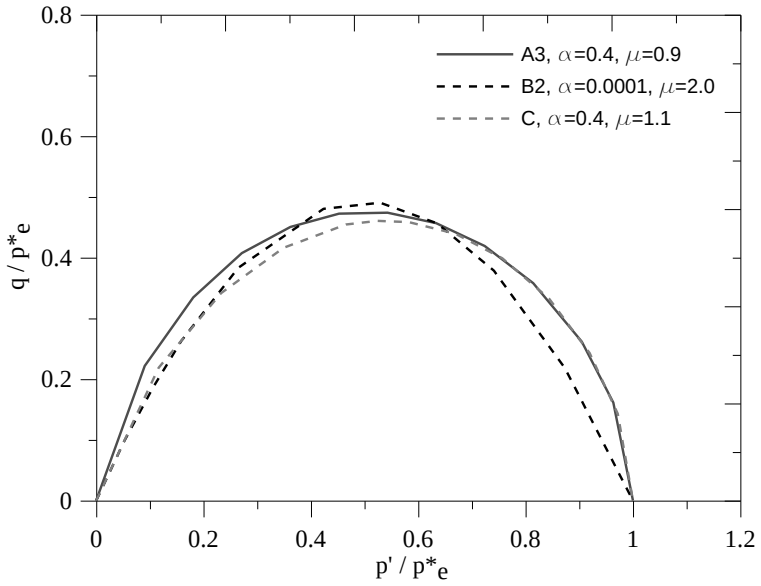


Figure 5.19: Normalised loading surfaces for lithological units B_2, A_3, and C

Unit	φ' (°)	$M_f = M_g$	$\alpha_f = \alpha_g$	$\mu_f = \mu_g$
C	22	0.8561	0.4	1.1
$B_{2(c)}$	25	0.9838	0.0001	2.0
$B_{2(b)}$	25	0.9838	0.0001	2.0
$B_{2(a)}$	25	0.9838	0.0001	2.0
A_3	24	0.9411	0.4	0.9

Table 5.2: ET Creep model parameters for London Clay: Parameters defining CSL and loading surface

5.6. SHEAR STIFFNESS FOR LABORATORY TESTS AND PILED FOUNDATIONS PROBLEMS

The elastic shear modulus G is an ET Creep model parameter. It is the second elastic parameter which, along with the slope of the instant time line, characterises the elastic response of the soil (see Section 4.4.7). Its importance is highlighted by the fact that the soil stress-strain behaviour is highly non-linear and therefore this has an important influence on the selection of design parameters for geotechnical design problems. The soil non-linearity is illustrated in Figure 5.20, where a typical stiffness-strain curve for soil is shown, indicating that at small strains stiffness is relatively large and close to failure at large strains stiffness is small.

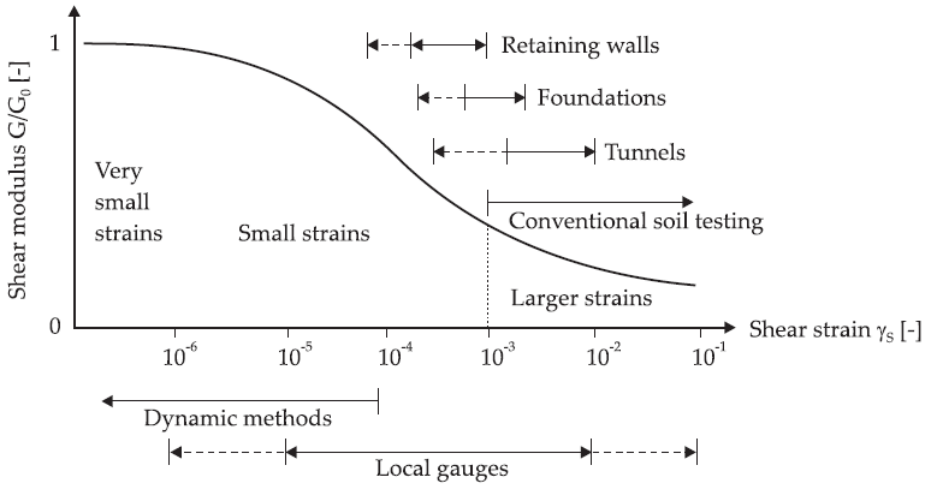


Figure 5.20: Characteristics stiffness-strain behaviour of soil with typical strain ranges for typical strain ranges for laboratory tests and structures (Atkinson, 2000)

In the ET Creep model, during shearing the shear stiffness initially up to yielding of the stress-strain curve is pseudo-linear for OC soils due to the pseudo-elastic behaviour of the model in the overconsolidated range of stress states. Therefore, it is anticipated that an appropriate value for the linear stiffness has to be chosen in order to reflect the strain ranges encountered. The lack of an appropriate shear stiffness value may result in overestimation or underestimation of deformation depending on the base at which the shear stiffness value is determined. For instance, if a value of stiffness reflecting the strain range of triaxial tests is utilised for analyses involving piled foundations, then a too soft response may be calculated for the piles load-settlement response, since the strain range involved are smaller than the strain range involved for a triaxial test. Therefore, referring to Figure 5.20, in foundations

problems neglecting the small strain stiffness may produce unrealistic results, whereas for triaxial tests at failure strains may be spot on, if a large strain stiffness is chosen as a model parameter.

Regarding the calibration of the ET Creep model parameters with London Clay behaviour, the shear stiffness values chosen for the different units (see Table 5.3) are consistent with a back analysis performed for a documented single pile load test in Heathrow (Unwin and Jessep, 2004) (see Section 6.3). The linear elastic stiffness values for the different units encountered at Heathrow required to match the field measurements are very close to the values of small strain stiffness (G_{hv}) presented by Gasparre (2005) in Figure 5.21. In Figure 5.21, the variation of G_{hv} and G_{hh} with depth is presented, where the strong anisotropy of small-strain stiffness of London Clay is evident.

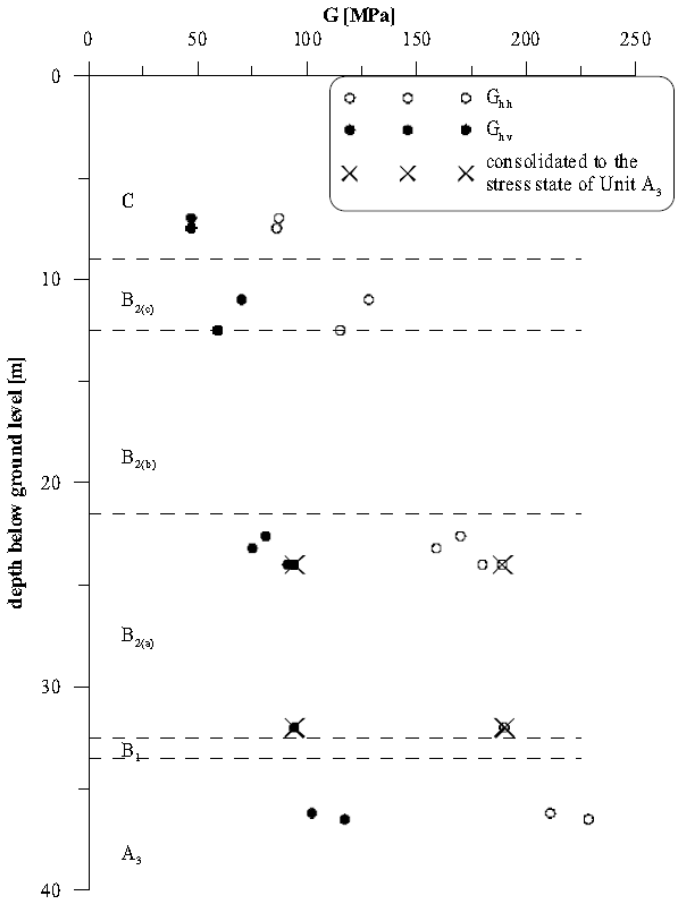


Figure 5.21: Variation with depth of shear moduli in vertical and horizontal planes (Gasparre, 2005)

Unit	Shear modulus, G (kPa)
C	50000.0
$B_{2(c)}$	55000.0
$B_{2(b)}$	70000.0
$B_{2(a)}$	90000.0
A_3	110000.0

Table 5.3: ET Creep model parameters for London Clay: Shear modulus **G**

5.7. MONOTONIC RATE BEHAVIOUR: CALIBRATION OF THE ET CREEP MODEL PARAMETERS

5.7.1. Oedometer tests: Units C, $B_{2(c)}$, $B_{2(b)}$, $B_{2(a)}$, A_3

Rotary-cored samples of London Clay from a range of depths retrieved from the site of the Heathrow Airport T5 were tested by Gasparre (2005) using a conventional load increment oedometer apparatus, in order to quantify the compressional behaviour of London Clay. Intact samples were tested, which were loaded from an initial vertical effective stress that was equal to their in situ stress. The tests were run by doubling the load for each increment and it involved swelling stages from different stress levels. The tests performed and utilised for the calibration of the ET Creep model parameters are summarised in Table 5.4 along with the main characteristics of the samples, as presented by Gasparre and Coop (2008).

Unit	Sample depth (m)	Initial void ratio	w_o (%)	LL (%)	PL (%)	PI (%)	CF (%)	A
C	7.0	0.68	24	66	25	37	53	69
$B_{2(c)}$	10.0	0.80	23	66	29	37		
$B_{2(b)}$	17.0	0.73	27	69	32	36	54	67
$B_{2(a)}$	28.0	0.74	25	71	23	48		
A_3	36.0	0.71	25	63	27	36	51	71

Note: A, activity; CF, clay fraction; LL, liquid limit; PI, plasticity index; PL, plastic limit; w_o, initial water content

Table 5.4: Main characteristics of London Clay samples tested in IL oedometer tests (Gasparre, 2005)

Single element axi-symmetric analyses were performed using ICFEP in order to simulate the incremental load oedometer tests performed on London Clay samples from the different lithological units encountered at Heathrow Airport T5. The single element was an 8-noded quadrilateral element of unit dimensions, whose displacement boundary conditions simulate one-dimensional compression. In particular, the bottom boundary was prescribed not to move vertically, whereas the left and right boundaries were restrained from moving in the horizontal direction. Boundary stresses were applied for each increment on the top boundary of the element. The analyses were fully drained and the simulation was axi-symmetric. A schematic diagram of the boundary conditions is shown in Figure 5.22.

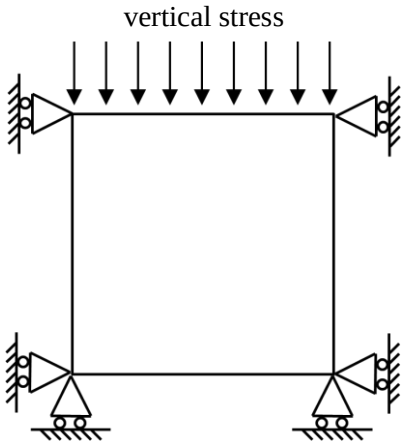


Figure 5.22: Single element boundary conditions for oedometer test

The parameters calibrated, by comparing the FE predictions and the laboratory results, were λ/V and κ/V along with the parameters defining structure (p_{s0}) and the rate of destructuration (ρ_s) upon loading, given the values of parameters G, α, μ and M already set. Parameters ψ_0/V, t_0 and $\varepsilon^{vp}_{vm,limit}$ depend on C_α and the initial void ratio, and were validated with the results from an oedometer creep test. Also, the initial stresses were set based on the data provided by Gasparre (2005) and the value of OCR from the calibration performed using the results from triaxial compression tests.

The samples tested were intact and therefore they were initially at an overconsolidated state. The initial compression path, along with the two swelling stages at different stress levels along the compression path, allows the approximate identification of the slope of the instant time line κ/V, which is used to define the elastic part of the ET Creep model. Also, the stress applied exceeding the yield stress allows the calibration and determination of the slope of the reference time line λ/V in the normally consolidated range of the compression path for the intact samples. Intact samples have a big component of post-sedimentation structure. Further

compression at higher levels of effective vertical stress results in destructuration, which is not fully visible due to the fact that larger stresses are required to fully break-down the structure of intact London Clay according to Gasparre et al. (2007). The destructuration observed in the compression paths allows the determination of the parameters p_{s0} and ρ_s for the different lithological units encountered in the London Clay.

The results of the laboratory tests along with the predictions of the ET Creep model employing the calibrated model parameters are presented in Figures 5.23 to 5.27. The model parameters calibrated from the oedometer tests for the different lithological units and sub-units are presented in Table 5.5.

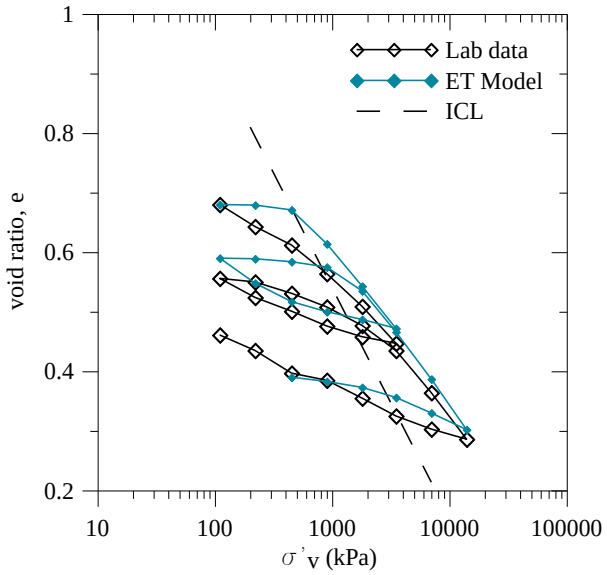


Figure 5.23: IL oedometer test on natural sample from unit C (7m)

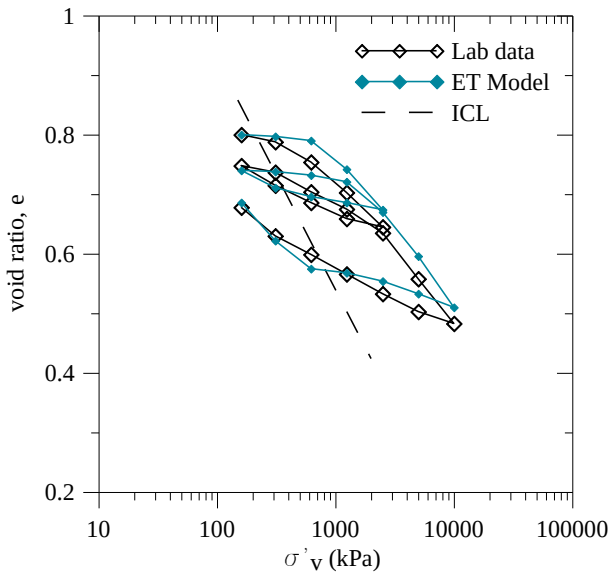


Figure 5.24: IL oedometer test on natural sample from unit $B_{2(c)}$ (10m)

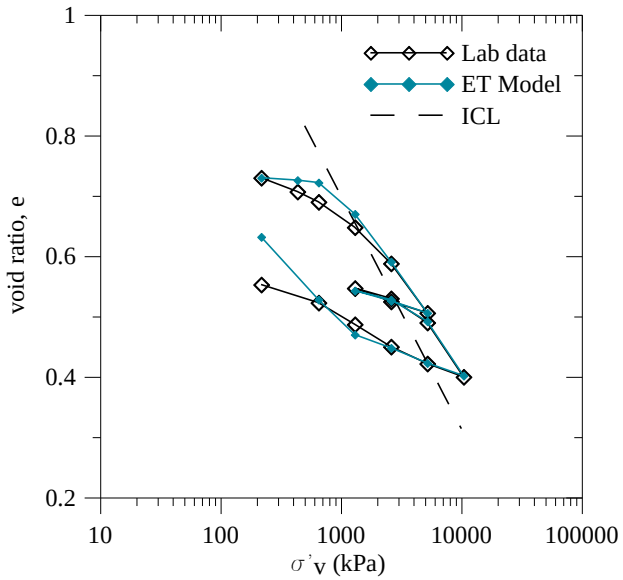


Figure 5.25: IL oedometer test on natural sample from unit $B_{2(b)}$ (17m)

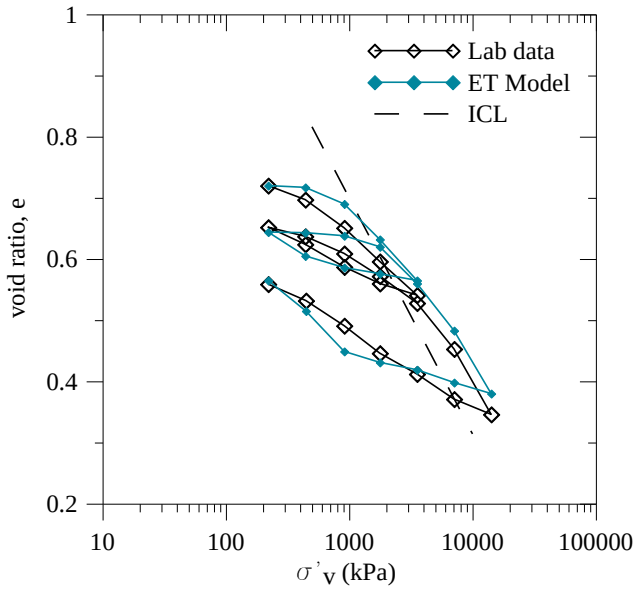


Figure 5.26: IL oedometer test on natural sample from unit $B_{2(a)}$ (28m)

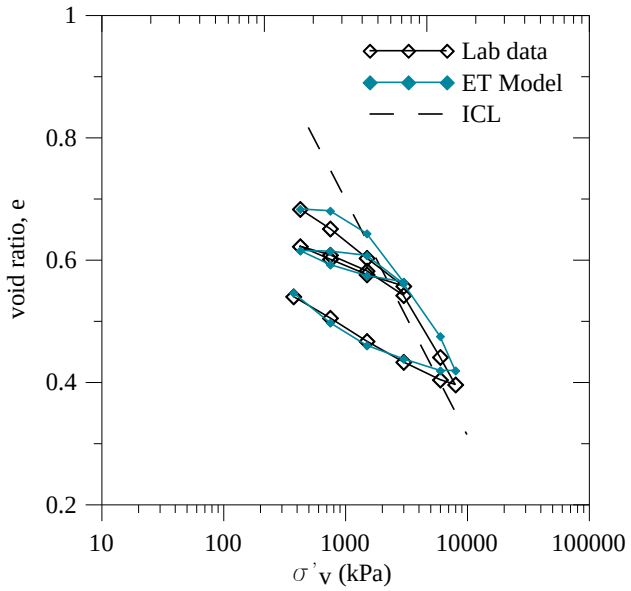


Figure 5.27: IL oedometer test on natural sample from unit A_3 (36m)

Unit	λ/V	κ/V	p_{s0}	ρ_s
C	0.062	0.030	-40.0	100.0
$B_{2(c)}$	0.055	0.025	-40.0	400.0
$B_{2(b)}$	0.065	0.050	-40.0	1500.0
$B_{2(a)}$	0.055	0.030	-70.0	500.0
A_3	0.070	0.045	-70.0	1600.0

Table 5.5: ET Creep model parameters for London Clay: Parameters defining compressibility

5.7.2. Triaxial tests: Units C, $B_{2(c)}$, $B_{2(b)}$, $B_{2(a)}$, A_3

Gasparre (2005) performed triaxial tests on intact samples of London Clay from a range of depths retrieved from the site of the Heathrow Airport T5, in order to examine several aspects of London Clay related to shear strength, including natural structure and sample size. The intact samples were consolidated either isotropically to their in situ mean effective stress level or to their estimated anisotropic in situ stress levels following approach paths that represented the site's recent geological history of erosion and gravel deposition. Triaxial compression was then followed in undrained conditions under strain control, allowing the quantification of shear strength. The tests utilised to calibrate the ET Creep model parameters are summarised in Table 5.6 along with the stress state before shearing. The main characteristics of each sample are assumed to be identical within each unit or sub-unit, including initial void ratio.

Unit	Sample depth (m)	p' (kPa)	q (kPa)
C	7.0	260	-86
$B_{2(c)}$	11.0	260	-86
$B_{2(b)}$	17.5	330	0
$B_{2(a)}$	28.5	400	0
A_3	38.0	600	0

Table 5.6: Triaxial tests on natural samples (Gasparre, 2005)

Single element axi-symmetric analyses were performed in order to simulate the triaxial compression tests on London Clay from the different lithological units encountered at Heathrow Airport T5. Displacement boundary conditions were applied in order to simulate triaxial compression; the bottom boundary and left boundary are prescribed not to move vertically and horizontally respectively. The analysis is axi-symmetric. Displacement based analysis is performed in order to simulate the undrained triaxial tests using an axial strain rate of 0.02%/h (Gasparre, 2005) from the respective in situ mean effective stress level or from their estimated anisotropic in situ stress levels. A schematic diagram of the boundary conditions is shown in Figure 5.28.

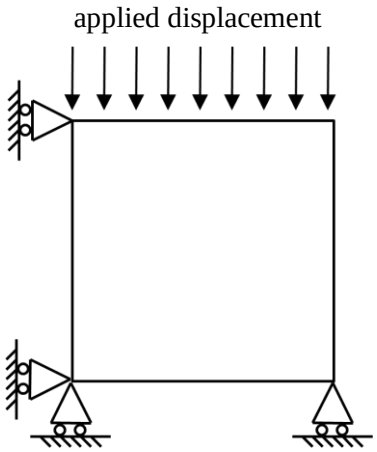


Figure 5.28: Single element displacement boundary conditions for triaxial test

The OCR value for each test is calibrated by comparing the FE predictions and the laboratory results, in order to give to the soil the required undrained shear strength, given the values of parameters obtained and calibrated, as detailed above. The process is regarded as iterative, due to the fact that the predicted compression paths in oedometer tests are influenced by the initial value of OCR and the predicted stress paths in triaxial compression tests are influenced by the values of λ/V and κ/V. The initial stresses of the triaxial tests are based on final stress levels following the initial consolidation of the intact samples to represent in situ stress levels and before undrained shearing.

The results of the laboratory tests along with the predictions of the ET Creep model employing the calibrated model parameters are presented in Figure 5.29 to 5.33. The stress paths indicate that the London Clay is anisotropic in stiffness, being indicative from the change in mean effective stress during undrained shearing. The anisotropy is not simulated in the ET Creep model; it assumes isotropic response. Also, the stress-strain curves indicate the soil stiffness non-linearity, which is also not simulated in the ET Creep model. The predicted stress-stain curves are stiffer that the ones obtained from the laboratory. This is due to the fact that a value of shear stiffness reflecting the small strains encountered in piled problems is employed (see Section 5.6).

The OCR values calibrated from the triaxial compression tests for the different lithological units and sub-units are presented in Table 5.7. These values represent the OCR in terms of mean effective stress and not in terms of vertical effective stress, indicating that the conventional OCR values in terms of vertical effective stress are larger than the tabulated values in terms of mean effective stress.

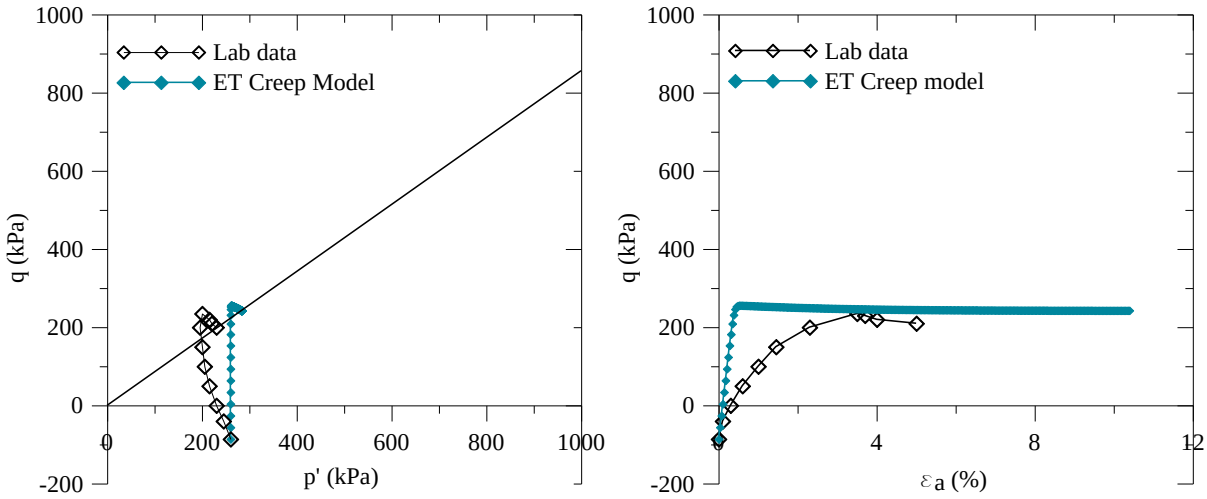


Figure 5.29: Undrained triaxial test on natural sample from unit C (7m)

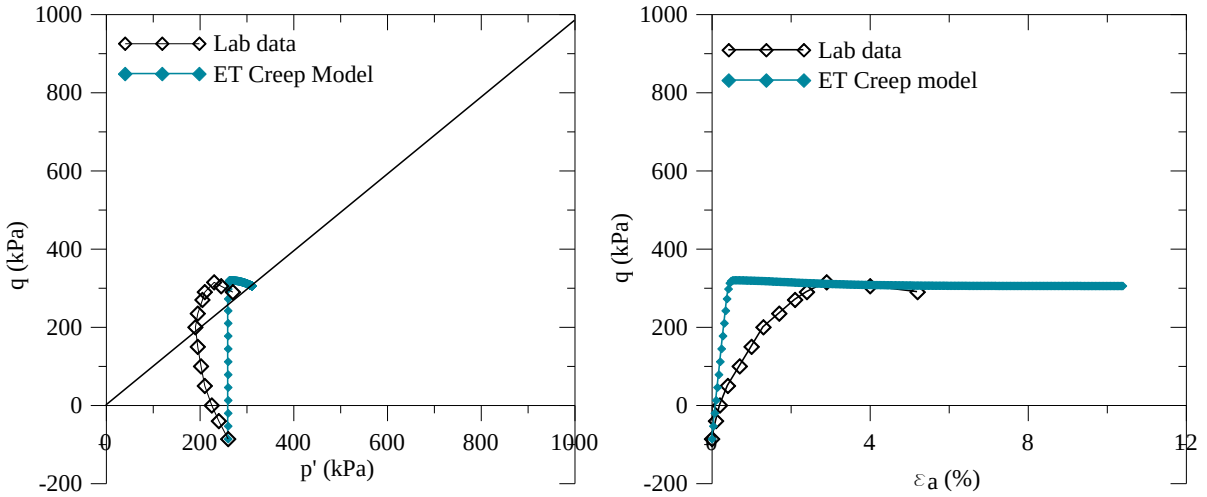


Figure 5.30: Undrained triaxial test on natural sample from unit $B_{2(c)}$ (11m)

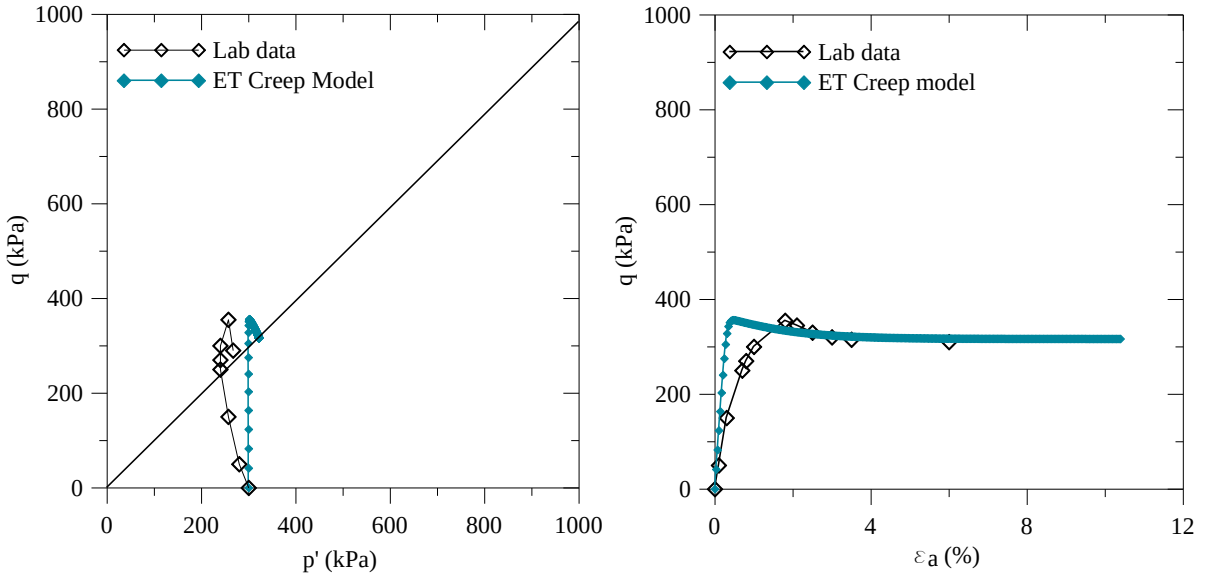


Figure 5.31: Undrained triaxial test on natural sample from unit $B_{2(b)}$ (17.5m)

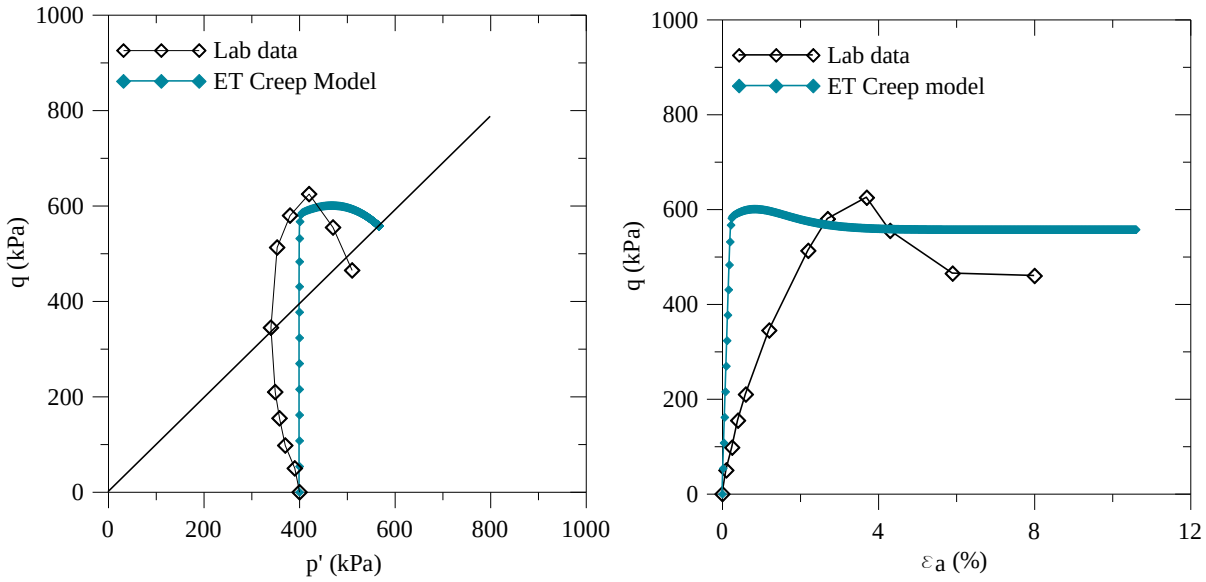


Figure 5.32: Undrained triaxial test on natural sample from unit $B_{2(a)}$ (28.5m)

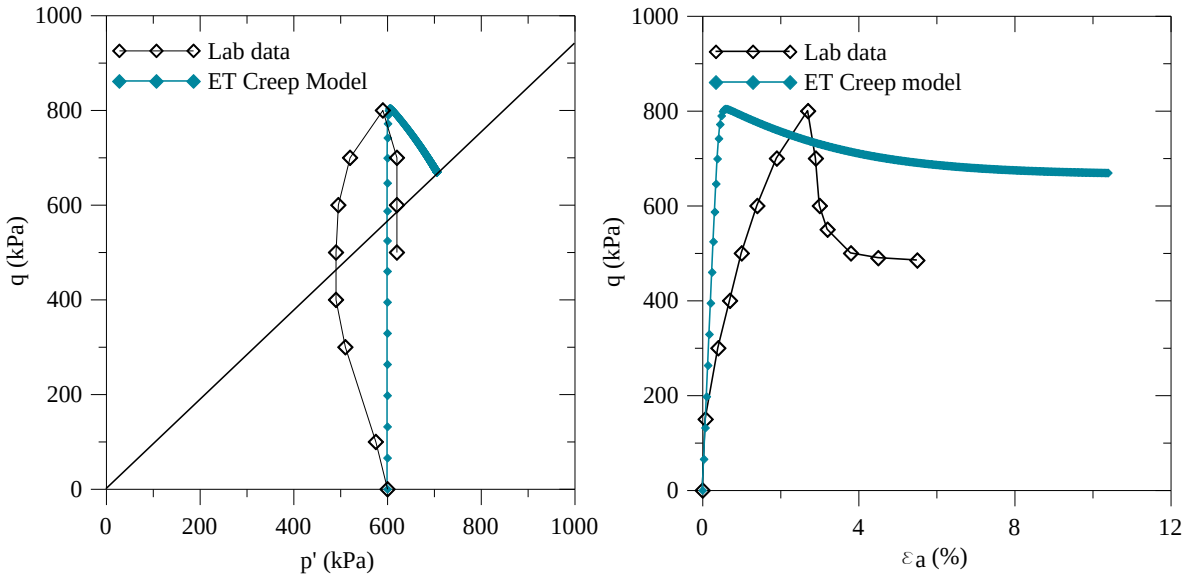


Figure 5.33: Undrained triaxial test on natural sample from unit A_3 (38m)

Unit	**OCR** (p'/p_i')
C	2.0
$B_{2(c)}$	2.7
$B_{2(b)}$	2.8
$B_{2(a)}$	3.8
A_3	3.1

Table 5.7: Calibrated OCR values in terms of mean effective stress for London Clay

5.8. TIME DEPENDENT BEHAVIOUR: CALIBRATION OF THE ET CREEP MODEL PARAMETERS

Sorensen (2006) performed a series of laboratory tests on London Clay samples from Heathrow Airport Terminal 5, in order to examine the time dependent behaviour of London Clay. In particular, he performed a series of tests on both intact and reconstituted samples of London Clay from the lithological unit $B_{2(b)}$, from which the time dependent parameters of the ET Creep model are calibrated. As foresaid in Section 5.4, the determination of the time dependent parameter C_α from intact samples is not straightforward. It is assumed that the value of C_α is independent of the soil's stress history and therefore the same value of C_α for both intact and reconstituted samples of London Clay applies.

In the following, a single element finite element analysis is performed, in order to simulate an oedometer creep test and validate the magnitude of the parameter C_α and the linear relationship between strain and logarithm of time during secondary compression represented by $m = 1$. In addition, a set of triaxial tests with different strain rates are simulated, in order to reproduce the strain rate effects of London Clay, as derived by Sorensen (2006) from an undrained triaxial test involving a stepwise change in stain rate. These sets of analyses are a continuation of the calibration of the monotonic rate behaviour of London Clay and therefore the same model parameters apply in the analyses.

5.8.1. Oedometer creep test: Unit $B_{2(b)}$

A single element finite element analysis was performed in order to simulate an IL oedometer creep test on a soil sample of London Clay from unit $B_{2(b)}$ retrieved from the Heathrow Airport T5 site. The model parameters are based on the calibration performed for the monotonic rate behaviour of London Clay for the same lithological unit. The aim is to verify whether the ET Creep model reproduces the magnitude of the viscoplastic strains developed during drained creep, i.e. after the completion of primary consolidation.

Similar displacement boundary conditions and loading conditions, to the oedometer tests performed by Gasparre (2005), were applied in the single element analyses (see Section 5.7.1). However, in order to simulate creep, a load increment at a stress level close to the normally consolidated range of the ET Creep model was maintained longer than 24 hours; the load being kept constant for 4 years. The stress level at which creep is taking place is close to the 'yield' stress level, in order to avoid the time delay (see Figure 4.16) in the results and

observe the linear logarithmic development of viscoplastic strains from a stress state close to the reference time line.

In Figure 5.34, the change in void ratio at a constant vertical effective stress level during elapsed time is observed. Also, the change in void ratio with the logarithm of time is presented in Figure 5.35 along with a straight line (i.e. m = 1) representing a C_α value equal to 0.016, which is the value applied in the FE analysis. By comparing the produced result and the C_α line, it is concluded that the ET Creep model reproduces well the development of viscoplastic strains with time at a stress level equivalent to the normally consolidated range of the soil, i.e. OCR equal to 1.

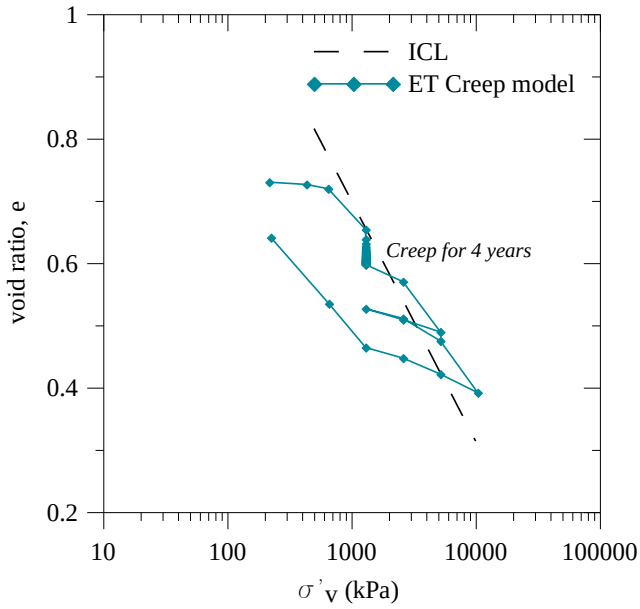


Figure 5.34: FE simulation of IL oedometer creep test

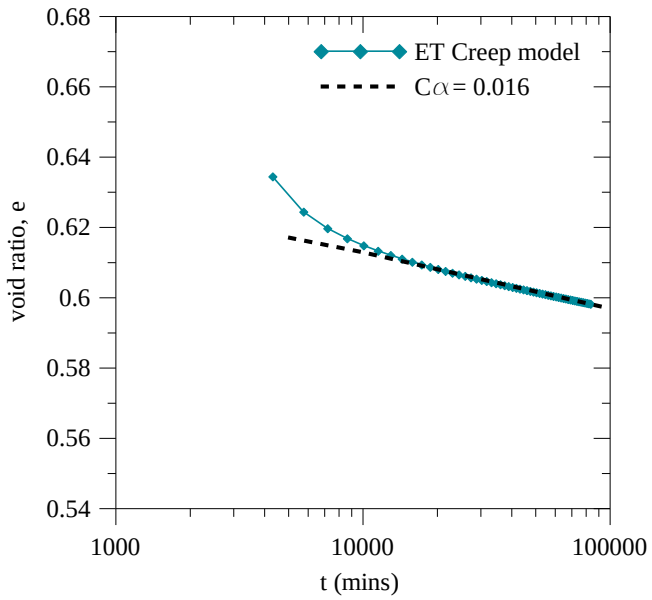


Figure 5.35: Development of viscoplastic strains with time at constant vertical effective stress

The time dependent ET Creep model parameters validated from the analyses are tabulated in Table 5.8. The validation applies for lithological unit $B_{2(b)}$, however it is assumed that for the rest of the lithological units the same value of C_α applies. Therefore, by considering the initial void ratio for the intact samples given in Table 5.4, the following parameters are obtained.

Unit	ψ/V	t_0 (h)	$\varepsilon^{vp}_{vm,limit}$
C	0.00414	24.0	0.405
$B_{2(c)}$	0.00386	24.0	0.444
$B_{2(b)}$	0.00402	24.0	0.422
$B_{2(a)}$	0.00404	24.0	0.419
A_3	0.00413	24.0	0.406

Table 5.8: ET Creep model parameters for London Clay: Parameters defining time dependency

5.8.2. Triaxial creep tests: Unit $B_{2(b)}$

Sorensen (2006) performed an undrained triaxial test on an intact sample of London Clay from unit $B_{2(b)}$ from Heathrow Airport T5, in order to examine the influence of strain rate on the stress-strain shearing path and stress path. The test was performed in a computer-controlled stress path triaxial apparatus with strain-controlled loading, using miniature linear variable differential transformers (LVDTs) for local strains measurements. The sample was isotropically compressed to a mean effective stress equal to 300 kPa and then it was sheared undrained in triaxial compression. To observe the strain rate effects in shearing, the axial strain rate was changed in a stepwise manner with strain rates of 0.05%/h, 0.2%/h and 0.9%/h, as shown in Figure 5.36. Three stress-strain curves were plotted, representing the stress-strain path for each stain rate applied in the triaxial test.

A set of undrained triaxial compression tests was simulated by a set of FE single element analyses, in order to reproduce the strain rate effects in London Clay and validate isotach viscosity. The FE analyses conditions were similar to those of Section 5.7.2. Model parameters are equal to those calibrated previously for the London Clay unit $B_{2(b)}$. Three simulations were performed, each one representing a strain rate applied in the triaxial compression tests performed by Sorensen (2006), allowing the comparison of the FE predicted results using the ET Creep model with the laboratory results. Figure 5.37 is

produced in order to show the stress-strain responses predicted from the FE analysis and those derived from the laboratory results. Also, the stress paths predicted for the three different strain rates are plotted in Figure 5.38, without the laboratory results for the former. These were described as unreliable due to a failed pore water pressure transducer.

Similar observations to those made in Chapter 4, including viscosity at small and large strains, are made. Regarding the effect of strain rate change, the ET Creep model overestimates the effect during shearing, since the predicted range of the peak stress for the strain rates applied is wider than the range recorded in the lab.

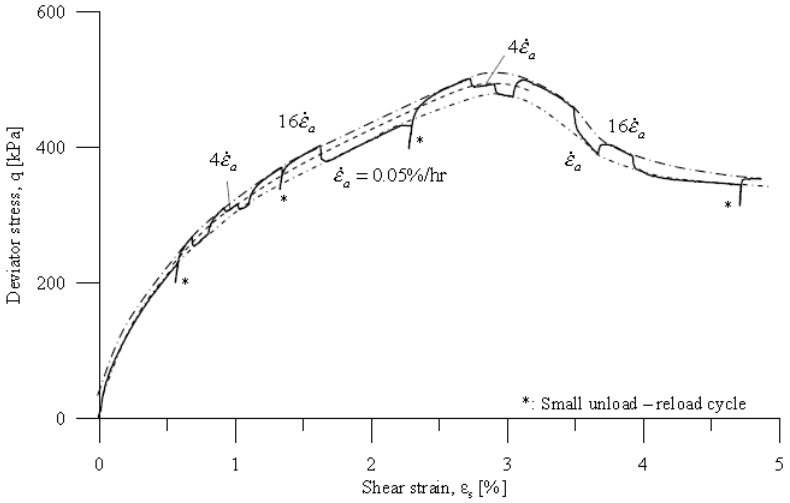


Figure 5.36: Effect of stepwise change in strain rate on undrained stress-strain shearing path of OC intact London Clay

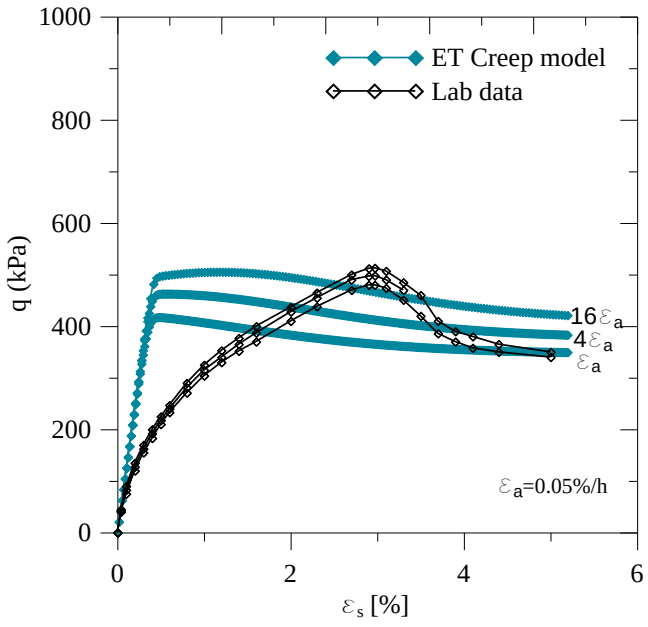


Figure 5.37: Effect of stain rate on undrained stress-strain shearing path of London Clay from unit B2b

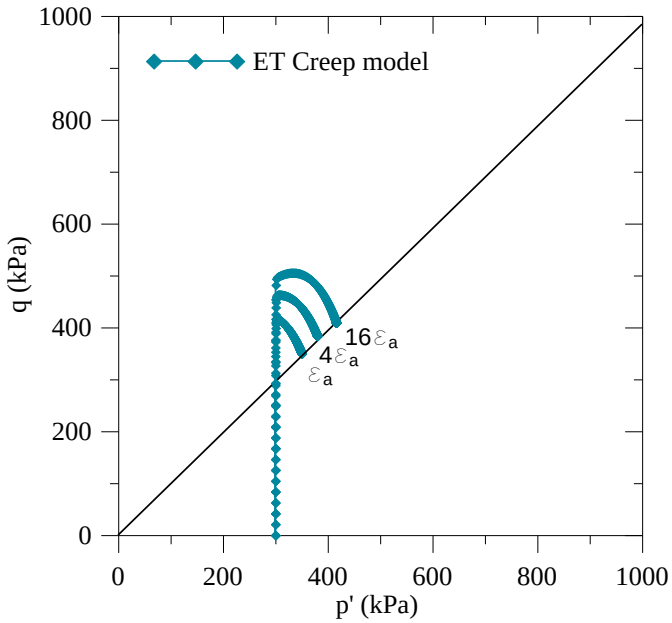


Figure 5.38: Effect of stain rate on undrained stress path of London Clay from unit B2b

5.9. SUMMARY AND CONCLUDING REMARKS

The Equivalent Time (ET) Creep model developed by Bodas Freitas (2008) is employed, in order to model the behaviour of London Clay and perform finite element analyses of piled raft foundations in London Clay. The required model parameters to model accurately both the monotonic rate and time dependent behaviour of London Clay are calibrated and validated using laboratory tests performed by Gasparre (2005) and Sorensen (2006) on London Clay samples from Heathrow Airport Terminal 5.

London Clay is a stiff overconsolidated marine clay of high plasticity and low sensitivity, whose macrofabric is characterised by the presence of fissures. It is heavily overconsolidated as a result of significant erosion events after deposition and also naturally structured from both sedimentation processes and post-sedimentation processes such as ageing. A series of sea level transgressive-regressive cycles have resulted in the formation of different lithological units. Laboratory tests, utilised to calibrate the ET Creep model parameters, involve tests from the majority of the units and sub-units encountered in Heathrow Airport Terminal 5.

The viscosity of natural London Clay is characterised as isotach and it is observed for both small and large strains in the pre- and post-peak regions during shearing. The peak strength is strain rate dependent, while the critical state appears to be independent of strain rate and

unique in the e-p'-q space. The value of C_α for natural London Clay is assumed to be equivalent to the value determined from tests on reconstituted samples and the relationship between the strain and the logarithm of time during secondary compression is regarded as linear for both volumetric and deviatoric creep conditions.

A summary of the ET Creep model parameters derived for London Clay is presented in Table 5.9. The value of C_α for natural London Clay is assumed to be equal to 0.016 for all lithological units. The shear stiffness values derived are based on the back-analysed values from a pile load test performed in the Heathrow Airport Terminal 5 area, detailed in Chapter 6. Oedometer tests and triaxial compression tests performed by Gasparre (2005) are utilised to calibrate the monotonic rate behaviour of London Clay and derive the model parameters that define compressibility and shear strength. In addition, an oedometer creep test and a triaxial compression test, involving a stepwise change of strain rate and performed by Sorensen (2006), are utilised to validate the model parameters defining the time dependency of London Clay.

Unit	$\mathbf{M_f = M_g}$	$\boldsymbol{\alpha_f = \alpha_g}$	$\boldsymbol{\mu_f = \mu_g}$	$\boldsymbol{\psi/V}$	$\mathbf{t_0}$	$\boldsymbol{\varepsilon_{vm,limit}^{vp}}$
C	0.8561	0.4	1.1	0.00414	24.0	0.405
$B_{2(c)}$	0.9838	0.0001	2.0	0.00386	24.0	0.444
$B_{2(b)}$	0.9838	0.0001	2.0	0.00402	24.0	0.422
$B_{2(a)}$	0.9838	0.0001	2.0	0.00404	24.0	0.419
A_3	0.9411	0.4	0.9	0.00413	24.0	0.406
Unit	$\boldsymbol{\lambda/V}$	$\boldsymbol{\kappa/V}$	$\mathbf{p_{s0}}$	$\boldsymbol{\rho_s}$	**G (kPa)**	**OCR**
C	0.062	0.030	-40.0	100.0	50000.0	+2.0
$B_{2(c)}$	0.055	0.025	-40.0	400.0	55000.0	+2.7
$B_{2(b)}$	0.065	0.050	-40.0	1500.0	70000.0	+2.8
$B_{2(a)}$	0.055	0.030	-70.0	500.0	90000.0	+3.8
A_3	0.070	0.045	-70.0	1600.0	110000.0	+3.1

Table 5.9: Summary of ET Creep model parameters for London Clay

Chapter 6

Numerical Model Calibration

6.1. INTRODUCTION

In this chapter, a preliminary analysis of the short-term and long-term behaviour of single piles founded in soft clay and stiff clay ground conditions is initially performed, before proceeding with the calibration of numerical models for piles installed in London Clay. The effect of preloading on the axial load capacity is examined. Then, documented case histories of single piles installed in London Clay on the response of single piles subjected to axial loading during pile load tests and on the performance of a piled raft foundation are utilised, in order to calibrate the numerical models which are subsequently used to investigate piled raft foundations. In particular, a documented single pile load test from Heathrow Airport Terminal 5 is back-analysed, in order to calibrate the model parameters and simulate the installation effects in the soil surrounding the piles. The pile load test is also used to obtain the shear modulus parameters of London Clay employed in the ET Creep model (see Section 5.6). Subsequently, research turns to a large scale project, Hiscocks House in Stonebridge Park founded on a piled raft foundation, where a pile load test performed before the erection of the building and another one performed after its demolition are utilised to calibrate the installation effects and validate the effects of time. Also, the documented performance of the piled raft foundation is utilised to verify the calibrated ET Creep model parameters, the boundary conditions and the numerical approximations of the analysis.

6.2. PRELIMINARY FINITE ELEMENT ANALYSES ON SINGLE PILES

Preliminary finite element analyses of the short-term and long-term behaviour of single piles founded in soft clay and stiff clay ground conditions is performed. The scope of these

analyses is to quantify the effects of time on the behaviour of piled foundations. The effect of preloading on the axial load capacity of piles is examined.

The short term capacity of a pile is usually the most critical in pile design and several approaches have been put forward, either analytical or empirical. However, a question remains about the capacity in the long term, if extra loading is applied on an existing piled foundation. Such a situation may arise when new floors are added to an existing structure, resulting in a load increase on existing piles. Previous studies on the effects of preloading and soil ageing on the bearing capacity of shallow foundations on soft clay, by Zdravkovic et al. (2003) and Bodas Freitas et al. (2007) respectively, have shown that the capacity of shallow foundations is significantly enhanced with time, however it remains a question whether this is the case for deep foundations.

Clearly, pre-loaded foundations have to sustain a certain load over a period of time, during which the soil is subjected to time-related processes of consolidation and creep. Both of these processes enhance the soil strength and stiffness compared to the initial conditions, and it remains a question whether these processes affect the long-term load capacity of single piles. In the literature (see Chapter 2), it has been reported that if a driven pile in soft clay has an adequate safety factor, as shown by a conventional short-term loading test, the effect of the permanent (i.e. long term) working load will be to increase the safety factor with time, as a result of creep and consolidation of the clay. In the same manner, for piles in stiff clay, it has been reported that an enhancement of the pile capacity by a lesser amount is expected at working load due to creep and consolidation, however no conclusive observations for the effects of sustained loading on piles have been published.

It is evident that the method of installation significantly affects the processes involved in the soil surrounding a pile. It has been described by several authors (see Chapter 2) that during pile installation and equilibration, the soil strength surrounding a pile may be enhanced or reduced depending on the method of installation or even the soil medium. However, these effects are ignored initially in the present study. Instead, the piles are wished in place. The effects of installation are omitted and the processes examined are those that take place after the effects of installation have stabilised. The effects of installation are considered numerically later in Section 6.3.

The effect of preloading on the behaviour of piles allows the assessment of the alternative design strategies of piles defined in Chapter 2, including conventional piles, ‘creep piles’ and ‘settlement reducing piles’. Conventional piles are designed with a factor of safety against

failure of the order of 2 to 3, implying a level of preloading of 50 and 33.3 % respectively. On the other hand, 'creep piles' or 'settlement reducing piles' are designed to utilise a significant part or their full load capacity under working conditions, implying levels of preloading larger than 50 %.

The problem is investigated by means of a series of coupled finite element analyses. Undrained analyses are also performed to establish the short term capacity. Two constitutive models, a form of the Modified Cam Clay (MCC) model (Potts & Zdravkovic, 1999) and the Equivalent Time (ET) Creep model (Bodas Freitas, 2008), both described in Chapter 4, are used in order to investigate the time effects on pile capacity in the long term. The MCC model accounts for the consolidation processes in the ground and can predict accurately the change of undrained shear strength during consolidation. The ET Creep model also takes account of the creep effects and can predict the change of undrained shear strength due to the development of viscoplastic strains, or creep strains, with time, along with the associated changes due to consolidation. Other time effects identified in Chapter 2 are not simulated, and therefore this study is limited to the effects of consolidation and creep on the long term behaviour of a preloaded pile.

6.2.1. Model parameters and soil conditions

The ground profiles adopted for this study include (a) a soft clay profile and (b) a stiff clay profile. The soft clay is more compressible and weaker than the stiff clay. Also, it is regarded as being more susceptible to creep as it is normally consolidated, allowing the development of larger creep deformations with time. In the following, a detailed description of the soil profiles adopted, and of the respective model parameters, is made. For the soft clay site, both the MCC and the ET Creep models are employed, whereas for the stiff clay site only the ET Creep model is utilised.

(a) Soft clay profile

The basic material properties employed for the behaviour of the soft clay are listed in Table 6.1. The material parameters and the ground profile adopted for the analysis are based on a site investigation and on laboratory data from a soft clay site in Grimbsy, Yorkshire (Mair et al. 1992). Similar soil conditions and model parameters to those adopted by Zdravkovic et al. (2003) and Bodas Freitas et al. (2007) for shallow foundations on the same soft clay site are used, in order to make the single pile and the footing analyses consistent.

φ'	κ	λ	G	γ	v_1	k
Degrees	-	-	kPa	kN/m^3	-	m/s
32	0.022	0.220	1700.0	17	3.00	5×10^{-10}

Table 6.1: Basic material properties for soft clay

The material properties tabulated are sufficient to define the constitutive behaviour of the MCC model.

To define the constitutive behaviour of the ET Creep model, additional time dependent parameters are required (see Chapter 4). The value of C_α adopted for the soft clay is equal to 0.01. This is regarded as conservative in terms of shear strength (the opposite for settlements) by Bodas Freitas et al. (2007). It is recognised, however, that according to Mesri and Castro (1987) the value of C_α for most inorganic soft clays ranges between 0.02 and 0.03. From Equation 4.61, the parameter ψ_0/V is set to 0.00217 and $t_0 = 1$ day. Also, a near linear logarithmic strain function is employed for the ET Creep model, therefore the value of $\varepsilon^{vp}_{vm,limit}$ represents strains at a level where voids no longer exist in the soil. The initial void ratio is set equal to 1.0 and the parameter $\varepsilon^{vp}_{vm,limit} = 0.5$.

The ET Creep model is assumed to be associated, with a common yield surface and plastic potential function. The shape of the yield surface and of the plastic potential for the ET Creep model are set to be similar to the MCC yield surface shape, with parameters α and μ being equal to 0.4 and 0.9 respectively in order to reproduce the elliptical yield surface.

Also, the parameters p_{s0} and ρ_s, which define the initial structure of the soil and the subsequent rate of structure loss with volumetric visco-plastic straining respectively, assume a stable structure; therefore, the parameters p_{s0} and ρ_s are set equal to zero.

The ET Creep model parameters employed for the soft clay are given in Table 6.2.

p'_{mio}	λ/V	κ/V	$M_f = M_g$	$\alpha_f = \alpha_g$	$\mu_f = \mu_g$
kPa	-	-	-	-	-
10.0	0.110	0.011	1.2872	0.4	0.9
G	ψ_0/V	t_0	$\varepsilon^{vp}_{vm,limit}$	p_{s0}	ρ_s
kPa	-	day	-	kPa	-
1700.0	0.00217	1.0	0.5	0.0	0.0

Table 6.2: ET Creep model parameters for soft clay

The ground profile at the site under investigation consists of normally consolidated clay, with 2 m thick stronger and overconsolidated crust above the ground water table. The soil above the water table is assumed to be saturated and able to sustain tensile pore water pressures. This gives a finite value of effective vertical stress, and therefore of undrained strength, at the ground surface.

Equation 4.17 is employed, where the values of OCR and K_o are varied, in order to obtain a realistic distribution of undrained strength (in triaxial compression). For depths below the ground water table, where the soil is normally consolidated, the input parameters listed in Table 6.1 give a ratio S_u/σ_v' of 0.3, a value typical of soft clays. In Figure 6.1, the S_u profile the assumed distribution of the OCR and K_o is shown.

For the ET Creep model, similar OCR, K_o and material properties to those of the MCC model are employed, however the undrained shear strength profile is not necessarily equal with the profile obtained from the MCC model. This is due to the fact that in the ET Creep model, the undrained shear strength is not only a function of the basic model parameters, as it is in the MCC model, but also a function of the shearing rate. Therefore, no closed form solution for S_u exists. In order to deal with this, a realistic pile loading rate is incorporated in the analyses, as described later.

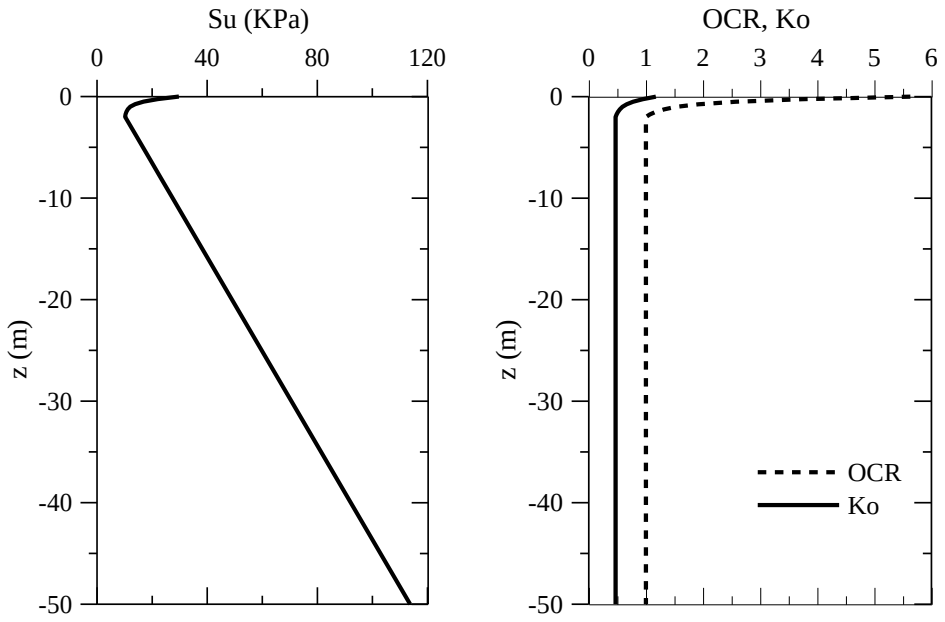


Figure 6.1: S_u, OCR and K_o profiles for soft clay site

(b) Stiff clay profile

The model parameters employed for the stiff clay are listed in Table 6.3. They are equivalent to those employed in the analyses in Chapter 4, for the validation of the ET Creep model for the behaviour of natural overconsolidated stiff clays. For the stiff clay pile analyses, the ET Creep model is employed only.

p'_{mio}	λ/V	κ/V	$M_f = M_g$	$\alpha_f = \alpha_g$	$\mu_f = \mu_g$
kPa	-	-	-	-	-
10.0	0.060	0.030	0.8985	0.4	0.9
G	ψ_0/V	t_0	$\varepsilon^{vp}_{vm,limit}$	p_{s0}	ρ_s
kPa	-	day	-	kPa	-
70000.0	0.00409	1.0	0.412	0.0	0.0

Table 6.3: ET Creep model parameters for stiff clay

The parameters λ/V, κ/V and G are based on the parameters calibrated for London Clay in Chapter 5. The value of λ/V is approximated from the compression curves of oedometer tests on undisturbed London Clay samples from different depths and units, whereas the values of κ/V and G are evaluated from unloading-reloading paths and considering the fact that the value of G has to be consistent with the stiffness range associated with the load-settlement response of piles.

The parameter ψ_0/V is calculated using Equation 4.62 with a value of C_α equal to 0.016, which is consistent with the value of C_α for London Clay employed in Chapter 5. According to the definition of C_α, the reference time t_0 is equal to 24 hours or 1 day, and therefore the visco-plastic volumetric strain rate on the reference time (Equation 4.37) is equal to 0.00409/day. A near linear logarithmic strain function is employed with the initial void ratio set equal to 0.7 and therefore the parameter $\varepsilon^{vp}_{vm,limit} = 0.412$.

The model is assumed to be associated, with a common yield surface and plastic potential function. Parameter M is calculated using Equation 4.57 with a value of φ' equal to 23^o, whereas parameters α and μ, which define the shape of the loading surface and plastic potential in the general stress space, are set equal to 0.4 and 0.9 respectively, which gives a MCC "ellipse".

As before the parameters p_{s0} and ρ_s are set equal to zero, representing a stable structure.

The stiff clay profile is assumed to be overconsolidated. A constant OCR value in terms of mean effective stress is employed equal to 4.0. The ground water table is set at 2.5 m below the ground level, and the soil above the water table is assumed to be saturated and able to sustain tensile pore water pressures. The K_o profile is set everywhere equal to 1.0. Regarding the S_u profile, as mentioned above, the undrained shear strength in the ET Creep model is not only a function of the basic model parameters, as it is in the MCC model, but also a function of the shearing rate. No closed form solution exists and, therefore, a realistic pile loading rate is incorporated in the analyses, as described later.

6.2.2. Problem geometry and boundary conditions

The single pile mesh used to perform the finite element analyses is shown in Figure 6.2. The analysis is axi-symmetric and the mesh domain is 50 m deep and 20 m wide. The single pile is 20 m long and its diameter is 1 m. The pile dimensions are chosen arbitrarily, however they are chosen such that they represent a typical friction pile. Full adhesion between the pile and soil is assumed.

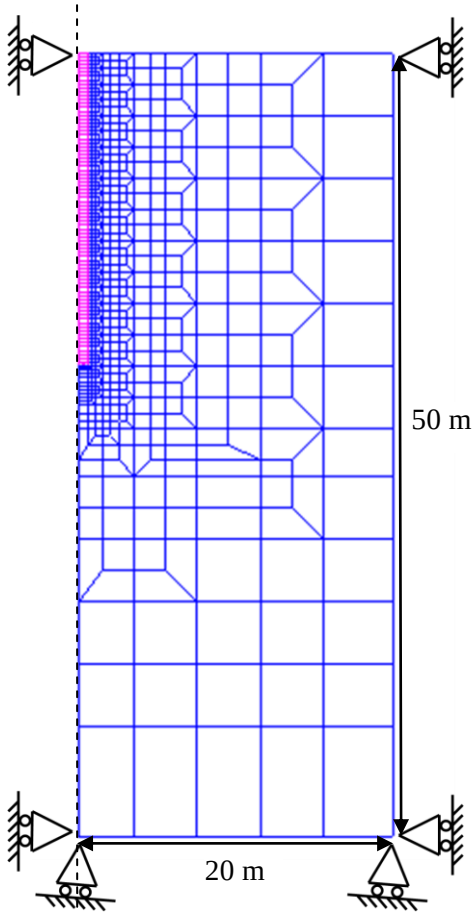


Figure 6.2: Mesh for preliminary finite element analyses on single piles

Both the pile and the soil are discretised. The pile is modelled as a very stiff elastic material ($E= 30\times10^6$ kPa, $\mu= 0.15$), which is able to transfer load from the pile head to the surrounding soil, whereas the soil is modelled either using the MCC or ET Creep models. The mesh consists of eight noded isoparametric elements with four pore pressures degrees of freedom at the corner nodes, and two displacement degrees of freedom at both corner and mid-side nodes.

The prescribed zero displacement boundary conditions prevent the base of the mesh from moving in the vertical and horizontal directions, while the vertical sides of the mesh are fixed in the horizontal direction but can move in the vertical direction.

The seepage boundary conditions applied for the coupled analyses allow no flow of water to the base of the mesh and to the left hand boundary of the mesh, while on the right hand boundary pore pressures are kept equal to their initial values, as determined by the water table 2 m (soft clay) or 2.5 m (stiff clay) below ground level.

6.2.3. Description of the analyses

The approach adopted to determine the effects of time on the axial load capacity of single piles is as follows: (1) the single pile is first loaded undrained to failure, in order to establish its initial short term (undrained) load capacity; (2) a further series of analyses is then performed, on the same single pile, in which the pile is first loaded undrained to a percentage (for instance 20, 40, 60, 80 or 100%) of its initial short term load capacity; (3) the load is then held constant at this value for a period of 50 years, during which it is ensured that all excess pore water pressures generated during initial loading have dissipated; and (4) additional load under undrained conditions is then applied until failure is reached to determine the new ultimate undrained load capacity.

This approach is followed for both the MCC and ET Creep analyses, however due to the time dependent nature of the latter a realistic loading rate is required. This rate is chosen to satisfy the assumption that the pile is loaded to failure under a constant displacement rate over a period of 6 months. It should be noted that, due to the development of viscoplastic strains and consolidation during loading, the failure load is not well defined for the ET Creep model analysis in soft clay. Therefore, a rule is adopted to define the displacement rate which initiates failure in six months. This is the rate where the increase in the sustained load between a pile displacement δ, after 6 months, and a pile displacement four times δ is smaller than 5%,

as shown in Figure 6.3. The displacement rate, which gives failure in 6 months, is equal to 0.0004 m/day and is kept constant for all ET Creep model analyses in soft clay.

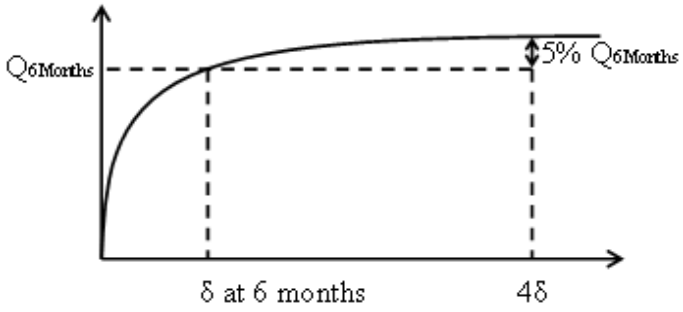


Figure 6.3: Soft clay analysis: definition of failure load for ET Creep analyses

On the other hand, for the analyses in stiff clay a peak resistance is reached, therefore a definite value for the pile load capacity is obtained. A displacement rate which also gives failure in 6 months is employed; this is equal to 0.00004 m/day and it is kept constant for all analyses in stiff clay.

In the ET Creep model, the initial stress state, with respect to the reference time line, is obtained through the value of the OCR. Therefore, the amount of viscoplastic strains is proportional to the OCR value. The soft clay is assumed normally consolidated, i.e. OCR equal to 1. However, such an OCR value represents the situation when the clay is first formed, resulting in unrealistic initial viscoplastic strains. In the soft clay analyses, the OCR is set equal to 1.05, which is consistent with the observations made by Schmertmann (1991). It is claimed that no real soil can be purely normally consolidated, since it has been in place for a certain period of time, during which creep has made the soil to appear "overconsolidated". This is usually termed as "aging preconsolidation".

For the MCC model, analyses to obtain the load capacity are undrained, since the interest is in the short term capacity. For those where the load is held constant until all excess pore water pressures dissipate, they are coupled to allow consolidation. On other hand, the ET Creep analyses are all coupled. This is due to the time dependent nature of the model and the relation of strain with time. It should be noted though, that rapid loading even in coupled conditions may be considered as undrained, since the period for full dissipation of excess pore water pressure is expected to be longer than the 6 month initial loading period.

6.2.4. Soft clay analyses

For the soft clay profile, two sets of analyses, with different constitutive models were performed; (a) the MCC analyses, where the effect of consolidation in the long term is observed, and (b) the ET Creep analyses, where both the effects of creep and consolidation are reproduced.

(a) MCC analyses

The first MCC analysis was on the behaviour of the single pile loaded under undrained conditions. In Figure 6.4, the load-settlement response is plotted for undrained loading. Failure is assumed to be reached when the curve reaches a plateau, which is at a displacement equivalent to 3.3 % of the pile diameter. The undrained load capacity of the single pile is 1615 kN. The contribution of the base and shaft resistances to the pile capacity is also presented in Figure 6.4, which shows that the pile works as a friction pile with the capacity mainly being provided by the shaft resistance. Contours of vertical shear stress at failure are plotted in Figure 6.5a, where the mechanism of shear resistance along the pile shaft is evident. Contours of excess pore water pressure at failure are also plotted in Figure 6.5b, being indicative of the soil area whose strength is enhanced during consolidation.

Subsequent analyses for different levels of preloading (20, 40, 60 and 80%) were performed, where the load settlement profiles are plotted in Figure 6.6. It is clear that there is little gain in capacity for all levels of preloading. The dissipation of excess water pressures generated during initial loading does not greatly enhance the pile capacity, even though settlements are larger for higher levels of preloading. This can be reconciled with the fact that the magnitudes of the excess pore water pressures, as well as their concentration around the pile toe (see Figure 6.5b), indicate that the soil's strength is enhanced primarily around the pile toe. Considering the contribution of the base in respect to the shaft to the load capacity (see Figure 6.4), it is concluded that the consolidation processes in the ground do not greatly affect the long term capacity of the piles founded in soft clays.

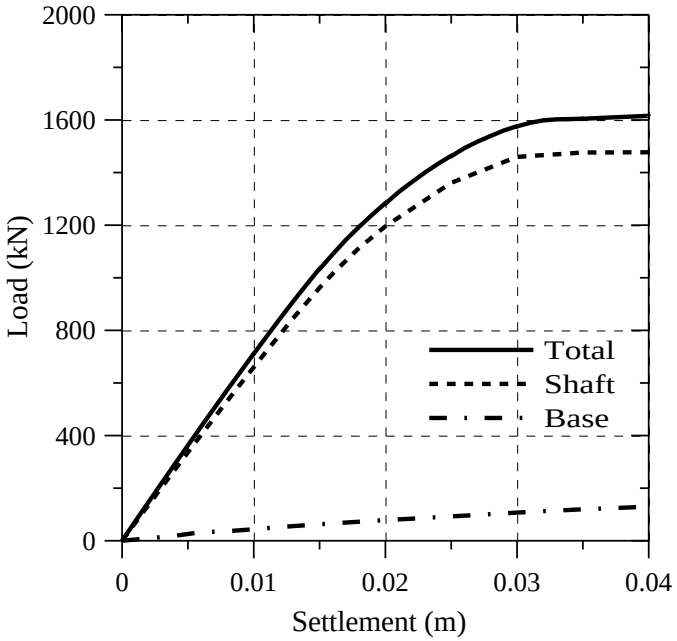


Figure 6.4: MCC soft clay analysis: load-settlement response for undrained loading

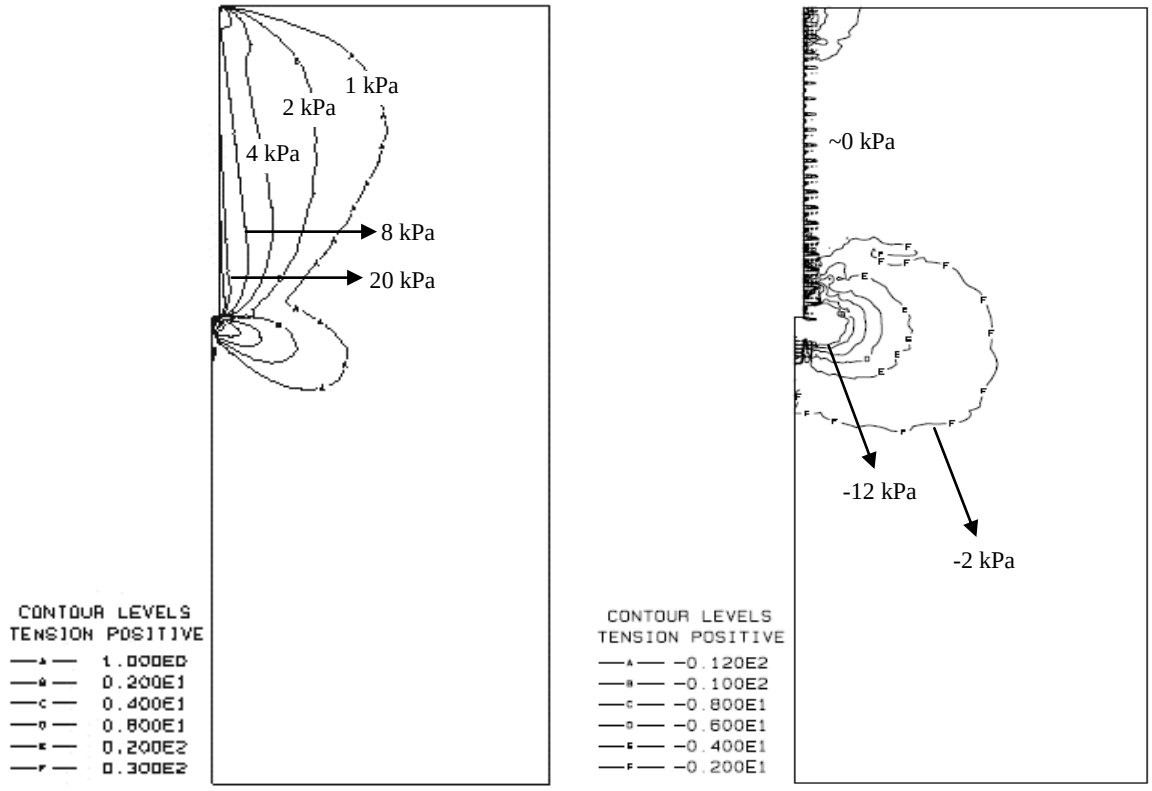


Figure 6.5: MCC soft clay analysis: contours at failure of (a) vertical shear stress, (b) excess pore water pressures

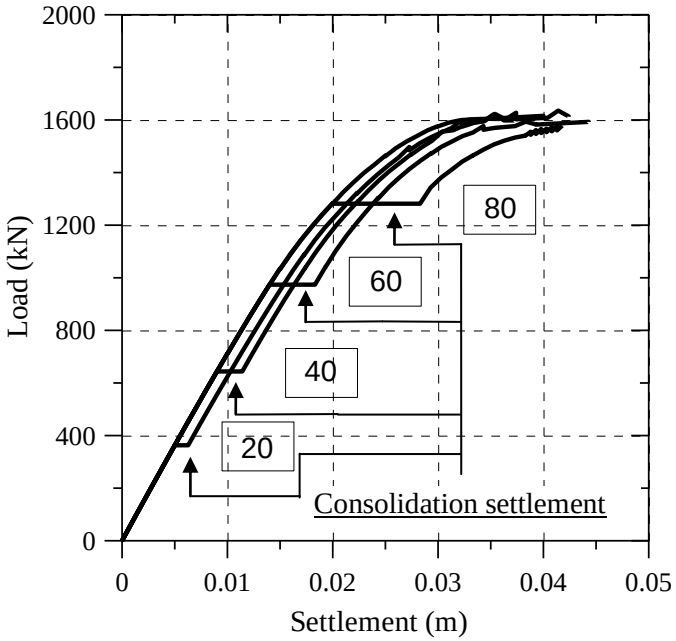


Figure 6.6: MCC soft clay analysis: load-settlement response for different levels of preloading

(b) ET Creep analyses

The first analysis employing the ET Creep model was to determine the initial short term load capacity of the single pile. A constant displacement rate initiating failure at 6 months was applied, which gave a load capacity equal to 2266 kN. This value is quite different to the value calculated in the MCC analysis. This is attributed to the difference of the plastic potential surface in the deviatoric plane between the two models. In particular, the ET Creep model assumes the Matsuoka-Nakai shape of the yield and plastic potential surfaces in the deviatoric plane, whereas the MCC model assumes that the yield and plastic potential surfaces are given by a Mohr Coulomb hexagon and a circle respectively. Such differences in the plastic potential in the deviatoric plane can cause significant discrepancy in the predicted failure loads (Potts & Gens, 1984). Thus, comparisons are made in terms of the proportional increase in load capacity observed in each set of analyses. Similar observations were made by Bodas Freitas et al. (2007) for the footing problem.

Analyses for different levels of preloading (20, 40, 60, 80 and 100%) were then performed. The load settlement profiles are plotted in Figure 6.7. The piles are preloaded for a period of 50 years and the results indicate that the load capacity of the piles is enhanced on subsequent loading. The gain in pile capacity is proportional to the level of pre-loading. This is due to the development of viscoplastic strains under constant deviatoric stress conditions along the pile shaft which enhances the soil's strength. During this preload period, due to the coupled nature

of the analyses, dissipation of the excess pore water pressures generated during initial loading also takes place. However, it has been shown (see MCC analysis) that this effect is not significant in enhancing the capacity of the pile.

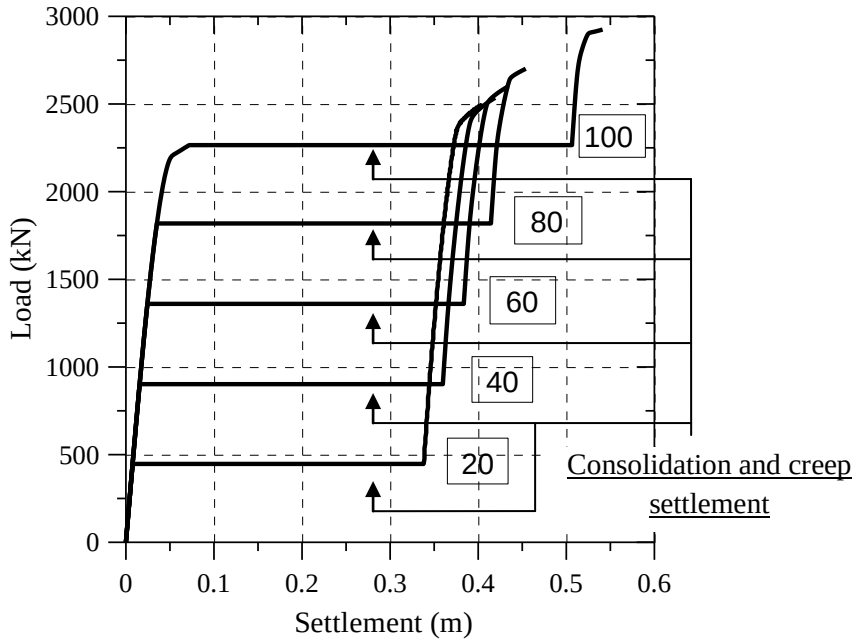


Figure 6.7: ET Creep soft clay analysis: load-settlement response for different levels of preloading

Viscoplastic strains enhance the undrained shear strength of the soil due to the changes in void ratio with time under constant deviatoric stress, making the soil appear preconsolidated. Higher values of pile preloading result in larger creep settlements and load capacities respectively on reloading. This is attributed to the fact that the larger the stress in the soil supporting the pile, the larger the development of strains and the subsequent reduction in void ratio with time due to creep.

(c) Discussion

The contribution of the consolidation settlement to the total settlement is very small compared to that of the creep settlement in the soft clay for a preloading period of 50 years. This is indicated in Figures 6.6 and 6.7, where the settlement for different levels of preloading is of the order of millimetres for the MCC analysis, whereas for the ET Creep analysis it is of the order of centimetres. Creep settlement results from: (a) settlement of the soil by its own weight, taking place in the entire soil domain, which is accumulated at the pile level, indicating probably that a larger OCR value than 1.05 should have been applied for the deeper

soil levels; and (b) settlement proportional to the level of preloading, where the larger the load on the pile, the larger the creep settlement.

In Figure 6.8, the normalised load capacity, as predicted by the ET Creep model, is plotted against the initial level of preloading. Figure 6.8 also includes the results of the MCC analysis. The results show that there is a significant increase in the load capacity of the preloaded piles when soil hardening due to creep is considered. In addition, the effect of creep is found to be more significant at higher levels of preloading, resulting in an additional increase in load capacity for instance up to 29.1% at 100% preload.

In Figure 6.9, the gain in bearing capacity, as predicted by Zdravkovic et al. (2003) and Bodas Freitas et al. (2007), for a preloaded footing in a similar set of analyses is shown. Both consolidation and creep enhance the capacity of footings depending on the level of preloading. In particular, dissipation of the excess pore water pressures generated during initial loading under undrained conditions results in a significant increase of the capacity, up to approximately 50% for a level of preloading of 100%. This conclusion is opposite to the findings of the single pile analysis which showed very little capacity increase due to the consolidation processes in the ground. This difference is attributed to the fact that in the footing analysis, due to the positive vertical compression of the soil beneath the footing, significant excess pore water pressures are generated, resulting in the subsequent increase in shear strength of the loaded soil volume during consolidation. On the other hand, the mechanism in piles is different. The load applied to the pile is mostly transferred to the surrounding soil through skin friction (interface shear between the pile shaft and the soil) and therefore insignificant excess pore water pressures are generated along the pile shaft (see Figure 6.5b).

In Figure 6.9, an additional gain in capacity due to creep is observed for the footing, which is proportional again to the level of preloading. Creep takes place due to the positive compression of the soil beneath the footing under volumetric creep conditions during and after the dissipation of excess pore water pressures. On the other hand, in single piles deviatoric creep takes place in the soil surrounding the pile shaft, due to the vertical shear of the soil. Both mechanisms result in soil hardening because of the development of viscoplastic strains with elapsed time under constant (or increasing due to consolidation) mean effective and deviatoric stress respectively.

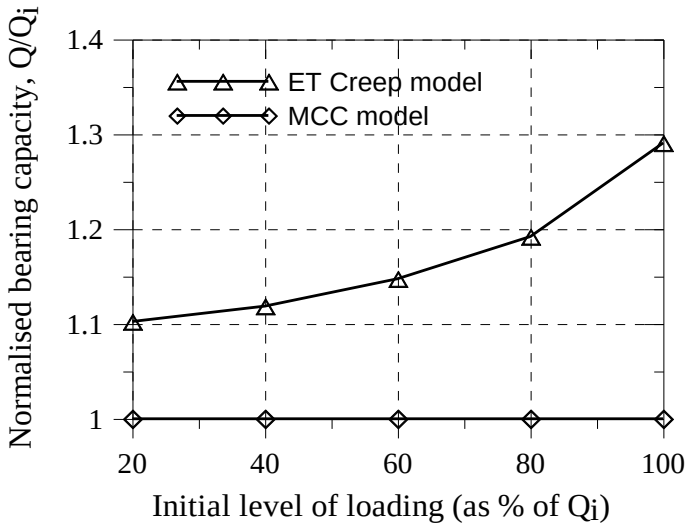


Figure 6.8: Soft clay analysis: gain in load capacity for different levels of preloading

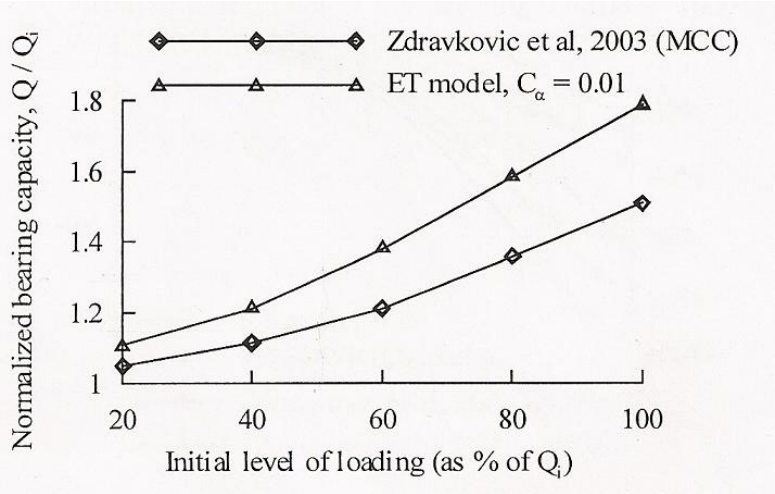


Figure 6.9: Gain in bearing capacity for preloaded footing (Bodas Freitas et al., 2007)

6.2.5. Stiff clay analyses

For the stiff clay analyses, the ET Creep model was employed as a constitutive model with the scope to quantify the effects of creep and consolidation on the behaviour of preloaded piles in an overconsolidated stiff clay profile. The aim of the first analysis was to determine the initial short term load capacity. A constant displacement rate for a period of 6 months was applied, and a well defined peak in the load-settlement response of the pile was obtained (Figure 6.11). The load capacity is equal to 5650 kN. Contours of excess pore water pressure at failure are plotted in Figure 6.10, where it is evident that excess pore water pressures are concentrated around the pile toe.

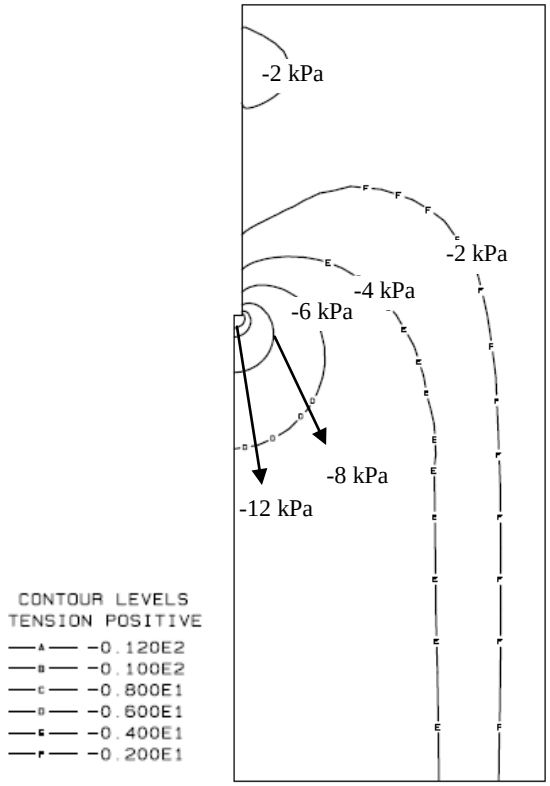


Figure 6.10: ET Creep stiff clay analysis: contours at failure of excess pore water pressures

Analyses for different levels of preloading (20-30-40-50-60-70-80-85%) were then performed. In Figure 6.11, the pile load-settlement response is shown, where it is evident that the pile load capacity is enhanced during the 50 year period of sustained load. The enhancement of the capacity is attributed to creep, and in particular to creep strains (viscoplastic strains) developed under constant deviatoric conditions in the soil surrounding the pile shaft, which enhances the shear strength of the soil.

The calculated settlements, both creep and consolidation, are proportional to the level of preloading. However, at levels of preloading close to the initial short term capacity (>70%), it is observed that settlement increases in a disproportional manner than at smaller levels of preloading. For instance, the deformation calculated for 85% of preloading is approximately 50% larger than the displacement for 80% of preloading. Additionally, further analyses performed at higher levels of preloading, not included in Figure 6.11, result in even larger deformations.

This observation is accompanied with a lower gain in the load capacity at higher levels of preloading than the gain observed at lower levels of preloading, as shown in Figure 6.12. In Figure 6.12, the normalised enhancement of load capacity against the level of preloading is plotted. Between 70 and 80% of preloading, the rate of increase of the capacity enhancement

is decreasing with respect to lower levels of preloading, where an increasing rate is observed. Furthermore, the rate becomes negative, as visualised between 80 and 85% of preloading, and for higher levels of preloading in the range of 90+%, creep settlement results in failure. At levels of preloading close to the initial short term capacity, the pile continuously deforms with time, indicating that failure is taking place due to deviatoric creep.

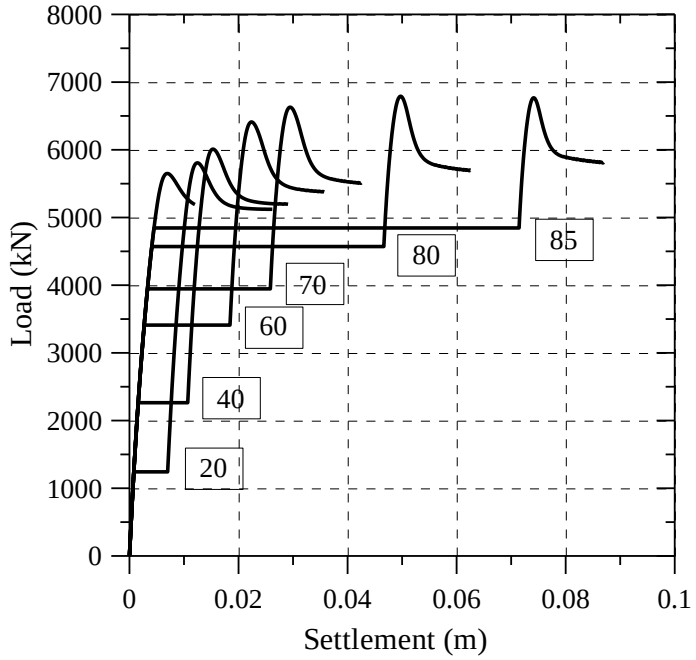


Figure 6.11: Stiff clay analysis: load-settlement response for different levels of preloading

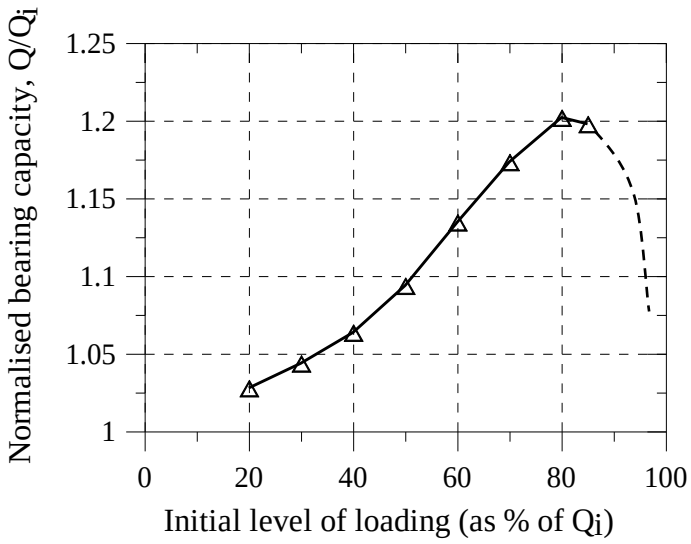
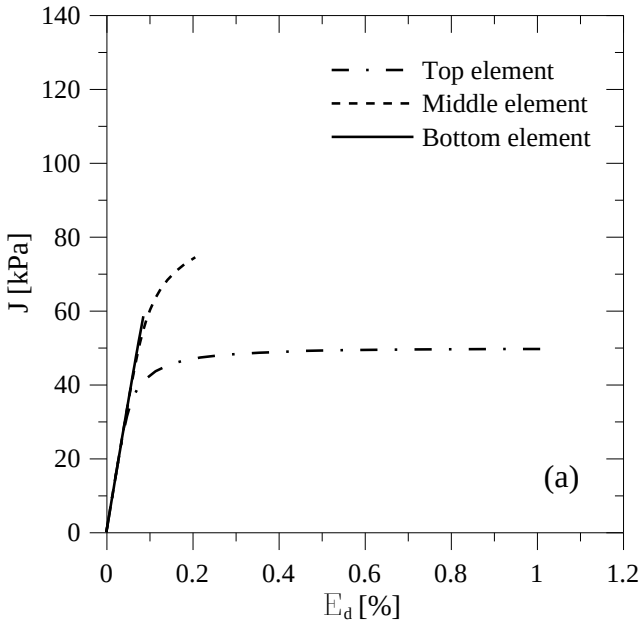


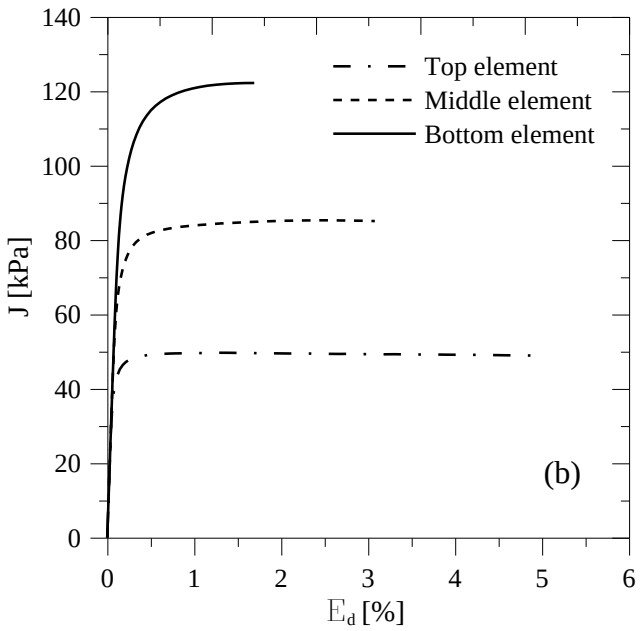
Figure 6.12: Stiff clay analysis: gain in load capacity for different levels of preloading

This effect is attributed to the progressive failure of the pile from top towards the bottom. Soil elements near the head of the pile mobilise their first, whereas deeper elements require larger movements (Figure 6.13). Therefore, at higher levels of preloading, the shear resistance of

soil elements near the pile head drops due to creep induced failure, associated with creep rupture at stress states close to the peak deviatoric stress. This intensifies at higher levels of preloading, close to the initial short term capacity, where a larger volume of soil fails due to creep and whose shear resistance drops with time.

Comparing the normalised enhancement of load capacity against the level of pre-loading for soft and stiff clay in Figures 6.8 and 6.12 respectively, it is observed that in the soft clay analyses the gain in capacity at levels of preloading close to the initial short term capacity is not reducing like in the stiff clay analyses. This is due to the fact that no creep induced failure is observed in the soft clay elements surrounding the pile during sustained loading in the ET Creep analysis. Comparison of the absolute values of capacity enhancement is not appropriate because of the different basic material properties assigned.





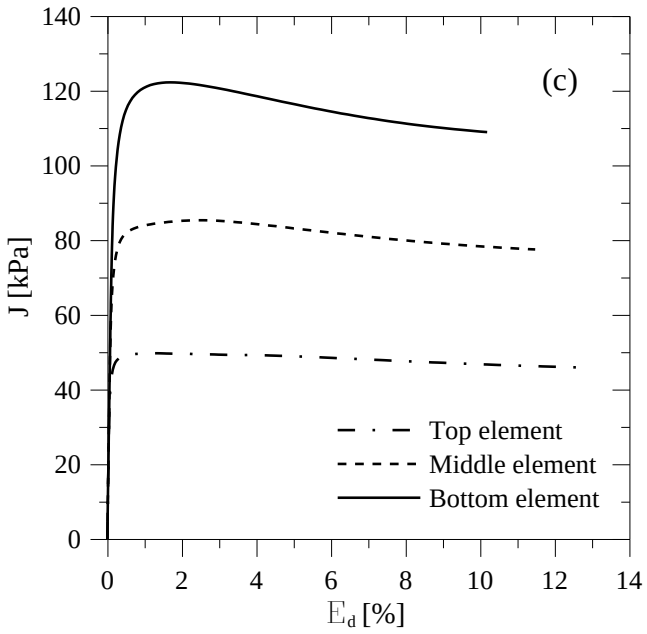


Figure 6.13: Deviatoric stress vs. deviatoric strain for elements adjacent to pile shaft: (a) below the failure load (66%), (b) at failure load, (c) after failure load

6.2.6. Discussion

In this preliminary study, the effects of time on the behaviour of single piles and the effect of preloading on the axial load capacity of piles in soft clay and stiff clay ground conditions is examined. The results allow the assessment of the alternative design strategies of piles defined in Chapter 2, including conventional piles, 'creep piles' and 'settlement reducing piles'. Conventional piles are designed with a factor of safety against failure of the order of 2 to 3, implying a level of preloading of 50 and 33.3% respectively, whereas 'creep piles' or 'settlement reducing piles' are designed to utilise a significant part or their full load capacity under working conditions, implying levels of preloading larger than 50%.

These preliminary finite element analyses highlight the potential of the load capacity to increase with time depending on the level of preloading, implying an increase in the factor of safety against failure with time. 'Creep piles' and 'settlement reducing piles" offer a larger potential for gain in capacity with time than conventional piles, and at the same time larger deformations are expected due to the higher level of preloading. 'Creep piles' have been used in Scandinavian countries where soft clay is present (see Chapter 2). They have been used in such a manner that they reduce the contact pressure between the raft and the soil. Therefore, a sufficient number of piles is required, in order to keep the net contact pressure below the preconsolidation pressure of the soil. Due to the large deformations involved, piles are designed to penetrate the soil until sufficient contact pressure between the raft and the soil is

reached. On the other hand, 'settlement reducing piles' or 'stress reducing piles' have been utilised in stiff clays, such as London Clay, locally under point loads, in order to reduce differential settlements or peak stresses respectively, and they are designed with a low factor of safety. Once again, the main element of support when utilising such piles is the raft, however the benefits of time on the pile load capacity are recognised.

In the context of piled raft foundations in stiff clays, this study highlights the potential benefit of designing 'settlement reducing piles' over the central area below a raft. These piles, if they are allowed to move plastically, so that they mobilise a significant part of their load capacity, with the overall factor of safety given by the raft, then the total long term capacity of the foundation system is expected to increase in the long term, without considering the positive effect from the contact pressure between the raft and the soil. At the same time, piles centrally located beneath a raft are expected to reduce settlements, both absolute and differential, at an acceptable level of serviceability, since they are usually utilised in order to reduce settlements, rather than as a means to provide load capacity.

6.3. BACK-ANALYSIS: PILE LOAD TEST AT HEATHROW

The results from a constant rate of penetration (CRP) pile load test on a large-diameter bored pile performed at the Heathrow Airport Terminal 5 site reported by Unwin and Jessep (2004) are back-analysed, in order to calibrate the numerical models for piles and provide design values for the working piles for the subsequent analyses. The ET Creep model parameter defining the shear modulus is back analysed, whereas the rest of the model parameters for the lithological units encountered at Heathrow Airport area are validated. The effects of pile installation (boring) on the soil surrounding the piles are also simulated by adopting in the analysis a "soft zone" around the pile, whose strength parameters are also back-analysed. The pile load test is performed in the same area where samples of London Clay were retrieved and tested in the laboratory by Gasparre (2005) and Sorensen (2006), and from which the ET Creep model parameters have been calibrated in Chapter 5.

6.3.1. Description of the pile load test

Unwin and Jessep (2004) performed a series of CRP pile load tests on large-diameter auger-bored test piles, constructed for the development of Heathrow Airport Terminal 5. The aim of

the tests was the investigation of the variation of the shaft resistance with time in London Clay. Four full-size, identical in dimension and construction, test piles were constructed.

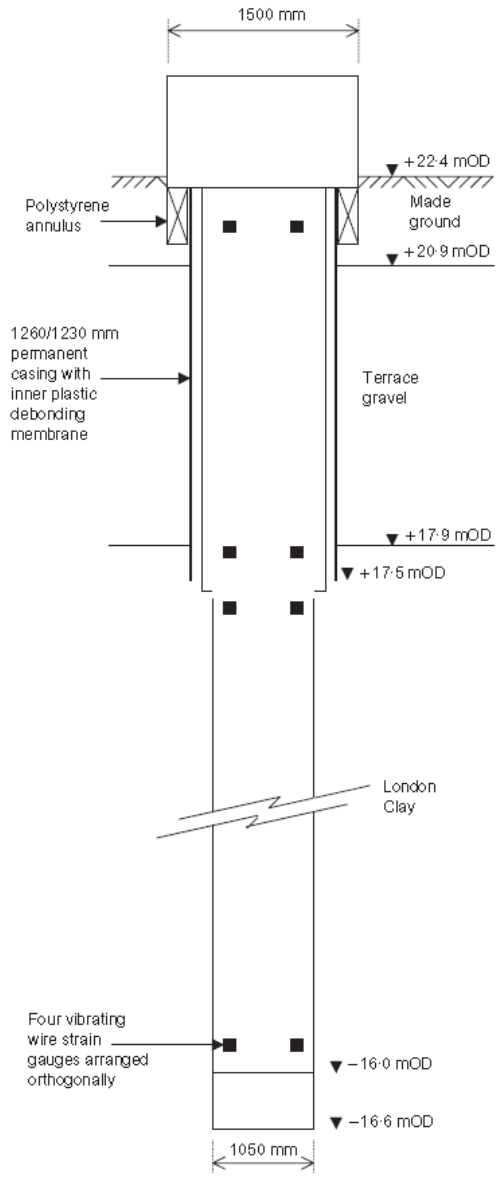


Figure 6.14: Test pile details performed in Heathrow Airport Terminal 5 (Unwin and Jessep, 2004)

The pile dimensions are shown in Figure 6.14. The test piles have a length of 39 m, their diameter is 1050 mm (for the region where no casing is in place) and they penetrate through three layers: Made Ground, Terrace Gravel and London Clay. The reaction force for each test pile was provided by four 1050 mm diameter tension piles. Several measures were taken, in order to isolate the shaft resistance component in the London Clay, including: (a) to minimise any bearing resistance from the bottom of the oversized pile cap (1500 mm in diameter) by installing an annular ring of polystyrene, (b) to eliminate the shaft resistance in the terrace

gravels and the made ground by applying a permanent casing with inner plastic debonding membrane, and (c) to limit the base resistance by applying a "soft toe".

The pile load tests performed were CRP tests with a 3 mm/h rate of displacement up to a displacement of between 100 mm and 150 mm. The piles were initially tested to failure after four ageing periods: 14 days, 3 months, 6 months and 12 months after their installation respectively. Then, the piles were re-tested at the subsequent test days following their installation test date, i.e. the first pile was initially tested 14 days after its installation and then re-tested three times at 3, 6 and 12 months, whereas the second pile was initially tested at 3 months and then re-tested twice at 6 and 12 months, and respectively for the rest. The objective of the testing programme was to investigate (a) the variation in initial response of the piles with age of test, (b) the variation in response of the piles to subsequent reloading with age of test, and (c) peak and critical state shaft resistances.

The first set of results obtained regarding the peak resistances for the four pile load tests, according to Unwin and Jessep (2004), are not indicative of the effect of time between installation and first loading. The peak resistance obtained for the first-time tested piles at 14 days and 12 months was similar, whereas for the other test days (3 and 6 months) the peak resistance was much smaller with the minimum being at 3 months. The fact that the peak resistances do not show a definite pattern is attributed to the sensitivity of the construction processes, including the period between boring and concreting, the fluid pressure exerted by the wet concrete, the degree of remoulding due to boring around the pile shaft interface, and the natural variation in soil. Also, it is postulated that possibly dilatancy and physico-chemical reactions may have played a role.

Unwin and Jessep (2004) present in Figure 6.15 the load-settlement response for the pile tested to failure 14 days after installation and then re-tested three times to failure. It is observed that only the first test shows a peak resistance, before dropping to a residual value at large strain. The peak resistance is mobilised at a displacement approximately of 15 mm (1.5% of the pile diameter), whereas the residual resistance is fully mobilised at a displacement around 40 mm (4.0% of the pile diameter). This pattern is observed, according to Unwin and Jessep (2004), in all tested piles.

The results from the initial test to failure of the first pile tested (Figure 6.15) are used, in order to calibrate the numerical model for piles in London Clay. The documented load-settlement response is back-analysed, using the calibrated ET Creep model parameters and data from the literature for the ground profile at Heathrow. Also, the second elastic ET Creep model

parameter, the shear modulus, is back analysed and calibrated along with the model parameter κ/V, which also defines the elastic part of the ET Creep model. The process is iterative and this analysis is considered as a continuation of the ET Creep model parameter calibration for London Clay behaviour performed in Chapter 5.

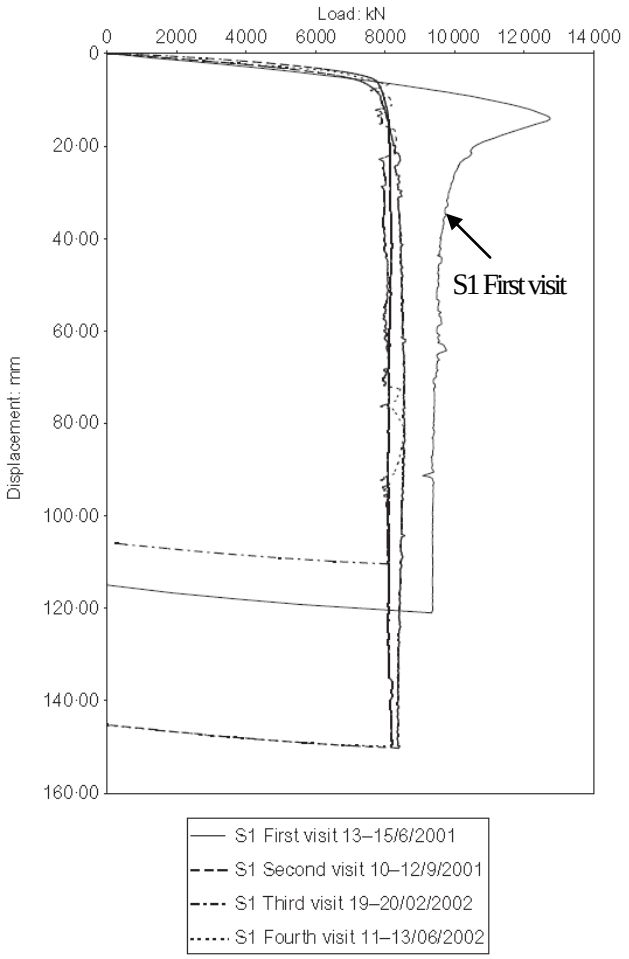


Figure 6.15: Pile head movement against load for test pile (Unwin and Jessep, 2004)

6.3.2. The stiff clay test site in Heathrow

The site where the pile load test was performed is at Heathrow Airport Terminal 5, which is the same area from which samples of London Clay were retrieved and tested in the laboratory by Gasparre (2005) and Sorensen (2006), and from which the ET Creep model parameters were obtained in Chapter 5. A site investigation on the project area of Terminal 5, performed by Hight et al. (2003), along with information provided by Unwin and Jessep (2004) on the site of testing, allows the identification of the soil layers and their respective properties.

The soil profile, as stated above, consists of Made Ground, Terrace Gravel and London Clay. The thickness of the made ground and the terrace gravel are identified by Unwin and Jessep

(2004) in Figure 6.14 equal to 1.5 and 3 m respectively. London Clay is considered by Unwin and Jessep (2004) as uniform, as stated by the model parameters employed for a preliminary axi-symmetric numerical analysis they performed. However, based on Hight et al. (2003), London Clay may be divided into three main lithological units (see Chapter 5), A, B and C, which in turn may be divided into several sub-units.

A soil profile with all the units identified in London Clay for the load test site is suggested in Figure 6.16, along with the geotechnical profile adopted in the numerical analysis. Units B_1, $A_{3(1)}$ and A_2 are omitted in the analysis, due to the fact that no laboratory data for these units were available. The thickness of unit B_1 is considered too small, therefore it is assumed that unit B_1 has the same properties as $B_{2(a)}$. In addition, units $A_{3(1)}$ and A_2 are assumed to have the same properties with $A_{3(2)}$, due to the lack of sufficient data to define these units. Finally, the Harwich Formation is not considered in the analysis, due to the fact that it is considered to be away from the zone of influence of the pile and, at the same time, if it were, no excess pore water pressures would build up due to its mainly sand formation.

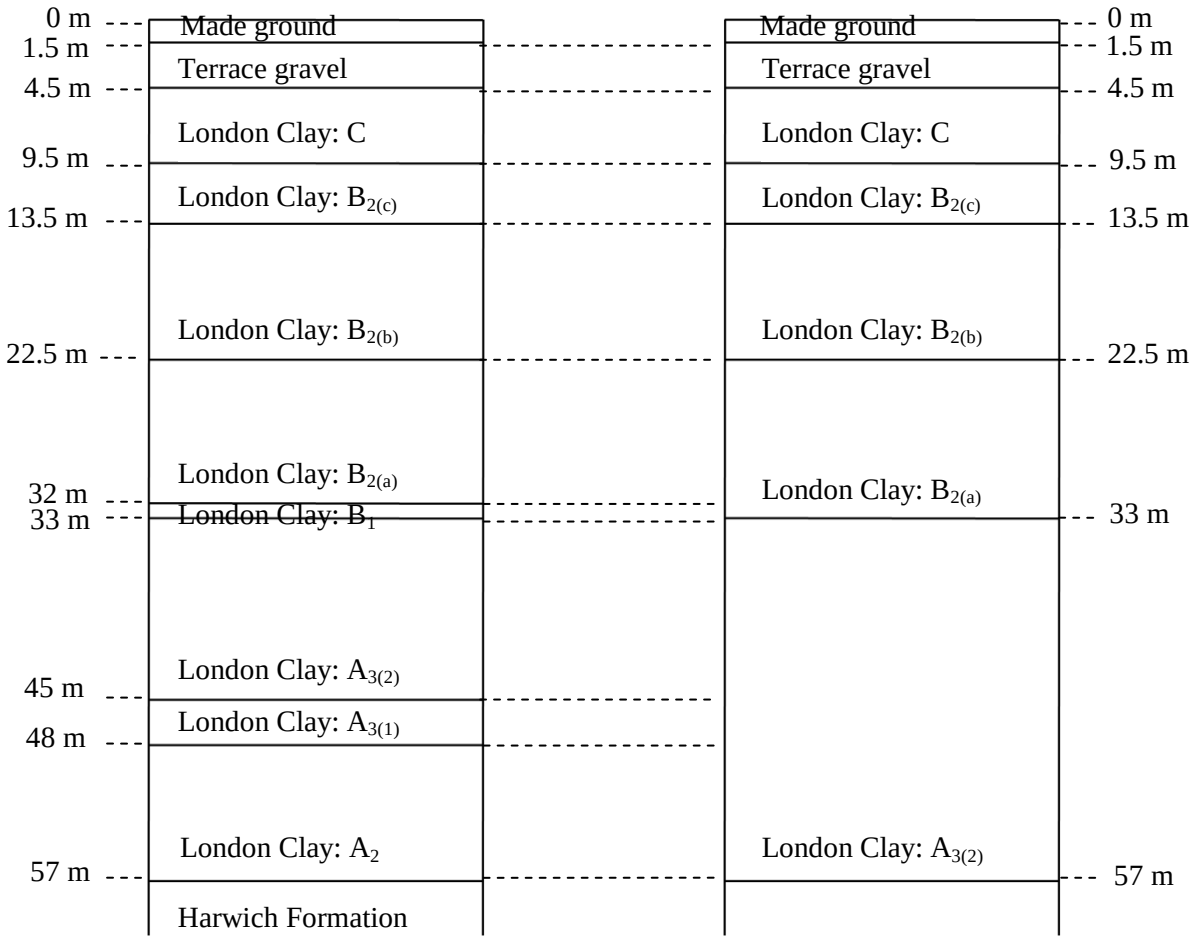


Figure 6.16: Pile load test site in Heathrow Airport T5: (a) suggested soil profile and, (b) adopted soil profile for the finite element simulation

The London Clay profile is an overconsolidated soil profile, which has been influenced by several deposition-erosion events throughout its history (see Chapter 5). As a result, stresses in the ground have been influenced by this deposition history. The current K_o profile at Heathrow Airport Terminal 5 site, as identified by Hight et al. (2007), is shown in Figure 6.17. The K_o profile with gravel surcharge is utilised to define the initial stresses in the numerical simulation. The water table is located 1.5 m above the top of the London Clay, within the Terrace Gravel, and the pore water pressure is assumed to vary hydrostatically with depth (Gasparre, 2005).

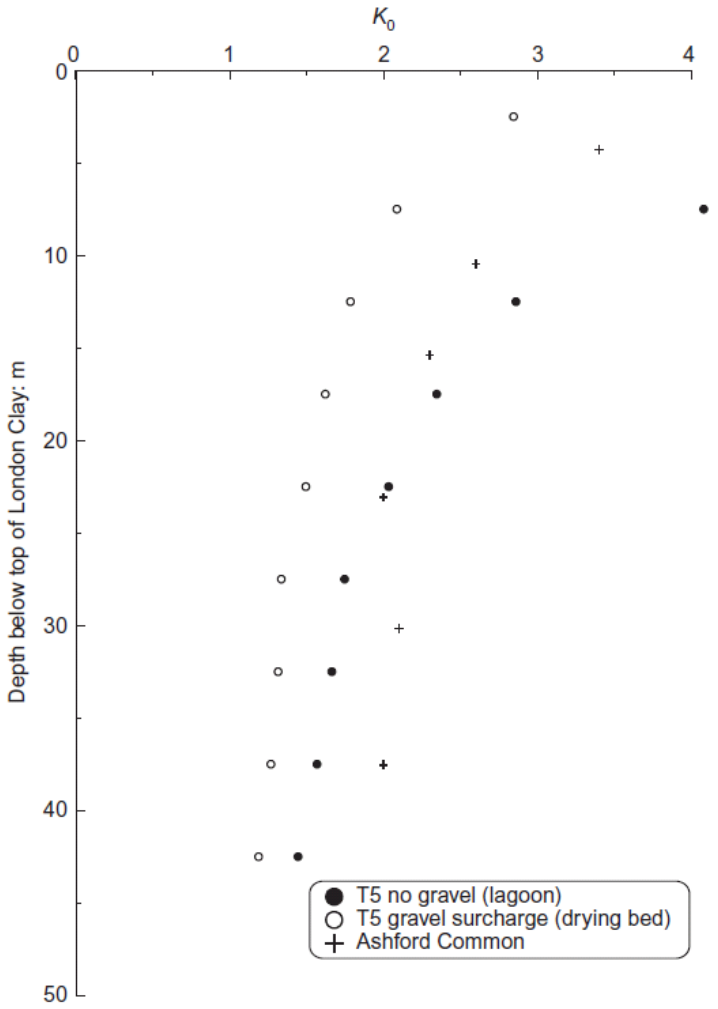


Figure 6.17: Ko profile estimated on basis of suction measurements (Hight et al., 2007)

In Figure 6.18, permeability measurements at the T5 site are presented after Hight et al. (2007), along with measurements from other London Clay sites. A constant value of isotropic permeability is assumed in the analysis of 1×10^{-10} m/s.

The variation of the shear moduli in the vertical and horizontal planes with depth from bender element tests is shown in Figure 6.19. A back-analysis of the shear modulus employed in the

analysis from the results of the pile load test is performed, as described later. The back-analysed values are also shown in Figure 6.19. Constant values are assumed along each unit, in an effort to represent the mean value of each lithological unit.

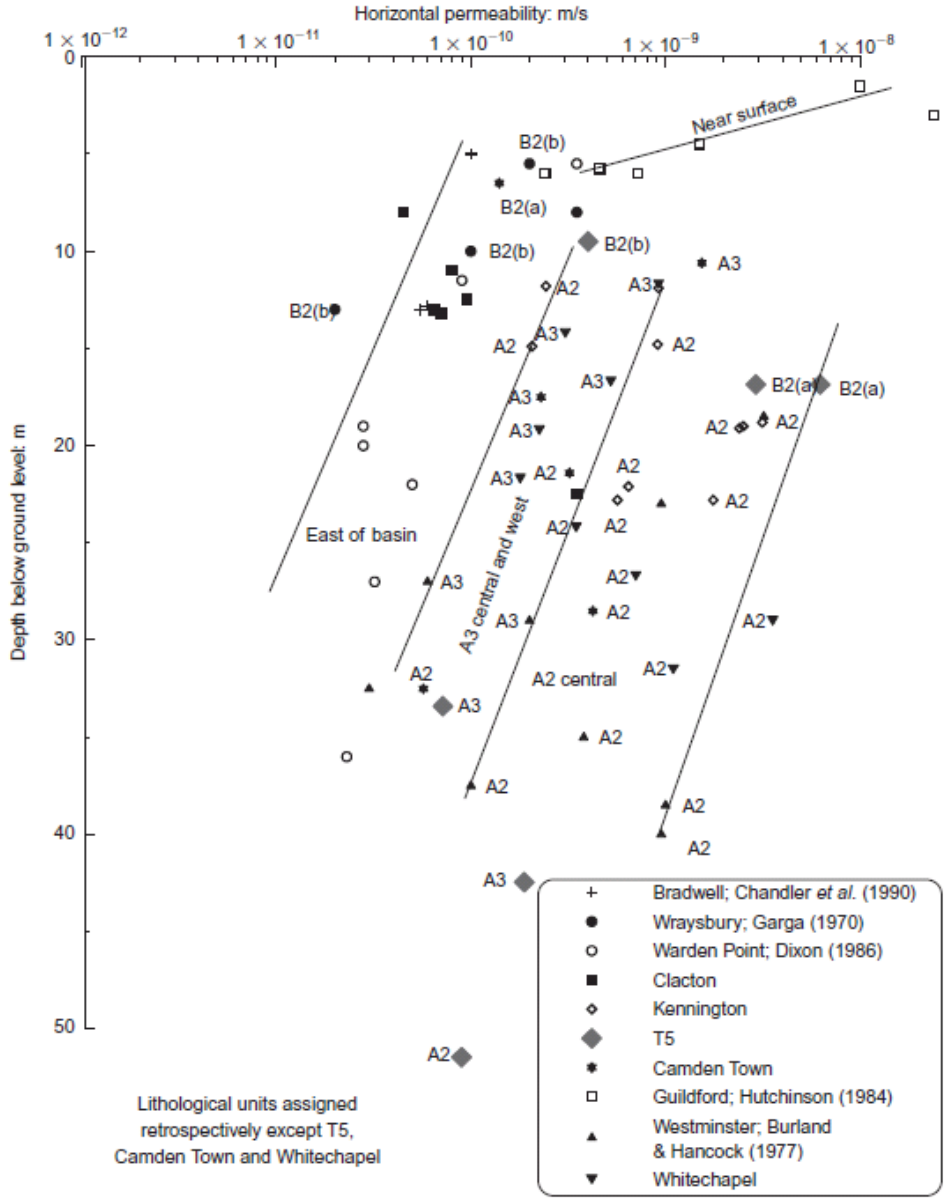


Figure 6.18: Permeability measurements at T5 using self-boring pressuremeter compared with database (Hight et al., 2007)

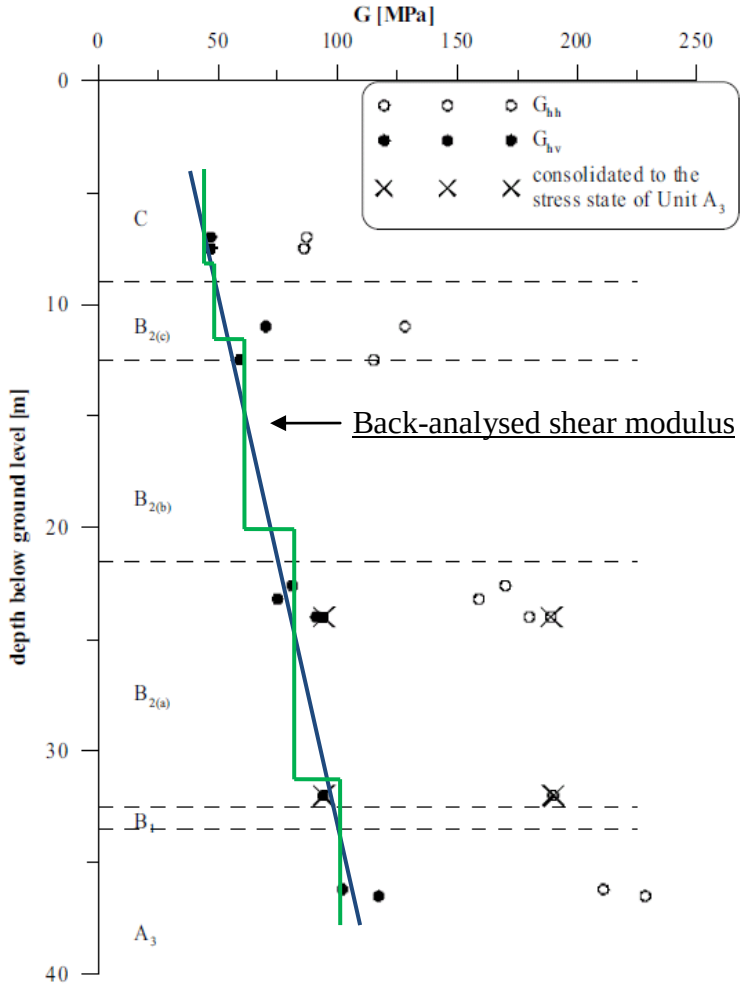


Figure 6.19: Variation with depth of shear moduli in vertical and horizontal planes (Gasparre, 2005)

6.3.3. Model parameters

The London Clay profile is modelled using the ET Creep model, and the model parameters assigned are those calibrated in Chapter 5 for the soil profile encountered at Heathrow Airport Terminal 5. The model parameters employed for London Clay are listed in Table 6.4. The Made Ground and the Terrace Gravel are both modelled using the Mohr-Coulomb model. The Made Ground is assigned the following parameters: $c' = 0$, $\varphi' = 25^o$ and $v = 12.5^o$. The Terrace Gravel is assigned respectively $c' = 0$, $\varphi' = 35^o$ and $v = 17.5^o$, where c' is the cohesion, φ' is the angle of shearing resistance, and v is the angle of dilation. Also, the Made Ground and the Terrace Gravel are assigned a Young modulus E' equal to 10000 kPa and 50000 kPa respectively, and a Poisson's ratio μ equal to 0.2 (Zdravkovic et al, 2005).

Unit	$\mathbf{M_f = M_g}$	$\boldsymbol{\alpha_f = \alpha_g}$	$\boldsymbol{\mu_f = \mu_g}$	$\boldsymbol{\psi/V}$	$\mathbf{t_0}$ **(h)**	$\boldsymbol{\varepsilon^{vp}_{vm,limit}}$
C	0.8561	0.4	1.1	0.00414	24.0	0.405
$B_{2(c)}$	0.9838	0.0001	2.0	0.00386	24.0	0.444
$B_{2(b)}$	0.9838	0.0001	2.0	0.00402	24.0	0.422
$B_{2(a)}$	0.9838	0.0001	2.0	0.00404	24.0	0.419
A_3	0.9411	0.4	0.9	0.00413	24.0	0.406
Unit	$\boldsymbol{\lambda/V}$	$\boldsymbol{\kappa/V}$	$\mathbf{p_{s0}}$ **(kPa)**	$\boldsymbol{\rho_s}$	**G (kPa)**	**OCR**
C	0.062	0.030	-40.0	100.0	50000.0	+2.0
$B_{2(c)}$	0.055	0.025	-40.0	400.0	55000.0	+2.7
$B_{2(b)}$	0.065	0.050	-40.0	1500.0	70000.0	+2.8
$B_{2(a)}$	0.055	0.030	-70.0	500.0	90000.0	+3.8
A_3	0.070	0.045	-70.0	1600.0	110000.0	+3.1

Table 6.4: ET Creep model parameters employed for the back-analysis of pile load test at Heathrow Airport Terminal 5

6.3.4. Considerations for the back-analysis

The numerical model for single piles is calibrated by back-analysing the results from the pile load test. Several aspects of the load test are considered in the finite element analysis, ranging from the effects of pile installation on the surrounding soil, to the several techniques applied in the test, including methods to isolate the shaft resistance component in the London Clay.

Tension piles providing the reaction force in pile load test are not discretised. The effects of pile installation on the surrounding soil are considered in the finite element analysis based on the literature review in Chapter 2.

(a) Shaft resistance isolation and tension piles

The bearing resistance of the oversized pile cap of 1500 mm diameter, as discussed above, is minimised by the adoption of an annular ring of polystyrene in the interface between the pile cap and soil near the pile head. In the analysis, it is assumed that the cap provides no resistance; therefore, the pile cap is not discretised and is omitted. The load is assumed to be applied directly on the pile head.

Shaft resistance in the Terrace Gravels and the Made Ground is eliminated by the application of a permanent lining in the interface between the concrete and the soil, which extends down to 4.5 m deep. This is modelled in the finite element analysis by the application of interface elements with almost zero shear stiffness. The values assigned for φ' and ν are similar to the values assigned for the solid elements, however the shear stiffness K_s in both the Terrace Gravels and the Made Ground is set equal to 10 kPa. The normal stiffness K_n is set equal to 27778 kPa and 5556 kPa respectively, based on the Young's modulus (E= 50000 kPa and 10000 kPa respectively) and the Poisson's ratio (μ= 0.2) assigned.

A "soft toe" method, described in detail by Unwin and Jessep (2004), is applied in the pile load test. The bearing resistance from the pile base is fixed to a known value, the minimum possible, however this value is not stated. In the finite element analysis, a very soft elastic area below the toe is modelled by prescribing a bulk (K) and shear (G) modulus equal to 10 kPa, in order to minimise the bearing resistance. Therefore, as the pile head is displaced axially, the resistance in mainly provided by the shaft.

Tension piles are known to provide the reaction force of the load test. In the analysis, tension piles are not discretised and are considered not be influential on the behaviour of the soil sheared around the test pile during the pile penetration. This allows simplification of the geometry and allows an axi-symmetric analysis to be performed.

(b) Effects of pile installation

The effects of pile installation on the soil surrounding the pile shaft are reviewed in Chapter 2. The adhesion between the clay and pile interface is considered to be significantly affected by the method of installation and the medium in which the pile is installed. For instance, referring to Figure 2.10, in soft clays full adhesion between the pile and the soil may be

assumed, unlike in stiff clays where adhesion is lost and the angle of skin friction reduces significantly. Driving or boring influences the processes taking place in the soil surrounding the piles. Driving generally enhances the soil's strength, whereas boring results in softening.

The pile under investigation is installed in London Clay by boring, which is known to have a softening effect on the surrounding soil and the loss of adhesion between the shaft and the soil. Boring in stiff clays also results in a relief of the lateral stresses and, therefore, the horizontal stresses exerted on the pile are considered to drop in magnitude. In numerical analysis, the reduction of skin friction is conventionally simulated with the use of interface elements. However, in this study interface elements are not employed due to the fact that the constitutive model used for London Clay is the ET Creep model, whose formulation is only for solid soil elements. If interface elements were to be applied, neither rate effects, nor changes in undrained shear strength, through the development of viscoplastic strains during creep, would be obtained. Therefore, the solution adopted was the inclusion of a "soft zone" of elements around the pile shaft, discretised in order to allow the modelling of the installation effects on the surrounding soil.

The "soft zone" of elements employed in the analysis around the pile shaft extends 9 cm from the pile shaft. This is based on the literature review of single piles in Chapter 2. The elements in the "soft zone" are modelled using the ET Creep model, and the model parameters assigned are equivalent to those applied to the remaining elements. However, in order to model the reduction of the angle of skin friction (δ'), a smaller angle of shearing resistance is applied in the model parameters ($\delta' < \varphi'$). This value is back-analysed using the documented load-settlement response of the pile load test.

Softening and change of moisture content is also observed around the pile during boring. This is simulated in the analysis by a reduction of the OCR in the "soft zone" around the pile shaft by 10%. The change in OCR reflects the resulting softening and swelling which makes the material more viscous and is an approximation.

Finally, the initial stresses in the "soft zone" are reduced, in order to simulate the relief of lateral pressures. Based on the literature review in Chapter 2, the value of K_o along the pile interface may drop below unity, in cases where delays occur between augering and forming of the piles. This is not considered to be the case in this study; pouring of concrete is assumed to take place quickly. However referring to Figure 2.3, the value of K_o is assumed to drop by 30%, as a result of boring for a radius of 0.5 m around the pile.

6.3.5. Problem geometry and boundary conditions

The single pile mesh, used in the finite element analyses, is shown in Figure 6.20. The analysis is axi-symmetric and the mesh domain is 57 m deep and 20 m wide. It extends down to the Harwich Formation, as shown in Figure 6.16. The single pile has a length of 39 m and its diameter is for the most part 1050 mm. For the upper region (4.9 m) where permanent casing is in place, the diameter is 1230 mm (see Figure 6.14). The finite element mesh is divided into several layers, representing the ground profile identified for the analysis (see Figure 6.16).

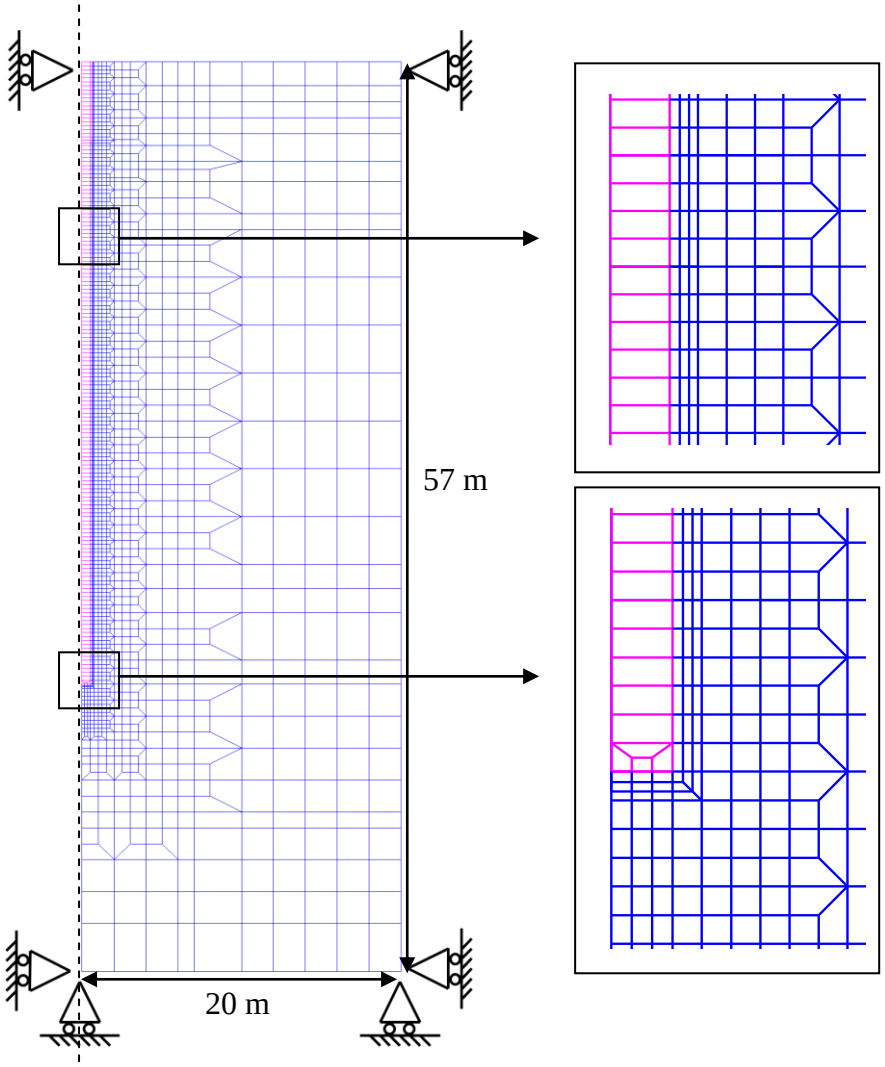


Figure 6.20: Single pile mesh for pile load test in Heathrow Airport Terminal 5

Both the pile and the soil are discretised. The pile is modelled as a very stiff elastic material ($E= 30\times10^6$ kPa, $\mu= 0.15$), which is able to transfer load from the pile head to the surrounding soil, whereas the soil is modelled using the ET Creep model for the London Clay units and the Mohr-Coulomb model for the Terrace Gravel and the Made Ground. The mesh consists of

eight noded isoparametric elements with four pore pressures degrees of freedom at the corner nodes (London Clay elements only), and two displacement degrees of freedom at both corner and mid-side nodes (all elements).

Full adhesion between the pile and the soil is assumed for the most part of the pile-soil interface. However, a "soft zone" of a thickness of 9 cm around the pile, with a lower angle of shear friction, is employed, in order to simulate numerically the loss of adhesion due to pile installation. Interface elements with zero thickness are employed in the upper region of the pile-soil interface, where the permanent casing is in place.

The prescribed zero displacement boundary conditions prevent the base of the mesh from moving in the vertical and horizontal directions, while the vertical sides of the mesh are fixed in the horizontal direction and can move in the vertical direction only.

The analysis is coupled. Consolidation takes place in the London Clay elements. The seepage boundary conditions applied allow no flow of water to the base and left hand boundary of the mesh, while on the right hand boundary up to the Terrace gravel layer pore pressures are kept equal to their initial values, as determined by the water table 3 m below ground level.

6.3.6. Description of analysis

A finite element analysis is performed, in order to determine the load-settlement response of the single pile in question and compare it with the documented results. The stiffness variation with depth and the angle of skin friction at the pile-soil interface ("soft zone") are back-analysed. A constant rate of penetration of 3 mm/h is applied to the pile head, in order to simulate the rate effects of the pile load test. This is numerically applied by applying increments of prescribed vertical displacement on top of the pile and by calculating the reaction given by the pile to the prescribed displacement.

The first step of the analysis is to determine the appropriate stiffness profile with depth. An iterative procedure is followed along with the calibration of the laboratory tests in Chapter 5, from which the stiffness profile giving a realistic load-settlement response is back-analysed. The analysis starts with the assumption that the shear modulus in the soil shall be close to the value of shear modulus at small strains measured in the laboratory. The analysis is repeated, if necessary, with a reduced stiffness profile until the predicted load-settlement response matches that measured in the field.

Next, the angle of skin friction is back-analysed for the "soft zone" discretised around the pile shaft. Considering the effects of softening and the lateral relief of pressures, the value of δ' is varied, in order to match the predicted shaft resistance with the measured one.

6.3.7. Results and discussion

The predicted load-settlement response of the single pile in question is shown in Figure 6.21, along with the measured load-settlement response of the pile load test at Heathrow Airport Terminal 5 performed by Unwin and Jessep (2004). The predicted results are obtained by calibrating the shear modulus variation with depth and the angle of interface friction in the "soft zone". The back-analysed stiffness profile is shown in Figure 6.19, which seems to plot along the G_{hv} shear modulus profile. The back-analysed angle of interface friction is $\delta_{ult}{}'$ = 12^o and $\delta_{peak}{}'$ is rate dependent.

The value of $\delta_{ult}{}'$ represents in the ET Creep model the angle of the critical state line in triaxial compression, which is equivalent to the post-rupture strength of soil samples when sheared undrained to failure after reaching the peak resistance. On the other hand, the $\delta_{peak}{}'$ angle, which is conventionally used for the determination of the shaft resistance, is rate dependent, due to the formulation of the ET Creep model and the time dependency of the peak strength. The angle $\delta_{ult}{}'$ is calculated close to the residual angle $\delta_r{}'$, which lies between 10^o and 12^o according to Hight et al. (2007). It should be noted that for bored piles in heavily consolidated clay, an angle of interface friction close to the residual angle is recommended in the literature, however, at the same time, it is considered that the angle of interface friction for bored piles is still subject to debate.

A "soft toe" is applied in the finite element analysis, in order to isolate the shaft resistance of the pile. Unwin and Jessep (2004) fixed the base resistance of the pile tested at a "known value", however the exact value is not stated. In the finite element analysis, the base resistance is determined equal to 808 kN. In a parallel analysis, performed without the application of a "soft toe", the base resistance is calculated equal to 2236 kN, indicating a significant reduction of the base resistance with the application of a "soft toe".

In Figure 6.22, the predicted load-settlement response without the effects of pile installation (original conditions) is plotted along with the final predicted results (calibrated). This allows the calculation of the conventional pile adhesion factor α. By comparing the peak axial load predicted from both analyses, the adhesion factor is calculated as 0.37. Skempton (1959)

recommends for bored piles in London Clay a value of 0.45. Other authors, as summarised in Figure 2.10, recommend for stiff clays values for the adhesion factor α lower than 0.4.

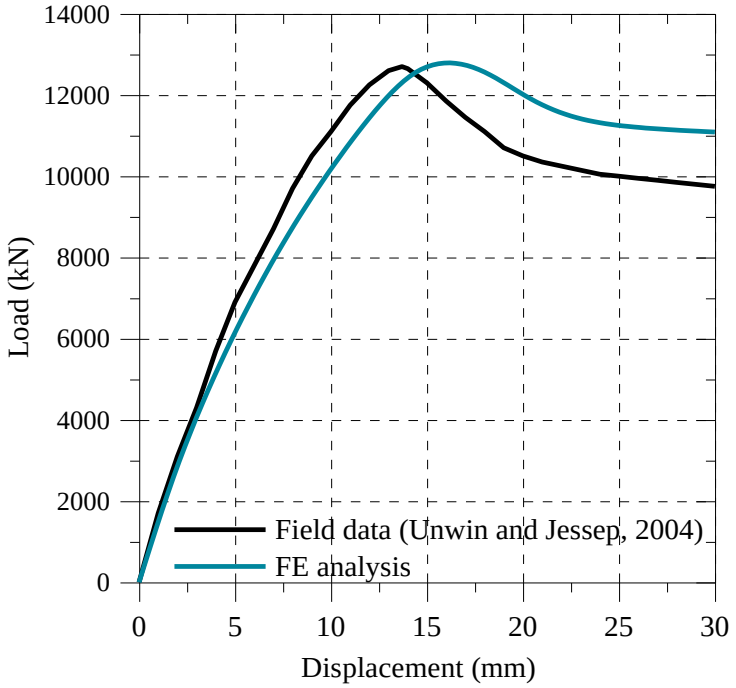


Figure 6.21: Predicted vs. measured load-settlement response of pile load test

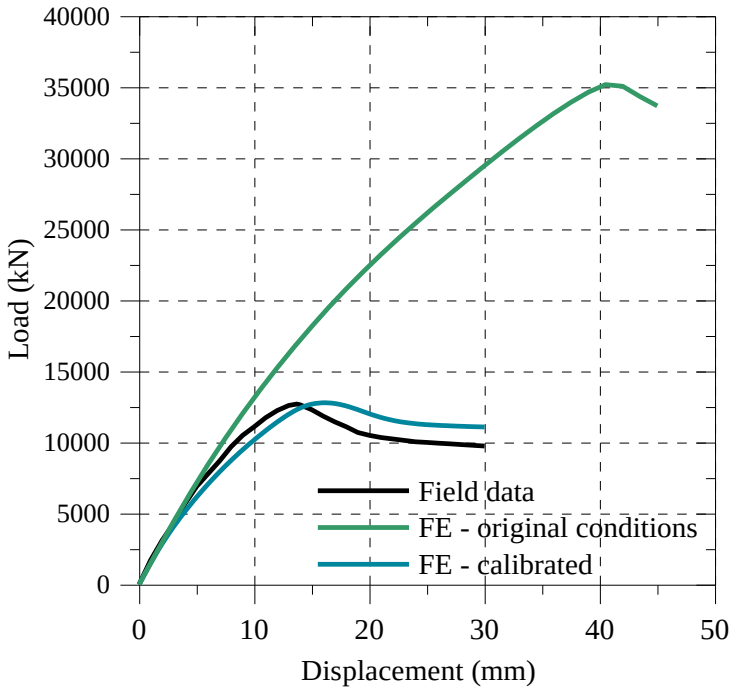


Figure 6.22: Predicted load-settlement response for original conditions vs. Calibrated

6.4. CASE HISTORY: HISCOCKS HOUSE, STONEBRIDGE PARK

A case history, which involves a piled raft foundation in London Clay, is Hiscocks House located in Stonebridge Park. Finite element predictions are compared with field measurements, in order to validate the constitutive and numerical models. The Hiscocks House case history involves documented measurements regarding the performance of a piled raft foundation, as well as the results from two pile load tests: one before the erection of the building and another after its demolition. The constitutive model employed is the ET Creep model, and the model parameters assigned are those calibrated for London Clay. Also, the installation effects, calibrated for a single pile at Heathrow, are employed in the analysis, in order to model the behaviour of individual piles.

This study allows the validation of the model parameters and of the numerical models for single piles and for large scale piled raft foundations, as well as the validation of the effects of sustained load on the load-settlement response of piles within pile groups. A description of the stiff clay site in Stonebridge Park is given in the following, along with the analysis considerations taken into account. The behaviour in the long term of the soil profile is examined. Subsequently, a simulation of a pile load test performed in 1972 is followed. Then, the focus turns to the piled raft foundation, where a 3D finite element analysis is performed, in order to compare the predicted behaviour with the documented one. Finally, a pile load test on a working pile after the demolition of Hiscocks House in 2005 is performed, in order to validate the time effects, in particular creep, during sustained loading.

6.4.1. Description of Hiscocks House

Hiscocks House is a 16 storey building located in the Stonebridge Park area of London and its foundation is a typical conventional piled raft. The dimensions of the piled raft are 43.3 m by 19.2 m and it consists of a heavily reinforced concrete raft (0.9 m thick) linking 351 bored concrete piles, which are installed on a square grid of 1.6 m distance centre to centre spacing. The piles are 13 m long and 0.45 m in diameter. The building was erected in 1975 and in 2004 it was demolished after 29 years of occupation, in order to redevelop the site (Cooke et al., 1981; Butcher and Skinner, 2006).

Hiscocks House is considered as a representative example of a conventional piled raft foundation. A detailed description of its performance and of the measurements made during construction and after the occupation is detailed in Chapter 2. In particular, data regarding the distribution of load between piles, the contribution of the raft to the foundation as a whole,

and the building settlements during construction and the first years of occupation are presented.

6.4.2. The stiff clay site in Stonebridge Park, London

(a) Ground profile

Cooke et al. (1981) gave an extensive description of the foundations of Hiscocks House and of their performance. Unfortunately, the information provided regarding the soil profile is limited. Therefore, it is considered appropriate to utilise records from other soil investigations performed in the Stonebridge Park area and assume that the variability in the soil profile within the area is limited. In this respect use has been made of the extensive soil investigation performed for the new Wembley stadium, as the Wembley stadium is located in the same area, approximately 1 mile away from Hiscocks House.

Cooke et al. (1981) describe, first of all, that the soil profile at Stonebridge Park consists only of London Clay. This is different to the Heathrow area, where a layer of Terrace gravel is found on top of the London Clay (see Section 6.3.2). That the London Clay outcrops at ground level is also supported by O'Brien et al. (2004) for the Wembley area. As a consequence the London Clay formation has a weathered layer close to the ground surface, as described later. Cooke et al. (1981) describe that the undrained shear strength profile with depth, used to calculate the required load capacity of piles, is equal to 100 kPa at 3 m and increases linearly to 260 kPa at a depth of 25 m. Other information about the soil profile at Stonebridge Park is not given.

In Figure 6.23, a satellite photo extracted from Google Earth shows the relative position of Hiscocks House, with respect to the Wembley new national stadium. Their relative distance, as shown, is 1.68 km. Figure 6.24, after Cheong (2007), presents the site geology at the eastern arch of the stadium roof, where six soil layers are identified: fill, upper and lower weathered London Clay, upper and lower unweathered London Clay, and the Lambeth Group. In the same manner, O'Brien et al. (2004) claim that the geology of the site at Wembley comprises London Clay, below made ground, with a varying thickness between 30 m and 40 m, which overlies the Lambeth Group at a depth between 10 m and 15 m OD. Chalk is the deepest layer at about -3 m OD. The London Clay profile at Wembley is divided into weathered and unweathered clay with weathering affecting the upper 8 to 10 m. The last remark made by O'Brien et al. (2004) about the soil profile is that the unweathered London

Clay becomes siltier and sandier at about 21 m OD, indicating a change from upper lithological unit B to lower unit A.



Figure 6.23: Plan view of Stonebridge Park and Wembley stadium area (Google Earth, 2010)

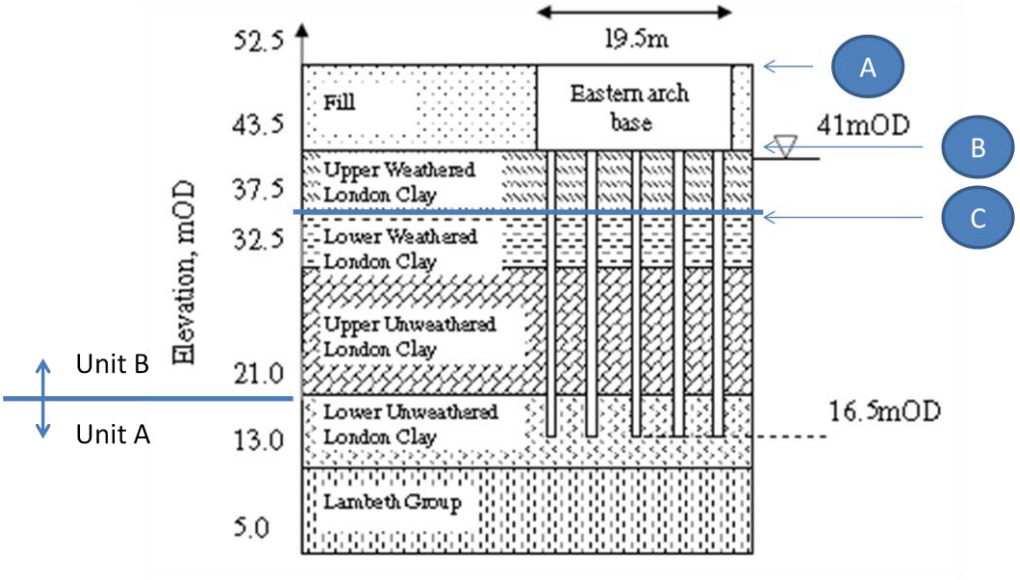


Figure 6.24: Schematic of the site geology in Wembley (Cheong, 2007)

In Figures 6.23 and 6.24, the elevations at ground surface level, based on Google Earth, at points of interest are shown. In particular, point A represents the elevation at Wembley stadium, point B the elevation south of the railway line crossing the area, and point C the elevation at Hiscocks House. The elevations at points A and B have been cross-checked with

published data for the development of Wembley new stadium and their accuracy has been confirmed. This approximation allows realistic identification of the soil profile at Stonebridge Park.

The adopted soil profile in the finite element analysis is shown in Figure 6.25. The boundary between units A and B is adopted at a depth of 16 m. The upper 4.5 m of unit B are regarded as weathered, while the rest 11.5 m as unweathered. Below unit A, a layer of Lambeth Group of 16 m thickness overlies Chalk. The water table is adopted at a depth of 3.5 m, based on Cooke et al. (1981).

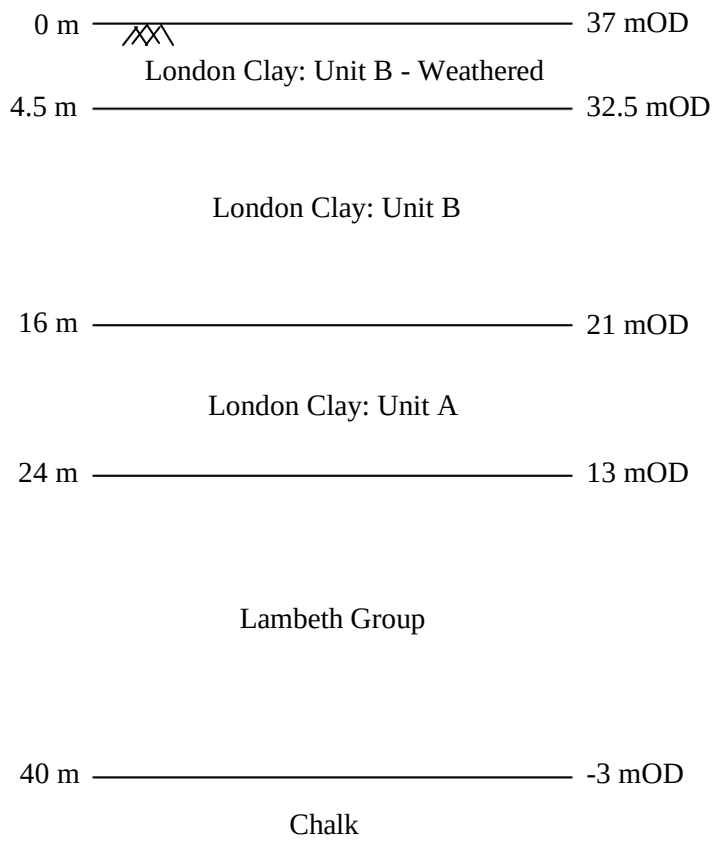


Figure 6.25: Hiscocks House: adopted soil profile for finite element simulation

Weathering of clays has been described in detail by Chandler (2000), allowing the identification of the dissimilarities between London Clay unit B unweathered and weathered layers. Weathering is known to affect the mechanical properties of clays. According to Chandler (2000), the most obvious evidence of weathering is the colour change from blue-grey to brown due to oxidation. The extent of oxidation can be down to a depth of 10 m below the present ground surface in the London Clay Formation, however in places where the London Clay underlies the terrace gravels it is recognised that little oxidation has occurred,

reflecting the fact that no weathering is observed at Heathrow. Weathering is accompanied by an increase in water content, which reflects the drop in undrained shear strength and an increase in global permeability. In addition, the weathered clay becomes softer and this process results in a weakened structure, quantified through a reduced Yield Stress Ratio (YSR) and elastic shear stiffness. The reduction in YSR is reflected in a reduced OCR input for the ET Creep model.

(b) Undrained shear strength profile

In Figure 6.26, the undrained shear strength profile with depth, based on Cooke et al. (1981), at the Hiscocks House site is given along with the adopted profile in the numerical simulation. The latter profile is based on the undrained shear strength profile at Wembley, given by O'Brien (2010), in Figure 6.27. Several observations can be made from this figure about the variation of shear strength with depth. The weathered material seems to have lower strength than the unweathered. The 'design line' adopted for the calculation of the piles' capacity at Wembley shows that close to the ground surface the gradient of the design line reduces compared to the gradient in the intact clay (between 10 and 30 m depth). In an opposite manner, the 'design line' in the Lambeth Group indicates a stronger material.

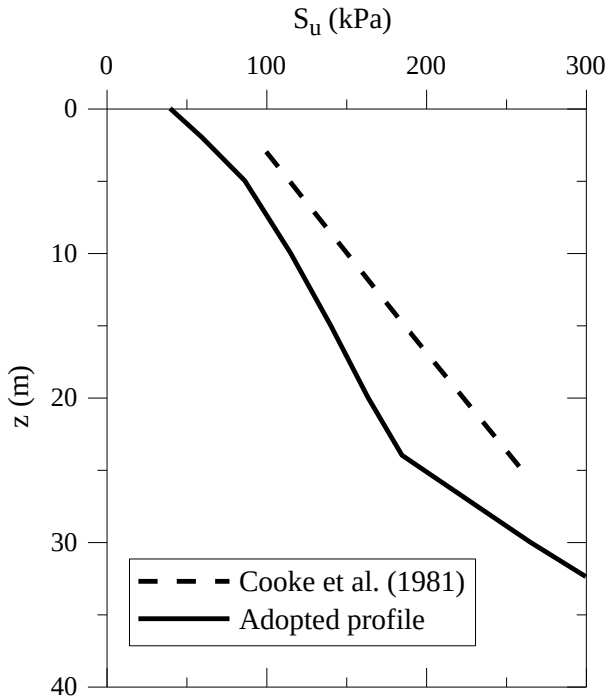


Figure 6.26: Stonebridge Park: undrained shear strength profile

In Figure 6.27, the S_u profile is quantified by multiple methods, including Self-Boring Pressuremeter (SBP) test, Standard Penetration Test (SPT), Cone Penetration Test (CPT),

theoretical approaches and TW/RC (Thin Wall/push-in or Rotary Core samples sheared) approach. O'Brien (2010) claims that these approaches give a limited scatter, allowing the identification of a "good" 'design line'. On the other hand, S_u values from conventional U100 QUT (Quick Undrained Triaxial tests) show a lot of scatter, with too high values at shallow depths, and at the same time the increase in shear strength with depth is regarded too small with respect to the other approaches. Also, the conventional U100 QUT plot higher than the other approaches defining the 'design line'. Therefore, these were ignored in the design, according to O'Brien (2010). The choice of a 'design line' lower than the one defined by conventional U100 QUT allowed the adoption of a higher adhesion factor of α = 0.6 for the design of piles, instead of the conventional value of 0.45. O'Brien (2010) claims that this approach has been confirmed from several pile load tests performed at the Wembley stadium site.

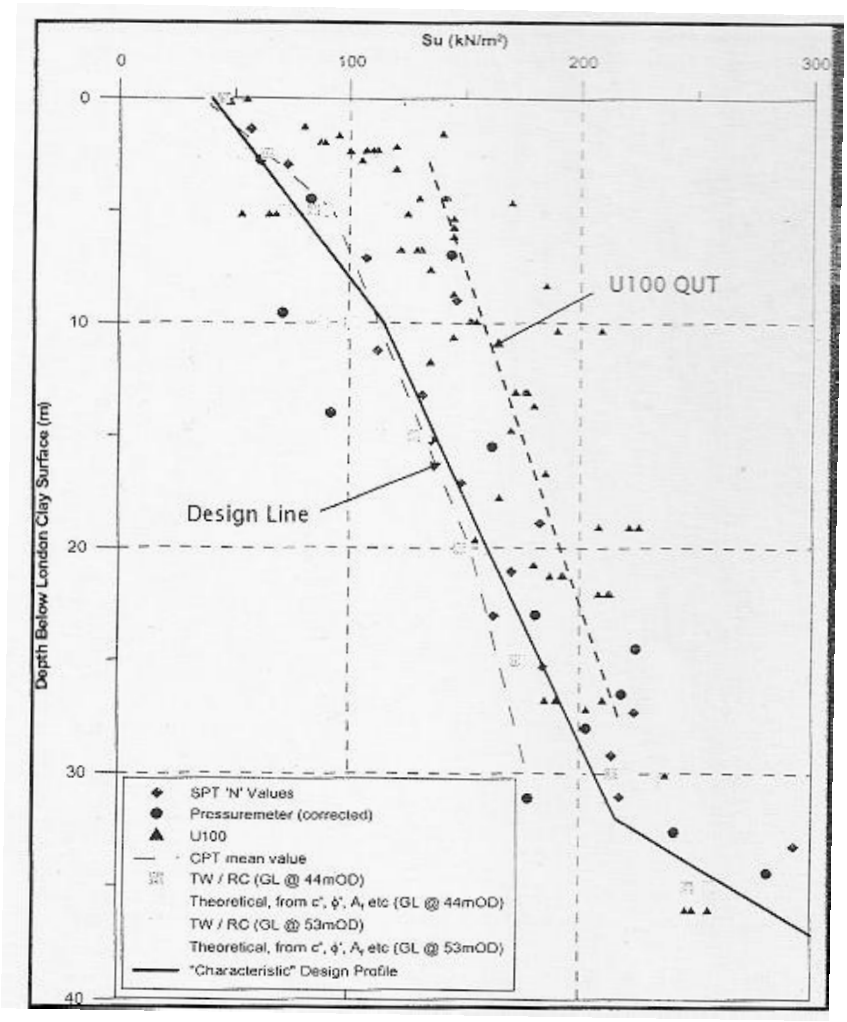


Figure 6.27: Wembley: undrained shear strength profile (O'Brien, 2010)

The variability of the S_u profile with the different methods applied shows that the α-method in pile design gives uncertainties and may lead to over-conservative designs, which has been

discussed in the literature review in Chapter 2. If the data from the Stonebridge Park and the Wembley stadium are compared in Figure 6.26, it is observed that the Stonebridge Park data plot on the right side of the adopted S_u profile. The approach to determine the S_u profile is not stated in Cooke et al. (1981). However, it is regarded that the means used in the 70's are less accurate than in the 21st century. Therefore, an allowance is made in terms of undrained shear strength, and therefore a lower S_u profile, than the one given by Cooke et al. (1981), is employed in the analyses, in order to be consistent with the findings at Wembley.

(c) Stiffness

Figure 6.28(a) presents the shear modulus variation with depth at the Wembley stadium, after O'Brien et al. (2004), where a near linear increase of shear modulus with depth is observed. It should be noted that in the Lambeth Group layer, the increase in shear modulus with depth is larger than in London Clay, indicating that it is stiffer than the overlying units. This measured variation with depth is utilised to determine the shear modulus profile in Stonebridge Park, as shown in Figure 6.28(b). The "adopted" profile indicates a constant shear stiffness for each of the soil layers identified in Figure 6.25.

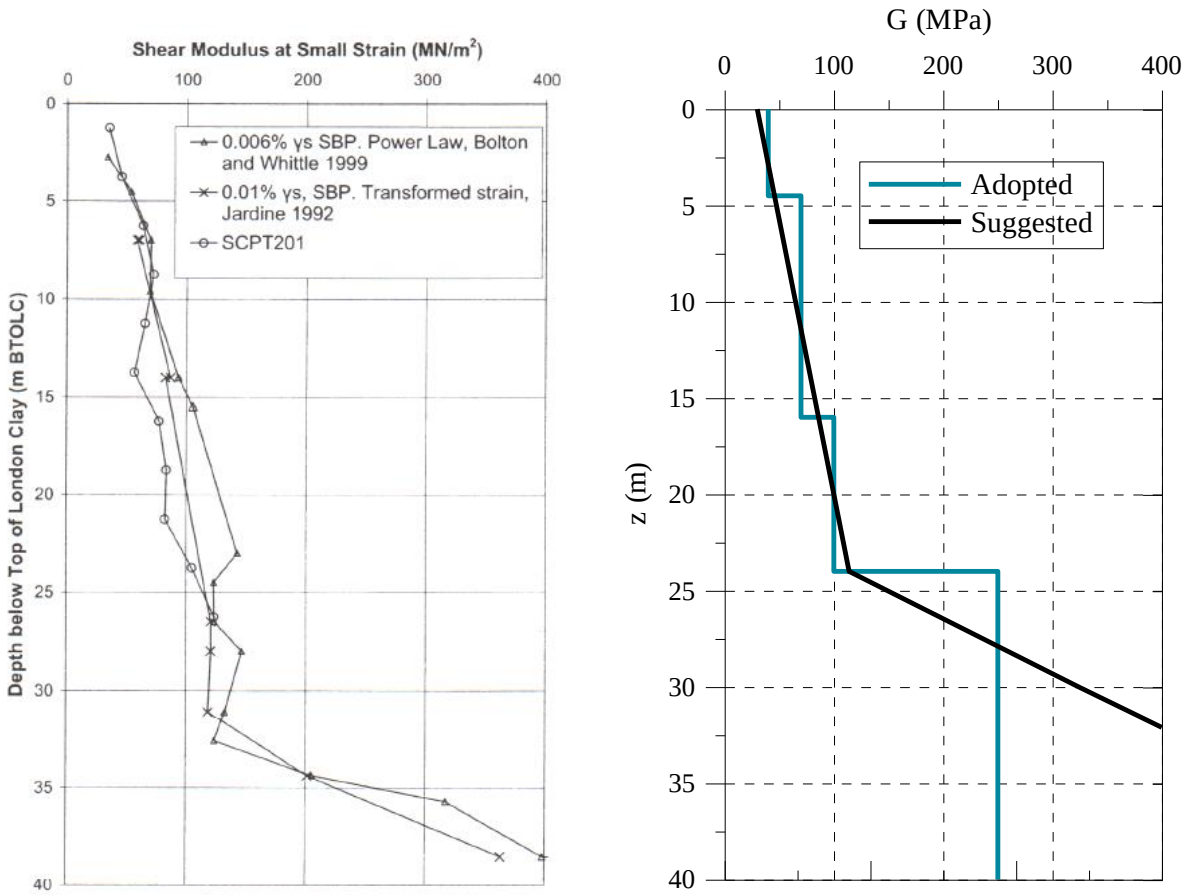


Figure 6.28: Shear modulus profile: (a) Wembley (O'Brien et al., 2004), (b) Stonebridge Park

(d) Initial stresses

The unit weight of London Clay is given by Cheong (2007) as equal to 20 kN/m^3, whereas for the Lambeth Group it is 20.5 kN/m^3. These values are adopted in the analysis, in order to determine the vertical effective stress. Regarding horizontal stresses, the K_o profile is not given in the literature. Therefore, the one adopted in Heathrow (Figure 6.17) is used as a first approximation for the initial stress conditions at Stonebridge. The adopted K_o profile for the analysis is obtained through the calibration of the soil profile for long term conditions, as described later.

Piezometer monitoring, according to O'Brien et al. (2004), indicated a water table 2.5 m below ground level. At Stonebridge Park, based on Cooke et al. (1981), the water table is adopted at a depth of 3.5 m. Also, O'Brien et al. (2004) suggest that pore water pressures increases with depth hydrostatically to 200 kN/m^2, at a level of about 20 mOD, and it remains approximately constant below 20 mOD, due to the presence of the Chalk under the Lambeth Group. A similar pore water pressure profile is employed for Stonebridge Park in the analysis, as shown later in Figure 6.32.

(e) Permeability

Data about permeability are given neither for Stonebridge Park nor for Wembley. Therefore data from Wongsaroj et al. (2007) for St James Park in Central London, where London Clay units B and A, and the Lambeth Group, are encountered (Figure 6.29), are utilised. In Figure 6.29, data from Burland and Hancock (1977), as well as the assumed profiles by Wongsaroj et al. (2007) are shown, including the profile assigned for Stonebridge Park. The profile at Stonebridge Park is calibrated for long term behaviour, as described later. It should be noted that for the weathered London Clay layer, a larger permeability equal to 2 x 10^{-9} m/s is applied in the analysis, in order to reflect weathering.

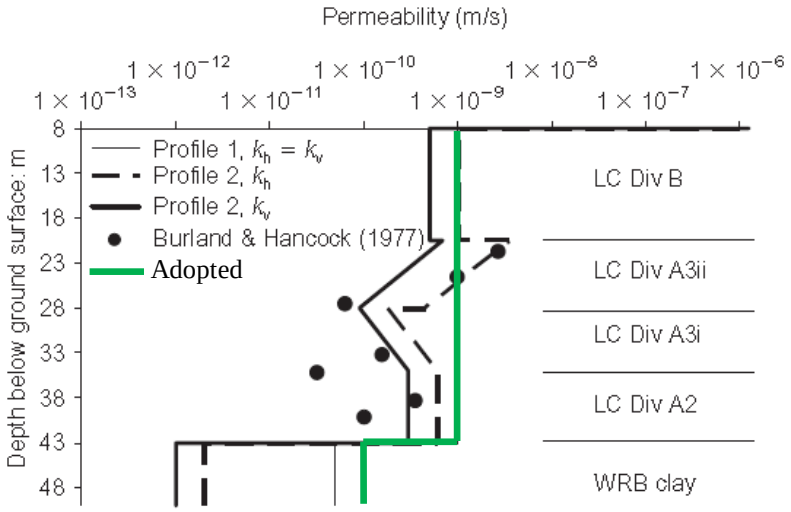


Figure 6.29: Assumed profiles in St James Park (Wongsaroj et al., 2007) and Stonebridge Park

6.4.3. Model parameters

The constitutive model employed for the analyses is the ET Creep model. The soil profile adopted for the Hiscocks House site is shown in Figure 6.25. It consists of four layers; London Clay unit B weathered, London Clay unit B, London Clay unit A, and the Lambeth Group (a clay formation). The ET Creep model parameters assigned for each layer at Stonebridge Park are similar to those assigned at Heathrow (see Chapter 5), considering local aspects such as weathering of the top layer. Specifically:

- *London Clay unit A*: it is assumed that it has the same material properties as unit A_3 at Heathrow;
- *London Clay unit B*: considering the fact that unit B is divided into units B_1 and B_2 ($B_{2(a)}$, $B_{2(b)}$, and $B_{2(c)}$), where the sub-units within unit B_2 have similar properties and B_1 is thin, the material properties assigned for the layer in question are chosen such that they satisfy and combine the properties of the three sub-units in unit B_2;
- *London Clay unit B weathered*: as above, however due to weathering the OCR (or YSR) is reduced (as shown by the S_u profile in Figure 6.26) and the initial void ratio is increased while the permeability increases too, and
- *Lambeth Group*: the clay at the top of the formation that is known to be stiffer than London Clay. The angle of shear resistance employed is based on Cheong (2007) and the shear stiffness employed is based on Figure 6.28. The remaining model parameters assigned are similar to unit A_3.

In summary, the model parameters assigned for the Hiscocks House site in Stonebridge Park are given in Table 6.5.

Unit	$\mathbf{M_f = M_g}$	$\boldsymbol{\alpha_f = \alpha_g}$	$\boldsymbol{\mu_f = \mu_g}$	$\boldsymbol{\psi/V}$	$\mathbf{t_0}$ **(h)**	$\boldsymbol{\varepsilon^{vp}_{vm,limit}}$
B - weathered	0.9838	0.0001	2.0	0.00397	24.0	0.429
B	0.9838	0.0001	2.0	0.00397	24.0	0.429
A	0.9411	0.4	0.9	0.00413	24.0	0.406
Lambeth Group	0.9411	0.4	0.9	0.00413	24.0	0.406
Unit	$\boldsymbol{\lambda/V}$	$\boldsymbol{\kappa/V}$	$\mathbf{p_{s0}}$ **(kPa)**	$\boldsymbol{\rho_s}$	**G (kPa)**	**OCR**
B - weathered	0.060	0.030	-10.0	500.0	40000.0	Fig. 6.30
B	0.060	0.030	-40.0	1000.0	70000.0	Fig. 6.30
A	0.070	0.045	-70.0	1500.0	100000.0	Fig. 6.30
Lambeth Group	0.070	0.045	-70.0	1500.0	250000.0	Fig. 6.30

Table 6.5: ET Creep model parameters for Stonebridge Park units

The shear modulus assigned for each layer is shown in Figure 6.28, whereas the OCR, which is input in the finite element analysis as a variation with depth, is determined by comparing the ET Creep model predictions for undrained shear strength with values of shear strength at characteristic depths, as shown in Figure 6.30. To achieve this, undrained triaxial compression tests are simulated by performing single element runs, in order to match the predicted undrained shear strength with the S_u profile identified for Stonebridge Park. In Figure 6.30, the OCR values and the respective undrained shear strength predicted at characteristic depths are plotted. The initial stresses applied for the single element analyses are those calibrated for the long term behaviour of the soil profile in Stonebridge, as described later.

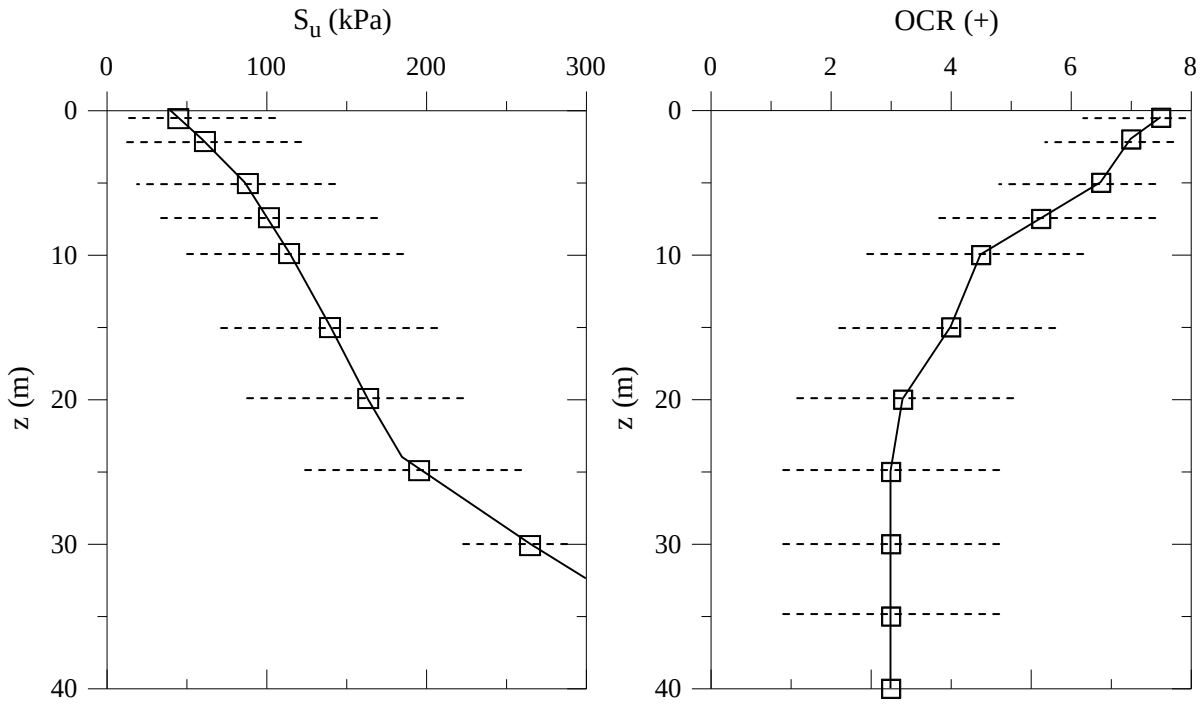


Figure 6.30: Determination of OCR profile in Stonebridge Park

6.4.4. Calibration of soil profile for long term analysis

The soil profile at Stonebridge Park is calibrated using a long term analysis, in order to check whether the initial stresses and pore water pressure profiles are in equilibrium with time. This is due to the time dependency of the ET Creep model, where it is recognised that, without any change in boundary conditions but with elapsed time only, stresses may change with time up to an equilibrium being consistent with the ET Creep model. Also, a change in pore water pressure profile may occur, if the permeability profile is not consistent with the pore water pressure profile.

An axi-symmetric column analysis is performed, in order to examine the long term behaviour of the soil profile and determine the appropriate initial stresses and permeability profiles that are consistent with the ET Creep model and with the initial pore water pressure profile respectively. The mesh used to perform the column analysis is shown in Figure 6.31. The mesh domain is 40 m deep and 10 m wide and is divided into several layers, representing the ground profile identified for the analysis in Figure 6.25. The mesh consists of eight noded isoparametric elements with four pore pressures degrees of freedom at the corner nodes, and two displacement degrees of freedom at both corner and mid-side nodes. The applied displacement boundary conditions prevent the base of the mesh from moving in the vertical and horizontal directions, while the vertical sides of the mesh are fixed in the horizontal direction and can move in the vertical direction only. The analysis is coupled due to the time

dependency. The seepage boundary conditions applied allow no flow on the left and right hand boundary of the mesh, while on the base and the top boundary of the mesh, pore pressures are kept equal to their initial values, as determined by the water table 3.5 m below ground level, representing one-dimensional flow.

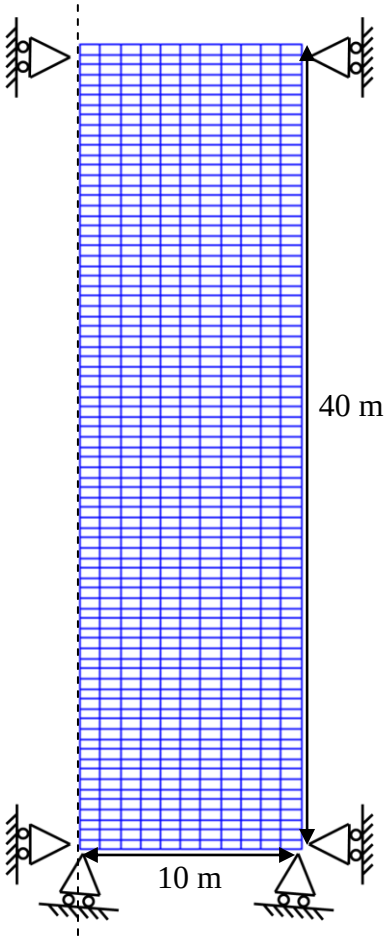


Figure 6.31: Column mesh used for calibration of soil profile for long term analysis

The first column analysis involves calibration of the permeability and pore water pressure profile. A linear elastic model is applied as a constitutive model, in order to isolate permeability and pore water pressures from other time effects. The pore water pressure profile identified in the literature is shown in Figure 6.32 (marked as 0y), where it is seen that, due to the presence of the Chalk (a very permeable unit) below the Lambeth Group unit, there is a relief of pore water pressures below the London Clay-Lambeth Group boundary at 24 m below ground surface. This is due to the past extraction of water during the industrial revolution.

The initial analysis is performed with a constant isotropic permeability of 1×10^{-9} m/s, where it is seen that the pore water pressure profile after 100 years changes dramatically. By applying different permeability profiles and based on Wongsaroj et al. (2007) (see Figure

6.29), the profile that satisfies (approximately) the pore water pressure profile in the long term is determined, which is plotted in Figure 6.33. It should be noted that a larger permeability is employed for the weathered layer, in order to be consistent with the observations made by Chandler (2000) on weathering.

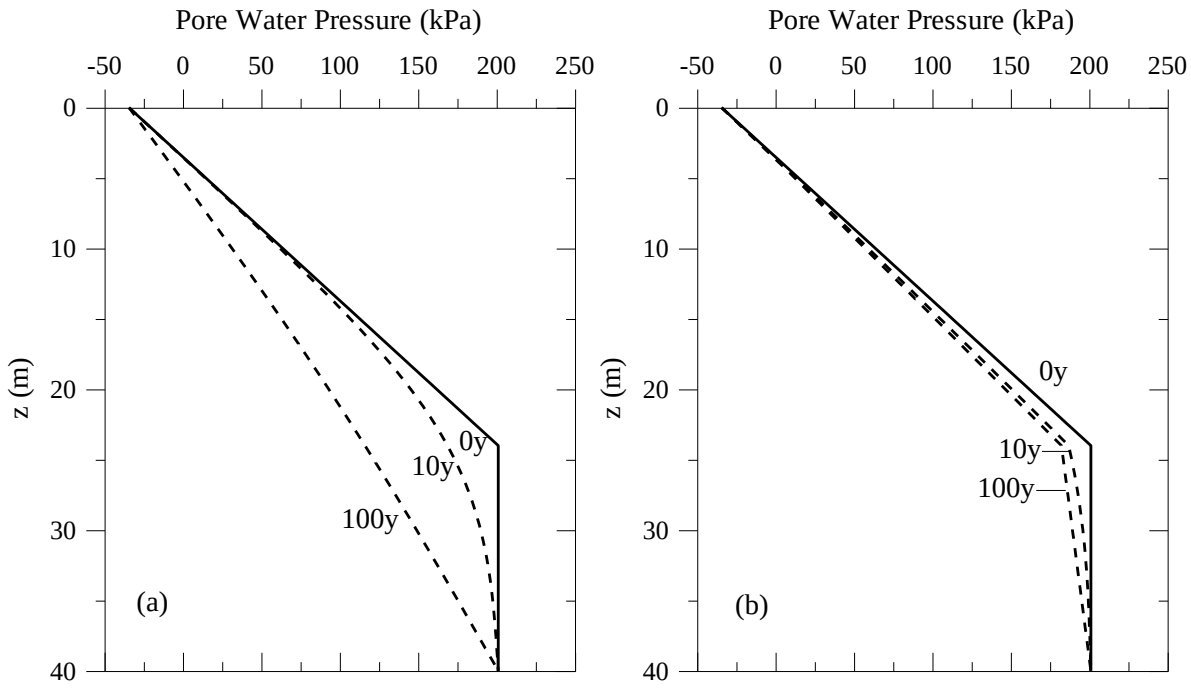


Figure 6.32: Pore water pressure profiles: (a) initial permeability, (b) calibrated permeability

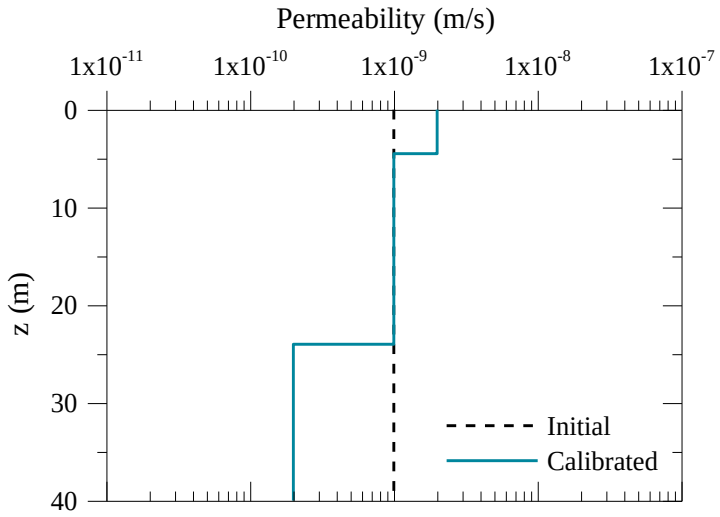


Figure 6.33: Isotropic permeability profile in Stonebridge Park

The second column analysis involves calibration of the initial stresses. Vertical effective stresses are calculated based on the unit weight of the London Clay and the Lambeth Group and on the water table 3.5 m below ground level. Horizontal stresses are calculated based on the K_o profile, where as a first approximation the one adopted at Heathrow (Figure 6.17) is

used for the initial column analysis. In Figure 6.34, the initial horizontal stress and K_o profiles are shown along with the profiles obtained after 100 years of elapsed time, where it is observed that the initial horizontal stress profile reduces with time. This is considered to be due to the development of viscoplastic strains with time, which result not only in vertical strains but in horizontal strains at the same time, having as a consequence the relief of horizontal stresses. The calibrated K_o profile is also shown in Figure 6.34, where after 100 years of elapsed time, no change in stresses take place.

Due to the change of initial stresses and in particular due to the drop of the horizontal stresses, there is a change in the initial stress state of the soil in terms of mean effective stress and deviatoric stress. The reduction in the K_o profile results in a reduction of the mean effective stress, affecting the undrained shear strength. In order to compensate this reduction in mean effective stress, the value of OCR in the ET Creep model is modified, in order to reflect the realistic undrained shear strength (see Section 6.4.3).

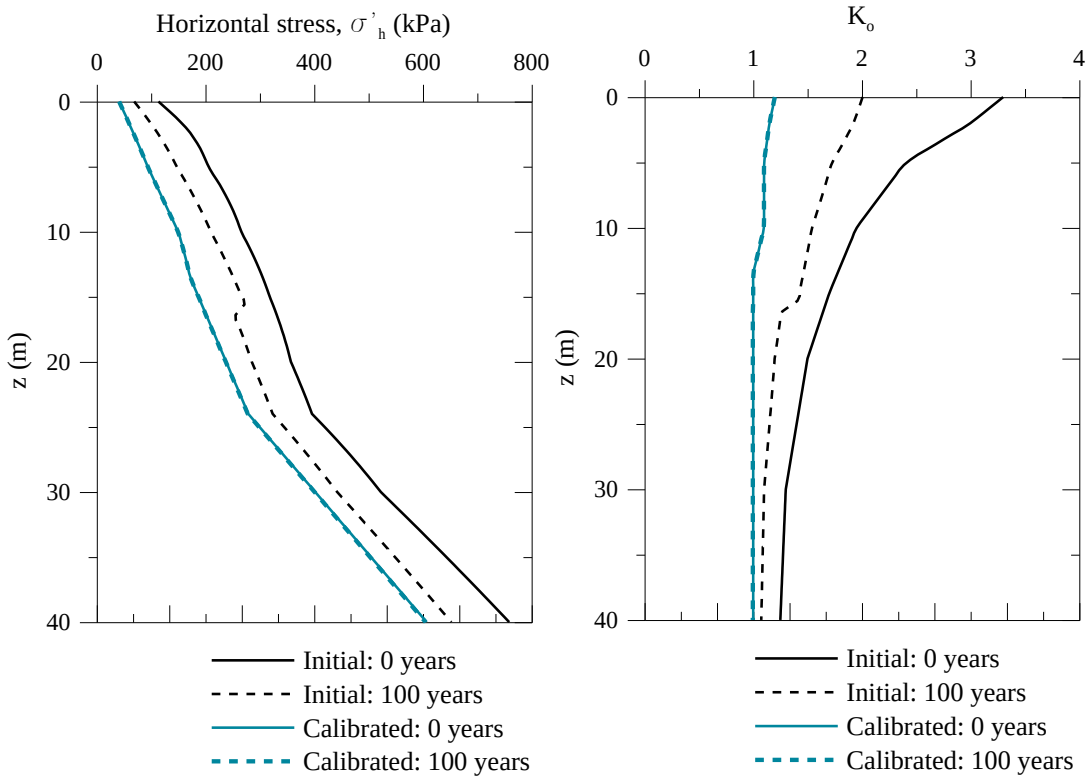


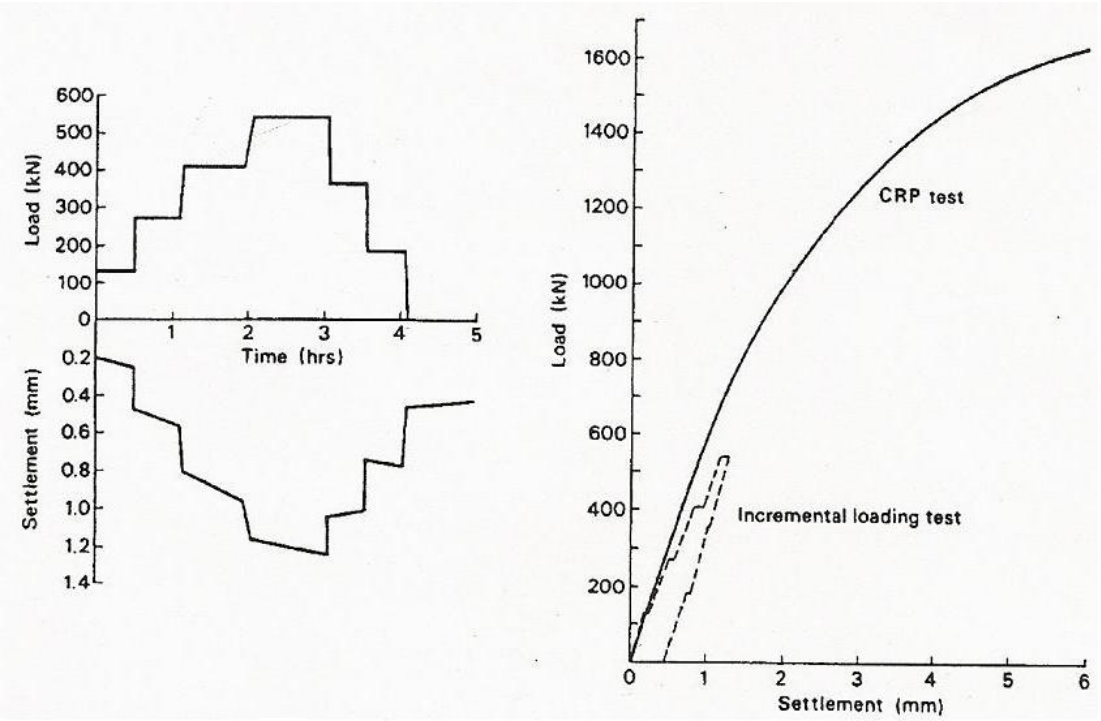
Figure 6.34: Initial and calibrated horizontal stress and K_o profiles

6.4.5. PILE LOAD TEST PRIOR CONSTRUCTION: 1972

6.4.5.1. Description of the pile load test

A load test on a preliminary test pile, similar to the piles used for the foundations of Hiscocks House, was performed in 1972 before the construction of the building, in order to verify the pile design, according to Cooke et al. (1981). The length of the test pile was 13 m and its diameter 0.45 m.

An incremental maintained load test and a subsequent constant rate of penetration (CRP) test were carried out on the test pile at the Stonebridge Park site. The incremental load test involved four load increments up to a maximum applied load of 540 kN and three increments of unloading, each being held for at least 30 minutes. In Figure 6.35(a), the load increments and the period for which they were held is shown, along with the results of the test in terms of settlement versus time. The load-settlement response is also shown in Figure 6.35(b), along with the results from the subsequent CRP test. Information regarding the rate of penetration is not given in Cooke et al. (1981).



(a) (b)

Figure 6.35: (a) Load-time and settlement-time curves from the incremental pile loading test; (b) load-settlement curves from the incremental and CRP tests (Cooke et al., 1981)

6.4.5.2. Problem geometry and boundary conditions

The single pile mesh, used to perform the finite element analysis, is shown in Figure 6.36. The analysis is axi-symmetric and the mesh domain is 40 m deep and 20 m wide. It extends down to the Chalk, as shown in Figure 6.25. The single pile is 13 m long and its diameter is 0.45 m. The finite element mesh is divided into several layers, representing the ground profile identified for the analysis earlier.

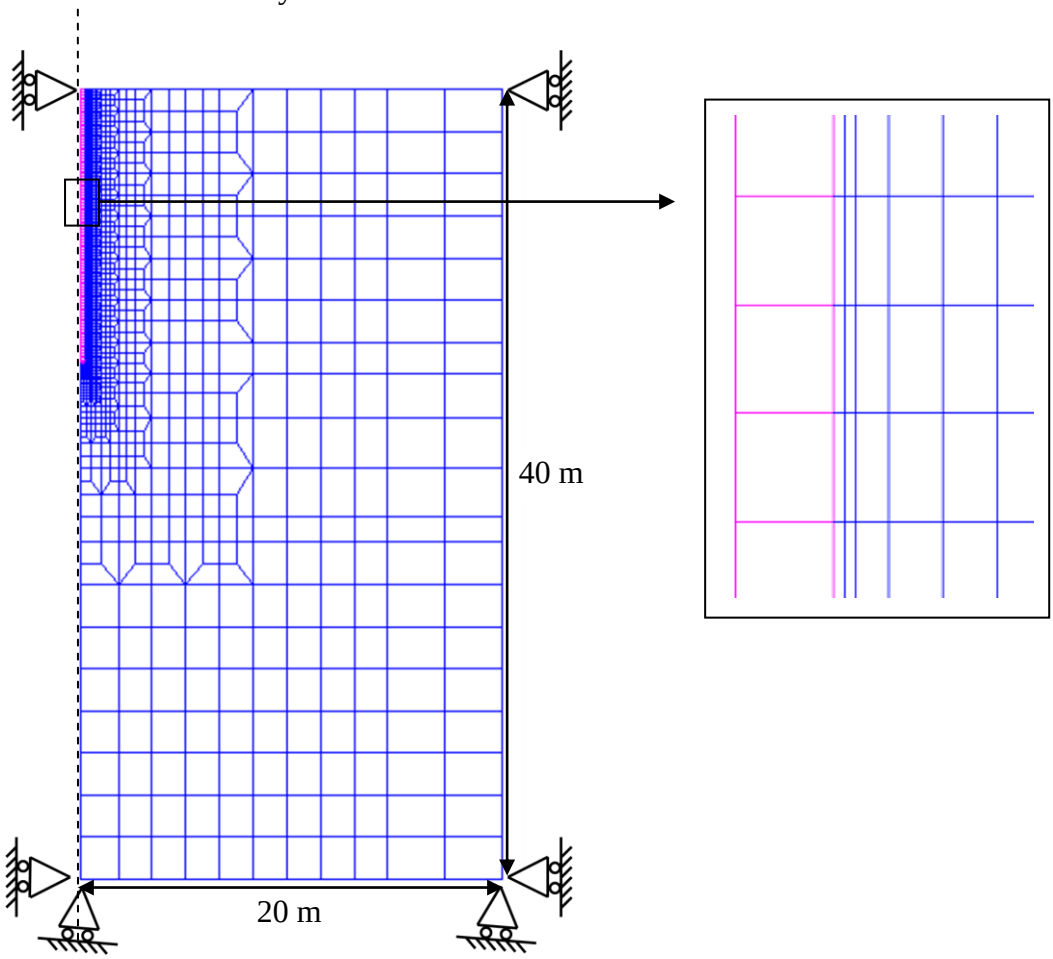


Figure 6.36: Single pile mesh for pile load test in Stonebridge Park

Both the pile and the soil are discretised. The pile is modelled as a very stiff elastic material ($E= 30\times10^6$ kPa, $\mu= 0.15$), which is able to transfer load from the pile head to the surrounding soil, whereas the soil is modelled using the ET Creep model. The mesh consists of eight noded isoparametric elements with four pore pressure degrees of freedom for consolidating elements at the corner nodes, and two displacement degrees of freedom at both corner and mid-side nodes for all elements.

A “soft zone” of a thickness of 4.5 cm around the pile with a lower angle of shear friction is employed, in order to simulate numerically the loss of adhesion on the pile-soil interface due to pile installation.

The applied displacement boundary conditions prevent the base of the mesh from moving in the vertical and horizontal directions, while the vertical sides of the mesh are fixed in the horizontal direction and can move in the vertical direction only. The analysis is coupled, i.e. consolidation takes place during the analysis. The seepage boundary conditions applied allow no flow into the pile and to the left hand boundary of the mesh, while on the base of the mesh, the right hand boundary and along the ground surface next to the pile, pore pressures are kept equal to their initial values, as determined by the water table 3.5 m below ground level.

6.4.5.3. Description of analysis

A finite element analysis is performed, in order to determine the load-settlement response of the single pile in question and compare it with the documented results. The angle of interface friction on the pile-soil interface ("soft zone") is back-analysed, considering the effects of pile installation on the surrounding soil.

The analysis consists of an incremental maintained load test and a CRP test. The incremental load test is simulated by prescribing boundary stresses on top of the pile, from which displacements are calculated, whereas the CRP test is simulated by applying prescribed displacements and by calculating the pile reaction. The magnitudes of the boundary stresses are obtained from Figure 6.35. For the CRP test, no information is given regarding the rate of penetration. Therefore, a constant displacement rate of 0.75 mm/min is applied based on BS 8004: 1986.

The angle of interface friction is back-analysed for the "soft zone" discretised around the pile shaft. Given the effects of softening (-10% in OCR in "soft zone") and the lateral relief of pressures (-20% for a radius of half pile diameter) which are simulated in the analysis, the value of δ' is varied, in order to match the predicted load-settlement response with the documented one.

An additional set of analyses is performed, in order to determine the adhesion factor α. This includes a finite element simulation of a CRP pile load test with the calibrated installation effects, being compared with the results of a CRP test, where no installation effects are considered. The rate of penetration applied is similar to the rate applied for the original pile load test, in order to make the analyses consistent.

6.4.5.4. Results and discussion

The predicted load-settlement response of the incremental pile load test and of the subsequent CRP test from the finite element analysis is shown in Figure 6.37, along with documented results from Cooke et al. (1981). The predicted results are obtained by calibrating the angle of interface friction in the "soft zone", which is back-analysed to be $\delta_{ult}{}' = 14^o$. This value of $\delta_{ult}{}'$ back-analysed for the load test in Stonebridge Park is larger than the value back-analysed at Heathrow, which was equal to 12^o.

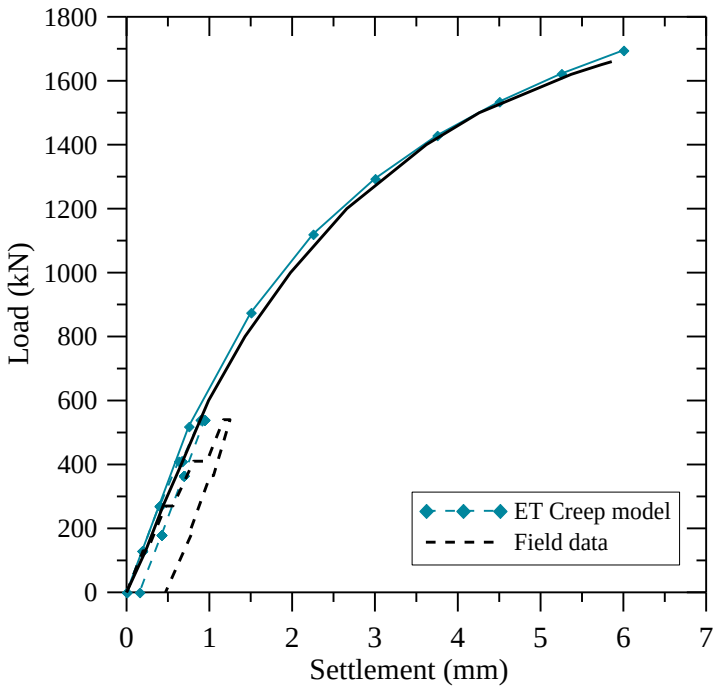


Figure 6.37: Load vs. settlement for the incremental and CRP pile load tests

Next, the magnitude and the duration of each load step of the incremental pile load test, as well as the predicted displacements, are shown in Figures 6.38 and 6.39, along with the documented results from Cooke et al. (1981). It is observed that the elastic response of the pile on the application of a boundary stress is well predicted. This is the predicted settlement for the increments where the boundary stress is applied instantly.

However, this is not the case for the predicted settlements during the elapsed time for each load step. The numerical analysis under-predicts the development of strains during the elapsed time, although the predictions are globally consistent with the expectation that larger displacement with time is predicted at larger stress levels. There is no obvious reason for this discrepancy. However, it is believed to be due to the disturbance and softening of the soil surrounding the pile during boring. In the unloading paths, the measured displacement during the elapsed time at different load levels indicates heave and compression at different load

steps, which is contradictory. The predicted results show insignificant heave during the elapsed time associated with the pile unloading. However, it should be noted that the measured settlements are negligibly small and therefore any discussion is inconclusive.

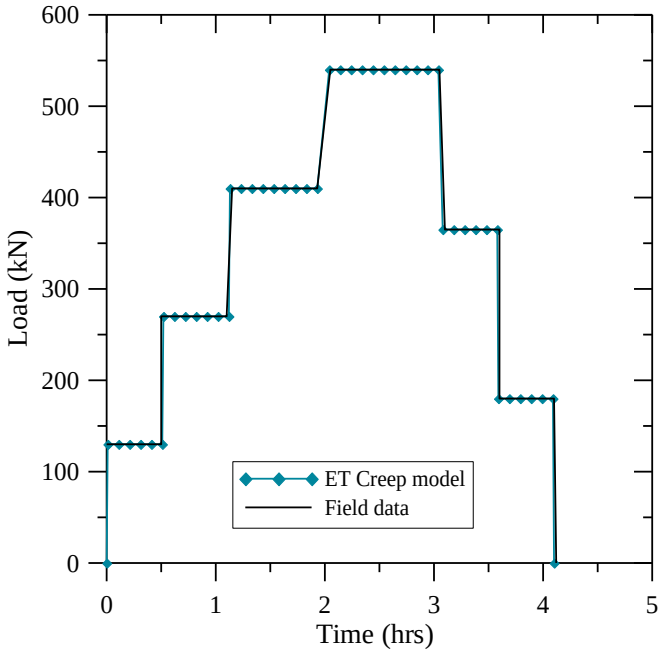


Figure 6.38: Load vs. time plot for the incremental pile load test

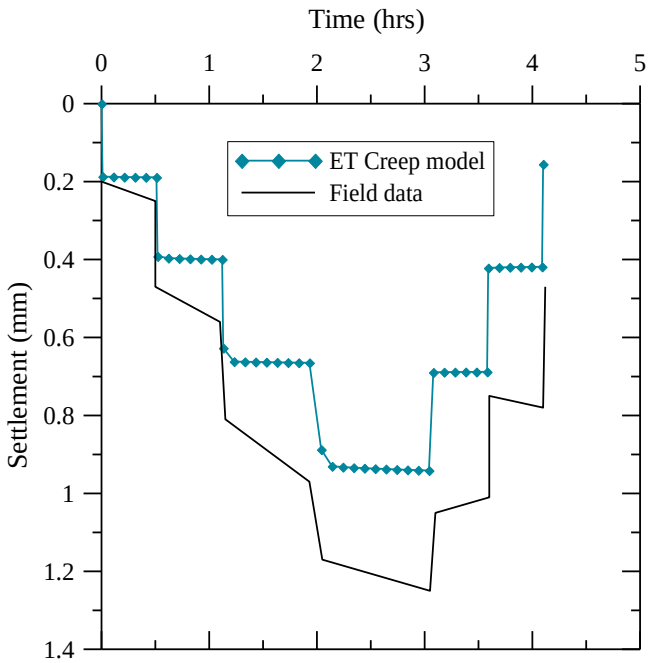


Figure 6.39: Settlement vs. time plot for the incremental pile load test

A further analysis is performed, in order to validate the value of the adhesion factor α in Stonebridge Park. It is expected to be larger than the one predicted at Heathrow and be consistent with the value predicted at Wembley. In Figure 6.40, the load-settlement responses

from two CRP tests, one considering pile installation and the other not considering it, are shown. Comparing the peak load capacity of the two tests, α= 0.5. This value is larger than the value predicted at Heathrow test (α= 0.37) and it is similar to the value suggested by O'Brien (2010), α= 0.6, from a series of pile load tests at Wembley. In the same manner, the value suggested by O'Brien (2010) is larger than the conventional α= 0.45.

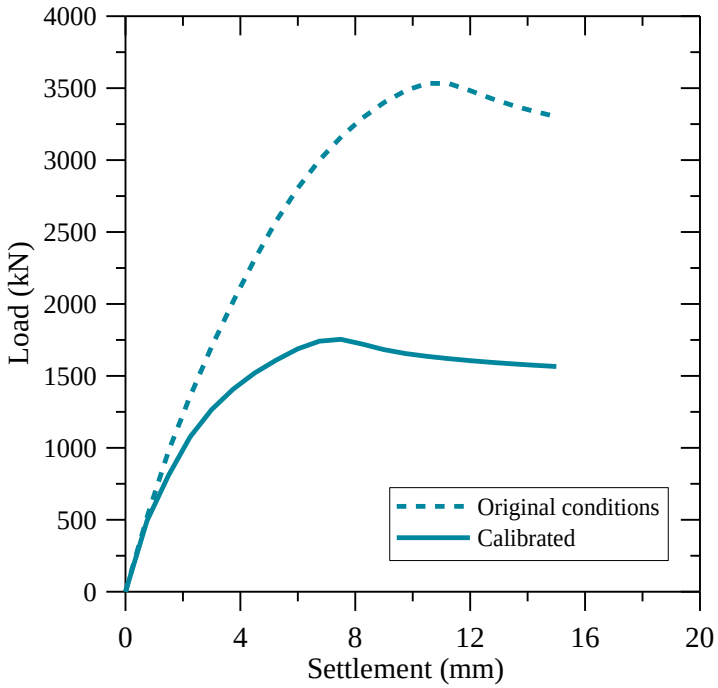


Figure 6.40: Load vs. settlement for the original conditions and calibrated CRP pile load tests

6.4.6. 3D MODELLING OF PILED RAFT FOUNDATION

6.4.6.1. Problem geometry and boundary conditions

The mesh created for the piled raft foundation problem is shown in Figure 6.41. The analysis is three-dimensional and the mesh domain is 100m x 50m x 40m in the X-Y-Z axes respectively. It extends down to the Chalk and includes all the units identified at Stonebridge Park (see Figure 6.25). The zone of influence of the piled raft foundation, as identified from Figure 2.20, is approximately 32 m below the raft and, therefore, the size of the mesh is regarded as sufficient. The ¼ of the problem is discretised into finite elements, due to the symmetry in foundation around the X and Y axes. The mesh consists of 20366 20-noded hexahedral finite elements.

In Figure 6.42, a 3D view of the piled raft foundation is shown. Both the piles and the raft are discretised. The dimensions of the raft are 43.3 m by 19.2 m and, due to the symmetry, ¼ of the raft is discretised, i.e. 21.65 m by 9.6 m. Piles are 13 m long and 0.45 m in diameter, while

the raft is 0.9 m thick. Both the piles and the raft are modelled as a linear elastic concrete material, with E = 30×10^6 kPa and μ= 0.15. The piles are installed on a square grid of 1.6 m distance centre to centre. A “soft zone” (see Figure 6.43), 7.5 cm thick, with a lower angle of shear friction, is discretised around the piles, in order to simulate the adhesion in the pile-soil interface.

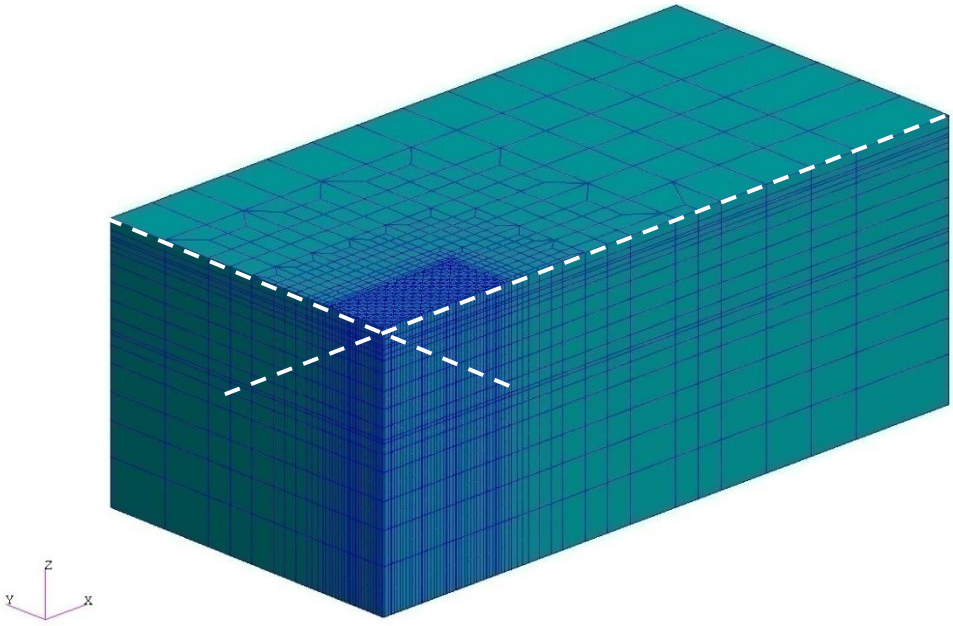


Figure 6.41: 3D mesh for the piled raft foundation of Hiscocks House

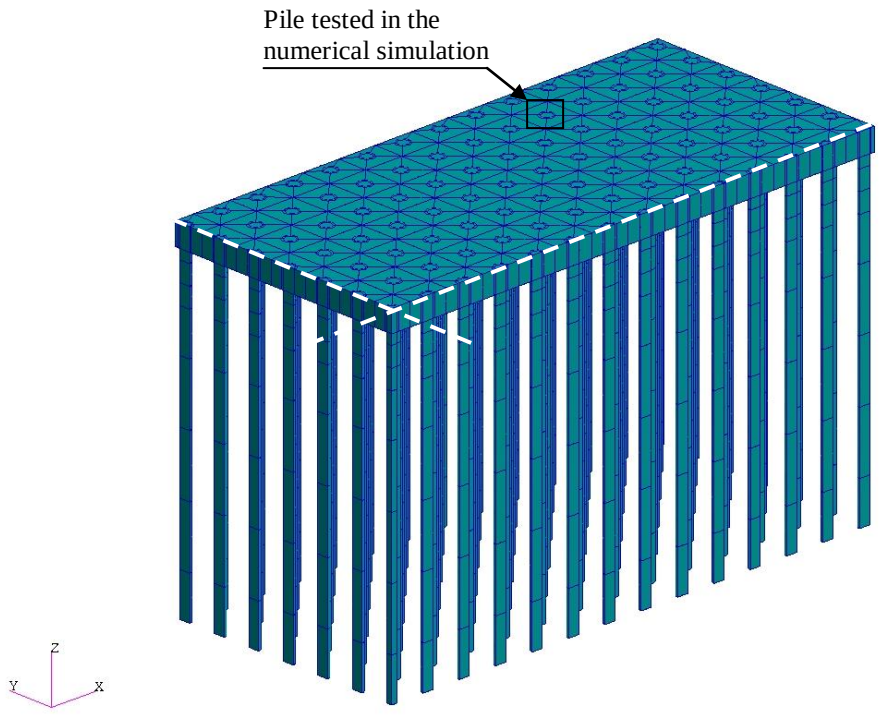


Figure 6.42: 3D view of the piled raft foundation of Hiscocks House

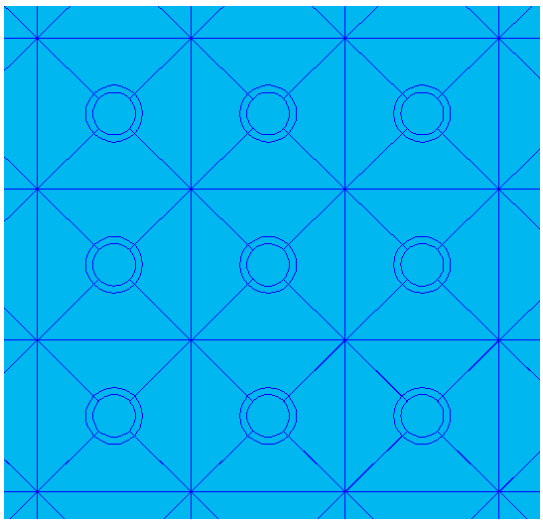


Figure 6.43: Plan view of piles detail of the piled raft foundation of Hiscocks House

The ET Creep model is employed to simulate the behaviour of the London Clay units and of the Lambeth Group, including the "soft zone" around the piles. Model parameters for each soil layer are set in Section 6.4.3 and the properties of the "soft zone" are identified in Section 6.4.5. The mesh consists of twenty noded isoparametric elements with eight pore pressure degrees of freedom at the corner nodes of the consolidating elements, and three displacement degrees of freedom at both corner and mid-side nodes for all elements.

The applied displacement boundary conditions prevent the base of the mesh from moving in the vertical (Z direction) and horizontal directions (X and Y directions), while the vertical sides of the mesh, whose face is not a plane of symmetry, are fixed in the horizontal directions and can move in the vertical direction only. Regarding the boundaries forming planes of symmetry, their vertical sides are fixed in the direction towards the plane of symmetry, i.e. the X-Z boundary is fixed in the Y direction and the Y-Z boundary in the X direction, whereas they are free to move in the remaining directions.

The analysis is coupled with consolidation taking place during the analysis. The seepage boundary conditions applied allow no flow across the planes of symmetry, while at the base of the mesh and the remaining vertical planes, pore pressures are maintained equal to their initial values, as determined by the water table 3.5 m below ground level.

6.4.6.2. Description of analysis

A finite element analysis is performed, in order to assess the performance of the piled raft foundation of Hiscocks House. The predicted results are compared with those documented by

Cooke et al. (1981). The finite element analysis simulates the life cycle of Hiscocks House, as identified by Cooke et al. (1981) and Butcher et al. (2006). It consists of:

- 100 years of elapsed time,
- the construction of the piled raft foundation, including pile installation, excavation and construction of the raft linking the piles,
- the construction of the structure on top of the foundation,
- the building life period of 29 years, and
- the demolition of Hiscocks House.

In Table 6.6, the sequence of the FE analysis is presented.

Increment	**Action**	**Stress (kPa)**	**Time (days)**
1	Soil profile	-	~ 0
2 – 6	Elapsed time	-	720.0
7 – 15	Elapsed time	-	3600.0
16	Pile installation	-	60.0
17 – 19	Excavation of raft	-	30.0
20	Construction of raft	24.0	30.0
21 – 23	Construction of structure	9.9	20.0
24 – 26	Construction of structure	-	45.0
27 – 31	Construction of structure	15.9	20.0
32	Construction of structure	-	30.0
33 – 35	Construction of structure	12.3	25.0
36 – 39	Construction of structure	-	37.5
40 – 43	Construction of structure	2.9	37.5
44 – 57	Building life	-	120.0
58 – 69	Building life	-	720.0
70 – 72	Demolition of building	-52.4	30.0
73	Excavation of raft	-	7.0

Table 6.6: Sequence of FE analysis for the piled raft foundation problem

A period of ***100 years elapsed time*** of the soil profile (increments 2 to 15) discretised in the 3D mesh is employed initially, in order to eliminate any small changes in the pore water pressure profile with time as identified in Section 6.4.4. This allows reaching equilibrium in pore water pressures, as shown in Figure 6.32, after a period of 100 years; a period set empirically, after which no changes in pore water pressures are identified.

The ***construction of the piled raft foundation*** (increments 16 to 20) follows the construction works, as described by Cooke et al. (1981). The installation of the 351 bored piles lasted for 2 months, from January to February 1973, whereas the excavation for the raft was carried out over the following 3 months and the subsequent construction of the raft lasted for a month, being completed by the end of June 1973.

The installation of the piles is simulated by changing the material properties of the appropriate elements from soil to concrete. At the same time, the "soft zone" around the piles is simulated, by changing also the material properties of the elements forming the "soft zone" and assigning a lower angle of shear resistance, as determined from the pile load test simulation. The relief of lateral pressures and the reduction in OCR are not simulated, unlike in the single pile tests. This is thought reasonable as lateral stresses are expected to recover with time after construction and here we are interested mainly in long term behaviour (see Figure 2.3).

Then, the excavation of the raft follows. A layer of 2.5 m is excavated over a period of 3 months, by removing the appropriate elements from the finite element mesh. Subsequently, the concrete raft is constructed in a period of 1 month. A layer of elements 0.9 m thick, representing the raft, is constructed on top of the excavated boundary over one increment with an elapsed time of 1 month. The raft is modelled with the material properties of concrete, as described above.

The ***construction of the super structure*** consisting of 16 storeys on top of the foundation (increments 21 to 43) is followed in the analysis, which lasted for a period of approximately 14 months, see Figure 2.20. Occupation was completed in August 1975, 2 years after the construction of the raft. The load from the structure is simulated through the application of boundary stresses on top of the raft, from which the respective displacements are calculated. Increments of elapsed time only are prescribed where it is required, according to the construction programme. The structure is recognised to be relatively rigid according to Padfield and Sharrock (1983). Therefore, a uniform load is assumed over the surface of the raft, which equates to 156,000 kN at occupation.

The ***building life*** of Hiscocks House lasted for 29 years. Increments of elapsed time are prescribed in the analysis (increments 44 to 69). The piled raft is loaded with the total stress prescribed in the previous increments of the analysis representing the total load of the structure. The settlements developing with time are calculated.

Finally, the ***demolition of Hiscocks House*** (increments 70 to 73) is simulated. Butcher and Skinner (2006) indicate that demolition works started in January 2004 and that 3 months were required to remove all floors. Subsequently, the raft was excavated in a period of a week. The former is achieved by prescribing negative boundary stresses on the raft representing unloading during demolition, while the latter is simulated by excavating the elements forming the raft, which were initially constructed during the analysis.

6.4.6.3. Results and discussion

The finite element predictions for the performance of the piled raft foundation of Hiscocks House are compared with the field measurements for the period during the construction and the first years after occupation. This allows the validation of the constitutive and numerical models employed in the 3D analysis. Moreover, the predicted behaviour in the long term for the whole life span of Hiscocks House is presented, from which several conclusions are drawn. In the following, predictions of absolute settlements, differential settlements, contact pressures between the raft and the soil, load share between individual piles, load share between the piles and the raft, and their evolution with time are presented.

In Figures 6.44 and 6.45, the application of load during construction and the development of ***absolute settlements*** predicted from the 3D analysis for a range of depths below the underside of the raft, at the point where an extensometer had been put in place originally (see Figure 6.46), are presented for the period during which measurements have been recorded, i.e. after the construction of the raft. Block deformation of the piled raft foundation is indicated by settlement profiles at depth levels of 0.4 m, 5 m and 10 m (see Figure 6.45) below the raft which are very close in magnitude (piles are 13 m long). In Figure 6.47, contours of accumulated displacement are shown, where it is visualised that the settlement is concentrated below the toe of the piles, while the displacement along the piles length is limited. The block deformation is an attribute of the conventional piled raft foundation type, as described in Chapter 2.

In Figure 6.48, predictions are compared with the measured settlements from Cooke et al. (1981) at representative depths below the underside of the raft (levelling observations at the

ground level are also shown), from which it can be concluded that good agreement between the measurements and predictions is generally achieved. The measured absolute settlements indicate, like the predicted ones, that the piled raft foundation is settling as a block with soil displacements being concentrated below the piles toe. However, the magnitude of the deformation with depth between the FE predictions and the measured results show some deviation for shallow depths. In particular, for depth levels up to 10 m it seems that the relative deformation is under-predicted from the FE analyses. It is evident that displacements are concentrated below the piles toe level.

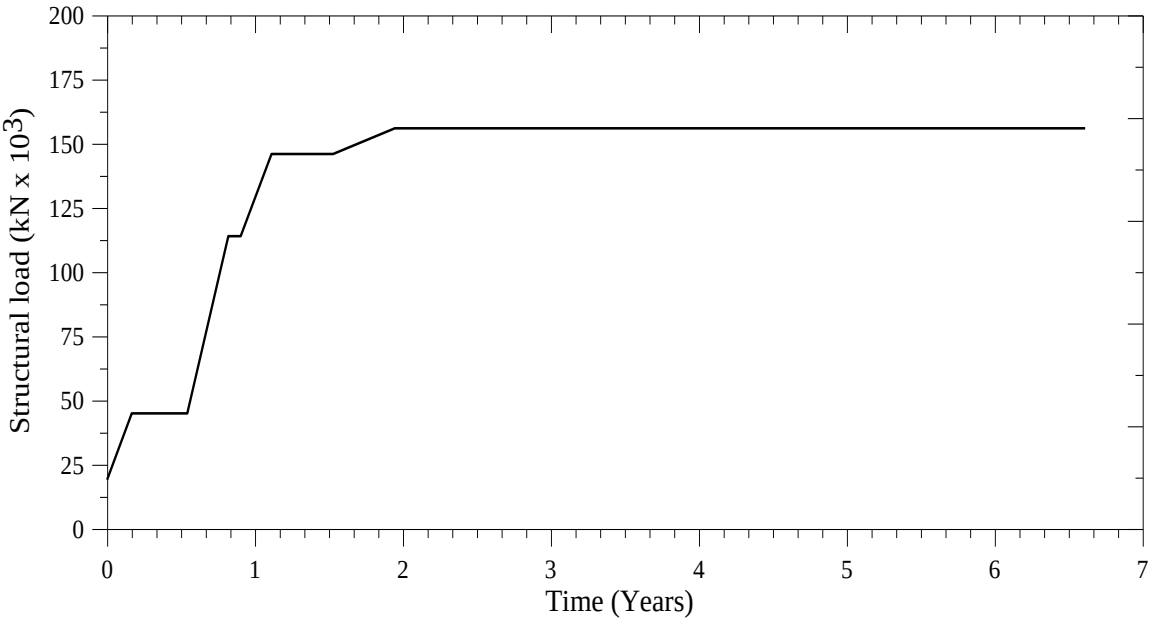


Figure 6.44: Structural load during construction of Hiscocks House

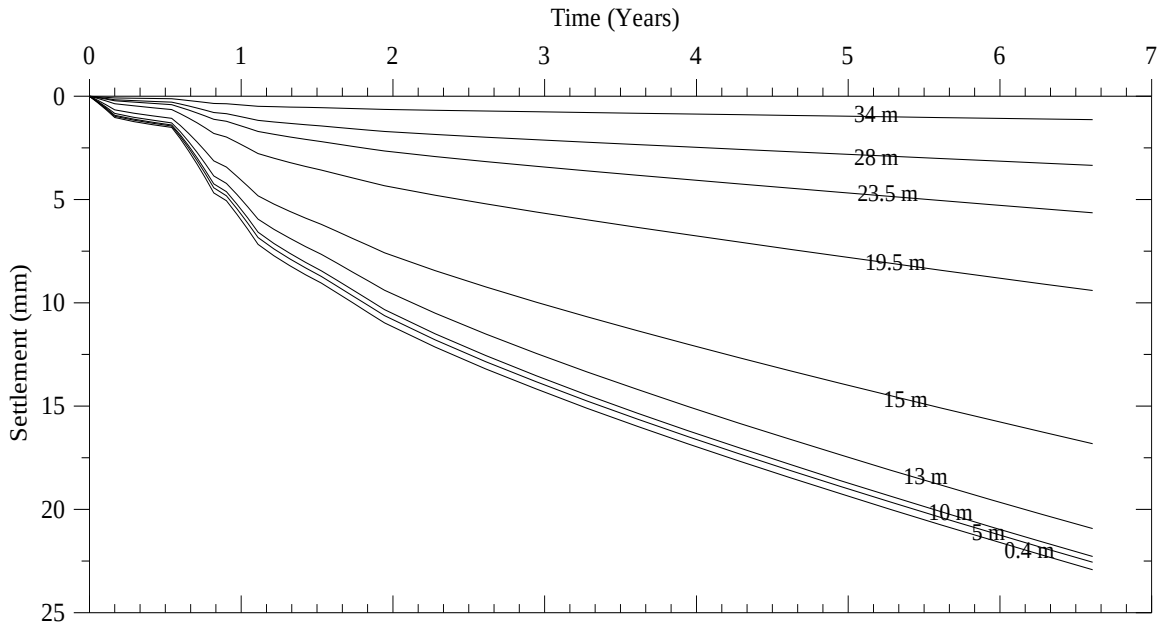


Figure 6.45: Development of absolute settlement for a range of depths below the underside of the raft

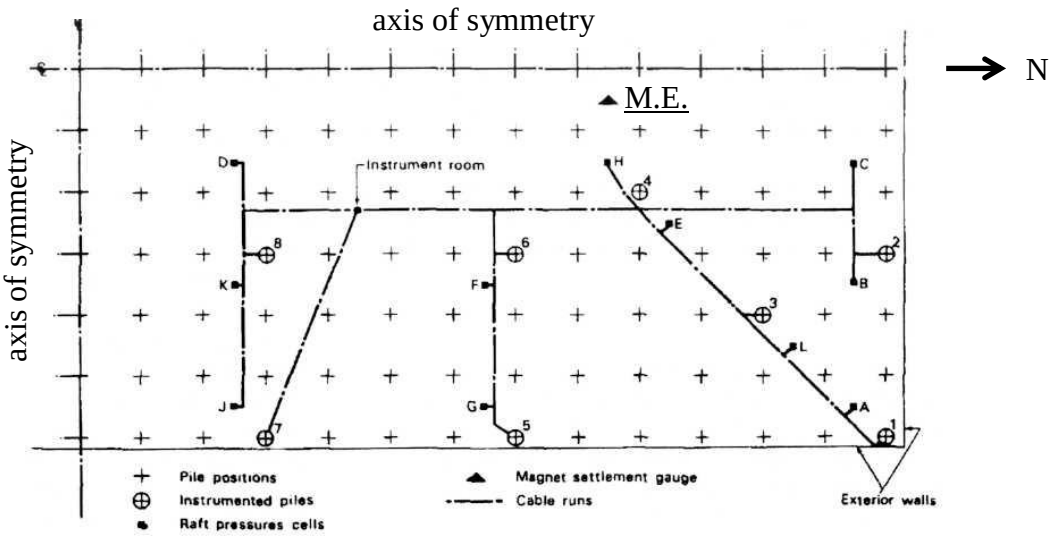


Figure 6.46: Foundation plan of north-east quarter showing positions of piles instrumented and of magnet extensometer (Cooke et al., 1981)

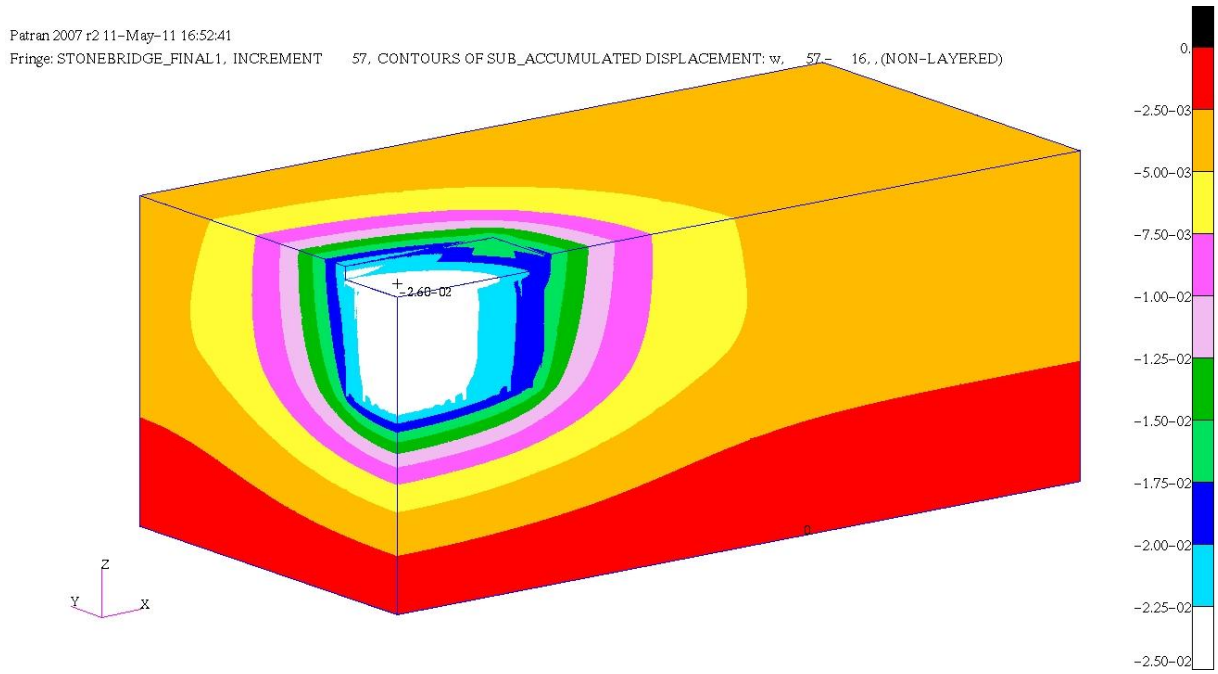


Figure 6.47: Contours of accumulated displacement for the period during which measurements have been reported by Cooke et al. (1981) (units in metres)

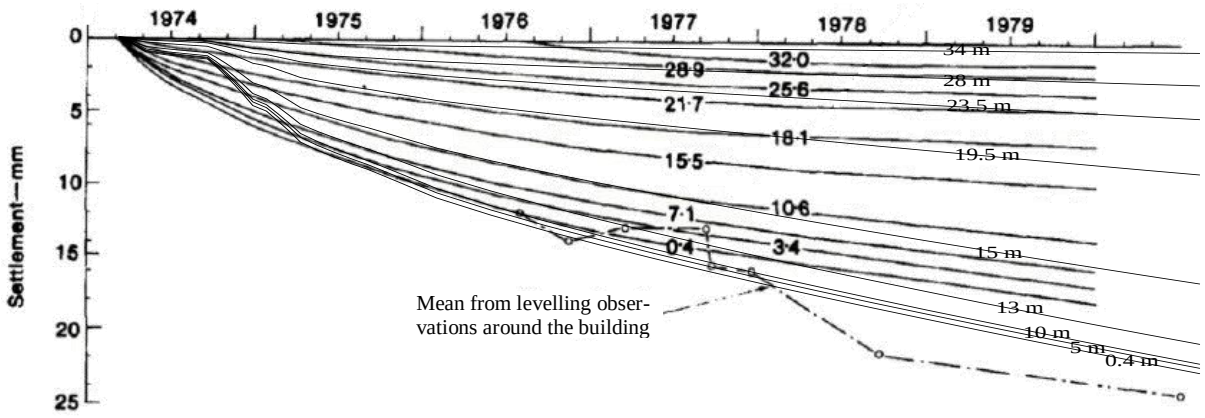


Figure 6.48: Comparison between FE predicted settlements with measured settlements from Cooke et al. (1981) at representative depths below the underside of the raft

In Figure 6.49, absolute settlements in the long term, i.e. during the life span of the building of 29 years, are plotted for a range of depths below the underside of the raft at the same point as above. The FE analysis predicts that settlement increases up to approximately 59 mm after the construction of the raft. Settlement consists of both consolidation and creep, whose rate is decreasing with elapsed time, being consistent with the formulation of the ET Creep model. Like in the short term, the piled raft foundation seems to settle as a block, with the majority of the displacements concentrated below the piles toe.

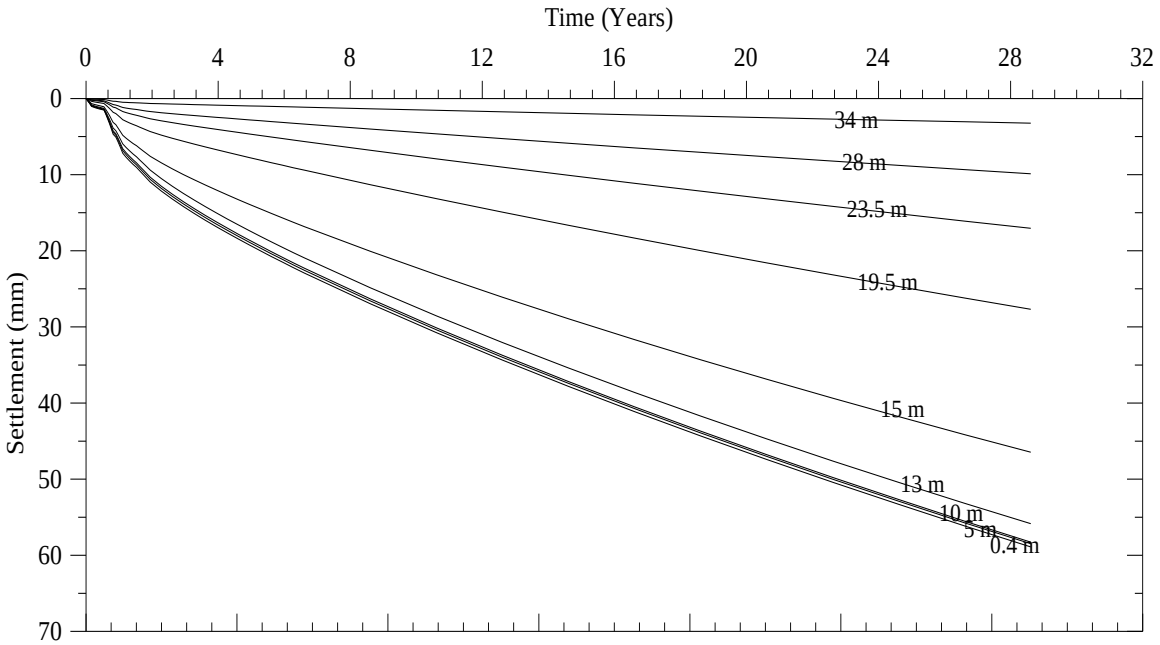


Figure 6.49: Development of absolute settlement for a range of depths below the underside of the raft in the long term

Regarding ***differential settlements***, finite element predictions are compared with measurements documented by Cooke et al. (1981). In Figure 6.50(a), contours of predicted settlement are presented, whose magnitude for the period recorded in-situ between 12 July 1976 and 24 June 1980 (increments 46-57) is shown. The magnitude of settlement ranges from 8.8 mm in the corner of the raft to 13.2 mm towards the centre of the raft. The predicted settlements indicate larger values in the centre of the raft compared to those along the edge and in the corner of the raft, as well as that the settlement along the edge is respectively larger than in the corner. Such behaviour is typical for conventional piled raft foundation, indicating that a smaller number of piles oriented towards the centre of the raft would be more beneficial in reducing differential settlement than a large number of piles uniformly distributed over the raft area.

The measured development of settlement under the raft area between 12 July 1976 and 24 June 1980 is shown in Figure 6.50(b). The settlement contours indicate, similar to the predicted results, that the absolute settlement is maximum in the centre with a value larger than 12.5 mm and minimum in the corners with values approximately between 7.5 mm and 10.0 mm. The maximum measured differential settlement corner-to-centre ranges between 3.0 and 6.0 mm, whereas the predicted maximum differential settlement centre-to-corner is equal to 4.4 mm.

Contours of settlement at the raft level, as predicted by the finite element analysis, at occupation and before demolition of Hiscocks House are plotted in Figure 6.51. These allow the amount of differential settlement at occupation and in the long term to be determined. Regarding the settlement contours at occupation in Figure 6.51(a), it is predicted that absolute settlement in the centre of the raft is equal to 12.5 mm, whereas in the corner it is 6.9 mm. Therefore, the differential settlement at occupation is estimated to be 5.6 mm. In the long term, after approximately 29 years of occupation, settlements increase due to consolidation and creep. The FE analysis predicts a settlement in the centre and in the corner of the raft equal to 62.0 mm and 41.3 mm respectively, with differential settlement therefore being equal to 20.7 mm (see Figure 6.51(b)). More on the evolution of the differential settlement with time and limits on differential settlement are given later in Chapter 7.

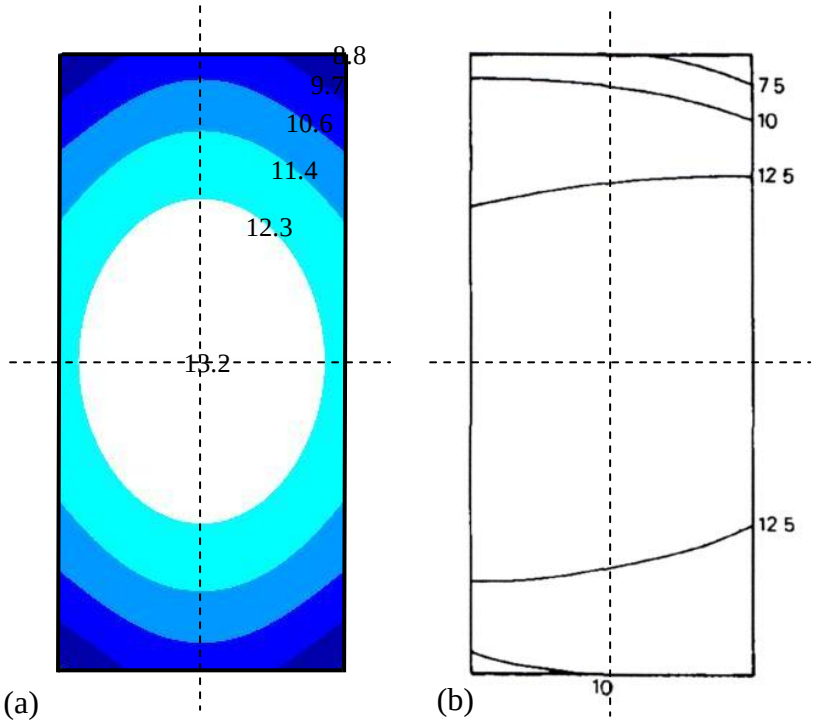


Figure 6.50: Contours of settlement at raft level between 12 July 1976 and 24 June 1980: (a) predicted, (b) measured

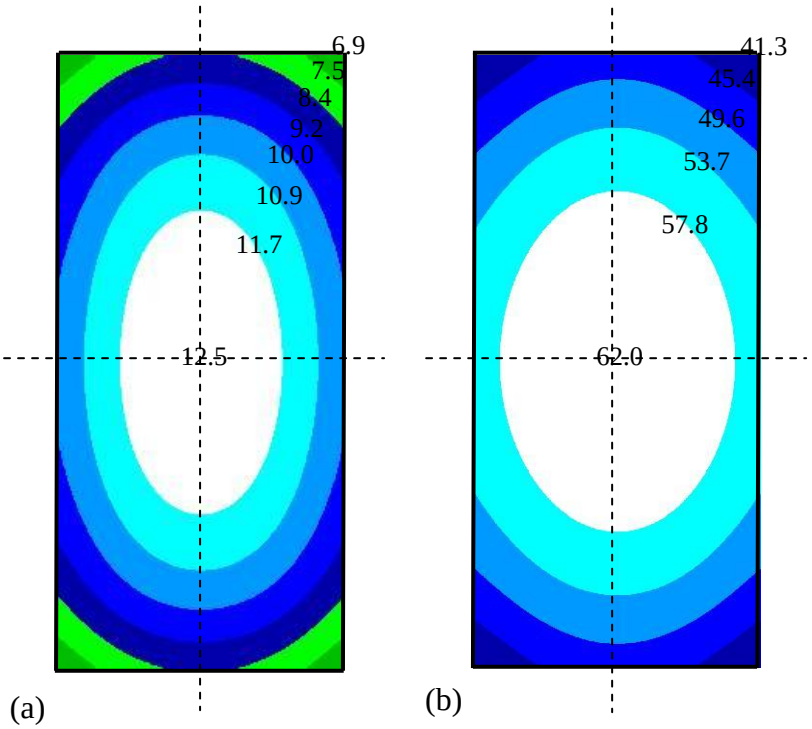


Figure 6.51: Predicted contours of settlement at raft level (a) at occupation of Hiscocks House, (b) after 29 years of occupation

Regarding the ***load share between piles***, the finite element predictions of the development of pile loading are compared with the measured development during the construction of Hiscocks House. As described in Chapter 2, pile load cells have been put in characteristic piles of the piled raft foundation (see Figure 6.46), in order to determine the load share between piles. In particular, one corner pile (pile 1), three edge piles (piles 2, 5 and 7) and four internal piles (piles 3, 4, 6 and 8) were instrumented.

In Figure 6.52, the development of load on the piles instrumented (see Figure 6.46) during construction as predicted from the finite element analysis, along with the average for each category of pile instrumented (corner, edge and internal piles), is plotted. It is observed that the corner pile and the edge piles attract more load than the internal piles. In particular, the corner pile receives approximately 50% more of the load received by the internal piles. This is attributed to the fact that the internal piles settle more than the piles at the periphery, as shown in Figure 6.51, and as a consequence the peripheral piles attract more loads than the internal piles.

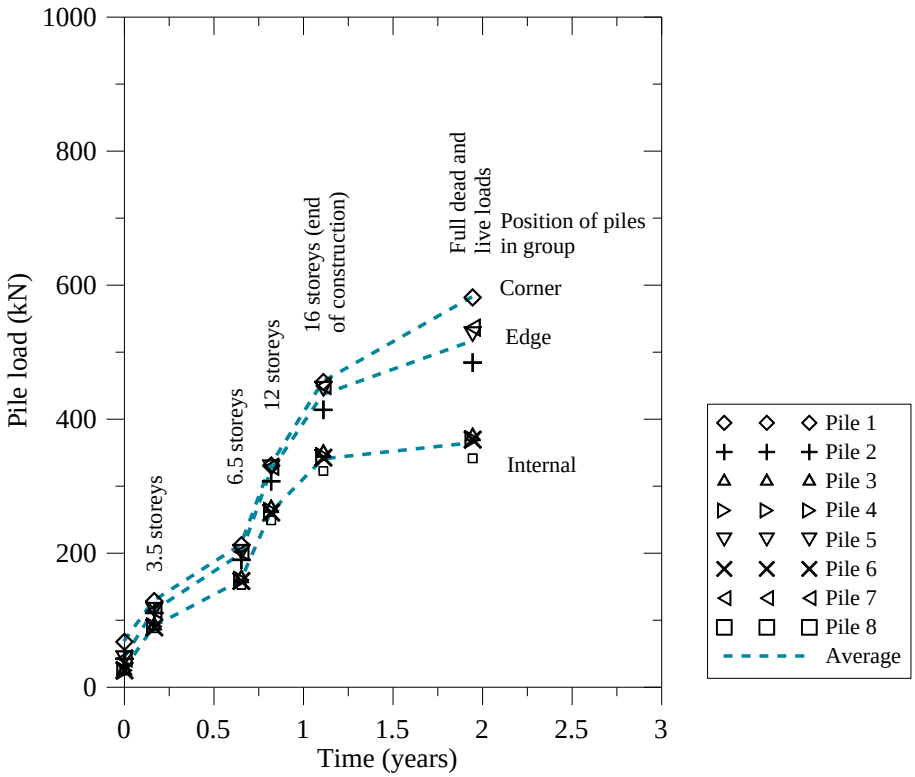


Figure 6.52: Development of predicted pile loading during erection of Hiscocks House, showing the distribution of loads carried by characteristic piles

In Figure 6.53, the average values predicted from the finite element analysis are compared with those measured in situ on the instrumented piles. Generally, good agreement is obtained. Corner and edge piles attract more load than internal piles. The predicted average magnitudes

for internal and edge piles are considered to be equivalent to the values obtained in situ, however it seems that the load on the corner pile is under-predicted. This is considered to be the result of the settlement on the instrumented corner pile (<7.5 mm), as shown in Figure 6.50(b), being smaller than the settlement on the other corner piles (~10 mm) resulting in a larger load being attracted on the instrumented corner pile than the other corner piles. The predicted settlement in the corner is 8.8 mm (see Figure 6.50(a)), therefore it is considered that less load than the in-situ pile would be attracted, which is the case.

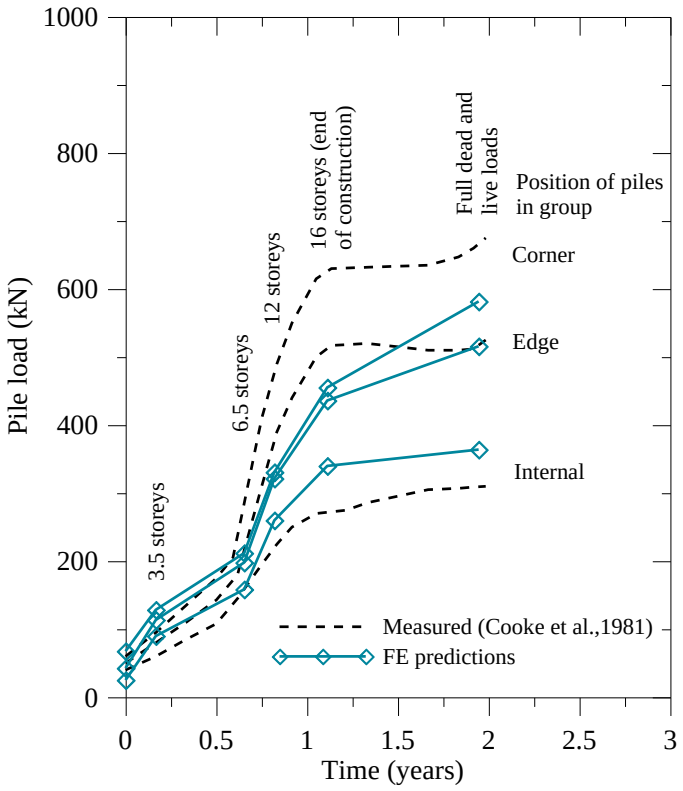


Figure 6.53: Comparison between the predicted average pile loading of characteristic piles and the measured values published by Cooke et al. (1981)

In Figure 6.54, the long term development of pile loading is presented, as predicted from the finite element analysis, for the lifespan of Hiscocks House. It is observed that the load share between piles changes with elapsed time. In particular, the load on the corner pile is increasing with a reducing rate as time elapses. This is also the case for edge piles, however the rate of increase is smaller than the rate observed for the corner pile. Unlike the corner and edge piles, the load attracted by the internal piles is reducing with time at a reducing rate. This contributes to the evolution of settlements on the raft and in particular to differential settlements, which influence the load share between the piles. The piles that settle the least attract the larger loads, whereas those that settle the most are loaded the least. Comparing the absolute settlements of the raft in Figure 6.51, differential settlements increase with time,

indicating that the load on the peripheral piles should increase in the long term, whereas the load on the internal piles should decrease. Therefore, it is concluded that the distribution of loads on the piles in the long term is dependent on the development of settlements of the raft with time.

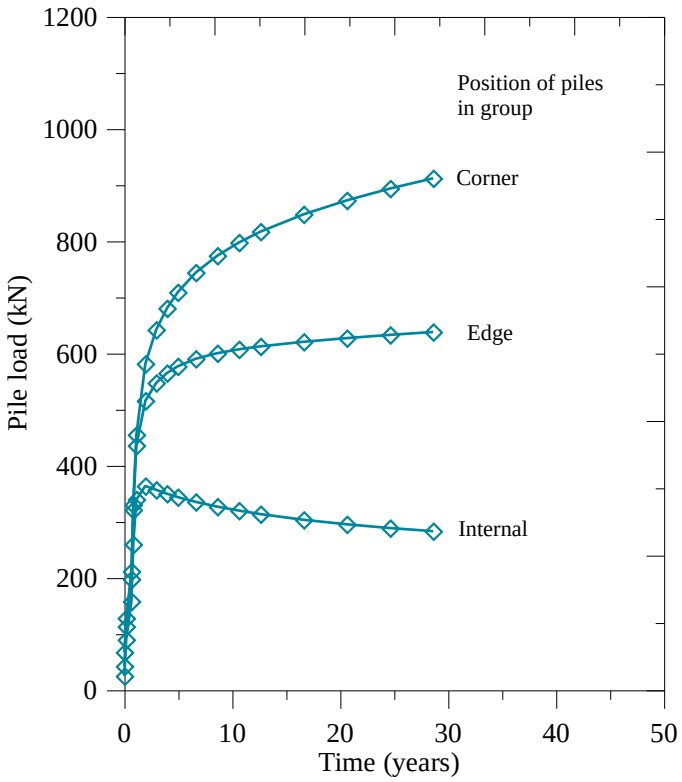


Figure 6.54: Development of predicted average pile loading of characteristic piles in the long term, showing the distribution of loads carried by characteristic piles

Regarding the ***contact pressure between the raft and the soil***, contours of vertical effective stress at the raft-soil interface are plotted in Figure 6.55. These are contours of the accumulated stresses applied from the construction of the raft up to the total building loading, which allow the determination of the variation of the contact pressure at the raft-soil interface. A much higher intensity of stresses from the raft to the soil around each pile is observed. The stress distribution around the piles is not symmetrical; it is concentrated around each pile with an orientation towards the centre of the raft. Larger magnitudes of vertical effective stress are predicted towards the periphery of the raft with a maximum contact stress obtained in the corner of the raft and a minimum in the centre of the raft. The contact stress distribution is equivalent, as in the load share of piles, to the settlement over the raft area, i.e. the larger the settlement the smaller the contact stress between the raft and the soil. Comparing the predicted results with the suggested contact stress distribution by Cooke et al. (1981) (Figure 2.22), good agreement is obtained in terms of the orientation of maximum and minimum

contact stress. Cooke et al. (1981) suggest contact stresses based on several approximations due to the difficulties involved in determining reliable contact stress. In addition, their suggestion is based on an insufficient number of pressure cells placed on the raft-soil interface. Therefore, absolute comparison of the values of contact stress predicted to those suggested is not a fair one, due to the approximations involved in the suggested values.

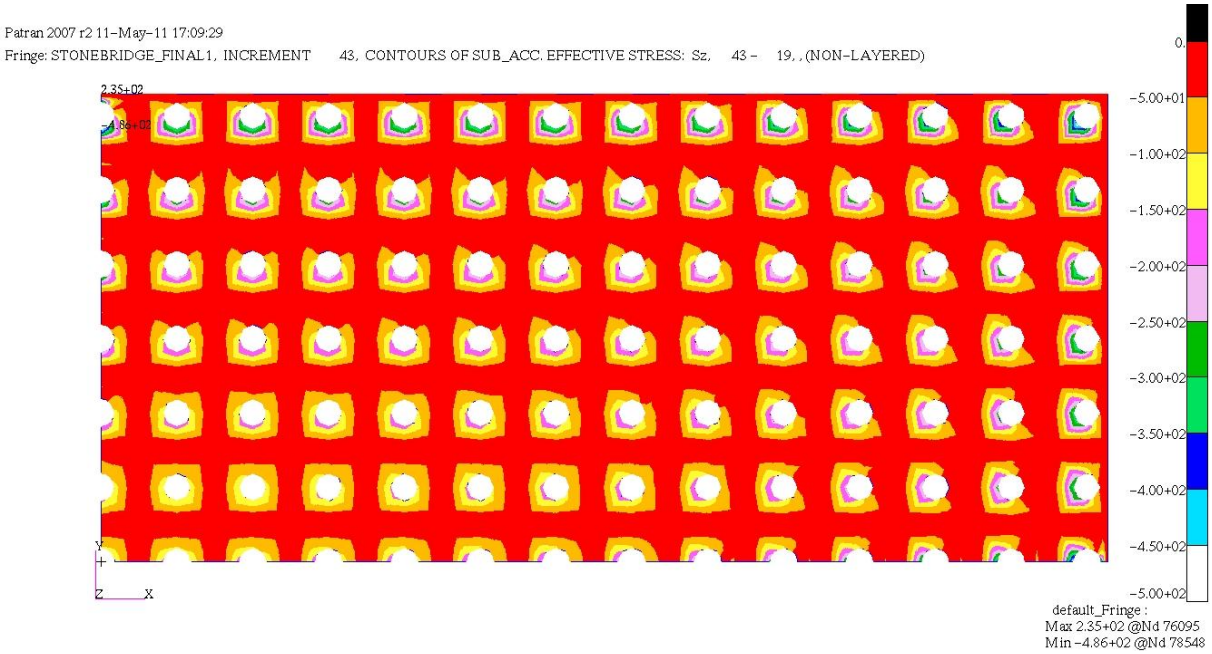


Figure 6.55: Contours of vertical effective stress at the raft-soil interface at occupation of Hiscocks House (units in kPa; sign convention tension positive)

Regarding the ***load share between piles and the raft***, the total load carried by the piles over the total structural load as a percentage of the total structural load is plotted in Figure 6.56, as predicted by the finite element analysis and as calculated (involving several approximations) by Cooke et al. (1981). The finite element predictions indicate that the load share of the piles increases with increasing structural load. The larger the structural load, the larger the proportion of load carried by the piles. In particular, the load share of the piles at a level of structural load of 3.5, 6.5, 12 and 16 storeys and at building occupation is 51.4, 66.5, 74.9, 79.7 and 83.4 % respectively. The predicted results are in good agreement with the calculated values by Cooke et al. (1981). The fact that the proportion of load carried by the piles increases with increasing structural load is explained by Cooke et al. (1981) by the fact that the supporting clay below the raft is consolidating with time, resulting in increased support by the piles. Therefore, as the soil beneath the piled raft consolidates and settles, some of the proportion of load previously carried by the raft is transferred to the piles.

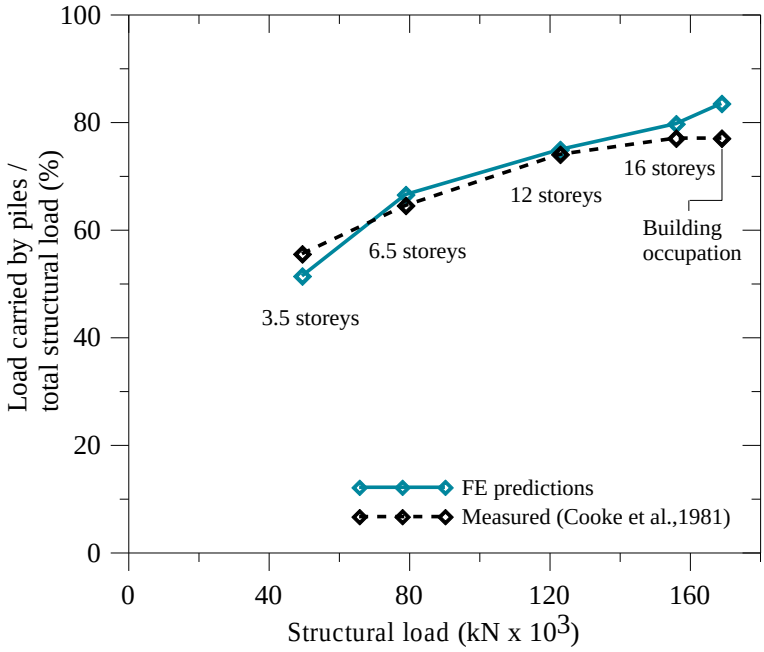


Figure 6.56: Proportion of total structural load carried by piles at various stages of construction

6.4.7. PILE LOAD TEST AFTER DEMOLITION: 2005

6.4.7.1. Description of the pile load test

A pile load test performed on a working pile of the piled raft foundation of Hiscocks House, after its demolition in 2005, is presented by Butcher et al. (2006). The load-settlement response of the pile tested in 2005 and of the pile tested in 1972 is compared, allowing the assessment of the behaviour of a fresh pile and a reused pile which had been under a working load for a long period of time. A discussion of the documented results was given in Chapter 2.

The recent test was designed to approximate the 1972 test. The pile chosen to perform the test is not identified by Butcher et al. (2006), however the structural load on the tested pile was estimated to be 400 kN (see Figure 2.14). The load on the pile was incremented in 100 kN steps with unload-reload cycles at 500, 1000 and 1500 kN. However, at 1300 kN one of the adjacent piles, used as anchor piles, failed and the test was terminated. The load-settlement response is given in Figure 2.14. Other information about the pile load test is not available.

6.4.7.2. Description of analysis

A finite element analysis of the pile load test is performed, in order to simulate the test performed in 2005 and to compare the predicted load-settlement response with the measured

one. The analysis is a continuation of the 3D analysis performed for the piled raft foundation problem. Due to the fact that the in-situ test failed during the test, an additional set of finite element analyses is performed involving CRP tests before the construction of Hiscocks House and after the demolition to assess the effects of sustained load on the load-settlement response. The simulated CRP tests are similar to the one performed originally in 1972 (Section 6.4.5), which was analysed as a single pile.

Information about the pile tested is not given by Butcher et al. (2006), however what is known is the level of estimated structural loading on the pile tested. This is 400 kN which, according to Figure 6.53, is consistent with the load carried by an internal pile close to the periphery of the foundation. The pile chosen for the numerical simulation is shown in Figure 6.42 and is known to carry 396 kN at occupation of Hiscocks House.

The first analysis consists of an incremental maintained load test. The incremental load test is simulated by prescribing boundary stresses on top of the pile, from which displacements are calculated. The magnitudes of the boundary stresses are set according to Butcher et al. (2006). The period of elapsed time during load increments is not specified. Therefore, an elapsed time period of 1 hour, similar to the test performed in 1972, is prescribed.

Regarding the CRP tests, a similar displacement rate to the one applied for the original CRP load test (see section 6.4.5) is applied. This is 0.75 mm/min, based on BS 8004:1986. The CRP tests are simulated by applying prescribed displacements and by calculating numerically the pile reaction.

6.4.7.3. Results and discussion

In Figure 6.57, the predicted load-settlement response of the pile tested is plotted, which is compared with the measured response reported by Butcher et al. (2006). The FE analysis simulates the 2005 in-situ test, and therefore the pile load test is interrupted at the load level the original pile load test was aborted due to the failure of one of the tension piles.

The pile is step loaded up to 500 and 1000 kN, from which levels it is unloaded and then reloaded to a higher load than previously experienced. During unloading from 500 and 1000 kN, the FE analysis predicts an elastic rebound accompanied with a permanent set of the pile, as shown in Figure 6.57. During reloading, a stiffer response than the one obtained at initial loading is predicted up to the load the pile had previously experienced (i.e. 500 and 1000 kN).

Comparing the predicted and the documented load-settlement response of the pile (Figure 6.57), a softer response than the one documented is predicted. It appears that the pile response during the instantaneous load increments is well predicted, however the development of strains during the elapsed time period between the load increments is over-predicted. The reason behind this softer response may be the fact that, in the real test, processes taking place during the structural life, other than those grouped in the viscous and consolidation effects (reproduced by the ET Creep model), may dominate the behaviour of the pile. These may include changes at the soil-shaft interface and the time-dependent structuration of the soil surrounding the pile as identified in Chapter 2, resulting in a stiffer soil. These additional effects are not simulated by the ET Creep model.

Numerically, the effects of installation in the short term may also play a role. These have been approximated in the FE analysis in Section 6.4.5, by prescribing a relief of lateral pressures around the pile and by a reduced OCR in the "soft zone". Finally, the elapsed time period between load steps is approximate, since no information is given in Butcher et al. (2006), and therefore the simulated elapsed period may be longer than the actual period resulting in larger deformations. In the following, both effects are investigated with the aim of quantifying the (a) the reduction of lateral stress and in OCR, and (b) the rate effects of the pile load test.

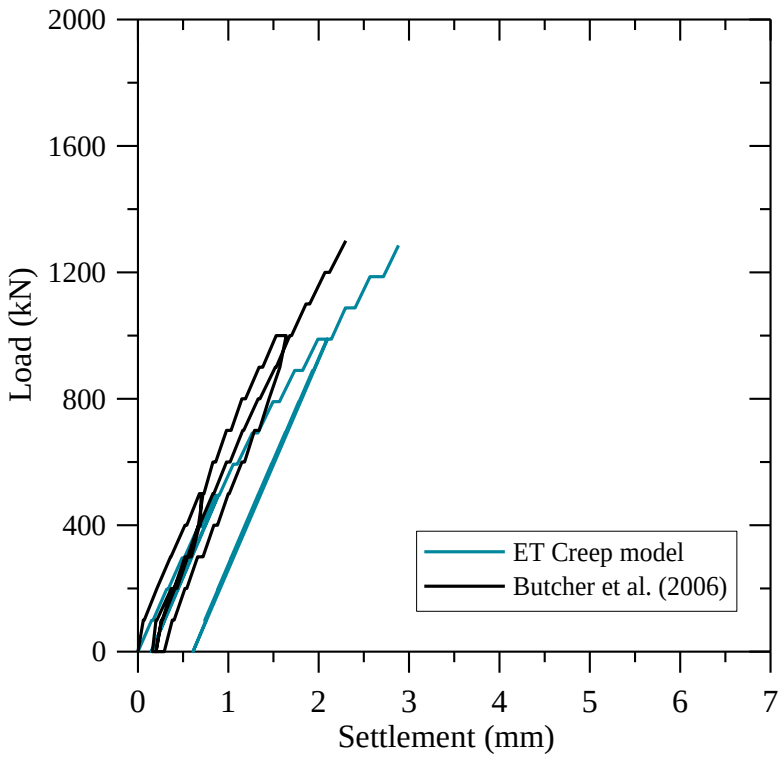


Figure 6.57: Comparison between the predicted and the documented (Burcher et al, 2006) load-settlement response of the pile tested in 2005

In Figure 6.58, the load-settlement response from a set of axi-symmetric finite element analyses of a single pile is presented, where the above effects are investigated. The single pile, the soil conditions and the boundary conditions are similar to those described in Section 6.4.5. Curve 1 represents the original conditions identified in Section 6.4.5, whereas Curve 2 represents the analysis with no reduced OCR and lateral stresses. Curve 3 represents the analysis with halved elapsed time between load steps compared to the original test. From Figure 6.58, the reduction in lateral stresses and in OCR (Curve 1 – original conditions) indicates a softer load-settlement response for the single pile than Curve 2. Also, a halved elapsed time between load steps (Curve 3) indicates a stiffer response than the original load-settlement Curve 1.

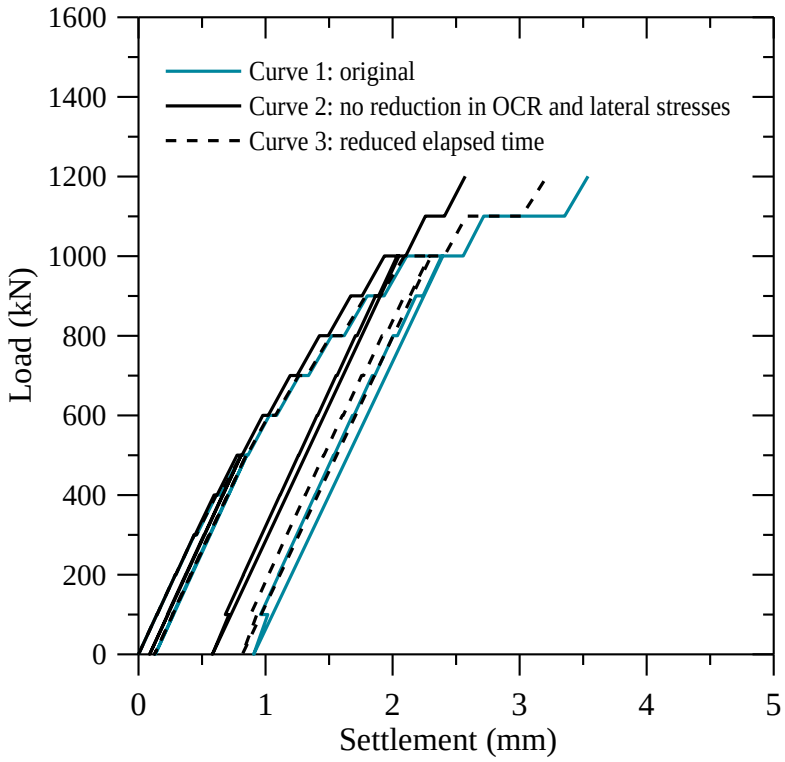


Figure 6.58: Comparison of the predicted load-settlement response of the pile testes in original conditions (Curve 1), with no reduced lateral stresses and OCR (Curve 2), and reduced elapsed time (Curve 3)

In Figure 6.59, the predicted load-settlement responses of the pile tested in 2005 (incremental load test - 3D analysis) and of the pile tested in 1972 (incremental and CRP load test - see section 6.4.5) is compared. This comparison highlights the significance of similar test procedures in pile load tests. Both simulations follow the pile load tests performed in the field and presented by Cooke et al. (1981) and Butcher et al. (2006), where different displacement rates were applied on the test piles.

At load levels lower than the load experienced from Hiscocks House (396 kN), the predicted load-settlement response of the 2005 test appears softer than the 1972 test. This would not be expected due to the unloading-reloading effect. However, the variation of the applied load rates between the 2005 and 1972 tests are considered to influence the pile response due to the rate effects encountered in the soils. In particular, in the 2005 test the pile is loaded up to 500 kN in five 1-hour increments, whereas in the 1972 test up to 540 kN in four 1-hour increments. Such difference in the applied load rates is considered to influence the development of strains with longer increments being associated with larger strains.

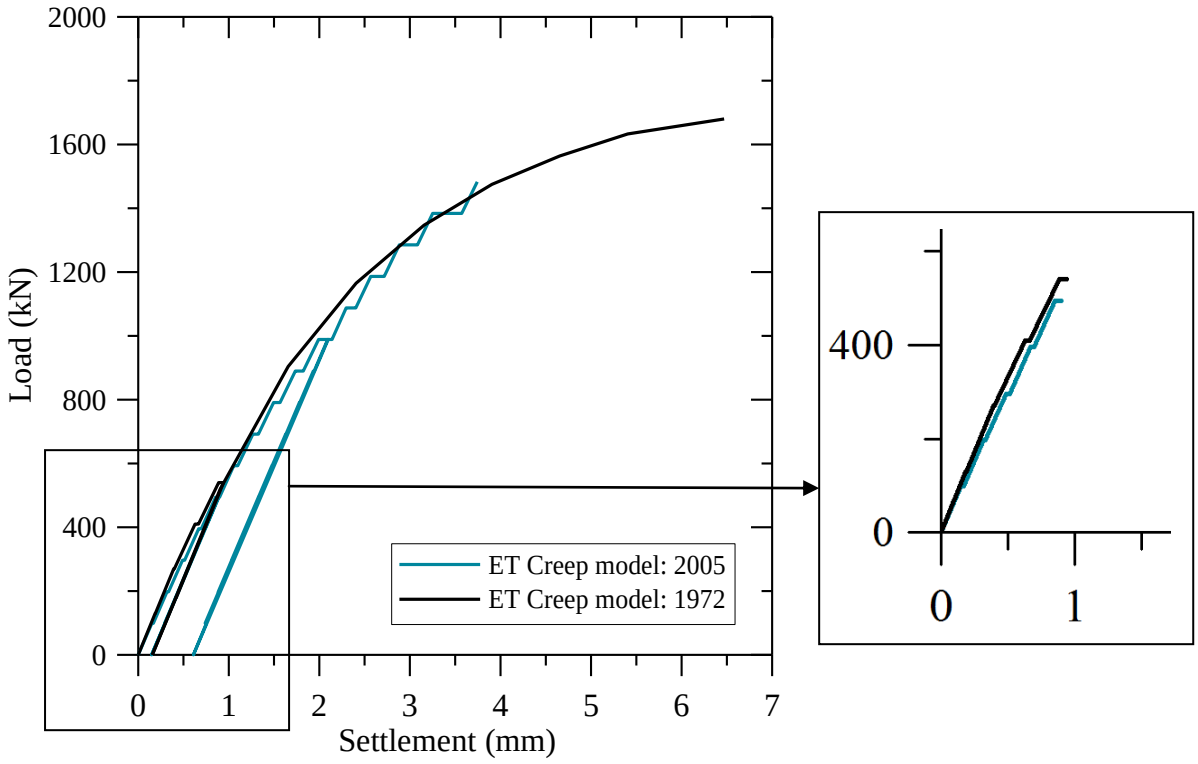


Figure 6.59: Predicted load-settlement response for pile load tests in 1972 and 2005

At higher levels of loading, when the load-settlement response of the static test in 2005 is compared with the CRP test in 1972 (Figure 6.59), a softer response is obtained up to a load level of 1000 kN, whereas for higher load levels a stiffer response is obtained. Once again, the applied load rates are influential. A CRP test is expected to give a stiffer response than a static test due to the higher displacement rate applied in the CRP test. This could compensate any creep or consolidation effects which result in stiffer responses, in particular for piles which are preloaded at low load levels where the effects of creep are limited. The fact that the recent test pile becomes stiffer at higher levels of loading may be attributed to the fact that numerically a higher K_o profile is prescribed around the pile in the 2005 test than in the 1972 test, in order to simulate the relief of later pressures during boring and the subsequent regain

in lateral stresses. Also, no effects of softening of the soil surrounding the pile are prescribed for the 2005 test.

In Figure 6.60, the load-settlement response of the two CRP pile load tests is plotted, from which the effect of sustained loading in the long term is observed. The rates applied in both tests are similar, therefore a valid assessment of the effects of time can be made. An almost negligible gain in capacity is observed in Figure 6.60. This is attributed to the fact that the piled raft foundation is settling as a block with the majority of support given by the base of the pile group. This has been observed in pile groups where the pile spacing is small. The block behaviour is also known to be enforced in the case where a ground contacting pile cap is employed even if quite large spacings are used. In the piled raft foundation, pile spacing is approximately 3.5D (D is the diameter of the pile), which is larger than the spacing of 2D to 3D suggested in most textbooks for piled foundations. However, it is considered that the effect of the raft on the piled raft foundation results in the observed block behaviour. It has been suggested that for piled raft foundations the critical pile spacing is larger that 4D. In addition, it should be acknowledged that the pile tested in axial loading fails individually with the shaft friction being mobilised, which is not the case when dealing with large pile groups behaving as a block unit. Also, the load level at which the pile has been preloaded (approximately 400 kN) is considered low in respect to the load capacity of the pile which is equal to approximately 2100 kN (based on the CRP test) resulting in limited creep strains.

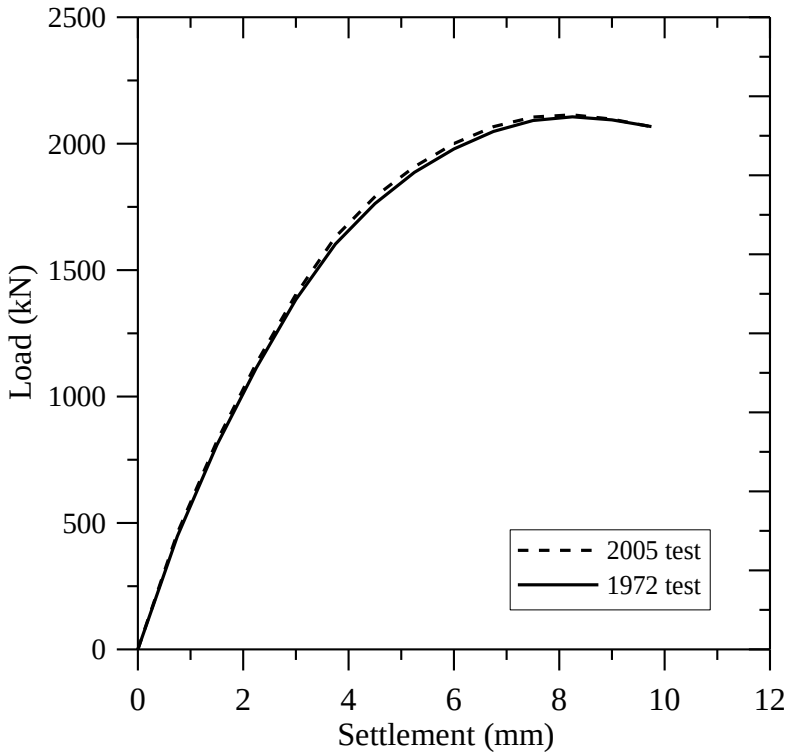


Figure 6.60: Predicted load-settlement response of a CRP test on a working pile in 1972 and in 2005

6.5. CONCLUDING REMARKS

An initial study of the short-term and long-term behaviour of single piles founded in soft clay and stiff clay ground conditions was performed from which it was concluded that consolidation effects do not enhance the long-term capacity of a preloaded friction pile. This is due to the concentration of excess pore water pressures below the pile base and the limited contribution of the pile base to the total load capacity of the friction pile. Creep in the soil surrounding the pile shaft is found to increase the shear strength of the soil due to the development of visco-plastic strains under a constant deviatoric stress. This results in increased shaft capacity with time. This is the case for both soft and stiff clays. In soft clays these effects are more evident than in stiff clays due to the larger development of viscoplastic strains in normally consolidated soils than in overconsolidated soils.

The enhancement of the load capacity is proportional to the level of preloading; the larger the preload, the larger the capacity enhancement. In stiff clays, there is a threshold level above which the enhancement of the load capacity drops associated with creep induced failure. It should be acknowledged that, despite the capacity enhancement with time at large levels of preloading, the limiting criterion in piled foundations is deformations rather than capacity.

Installation effects are not considered in the initial analysis and the single piles are assumed to be wished-in-place. A back-analysis of documented pile load tests from Heathrow and Stonebridge Park is performed in order to quantify the effects of installation, in particular of boring, on the surrounding soil. The model parameters of the ET Creep model for the lithological units in the London Clay are calibrated and validated with the documented results. Numerically, a "soft zone" around the pile shaft was discretised in order to quantify the reduction in the angle of interface friction due to the boring and the resulting softening. The relief of lateral pressures and the softening associated with the disturbance of the intact London Clay were also simulated. The angle of interface friction $\delta_{ult}{}'$ in the "soft zone" was back-analysed and it was found close to the residual angle of shear resistance.

The behaviour of a large piled raft foundation at Stonebridge Park designed conventionally was simulated by performing a 3D analysis. The results have been validated with the field observations of Cooke et al. (1981) for the foundation's performance. It has been validated that the foundation settles more towards the centre of the foundation with the minimum settlement being predicted and recorded at the corner. Respectively, the piles towards the periphery of the foundation attract more load than internal piles. This is also the case for the

contact stress between the raft and the soil; the maximum is at the corner and the minimum at the centre of the raft. The load share between the piles and the raft was also validated. The majority of the support is provided by the piles with the raft providing approximately 20 % of the total support, a typical value for a conventional piled raft.

The foundation is found to settle as a block unit, a common behaviour for pile groups with small spacing. This behaviour is enhanced by the presence of the raft. The majority of the settlement is accumulated at a depth level below the piles toe. Short- and medium-term settlement recordings are provided by Cooke et al. (1981), which are validated with the numerical results. A pile load test on a working pile after the demolition of the superstructure indicated insignificant enhancement of the pile stiffness and capacity. This is believed to be associated with the fact that the foundation is settling as a block with the majority of the resistance being provided by the piles base and not through shaft friction of each individual pile.

The significance of the rate effects in single pile load testing were revealed through the analysis of the recent pile load test after the demolition of the supported structure. Comparison between pile load tests should be for tests with similar loading rates. The comparison of the load-settlement response of a recent pile load test with the documented case indicates that processes other than creep and consolidation may affect the long-term behaviour of piles including changes at the soil-shaft interface and the time-dependent structuration of the soil surrounding the pile.

Chapter 7

Parametric Analyses of Piled Raft Foundations

7.1. INTRODUCTION

A series of 3D parametric finite element analyses was performed, in order to examine the reuse of piled raft foundations and optimise their design. The key design decisions for piled raft foundations are considered to be the raft thickness, the type of piles, the number of piles, the size of piles and their location underneath the raft. These design decisions shape the performance of the piled raft foundation and, therefore, the better they are, the more efficient and optimum the design is likely to be.

In this chapter, an initial study on a hypothetical piled raft foundation in London Clay is performed in order to assess the concept of locating piles in the central region of the raft. Three different foundations are examined: a raft foundation, a piled raft foundation with a uniform distribution of piles and a piled raft foundation with central pile support. The effect of preloading and the potential for increased load capacity are also assessed. Subsequently, optimisation of the performance of the piled raft foundation in Stonebridge Park is attempted by examining several pile arrangements, consistent with the findings from the literature review on piled raft foundations. In particular, the limitations of employing a raft foundation for Hiscocks House and the lack of cost-efficiency of the original design are demonstrated. A parametric study of the foundations of Hiscocks House is performed by varying the raft thickness, the number of piles and the pile length, as well as the pile geometry underneath the raft. Finally, the effects of time on the performance of the original piled raft foundation for Hiscocks House are examined.

7.2. HYPOTHETICAL PILED RAFT FOUNDATION IN LONDON CLAY

A parametric study of a hypothetical piled raft foundation is performed in order to assess whether a central support consisting of a limited number of piles underneath the raft is more beneficial than a uniform distribution of piles with more piles. Also, the effect of preloading on the piled raft behaviour for each parametric case is examined.

The number of piles, the geometry and the level of preloading are varied, in order to assess the most optimum solution in terms of differential settlement and the gain in load capacity. Three types of foundations are modelled: a raft foundation, a piled raft foundation with uniform distribution of piles and a piled raft foundation with piles centrally located under the raft. The raft is square with sides 20.0 m long and is 0.5 m thick. The raft is founded at 0.5 m depth. The uniform piled raft foundation consists of 25 piles uniformly distributed (12.5 m long with 0.5 m diameter), whereas the piled raft foundation with central support consists of 5 piles of similar dimensions centrally located under the raft.

7.2.1. Problem geometry and boundary conditions

The mesh created to perform the parametric analyses for the raft foundation problem is shown in Figure 7.1. The analysis is three-dimensional and the mesh domain is 50m x 50m x 40m in the X-Y-Z axes. The soil profile adopted for the analysis is the one identified for Stonebridge Park in Chapter 6 (see Figure 6.23). Only a ¼ of the problem is discretised into finite elements, due to the symmetry of the foundation around the X and Y axes. The mesh consists of 5096 20-noded hexahedral finite elements.

In Figure 7.2, a 3D view of the discretised (a) raft foundation, (b) uniform piled raft foundation, and (c) piled raft foundation with central pile support, is shown. The dimensions of the raft are 20.0 m by 20.0 m and, due to the symmetry, ¼ of the raft is discretised, i.e. 10.0 m by 10.0 m. Piles are 12.5 m long and 0.5 m in diameter, while the raft is 0.5 m thick. Both the piles and the raft are modelled as a linear elastic material representing the stiffness of concrete, where $E = 30 \times 10^6$ kPa and $\mu = 0.15$. Piles are installed on a square grid of 4.0 m distance centre to centre. A "soft zone" (see Figure 7.3), 5 cm thick, with a lower angle of shearing resistance, is discretised around the piles, in order to simulate the adhesion at the pile-soil interface.

The ET Creep model is employed to model the behaviour of London Clay units and of Lambeth Group, including the "soft zone" around the piles. The model parameters for each

soil layer are those set for Stonebridge Park in Chapter 6. The mesh consists of twenty noded isoparametric elements with eight pore pressures degrees of freedom at the corner nodes of the consolidating elements, and three displacement degrees of freedom at both corner and mid-side nodes of all elements.

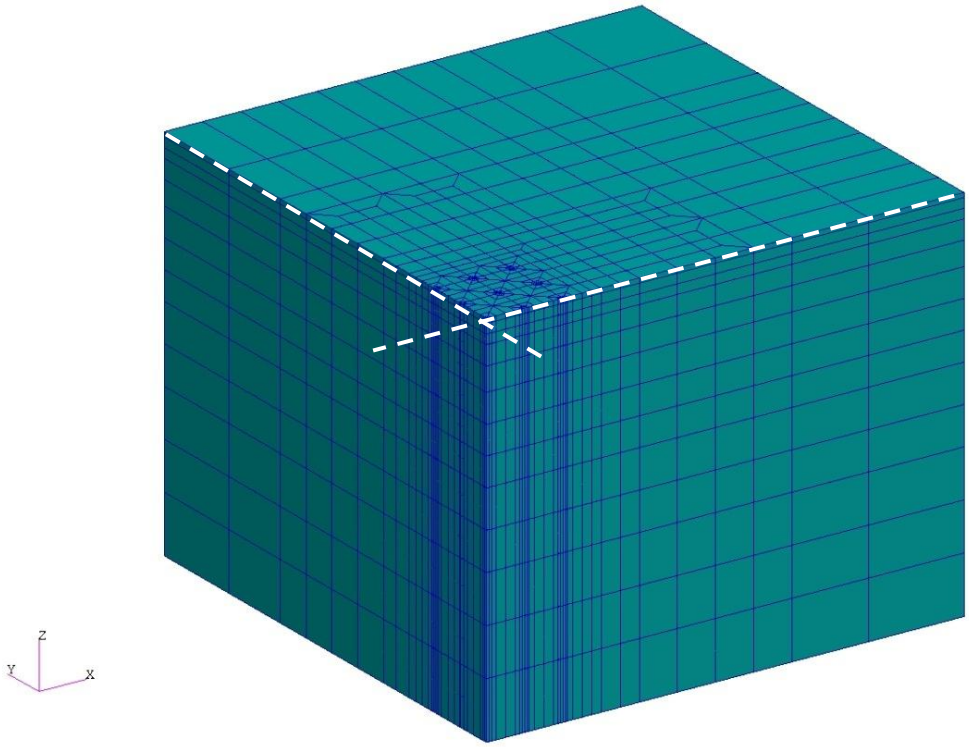


Figure 7.1: 3D mesh for hypothetical foundation problem

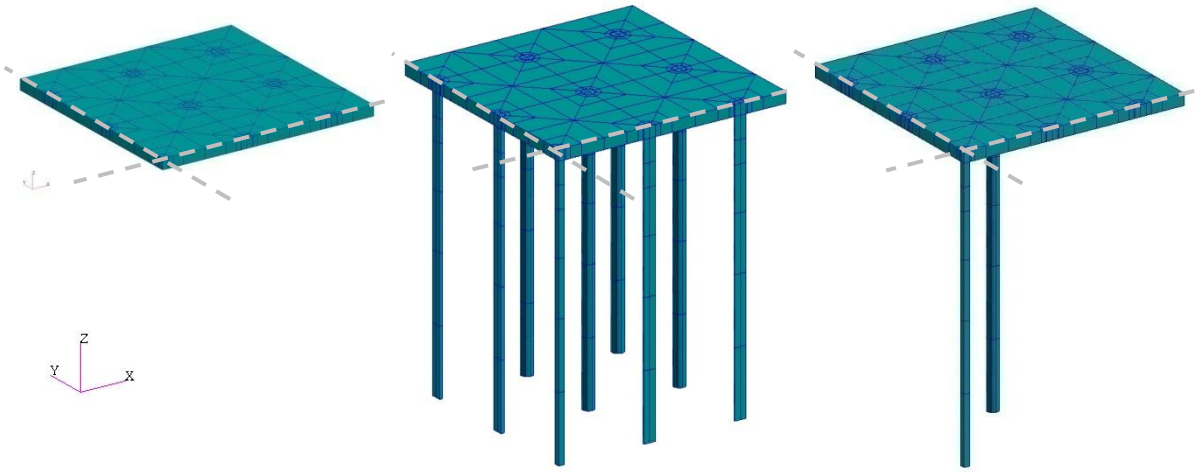


Figure 7.2: 3D view of the discretised (a) raft foundation, (b) uniform piled raft foundation, and (c) piled raft foundation with central pile support

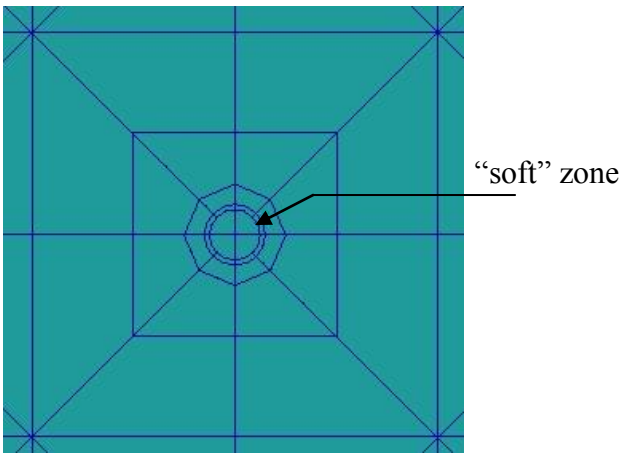


Figure 7.3: Plan view of piles detail of hypothetical piled foundations

The applied displacement boundary conditions prevent the base of the mesh from moving in the vertical (Z direction) and horizontal directions (X and Y directions), while the vertical sides of the mesh, whose face is not on one of the planes of symmetry, are fixed in the horizontal directions and can move in the vertical direction only. Regarding the boundaries forming the planes of symmetry, their vertical sides are fixed in the horizontal direction normal to the plane of symmetry, i.e. the X-Z boundary is fixed in the Y direction and the Y-Z boundary in the X direction, whereas they are free to move in the remaining directions.

The analysis is coupled with consolidation taking place during the analysis. The hydraulic boundary conditions applied allow no flow of water through the planes of symmetry and the ground surface, while on the base of the mesh and the remaining vertical planes, pore pressures are maintained equal to their initial values, as determined by the water table 3.5 m below ground level. The permeability for each soil layer is that set for Stonebridge Park in Chapter 6.

7.2.2. Description of analyses

A series of 3D parametric finite element analyses is performed on a hypothetical (a) raft foundation, (b) uniform piled raft foundation and (c) piled raft foundation with central pile support. The development of settlement and the effect of preloading are assessed. The soil profile employed for the analyses is London Clay and in particular the soil profile at Stonebridge Park. The finite element analysis follows the construction sequence of a typical development, with an initial 100 years of elapsed time in order to make sure there is no discrepancy between the initial under-drained pore water pressure profile and the permeabilities assumed (see Chapter 6).

After the initial 100 years period of elapsed time, the construction of the piled raft foundation follows, including pile installation (for piled foundations), excavation and construction of the raft. The installation of the piles is achieved by changing the material properties of the elements forming the piles from soil to concrete. At the same time, a "soft zone" around the piles is simulated by also changing the material properties of the elements forming the "soft zone" and assigning a lower angle of shearing resistance, as determined in Chapter 6.

The excavation of the raft, founded at a depth of 0.5 m below the ground level, follows. It takes 3 months to complete, whereas the subsequent construction of the raft lasts for a month. The excavation of the raft, numerically, is simulated by removing the elements from the finite element mesh. The subsequent construction of the raft, 0.5 m thick, takes place on top of the excavation boundary over one increment with an elapsed time of 1 month; the raft is modelled with the material properties of concrete, as described above.

The loading from the structure is followed, which is simulated through the application of uniform boundary stresses on top of the raft, from which the respective displacements are calculated. All foundations are initially loaded up to failure at a constant rate of 0.65 kPa/day in order to obtain their load capacity. The failure criterion applied, due to the nature of the analyses and the employment of the ET Creep model, is set as equal to 700 kN per mm of maximum displacement.

A series of analyses is followed in order to determine the effect of preloading on the total load capacity of the foundation. In particular, the foundations are preloaded for a period of 50 years at different total load levels. The preloading period of 50 years is simulated through the application of elapsed time increments. After the 50 years period, the foundations are reloaded in order to determine the new total load capacity by applying boundary stresses. Loading rates are maintained equal to the initial loading rate.

7.2.3. Results and discussion

The results of the parametric analyses of the different foundation solutions are presented, allowing the assessment of central pile support on the performance of a piled raft foundation. Initially, the load-settlement response of each foundation type up to failure is presented along with contours of settlement in order to determine the differential settlement for each foundation type. Subsequently, the effect of preloading for each foundation type for a period of 50 years is assessed, allowing the determination of the possible enhancement of the overall capacity of a reused piled raft foundation.

In Figure 7.4, the predicted ***load-settlement response*** of each foundation type in the centre of the raft up to the failure load (as identified above) is presented. It is evident that the addition of piles enhances the overall stiffness of the foundation. The raft foundation gives the softest response, whereas the piled raft foundation with 25 piles gives the stiffest response. This indicates that the required settlement may be obtained by varying the number of piles (or total pile length). Also, the contribution of the piles to the overall load capacity is limited in respect to the contribution of the raft. This is observed by the limited capacity increase, due to the addition of 5 and 25 piles respectively, in the load-settlement curves in Figure 7.4.

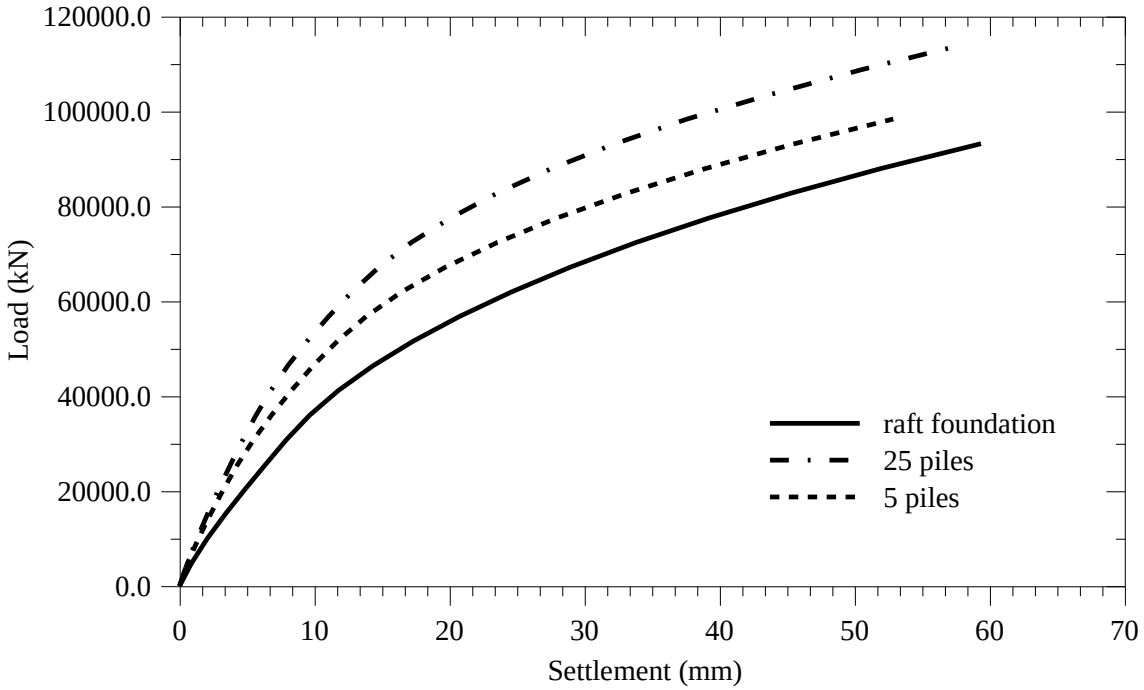


Figure 7.4: Load-settlement response of hypothetical foundations up to failure load

In Figures 7.5 and 7.6, ***the load on piles and their load share*** to the overall piled raft foundation resistance at different applied load levels is presented for both the piled raft foundations with 25 and 5 piles. The resistance provided by the piled raft foundation with 25 piles is larger than the resistance provided by the piled raft foundation with 5 piles. For the case with the 25 piles, for low levels of applied load, the piles resistance increases up to an applied load level where the piles resistance is fully mobilised. After the peak resistance of the piles, the total pile resistance reduces marginally with increasing applied load, demonstrating the possibility of small amount of 'undrained' post-peak softening behaviour of London Clay. For the case with 5 piles, due to the limited number of piles, the capacity of the piles mobilises at much smaller applied load levels, as shown in Figure 7.5.

Regarding the load share of the piles to the overall resistance of the piled raft foundation, the load share of the piled raft with 25 piles is larger than the load share of the piled raft with 5 piles. For the 25 piles, the load share is increasing with increasing applied load up to the full mobilisation of the piles load capacity, from which point the load share starts reducing. For the 5 piles, the load share is reducing with increasing applied load, demonstrating that the piles load capacity is already mobilised at the applied load levels examined.

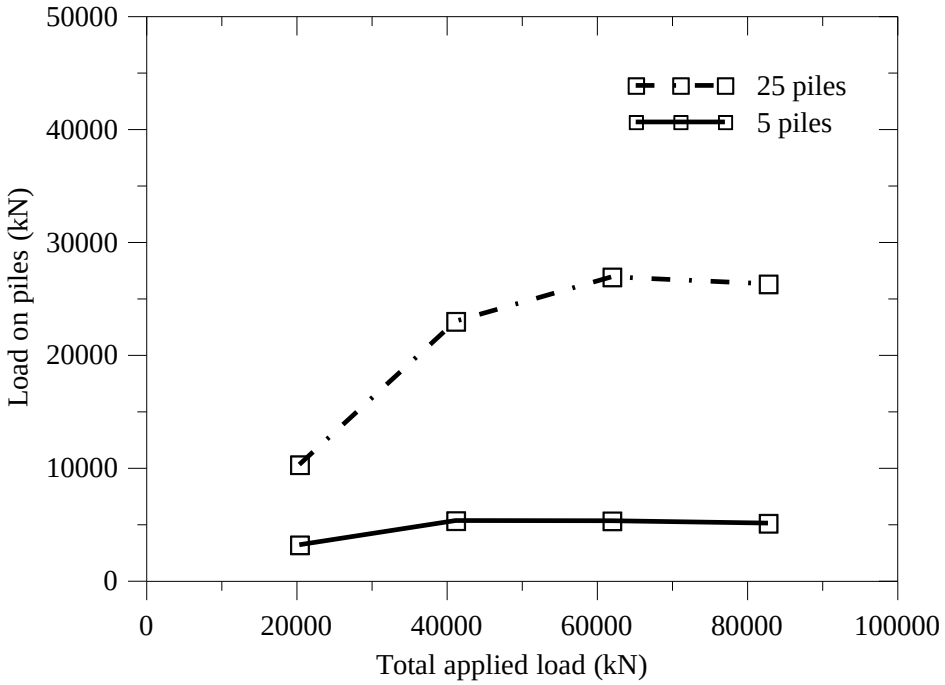


Figure 7.5: Load on piles for piled raft foundations with 25 and 5 piles

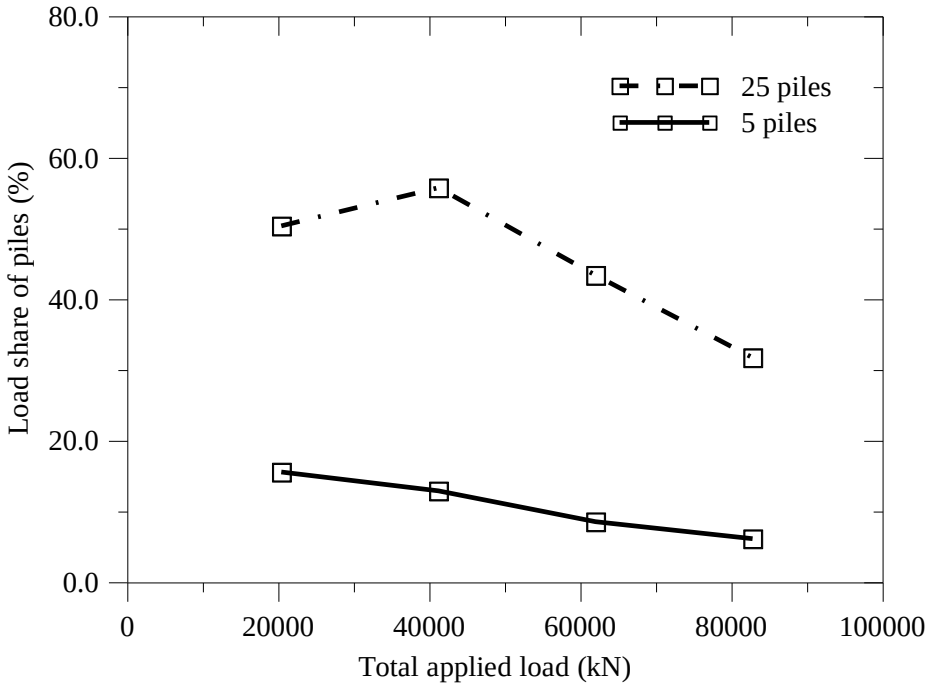


Figure 7.6: Load share of piles for piled raft foundations with 25 and 5 piles

In Figure 7.7, ***contours of settlement*** are presented for the three foundations examined in this set of analyses. Contours are plotted at a level of total load of 41.2 MN. Contours of settlement indicate that, unlike the piled raft foundation in Stonebridge Park (see Chapter 6), the piled raft foundation with the 25 piles uniformly, distributed at a larger distance between piles, mobilises the shaft capacity of the piles and a block settlement behaviour is avoided, improving the efficiency of the individual piles. This is visualised by the contours of settlement in Figure 7.7(b) where the soil around the piles is dragged down by the piles and, as a result, the shaft friction is mobilised. This is attributed to the large spacing (=8.0d) applied in this foundation, which is greater than the pile spacing in the piled raft foundation of Hiscocks House (=3.5d).

In Figure 7.8, contours of settlement at the raft level are presented for all parametric cases at a load level of 41.2 MN (a) at zero elapsed time after the application of the last load increment (short term) and (b) after 50 years of consolidation and creep respectively (long term).

Regarding the settlement contours of the raft foundation plotted in Figures 7.8(a) and 7.8(b), the minimum settlement at zero elapsed time is in the corner (6.1 mm) and the maximum settlement is in the centre of the raft (11.4 mm). After 50 years of consolidation and creep, the minimum settlement in the corner of the raft is equal to 130.0 mm and the maximum settlement in the centre is equal to 185.0 mm. The predicted settlements indicate that the raft foundation is sagging in the centre with an initial differential settlement centre-to-corner at zero elapsed time equal to 5.3 mm increasing to 55.0 mm after 50 years of consolidation and creep.

In Figures 7.8(c) and 7.8(d), settlement contours of the piled raft foundation with 25 piles uniformly distributed are plotted. The minimum settlement at zero elapsed time is in the corner of the raft and is equal to 5.0 mm, whereas the maximum settlement in the centre is equal to 7.1 mm. The piled raft foundation is sagging in the centre with a differential settlement centre-to-corner equal to 2.1 mm. In the long-term, after 50 years of consolidation and creep, the minimum settlement on the raft is equal to 87.0 mm and the maximum 94.6 mm, giving a differential settlement of 7.6 mm. The significant reduction of the differential settlement in respect to the raft foundation in the short term from 5.3 mm to 2.1 mm and in the long term from to 55.0 mm to 7.6 mm is attributed to the addition of piles and demonstrates the significant contribution of the piles in reducing settlement.

Regarding the settlement contours in Figures 7.8(e) and 7.8(f) for the piled raft foundation with the 5 piles centrally located, it is observed that at zero elapsed time a non-uniform

distribution of the settlement profile from corner-to-centre is obtained, unlike the raft foundation and the piled raft foundation with the 25 piles uniformly distributed. In particular, as shown in Figure 7.8(e) the piled raft in the corner has a settlement of 7.3 mm and the settlement is increasing towards the centre of the piled raft up to the region where the piles are included. Piles in the central region of the raft reduce the local settlement resulting in hogging. Settlement in the centre of the piled raft is equal to 8.2 mm, giving a differential settlement centre-to-corner of the piled raft equal to 0.9 mm. This differential settlement is smaller than the one predicted for the piled raft foundation with 25 piles uniformly distributed, despite the fact that absolute settlements for the piled raft foundation with 5 piles centrally located are larger. This demonstrates that in the short term locating piles in the central region is more efficient in reducing differential settlements than uniformly distributed piles.

Regarding the settlement contours in the long term in Figure 7.8(f), a different picture to that in the short term is obtained. No hogging is observed in the raft; minimum settlement is in the corner (129.0 mm) and maximum settlement in the centre (153.0 mm) of the raft. Differential settlement centre-to-corner is equal to 24.0 mm. This is attributed to creep, where creep deformations in the long term result in increased settlement of the piles. Creep is significant on the piles due to the increased loading on the piles, which mobilises the full load capacity of the 5 piles. It has been shown in Chapter 6 that at high levels of preloading significant creep deformations are induced. The small number of piles in the piled raft foundation indicates that the primary function of piles is to reduce settlement rather than to provide load capacity. However, the fact that they are loaded up to their ultimate load capacity results in increased deformations with time due to creep, reducing their efficiency in reducing settlements. This is also the case for the uniform piled raft with 25 piles, where the piles are loaded close to their ultimate load capacity (see Figure 7.5), however this is not shown in the results due to the uniform distribution of the piles. Therefore, it may be concluded that depending on the level of the piles shaft friction mobilisation, the benefits observed in the short term in piles centrally located may reduce in the long term.

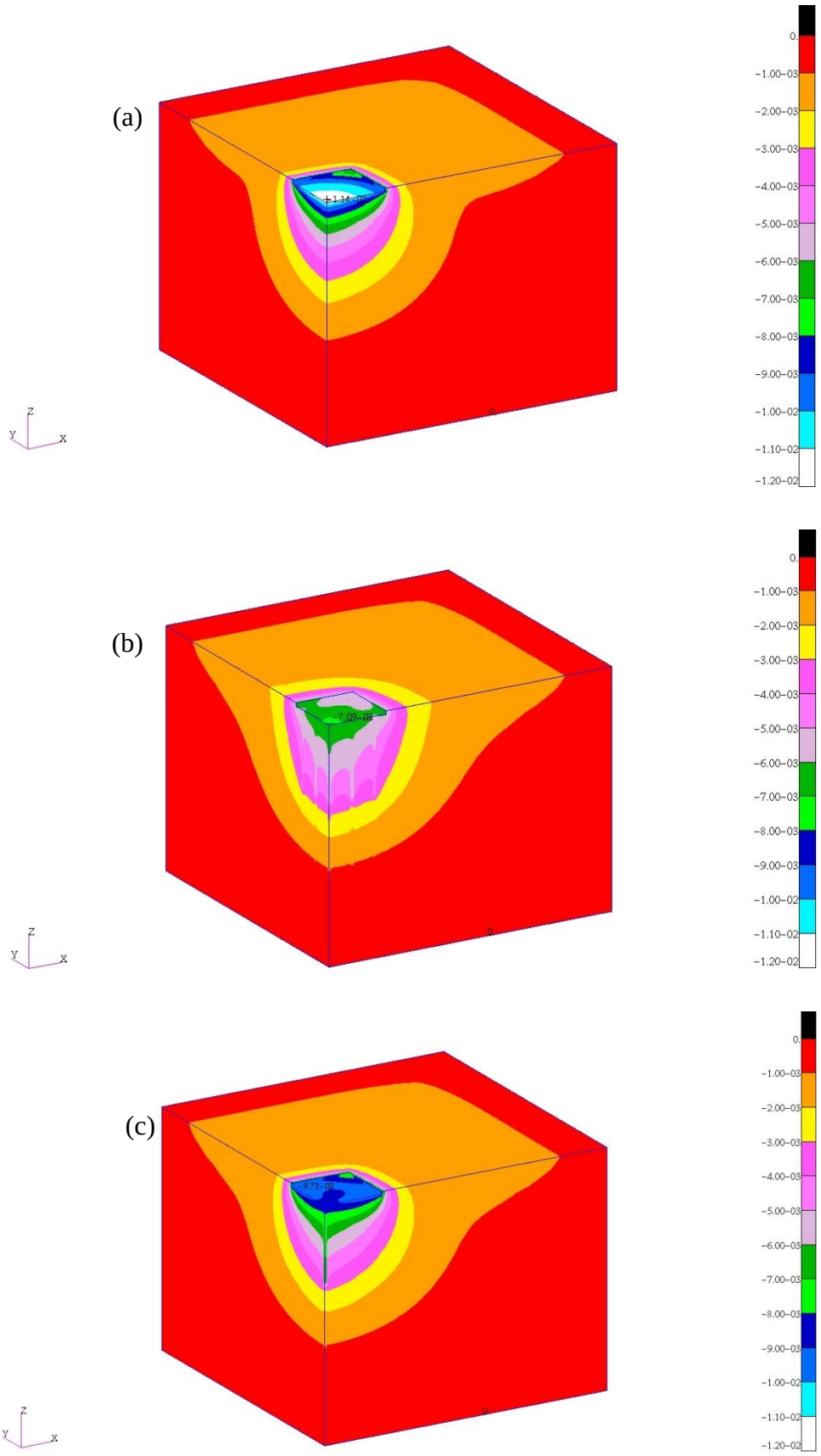


Figure 7.7: Contours of settlement at a load level of 41.2 MN for the (a) raft foundation, (b) piled raft foundation with 25 piles, and (c) piled raft foundation with 5 piles (units in m)

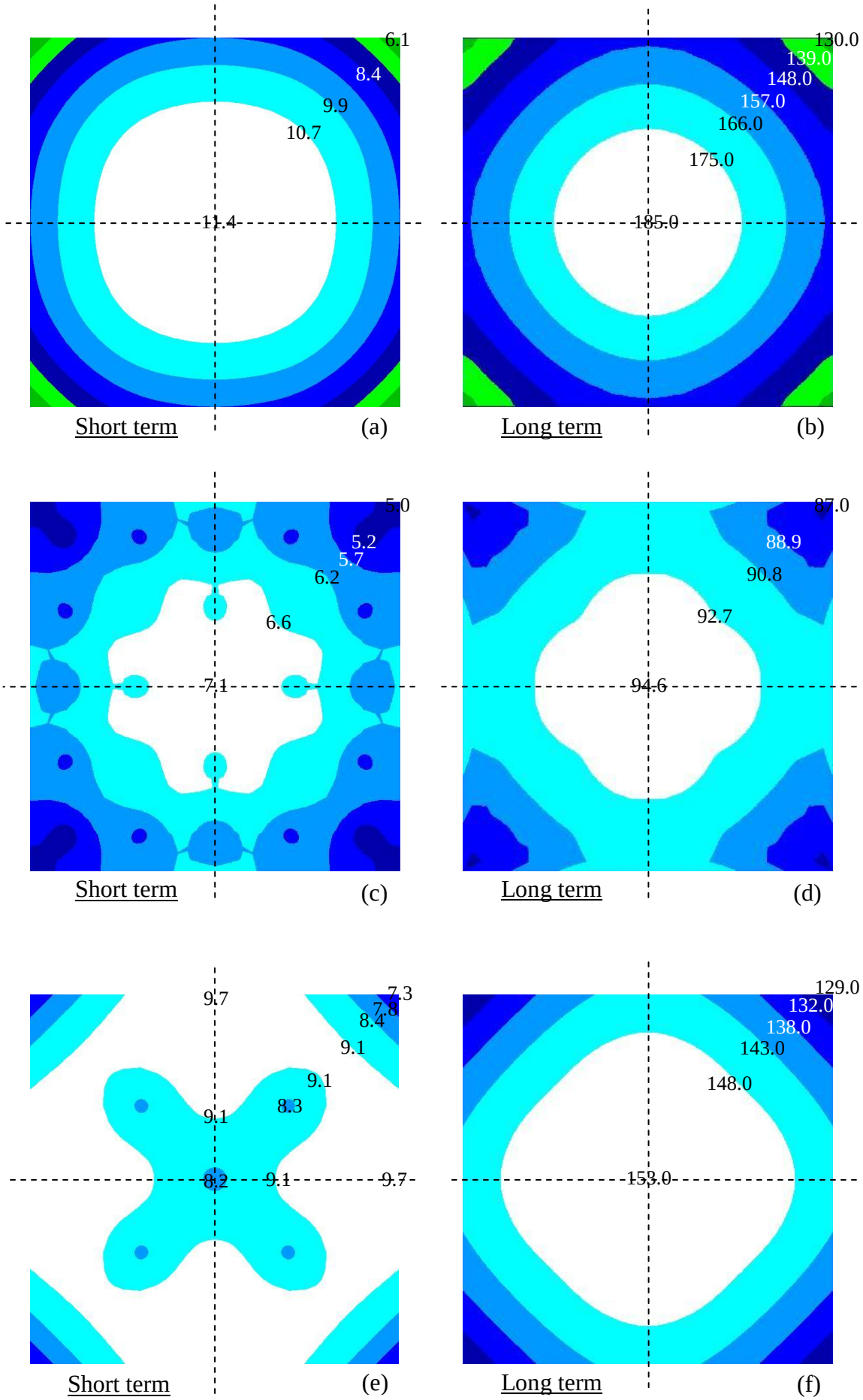


Figure 7.8: Contours of settlement at a load level of 41.2 MN for the (a-b) raft foundation (c-d) piled raft foundation with 25 piles, and (e-f) piled raft foundation with 5 piles (units in mm)

In Figures 7.9 to 7.11, the ***effect of preloading*** on the overall load capacity of the parametric cases examined is presented. In particular, the load-settlement response for (a) the un-piled raft foundation, (b) the piled raft foundation with 25 piles uniformly distributed and (c) the piled raft foundation with 5 piles centrally located under the raft for a preloading of 50 years at different levels of preloading is presented. A gain in capacity depending on the level of preloading is determined for each type of foundation. Also, the settlement during the 50 years period of elapsed time is proportional to the level of preloading; the larger the applied load, the larger the settlement. Settlement is due to consolidation and creep.

In Figure 7.12, the normalised gain in the overall load capacity of each foundation type at different levels of preloading of 50 years is plotted. The results show that there is a significant increase in the overall load capacity of the foundations. The effects of time are more significant at higher levels of preloading. It is also evident that the gain in capacity for the un-piled raft is larger than the gain in capacity for the piled rafts. For instance, at a working load level of 41.2 MN, the gain in capacity is equal to 22.3, 15.9 and 10.0 % for the un-piled raft, the piled raft with 5 piles and the piled raft with 25 piles respectively. It should be noted that at this level of preloading the shaft resistance of the piles is fully mobilised. Such a fact indicates that the gain in capacity is attributed mainly to the capacity provided by the raft foundation, since it has already been shown that at high levels of preloading piles in stiff clays, such as London Clay, lose their potential for increased load capacity (see section 6.2).

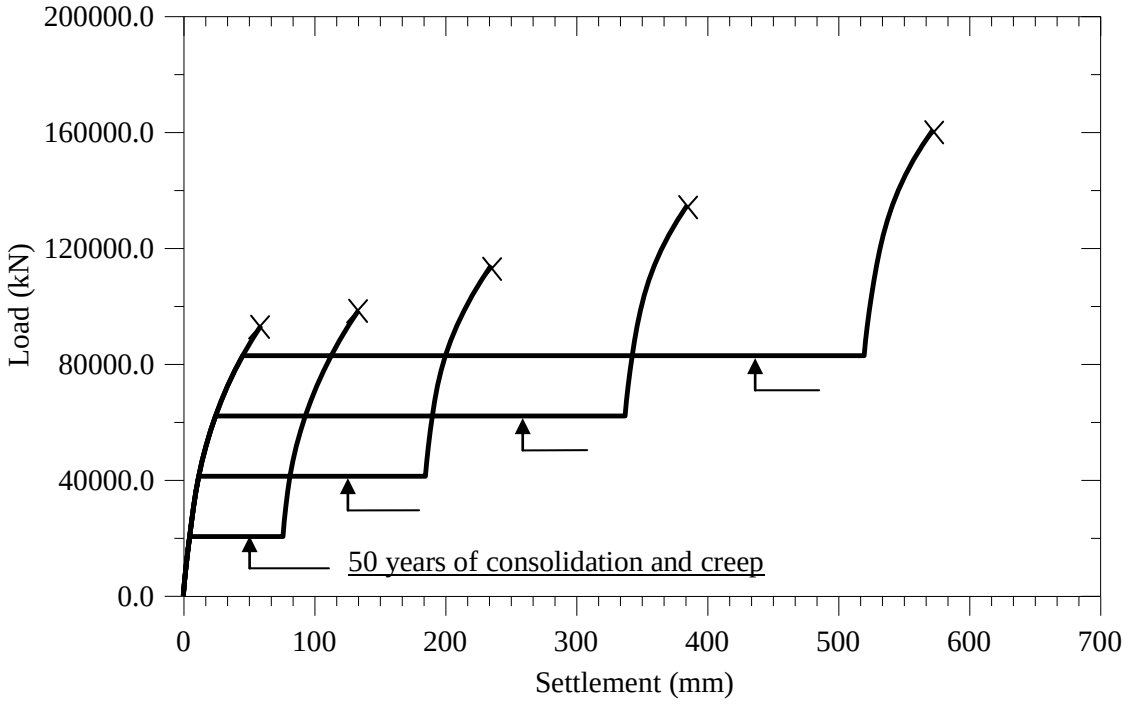


Figure 7.9: Load-settlement response for different levels of preloading for raft foundation

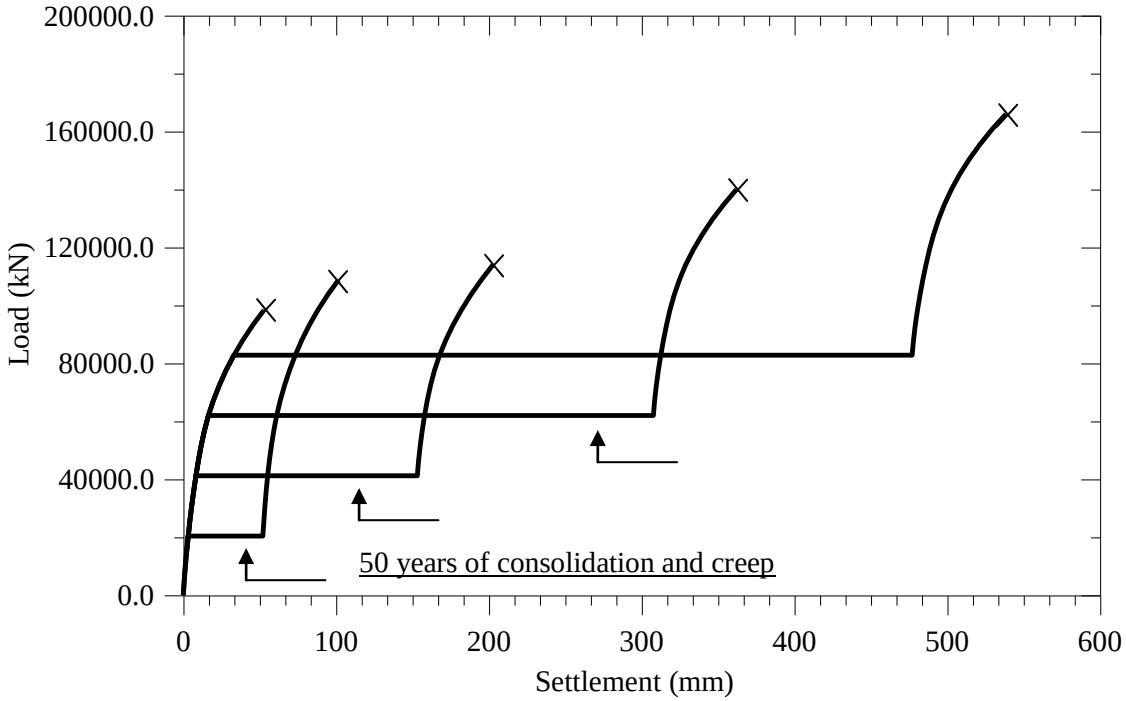


Figure 7.10: Load-settlement response for different levels of preloading for piled raft foundation with 25 piles uniformly distributed

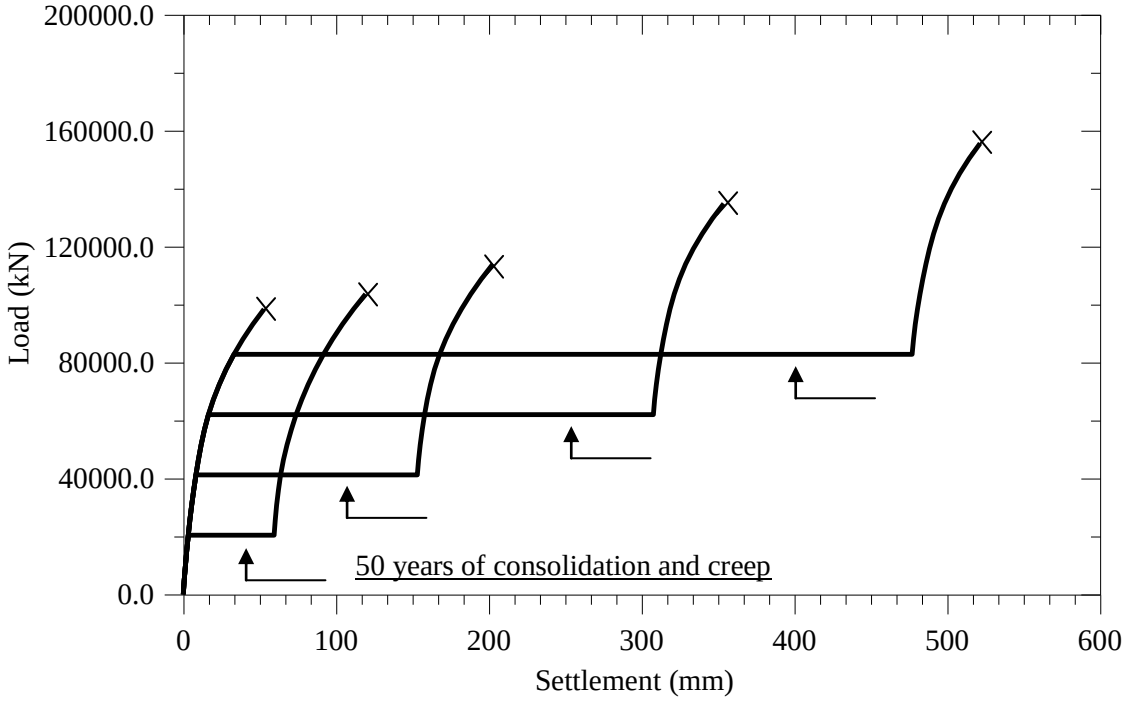


Figure 7.11: Load-settlement response for different levels of preloading for piled raft foundation with 5 piles in the central region of the raft

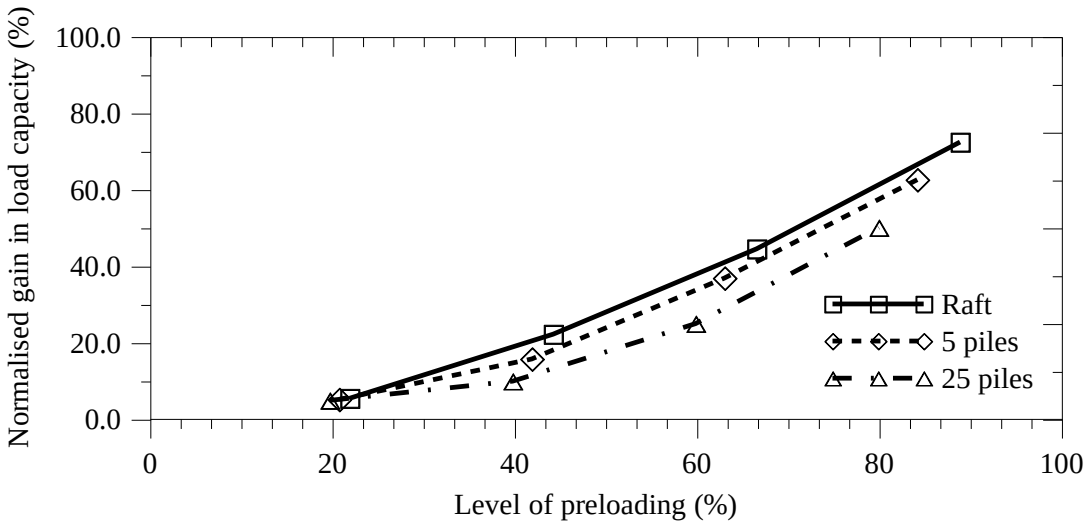


Figure 7.12: Gain in overall load capacity after 50 years of preloading for the raft foundation, the piled raft foundation with 25 piles and the piled raft foundation with 5 piles

7.3. OPTIMISED FOUNDATION DESIGN OF HISCOCKS HOUSE

In the literature, it has been shown that the foundation design of Hiscocks House in Stonebridge Park is conservative (see Chapter 2). The foundations fall into the category of conventional piled raft foundations, where the foundations are designed essentially as a conventional pile group, however some allowance is made for the contribution of the raft to the foundation performance, primarily in terms of ultimate load capacity. Such foundation design has been shown not to be cost-efficient and significant savings could be made, if less piles located centrally underneath the raft were installed.

In the following, an attempt is made to optimise the foundations of Hiscocks House by employing the time dependent ET Creep model validated in Chapter 5 and 6. The process followed is the one described in Chapter 2 for the effective choice of foundation type. Initially, the performance of a raft foundation alone, without piles, is assessed, in order to determine whether a raft foundation alone is sufficient to provide support and keep settlements within the design limits. Although in practice, bending stress in the raft due to concentrated loading from columns can be an issue, in this case study uniform loading from Hiscocks House on the raft is assumed. It is expected that the raft alone provides sufficient load capacity with settlements though being excessive. Such performance has been recorded in the literature for raft foundations in stiff clays (see Chapter 2), and this remains to be confirmed in the following.

Then, focus turns on piled raft foundations. The original design of the foundations of Hiscocks House is assessed in terms of load capacity and settlements. Then, the conceptual design process as identified in Chapter 2 is followed, in order to adopt an efficient type of piled raft foundation. Different piled raft foundations are employed numerically ranging from the conventional design to settlement reducing approaches, in order to obtain an optimum design. Generally, it is known that if the raft alone provides only a small proportion of the required load capacity ('small' raft), then the conventional approach is most feasible to adopt. On the other hand, if enough load capacity is provided ('large' raft), but at the same time settlements exceed the design limits, then the settlement reducing approaches may be adopted. It remains to validate this in the following by the employment of the time dependent ET Creep model, which is able to reproduce the time dependent behaviour of soils.

Design criteria have been described by several authors, including Skempton and MacDonald (1956), Bjerrum (1963), Burland and Wroth (1974), Burland et al. (1977), etc. It is recognised that settlements, and in particular differential settlement resulting in angular distortion β and deflection ratio Δ/L (see Figure 7.13), are the limiting criteria rather than bearing capacity. This is due to the fact that serviceability limits, including cracking and overstressing of the structure, are usually reached well before bearing capacity failure. The angular distortion between two points is equal to the differential settlement between two points divided by the distance between them, i.e. $\beta_{max} = \Delta_{max} / L_{AC}$ in Figure 7.13.

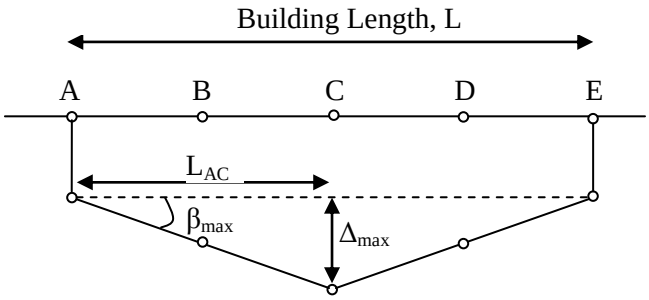


Figure 7.13: Definitions of foundation movement

In Tables 7.1 and 7.2, commonly adopted limits given by the Institution of Structural Engineers (1989) and by Bjerrum (1963) respectively for angular distortion are presented. The empirical limit suggested for angular distortion affecting serviceability of framed buildings is 1/500, whereas severe structural damage is recognised to occur if the angular distortion is larger than 1/150. Design limits are known to vary depending on the structural stiffness and the maximum tensile strain of structural materials. Absolute settlements are recognised not to be responsible for damage in structures, however large settlements (ρ > 150 mm) may cause

damage in facility connections (drains, gas pipelines, etc.). Tilting resulting from the non-uniformity of the supporting soil is another criterion, which may affect mainly the visual appearance of the building. However, it is recognised that in the finite element simulation non-uniformities are not reproduced. Last, regarding the factor of safety against bearing capacity failure, it is conventionally set between 2 to 3, with the latter value being adopted if limited information about the ground is available.

	Skempton & MacDonald (1956)	Meyerhof (1956)	Polshin & Tokar (1957)	Bjerrum (1963)
Structural damage	1/150	1/250	1/200	1/150
Cracking in walls and partitions	1/300 (but 1/500 recommended)	1/500	1/500	1/500

Table 7.1: Summary of limiting values of angular distortion for framed buildings and reinforced load bearing walls (Institution of Structural Engineers, 1989)

Structural situation	Angular distortion limit
Difficulties with machines sensitive to settlement	1/750
Overstressing of structural frames with diagonals	1/600
Limit for buildings in which cracking is not permissible	1/500
Cracking in panel walls expected	1/300
Tilting of high rigid buildings noticeable	1/250
Structural damage of general buildings expected	1/150

Table 7.2: Angular distortion limits after Bjerrum (1963)

7.3.1. DESIGN OF RAFT FOUNDATION: parametric study of raft thickness

A parametric study of raft thickness on the behaviour of a raft foundation designed to support Hiscocks House is performed, in order to examine whether a raft solution is feasible for the foundations of Hiscocks House. The original raft thickness of 0.9 m and two raft thicknesses of 1.5 m and 2.5 m are employed, in order to assess whether a raft foundation solution would be feasible.

7.3.1.1. Problem geometry and boundary conditions

The mesh created to run the parametric analyses for the raft foundation problem is shown in Figure 7.14. The analysis is three-dimensional and the mesh domain is 100m x 50m x 40m in the X-Y-Z axes respectively. The soil profile adopted for the analysis is the one identified for Stonebridge Park in Chapter 6 (see Figure 6.23). A ¼ of the problem is discretised into finite elements, due to the symmetry of the foundation around the X and Y axes. The mesh consists of 11904 20-noded hexahedral finite elements.

In Figure 7.15, a 3D view of the discretised raft foundation (0.9 m thick case) is shown. The dimensions of the raft are 43.3 m by 19.2 m and, due to the symmetry, ¼ of the raft is discretised, i.e. 21.65 m by 9.6 m. The thickness of the raft is 0.9 m, 1.5 m and 2.5 m for each parametric analysis respectively. The raft is modelled as a linear elastic concrete material, with E = 30×10^6 kPa and μ= 0.15.

The ET Creep model is employed to simulate the behaviour of the London Clay units and of the Lambeth Group. Model parameters for each soil layer are set in Chapter 6. The mesh consists of twenty noded isoparametric elements with eight pore pressures degrees of freedom at the corner nodes of the consolidating elements, and three displacement degrees of freedom at both corner and mid-side nodes for all elements.

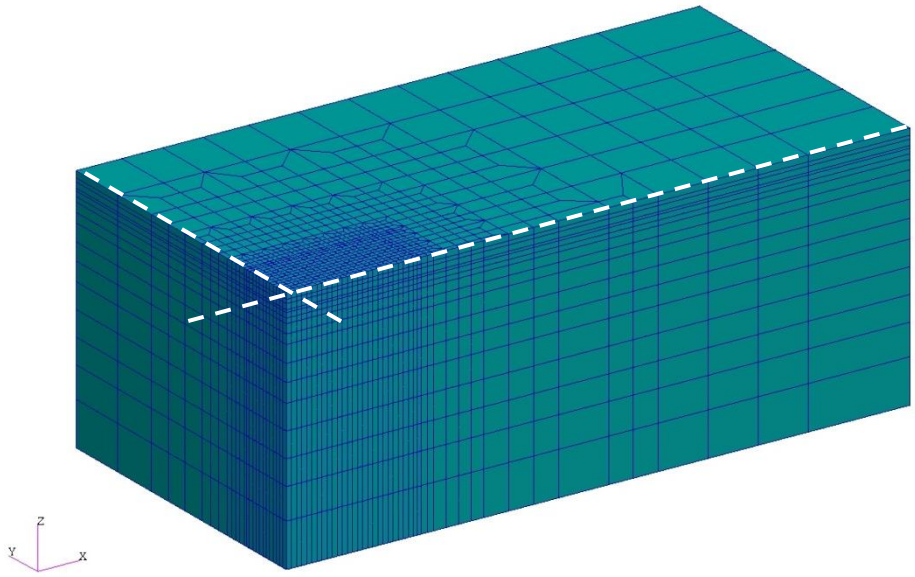


Figure 7.14: 3D mesh for the raft foundation

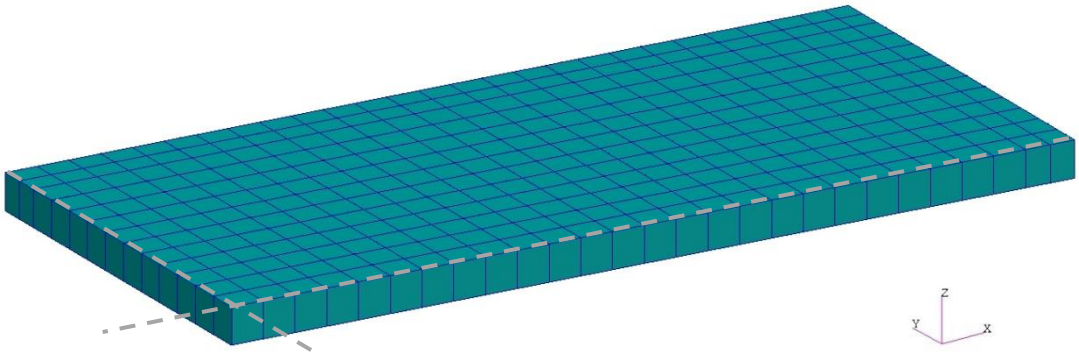


Figure 7.15: 3D view of the raft foundation (0.9 m thick case)

The applied displacement boundary conditions prevent the base of the mesh from moving in the vertical (Z direction) and horizontal directions (X and Y directions), while the vertical sides of the mesh, whose face is not a plane of symmetry, are fixed in the horizontal directions and can move in the vertical direction only. Regarding the boundaries forming planes of symmetry, their vertical sides are fixed in the horizontal direction normal to the plane of symmetry, i.e. the X-Z boundary is fixed in the Y direction and the Y-Z boundary in the X direction, whereas they are free to move in the remaining directions.

The analysis is coupled with consolidation taking place during the analysis. The hydraulic boundary conditions applied prevented flow of water across the planes of symmetry and the ground surface, while at the base of the mesh and the remaining vertical planes, pore pressures are maintained equal to their initial values, as determined by the water table 3.5 m below ground level.

7.3.1.2. Description of analysis

A 3D finite element analysis is performed, in order to assess the performance of a raft foundation for Hiscocks House. The analysis is parametric, with the varying parameter being the raft thickness. The finite element analysis follows the construction sequence of Hiscocks House, with an initial 100 years of elapsed time in order to make sure there is no discrepancy between the initial under-drained pore water pressure profile and the permeabilities assumed.

After the initial 100 years period of elapsed time, the finite element analysis follows mainly the construction programme of the original Hiscocks House, as described by Cooke et al. (1981), without including the installation of piles. The excavation of the raft, which is founded at a depth of 2.5 m below ground level, takes 3 months to complete, and the

subsequent construction of the raft lasts for a month. The excavation of the raft, numerically, is simulated by removing the elements from the finite element mesh and applying, in increments, nodal forces on the element nodes of the new boundary. The subsequent construction of the raft, 0.9 m, 1.5 m and 2.5 m thick depending on the analysis, takes place on top of the excavation boundary in one increment with an elapsed time of 1 month. The raft is modelled with the material properties of concrete, as described above.

Loading from the structure is followed, which is simulated through the application of uniform boundary stresses on top of the raft, from which the respective displacements are calculated. The increments of loading are equivalent to those employed for the original piled raft foundation in Chapter 6. All parametric cases are loaded up to the building load level, in order to examine the response of the raft at working conditions and assess its performance. Additionally, for the original raft thickness of 0.9 m, the analysis continues up to bearing capacity failure, in order to determine the factor of safety against bearing failure. The failure criterion applied is set as equal to 700 kN per mm of maximum displacement.

Finally, a period of elapsed time of 30 years is employed in the analysis, in order to determine the development of settlements with time. Increments of elapsed time are prescribed in the analysis during which consolidation and creep takes place due to the coupled nature of the analysis.

7.3.1.3. Results and discussion

The results of the parametric analysis of a raft foundation with a varying raft thickness, employed to provide support to Hiscocks House, are presented. This allows the assessment of the feasibility to adopt a raft foundation as a foundation solution for Hiscocks House. Initially, the results for the analysis of the raft foundation with the original raft thickness are presented, including bearing capacity and settlements, both absolute and differential. Subsequently, the results in terms of differential settlement for a varying raft thickness are presented, where the rigidity of the raft is assessed.

The ***factor of safety*** against bearing capacity failure is calculated in order assess whether a raft foundation solution would provide enough load capacity to Hiscocks House, and whether the raft is a ‘large’ or ‘small’ raft. In Figure 7.16, the load-settlement response for the raft foundation with raft thickness equal to 0.9 m is plotted, from which the factor of safety against bearing capacity failure is obtained. The limiting load is equal to 461.3 MN, which gives a factor of safety equal to 2.96, based on the total structural load which is equal to 156

MN. This satisfies the design limits set above. Thus, it remains to assess whether settlements at working conditions are excessive or not.

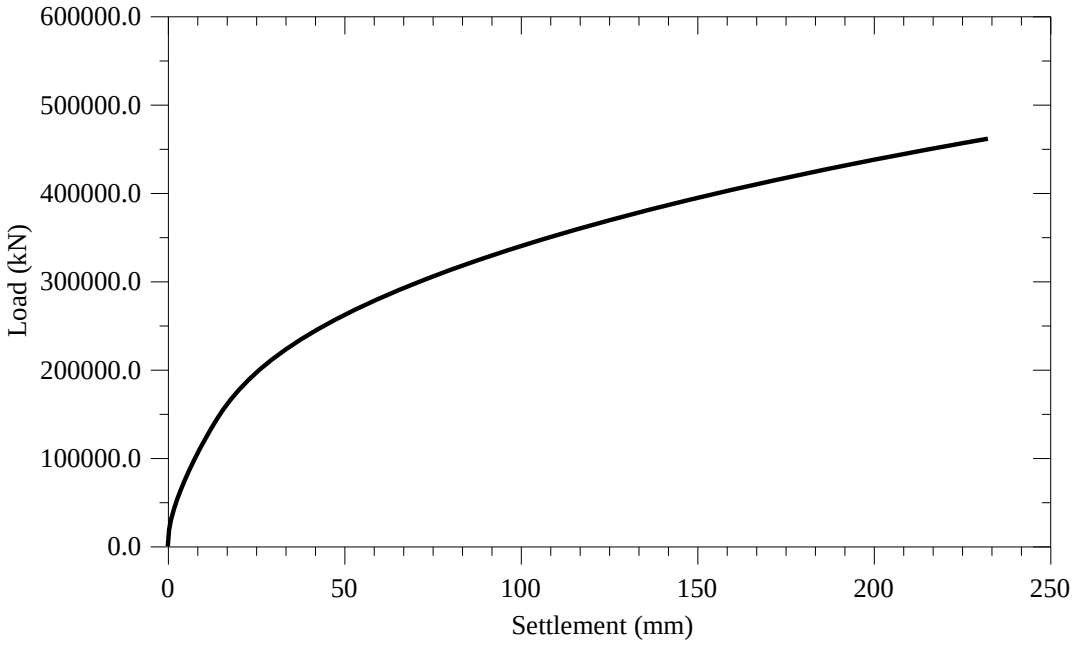


Figure 7.16: Load-settlement response of raft foundation loaded to failure

In Figure 7.17, the development of structural load with time for the analysis with the original thickness is presented. The raft is loaded up to the load level of Hiscocks House with a realistic load rate and then it is maintained constant for a period of 30 years, representing the lifespan of Hiscocks House. The analysis is coupled, therefore consolidation initiates from the beginning. However, it is anticipated that consolidation lasts much longer than the period of construction, and therefore the construction is considered as an undrained process.

In Figure 7.18, the development of ***absolute settlements*** at the centre of the raft (i.e. corner of the discretised raft) for a range of depths below the underside of the raft for the original raft thickness is plotted. Unlike the original piled raft foundation which is settling as a block, the predicted absolute settlements indicate that the raft foundation is settling uniformly with depth, with larger displacements obtained close to the surface. In Figure 7.19, contours of excess pore water pressures at the end of the application of the structural load are plotted, which are indicative of the amount of stress applied to the soil below the raft. Figure 7.20 presents the accumulation of settlement, below the centre of the raft, from the bottom of the mesh up to the foundation level in the long term. This indicates that close to the surface larger displacements are accumulated with time, being proportional to the effective stress applied on the soil below the raft foundation.

Referring to the design limits for absolute settlements, the maximum absolute settlement of the raft at the end of construction and after 30 years of elapsed time is equal to 40.3 mm and 182.9 mm respectively. A settlement larger than 150 mm does not fulfil the serviceability requirements (see Section 7.3). Therefore, the predicted settlement of 182.9 mm in the long term indicates that the magnitude of absolute settlement is intolerable for this foundation scheme.

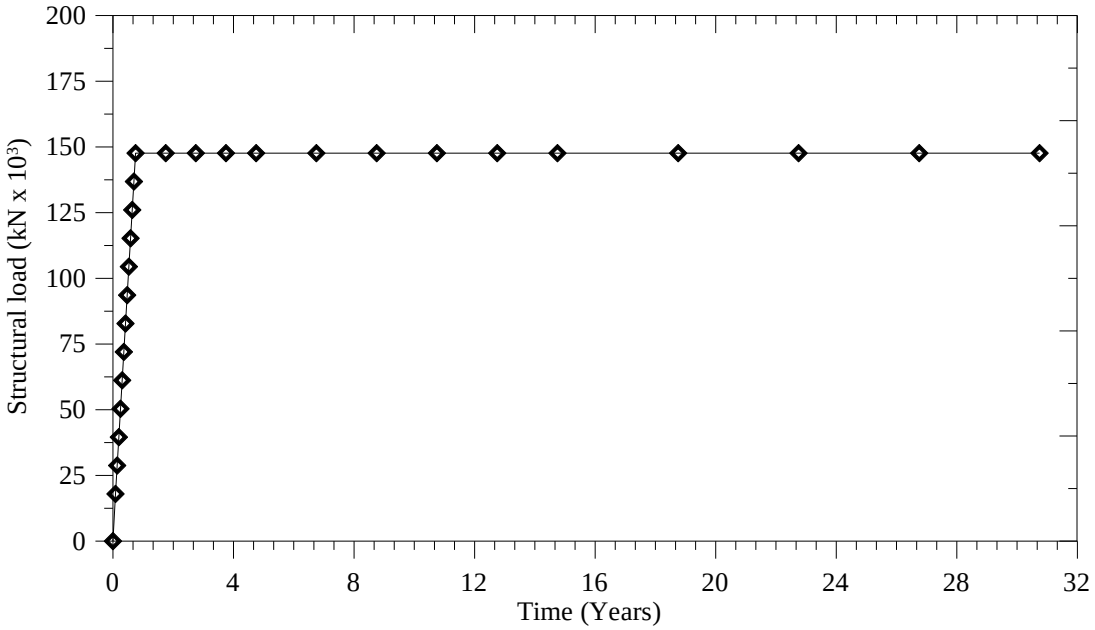


Figure 7.17: Development of structural load with time for the raft foundation with the original thickness

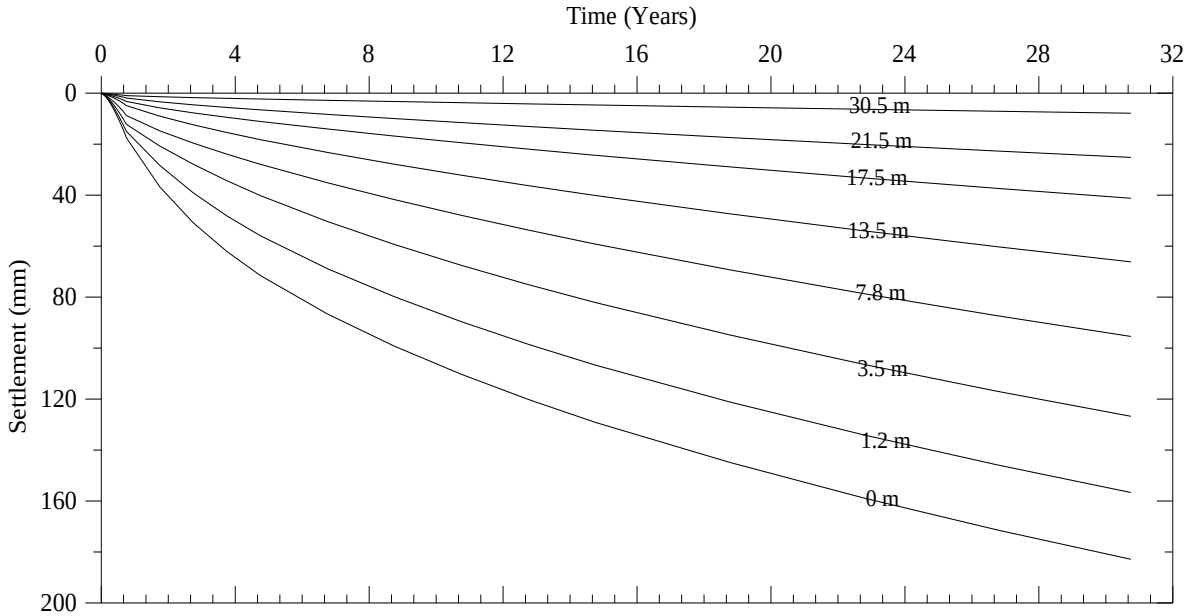


Figure 7.18: Development of absolute settlements at the centre of the raft for a range of depths below the underside of the raft for the original raft thickness

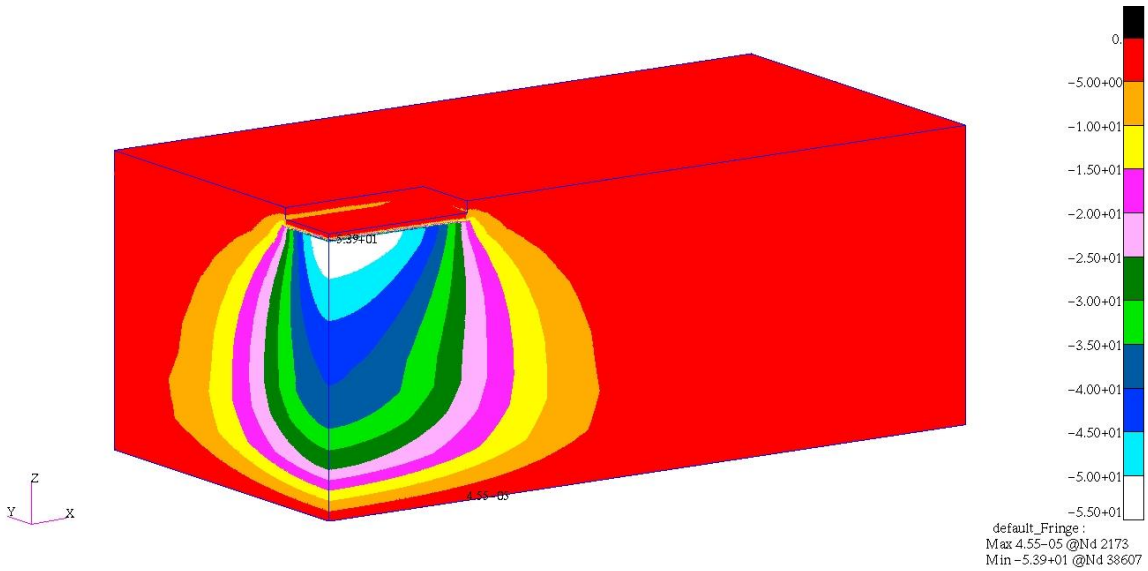


Figure 7.19: Contours of excess pore water pressures at the end of the structural load application for the raft foundation with the original raft thickness (units in kPa)

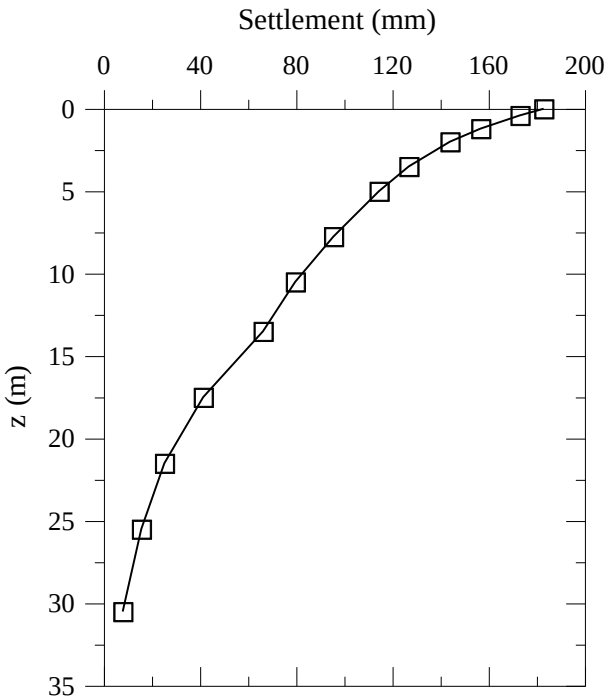


Figure 7.20: Settlement profile with depth in the long term for the raft foundation with the original raft thickness

Regarding ***differential settlements***, contours of settlement as predicted by the finite element analysis in the long term (after 30 years) for each parametric case are plotted in Figure 7.21. For the original raft thickens (Figure 7.21a), it is observed that the absolute settlement in the centre of the raft is at maximum and is equal to 182 mm, whereas the absolute settlement in the corner is at minimum and equal to 110 mm. Such displacements indicate that the raft is sagging towards the centre, being indicative of the area where the performance of the raft

foundation should be enhanced in the situation where the differential settlements are deemed excessive. Similar observations about the thicker rafts are made. However, it is observed that the amount of differential settlement drops with increased raft thickness reflecting the increased rigidity. At the same time, the amount of absolute settlement increases with increased raft thickness reflecting the increase of the weight of the thicker rafts. In particular, for the 1.5 m thick raft foundation the settlement in the centre is equal to 198 mm and in the corner 156 mm (Figure 7.21b). For the 2.5 m thick raft foundation the settlement in the centre is 242 mm and in the corner 226 mm (Figure 7.21c).

In Figure 7.22, the development of differential settlement centre-to-corner with time for each parametric case is plotted. Differential settlement increases with time, which is proportional to the accumulation of absolute settlements due to consolidation and creep. Larger differential settlements are obtained for the thinner rafts. The reason behind this is the raft stiffness which is proportional to the raft thickness. A thinner raft reflects a flexible foundation, whereas a thicker raft reflects a rigid foundation with less distortion.

Referring to the design limits for angular distortion, the maximum angular distortion in the raft with the original raft thickness after 30 years of elapsed time after the initial loading is equal to 1/330 (Figure 7.23). Such distortion is expected to result in increased tensile strains in the structure materials, resulting in cracking to walls and even to structural damage. Regarding the other raft thicknesses employed in the analysis, the angular distortion after 30 years significantly reduces. In particular, for the raft thickness of 1.5 m the angular distortion is equal to 1/580, and for the raft thickness of 2.5 m it is equal to 1/1470. Both raft thicknesses indicate that an increased raft thickness would keep differential settlement within design limits.

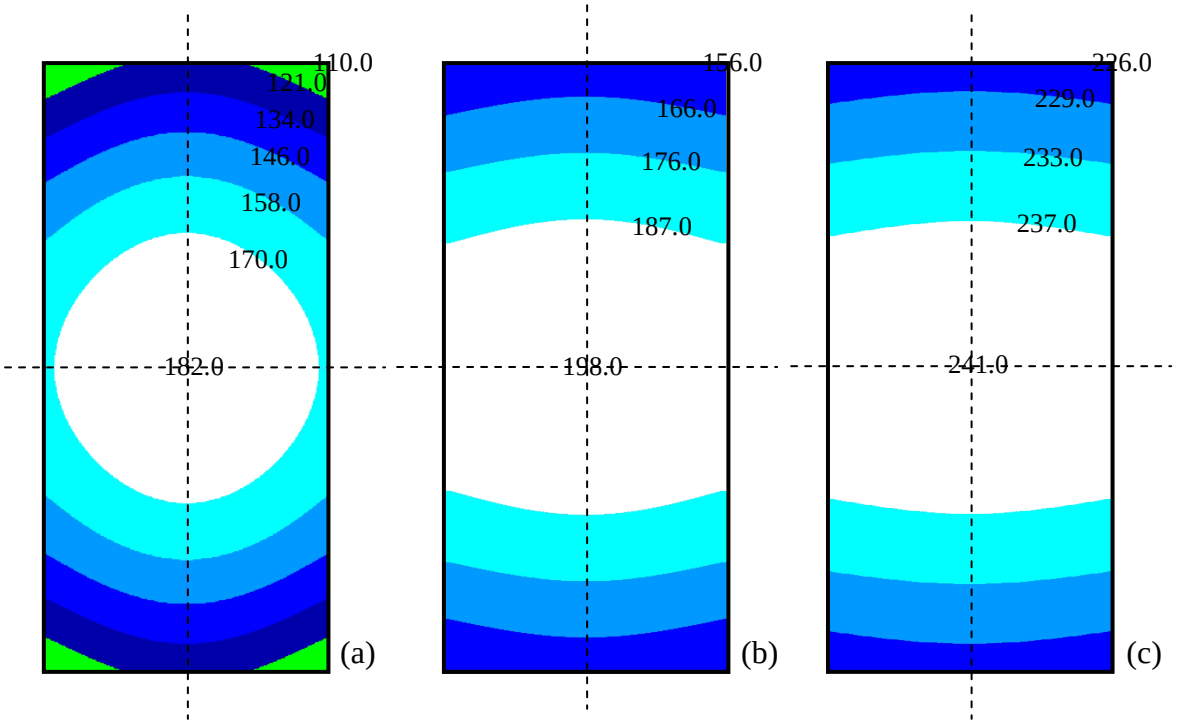


Figure 7.21: Contours of settlement of the raft foundation with raft thickness equal to: (a) 0.9 m, (b) 1.5 m, and (c) 2.5 m (units in mm)

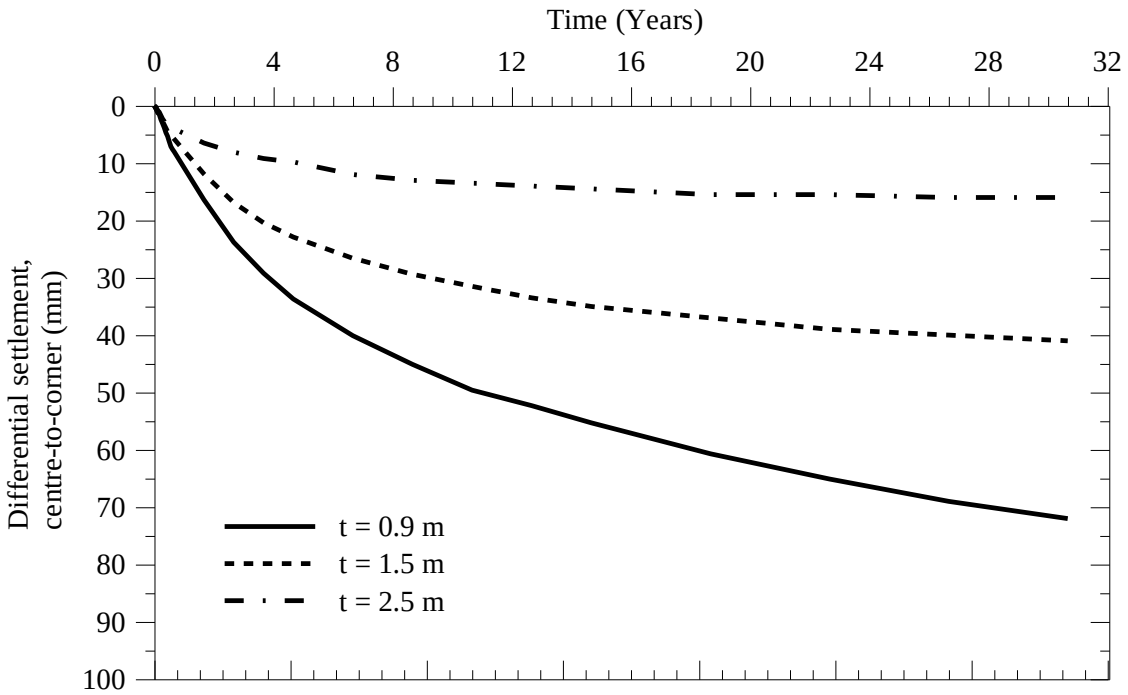


Figure 7.22: Development of differential settlement centre-to-corner with time for the raft foundation examined parametrically

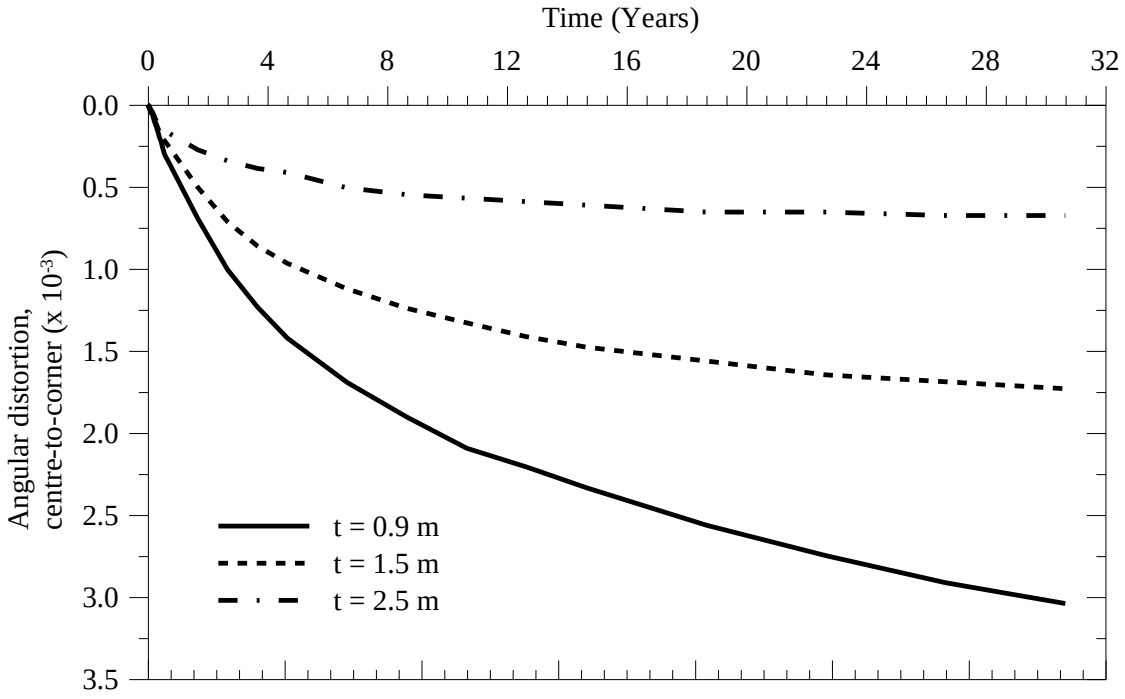


Figure 7.23: Development of maximum angular distortion with time for the raft foundation examined parametrically

7.3.2. ORIGINAL DESIGN OF PILED RAFT FOUNDATION

In Chapter 6, the performance of the original foundations of Hiscocks House, as documented by Cooke et al. (1981), is compared with the finite element predictions, allowing the validation of the numerical and constitutive models employed in the FE analyses. The scope of the following is to determine the factor of safety against bearing failure and assess also the long-term predicted settlements at working conditions. In addition, the effect of preloading is examined in order to quantify the enhancement of the overall load capacity of the piled raft foundation in the long-term.

The problem geometry of this analysis is described in Chapter 6, along with the boundary conditions. In the following, a description of the analysis performed and the results obtained are discussed.

7.3.2.1. Description of analysis

This analysis is considered as a continuation of the analysis performed in Chapter 6. The piled raft foundation is loaded up to failure, in order to determine the factor of safety against bearing failure. The failure criterion applied is set as equal to 700 kN per mm of maximum displacement. Increments of boundary stress on the raft are prescribed with a rate equivalent to the construction of the 16 storeys of the Hiscocks House.

In order to quantify the effect of preloading, an additional analysis is run where the piled raft foundation is loaded to failure after 30 years of elapsed time at working conditions. Similar loading rates to that used in the analysis employed to determine the initial load capacity are employed, in order to isolate any rate effects. The failure criterion applied is the same as above, i.e. 700 kN per mm of maximum displacement.

7.3.2.2. Results and discussion

In Figure 7.24, the load-settlement response for the original piled raft foundation is plotted, from which the ***factor of safety*** against bearing capacity failure is obtained. The limiting load is equal to 549.6 MN, which gives a factor of safety equal to 3.52, based on the total structural load which is equal to 156 MN. The predicted factor of safety satisfies the design limits set above, however the value predicted is considered very conservative. It remains to assess the settlements, in order to conclude whether the design is conservative.

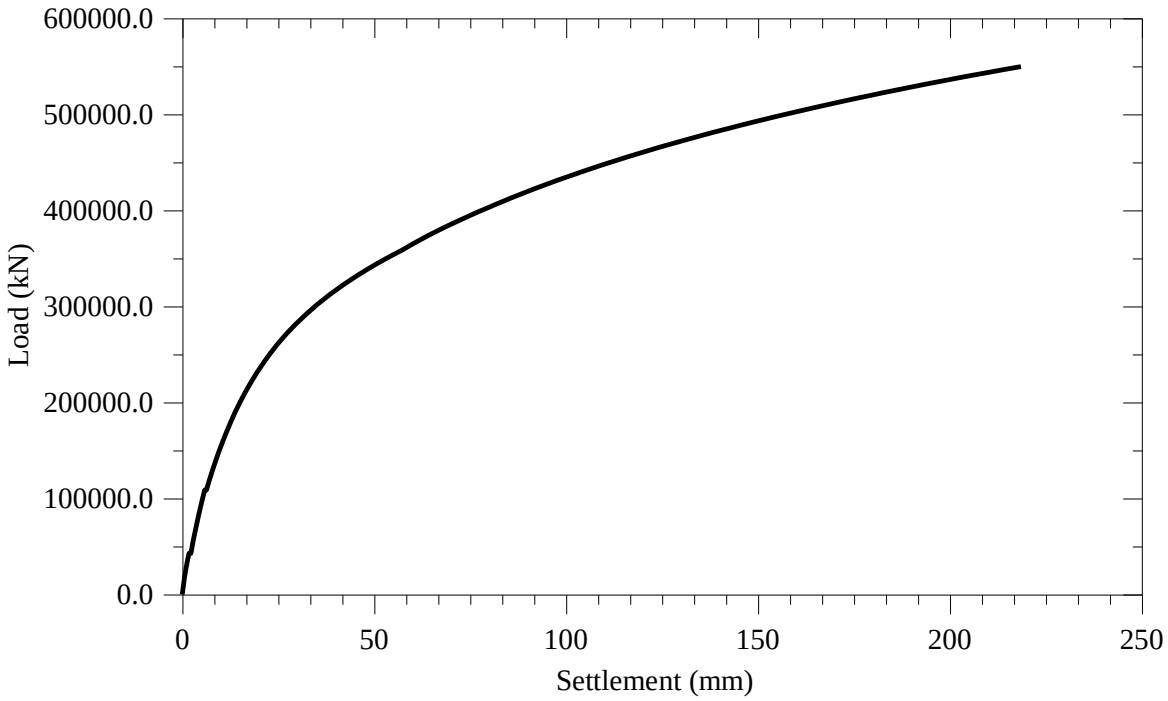


Figure 7.24: Load-settlement response of original piled raft foundation loaded to failure

Regarding absolute settlements, a ***maximum settlement*** of 62.0 mm in the centre of the raft after approximately 30 years of structural life is predicted. This satisfies the suggested maximum tolerable absolute settlement of 150 mm. In Figure 7.25, the evolution of ***differential settlement*** centre-to-corner with time for the original piled raft foundation is plotted. This, along with the dimensions of the foundation, allows the determination of the angular distortion and its development with time (Figure 7.26). The maximum angular

distortion at the end of Hiscocks House life is calculated equal to 1/1060. This value satisfies the design limits set in Tables 7.1 and 7.2, where a limit of 1/500 is recommended. The predicted angular distortion, along with the factor of safety against bearing failure, indicates that the original foundation design is conservative, allowing for more cost-efficient solutions.

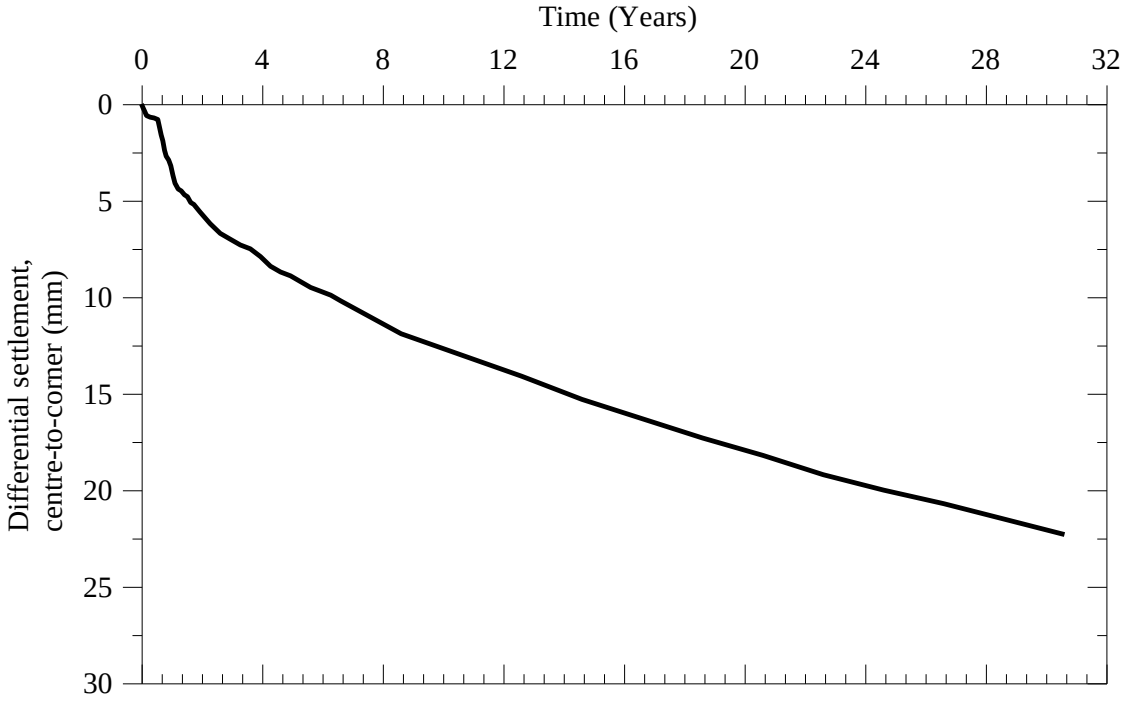


Figure 7.25: Development of differential settlement centre-to-corner with time for the raft foundation examined parametrically

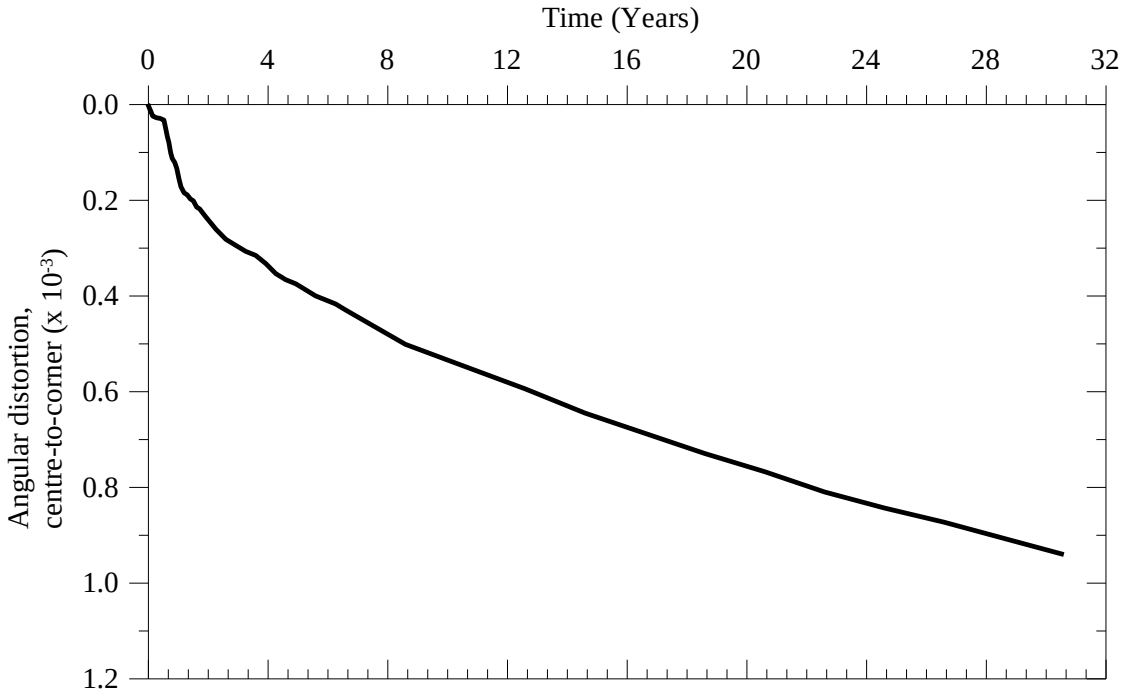


Figure 7.26: Development of maximum angular distortion with time for the raft foundation examined parametrically

In Figure 7.27, the effect of preloading on the long-term behaviour of the original foundations of Hiscocks House is presented. In particular, the load-settlement response of the piled raft foundation loaded to failure (a) during initial construction and (b) after 30 years of elapsed time at working conditions is presented. As noted above, the initial overall load capacity of the foundation was determined equal to 549.6 MN. The new overall load capacity after 30 years of consolidation and creep is predicted equal to 607.4 MN, indicating an enhancement of capacity equal to 10.5 %. Such enhancement indicates that the factor of safety increases with time, allowing for additional loading on the foundations. Also, an enhancement of the overall stiffness of the foundations is predicted after 30 years of consolidation and creep, as observed in Figure 7.27 by the steeper response of the preloading curve after the elapsed period.

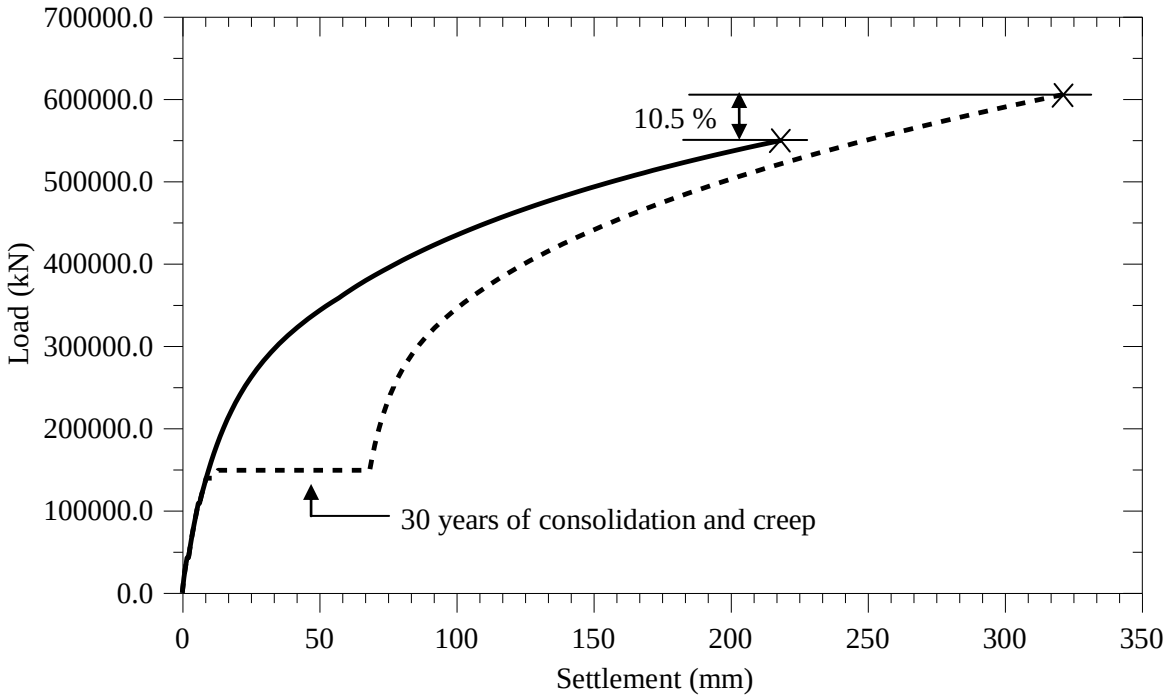


Figure 7.27: Load-settlement response of original piled raft foundation loaded to failure during construction and after 30 years of elapsed time at working conditions

7.3.3. DESIGN OF PILED RAFT FOUNDATION: parametric study varying the number and length of piles

A parametric study investigating the effect of the number and the length of piles on the behaviour of a piled raft foundation employed to support Hiscocks House is performed, in order to optimise the design of the Hiscocks House foundations. It has been shown that the original design of a piled raft foundation is very conservative and cost-ineffective on the one hand, on the other hand a raft foundation, despite providing enough load capacity, produces

excessive settlements. This suggests the use of a piled raft foundation, whose piles are utilised to reduce settlements rather than to provide load support, i.e. a settlement reducing approach.

Differential settlement is the most critical criterion in design. A series of parametric analyses is performed, where piles are installed following the design concept that piles installed in the central region under the raft area are more effective in reducing differential settlements, than if they were uniformly distributed.

7.3.3.1. Parametric cases

A series of parametric analyses was performed, where the number of piles and their length were varied, in order to obtain the most optimum solution in terms of differential settlement. A total of 9 analyses were performed, where the number of piles, their length and the total pile length for each parametric case are presented in Table 7.3. In Figure 7.28, the location of the piles for each parametric analysis is shown. Piles are located in the central region of the raft area, keeping the original pile grid 1.6 m centre to centre (~3.5d).

Parametric case	Number of piles	Pile length (m)	Total pile length (m)
1	185	17.5	3238
2	185	13.0	2405
3	185	8.75	1619
4	107	17.5	1873
5	107	13.0	1391
6	107	8.75	936
7	55	17.5	963
8	55	13.0	715
9	55	8.75	481

Table 7.3: Parametric cases with varying number of piles and pile length

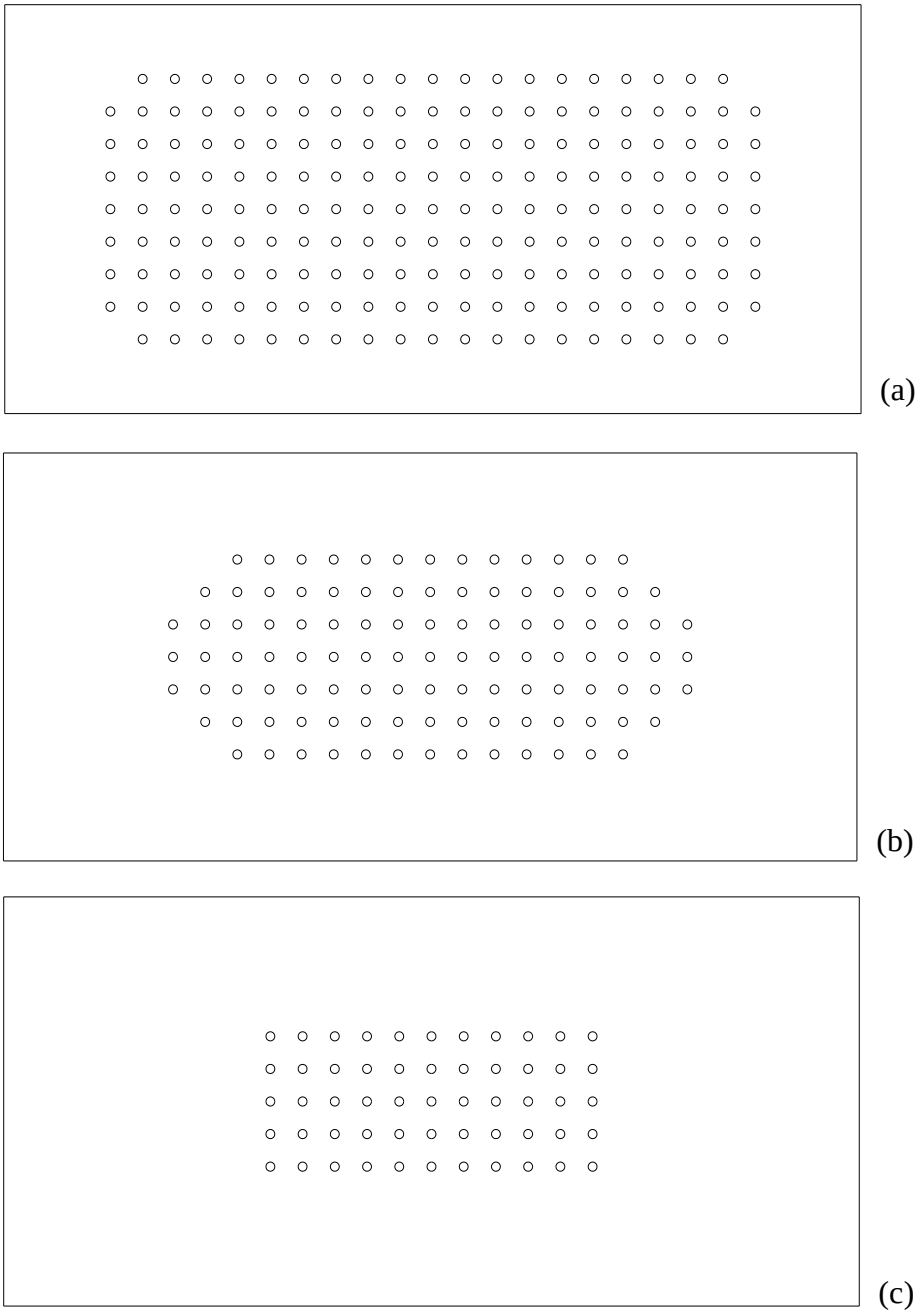


Figure 7.28: Location of piles for parametric case with (a) 185 piles, (b) 107 piles, and (c) 55 piles

7.3.3.2. Problem geometry and boundary conditions

The mesh created to run the parametric analyses is shown in Figure 7.29. It is similar to the mesh created for the original design of the piled raft foundation of Hiscocks House. The analysis is three-dimensional and the mesh domain is 100m x 50m x 40m in the X-Y-Z axes respectively. The soil profile adopted for the analysis is the one identified for Stonebridge Park in Chapter 6 (Figure 6.23). A ¼ of the problem is discretised into finite elements, due to

the symmetry of the foundation around the X and Y axes. The mesh consists of 20366 20-noded hexahedral finite elements.

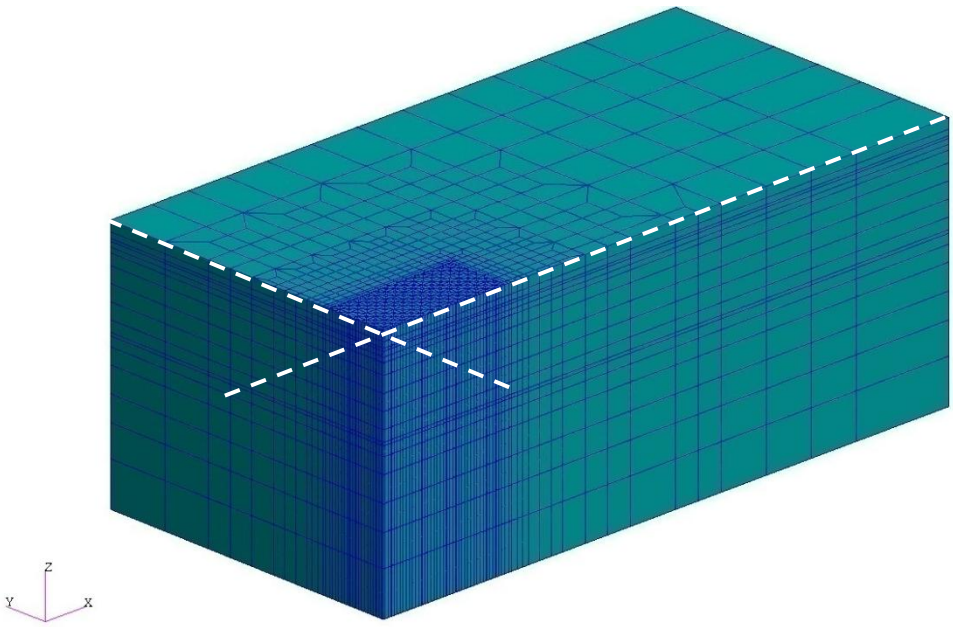


Figure 7.29: 3D mesh for the piled raft foundation

The mesh shown in Figure 7.29 is employed for all parametric analyses. Both the piles and the raft are discretised. The dimensions of the raft are 43.3 m by 19.2 m and, due to symmetry, ¼ of the raft is discretised, i.e. 21.65 m by 9.6 m. The pile length varies depending on each parametric case (Table 7.3) and the pile diameter is equal to 0.45 m, while the thickness of the raft is 0.9 m. The location of the piles depends on each parametric case as shown in Figure 7.28. Both the piles and the raft are modelled as a linear elastic concrete material, with E = 30×10^6 kPa and μ= 0.15. The piles are installed on a square grid of 1.6 m distance centre to centre. A "soft zone", 7.5 cm thick, with a lower angle of shearing resistance, is discretised around the piles, in order to simulate the adhesion at the pile-soil interface.

The ET Creep model is employed to simulate the behaviour of the London Clay units and of the Lambeth Group. Model parameters for each soil layer are set in Chapter 6. The mesh consists of twenty noded isoparametric elements with eight pore pressures degrees of freedom at the corner nodes of the consolidating elements, and three displacement degrees of freedom at both corner and mid-side nodes for all elements.

The applied displacement boundary conditions prevent the base of the mesh from moving in the vertical (Z direction) and horizontal directions (X and Y directions), while the vertical

sides of the mesh, whose face is not a plane of symmetry, are fixed in the horizontal directions and can move in the vertical direction only. Regarding the boundaries forming planes of symmetry, their vertical sides are fixed in the horizontal direction perpendicular to the plane of symmetry, i.e. the X-Z boundary is fixed in the Y direction and the Y-Z boundary in the X direction, whereas they are free to move in the remaining directions.

The analysis is coupled with consolidation taking place during the analysis. The hydraulic boundary conditions applied allow no pore water flow across the planes of symmetry and the ground surface, while at the base of the mesh and the remaining vertical planes, pore pressures are maintained equal to their initial values, as determined by the water table 3.5 m below ground level.

7.3.3.3. Description of analysis

A series of 3D parametric finite element analyses is performed, in order to optimise the performance of the foundations of Hiscocks House. The varying parameters are the number of piles and the length of the piles. The finite element analysis follows the construction sequence of Hiscocks House, with an initial 100 years of elapsed time in order to make sure there is no discrepancy between the initial under-drained pore water pressure profile and the permeabilities assumed (see Chapter 6).

After the initial 100 years period of elapsed time, the finite element analysis follows the construction programme of the original Hiscocks House, as described by Cooke et al. (1981). The piled raft foundation for each parametric case is constructed. The installation of the piles is simulated by changing the material properties of the appropriate elements from soil to concrete for each parametric case. At the same time, the "soft zone" around the piles is simulated, by changing also the material properties of the elements forming the "soft zone" and assigning a lower angle of shear resistance, as determined in Chapter 6.

The excavation of the raft, founded at a depth of 2.5 m below ground level, follows. The excavation of the raft is achieved by removing the appropriate elements from the finite element mesh. Then, a layer of elements 0.9 m thick, representing the raft, is constructed on top of the excavated boundary. The raft is modelled with the material properties of concrete, as described above.

The construction of the super structure consisting of 16 storeys on top of the foundation is followed, which is simulated through the application of uniform boundary stresses on top of the raft, from which the respective displacements are calculated. The increments of loading

are equivalent to those employed for the original piled raft foundation in Chapter 6. All parametric cases are loaded up to the building load level, in order to examine the performance of the piled raft foundation at working conditions.

Finally, a period of elapsed time of 30 years is prescribed in the analysis. The piled raft is loaded with the total stress prescribed in the previous increments of the analysis representing the total load of the structure. The settlements developing with time are calculated.

7.3.3.4. Results and discussion

Plots of contours of settlements at the raft level are plotted for each parametric case, in order to assess the settlement profile over the raft area and the differential settlements developed. Also, the differential settlement centre-to-corner of each parametric case is determined, allowing the comparison and the determination of the most optimum design for the foundations of Hiscocks House. Finally, the load share between the piles and the raft is evaluated, in order to assess the contribution of the raft and of the piles on the piled raft foundation.

In Figures 7.30 to 7.32, ***contours of settlement*** at the raft level after 30 years of elapsed time are plotted for each parametric case. The location of the piles is also shown in the figures. In Figure 7.30, settlement contours for the parametric cases with 185 piles are plotted with a varying pile length as annotated in the figure. The contours of settlement indicate that the maximum settlement of the raft is on the periphery of the raft, which is equal to 71.5, 85.9 and 102.0 mm for a pile length of 17.5, 13.0 and 8.75 m respectively. This is opposite to the observations made for the conventional piled raft foundation of Hiscocks House, where the foundations were found to sag in the centre. The observed hogging is attributed to the fact that the loading on the foundation is uniform and therefore the compression applied by the area of the raft, which is not piled, to the supporting soil results in increased settlement of the soil. Settlement in the central region where the piles are located is less than in the periphery, due to the fact that the stress applied is transferred to deeper levels where the soil is less compressible. Another point is that piles are installed before the raft excavation. Thus, during excavation the piles work as tension piles and, consequently, the soil in the piled area heaves less than the soil in the un-piled area of the raft. On subsequent structural loading, the heaved soil in the periphery settles more than the soil in the piled area. Regarding the minimum settlement, it is observed that it is not in the centre of the raft, but in an area close to the short side of the piled area of the raft. Such a settlement profile is attributed to the superposition of

the accumulated settlements in the un-piled and the piled raft area, where the central area tends to sag, as observed in the conventional piled raft foundation in Chapter 6.

In Figure 7.31, settlement contours for the parametric cases with 107 piles are plotted with a varying pile length as annotated in the figure. Maximum settlement is on the periphery of the raft and minimum settlement in the centre; the raft is hogging. The maximum settlement is equal to 103.0, 116.0 and 125.0 mm and the minimum settlement is equal to 68.1, 87.2 and 109.0 mm for a pile length of 17.5, 13.0 and 8.75 m respectively. In this set of parametric analyses, the minimum settlement is exactly in the centre of the raft, unlike the cases with 185 piles. This due to the fact that the area occupied by the piles is significantly less than the area occupied in the parametric cases with 185 piles, and therefore the sagging effect is not dominant in the centre of the raft.

In Figure 7.32, settlement contours for the parametric cases with 55 piles are plotted with a varying pile length as annotated in the figure. Similar observations for a pile length of 17.5 and 13.0 m are made in terms of settlement with the other parametric cases, i.e. minimum settlement in the centre and maximum in the periphery of the raft. However, for the case with a pile length of 8.75 m a varying settlement profile is observed with the periphery of the raft sagging and the centre of the raft, where piles are included, hogging. Such a settlement profile indicates that the piles are not dominating the behaviour of the foundation, like the other parametric cases. Piles are utilised to improve the performance of the foundation and therefore their function is to reduce the settlement, i.e. piles work as settlement reducers.

Regarding the overall effect of pile length on the piled raft foundation performance, the longer the piles the less settlement and vice versa. This is observed in all parametric cases. Comparing the settlement contours of the different piled raft foundations with those of a raft foundation (see Figure 7.21), it is observed that the addition of piles in the central area of the raft reduces the settlement in the central area resulting in hogging instead of the observed sagging in raft and conventional piled raft foundations. However, for the case of 55 piles with piles length equal to 8.75 m, piles do not dominate the behaviour of the foundation, as foresaid, and a more uniform settlement profile is obtained. In this case, piles work as settlement reducers and therefore they limit the observed sagging in the raft foundation analysis.

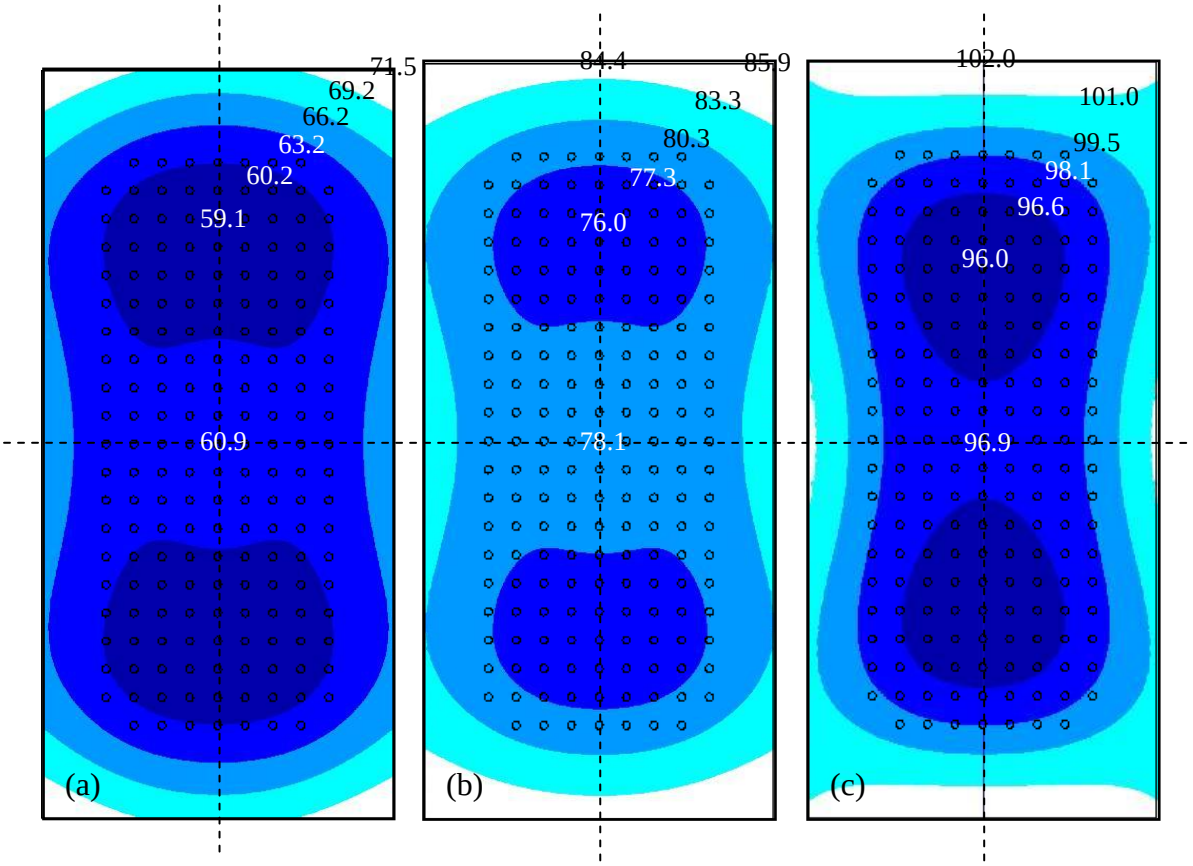


Figure 7.30: Contours of settlement for the parametric cases with 185 piles and pile length (a) 17.5 m, (b) 13.0 m, and (c) 8.75 m (units in mm)

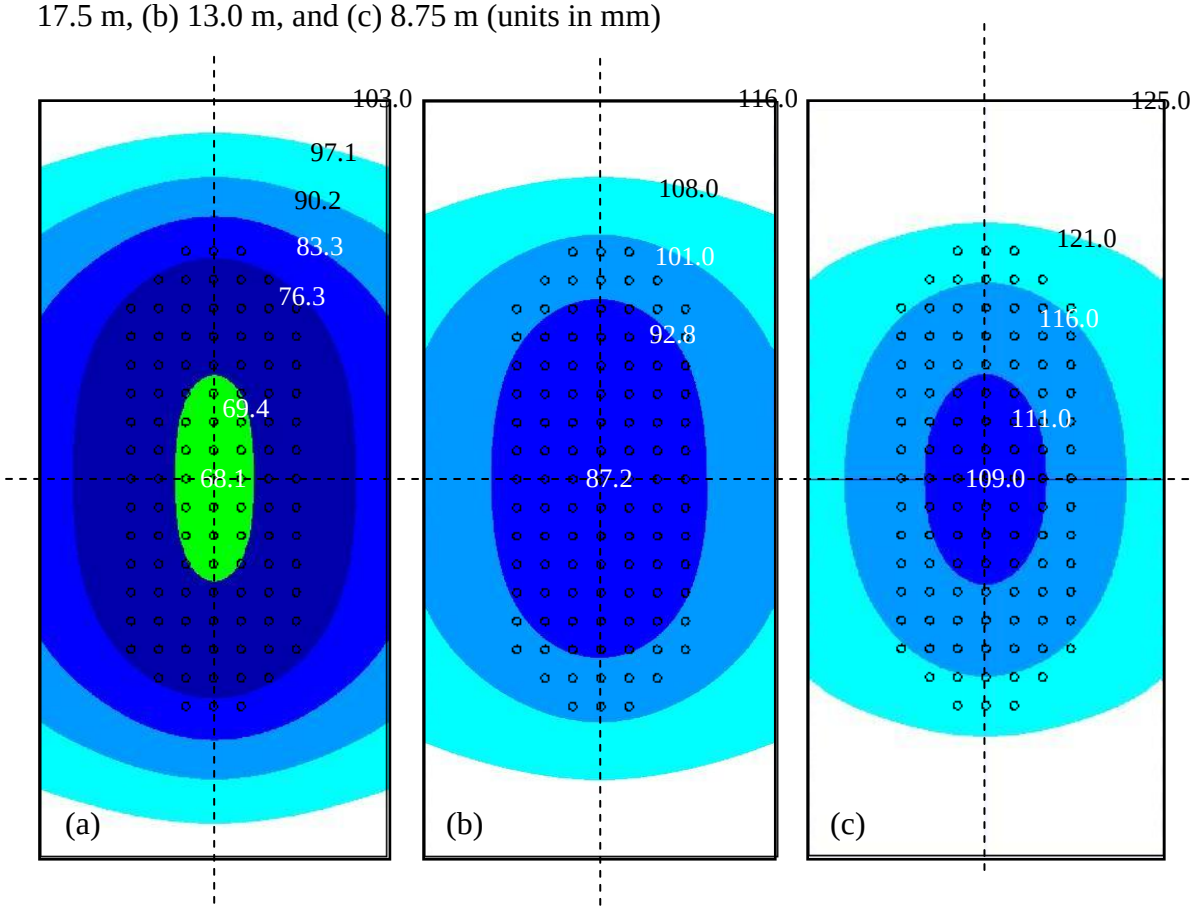


Figure 7.31: Contours of settlement for the parametric cases with 107 piles and pile length (a) 17.5 m, (b) 13.0 m, and (c) 8.75 m (units in mm)

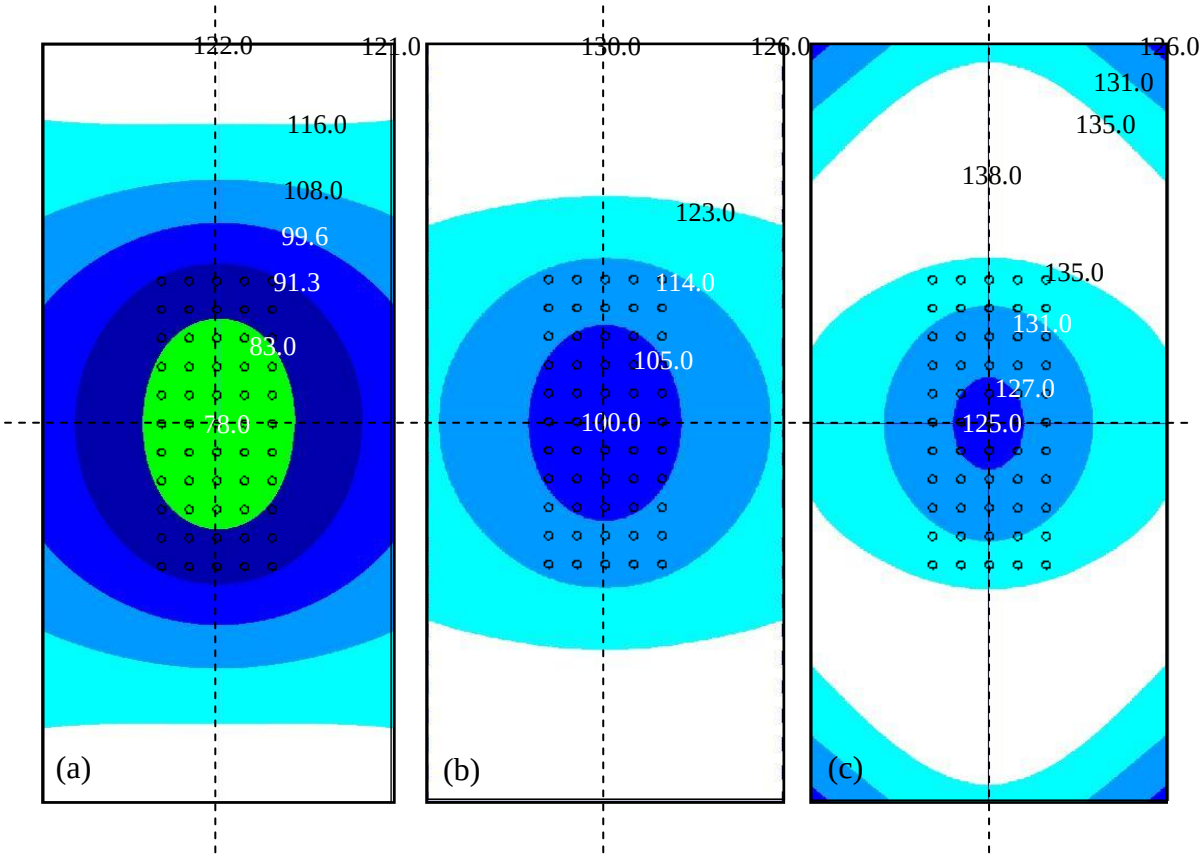


Figure 7.32: Contours of settlement for the parametric cases with 55 piles and pile length (a) 17.5 m, (b) 13.0 m, and (c) 8.75 m (units in mm)

In Figure 7.33, the ***differential settlement*** centre-to-corner for each parametric case after 30 years of elapsed time against the total pile length is plotted. The differential settlement determined for the original piled raft foundation of Hiscocks House and for a raft foundation with the original thickness is also presented for the same time period. This allows the determination of the most optimum design in terms of differential settlement and total pile length. The results indicate that the concentration of the piles in the central region results in a hogging effect (i.e. negative values for differential settlement), which was not observed in the piled foundation with a uniform distribution of piles and in the raft foundation. The reasons for this have already been explored.

The results show that a more efficient and cost-effective solution could be obtained for the design of the foundations of Hiscocks House. Reducing the number of piles may be beneficial in terms of differential settlement, depending on the piles length. In particular, 185 piles centrally located and occupying approximately 53% of the raft area give smaller differential settlement (-7.8 mm) than the settlement of 351 piles uniformly distributed (20.7 mm). In particular, 55 piles centrally located may minimise the differential settlement close to zero and, at the same time, keep absolute settlements and the factor of safety against bearing failure within the design limits.

Generally, the longer the piles are for a constant number of piles, the smaller the absolute settlement in the central region of the raft and therefore the larger the negative differential settlement. Comparing the parametric cases with different number of piles but with an equal total pile length, a smaller number of longer piles decrease the settlement in the central region more effectively than shorter piles. This is observed in Figure 7.33 by the increased negative differential settlement of piled foundations with a smaller number of piles, but with the same total pile length with other parametric cases. For instance, for a total pile length of 1000 m, for 107 piles centrally located under the raft the differential settlement centre-to-corner is predicted approximately -18.0 mm, whereas for 55 piles it is predicted approximately -45.0 mm.

Regarding the influence of the variation in pile length on differential settlement, the fewer the number of piles, the larger the influence of the pile length. In particular, for the parametric cases with 185 piles the differential settlement varies from -10.6 mm to -5.1 mm for pile lengths 17.5 m to 8.75 m, whereas for the cases with 55 piles the differential settlements varies from -44.0 mm to -1.0 mm, indicating that for a smaller number of piles the piled raft foundation performance is more sensitive to pile length changes.

Finally, the results indicate a significant hogging effect in the central region of the raft where piles are located suggesting that, in order to minimise differential settlement, a more sensible approach would be the uniform distribution of piles over the raft area and the variation of the pile length with longer piles in the central region and shorter piles in the periphery. Also, the pile spacing used in the analyses is the original spacing of the piles used to support Hiscocks House, which were shown to initiate block behaviour. Such behaviour reduces the efficiency of the individual piles in the piled raft foundation, and therefore a larger spacing of piles would provide a more cost-effective solution.

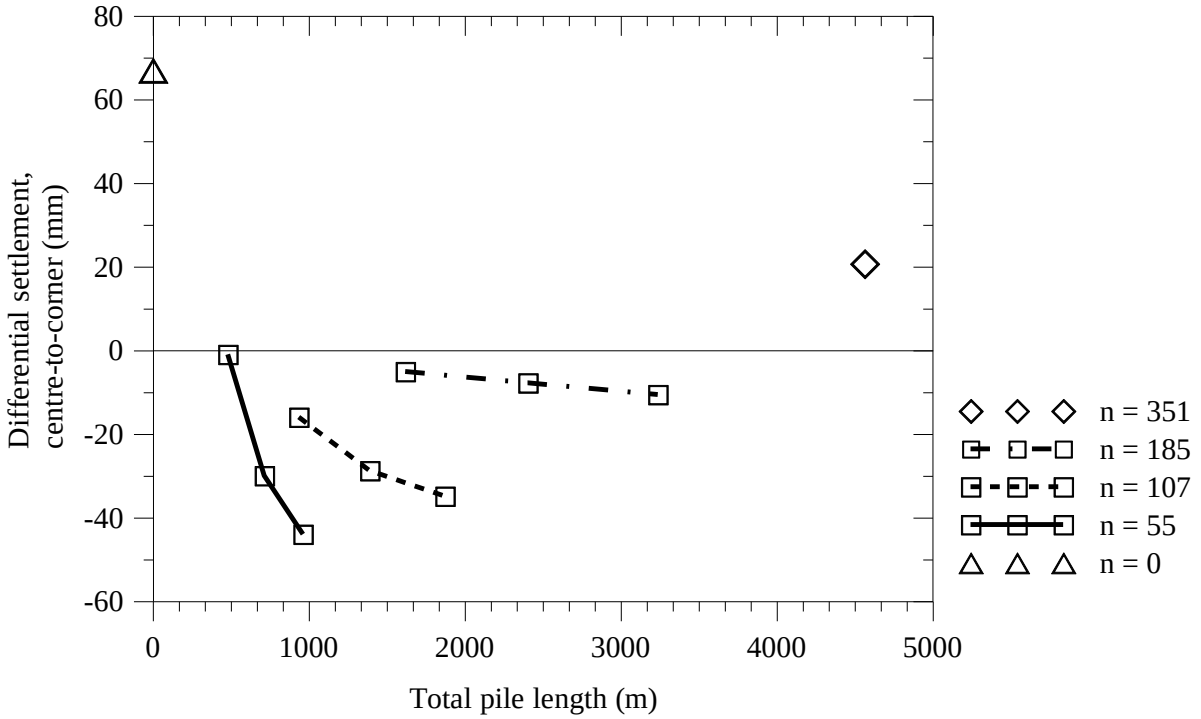


Figure 7.33: Differential settlement centre-to-corner for each parametric case against total pile length

In Figure 7.34, the ***load share of piles*** against the total pile length for each parametric case is plotted. Generally, the larger the total pile length for a constant number of piles, the larger the contribution of the piles to the overall foundation resistance. For instance, for the parametric cases with 185 piles, a pile length of 8.75 m results in a pile load share of 57.9 %, whereas for a pile length of 17.5 m the load share is 70.8 %. Comparing the parametric cases with different number of piles but with an equal total pile length, it is observed that the larger number of piles, the larger the load share of the piles. In particular, for a total pile length equal to 1800 m, 107 piles have a load share of 50 % approximately, whereas 185 piles have a load share of 60 % approximately.

The load share of piles and the contribution of the raft to the overall resistance of the foundation has an important influence in the design. A foundation design with 185 piles may be considered as a conventional piled raft where the majority of the resistance is provided by the piles. In the case where the raft provides enough load capacity, such design is considered as not cost-effective. This is the case for Hiscocks House. On the other hand, the parametric case studies with 55 piles indicate that piles are utilised mainly as settlement reducers and not as a means to provide load capacity, since the load share of the piles varies from 25.2 to 34.1% depending on the pile length. Therefore, considering the fact that the raft alone provides sufficient load capacity it is evident that a solution with the least number of piles strategically located under the raft is considered as the most cost-effective solution.

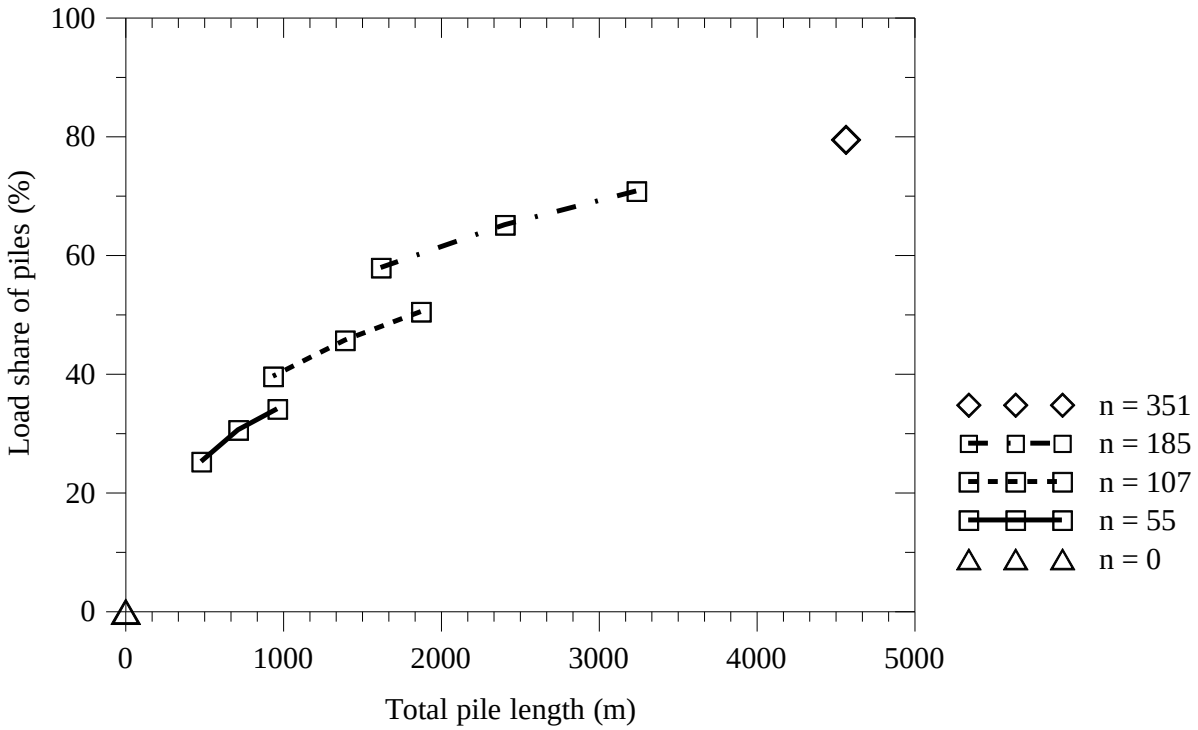


Figure 7.34: Load share of piles for each parametric case study against total pile length

7.4. SUMMARY AND CONCLUDING REMARKS

An initial study on a hypothetical piled raft foundation in London Clay was performed in order to assess the concept of locating piles in the central region of the raft. Three different foundations were examined: a raft foundation, a piled raft foundation with a uniform distribution of piles and a piled raft foundation with central pile support.

In both piled foundations, the contribution of the piles to the overall load capacity was limited in respect to the contribution of the raft. The spacing of piles was set equal to 8.0D, which prevented the settlement block behaviour observed in the piled raft foundation of Hiscocks House with 3.5D pile spacing.

The raft foundation was found to sag towards the centre of the raft with the maximum settlement predicted in the centre and the minimum settlement in the corner of the raft. This was also the case for the piled raft foundation with the uniform distribution of piles. The significant contribution of the piles at a realistic load level in reducing absolute settlements on the raft was demonstrated.

Central pile support resulted in a non-uniform settlement profile in the short term. Pile support in the central region of the raft reduced local settlement resulting in local hogging and

reduced centre-to-corner differential settlement in respect to the uniform piled raft foundation, despite the fact that absolute settlements were predicted to be larger.

In the long term, no hogging in the centre of the raft was observed. This is attributed to creep and the resulting deformations with time. The fact that piles were loaded very close to their ultimate load capacity resulted in increased deformations with time due to creep, reducing their efficiency in reducing settlements. This demonstrates that, depending on the level of pile shaft friction mobilisation, the benefits observed in the short term in piles centrally located under the raft may reduce in the long term due to creep.

The effect of preloading on the overall load capacity was quantified. The gain in load capacity and the development of settlements due to consolidation and creep increase with the level of preloading. The larger the applied load, the larger the settlement and the gain in capacity after 50 years of elapsed time. Also, the normalised gain in capacity is larger for the un-piled raft foundation than in the piled raft foundations. This is attributed to the fact that piles shaft friction is fully mobilised at the applied load level, resulting in a limited gain in pile capacity.

Subsequently, optimisation of the performance of the piled raft foundation in Stonebridge Park was attempted by examining several pile arrangements. The limitations for employing a raft foundation for Hiscocks House and the lack of cost-efficiency of the original design were demonstrated.

The parametric analysis on a raft foundation to support the Hiscocks House, with the varying parameter being the raft thickness, indicated that the raft foundation provides enough load capacity with a factor of safety equal to 2.96 for the original raft. Such raft foundation is characterised as a ‘large’ raft. Absolute settlements 30 years after the application of the total structural load on the raft were excessive, resulting in serviceability problems. Differential settlements for the original raft thickness gave an angular distortion that could result in cracking of walls and possible structural damage. Thicker raft foundations limited the angular distortion to tolerable values, however it is anticipated that thicker rafts result in larger absolute settlements due to the increased raft weight.

The adoption of a fully piled foundation with 351 piles is considered as over-conservative. A factor of safety against bearing failure equal to 3.52 and an angular distortion 30 years after the application of the total structural load equal to 1/1060 were calculated, which are both above the design limits.

A parametric study varying the number and length of piles allowed the assessment of a more optimum and more cost-effective solution than the one adopted originally for the foundations of Hiscocks House. The fact that the raft alone provided enough load capacity indicates that piles may be introduced below the raft only in order to reduce settlement. The results from the parametric analysis showed that a more efficient, in terms of differential settlement, and cost-effective solution, in terms of the number of piles and the total pile length, may be obtained with a smaller number of piles located in the central region of the raft. In particular, 55 piles (8.75 m long) in the central region of the raft may reduce the differential settlement to almost zero and, at the same time, keep absolute settlements and the factor of safety against bearing failure within the design limits. The load share of the 55 piles is 25.2%, indicating that despite the main function of the piles being to reduce settlement, there is a significant contribution to the overall load capacity of the piled raft foundation.

Finally, the effects of time on the performance of the original piled raft foundation for Hiscocks House were examined, from which an enhancement of capacity equal to 10.5 % was evaluated after 30 years of consolidation and creep. Such enhancement indicates that the factor of safety against bearing failure increases with time, allowing for additional loading on the foundations. Also, an enhancement of the overall stiffness of the foundations was predicted after 30 years of consolidation and creep.

Chapter 8

Conclusions and Recommendations

8.1. GENERAL REMARKS ON THE RESEARCH

The overall objective of this research was to contribute towards the optimum design of foundations considering their past, their present and their future. Foundations of old buildings were considered, in order to examine the time effects on them, and at the same time an effort was made to provide sustainable foundation solutions for future developments, considering their geometry and the time factor. This thesis considers the reuse of piled raft foundations and, in particular, the optimised design of piled foundations to support successive buildings using numerical analysis.

The key objectives of this research were:

- to realistically reproduce the time dependent behaviour of natural stiff clays,
- to quantify the effects of time, including consolidation and creep, on the performance of piled foundations in clays,
- to optimise the design of foundations in stiff clays.

The research involved advanced finite element analyses using the Soil Mechanics Section's finite element program ICFEP. The analyses were coupled, thus taking account of consolidation processes in the ground. Two advanced constitutive models were employed to model the behaviour of saturated clays: a form of the Modified Cam Clay (MCC) model and the Equivalent Time (ET) Creep model. The latter accounts for soil viscous behaviour and can reproduce soil behaviour due to creep.

The research consisted of four main parts: (a) a literature review on piles, piled raft foundations and time dependent behaviour of soils, (b) a description of an appropriate

constitutive model and calibration of the model parameters with laboratory tests on London Clay, (c) preliminary finite element analyses of single piles and calibration of numerical models, including single piles and piled raft foundations, with field data from case histories in London clay, and (d) parametric analyses to optimise the design and the reuse of piled raft foundations.

Initially, a literature review on piles and on piled raft foundations was performed. It was concluded that a raft foundation, with a limited number of piles located strategically beneath the raft and utilising their ultimate load capacity, is the most efficient design when the raft foundation alone provides sufficient load capacity, but at the same time settlements are excessive. This is the case in high plasticity stiff clays such as London Clay. It was also identified that when building on old piles, piles had to sustain a certain load from the previous structure over a period of time, during which the soil is subjected to the time-related processes of consolidation and creep. Also, several other processes, which affect the frictional resistance of piles, were identified in the literature.

A literature review on the time dependent behaviour of soils then followed. As a consequence of the review, a time dependent constitutive model, the ET Creep model, was employed in the author's analyses. This model is capable of reproducing several aspects of the time dependent behaviour of soils including creep. The model parameters were then calibrated with the results of laboratory tests on London Clay sampled from Heathrow Terminal 5.

Then, preliminary analyses of single piles were performed, in order to assess the time effects on the performance of single piles. Numerical model calibration was made with documented single pile load tests, both maintained load and CRP tests, as well as with a well instrumented piled raft foundation at Stonebridge Park, London. The single pile load tests included a test at Heathrow T5 and load tests on piles from the Stonebridge Park foundation before the construction of the building and after its demolition approximately 30 years later, allowing the assessment of the time effects on piles preloaded during a long period under working load.

3D parametric analyses were then performed in order to assess the appropriate location and dimensions of piles and raft thickness. The performance of piled raft foundations with time was assessed parametrically at different levels of preloading. Subsequently, optimisation of the performance of the piled raft foundation at Stonebridge Park was attempted by examining several pile arrangements.

8.2. TIME DEPENDENCY AND CONSITUTIVE MODELLING OF NATURAL STIFF CLAYS

One of the initial objectives of this research was to review the time dependent behaviour of soils, and in particular of saturated clays, in order to assess the main aspects required to be reproduced in numerical analysis of piled foundations. Time effects include consolidation, soil viscosity and time dependent structuration (soil ageing). In terms of constitutive modelling, an important feature of soils is strain rate effects and whether soils exhibit isotach or non-isotach viscosity. Isotach viscosity implies a unique stress-strain-strain rate relationship, whereas non-isotach viscosity, including pure and general TESRA behaviour, does not. In general, clays are known to exhibit isotach viscosity.

In this thesis, two constitutive models were employed to model the behaviour of saturated clays, including a form of the elasto-plastic Modified Cam Clay model and the visco-plastic Equivalent Time (ET) Creep model developed by Bodas Freitas (2008). A series of finite element analyses employing the ET Creep model were performed by Bodas Freitas (2008), primarily for normally consolidated soft clays, in order to validate the formulation of the model by comparing the model predictions with the observed experimental trends. Further validation of the ET Creep model was performed in this research for the time dependent behaviour of natural overconsolidated stiff clays. This leads to the following conclusions:

- Isotach viscosity in the normally consolidated range in one-dimensional compression, as well as strain rate dependency of the peak deviatoric stress in undrained triaxial compression, is well predicted by the ET Creep model.
- Strain rate dependency at low deviatoric stresses during undrained triaxial compression and in the overconsolidated range during one-dimensional compression agrees also with isotach viscosity.
- Development of creep strains in one-dimensional compression and undrained triaxial compression is well predicted.
- The failure initiated at stress states close to the peak deviatoric stress under constant deviatoric creep associated with creep rupture is well predicted.
- The presence of structure in natural overconsolidated stiff clays and it degradation upon loading can be employed in the ET Creep model. However, no development of structure with time during creep can be reproduced.

In order to perform finite element analyses of piled raft foundations in London Clay, the ET Creep model is employed to simulate the time dependent behaviour of London Clay. The ET Creep model can realistically reproduce the basic features of viscosity and rate dependency of intact London Clay. The viscosity of London Clay in its natural state is characterised as isotach. In particular,

- Isotach viscosity is observed for both small and large strains in the pre- and post-peak regions during shearing.
- The peak strength is strain rate dependent.
- The critical state appears to be independent of strain rate and unique in the e-p'-q space.
- The relationship between the strain and the logarithm of time during secondary compression is regarded as linear for both volumetric and deviatoric creep conditions.

The required model parameters to model accurately both the monotonic rate and time dependent behaviour of London Clay were calibrated and validated using laboratory tests performed by Gasparre (2005) and Sorensen (2006) on London Clay samples from Heathrow Airport Terminal 5.

The coefficient of secondary compression (C_α), a major time dependent parameter of the ET Creep model, for natural London Clay was assumed to be equivalent to the value determined from tests on reconstituted samples. This is due to the fact that the value of C_α cannot be calibrated from creep tests on intact samples at stress levels which are similar to the in-situ stresses, due to swelling and sample disturbance during sampling, affecting the soil structure and subsequent creep during loading. Therefore, no time delay due to creep history is observed.

Oedometer tests and triaxial compression tests were utilised to calibrate the monotonic rate behaviour of London Clay and derive the model parameters that define compressibility, shear strength and structure of the different lithological units encountered at Heathrow. The elastic shear modulus, the second elastic parameter of the ET Creep model, was back-analysed from a pile load test performed at the Heathrow Airport Terminal 5 site. In addition, an oedometer creep test and a triaxial compression test, involving a stepwise change of strain rate, were utilised to validate the model parameters defining the time dependency of London Clay. From these, it was concluded that the ET Creep model reproduces well the development of viscoplastic strains with time at a stress level equivalent to the normally consolidated range of the soil. Also, similar observations to those made from the model validation for natural

overconsolidated stiff clays, including the viscosity at small and large strains, were made. However, it was concluded that the ET Creep model overestimates the effect of strain rate change during shearing.

8.3. TIME EFFECTS AND OPTIMUM DESIGN OF PILED RAFT FOUNDATIONS

Time effects and the optimum design of piled raft foundations were based on:

- a series of FE analyses of single piles in soft and stiff clays,
- back-analyses of pile load tests in London Clay,
- numerical analyses of a piled raft foundation in London Clay (Hiscocks House),
- numerical analyses of a hypothetical pile raft foundation in London Clay.

In the following, a brief description of the objectives, achievements and conclusions is made.

FE analyses of single piles in soft and stiff clay

Preliminary finite element analyses of the short-term and long-term behaviour of single piles founded in soft clay and stiff clay ground conditions were performed. The scope of these analyses was to quantify the effects of time on the behaviour of piled foundations. The effect of preloading on the axial load capacity of piles was examined. The results allow the assessment of the alternative design strategies for piles including conventional piles, 'creep piles' and 'settlement reducing piles'.

The single pile examined numerically was a typical friction pile, 20 m long and 1 m in diameter. The single pile was assumed wished in place with full adhesion between the pile and soil. Therefore, the effects of installation were omitted and the processes examined were those that take place after the effects of installation have stabilised.

Two constitutive models, a form of the Modified Cam Clay (MCC) model (Potts & Zdravkovic, 1999) and the Equivalent Time (ET) Creep model (Bodas Freitas, 2008) were employed. The MCC model accounts for the consolidation processes in the ground and can predict accurately the change of undrained shear strength during consolidation. The ET Creep model also accounts for consolidation and in addition accounts for creep effects. It can predict the change of undrained shear strength due to the development of viscoplastic strains, or creep strains, with time, along with the associated changes due to consolidation.

The ground profiles adopted for this study included (a) a soft clay profile and (b) a stiff clay profile. Similar soil conditions and model parameters to those adopted by Zdravkovic et al. (2003) and Bodas Freitas et al. (2007) for a footing problem on the same soft clay site were used, in order to make the single pile and the footing analyses consistent. For the stiff clay site, the material properties were assumed to be those of a typical natural overconsolidated stiff clay.

The following conclusions arise from the MCC soft clay analyses:

- The single pile works as a friction pile with the capacity mainly being provided by shaft resistance.
- Analyses for different levels of preloading (20, 40, 60 and 80%) indicate that there is little gain in capacity for all levels of preloading due to the dissipation of excess water pressures generated during initial loading.

The following conclusions arise from the ET Creep model soft clay analyses:

- A realistic loading rate of the single pile is required due to the time dependent nature of the ET Creep model.
- The initial short term load capacity of the single pile (2266 kN) is quite different to the value calculated in the MCC analysis (1615 kN). This is attributed to the difference of the plastic potential surface in the deviatoric plane between the ET Creep and the MCC models.
- Preloading the single pile for a period of 50 years results in increased load capacity on subsequent loading. The gain in pile capacity increases with the level of pre-loading. This is due to the development of viscoplastic strains (creep strains) under constant deviatoric stress conditions along the pile shaft, which enhances the soil's strength.

The following conclusions arise from the ET Creep model stiff clay analyses:

- Excess pore water pressures during initial loading are concentrated around the pile toe, similar to the soft clay analysis implying limited gain in capacity due to the consolidation processes.
- Preloading at different levels of the initial load capacity results in increased load capacity after a 50 year period of sustained load. The enhancement of the capacity is attributed to creep, and in particular to creep strains (viscoplastic strains) developed under constant deviatoric stress conditions in the soil surrounding the pile shaft, which enhances the shear strength of the soil.

- The calculated settlements, both creep and consolidation, increase with the level of preloading. However, at levels of preloading close to the initial short term capacity (>70%), it is observed that settlement increases in a disproportional manner than at smaller levels of preloading.
- A lower gain in the load capacity at higher levels of preloading than the gain observed at lower levels of preloading is predicted. Between 70 and 80% of preloading of the initial load capacity, the rate of increase of the capacity enhancement is decreasing with respect to lower levels of preloading, where an increasing rate is observed. Between 80 and 85% of preloading, the rate becomes negative and for higher levels of preloading in the range of 90+%, creep settlement results in failure. This effect is attributed to the progressive failure of the pile from top towards the bottom.

Comparison of the soft clay and stiff clay analyses leads to the following conclusions:

- In soft clays, the gain in pile capacity at levels of preloading close to the initial short term capacity does not reduce like that predicted for stiff clays when considering creep. This is due to the fact that no creep induced failure is observed in the soft clay elements surrounding the pile during sustained loading.
- The creep effects are more evident in soft clays than in stiff clays, due to the larger development of viscoplastic strains in normally consolidated soils than in overconsolidated soils.

Back-analysis of pile load tests in London Clay

A back-analysis of the documented pile load tests from Heathrow and Stonebridge Park was performed in order to quantify the effects of installation on the surrounding soil. The pile load test at the Heathrow Airport Terminal 5 site involved a CRP test, whereas the load test at Stonebridge Park involved an initial incremental maintained load test followed by a CRP test. The main objectives of the back-analysis were:

- to back-analyse the ET Creep model parameter defining the elastic shear modulus and validate the rest of the model parameters for the lithological units encountered at the Heathrow Airport area and those assumed for Stonebridge Park, and
- to back-analyse the angle of interface friction (δ') between the soil and the pile and quantify the resulting softening around the pile shaft due to boring.

Regarding the pile load test at Heathrow, several aspects of the load test were considered in the finite element analysis, ranging from the effects of pile installation on the surrounding soil to the several techniques applied in the test.

The London Clay profile at Heathrow adopted in the numerical analysis was divided into three main lithological units, A, B and C, which in turn were divided into several sub-units. The Harwich Formation was not considered in the analysis. The London Clay profile was modelled using the ET Creep model, and the model parameters assigned were those calibrated from the results of laboratory tests on samples from the Heathrow Airport Terminal 5 site. The Made Ground and the Terrace Gravel on top of London Clay were both modelled using the Mohr-Coulomb model.

In the numerical simulation, the appropriate shear modulus profile with depth was back-analysed by following an iterative procedure along with the calibration of the ET Creep model parameters with the results from the laboratory tests, in order to match the predicted load-settlement response with the recorded response. The back-analysed shear modulus profile plots along the small strain G_{hv} shear modulus profile obtained from the laboratory tests.

The pile under investigation was installed in London Clay by boring. Numerically, a "soft zone" around the pile shaft was adopted. The thickness of the "soft zone" of elements was proportional to the pile diameter. The elements in the "soft zone" were modelled using the ET Creep model.

The reduction of the angle of skin friction (δ') was simulated by the adoption of a lower angle of shearing resistance in the model parameters ($\delta' < \varphi'$). This value was back-analysed using the documented load-settlement response of the pile load test and it was found to be close to the residual angle of shearing resistance. The back-analysed angle of skin friction was $\delta_{ult}{}'$ = 12^{o}. The $\delta_{peak}{}'$ angle is rate dependent due to the formulation of the ET Creep model and the time dependency of the peak strength. The adopted angle of skin friction, and the assumed relief of lateral stresses and softening, gave a pile adhesion factor α equal to 0.37.

Regarding the pile load tests at Stonebridge Park, similar considerations to those adopted for the Heathrow pile test concerning the effects of installation were made. A "soft zone" around the pile with a lower angle of shear friction was employed. The model parameters were similar to those employed for the Heathrow pile test for the lithological units encountered in Stonebridge based on a soil investigation at Wembley.

The load-settlement response of the single pile in question was compared with the documented results, where a good match of the load-settlement response was obtained for the adopted shear modulus profile based on data from Wembley. The angle of interface friction in the "soft zone" was back-analysed to give $\delta_{ult}{}' = 14^{o}$. An adhesion factor α equal to 0.5 was obtained.

Numerical analysis of a piled raft foundation in London Clay – Hiscocks House in Stonebridge Park

A series of 3D finite element analyses of a piled raft foundation in London Clay at Stonebridge Park was performed. Initially, the results of the analysis for the conventional piled raft foundation of Hiscocks House were validated with the field observations of Cooke et al. (1981). Subsequently, a series of parametric analysis were performed by varying the raft thickness, the number of piles and the pile length, as well as the pile geometry underneath the raft. The effects of time on the performance of the original piled raft foundation for Hiscocks House were also examined.

The dimensions of the conventional piled raft are 43.3 m by 19.2 m, with a thickness of 0.9 m. The piles are 13 m long and 0.45 m in diameter, and are installed on a square grid of 1.6 m distance centre to centre. Both the piles and the raft were modelled as a linear elastic concrete material. A "soft zone" with a lower angle of shearing resistance, was discretised around the piles. The ET Creep model was employed to simulate the behaviour of the London Clay units and of the Lambeth Group identified at Stonebridge Park, including the "soft zone" around the piles.

Initially, the performance of the original foundations of Hiscocks House, as documented by Cooke et al. (1981), was compared with the finite element predictions, allowing the validation of the numerical and constitutive models employed in the FE analyses. The following conclusions were made:

- The foundation settles as a block unit. This behaviour is enhanced by the presence of the raft. The majority of the settlement accumulates at a depth level below the pile toe.
- The foundation settles more in its centre, with the minimum settlement being predicted and recorded in the corners. This is typical of conventional piled raft foundations, implying that a smaller number of piles oriented towards the centre of the raft would be more beneficial in reducing differential settlement than a large number of piles uniformly distributed over the raft area.

- The piles close to the periphery of the foundation attract more load than internal piles. This is attributed to the fact that the relative settlement of the internal piles is larger than the relative settlement of the piles at the periphery.
- The load share between piles depends on the relative settlement of each individual pile. The piles that settle the least in the foundation system attract the larger loads, whereas those that settle the most are loaded the least. In the Hiscocks House case, the loads on the corner piles and on the edge piles are increasing, whereas the loads attracted by the internal piles are reducing with elapsed time. This is attributed to the evolution of settlements, in particular to increasing differential settlements, at the raft level.
- The contact stress between the raft and the soil is maximum at the corners and minimum at the centre of the raft, similarly to the pile load distribution.
- The majority of the support is provided by the piles (~80%) with the raft providing approximately 20% of the total support, a typical value for a conventional piled raft. The load share of the piles increases with increasing structural load. The larger the structural load, the larger the proportion of load carried by the piles. For instance, the load share of the piles at a level of structural load of 3.5, 6.5, 12 and 16 storeys and at building occupation is 51.4, 66.5, 74.9, 79.7 and 83.4 % respectively. This is due to the fact that the supporting clay below the raft is consolidating with time, resulting in increased support by the piles.

Next, the factor of safety against bearing failure and the long-term predicted settlements at working conditions were determined, in order to assess whether the design of the conventional piled raft is cost-effective. The following were concluded:

- A factor of safety equal to 3.52 was predicted, which satisfies the conventional design limits. However, the predicted value is considered to be conservative.
- The maximum settlement in the centre of the raft after approximately 30 years of structural life was predicted to be 62.0 mm. This is well below the suggested maximum tolerable absolute settlement of 150 mm.
- The maximum angular distortion at the end of Hiscocks House life, determined by the differential settlement centre-to-corner, was calculated to be 1/1060. This value satisfies the recommended design limit of 1/500 and is considered conservative.

A parametric study of raft thickness on the behaviour of a raft foundation designed to support Hiscocks House was performed, in order to examine whether a raft solution would be feasible for the foundations of Hiscocks House. The original raft thickness of 0.9 m and two raft

thicknesses of 1.5 m and 2.5 m were employed in the analyses. The following were concluded:

- The un-piled raft foundation with the original thickness provides sufficient load capacity with a factor of safety equal to 2.96. This satisfies the conventional design limit, and therefore such a raft foundation is characterised as a 'large' raft.
- For all parametric cases, the raft is sagging towards the centre, being indicative of the area where the performance of the raft foundation should be enhanced if differential settlements are deemed excessive.
- Absolute settlements, 30 years after the application of the total structural load on the raft, are excessive, resulting in potential serviceability problems. The amount of absolute settlement increases with increased raft thickness, reflecting the increase of the weight of the thicker rafts.
- Differential settlements for the original raft thickness result in an angular distortion equal to 1/330. Such distortion is expected to result in increased tensile strains in the structural materials, resulting in cracking to walls and even to structural damage. The amount of differential settlement drops with increased raft thickness, reflecting the increased rigidity of the raft. Thicker raft foundations limit angular distortion into tolerable angles of 1/580 and 1/1470 for 1.5 and 2.5 m thickness respectively.

A parametric study on the number of piles (185, 107 and 55 piles) and the piles length (17.5, 13.0 and 8.75 m) allowed the assessment of a more optimum and more cost-effective solution than the one adopted originally for the foundations of Hiscocks House. The fact that the raft alone provides enough load capacity indicates that piles may be introduced below the raft only in order to reduce settlement. Piles were located in the central region of the raft area, keeping the original pile grid 1.6 m centre to centre (~3.5d).

Each parametric case was loaded up to the load level of Hiscocks House and approximately 30 years of elapsed time was applied. The following conclusions are drawn:

- The addition of piles under the central area of the raft reduces the settlement in the central area, resulting in hogging (i.e. negative values for differential settlement) instead of the predicted sagging in raft and conventional piled raft foundations. For the majority of the parametric cases, the maximum settlement of the raft is on the periphery of the raft, whereas the minimum settlement is in the centre or close to the centre of the raft.

- For the case of 55 piles with pile lengths of 8.75 m, the piles do not dominate the behaviour of the foundation, and a more uniform settlement profile is obtained with the periphery of the raft sagging and the centre of the raft, where the piles are present, hogging. This design is considered as the most efficient, due to the fact that it minimizes differential settlement centre-to-corner close to zero, and implies a potential saving in piling costs.
- For equal total pile length but with different number of piles, a smaller number of longer piles decrease the settlement in the central region more effectively than a larger number of shorter piles.
- The smaller the number of piles, the larger the influence of the piles length on differential settlement. For a smaller number of piles the piled raft foundation performance is more sensitive to pile length changes.
- A more sensible approach would be the uniform distribution of piles under the raft area but with a variation of the pile lengths with longer piles in the central region and shorter piles at the periphery, in order to avoid the hogging effect and minimise differential settlement.
- The pile spacing employed in the analysis is the original spacing of Hiscocks House, which initiates block settlement behaviour. Such behaviour reduces the efficiency of the individual piles in the piled raft foundation, and therefore a larger spacing of piles would provide a more cost-effective solution.

The effects of time on the performance of the original piled raft foundation for Hiscocks House were examined. In particular, the effect of sustained loading on the long-term behaviour of the original foundations and the results of two pile load tests, on a test pile before the erection of Hiscocks House and on a working pile after the demolition of Hiscocks House, were assessed.

The following are concluded from 30 years of sustained loading on the piled raft foundation:

- The overall load capacity is enhanced by 10.5 % after 30 years of consolidation and creep. Such enhancement indicates that the factor of safety against bearing failure increases with time, allowing for additional loading on the foundations.
- An enhancement to the overall stiffness of the foundations is predicted after 30 years of consolidation and creep.

The following are concluded from the simulation of the pile load tests:

- The pile load test on a working pile after the demolition of the superstructure indicated insignificant enhancement of the pile stiffness and capacity in respect to the test before the erection of the superstructure. This is believed to be associated with the fact that the foundation is settling as a block with the majority of the resistance being provided by the piles base and not through shaft friction of each individual pile.
- The rate effects in single pile load testing are significant. Comparison between pile load tests should be for tests with similar loading rates.
- Other processes than creep and consolidation may affect the long-term behaviour of piles, including changes at the soil-shaft interface and the time-dependent structuration of the soil surrounding the pile.

Numerical analysis of a hypothetical piled raft foundation in London Clay

A parametric study of a hypothetical piled raft foundation was performed, in order to:

- assess whether a central support of piles underneath the raft with less piles is more beneficial than a uniform distribution of piles with more piles, and
- examine the effect of preloading on the piled raft behaviour for each parametric case.

The number of piles, the geometry and the level of preloading were varied. Three types of foundations were modelled:

(a) a raft foundation,
(b) a piled raft foundation with uniform distribution of piles, and
(c) a piled raft foundation with central pile support.

The raft was a square raft 20.0 m by 20.0 m and 0.5 m thick, founded at 0.5 m deep. The uniform piled raft foundation consisted of 25 piles uniformly distributed (12.5 m long with 0.5 m diameter), whereas the piled raft foundation with central support consisted of 5 piles of similar dimensions centrally located under the raft. Piles were installed on a square grid of 4.0 m distance centre to centre for both piled cases.

Both the piles and the raft were modelled as a linear elastic material representing the stiffness of concrete. A “soft zone” with a lower angle of shearing resistance, was discretised around the piles. The ET Creep model was employed to model the behaviour London Clay units and of the Lambeth Group, including the “soft zone” around the piles. Model parameters for each soil layer were those set for Stonebridge Park.

The following conclusions are drawn from the results of the parametric analysis:

- The overall load capacity of the piled raft foundation with 25 piles is larger than the capacity of the piled raft foundation with 5 piles and the un-piled raft foundation respectively.
- The addition of piles enhances the overall stiffness of the foundation. The un-piled raft foundation gives the softest response, whereas the piled raft foundation with 25 piles gives the stiffest response.
- The contribution of the piles to the overall load capacity is limited in respect to the contribution of the raft. The piles load share for the piled raft with 25 piles is approximately 50% and for the piled raft with 5 piles is approximately 15%. The piles load share, however, is varying depending on the applied load level and the level of mobilisation of the piles resistance.
- For the case with the 25 piles, for low levels of applied load, the piles' resistance increases up to an applied load level where the piles' resistance is fully mobilised and the ultimate load capacity of the piles is reached. After the peak resistance of the piles, the total pile resistance reduces marginally with increasing applied load, demonstrating the possibility of small amount of 'undrained' post-peak softening behaviour of London Clay. For the case with 5 piles, due to the limited number of piles, the piles mobilise at much lower applied load levels.

Contours of settlement at a realistic level of loading in the short term and in the long term allow the following to be concluded:

- The piled raft foundation with the uniform distribution of 25 piles mobilises the shaft capacity of the piles and a block settlement behaviour is avoided. This is attributed to the large spacing of the piles (= 8.0d).
- The significant contribution of the piles in reducing absolute settlements of the raft is demonstrated.
- The raft foundation is sagging towards the centre of the raft with the maximum settlement in the centre and the minimum settlement in the corner of the raft. This is also the case for the piled raft foundation with the uniform distribution of piles.
- Central pile support results in a non-uniform settlement profile in the short term. Pile support in the central region of the raft reduces local settlement, resulting in local hogging and reduced centre-to-corner differential settlement in respect to the uniform piled raft foundation, despite the fact the absolute settlements are larger.

- In the long term, no hogging in the centre of the raft is observed for the piled raft foundation with central support. This is attributed to creep and the resulting deformations with time. The fact that piles are loaded very close to their ultimate load capacity results in increased deformations with time due to creep, reducing their efficiency in reducing settlements.

Preloading the foundations for a period of 50 years, allows the following conclusions to be drawn:

- The gain in load capacity and the development of settlements due to consolidation and creep are increasing with the level of preloading. The larger the applied load, the larger the settlement and the gain in capacity after 50 years of elapsed time.
- The normalised gain in capacity is larger for the un-piled raft foundation than in the piled raft foundations. This is attributed to the fact that the piles shaft friction is fully mobilised at the applied load level, resulting to limited gain in pile capacity with time.

8.4. RECOMMENDATIONS FOR FURTHER RESEARCH

The research presented in this thesis has demonstrated the importance of the time dependent behaviour of soils in piled foundation problems. The time dependent ET Creep model was employed for the analysis of piled foundations and the simulation of the behaviour of natural stiff clays, including London Clay. This research demonstrated several aspects that require further examination, including aspects related to the ET Creep model, the design and reuse of piled raft foundations.

The following aspects in terms of the ET Creep model are recommended for further research:

- Incorporate a small strain stiffness facility to the model formulation of the ET Creep model to describe the elastic part of the model. In the ET Creep model, the elastic shear modulus, along with the slope of instant time line, characterises the elastic response of the soil. For overconsolidated soils, the elastic shear modulus is pseudo-linear up to yielding due to the pseudo-elastic behaviour of the model in the overconsolidated range of stress states, and therefore an appropriate value has to be assigned in order to reflect the strain ranges encountered. Considering the fact that the soil stress-strain behaviour is highly non-linear, this may result in overestimation or underestimation of deformation.

- Incorporate a mechanism for structure development with time. In the literature, it has been shown that time dependent structuration is an important mechanism that may affect the compressional behaviour of clays. The ET Creep model can only predict destructuration due to the development of visco-plastic volumetric strains.
- Incorporate a structure mechanism in which the structure degradation law is a function of both deviatoric and volumetric visco-plastic strain components.
- Incorporate in the model formulation of the ET Creep model a rotation of the yield and plastic potential surfaces in J-p′ stress space to account for anisotropy. Anisotropy is considered to play an important role in stiff overconsolidated clay, such as London Clay, during shearing.

The following aspects in terms of the design and reuse of piled raft foundations are recommended for further research:

- Examine the effect of pile spacing in the design of piled raft foundations. Small pile spacings result in block settlement behaviour, where the efficiency of each individual pile is reduced. Also, the raft linking the piles is known to enhance this block settlement behaviour. Therefore, the combined effect of the presence of the raft with pile spacing should be considered in the design of piled raft foundations.
- Uniform loading was assumed in this research as an idealisation for the structural loading on the foundations. In practice, concentrated column loading is applied on rafts which may result in increased bending stress in the raft. In addition, new developments tend to have a central core, where the majority of the load is concentrated. The concentration of loading in the central zone would result in even larger deformations in the central region of the raft. Therefore, this should be considered when designing the pile support under the raft.
- The effects of boring on the surrounding soil were simulated in the numerical analyses of piled raft foundations in this research. The installation effects were quantified through a back analysis of documented pile load tests. Pile driving is another method of installation, which was not considered in the analyses in this research. A back analysis of pile load tests on driven piles could be performed in the future.
- The ET Creep model was employed for the analysis of piled raft foundations, which accounts for both consolidation and creep. Another constitutive model could be employed, which accounts only for consolidation, such as the MCC model, in order to differentiate the effects of consolidation and creep on the long term behaviour of piled raft foundations.

- In this research, the reuse of piled raft foundations has been examined without considering the addition of fresh piles along with the reused piles. Fresh piles may be required, if the new structural load is significantly larger than the previous one. Also, if the structural loading on the piled raft foundation changes or if the existing structure is extended, additional piles may be required, in order to enhance the piled raft foundation performance in certain areas.

References

Aboshi, H. (2004). Long-term effect of secondary consolidation on consolidation settlement of marine clays. *Advances in Geotechnical Engineering: The Skempton Conference.* London: Thomas Telford.

American Petroleum Institute. (1986). RP2A: Recommended practice of planning, designing and constructing fixed offshore platforms. *16th*, 59-61. Washigton.

Anderson, S. A., Bird, J. F., & Chapman, T. J. (2006). Assessment of risks and opportunities of foundation reuse. *Reuse of Foundations for Urban Sites: Proceedings of International Conference.* Watford, UK.

Arulanandan, K., Shen, C. K., & Young, R. B. (1971). Undrained creep behaviour of a coastal organic silty clay. *Geotechnique, 21* (4), 359-375.

Atkinson, J. H. (2000). Non-linear soil stiffness in routine design. *Geotechnique, 50* (5), 487-508.

Augustesen, A. H. (2006). *The effects of time on soil behaviour and pile capacity*. PhD thesis. Aalborg University, Denmark.

Augustesen, A., Liingaard, M., & Lade, P. V. (2004). Evaluation of time-dependent behaviour of soils. *International Journal of Geomechanics , 4* (3), 137-156.

BCA/BSRIA. (1999). *Refurbishment of concrete buildings: structural and services Guidance note GN8./99.* Bracknell, UK: The Building Services Research and Information Association.

Biot, M. A. (1941). General theory of three-dimensional consolidation. *Jnl. Appl. Phys. , 12*, 155-164.

Bishop, A. W. (1966). The strength of soils as engineering materials. In *Milestones in Soil Mechanics* (pp. 131-172). Thomas Telford.

Bishop, A. W., Webb, D. L., & Lewin, P. I. (1965). Undisturbed samples of London Clay from the Ashford Common shaft: strength-effective stress relationships. *Geotechnique , 15* (1), 1-31.

Bjerrum, L. (1963). Discussion. *Proceedings European Conference SMFE, 3*, pp. 135-137. Wiesbaden.

Bjerrum, L. (1967). Engineering geology of Norwegian normally consolidated marine clays as related to the settlements of buildings. *Geotechnique, 17* (2), 83-118.

Bjerrum, L. (1973). Problems of soil mechanics and construction in soft clay. *Proceedings of the 8th International Conference, ISSMFE, 3*, pp. 150-157. Moscow.

Bodas Freitas, T. M. (2008). *Numerical modelling of the time dependent behaviour of soils*. PhD thesis. University of London (Imperial College London).

Bodas Freitas, T. M., Potts, D. M., & Zdravkovic, L. (2007). A numerical study on the effect of ageing on undrained bearing capacity. *10th International Symposium on Numerical Models in Geomechanics*, (pp. 419-424).

British Geological Survey. (2004). *Geology of London, Special Memoir 256, 257, 270 and 271 (England and Wales).* Keyworth, Nottingham.

British Standards Institution. (1986). BS 8004:1986. *Code of practice for foundations* . British Standards Institution.

Brown, P. T., & Wiesner, T. J. (1975). The behaviour of uniformly loaded piled strip footings. *Soils and Foundations, 15*, 13-21.

Bullock, P. J., Schmertmann, J. H., McVay, M. C., & Townsend, F. C. (2005a). Side shear setup. I: Test piles driven in Florida. *Journal of Geotechnical and Geoenvironmental Engineering, 131* (3), 292-300.

Bullock, P. J., Schmertmann, J. H., McVay, M. C., & Townsend, F. C. (2005b). Side shear setup. II: Results from Florida test piles. *Journal of Geotechnical and Geoenvironmental Engineering, 131* (3), 301-310.

Burland. (1973). Shaft friction of piles in clay - a simple fundamental approach. *Ground Engineering, 6* (3), 30-42.

Burland, J. B. (1995). Piles as settlement reducers. *19th Italian Cong. Soil Mech.*, (pp. 21-34). Pavia, Italy.

Burland, J. B., & Hancock, R. J. (1977). Underground car park at the House of Commons, London: geotechnical aspects. *Struct. Engr, 55* (2), 87-100.

Burland, J. B., & Kalra, J. C. (1986). Queen Elizabeth II Conference Centre: geotechnical aspects. *Proc. Instn. Civ. Engrs, 80* (Part I), 1479-1503.

Burland, J. B., & Twine, D. (1988). The shaft friction of bored piles in terms of effective strength. *Proc. 1st Int. Geot. Sem. on Deep Foundations on Bored and Auger Piles*, (pp. 411-420). Ghent.

Burland, J. B., & Wroth, C. P. (1974). Settlement of buildings and associated damage. *Proc. Conf. Settlement of Structures* (pp. 611-651). Cambridge: Pentech Press.

Burland, J. B., Broms, B. B., & De Mello, V. F. (1977). Behaviour of foundations and structures. *Proceedings of the 9th International Conference of Soil Mechanics and Foundation Engineering, 2,* pp. 495-546. Tokyo.

Bustamante, M., & Gianeselli, L. (1982). Pile bearing capacity by means of static penetrometer CPT. *Proceedings of the 2nd European Symposium on Penetration Testing,* (pp. 493-500). Amsterdam.

Butcher, A. P., & Skinner, H. D. (2006). Stonebridge Park a demolition case-study. *Reuse of Foundations for Urban Sites: Proceedings of International Conference.* Watford, UK.

Butcher, A. P., Powell, J. J., & Skinner, H. D. (Eds.). (2006a). *Reuse of Foundations for Urban Sites: Proceedings of the International Conference.* IHS BRE Press.

Butcher, A. P., Powell, J. J., & Skinner, H. D. (Eds.). (2006b). *Reuse of foundations for urban sites: A best practice handbook.* IHS BRE Press.

Butterfield, R., & Banerjee, P. K. (1971). The elastic analysis of compressible piles and pile groups. *Geotechnique, 21* (1), 43-60.

Chandler, R. J. (2000). Clay sediments in depositional basins: the geotechnical cycle. *Quarterly Journal of Engineering Geology and Hydrogeology, 33,* 7-39.

Chandler, R. J. (1968). The shaft friction of piles in cohesive soils in terms of effective stress. *Civil Eng. And Public Works Review, 63,* 48-51.

Chapman, T. J., Marsh, B., & Foster, A. (February 2001). Foundations for the future. *Proc ICE, Civil Engineering, 144,* pp. 36-41.

Chapman, T., Anderson, S., & Windle, J. (2007). *Reuse of foundations.* CIRIA C653, Classic House, 174-180 Old Streer, London EC1V 9BP, UK.

Cheong, M. T. (2007). Case Study: Negative Skin Friction Development on Large Pile Groups for the New Wembley Stadium. *18th European Young Geotechnical Engineers' Conference.* Ancona, Italy.

Chow, F. C. (1997). *Investigations into displacement pile behaviour for offshore foundations*. PhD Thesis. University of London (Imperial College).

Clancy, P., & Randolph, M. F. (1993). An approximate analysis procedure for piled raft foundations. *Int. J. Numer. Anal. Methods Geomech , 17,* 849-869.

Cooke, R. W. (1986). Piled raft foundations on stiff clays: a contribution to design philosophy. *Geotechnique, 36* (2), 169-203.

Cooke, R. W., Bryden-Smith, D. W., Gooch, M. N., & Sillet, D. F. (1981). Some observations of the foundation loading and settlement of a multi-storey building on a piled raft foundation in London Clay. *Proc. ICE, Part 1, 70,* pp. 433-460.

Cooling, I. F., & Gibson, R. E. (1955). Settlement studies on structures in England. *Proc. Conf. Correlation of Calculated and Observed Stresses and Deformation in Structures*, (pp. 295-317). London.

Council of Europe. (1992). European convention on the protection of the archaeological heritage (revised). Valleta, Malta.

Craig, R. F. (1997). *Soil mechanics* (6th ed.). London and New York: Spon Press.

Davies, P. (1975). *Creep characteristics of three undisturbed clays*. PhD Thesis. Imperial College London.

De Cock, & Legrand. (1997). Design of Axially Loaded Piles - European Practice. In D. Cock, & Legrand (Ed.), *Proceedings of the ERTC3 (The ISSMFE European Regional Technical Committee 4 "Piles"), Design of Axially Loaded Piles - European Practice.* Rotterdam: Balkema.

den Haan, E. J. (1994). Summary of session 1: One-dimensional behaviour. *Proceedings of the International Workshop on Advances in Understanding and Modelling the Mechanical Behaviour of Peat* (pp. 131-140). Rotterdam: Balkema.

Desai, C. S. (1974). Numerical design-analysis for piles in sands. *Jnl. Geot. Eng. Divn., ASCE, 100* (GT6), 613-635.

English Architectural Glazing. (2008). *Juxon House [image]*. Retrieved September 8, 2008, from http://www.eag.uk.com/portofolio/juxon_house.php

Fleming, K., Weltman, A., Randolph, M., & Elson, K. (2009). *Piling Engineering* (3rd ed.). Taylor & Francis Group.

Fleming, W. G., & Thorburn, S. (1983). Recent piling advances, State of the Art Report. *Proc. Conf. on Advances in Piling and Ground Treatment for Foundations.* London: ICE.

Fleming, W. G., Weltman, A. J., Randolph, M. F., & Elson, W. K. (1992). *Piling Engineering* (2nd ed.). Surrey University Press.

Franke, E., Lutz, B., & El-Mossallamy, Y. (1994). Measurements and numerical modelling of high-rise building foundations on Frankfurt clay. *Vertical and Horizontal Deformations of Foundations and Embankments, ASCE Geot. Spec. Pub., 40* (2), 1325-1336.

Fraser, R. A., & Wardle, L. J. (1976). Numerical analysis of rectangular rafts on layered foundations. *Geotechnique, 26* (4), 613.

Gasparre, A. (2005). *Advanced laboratory investigation of London Clay*. PhD thesis. Imperial College of Science Technology and Medicine, University of London.

Gasparre, A., & Coop, M. R. (2008). Quantification of the effects of structure on the compression of a stiff clay. *Canadian Geotechnical Journal, 45* (9), 1324-1334.

Gasparre, A., Nishimura, S., Minh, N. A., Coop, M. R., & Jardine, R. J. (2007). The stiffness of natural London Clay. *Geotechnique, 57* (1), 33-47.

Hain, S. J., & Lee, I. K. (1978). The analysis of flexible pile-raft systems. *Geotechnique, 28* (1), 65-83.

Hansbo, S. (1984). Foundations on friction creep piles in soft clays. *Proceedings of the International Conference on Case Histories in Geotechnical Engineering, 2*, pp. 913-922. St Louis.

Hansbo, S. (1993). Interaction problems related to the installation of pile groups. *International Geotechnical Seminar on Deep Foundations on Bored and Auger Piles*, (pp. 59-66). Ghent.

Havel, F. (2004). *Creep in soft soils*. PhD thesis. Norwegian University of Science and Technology, Trondheim.

Hight, D. W., Gasparre, A., Nishimura, S., Minh, N. A., Jardine, R. J., & Coop, M. R. (2007). Characteristics of the London Clay from the Terminal 5 site at Heathrow Airport. *Geotechnique, 57* (1), 3-18.

Hight, D. W., McMillan, F., Powell, J. J., Jardine, R. J., & Allenou, C. P. (2003). Some characteristics of London Clay. In T. S. Tan, K. K. Phoon, D. W. Hight, & S. Lerouil (Ed.), *Proc. Conf. Characterisation and Engineering. 2*, pp. 851-908. Balkema: National University Singapore.

Hooper, J. A. (1973). Observations on the behaviour of piled-raft foundation on London Clay. *Proc. ICE, 55* (2), 77-90.

Institution of Structural Engineers. (1989). *Soil-structure interaction: The real behaviour of structures.* London, UK.

Jardine, R. J., & Chow, F. C. (1996). *New Design Method for Offshore Piles, Report MTD 96/103.* Marine Technology Directorate ltd.

Jardine, R. J., & Christoulas. (1991). Recent developments in defining and measuring static piling parameters. *Proc. Conf. Foundations Profondes* (pp. 713-745). Paris: Presse de l'ENPC.

Jardine, R., Chow, F., Overy, R., & Standing, J. (2005). *ICP design methods for driven piles in sands and clays.* London: Thomas Telford.

Katzenbach, R., Arslan, U., Moorman, C., & Reul, O. (1998). Piled raft foundation: interaction between piles and raft. *Darmstadt Geotechnics, 4*, 279-296.

King, C. (1981). The stratigraphy of the London Basin and associated deposits. *Tertiary Research Special Paper, 6* . Rotterdam: Backhuys.

Komurka, V. A., Wagner, A. B., & Edil, T. B. (2003). *Estimating soil/pile set-up.* Wisconsin HighWay Research Program Contract No. 0092-00-14, Report No. 0305.

Kuwabara, F. (1989). An elastic analysis for piled raft foundations in a homogeneous soil. *Soils and Foundations, 28* (1), 82-92.

Lacerda, W. A., & Houston, W. N. (1973). Stress relaxation in soils. *Proceedings of 8th International Conference on Soil Mechanics and Foundation Engineering, 1*, pp. 221-227. Moscow.

Lagioia, R., & Nova, R. (1995). An experimental and theoretical study of the behaviour of a calcarenite in triaxial compression. *Geotechnique, 45* (4), 633-648.

Lagioia, R., Puzrin, A. M., & Potts, D. M. (1996). A new versatile expression for yield and plastic potential surfaces. *Computers and Geotechnics, 19* (3), 171-191.

Leroueil, S. (1995). Could it be that clays have no unique way of behaving during consolidation? In *Compression and Consolidation of Clays* (pp. 1039-1048). Yoshikuni & Kusakabe eds., Balkema.

Leroueil, S., Perret, D., & Locat, J. (1996). Strain rate and structuring effects on the compressibility of a young clay. *ASCE Geotechnical Special Publication, 61*, 137-150.

London, U. K. (2010). *Google Earth [online, satellite]*. Retrieved January 2010, from http://www.maps.google.com.

Love, J. P. (2003). Use of settlement reducing piles to support a raft structure. *Proceedings of the Institution of Civil Engineers, Geotechnical Engineering, 156* (GE4), 177-181.

Lovenbury, H. T. (1969). *Creep characteristics of London clay*. PhD Thesis. Imperial College London.

MacDonald, D. H., & Skempton, A. W. (1955). A survey of comparisons between calculated and observed settlements of structures on clay. *Proc. Conf. Correlation of Calculated and Observed Stresses and Deformation in Structures*, (pp. 318-337). London.

Mair, R. J., Hight, D. W., & Potts, D. M. (1992). Finite element analyses of settlements above a tunnel in soft ground. *Contractors Rep. 265.* Crowthorne, England: Transport and Road Research Laboratory.

Mayne, P. W., & Poulos, H. G. (1999). Approximate displacement influence factors for elastic shallow foundations. *Jnl. Geot. & Geoenv. Eng. ASCE, 125* (6), 453-460.

Mesri, G., & Castro, A. (1987). Ca/Cc concept and Ko during secondary compression. *Journal of Geotechnical Engineering, 113* (3), 230-247.

Meyerhof, G. G. (1976). Bearing capacity and settlement of pile foundations. *ASCE Jnl. Geotechnical Eng. Div., 102* (GT3), 197-228.

Meyerhof, G. G. (1956). Discussion paper by Skempton et al. "Settlement analysis of six structures in Chicago and London". *Proc. ICE*, 774-775.

Meyerhof, G. G., & Murdock, L. J. (1953). An investigation of the bearing capacity of some bored and driven piles in London Clay. *Geotechnique, 3*, 267-282.

Mitchell, J. K. (1993). *Fundamentals of soil behaviour* (2nd ed.). New York: John Wiley & Sons.

Mitchell, J. K., Baxter, C. D., & Soga, K. (1997). Time effects on the stress deformation behaviour of soils. *Proceedings of Professor Sakuro Murayama Memorial Symposium* (pp. 1-64). Kyoto University.

Momoya, Y. (1998). *Effects of the period and stress path of consolidation on consolidation characteristics of clays*. MSc thesis. University of Tokyo (in Japanese).

Nash, D. F. (2010). Influence of destructuration of soft clay on time-dependant settlements. In T. Benz, & S. Nordal (Ed.), *Proceedings of the 7th European Conference on Numerical Methods in Geotechnical Engineering* (pp. 75-80). Trondheim, Norway: CRC Press, Taylor & Francis Group.

Naylor, D. J., & Hooper, J. A. (1974). An effective stress finite element analysis to predict the short term and long term behaviour of a piled-raft foundation on London Clay. *Proceedings of Conference on Settlement of Structures*, (pp. 394-402). Cambridge.

O'Brein, A. S. (2010). Visiting Lecture at Imperial College London (9th March 2010). *Pile group design for major structures - Pitfalls and opportunites*. London.

O'Brien, A. S., Hardy, S., Farooq, I., & Ellis, E. A. (2004). Foundation Engineering for the UK's New National Stadium at Wembley. *Proc. 16th Int. Conf. on Soil Mechanics and Geotech. Eng., 2*, p. 1533. Osaka, Japan.

Ottaviani, M. (1975). Three-dimensional finite element analysis of vertically loaded pile groups. *Geotechnique, 25* (2), 159-174.

Padfield, C. J., & Sharrock, M. J. (1983). *Settlement of structures on clay soils* (Vol. 27). London: CIRIA special publication.

Pellew, A. (2002). *Field investigations into pile behaviour in clay*. PhD thesis. University of London (Imperial College of Science, Technology and Medicine).

Perret, D., Locat, J., & Leroueil, S. (1995). Strength development with burial in fine-grained sediments from the Saguenay Fjord, Quebec. *Canadian Geotechnical Journal, 32*, 247-262.

Perzyna, P. (1963). The constitutive equations for work-hardening and rate sensitive plastic materials. *Proc. of vibrational problems, 4* (3), 281-290.

Polshin, D. E., & Tokar, R. A. (1957). Maximum allowable non-uniform settlement of structures. *Proc. 4th ICSMFE. 1*, pp. 402-405. London: Butterwoths.

Potts, D. M., & Gens, A. (1984). The effect of the plastic potential in boundary value problems involving plane strain deformations. *Int Journal Numerical Analytical Methods Geomechanics, 8*, 259-286.

Potts, D. M., & Zdravkovic, L. (2001). *Finite element analysis in geotechnical engineering: Application.* London: Thomas Telford.

Potts, D. M., & Zdravkovic, L. (1999). *Finite element analysis in geotechnical engineering: Theory.* London: Thomas Telford.

Poulos, H. G. (1994). An approximate numerical analysis of pile-raft interaction. *Int. Jnl. Num. Anal. Meths. In Geomechs., 18*, 73-92.

Poulos, H. G. (1991). Analysis of piled strip foundations. In Beer (Ed.), *Comp. Methods & Advances in Geomechanics, 1*, pp. 183-191. Balkema, Rotterdam.

Poulos, H. G. (1990). *DEFPIG users' manual.* University of Sydney, Australia.

Poulos, H. G. (1984). Parametric solutions for strip footings on swelling and shrinking soils. *Proceedings of the 3th International Conference on expansive soils*, (pp. 149-153). Adelaide.

Poulos, H. G. (1989). Pile behaviour - Theory and application. *Geotechnique, 39* (3), 365-415.

Poulos, H. G. (2001). Piled raft foundations: design and applications. *Geotechnique, 51* (2), 95-113.

Poulos, H. G. (1993). Piled rafts in swelling or consolidating soils. *Jnl. Geot. Eng., ASCE , 119* (2), 374-380.

Poulos, H. G. (2002). *Simplified Design Procedure for Piled Raft Foundations.* Coffey Geosciences & University of Sydney (Australia).

Poulos, H. G., & Davis, E. H. (1980). *Pile Foundation Analysis and Design.* New York: John Wiley and Sons.

Poulos, H. G., Small, J. C., Ta, L. D., Sinha, J., & Chen, L. (1997). Comparison of some methods for analysis of piled rafts. *Proceedings of the 14th International Conference of Soil Mechanics and Foundation Engineering, 2*, pp. 1119-1124. Hamburg.

Powell, J. J., & Skinner, H. D. (2006). Capacity changes of bored piles with time. In A. P. Butcher, J. J. Powell, & H. D. Skinner (Ed.), *Reuse of Foundations for Urban Sites: Proceedings of International Conference.* Watford, UK: HIS BRE Press.

Powell, J. J., Butcher, A. P., & Pellew, A. (2003). Capacity of driven piles with time - implications for reuse. *Proc XIIIth ECSMFE. 2*, pp. 335-340. Prague: Millpress.

Randolph, M. F. (1994). Design methods for pile groups and piled rafts. *Proceedings of the 13th International Conference of Soil Mechanics and Foundation Engineering, 5*, pp. 61-82. New Delhi.

Randolph, M. F. (1983). Design of piled raft foundations. *Proceedings of the International Symposium on Recent Developments in Laboratory and Field Tests and Analysis of Geotechnical Problems*, (pp. 525-537). Bangkok.

Randolph, M. F. (2003). Science and empiricism in pile foundation design. *Geotechnique, 53* (10), 847-875.

Randolph, M. F., & Clancy, P. (1993). Efficient design of piled rafts. *Proc. 2nd Int. Geotech Semin. Deep Fdns Bored Auger Piles*, (pp. 119-130). Ghent.

Randolph, M. F., & Wroth, C. P. (1978). Analysis of deformation of vertically loaded piles. *J. Geotech. Engng. Div. ASCE, 104* (GT12), 1465-1488.

Reul, O., & Randolph, M. F. (2003). Piled rafts in overconsolidated clay: comparison of in situ measurements and numerical analyses. *Geotechnique , 53* (3), 301-315.

Roscoe, K. H., & Burland, J. B. (1968). On the generalised stress-strain behaviour of 'wet' clay. *Eng. plasticity* (pp. 535-609). Cambridge Univ. Press.

Roscoe, K. H., & Schofield, A. N. (1963). Mechanical behaviour of an idealised 'wet' clay. *2nd ECSMFE*, *1*, pp. 47-54. Wiesbaden.

Santucci de Magistris, F., Tatsuoka, F., Sato, T., & Koseki, J. (1998). Effects of strain rate and ageing on small strain behaviour on compacted silty sand. *Proceedings of 2nd International Symposium of Hard Soils and Soft Rocks, 1,* pp. 843-854. Balkema, Rotterdam.

Schmertmann, J. H. (1991). The mechanical ageing of soils. *Journal of Geotechnical Engineering, 117* (9), 1228-1330.

Schofield, A. N., & Wroth, C. P. (1968). *Critical state soil mechanics.* London: McGraw Hill.

Singh, A., & Mitchell, J. K. (1968). General stress-strain-time function for soils. *Journal Soils Mechanics and Foundations Division, ASCE, 94* (1), 21-46.

Sinha, J. (1997). *Piled raft foundations subjected to swelling and shrinking soils*. PhD Thesis. Australia: University of Sydney.

Skempton, A. W. (1959). Cast in situ bored piles in London clay. *Geotechnique, 9*, 153-173.

Skempton, A. W. (1961). Horizontal stresses in an overconsolidated Eocene clay. *Proceedings of the 5th International Conference of Soil Mechanics and Foundation Engineering, 1*, pp. 351-357. Paris.

Skempton, A. W. (1951). The Bearing Capacity of Clays. *Building Research Congress* (pp. 180-189). London: ICE.

Skempton, A. W., & MacDonald, D. H. (1956). Allowable settlement of buildings. *Proceedings ICE, 5* (Part 3), 727-768.

Skempton, A. W., Schuster, F. R., & Petley, D. J. (1969). Joints and fissures in the London Clay at Wraysbury and Edgware. *Geotechnique, 19* (2), 205-217.

Skyscrapernews.com. (2008). *Empress state building [image]*. Retrieved September 8, 2008, from http://www.skyscrapernews.com/buildings.php?id=80

Som, N. N. (1968). *The effects of stress path on deformation and consolidation of London Clay*. PhD thesis. Imperial College, University of London.

Sommer, H. (1991). Entwicklung der Hochhausgrundungen in Frankfurt/Main. *Festkolloquium 20 Jahre Grundbauinstitut Prof. Dr. Ing H. Sommer und Partner*, (pp. 47-62). Germany.

Sommer, H., Tamaro, G., & DeBeneditis, C. (1991). Messe Turm, foundations for the tallest building in Europe. *Proceedings of the 4th International Conference in Piling and Deep Foundations*, (pp. 139-145).

Sommer, H., Wittman, P., & Ripper, P. (1985). Piled raft foundation of a tall building in Frankfurt clay. *Proceedings of the 11th International Conference of Soil Mechanics and Foundation Engineering, 4*, pp. 2253-2257. San Francisco.

Sorensen, K. K., Baudet, B. A., & Simpson, B. (2007). Influence of structure on the time-dependent behaviour of a stiff sedimentary clay. *Geotechnique, 57* (1), 113-124.

Sorrensen, K. K. (2006). *Influence of viscosity and ageing on the behaviour of clays*. PhD thesis. University of London.

St John, H. D., & Chow, F. C. (2006). Reusing piled foundations - two case studies. In A. P. Butcher, J. J. Powell, & H. D. Skinner (Ed.), *Reuse of Foundations for Urban Sites: Proceedings of International Conference.* Watford, UK: HIS BRE Press.

Standing, J. R., & Burland, J. B. (2006). Unexpected tunnelling volume losses in the Westminster area. *Geotechnique, 56*, 11-26.

Starzec, P., Norman, J., Chapman, T. J., & Anderson, S. A. (2006). Foundation reuse decision model. Part I: model structure. In A. P. Butcher, J. J. Powell, & H. D. Skinner (Ed.), *Reuse of Foundations for Urban Sites: Proceedings of International Conference.* Watford, UK: HIS BRE Press.

Tatsuoka, F. (2003). Effects of viscous properties and ageing on the stress-strain behaviour of geomaterials. *ASCE Geotechnical Special Publication, 143*, 1-60.

Tatsuoka, F., Ishihara, M., Di Benedetto, H., & Kuwano, R. (2002). Time-dependent shear deformation characteristics of geomaterials and their simulation. *Sois and Foundations, 42* (2), 103-129.

Tatsuoka, F., Santucci de Magistris, F., Hayano, K., Koseki, J., & Momoya, Y. (1998). Some new aspects of time effects on the stress-strain behaviour of stiff geomaterials. *Proceedings of the 2nd International Symposium of Hard Soils and Soft Rocks, 3*, pp. 1285-1371. Balkema, Rotterdam.

Tavenas, F., & Leroueil, S. (1977). Effects of stresses and time on yielding of clays. *9th International Conference of Soil Mechanics and Foundation Engineering, 1*, pp. 319-326. Tokyo.

Tavenas, F., Leroueil, S., La Rochelle, P., & Roy, M. (1978). Creep behaviour of an undisturbed lightly overconsolidated clay. *Canadian Geotechnical Journal , 15* (3), 402-423.

Taylor, P. T. (1966). *Age effect on shaft resistance and effect of loading rate on load distribution of bored piles*. PhD thesis. University of Sheffield.

Tomlinson, M., & Woodward, J. (2009). *Pile Design and Construction Practice* (5th ed.). London, UK: Taylor & Francis.

Unwin, H., & Jessep, R. A. (2004). Long term pile testing in London Clay: a case study. *Geotechnical Engineering, Proc. ICE* (GE2), 57-63.

Vaid, Y. P., & Campanella, R. G. (1977). Time-dependent behaviour of undisturbed clay. *J. Geotech. Div., ASCE, 103* (7), 693-709.

Van Impe, W. F., & Clerq, L. (1995). A piled raft interaction model. *Geotechnica, 73*, 1-23.

Vaziri, M., & Windle, J. (2006). Testing strategy for the reuse of existing piles: case study at Belgrave House, London. In A. P. Butcher, J. J. Powell, & H. D. Skinner (Ed.), *Reuse of Foundations for Urban Sites: Proceedings of International Conference.* Watford, UK: HIS BRE Press.

Viggiani, C. (2001). Analysis and design of piled foundations: First Arrigo Croce Lecture. *Riv. Ital. di Geotechnica, 35* (1), 47-75.

Viggiani, C. (1998). Pile groups and piled rafts behaviour. In v. Impe, & Haegman (Eds.), *Deep foundations on bored and auger piles* (pp. 77-90). Rotterdam: Balkema.

Whitaker, T., & Cooke, R. W. (1966). An investigation of the shaft and base resistance of large bored piles in London Clay. *Symposium on Large Bored Piles* (pp. 7-49). ICE.

Wiesner, T. J., & Brown, P. T. (1976). Behaviour of piled strip footings subject to concentrated loads. *Aust. Geomechs. Jnl., G6*, 1-5.

Wikipedia. (2008). *Empress state building [photograph]*. Retrieved September 8, 2008, from http://en.wikipedia.org/wiki/Empress_State_Building

Williams, J. (2006). Archaelogy and historic buildings as drivers for foundation reuse. In A. P. Butcher, J. J. Powell, & H. D. Skinner (Ed.), *Reuse of Foundations for Urban Sites: Proceedings of International Conference.* Watford, UK: HIS BRE Press.

Wongsaroj, J., Soga, K., & Mair, R. J. (2007). Modelling of long-term ground response to tunnelling under St James's Park, London. *Geotechnique, 57* (1), 75-90.

Yamashita, K., Kakurai, M., & Yamada, T. (1994). Investigation of a piled raft foundation on stiff clay. *Proceedings of the 13th International Conference of Soil Mechanics and Foundation Engineering, 2*, pp. 543-546. New Delhi.

Yamashita, K., Kamurai, M., Yamada, T., & Kuwabara, F. (1993). Settlement behaviour of a five-storey building on a piled raft foundation. *Proceedings of the 2nd International Geotechnical Seminar on Deep Foundations and on Bored and Auger Piles* (pp. 3512-3560). Ghent: Balkema, Rotterdam.

Yin, J. H., & Graham, J. (1989). Viscous-elastic-plastic modelling of one-dimensional time-dependent behaviour of clays. *Canadian Geotechnical Journal, 26*, 199-209.

Yin, J. H., Zhu, J. G., & Graham, J. (2002). A new elastic visco-plastic model for time-dependent behaviour of normally and overconsolidated clays: theory and verification. *Canadian Geotechnical Journal, 39*, 157-173.

Zdravkovic, L., Potts, D. M., & Jackson, C. (2003). Numerical study of the effect of preloading on undrained bearing capacity. *International Journal of Geomechanics, 3* (1), 1-10.

Zdravkovic, L., Potts, D. M., & St John, H. D. (2005). Modelling of a 3D excavation in finite element analysis. *Geotechnique, 55*, 497-513.

Ziegler, P. A. (1990). *Geological Atlas of Western and Central Europe* (2nd ed.). Den Haag, Netherlands: Shell Internationale Petroleum Maatschappij B.V.